



ON THE DESIGN AND FURTHER APPLICATIONS OF
IRIDIUM(I) COMPLEXES IN HYDROGEN ISOTOPE
EXCHANGE PROCESSES

Marc Reid

PhD Thesis

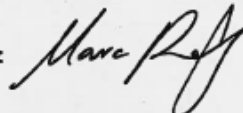
2015

Declaration of Authenticity and Author's Rights

This thesis is the result of the author's original research. It has been composed by the author and has not been previously submitted for examination which has led to the award of a degree.

The copyright of this thesis belongs to the author under the terms of the United Kingdom Copyright Acts as qualified by University of Strathclyde Regulation 3.50. Due acknowledgement must always be made of the use of any material contained in, or derived from, this thesis.

Signed:



Date:

18/06/15

“It doesn't matter how beautiful your theory is, it doesn't matter how smart you are. If it doesn't agree with experiment, it's wrong.”

“The Prize is the pleasure of finding the thing out.”

Richard P. Feynman

Abstract

A new synthetic procedure for isolation of three established Kerr group catalysts has been successfully developed. The final yield of these catalysts has now been improved beyond those published in the literature, and has allowed for the commercialisation of such catalysts for the first time.

The synthesis of a series of iridium(I) complexes of the type [(COD)Ir(IMes)(PPh₃)]X (X = BF₄, OTf, and BArF) has been established. Application of these species in hydrogen isotope exchange (HIE) processes revealed more efficient catalysis and a wider solvent scope when X = BArF. Additionally, these findings have allowed for the development of a novel method for *ortho*-HIE in unprotected tetrazoles under basic conditions, revealing a rare account of *N*-H tetrazole C-H activation and a new mode of reactivity for Kerr group HIE catalysts.

Towards predictive catalyst design, a combined experimental and theoretical model has been developed to describe the impact of ligand *combinations* on catalyst performance. Experimentally, this has resulted in a further broad range of novel NHC/phosphine iridium carbonyl complexes, as well as a catalyst ‘quick screen’ method based on *in-situ* formation of Ir dihydride complexes. Computationally, novel parameters have been assessed, culminating in a combined ligand map derived from Principal Component Analysis (PCA) of 140 DFT-optimised iridium complexes. Ligand mapping methods have been employed to assess the use of natural product *Lepidiline A* as a NHC ligand precursor in novel HIE catalysts, revealing the almost purely electronic influence of 4,5-dimethyl substitution on the imidaz-2-ylidene ring. The PCA model has also highlighted complexes of the type [(COD)Ir(NHC)Cl] to be promising in delivering orthogonal reactivity to the now traditional NHC/phosphine pairing. This analysis has led to the realisation of the first regio- and chemoselective catalytic labelling methods for primary sulfonamides and aldehydes.

Finally, a novel, one-parameter approach has been developed to describe chelating and monodentate ligand spheres on the same comparable and quantifiable footing. Chelating NHC/phosphine-ligated iridium catalysts have been designed, synthesised, and successfully applied to *ortho*-labelling of previously inaccessible sulfones, secondary sulfonamides, and bulky tertiary amides.

Abbreviations

°C	Degrees Celcius
ADMET	Adsorption, Distribution, Metabolism, Excretion, and Toxicity
BArF	Tetrakis[3,5-bis(trifluoromethyl)phenyl]borate; B(3,5-CF ₃ -C ₆ H ₃) ₄
Bn	Benzyl; PhCH ₂ -
ⁿ Bu	<i>n</i> -Butyl; CH ₃ (CH ₂) ₃ -
COD	Cycloocta-1,5-diene; C ₈ H ₁₂
CPME	Cyclopentyl methyl ether
Cy	Cyclohexyl; C ₆ H ₁₁ -
DCM	Dichloromethane; CH ₂ Cl ₂
DFT	Density Functional Theory
DMF	<i>N,N</i> -Dimethylformamide
DMSO	Dimethylsulfoxide
Et	Ethyl; CH ₃ CH ₂ -
g	Grammes
h	Hours
HIE	Hydrogen Isotope Exchange
Hz	Hertz
IMe	1,3-Bis(methyl)imidazol-2-ylidene
IMes	1,3-Bis(2,4,6-trimethylphenyl)imidazol-2-ylidene
ⁱ Pr	1,3-Bis(2,6-diisopropylphenyl)imidazol-2-ylidene
ⁱ Pr	<i>iso</i> -Propyl; (CH ₃) ₂ CH-
IPA	<i>iso</i> -Propyl alcohol
IR	Infrared
<i>J</i>	Coupling Constant
L	Ligand
Me	Methyl; CH ₃ -
Mes	Mesityl
mg	Milligrammes
MHz	Megahertz
min	Minutes

mL	Millilitres
mmi	Membered Metallocyclic Intermediate
mmol	Millimoles
MPa	Mega Pascals
mol	Moles
NCE	New Chemical Entity
NHC	<i>N</i> -Heterocyclic Carbene
NMR	Nuclear Magnetic Resonance
	s – singlet
	d – doublet
	t – triplet
	q – quartet
	m – multiplet
	b – broad
Pa	Pascals
PES	Potential Energy Surface
PCA	Principle Components Analysis
Ph	Phenyl; C ₆ H ₅ -
ppm	Parts Per Million
psi	Pounds Per Square Inch
py	Pyridine
r.t.	Room Temperature
S	Solvent
SIMes	1,3-Bis(2,4,6-trimethylphenyl)-4,5-dihydroimidazol-2-ylidene
^t Bu	<i>tert</i> -Butyl; (CH ₃) ₃ C-
Temp.	Temperature
TEP	Tolman Electronic Parameter
<i>tert</i>	Tertiary
THF	Tetrahydrofuran

Acknowledgments

Firstly, I am grateful to Professor Billy Kerr for kindly welcoming me into his research team. For your untiring determination to help and motivate me, I offer my sincere thanks. I will never look at a broadsheet in the same way again!

For their friendship, support, interest, and contributions to a wonderfully R-rated viva t-shirt, I thank members of the Kerr group. From the Old Guard, I thank: Drs Calumbo, Malky, Weber-Weber, R-Bo, Goldie, Monksy-Moo, Ali, Chief, and Linsey. From the New Age Alcoholics, I tip the bunnet to: Murali, Muddster, Andy Malcolm, and Flounder.

For the fun reminder that age creeps up fast, I thank the undergraduates I've worked with over the years: Tim, Jenny, Jen, Kirsty, Rory, and Patrick. May they rest in peace.

I would also like to thank Drs L-Patz and Monty for their X-ray vision and enviable ability to spot the mistakes that the rest of us mere mortals miss!

My interest in the computational aspects of chemical research would have come to nothing without the enviable, Feynmann-esque mathematical knowledge of Dr Tell Tuttle. For his guidance and support, I offer my genuine thanks. Thanks must also go to TuttleLab members Dr Bhaskar Mondal, Daniel Cannon, Ivan Ramos-Sasselli, and Greg Anderson for their patience in showing me the footery ropes of DFT-based calculations. How many basketballs can you guys count?

Having solved all crystal structures in this thesis (and many others not included herein), I thank the skill, enthusiasm, and 'on tap' assistance from Dr Alan Kennedy.

For hosting my fun, productive, and memorable industrial research project, I offer my thanks to Dr Jens Atzrodt, Dr Volker Derdau, Remo Weck, and fellow colleagues at Sanofi. May I never encounter Handkäs mit Musik ever again!

Lastly, I reserve my deepest and most enduring thanks for my fiancée (and soon to be wife), Amanda. For displaying an inhuman level of patience and accommodation for my work, I thank you to no end. Weekends are back!

List of Publications

Stated below are the works from (or associated with) this thesis that have been accepted for publication in the primary literature. A number of additional publications are planned for 2015-16. Authorship is recorded alphabetically or by institution rather than by individual author contributions.

A. R. Cochrane, S. Irvine, W. J. Kerr, M. Reid, S. Andersson, G. N. Nilsson, *J. Label. Compd. Radiopharm.* **2013**, *56*, 451 – 454. [Invited paper]

A. R. Kennedy, W. J. Kerr, M. Reid, R. Moir, *Org. Biomol. Chem.* **2014**, *12*, 7927 – 7931.

J. A. Brown, A. R. Cochrane, S. Irvine, B. Mondal, J. A. Parkinson, L. C. Paterson, M. Reid, T. Tuttle, S. Andersson, G. N. Nilsson, *Adv. Synth. Catal.* **2014**, *356*, 3551 – 3562.

W. J. Kerr, M. Reid, T. Tuttle, *ACS Catal.* **2015**, *5*, 402 – 410.

J. Atzrodt, V. Derdau, W. J. Kerr, M. Reid, P. Rojahn, R. Weck, *Tetrahedron* **2015**, *71*, 1924 – 1929.

J. Devlin, W. J. Kerr, D. M. Lindsay, T. J. D. McCabe, M. Reid and T. Tuttle, *Molecules* **2015**, *20*, 11676 – 11698. [Invited paper]

CONTENTS

1. INTRODUCTION	11
1.1 PHARMACEUTICAL INDUSTRY AND DRUG DEVELOPMENT	11
1.2 ISOTOPIC LABELLING IN EARLY STAGE DRUG DESIGN	12
1.3 HETEROGENEOUS HIE CATALYSIS	13
1.4 HOMOGENEOUS HIE CATALYSIS.....	15
1.4.1 Platinum.....	15
1.4.2 Rhodium.....	16
1.4.3 Ruthenium.....	23
1.4.4 Palladium.....	29
1.4.5 Iridium	32
1.5 KEY CONCEPTS IN SELECTED LIGAND DESIGN	42
1.5.1 Phosphines as Ligands.....	42
1.5.2 N-Heterocyclic Carbenes as Ligands.....	45
2. PROPOSED WORK	50
3. EXPANDING THE APPLICABILITY OF [(COD)Ir(NHC)(PR₃)]X COMPLEXES IN HIE PROCESSES.....	56
3.1 ALTERNATIVE SYNTHETIC ROUTE TO [(COD)Ir(IMes)(PR ₃)]PF ₆	56
3.2 ANION EFFECTS IN IRIIDIUM-CATALYSED ISOTOPE EXCHANGE PROCESSES.....	59
3.3 BASE-SENSITIVE HIE: <i>ORTHO</i> -DIRECTED LABELLING OF UNPROTECTED TETRAZOLES.....	69
4. EXPERIMENTAL & THEORETICAL LIGAND DESIGN METHODS IN HIE PROCESSES.....	79
4.1 EXPERIMENTAL EVIDENCE FOR OBSERVABLE LIGAND PAIRING BEHAVIOUR	79
4.1.1 Ir(I) Di- & Tricarbonyl Complexes in the Assessment of Combined Ligand Sterics	79
4.1.2 Ir(I) Chloro-carbonyl Complexes in the Study of Combined Ligand Electronics.....	82
4.1.3 Ir(III) Dihydride Complexes in the Study of Combined Ligand Electronics.....	85
4.2 THEORETICAL LIGAND DESIGN METHODS IN HIE PROCESSES	87
5. COMBINED EXPERIMENTAL & THEORETICAL APPROACH TO UNSOLVED CHALLENGES IN HIE	92
5.1 ALTERNATIVE NHC LIGANDS IN HIE CATALYST MOTIF [(COD)Ir(NHC)(PR ₃)]X	92
5.2 <i>ORTHO</i> -DEUTERATION OF 1° SULFONAMIDES – AN EXPERIMENTAL & COMPUTATIONAL STUDY.....	109
5.3 REGIOSELECTIVE CONTROL IN THE DEUTERATION OF AROMATIC ALDEHYDES – AN EXPERIMENTAL & COMPUTATIONAL STUDY	127
5.4 ON THE FUNDAMENTALS OF CHELATING LIGAND DESIGN TOWARDS NOVEL HIE TECHNOLOGIES.....	141
6. CONCLUSIONS.....	150
7. FUTURE WORK.....	155
8. EXPERIMENTAL.....	162

9. COMPUTATIONAL DETAILS	321
10. REFERENCES	327

1. Introduction

1.1 Pharmaceutical Industry and Drug Development

With the world's population now in excess of 7 billion,¹ modern society is increasingly dependent on the ever-evolving chemical sciences and, more specifically, the pharmaceutical industry. In 2012, it was believed that the global pharmaceutical market value reached \$962 billion; a value which increased by a further 3.3% in 2013.² Such intimidating financial figures can be attributed to the constant need for new medicines capable of fighting new viruses, as well as the desire to eradicate existing diseases.

Despite the apparent growth in the industry, pharmaceutical companies are burdened by extensive costs in designing, manufacturing, and marketing drugs. The development of just one new chemical entity (NCE) from conception to marketplace is estimated to cost a staggering \$1.3 billion over a period as long as fifteen years (**Figure 1**).^{3,4} Why is expenditure so high? With around 98% of all NCEs failing in pre-clinical trials, it is evident that the majority of potential drug molecules that are synthesised possess inherently poor pharmacokinetics. Indeed, if the efficacy of characterising the pharmacokinetic properties of a potential drug molecule was increased by a mere 10%, savings of approximately \$100 million per drug could be realised.⁵ It is the adsorption, distribution, metabolism, excretion, and toxicological (ADMET) properties of these molecules that are central to the work of the medicinal chemist, and the earlier in a drug discovery project these properties are understood, the greater the potential cost saving overall.

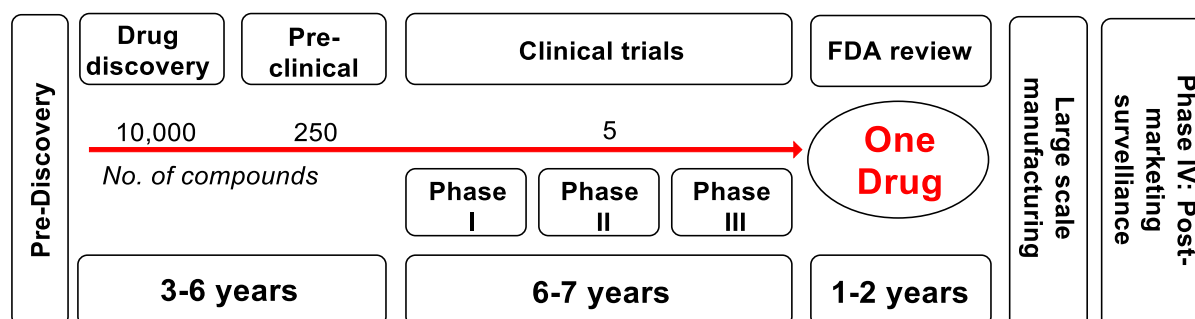


Figure 1. Simplified diagram showing the interwoven aspects of a drug design project.

1.2 Isotopic Labelling in Early Stage Drug Design

To assess a drug candidate's metabolic fate, the chemist must first have a flexible technique with which to study it. For example, significant investment has been made in LC-MS techniques coupled with structure prediction software.⁶ However, this method is heavily dependent on the ionisation properties of the drug and its associated metabolites. Alternatively, as a marine biologist may physically tag a whale to monitor migration patterns, a chemist can deliver a radioactive 'tag' or 'label' to a drug molecule in order to gain vital information on its ADMET properties. This method is not dependent on the ionisation of the parent drug or its metabolites. It can also be used to detect where an unreacted drug is stored *in vivo* without necessarily knowing how the drug is bound. Consequently, *isotopic labelling* is the gold standard method by which early stage drug discovery processes are optimised.

Isotopes of a particular element have an identical number of protons in their respective nuclei but possess an unequal number of neutrons. Namely, they share the same atomic number but have different mass numbers, as exemplified for hydrogen (**Figure 2**).⁷ The stability of an isotope is governed by the ratio of neutrons to protons within the nucleus, thus giving rise to two possible circumstances. Firstly, a *heavy isotope* of an element, such as ^2H or ^{13}C , has a stable nucleus and tends to be found in nature, albeit at lower abundances than their more common counterparts, ^1H and ^{12}C , respectively. In the alternative case, *radioisotopes*, such as ^3H or ^{14}C , have an unstable neutron/proton ratio and decay, *via* emission of radiation or particles, to form other elements, or different isotopes of the parent element.

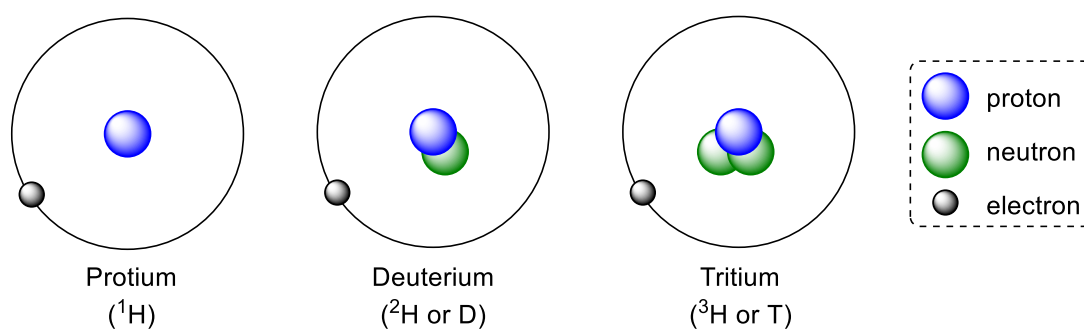


Figure 2. Simplified Bohr representations of the isotopes of hydrogen.

Undoubtedly, the synthesis and supply of isotopically-labelled molecules has a sustained importance in the study of the aforementioned metabolic processes. It is therefore unsurprising that there is a large and growing body of research dedicated to the synthesis of

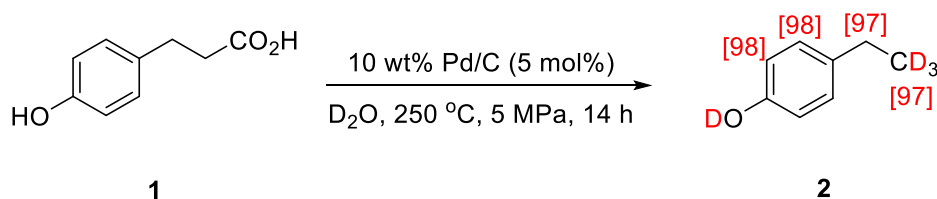
isotopically-labelled compounds. The labelling of molecules with ^{13}C or ^{14}C is most readily achieved through the use of commercially available, isotopically-enriched starting materials. While such a technique ensures a regiospecific label will be present in the desired target molecule, it ultimately comes at the price of unwanted additional steps in the synthesis.⁶

Research into deuterium (^2H or D) and tritium (^3H or T) labelling is more substantial than that for other isotopes, and has been developed on a number of fronts over the past 60 years.^{6,8-16} Further to this, key developments in synthetic strategies and analytical techniques over the past three decades is gradually making tritium labelling the preferred technique in many ADMET studies.¹¹ In one particularly active branch of such research, *hydrogen isotope exchange* (HIE) is commonly employed to deliver deuterium or radioactive tritium to pharmaceutical drug candidates in one synthetic step. As well as circumventing the requirement for isotopically-enriched starting materials in synthesising tritiated drug candidates,^{6,11} HIE can also provide analogous deuterated compounds for use as internal standards for mass spectrometry,^{17,18} for kinetic isotope studies,^{19,20} and for the alteration of reaction pathways in total syntheses.²¹

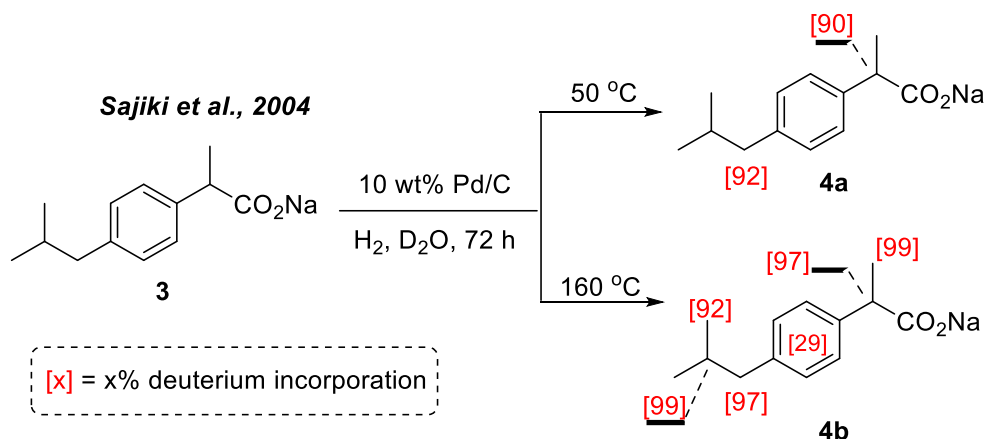
1.3 Heterogeneous HIE Catalysis

By means of heterogeneous catalysis, Pd/C, PdO/Ba₂SO₄, Rh black, Ru black, and Raney Nickel have all been employed with various deuterium and tritium sources to label organic molecules *via* HIE.^{9,13,22-27} Such methods appear attractive, as the catalyst can be separated from the reaction mixture by simple filtration; however, isotopic labelling employing such catalyst systems often requires elaborate and harsh reaction conditions. In addition to this, molecules are often labelled in a non-regioselective manner, under forceful and (partially) reductive conditions, as illustrated in the deuteration of the substituted phenol, **1**, by Mastubara and co-workers (**Scheme 1**, top).^{24,25} There are, however, some especially attractive developments in the field of heterogeneous labelling. Of particular note, Sajiki has shown the highly regioselective labelling of the benzylic positions in the sodium salt of Ibuprofen, **3**, using D₂ generated *in-situ* from D₂O and H₂ as an inexpensive source of the heavy isotope, albeit with long reaction times (**Scheme 1**, bottom).¹³ Global labelling of the same compound could be readily achieved at higher temperatures.

Matsubara et al., 2004



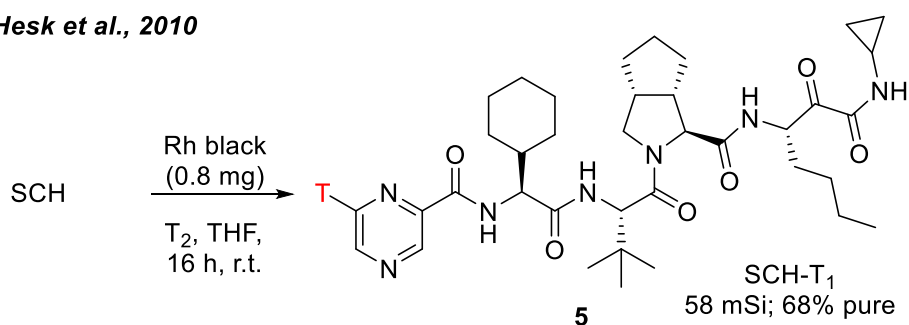
Sajiki et al., 2004



Scheme 1. HIE using heterogeneous transition metal catalysis.

Alternatively, aromatic labelling selectivity using a heterogeneous catalyst was demonstrated by Hesk and co-workers, using Rh black and tritium gas to install a single isotopic label on the pyrazine ring of the Merck drug candidate, SCH, **5** (Scheme 2).²⁸

Hesk et al., 2010



Scheme 2. Selective aromatic tritiation using heterogeneous Rh catalysis.

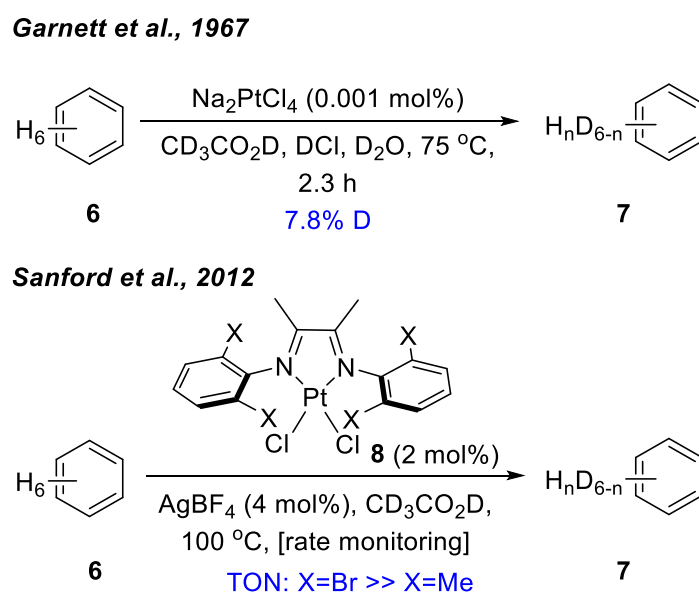
Above all else, the major limitation of heterogeneous HIE is the lack of predictability in where the isotopic label will be placed on the molecule of interest. The chemist may wish to track and follow different metabolic fragments of the parent drug at different times. As a result, the greatest progress in flexible and predictable HIE methods has come from homogeneous transition metal catalysis, and is the main focus of the work presented herein.

1.4 Homogeneous HIE Catalysis

The study of the d-block metals for homogeneous catalysis is extremely diverse and has had a major impact on organic synthesis and catalysis.^{29,30} As homogeneous catalysts are often single molecule species, their catalytic properties can be tuned by judicious manipulation of the ligands bound to the reactive metal centre. Furthermore, this mode of catalysis often leads to very mild and industrially attractive reaction conditions. Therefore, despite advances in heterogeneous catalysis (*vide supra*), acid/base-mediated HIE,¹⁴ and even organocatalytic HIE methods,³¹ it is homogeneous catalysis that dominates modern research in HIE.

1.4.1 Platinum

In 1967, Garnett and Hodges reported one of the first examples of HIE employing homogeneous catalysts.³² Using Pt(II) salts, in the presence of deuterated acetic acid, water and hydrochloric acid, various arenes were labelled, albeit in a non-regioselective manner (**Scheme 3**, top). Many years later, Sanford and co-workers explored a similar deuterium labelling strategy using diimine-ligated Pt(II) catalysts, **8** (**Scheme 3**, bottom).^{33,34} It was found that a bromo- rather than methyl-substituted ligand provided the most active catalyst, with this being hypothesised to originate from the greater propensity of the bromine to coordinate to and stabilise the metal centre.³⁴

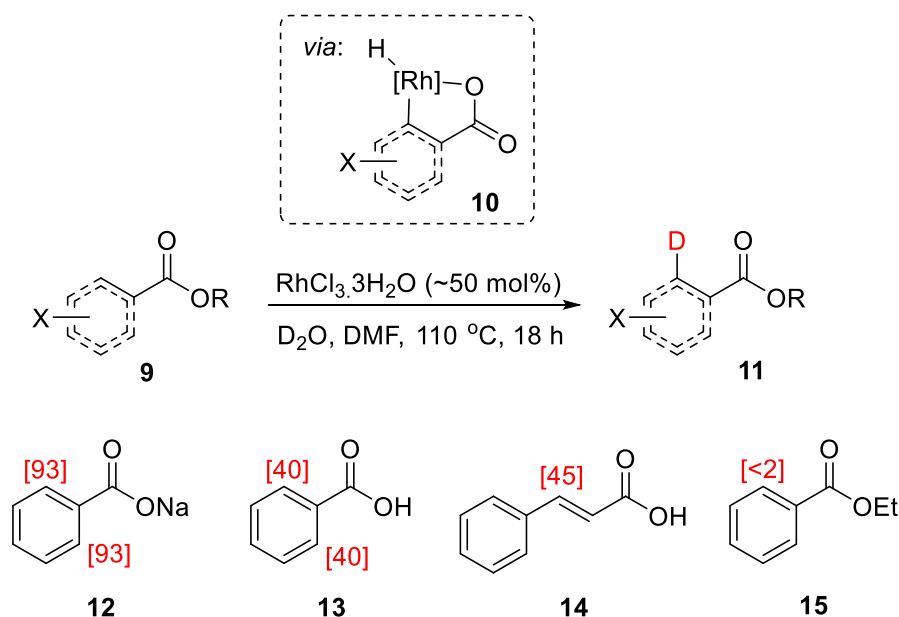


Scheme 3. Global aromatic HIE *via* homogeneous Pt(II) catalysis.

1.4.2 Rhodium

After his initial work with Pt(II), Garnett later detailed the first use of $\text{RhCl}_3 \cdot 3\text{H}_2\text{O}$ as a homogeneous catalyst in HIE.³⁵ Although aromatic deuteration was, again, accomplished non-regioselectively, important advantages over earlier work in *heterogeneous* catalytic methods were discussed, supporting the rigorous area of research that homogeneous HIE catalysis has become.

In 1982, a new dimension was added to the study of deuterium incorporation in organic molecules when Lockley demonstrated that aromatic and α,β -unsaturated carboxylic acids could be labelled regioselectively using $\text{RhCl}_3 \cdot 3\text{H}_2\text{O}$ (**Scheme 4**).³⁶ In contrast to Garnett's work, which had *not* illustrated any preference with respect to the site of labelling, Lockley's introduction of the carboxyl functionality to the substrate demonstrated a clearly *ortho*-directed deuteration process. The chosen catalyst was the most active of several platinum group metal species tested, including $\text{IrCl}_3 \cdot 3\text{H}_2\text{O}$ and $\text{Ru}(\text{acac})_3$. During the study, it was noted that sodium benzoate, **12**, was labelled at a rate faster than the free carboxylic acid, **13**, and *trans*-cinnamic acid, **14**. Furthermore, labelling of the more weakly coordinating ethyl ester derivative, **15**, did not proceed under the reaction conditions employed. Armed with these observations, Lockley postulated that the observed regioselectivity in the isotope exchange process resulted from prior complexation of the substrate to the rhodium centre through the lone pair of electrons on the carbonyl group (**10, Scheme 4**).³⁶ Such coordination would enable the *ortho*-positions of the substrate to be selectively deuterated due to their close proximity to the reactive metal centre. This theory was strengthened by the additional observation that a reduction in the volume of DMF co-solvent employed *increased* the level of deuterium incorporation achieved, most likely due to removal of a strong competitor for coordination.



Lockley's methodology was later extended to explore the regioselective deuteration of aromatic amines, amides, and anilides.^{37,38} Significant *ortho*-directed deuterium incorporation was detected for primary and secondary derivatives of each substrate, but reduced activity was noted for bulkier tertiary derivatives (**Figure 3**). It was believed that the rate of catalyst degradation competed with the rate of labelling for the tertiary substrates, ultimately limiting the attraction of RhCl_3 as a catalyst for directed HIE processes. Nonetheless, further extension of this work into tritiation chemistry was later documented by Hesk, Jones, and Lockley who demonstrated that *N*-heterocycles such as pyridines and pyrazoles could also act as viable handles for *ortho*-directed labelling.³⁹

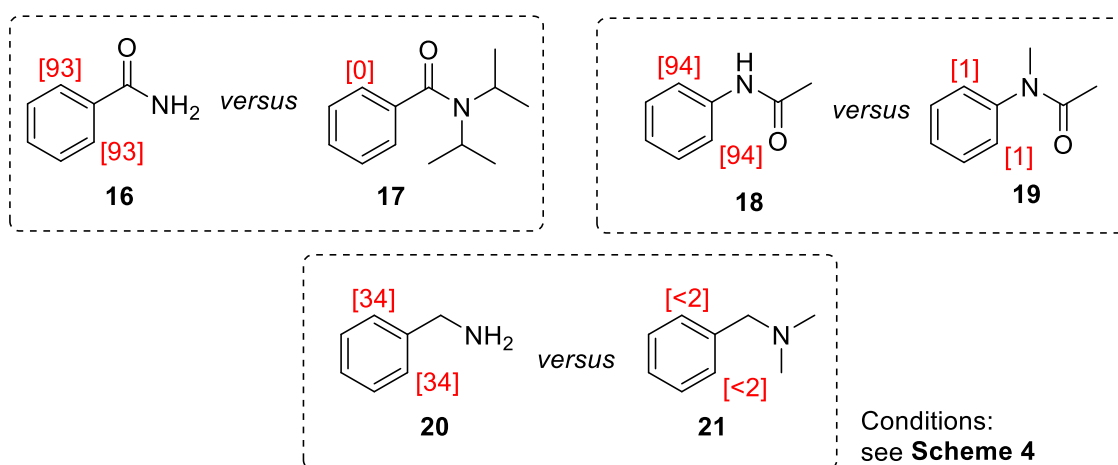
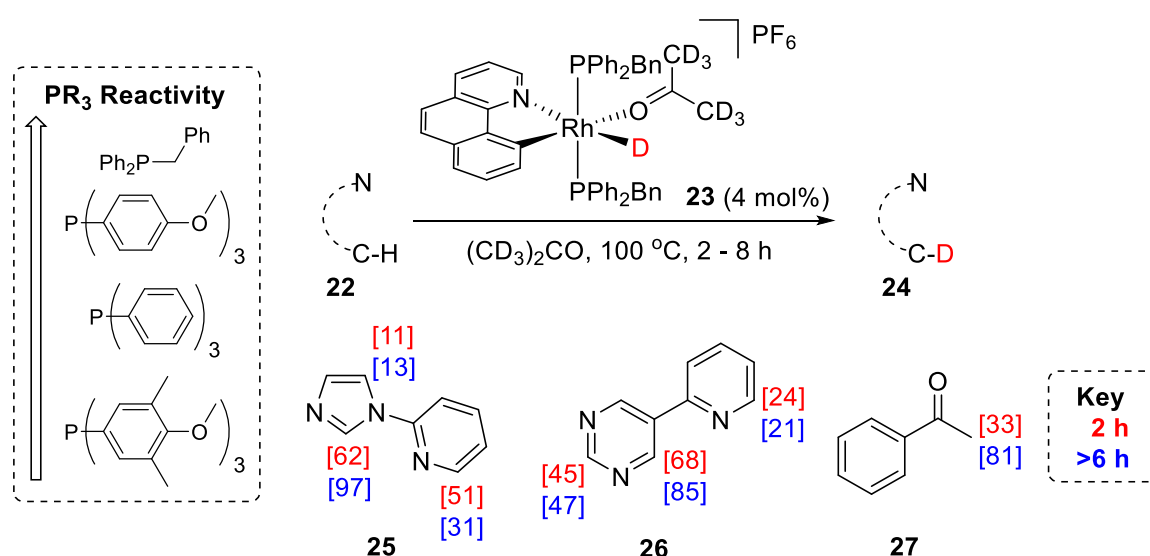


Figure 3. Free *versus* protected nitrogen directing groups in Rh(III)-catalysed HIE.

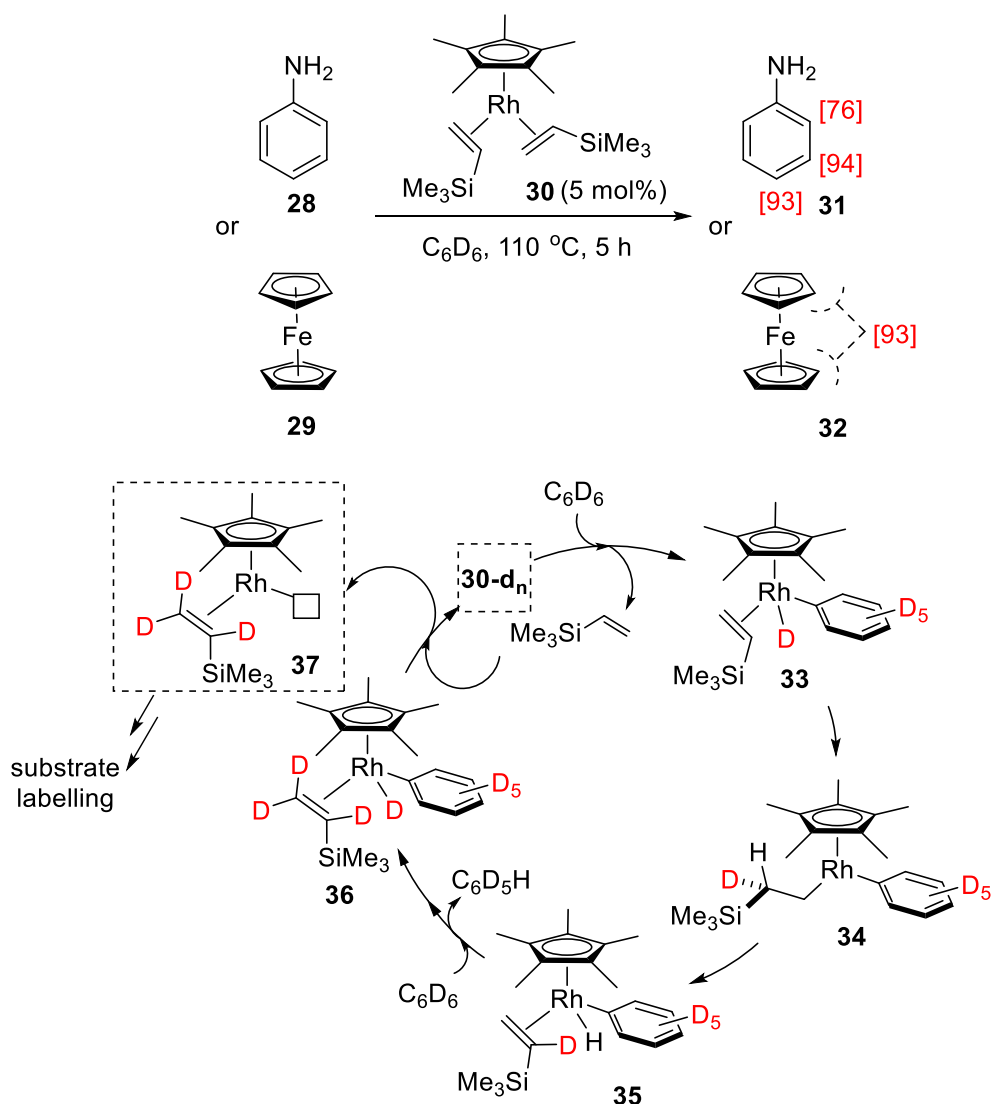
The same principles applied by Lockely, Hesk, and Jones were later put to use by Li and co-workers using a bis-phosphine, chelation-assisted Rh(III) catalyst series, led by **23**, in the directed labelling of various *N*-heterocycles (**Scheme 5**).⁴⁰ The catalyst structure was optimised by simple screening of available phosphine ligands. In general, more electron-donating phosphines provided more active catalysts, with **23** being optimal. Excessively large phosphines were less active and thought to hinder necessary coordination of substrate to Rh. Intriguingly, only those labelling sites most easily accessed *via* a metal-coordinating atom were found to have significantly increased D-incorporation with longer reaction times (**25** and **26**), with some base-sensitive sites even being subject to *decreased* D-incorporation. This demonstrated an element of thermodynamic selectivity rarely encountered in HIE catalysis. The alkaline nature (and ultimate limitation) of Li's catalysts was demonstrated in labelling acetophenone, **27**, where only the acid-sensitive alkyl sites were exchanged.



Scheme 5. Directed HIE using basic chelation-assisted Rh(III)-catalysts.

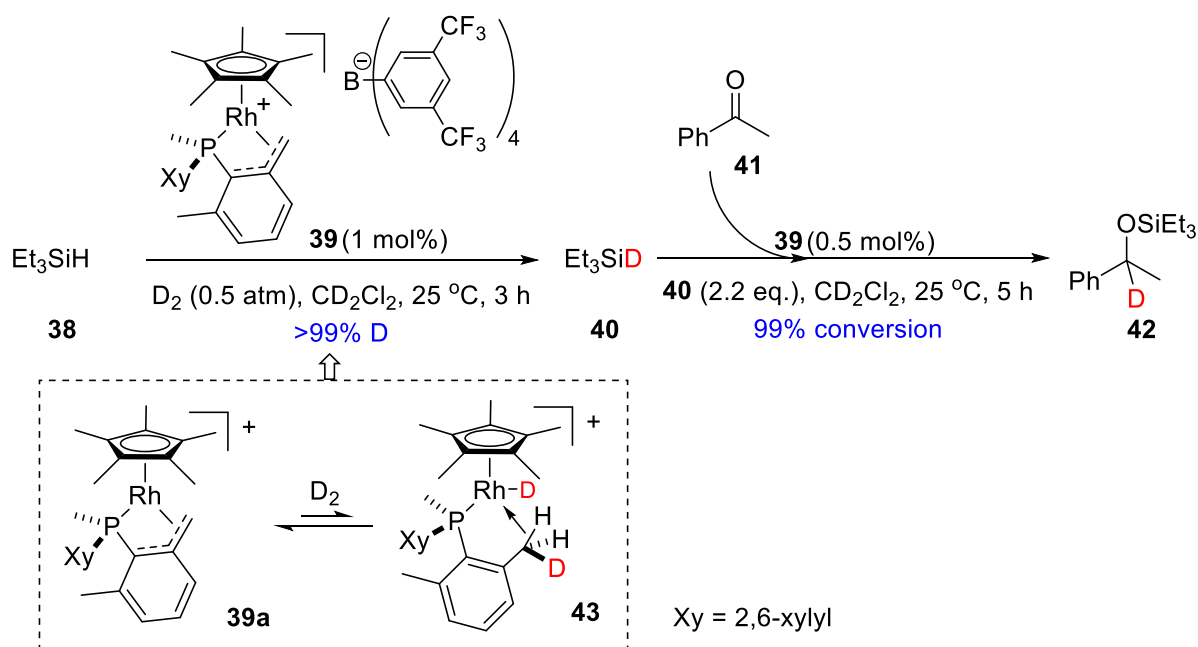
HIE processes *via* Rh(III) catalysis have since been developed on several complementary fronts by means of altering the ligand design. For example, based on fundamental C-H activation studies by Jones,⁴¹ a series of pentamethylcyclopentadienyl (Cp*)-ligated complexes has emerged that catalyse several useful HIE processes. Firstly, Brookhart and co-workers showed that the Rh(I) bis-olefin precatalyst, **30**, can be activated in the presence of C₆D₆ to deliver global aromatic deuteration of molecules such as aniline, **28**, and ferrocene, **29** (**Scheme 6**).⁴² Although the specific nature of the substrate labelling process was not discussed in detail, in-depth studies into intramolecular deuteration of the vinyl silane ligands

lead to the reasonable postulation that loss of one vinyl silane from **30** and subsequent oxidative addition across C_6D_6 gives the first Rh(III) intermediate, **33**. Migratory insertion of the olefin across the Rh-D bond gives **34**; anti-Markovnikov insertion occurs first *via* kinetic (steric) control. Next, β -hydride elimination gives hydride intermediate **35**, showing the first complete transfer of a D-atom from aryl to olefinic ligand, and an important example of metal-ligand cooperation.⁴³ The process can repeat until the silane is per-deuterated, as in **36**, which can then reductively eliminate benzene to recycle the Rh(I) pre-catalyst, **30**. Alternatively, the unsaturated Rh(I) species, **37**, can be intercepted by an external substrate molecule (such as **28** or **29**) to form a series of new Rh(III) intermediates that lead to the desired substrate deuteration.



Scheme 6. Rh(III)-catalysed aromatic HIE and proposed catalyst activation mechanism.

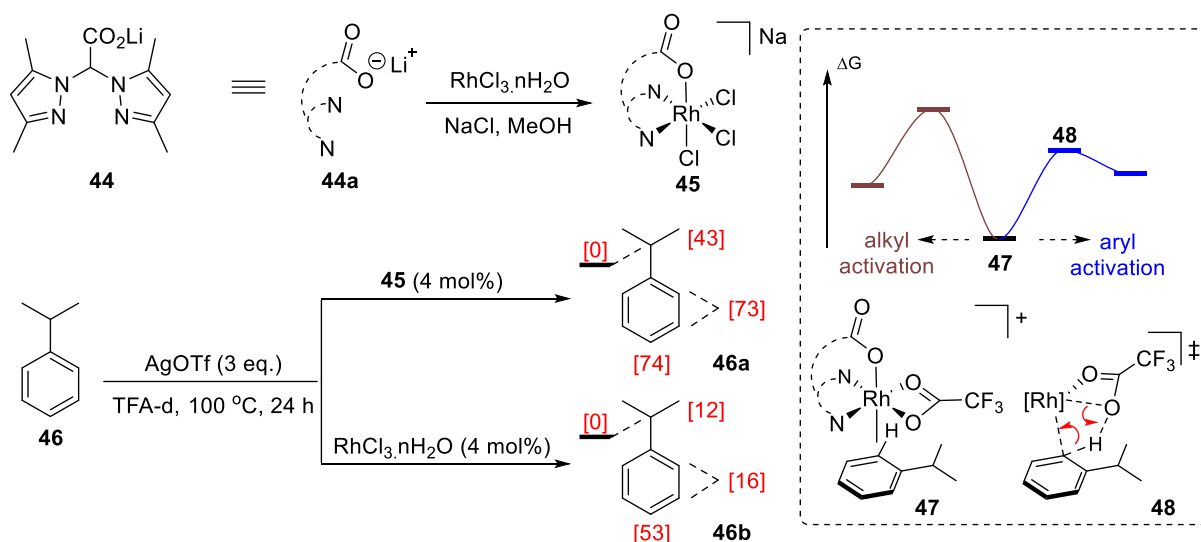
The HIE behaviour of Cp*Rh(III) complexes has also been investigated by Carmona and co-workers.^{44,45} Employing an unusual cyclometallated phosphine complex, **39**, silane deuteration - relatively less well explored with respect to aryl/alkyl labelling - could be achieved under extremely mild conditions for mono-, di-, and trisilanes using D₂ or T₂ as the isotope source (for example, see **38**→**40**, **Scheme 7**).⁴⁴ In an impressive application of this work, the deuterated silanes were later employed with the *same catalyst* as starting materials in the large-scale production of α-deuterated silyl protected alcohols and amines (for example, **41**→**42**).⁴⁵ With observable solution-phase ligand fluxionality in **39**, and its recovery unchanged after catalysis, D₂ (or T₂) gas was proposed to be activated by the ligand and metal together (**39a**→**43**). This example of metal-ligand cooperation to shuttle an isotopic label is complementary to that of Brookhart (**Scheme 6**, *vide supra*).⁴²



Scheme 7. Rh(III)-catalysed deuteration of silanes and application in hydrosilylation.

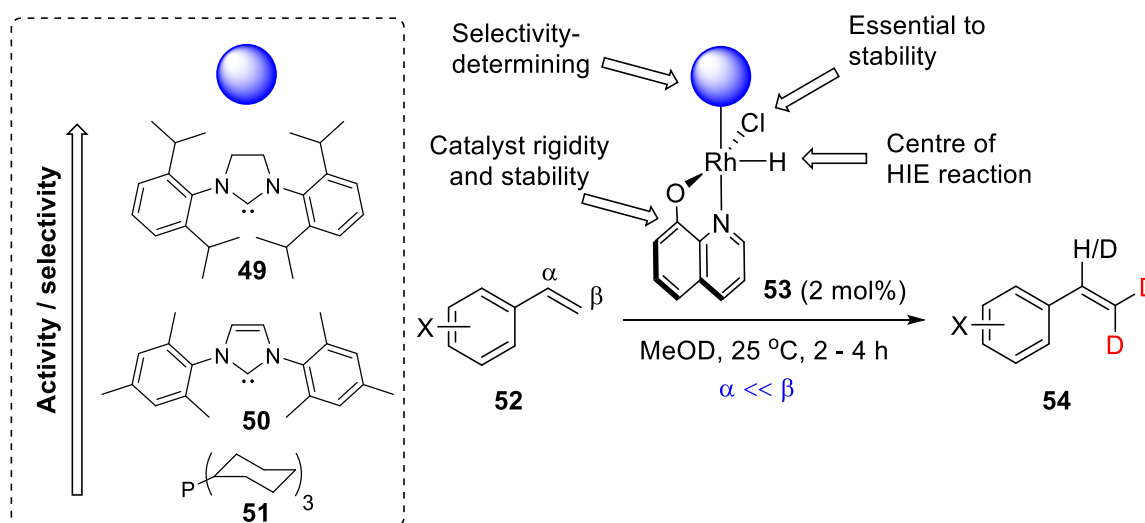
In more recent times, the RhCl₃ catalyst was used as a precursor to a catalyst with complementary reactivity to Lockley's system. More specifically, the bis(3,5-dimethylpyrazol-1-yl) acetate (bdmpza) ligand, **44**, delivered an anionic Rh(III)-centred pre-catalyst, **45**, that was able to deuterate both aryl and β-alkyl positions of substrates bearing no strong directing group (**46**→**46a**, **Scheme 8**).⁴⁶ Under identical conditions, the parent RhCl₃.H₂O was more selective for aryl deuteration (**46**→**46b**). A combined experimental and density functional theory (DFT) investigation into the operative reaction mechanism using **45**

revealed that aryl labelling was kinetically favoured over alkyl labelling by 9.0 kcal/mol *via* the shared catalyst resting state, **47**. Additionally, C-H bond breaking was postulated to occur *via* a trifluoroacetate-assisted and redox neutral concerted metalation-deprotonation (CMD), transition state **48**.⁴⁷



Scheme 8. Rh(III)-catalysed HIE *via* CMD in the absence of directing groups.

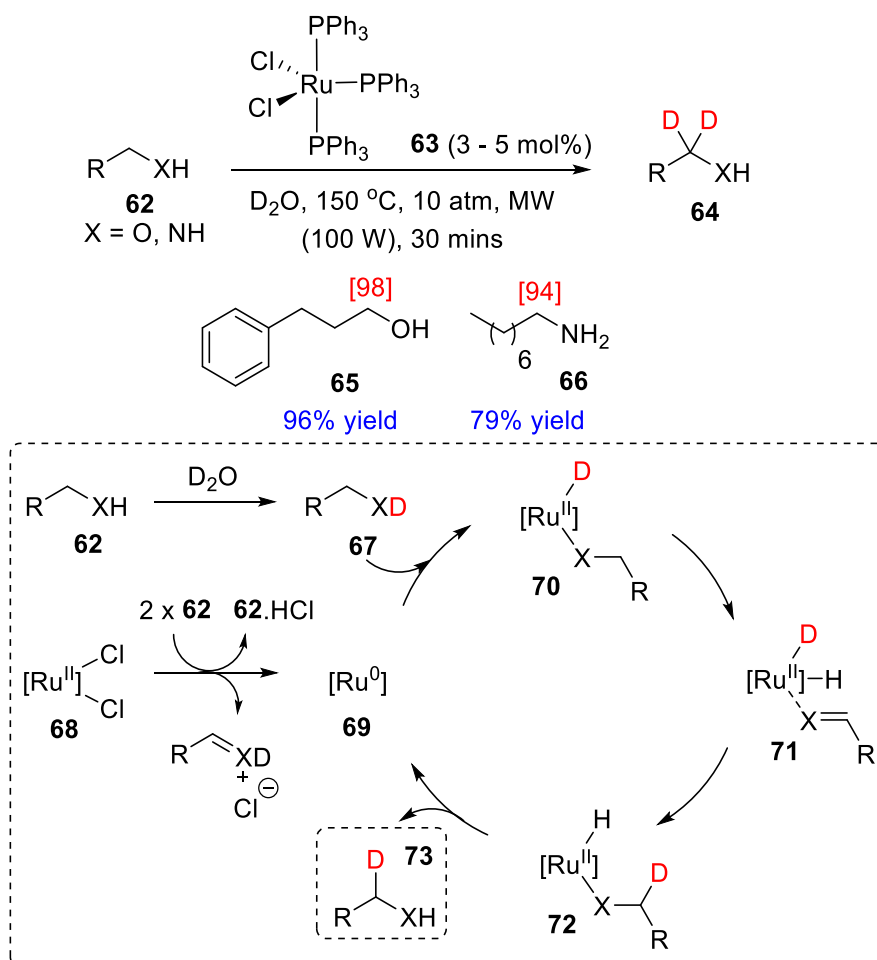
In the final and (to date) most recent example of Rh(III)-catalysed HIE, Castarlenas and Oro reported a beautifully detailed method for the β -selective deuteration of styrenes (**52**→**54**) using *N*-heterocyclic carbene (NHC) and quinoline *N*-oxide ligated catalysts, **53** (Scheme 9).^{48,49}



Scheme 9. Rh(III)-catalysed β -selective deuteration of styrenes.

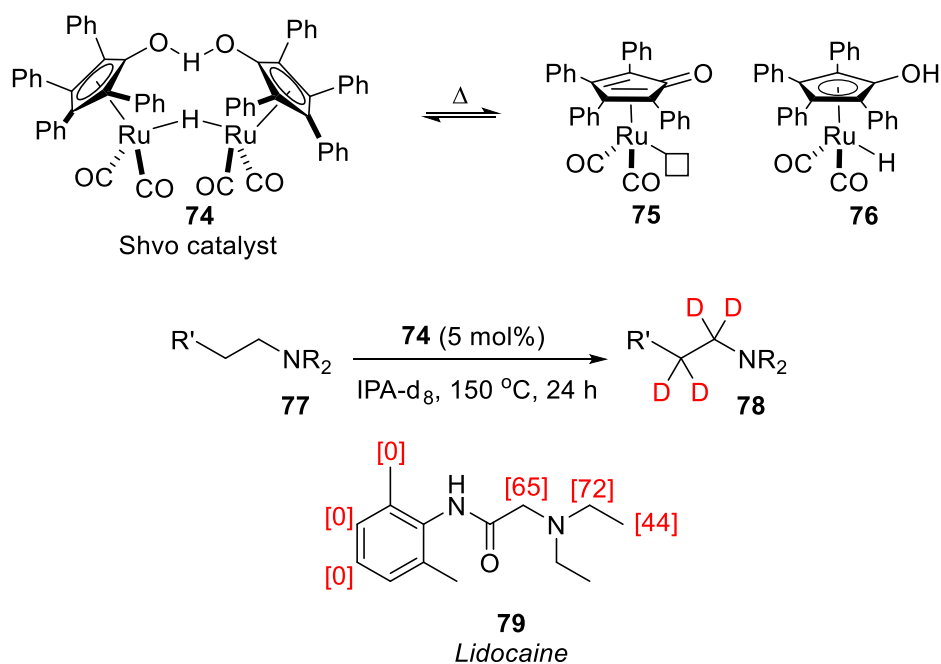
1.4.3 Ruthenium

Among the growing selection of available homogeneous HIE catalysts, ruthenium-based methods have also played a notable role.²⁸ Firstly, Matsubara and co-workers have demonstrated the use of precatalyst $\text{RuCl}_2(\text{PPh}_3)_3$, **63**, in the Ru(0)-catalysed α -deuteration of alcohols and amines (**Scheme 11**, top).⁵⁰ Based on literature precedent,⁵¹ the authors proposed that substrate **62** first exchanges with D_2O to give **67**. The precatalyst, **68**, can be activated *via* coordination and β -hydride elimination of the substrate, followed by reductive elimination of HCl to give Ru(0) catalyst, **69**. The low-valent catalyst can undergo oxidative addition with **67** to give Ru(II) intermediate, **70**, then **71** after a β -hydride elimination step. The coordinated aldehyde or imine is then susceptible to intramolecular nucleophilic attack from a Ru-deuteride, producing **72**. The desired product, **73**, is then obtained after reductive elimination. Despite the harsh conditions, this method was able to deliver simple deuterated alcohols and amines in good to excellent yield, and excellent labelling selectivity.



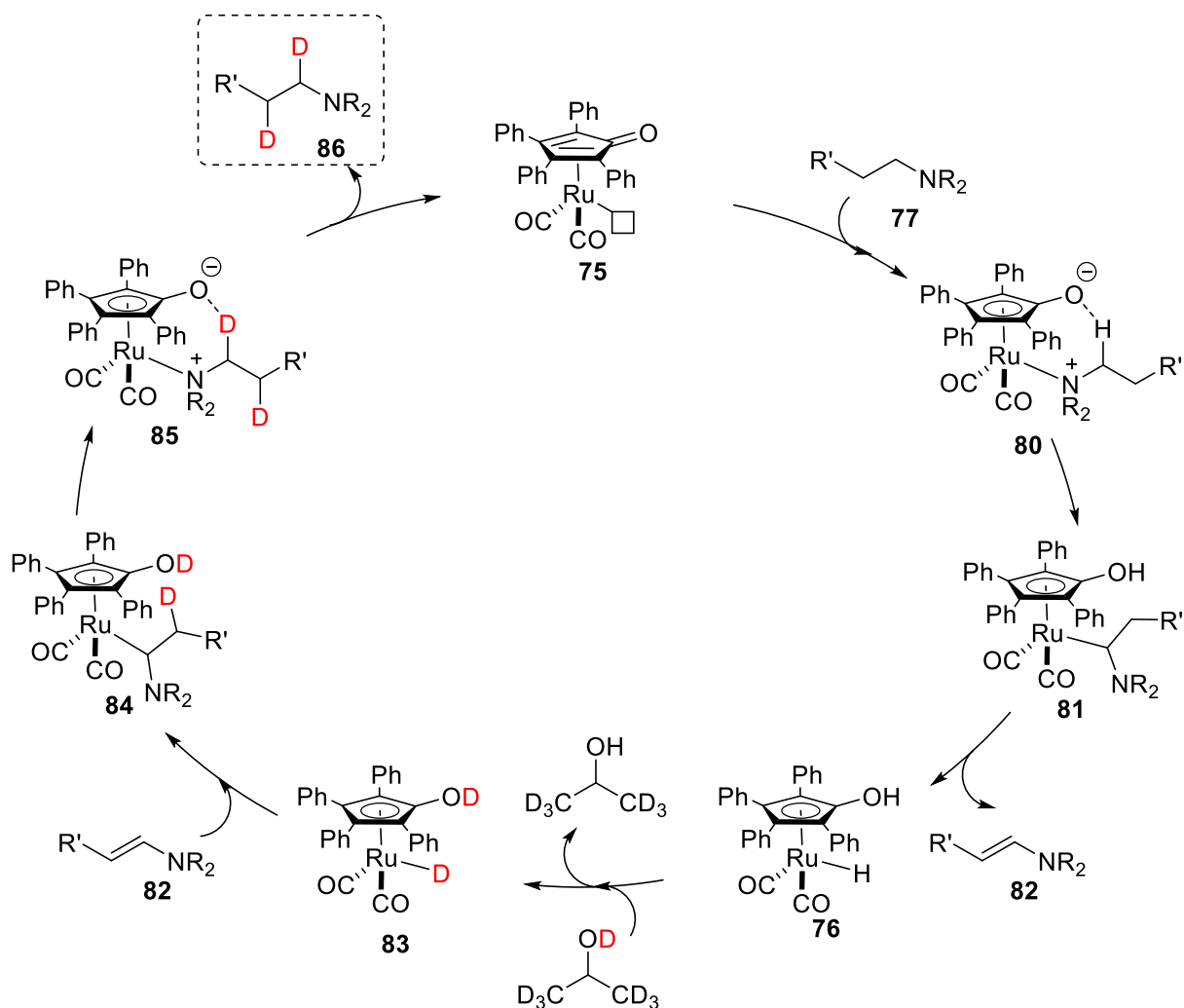
Scheme 11. Ru(0)-catalysed α -deuteration of alcohols and amines.

In a more complex variant of the above reaction, Beller and co-workers were able to exploit the unusual and so-called Shvo catalyst,⁵² **74**, in the α,β -deuteration of biologically-relevant amine molecules (**Scheme 12**).⁵³ On heating, the Shvo catalyst dimer breaks down into two distinct, catalytically active monomers: dehydrogenated form **75**, and hydrogenated form, **76**. Together, they catalyse the reaction of **77** to **78** using deuterated *iso*-propanol (IPA-d₈) as the isotope source. This method was applied to a host of drug-type molecules, including **79**.



Scheme 12. Ru-catalysed α,β -deuteration of biologically-relevant amines.

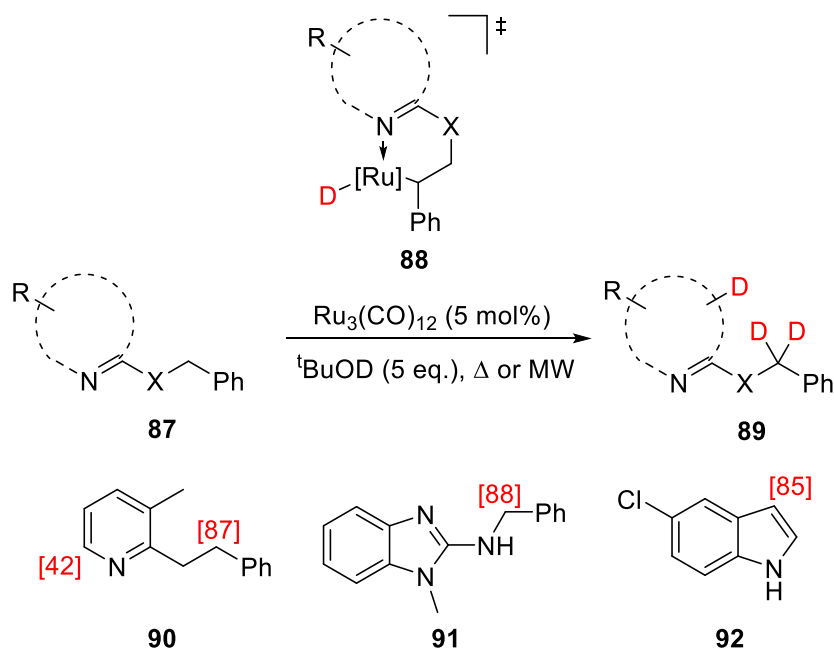
The full significance of both monomeric forms of the Shvo catalyst becomes fully apparent in the reaction mechanism proposed by the authors (**Scheme 13**). Amine substrate, **77**, first coordinates to the dehydrogenated catalyst monomer, **75**, producing the zwitterion, **80**. In a ligand-assisted step, the amine is deprotonated, thus switching from a nitrogen- to carbon-centred coordination mode in **81**. Subsequent β -hydride elimination produces enamine **82** and the hydrogenated form of the Shvo catalyst, **76**. In this form, isotope exchange with IPA-d₈ gives the deuterated catalyst, **83**. The aforementioned enamine, **82**, undergoes migratory insertion with **83** to deliver the β -label in intermediate **84**. Deprotonation of the cyclopentadienyl ligand by the metallated amine gives **85**, installing the α -label in final product amine, **86**, eventually recycling **75**.



Scheme 13. Proposed mechanism for α,β -deuteration of amines with the Shvo catalyst.

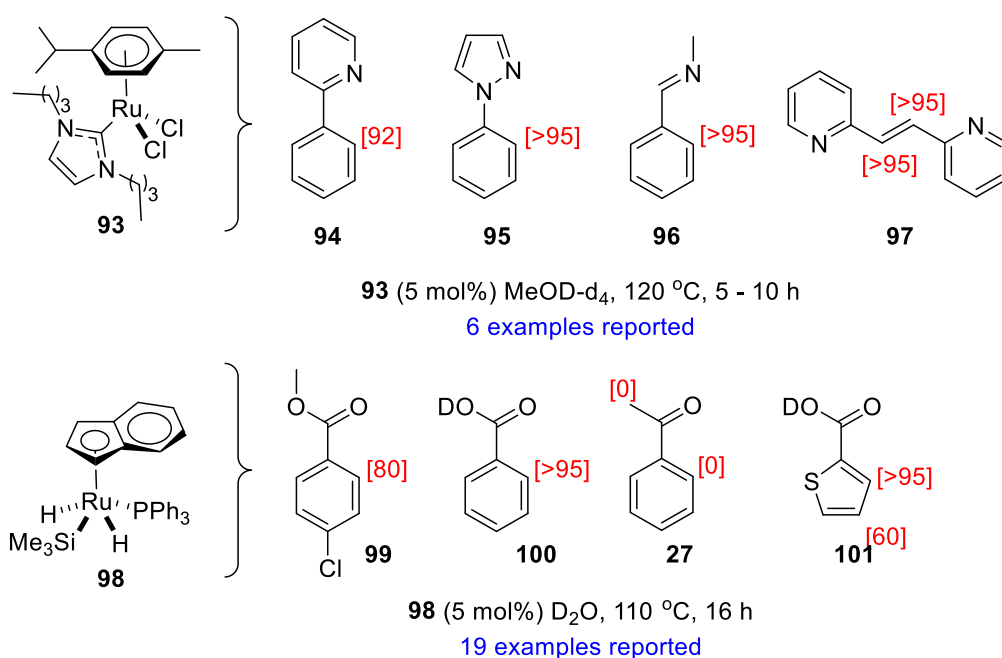
Regioselective Ru-catalysed HIE processes have also been exploited in the labelling of aromatic and *N*-heterocyclic substrates. In 2012, Schnürch and co-workers reported the regioselective deuteration of *N*-heterocycles using the Ru(0) cluster, $\text{Ru}_3(\text{CO})_{12}$, and $^t\text{BuOD}$ as the deuterium source ($87 \rightarrow 89$, via 88).⁵⁴ In some substrates, deuteration occurred at aromatic and benzylic positions accessible *via* nitrogen coordination, favouring the latter when both were available (molecules **90** and **91**, **Scheme 14**). Conversely, indole-derived structures were deuterated at the electron-rich 3-position (**92**, **Scheme 14**). No in-depth mechanistic analysis was carried out by the authors, however, it was speculated that labelling of substrates like **90** or **91** is likely to occur *via* a deuterated ruthenacycle such as **88**. The mechanism for the labelling of indoles such as **92** remains altogether unclear.

Developments in exclusively *ortho*-directed HIE reaction using ruthenium catalysts has also been advanced in recent years. In the first of two key examples, the Peris group showed that



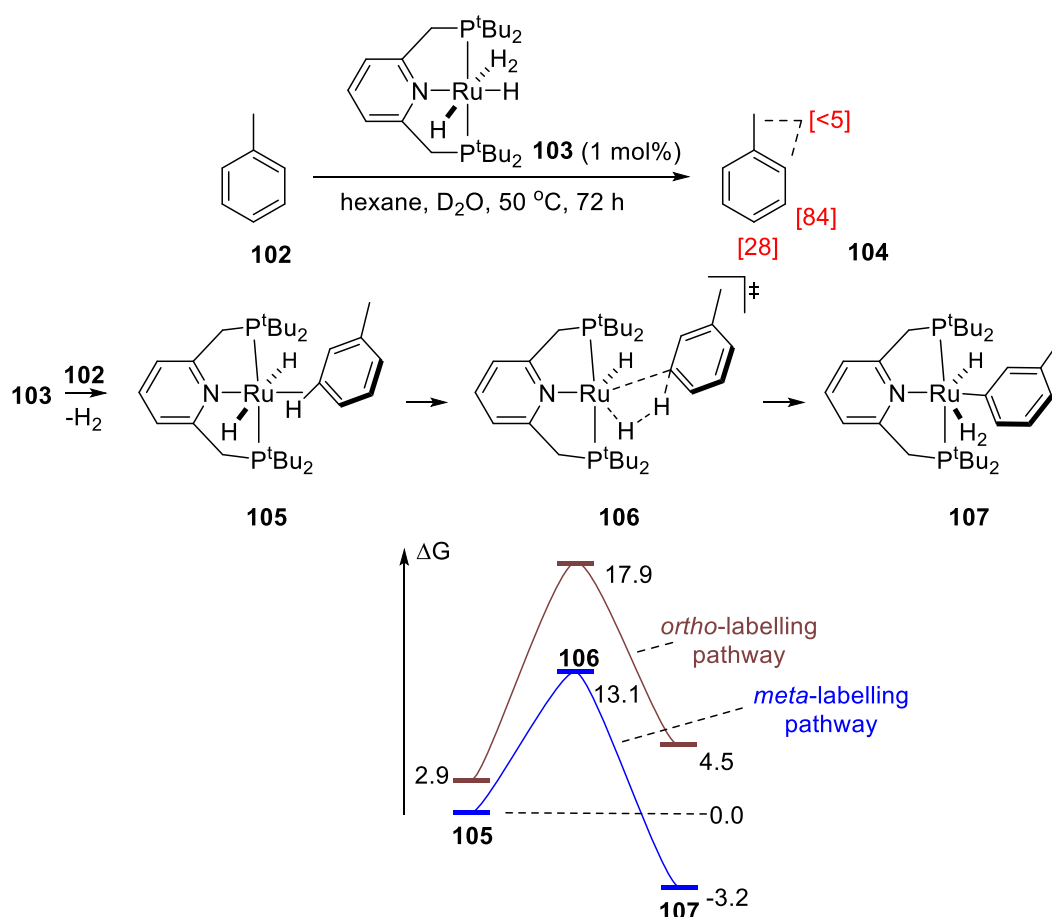
Scheme 14. Benzylic and aromatic deuteration of *N*-heterocycles using $\text{Ru}_3\text{CO}_{12}$.

the Ru(II) NHC complex, **93**, could efficiently catalyse the *ortho*-directed deuteration of various *N*-heterocycles (**94** - **97**) in the presence of MeOD (**Scheme 15**, top).⁵⁵ In a similar fashion, Nolan and co-workers recently divulged the directed deuteration of a significantly broader range of coordinating functionalities (**99** – **101**; note no labelling on **27**) using the Ru phosphine complex, **98**, and D_2O as the key main isotope source (**Scheme 15**, bottom).⁵⁶



Scheme 15. Directed HIE involving Ru(II) catalysts by Peris (top) and Nolan (bottom).

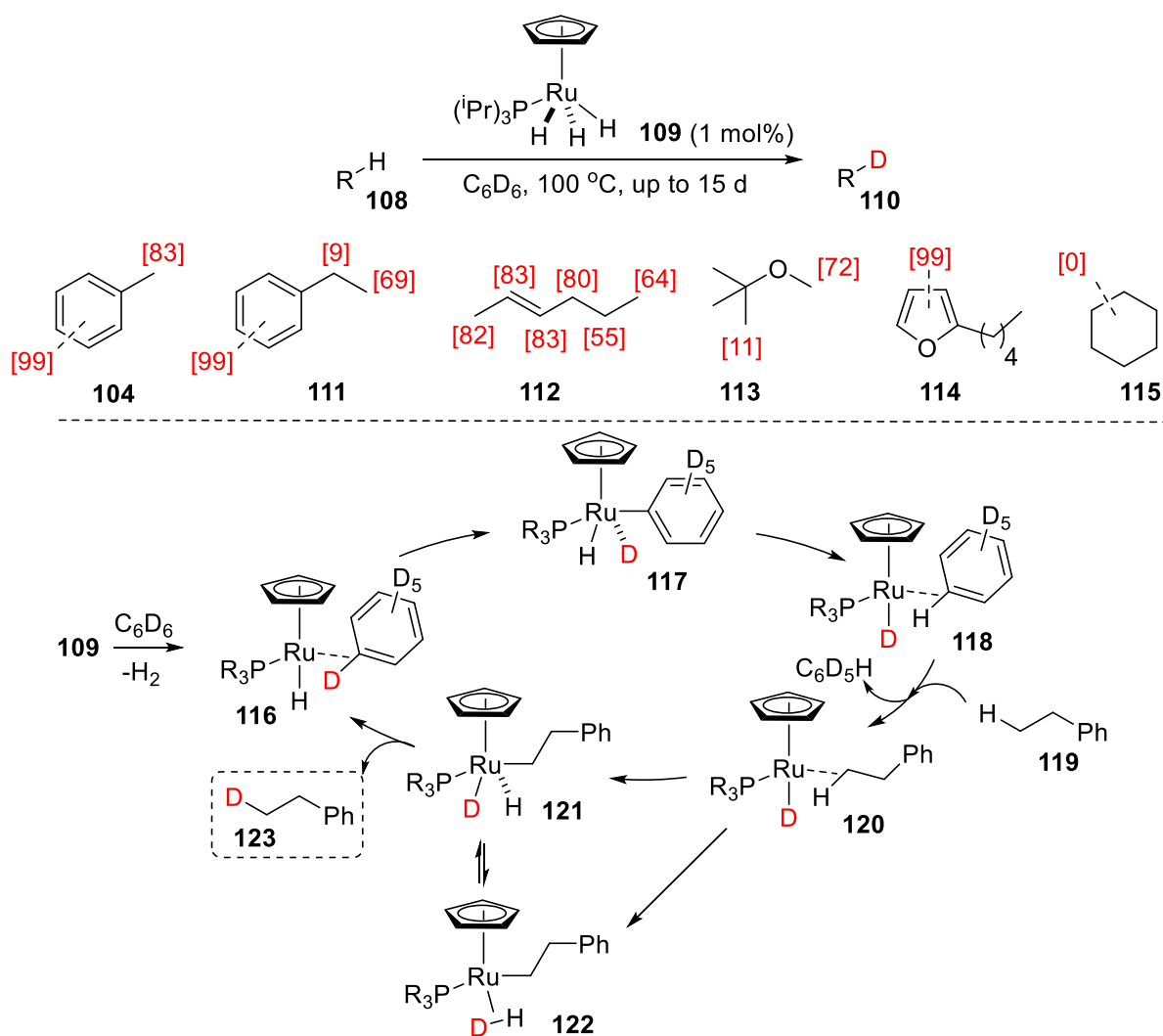
A number of ruthenium catalysts have been developed to affect the deuterium labelling of molecules which lack strong coordinating functionalities. Among these, Leitner has reported the D-labelling of benzene derivatives (**102**→**104**, for example) and heteroaromatic compounds using the Ru(II) pincer complex, **103**, under relatively mild, albeit time-consuming, conditions (**Scheme 16**, top).⁵⁷ A combined experimental and DFT study revealed that site selectivity in labelling was largely based on steric effects. Mechanistically, after the loss of the dihydrogen ligand and agnostic coordination of the unlabelled substrate (**105**, **Scheme 16**) the key step in the mechanism was reported to involve a σ -bond metathesis between the substrate C-H and one of the hydride ligands on Ru(II) (**105**→**107** via **106**). DFT-calculated energies showed that *ortho*-labelling was disfavoured both thermodynamically and kinetically (as shown *versus meta*-labelling in the PES, **Scheme 16**).



Scheme 16. Sterically-selective labelling of toluene using Leitner's Ru(II) pincer catalyst.

In a similar approach (where loss of a labile dihydrogen ligand is necessary for catalysis), Gorelsky and Nikonov reported the use of Ru(IV) trihydride precatalyst, **109**, in the Ru(II)-

catalysed labelling of unactivated molecules, using C_6D_6 (**Scheme 17**).⁵⁸ In all cases, aryl and heteroaryl positions were labelled fastest (**104**, **111**, and **114**). In alkyl species, the extent of labelling varied markedly depending on the exact nature of the rest of the molecule, and required at least some weakly coordinating functionality to operate at all (for example, **115** *versus* **112** and **113**). Potential reaction mechanisms were studied by DFT (**Scheme 17**, bottom). Catalyst activation *via* reductive loss of H_2 and coordination of C_6D_6 (**109**→**116**) was found to be favourable over alternative pathways involving loss of the phosphine ligand. Subsequent oxidative addition across benzene gives Ru(IV) intermediate **117**, then Ru(II) monodeuteride intermediate **118**, following reductive elimination of benzene. After complexation of exemplar substrate, **119**, to give **120**, rate-limiting C-H bond cleavage was predicted to occur towards Ru(IV) complex, **121**, or Ru(II) complex, **122**, depending on the specific substrate in question. Finally, reductive elimination delivers labelled substrate, **123**.



Scheme 17. Ru(II)-catalysed D-labelling of aryl, heteroaryl, and alkyl groups, using C_6D_6 .

Beyond the illustrative examples described, other, less-widely applied Ru-^{28,59-61} and related Os-catalysed⁶⁰ HIE methods have been reported, and the relevant catalyst structures are summarised in **124** – **127** (**Figure 4**).

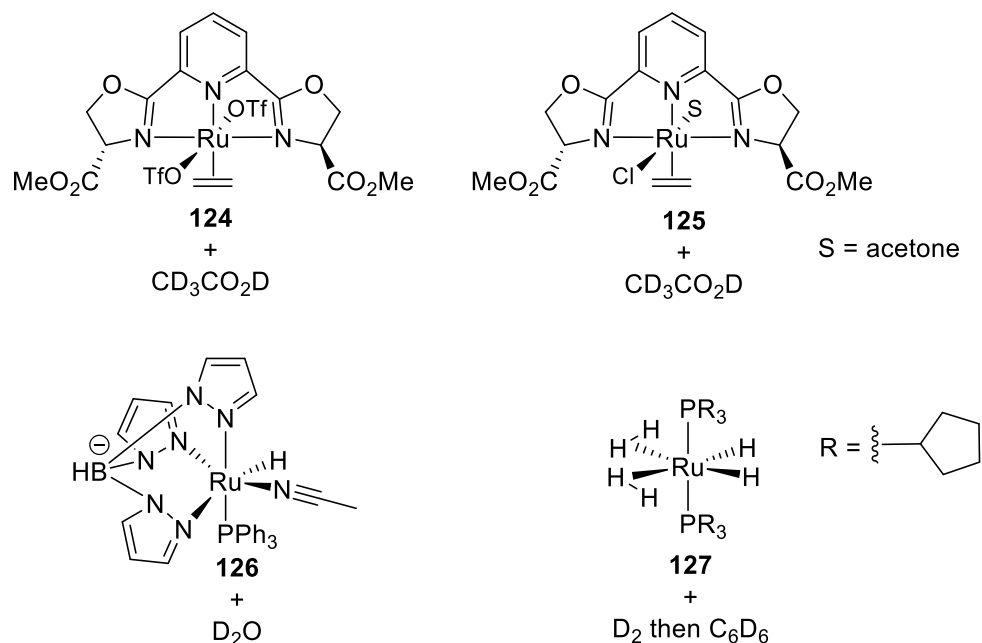
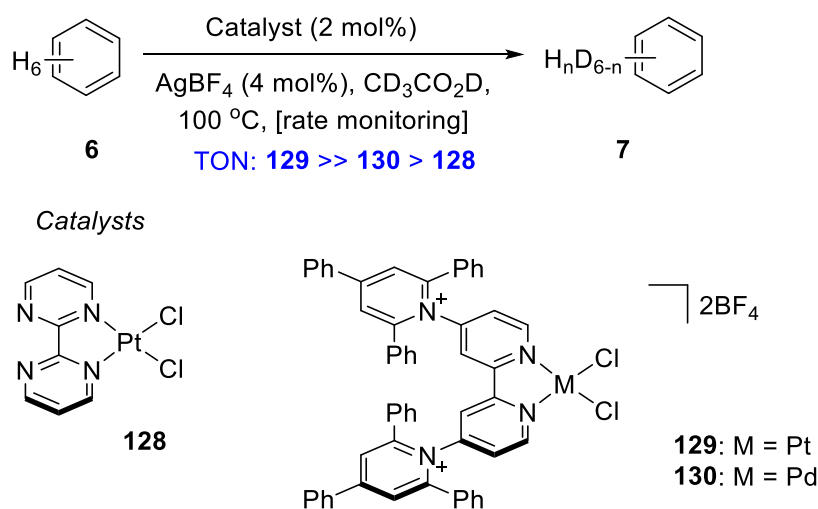


Figure 4. Further examples of homogeneous Ru-based catalysts used in HIE processes.

1.4.4 Palladium

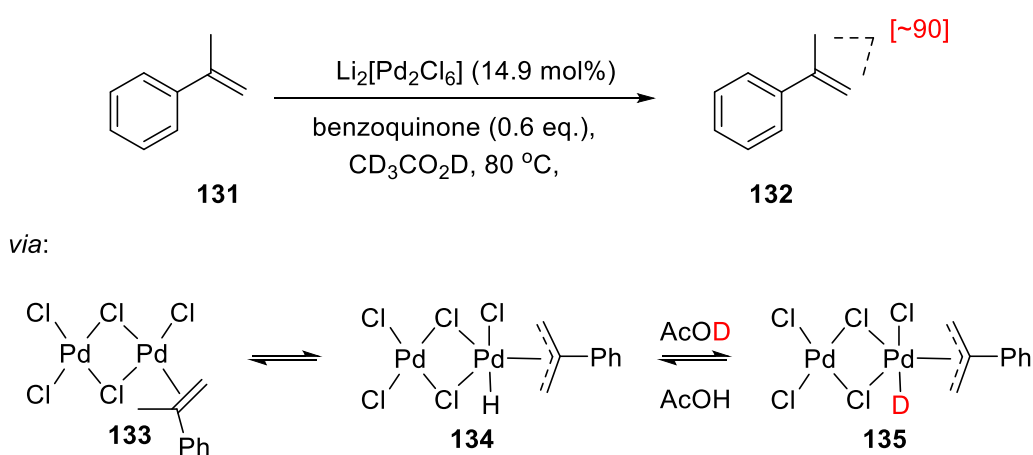
The study of homogeneous palladium complexes in HIE processes has often been compared to analogous platinum complexes. Indeed, this was the case in the earlier of Sanford's aforementioned deuterium labelling studies, where cationic bipyridine ligands were employed to produce advantageously Lewis acidic catalysts, **129** and **130**, for the deuterium labelling of benzene in the presence of CD₃CO₂D (**Scheme 18**).³³ Although both metals produced highly active HIE catalysts compared to the parent catalyst of the study, **128**, Pt was more useful than Pd as it delivered the most highly acidic catalyst.

Homogeneous palladium catalysis has also been explored more fully in its own right for HIE processes. Despite prior reports,⁶² work by Ryabov, Eliseev, and Yatsimirsky on H/D-exchange with styrenes best represents an early example of homogeneous Pd-catalysed HIE.⁶³ In the 1988 study, it was shown that, in the presence of CD₃CO₂D and benzoquinone,



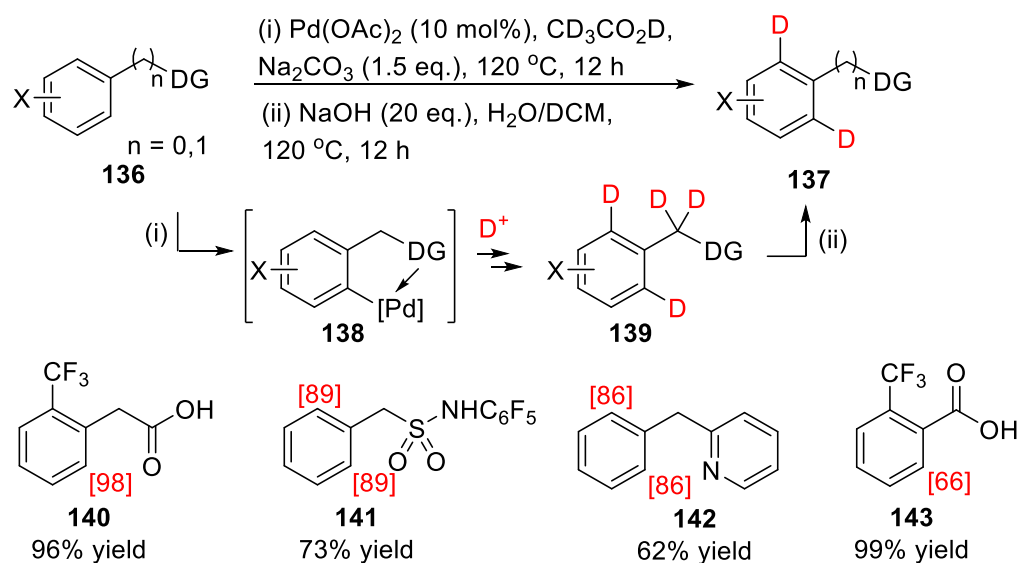
Scheme 18. Palladium *versus* platinum homogeneous catalysts in global aromatic HIE.

$\text{Li}_2[\text{Pd}_2\text{Cl}_6]$ could efficiently catalyse the H/D-exchange of the allyl and vinyl positions in α -methylstyrene, **131** (**Scheme 19**). Detailed kinetic experiments revealed that the reaction was most likely to proceed *via* a Pd(II)/Pd(IV) cycle, with key steps including oxidative addition of **131** across one Pd atom in the active all Pd(II) dimer, **133**. In the resultant mixed Pd(II)/Pd(IV) complex, **134**, the hydride ligand (assumed to be acidic) exchanges with the deuterium source to give **135**. Subsequent acidic H/D-exchange steps then result in equal deuterium labelling across the allyl and vinyl positions of product **132**.



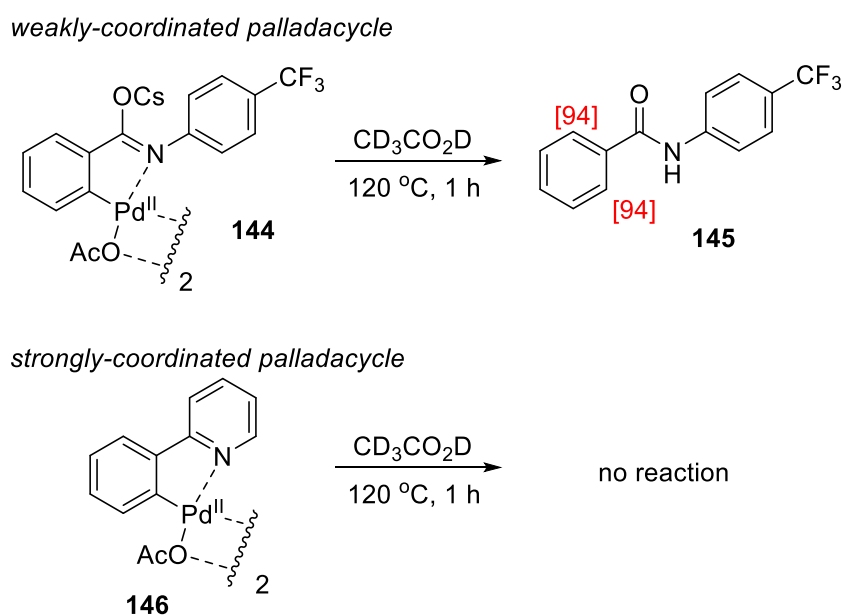
Scheme 19. Pd(II)-catalysed regioselective deuterium labelling of α -methylstyrene.

In far more recent times, Yu and co-workers demonstrated that Pd(II)-catalysis can be effectively employed in *ortho*-directed HIE processes.⁶⁴ Using $\text{Pd}(\text{OAc})_2$ under basic conditions in the presence of $\text{CD}_3\text{CO}_2\text{D}$, various weakly coordinating functionalities were able to affect *ortho*-deuterium labelling and in moderate to excellent yield (**Scheme 20**).



Scheme 20. Pd-catalysed *ortho*-deuteration of aromatic compounds using weakly-coordinating directing groups.

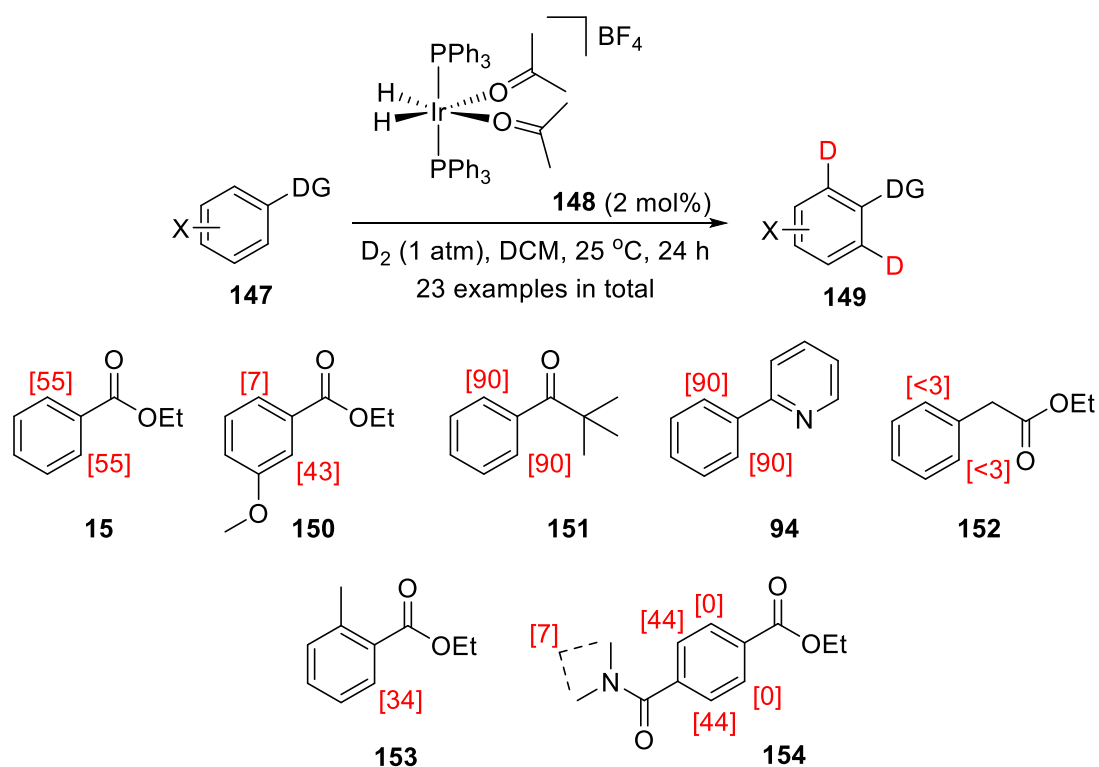
Some notable observations were made by Yu from the same study. Firstly, more weakly coordinating directing groups proved to be most reactive (for example, **140** versus **142**). This analysis was strengthened by the D-labelling results of stoichiometric experiments with weakly and strongly coordinating palladacycles, **144** and **146**, respectively (**Scheme 21**). Furthermore, labelling *via* a six-membered metallocyclic intermediate (6-mmi) was found to be more efficient than the analogous 5-mmi (for example, **140** versus **143**, **Scheme 20**).



Scheme 21. Discriminating reactivity of weak and strong palladacycles in *ortho*-deuteration.

1.4.5 Iridium

Among all transition metals employed in homogeneous HIE methods, iridium is arguably the most widely studied,^{8,11,12,65-69} which is, in part, due to the vast and ever-expanding literature precedent in related hydrogenation reactions.⁷⁰⁻⁸⁶ Despite interesting alternative Ir-catalysed HIE methods, such as for silanes,⁸⁷ boranes,⁸⁸ olefins,⁸⁹ and global aryl labelling,^{90,91} there is a clear dominance of *ortho*-HIE in the iridium literature. In 1992, Heys demonstrated the successful *ortho*-directed deuteration of several substituted aromatic compounds using the 18-electron Ir(III) bisphosphine dihydride complex **148**⁹² under very mild conditions (**147**→**149**, **Scheme 22**).⁹³ Crucially for the time, Heys' investigations marked a significant advancement from Lockley's *ortho*-labelling work (*vide supra*).³⁶⁻³⁸ D₂ gas replaced D₂O as the deuterium source (an advantage when considering the use of tritium), reactions operated efficiently at room temperature and, perhaps most importantly, catalyst loadings were significantly reduced from 50 mol% to 2 mol%. Interestingly, it was noted that labelling was significantly affected by steric or electronic aspects of the aryl substituents present. For example, *meta*-substituted ethyl benzoates, such as **150**, showed a consistent preference for labelling at C-2 over the less hindered C-6 position, presumably due to additional coordination assistance from *meta*-substituent lone pairs.⁹⁴ Steric hindrance from *ortho*-substitution reduced labelling efficiency (**153** *versus* **15**), however bulky α -substituted ketones were not so adversely affected (**151** *versus* **15**). Further to this, where substrates possessed more than one carbonyl directing group, the labelling site(s) changed according to which substituent could coordinate to the catalyst to the greatest extent (for example, **154** *versus* **15**).



Scheme 22. Heys' Ir-catalysed *ortho*-directed deuteration of aromatic compounds.

The mild labelling conditions pioneered by Heys and co-workers, coupled with intriguing substrate-dependent regioselectivity, captured the combined interest of the industrial and academic labelling communities, resulting in a large number of subsequent studies aimed at understanding the catalytic properties of **148** and related Ir-based HIE catalysts. Firstly, Heys followed up his initial study with a more in-depth assessment of the aryl substituent effects in the labelling efficiency of ethyl benzoates and *N,N*-dimethyl benzamide substrates.⁹⁵ In a rather unexpected outcome, *para*-substitution improved the rate of labelling in both substrate types, *irrespective of substituent electronics* (for example, **155a** versus **155b** and **155c**, **Figure 5**). In an attempt to explain this effect, Heys monitored the rate of labelling in both rings of several monosubstituted benzophenones.⁹⁵ In a manner similar to the results discussed previously, the substituted ring was labelled faster in every instance (**156a** - **156c**, **Figure 5**). As both rings are connected to the same carbonyl functionality, it appeared that the rate-limiting step of the overall reaction could *not* be ascribed to the initial coordination of the substrate, nor the fluxionality step (**171**→**172**), *vide infra*.⁹⁶ Instead, Heys suspected that some aspect of the C-H bond cleavage was rate-limiting, proposing key intermediates **157** and **158** based on available literature. At this time, the formal oxidation state of iridium intermediates involved in the C-H bond cleavage ($\text{Ir}^{\text{I}}/\text{Ir}^{\text{III}}$ or $\text{Ir}^{\text{III}}/\text{Ir}^{\text{V}}$) was not clear.

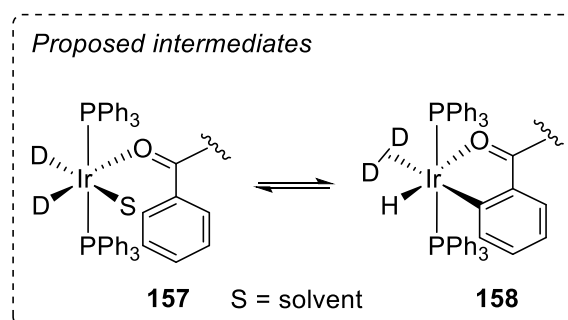
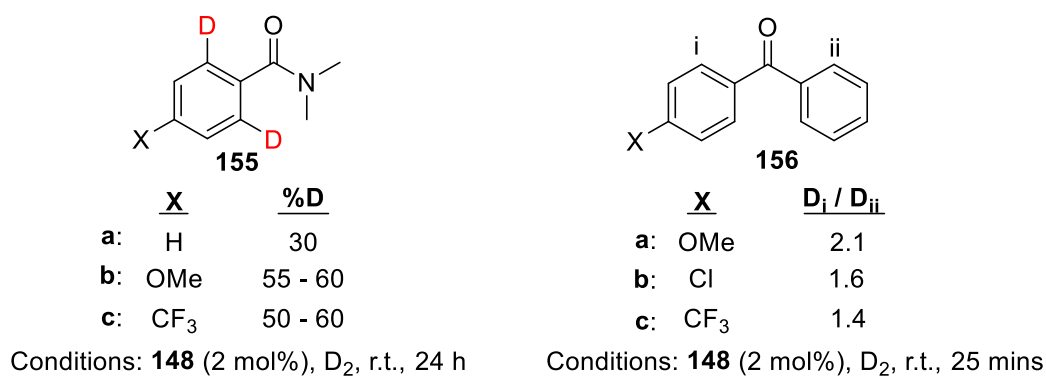
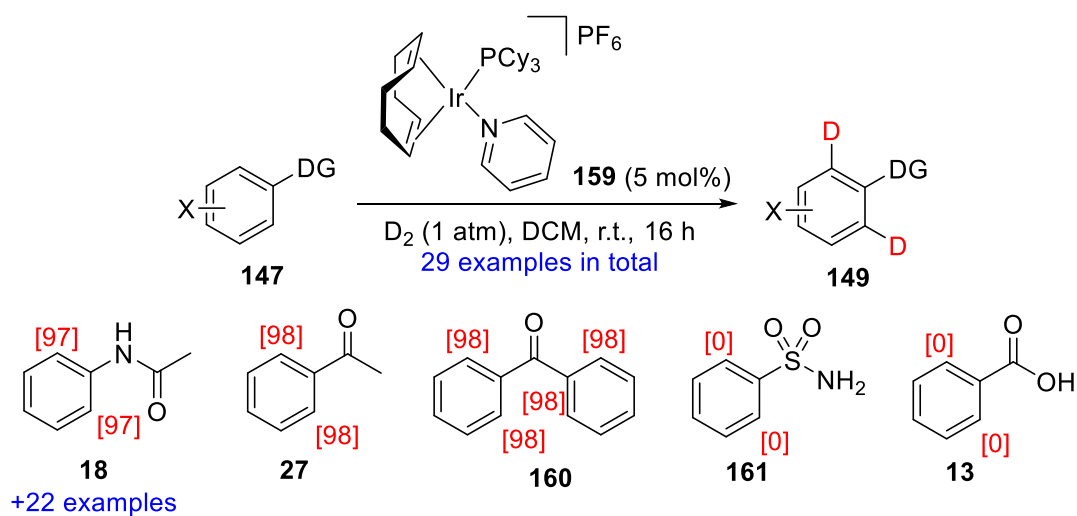


Figure 5. Mechanistic investigations into Heys' Ir-catalysed HIE protocol.

Inspired by Heys, Hesk and co-workers probed the efficacy of the commercially available Crabtree hydrogenation catalyst, **159**,⁷⁰ in labelling acetanilide derivatives, the first such substrates to be effectively labelled *via* a 6-*mmi*.⁹⁷ Consistent with Heys' work, deuteration was directed *ortho* to the coordinating functionality, and no clear relationship emerged regarding the electronics of *para*-substituents. Ketones **27** and **160** were also compatible with this mild labelling method, however, weakly coordinating substrates **161** and **13** were not.



Scheme 23. Hesk's application of Crabtree's catalyst in *ortho*-HIE.

Since Heys' and Hesk's respective discoveries of iridium catalysts for *ortho*-directed HIE, complexes **148** and **159** (and derivatives thereof, *vide infra*) have remained topics of high interest in HIE research.^{65,66,94,98-103} In a further key development by Heys, **162**, a precatalytic Ir(I) variant of Ir(III) catalyst **148** was compared to related bidentate precatalyst, **163** (**Figure 6**). By the mid-1990s, it had already been hypothesised by several researchers that both 5- and 6-mmis could be formed during the C-H bond cleavage step in the *ortho*-deuteration process (**164** *versus* **165**), depending on the substrate being studied; this was to be the platform on which to compare **162** and **163**.

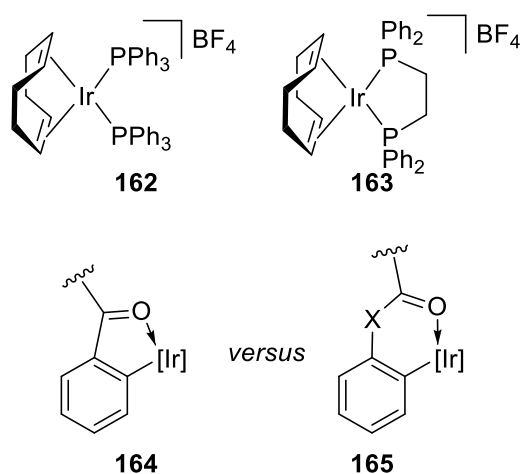
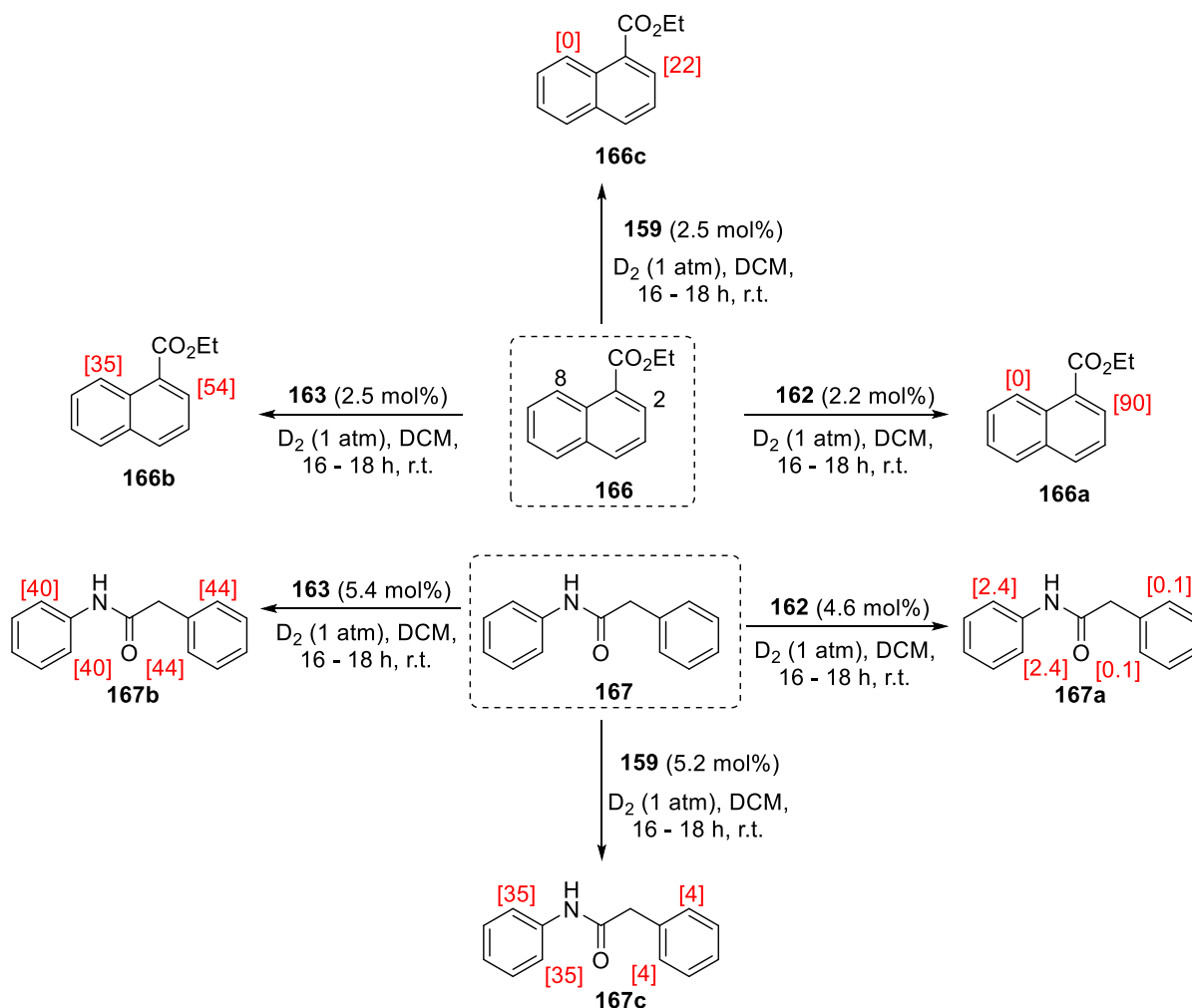


Figure 6. Mono- *versus* bidentate Ir-phosphine catalysts to study *ortho*-deuteration via 5- and 6-mmis.

Labelling a range of substrates enabled a comparison of the mono- and bidentate phosphine complexes to be made, highlighting a preference for **162** to react through a 5-mmi only, whereas **163** could react through both a 5- and a 6-mmi. This was exemplified in the labelling of ethyl 1-naphthoate, **166** (**Scheme 24**, top). Of the two available labelling sites, the monodentate complex, **162**, labelled solely at C-2. Conversely, bidentate complex **163** demonstrated the capability to direct labelling at both C-2 and C-8. When Crabtree's catalyst, **159**, was exposed to similar reaction conditions, the regioselectivity in labelling was similar to monodentate complex **162**, albeit with reduced labelling efficiency. Labelling through a 6-mmi only was also investigated. Perhaps the most remarkable findings from this study were those concerning the labelling of *N*-phenyl phenylacetamide, **167** (**Scheme 24**, bottom). Interestingly, the less active monodentate complex, **162**, showed selectivity for the aromatic ring adjacent to the nitrogen, **167a**, an effect emulated more efficiently by Crabtree's catalyst in **167c**. However, the bidentate catalyst, **163**, was able to label both rings of **167** almost

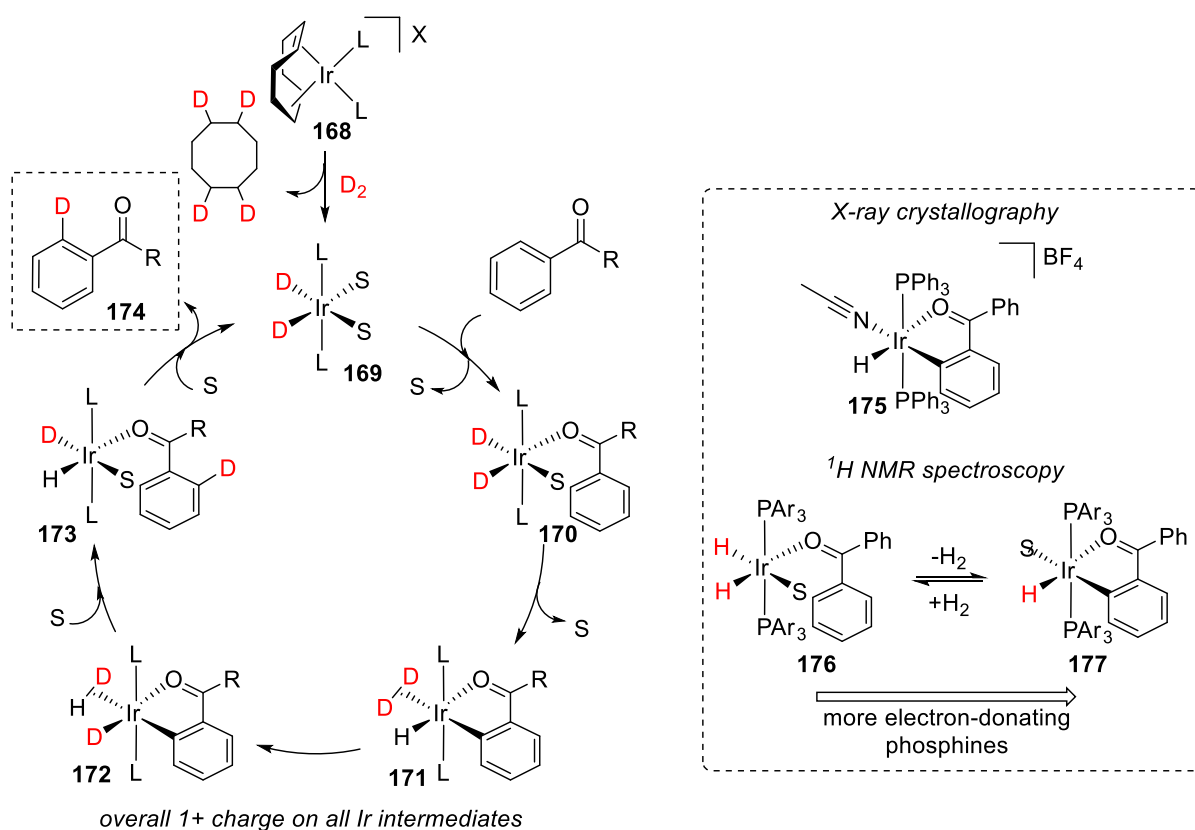
indiscriminately (see **167b**). This served to show that there was potential to distinguish not only between a 5 or 6-mmi, but also between different *types* of 6-mmi, depending on the ancillary ligands employed.



Scheme 24. Heys' versus Hesk's *ortho*-HIE methods for 5- and 6-mmi substrates.

On accumulation of these data, Heys proposed a catalytic cycle by which these iridium complexes may be affecting the observed regioselective hydrogen isotope exchange (**Scheme 25**).⁹⁸ Upon treatment of the Ir(I) pre-catalyst, **168**, with deuterium gas, hydrogenolysis of COD as d_4 -cyclooctane generates the active Ir(III) catalyst, **169**, where ligands (L) are assumed to be arranged *trans* to one another when monodentate. Coordination of substrate displaces a solvent molecule (S), and is thus accepted into the coordination sphere of the iridium catalyst to give **170**. A second solvent molecule can then be displaced, allowing iridium to cleave the nearby *ortho* C-H bond of the aryl ring to yield **171**. Transformation of species **171** to **172** is driven by a process known as *hydride fluxionality*, and is central to the

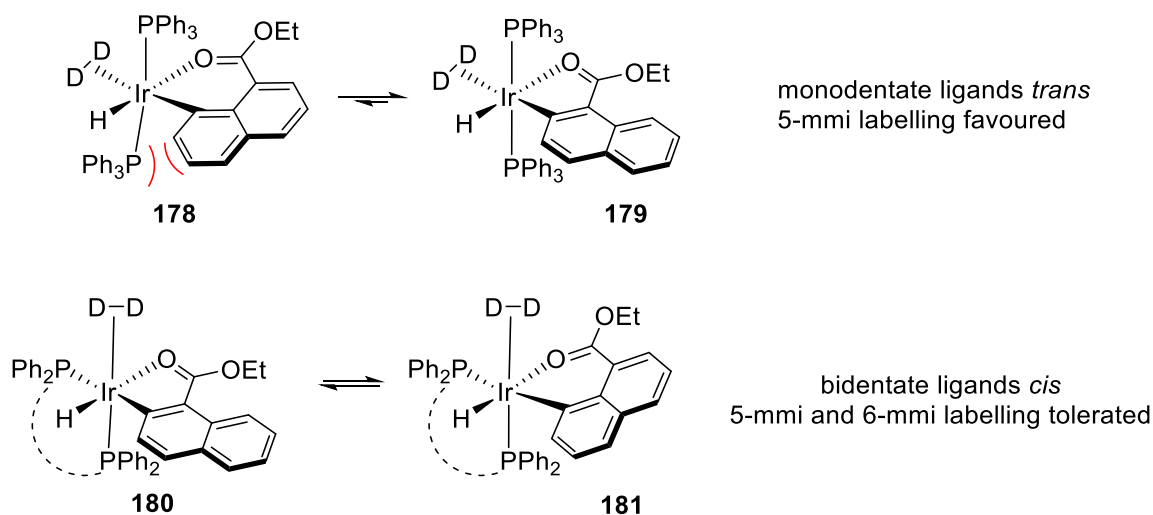
isotope exchange process.⁹⁶ The overall effect brings a deuteride and the activated aryl carbon into a *cis* arrangement. Subsequent elimination furnishes **173**, with a deuterium atom now installed *ortho* to the directing group. Finally, the release of deuterated substrate, **174**, regenerates the resting catalytic intermediate, **169**. This mechanism invokes an all-Ir(III) catalytic cycle with C-H activation as the rate-limiting step, supporting evidence for which would take another decade to accumulate. Said evidence involved isolation and crystallographic characterisation of **175** (an acetonitrile-solvated analogue of **171**), and spectroscopic studies on the evolving nature of Ir hydride equilibria as a function of ancillary ligand electronics (Scheme 25, inset).¹⁰



Scheme 25. Heys' mechanistic analysis for homogeneous Ir-catalysed *ortho*-HIE.

In an extension of this theory, Heys postulated that the preference for the monodentate phosphine complex, **162**, to react only *via* a 5-mmi, **179**, as opposed to a 6-mmi, **178**, was based on steric effects (Scheme 26).⁹⁸ By contrast, the bidentate complex, **163**, is forced to arrange the phosphines *cis* to one another. For substrates such as **166**, this opens up a second face on the complex, offering greater spatial freedom for the formation of the less planar 6-mmi, **181**, as well as the 5-mmi, **180**. By the same thought, the monodentate Crabtree

catalyst, **159**, can facilitate labelling through a 6-mmi as the pyridine and tricyclohexylphosphine ligands present less steric bulk than the two triphenylphosphine ligands of complex **162**, and may thus exist in *cis* or *trans* form. Herbert later capitalised on this rationale to further improve bidentate catalyst **163** in the labelling of 6-mmi substrates, changing the diphenylphosphinoethane (dppe) ligand for the sterically less encumbered arsine analogue.¹⁰²

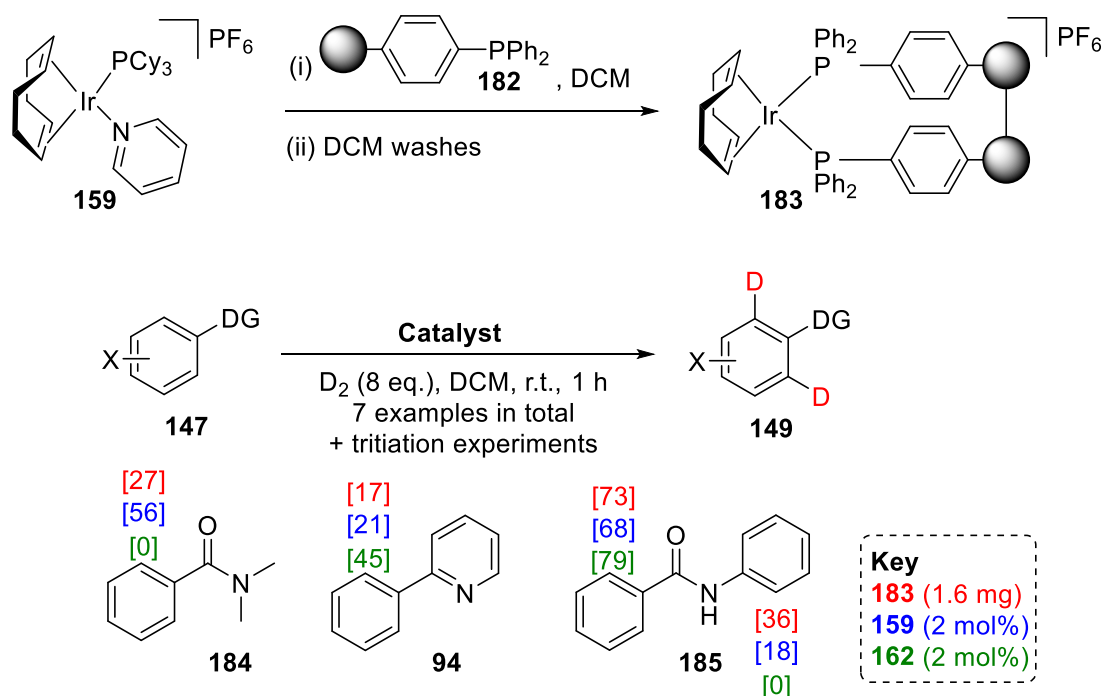


Scheme 26. Rationale for 5- versus 6-mmi labelling selectivity with mono-/bidentate phosphine catalysts.

Further synthetic developments by Herbert^{67,101,104} and later Salter⁶⁶ showed that bis-phosphine catalysts like **163** may be generated *in-situ* from the relevant free phosphine and commercial iridium dimer, $[\text{Ir}(\text{COD})\text{Cl}]_2$, with comparable activity to the isolated complexes. The same authors are also separately responsible for detailed studies into alteration of the phosphine structure.^{66,101,102} However, both parties have remarked that strong correlations between ligand properties (such as sterics or electronics) and catalyst activity are difficult to detect.

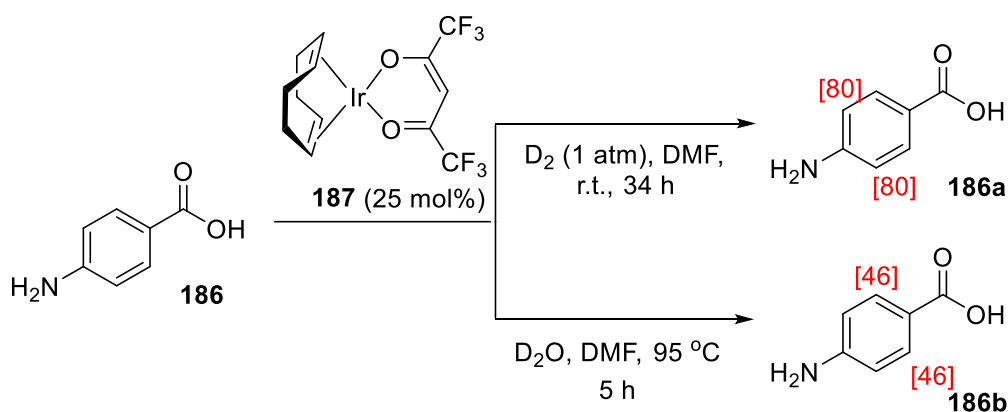
In parallel with the bis-phosphine systems, Crabtree's catalyst has also been the subject of intense study in deuteration and tritiation since Hesk's discovery.^{8,94,104-106} In the largest of any such study, Herbert explored an expansive substrate scope, including ketones, amides, anilides, and various heterocycles.¹⁰⁴ Despite the impressive array of examples reported, this study employed *at least* stoichiometric quantities of **159** and a dual $\text{D}_2/\text{D}_2\text{O}$ isotope source, making comparisons to related *ortho*-labelling methods difficult.

In a notably singular crossover between bis-phosphine catalysts and Crabtree's catalyst, Hickey and co-workers developed a polymer-supported variant of Heys' bis-phosphine catalyst, **183**, which showed comparable *ortho*-HIE activity to **159** and **162**, but with the practical benefit of simple catalyst filtration at the end of the reaction (**Scheme 27**).^{15,103}



Scheme 27. Polymer-supported Ir catalyst in *ortho*-HIE.

At a slightly earlier time, Lockley reported the application of hexafluoroacetoacetate (hfacac)-ligated Ir(I) complex, **187**, in *ortho*-HIE (**Scheme 28**).^{8,11,68,107,108} This catalyst has been successfully applied in the labelling of benzylic amines, benzoic acids, and primary sulfonamides, where few other Ir-based HIE catalysts have succeeded. The catalyst is one of few iridium HIE catalysts operational in highly polar solvents such as DMF (desirable for poorly soluble drug molecules), and displays different labelling regioselectivities depending on the choice of isotope source (water or gas, see **186a** versus **186b**).



Scheme 28. Ir(I)-hfacac *ortho*-HIE catalyst and isotope source-dependent regioselectivity switch.

Increasing interest in Crabtree's catalyst, **159**, in HIE has been paralleled by investigations by other researchers to improve its efficiency and chemoselectivity in olefin hydrogenation reactions.⁸⁴ Despite its widely reported success, **159** is known to suffer from thermal deactivation *via* the formation of inactive, hydride-bridged, iridium clusters (**188**, **Figure 7**).⁷¹ Similar effects have been documented for other iridium-based complexes.^{74,82}

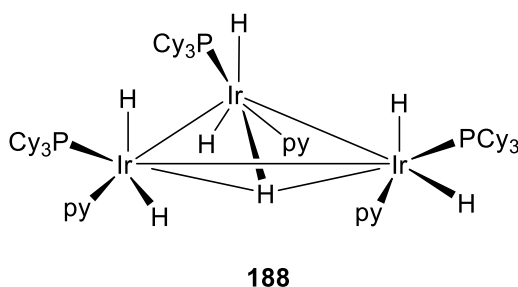


Figure 7. Trimeric Ir cluster formed from thermal deactivation of Crabtree's catalyst.

Between 2001-06, separate investigations by Nolan⁷² and Buriak¹⁰⁹ towards improved thermal stability and predictable chemoselectivity of Crabtree-like hydrogenation catalysts resulted in a plethora of highly promising electron-rich, NHC-ligated catalysts (**Figure 8**). Such species were first applied and published in *ortho*-HIE processes by Powell and co-workers.¹¹⁰ In the study, complexes **194a** and **195a** – **195c** were employed under stoichiometric ('tritiation-like') conditions, with the most active variant, **195c**, shown to be superior to Crabtree's catalyst across the entire substrate range.

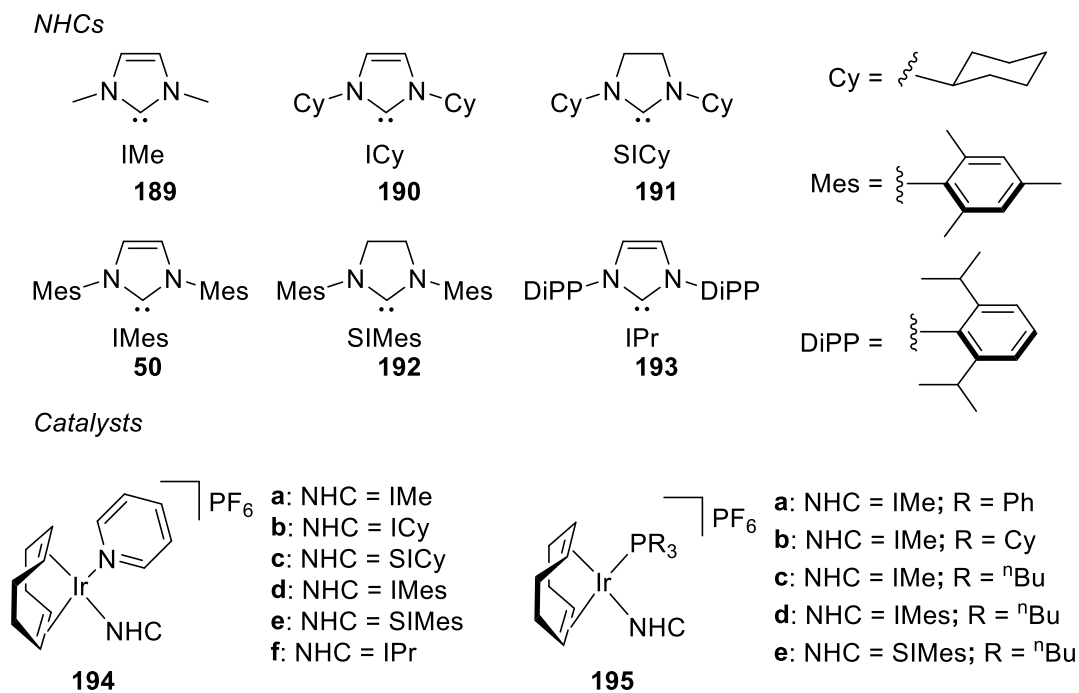
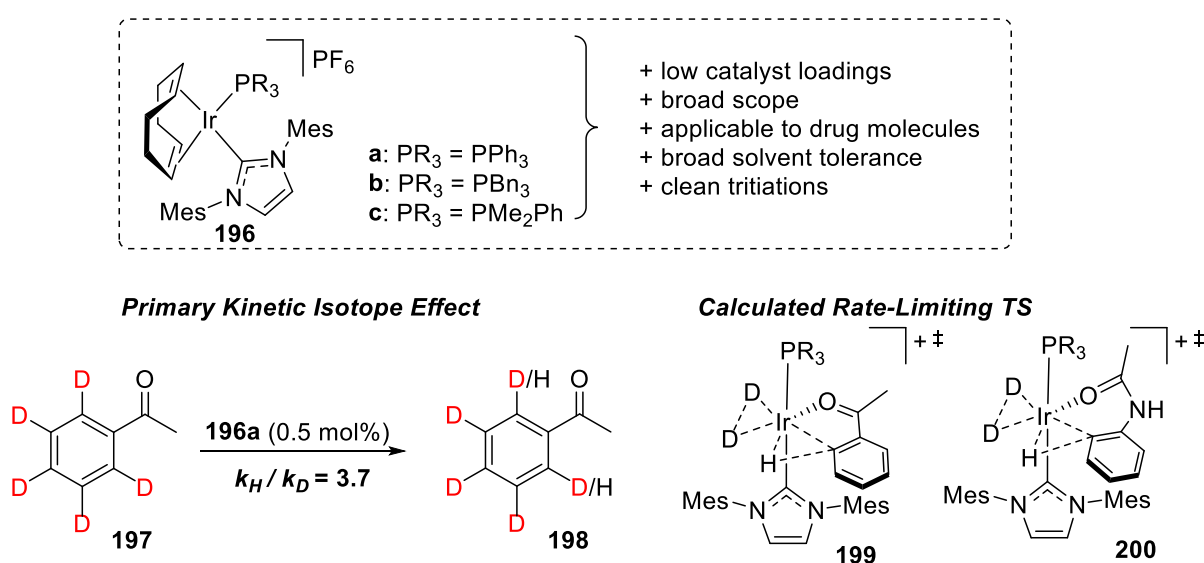


Figure 8. NHC-ligated Ir catalysts for hydrogenation later explored by HIE chemists.

In a more interesting variant of this work, Kerr and co-workers studied the *catalytic* activity of complexes **194b** – **194f**, showing most active complex, **194e**, to be highly active over an appreciable substrate scope (5 mol% [Ir], 16 h, r.t.), and displaying a higher turnover frequency (TOF) than Heys' bis-phosphine catalyst, **162**. Interestingly, the smaller complexes in the series studied by Kerr (**194b** and **194c**) were completely inactive as HIE catalysts.¹¹¹ Similar investigations by the same group later led to the discovery that small NHC/phosphine complexes such as **195c** were inactive as HIE catalysts, but larger variants **195d** and **195e** was active across a limited substrate scope.¹¹²

The exploration of NHC-ligated Ir HIE catalysts had revealed promising (proof-of-concept) developments beyond the popular and established works of Hesk and Heys. Keen to fully explore such developments in HIE chemistry, Kerr and co-workers later developed a synthesis of previously unattainable complexes **196a** – **196c**, bearing large phosphine *and* NHC ligands (**Scheme 29**).¹¹³ These complexes have proven seminal within the *ortho*-HIE domain, and have among the highest activity,¹¹⁴ substrate/solvent scope,^{115,116} and tritiation reaction cleanliness¹² of any such catalyst reported to date. Additionally, *ortho*-HIE process with these complexes have been studied experimentally and computationally, strengthening the case for a Ir(III)-based reaction mechanism akin to that proposed by Heys.¹¹⁴ More

specifically, kinetic isotope effect (KIE) measurements¹¹⁷ revealed that C-H bond cleavage was the rate-limiting step of the reaction, and detailed NMR studies revealed the *trans*-geometry of the ancillary ligands.¹¹⁴ The same study was also able to reveal the origins of the selective reactivity of such catalysts for 5- over 6-mm substrate, citing dual kinetic and thermodynamic favourability for the 5-mm. Building on Kerr's work, Ir(III)-catalysed *ortho*-HIE has continued to flourish, and a recent contribution from Pfaltz and Muri has shown the application of *P,N*-derived bidentate ligands. Most notably, these latest Ir-based HIE catalysts have been developed to be able to label *ortho* to secondary benzenesulfonamides for the first time, albeit using high temperatures and synthetically intricate ligands.¹¹⁸



Scheme 29. Highly-active NHC/phosphine Ir *ortho*-HIE catalysts.

1.5 Key Concepts in Selected Ligand Design

1.5.1 Phosphines as Ligands

In transition metal catalysis, ligand choice and ligand design are fundamental to the success of a catalyst in its desired function. In this respect, phosphines, and indeed phosphites, rank among the most widely employed ligand types in organometallic chemistry. The principle reason leading to their popularity is the ease with which their steric and electronic properties can be controlled by altering the substituents present on the phosphorus atom.²⁹

Electronically, phosphines bind to the metal centre by σ -donation from a lone pair of electrons on the central phosphorus atom into an empty d-orbital on the metal. In a complementary fashion, phosphines also participate in π -backbonding, accepting electron density into an empty P-R σ^* -orbital from a filled metal d-orbital (**Figure 9**).³⁰

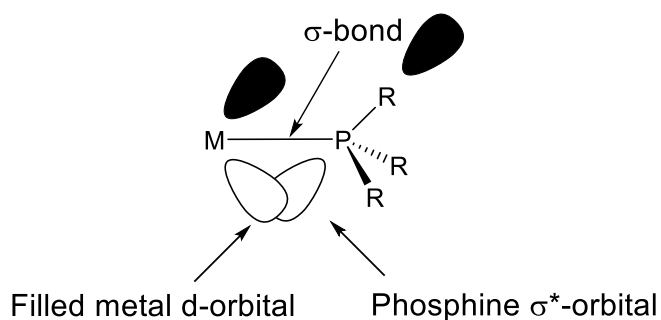


Figure 9. Metal to phosphine π -backbonding through P-R σ^* -orbital.

In general, the Lewis basicity of phosphines and phosphites is inversely proportional to the electron-withdrawing capability of the surrounding R groups. To that effect, the generally accepted scale for the σ -donating nature of these ligands is as expressed below in **Figure 10**.

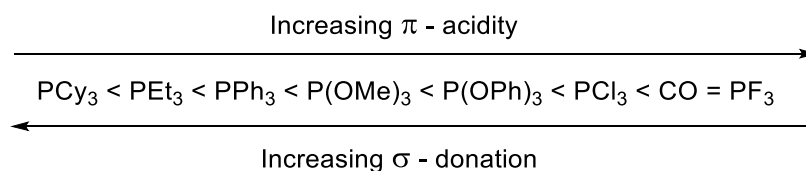


Figure 10. A didactic scale of the electronic characteristics of common phosphine ligands.

In 1970, seminal work by Tolman helped quantify the electronic nature of these ligands for the first time, measuring the CO stretching frequencies of a series of $[\text{Ni}(\text{CO})_3\text{PR}_3]$ complexes.¹¹⁹ Increased σ -donation from the phosphine/phosphite increases the electron density on the metal and thus increases the level of back donation into the CO π^* -orbital. Such an increased level of back bonding weakens the CO triple bond and lowers the observed IR stretching frequencies for the CO ligands. This method of quantification was later named the *Tolman Electronic Parameter* (TEP). In more recent times, Nolan has expanded this methodology to include TEP measurements from $[\text{Ir}(\text{CO})_2(\text{L})\text{Cl}]$, allowing direct comparisons to be drawn between phosphine and NHC ligands.^{120,121}

Due to the substantial variety of phosphine and phosphite substituents available, the steric bulk of the ligand is of equal importance to the aforementioned electronic character. Additional investigations by Tolman led to the concept of the *cone angle*, θ , enabling the steric properties of the phosphine to be quantified.¹²² By setting the M-P bond length to 2.28 Å, the cone angle was defined as the minimum apex angle set out by three identical R groups on the phosphorus atom (**Figure 11**). The bulkier the ligands around phosphorus are, the larger the cone angle.

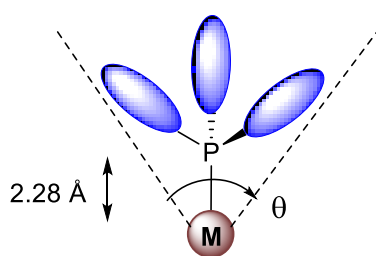


Figure 11. Simplified representation of the Tolman Cone Angle model.

To assess the suitability of his descriptor experimentally, Tolman correlated the cone angle of certain phosphine/phosphite ligands with the degree of CO substitution in a reaction with $\text{Ni}(\text{CO})_4$ (**Table 1**).

Table 1. Substitution reaction on $\text{Ni}(\text{CO})_4$ as a measure of ligand steric impact.



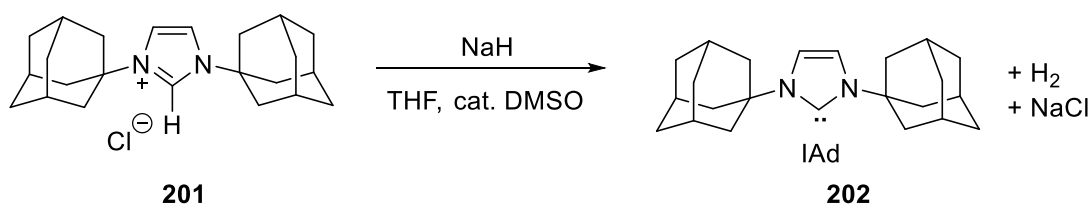
<i>L</i>	<i>Cone Angle</i> (°)	<i>Degree of CO Substitution</i> (<i>n</i>) ^a
$\text{P}(\text{OMe})_3$	107	3.0
$\text{P}(\text{OPh})_3$	121	2.7
P^iBu_3	130	2.2
PPh_3	145	2.0
PCy_3	179	1.5

^a $4 \geq n \geq 0$

It was evident that the level of CO displacement became lower with increased steric bulk of the ligand substituents. Indeed, Tolman postulated that, in general, the *steric* influence of the incoming ligand exerted a greater influence on ligand substitution than its *electronic* nature.¹²²

1.5.2 *N*-Heterocyclic Carbenes as Ligands

In the past quarter century, *N*-heterocyclic carbenes (NHCs) have come under significant scrutiny as ligands in transition metal catalysis.^{121,123–129} The first crystalline NHC was reported in 1991 by Arduengo, who isolated 1,3-diadamantylimidazol-2-ylidene (IAd), **202**, *via* deprotonation of the parent imidazolium salt, **201** (Scheme 30).¹³⁰



Scheme 30. The synthetic method used to isolate IAd.

Since Arduengo's early work, NHCs have been employed as ligands to help both stabilise and activate the metal centre to which they are bound. Their success in transition metal catalysis is now evident across a spectrum of reaction classes, including olefin metathesis,¹³¹ borylation,¹³² and cross-coupling,^{133,134} as well as hydrogen isotope exchange.¹² In a similar fashion to phosphines, the inherent properties of these ligands can be understood by knowledge of their electronic properties.^{121,126} NHCs are singlet carbenes which possess a lone pair of electrons in a sp^2 -hybridised orbital in the plane of the ring (**Figure 12**).³⁰ With specific reference to imidazole derivatives, the empty p-orbital on the carbenic carbon is stabilised by π -donation from the lone pairs of electrons on the adjacent nitrogen atoms. Delocalisation of this type is extended when a double bond is present in the ring, the 6 π -electrons providing *pseudo*-aromaticity.

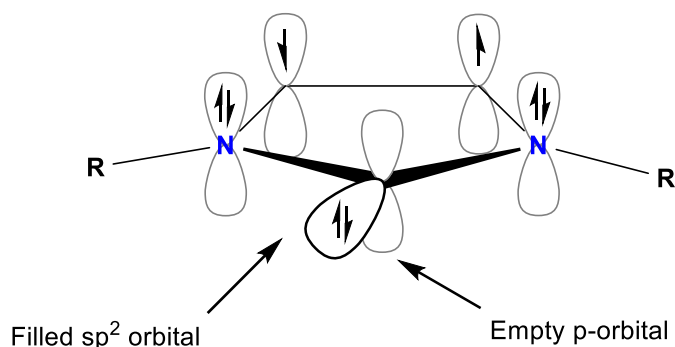


Figure 12. Simplified representation of bonding in imidazole-derived NHCs.

NHCs have often been compared with phosphine ligands in bonding to transition metals, notably due to the apparent similarity in their σ -donor and π -acceptor capabilities. In 2008, Nolan's analysis of the carbonyl stretching frequency in a series of iridium complexes, $[\text{Ir}(\text{CO})_2(\text{L})\text{Cl}]$, revealed NHCs to be stronger σ -donators than even the most Lewis basic of tertiary phosphines (**Table 2**).¹²⁰

Table 2. Exemplar comparison of NHC and phosphine TEP values.

<i>L</i>	<i>TEP</i> (cm^{-1})
IAd	2049.5
IMes	2050.7
SIMes	2051.5
IPr	2051.5
PCy ₃	2056.4
PPh ₃	2068.9

The study of iridium carbonyl complexes fell in agreement with an earlier study on complexes of the type $[\text{Ni}(\text{CO})_3(\text{L})]$ and served to show that, although electronic properties can be tuned by substitution on the nitrogen atoms, there seemed a surprising lack of variation in the σ -donating capabilities of NHCs.¹³⁵ Indeed, it is only within the past few years that such a view has been challenged. For instance, in 2012, Sato and co-workers characterised electron-poor NHC, **203** (IDNP), showing that, when bound to rhodium in **204**, it was identical to PPh₃ in terms of its electron-donating capabilities (**Figure 13**).

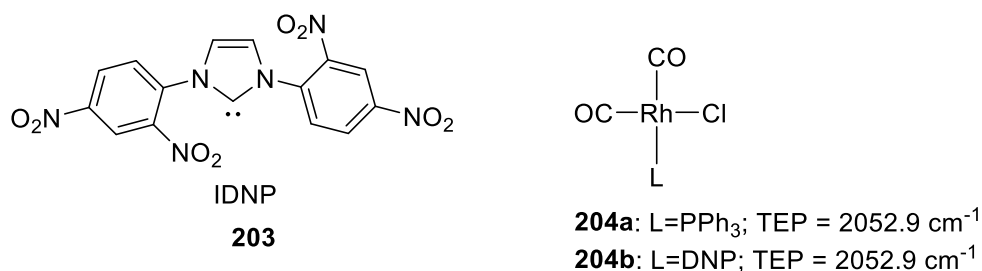


Figure 13. An example of an electron-poor NHC equal in measure to PPh₃.

In addition to all of the above, the level of back bonding in NHCs has been the subject of intense questioning in recent years. It has previously been theorised that the NHC-metal interaction is primarily of single bond character, with little or no back donation into the p-orbital on the NHC, which is already stabilised by interaction with the flanking nitrogen atoms. Despite this, there exists a growing body of evidence to the contrary. Most recently, experimental techniques have been developed using NHC adducts of phosphinidenes¹³⁶ and selenium (**Figure 14**, top and bottom, respectively), showing a measurable range of NHC Lewis acidity.¹³⁷ It is therefore unlikely that π -back bonding in NHCs can be ignored.

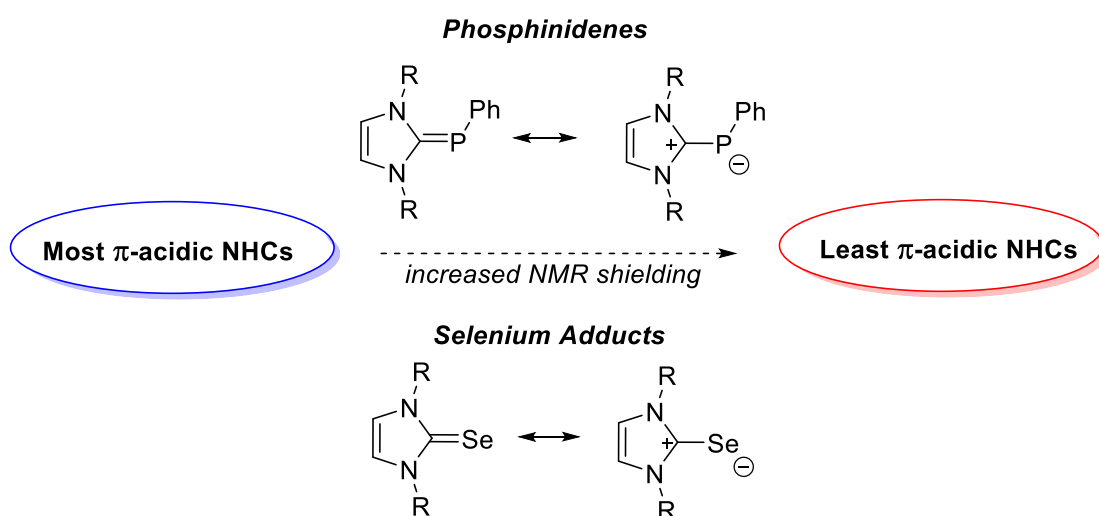


Figure 14. Basic representation of phosphinidene and selenium adduct methods for determining NHC back bonding capability.

Nolan believed that, like phosphines, the steric influence of NHCs generally outweighs that of its electronic parameter.¹³⁵ In a development similar to the pioneering work of Tolman, Nolan and Cavallo introduced the *Percent Buried Volume*, % V_{bur} concept.^{128,138} Although it is by no means the only model in existence for describing NHC steric bulk,^{139,140} it remains one of the most widely utilised, especially in terms of comparing NHC and phosphine ligands on

the same basis. In a sphere centred on the metal atom, whose radius, r , is fixed, $\%V_{bur}$ is defined as the fraction of the sphere occupied by the ligand (**Figure 15**). As with Tolman's cone angle, Nolan fixed the NHC-metal bond distance, d ; however, this could be varied for different metal systems.

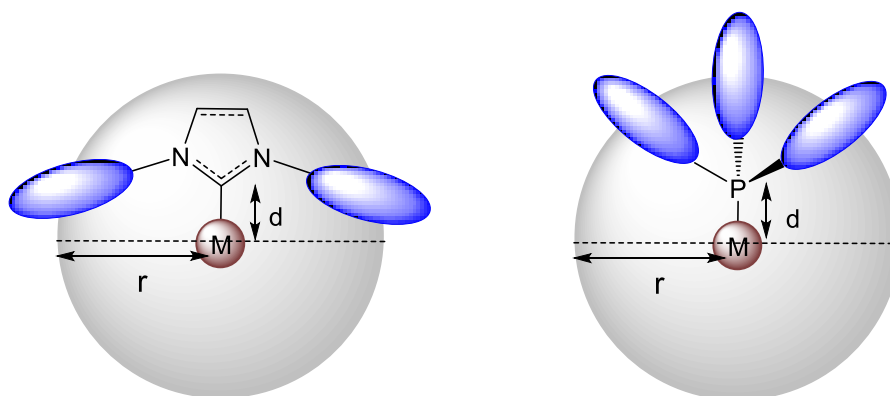


Figure 15. Simplified representation of the Percent Buried Volume concept as applied to NHCs and phosphines.

Nolan and Cavallo's steric parameter has been successfully correlated with the cone angle of phosphines (**Table 3, Entries 1 - 4**); however, phosphites do not generally fit this model due to their greater ligand flexibility.¹²⁰ NHCs have been classed in this manner using a range of NHC-metal species, including Nolan's hydrogenation catalysts, **194d - 194f** (**Entries 5 - 7**).¹²⁸

Table 3. Exemplar comparisons between Cone Angle and Percent Buried Volume values.

<i>Entry</i>	PR_3	<i>Cone Angle</i> (°)	$\%V_{bur}$ for $M-L$ of 2.28 Å
1 ^a	P^tBu_3	132	25.9
2 ^a	PPh_3	145	29.6
3 ^a	PCy_3	170	31.8
4 ^a	$P(OPh)_3$	128	30.7
5	IMes	-	27.4
6	SIMes	-	28.3
7	IPr	-	30.2

^a Derived for a range of complexes. See reference for full details.

As

mentioned previously, this more universal quantification of ligand sterics allows for an easier

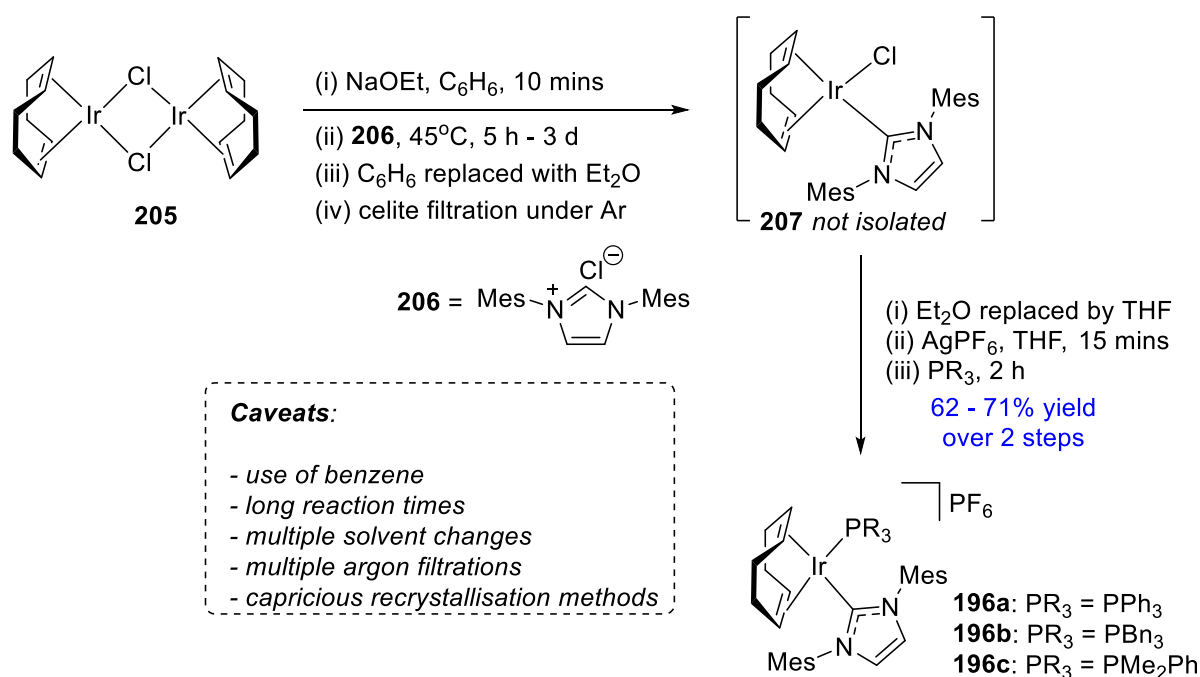
comparison between phosphines and NHCs to be made. However, such calculations are based on crystallographic or DFT-derived data and, as they do not describe solution structure, this is recognised as one of the main limitations of this approach.

1.6 Concluding Introductory Remarks

The field of hydrogen isotope exchange using homogeneous transition metal catalysis has undergone a remarkable evolution since its inauspicious beginnings in platinum and rhodium chemistry. Developments in metal choice, ligand design, and isotope source over the ensuing 50 years have led to a deeper appreciation of the operative mechanisms behind such labelling reactions. The most recent developments in the area have shown unprecedented levels of activity and regioselectivity under ambient conditions using a new generation of iridium(I) phosphine/NHC complexes.^{113,114} Nonetheless, it is clear that, as the substrate base continues to expand, there remains the potential to further improve on current successes. Indeed, it is the search for a wider range of applicable catalysts and reaction conditions that form the basis of the research presented herein.

2. Proposed Work

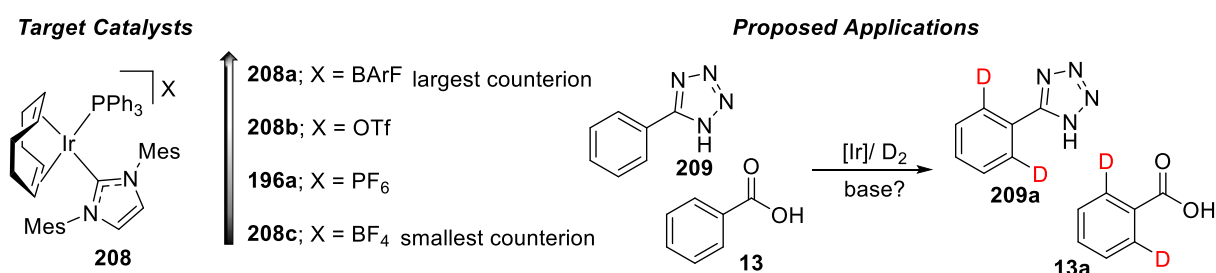
Within the Kerr laboratory, several novel complexes of the type [(COD)Ir(PR₃)(NHC)]PF₆, **196**, have been synthesised and successfully applied to homogeneous *ortho*-directed HIE processes.^{12,113,114,116} As these complexes are emerging as an industry standard in HIE chemistry, it is vital that their synthesis and use be made accessible to the broadest possible audience. As such, the first aim of this project will be to improve on the current published synthesis of complexes **196a** – **196c** (Scheme 31),¹¹³ allowing for enhanced reaction scalability and more attractive operational simplicity. A faster, more scalable route towards key intermediate [(COD)Ir(IMes)Cl], **207**, from **205** is believed to be crucial to this goal, as it is diversification from this complex that leads to the desired catalysts. Current efforts will thus focus on eliminating long reaction times and the carcinogenic solvent, benzene, from the syntheses of **196a** – **196c**.



Scheme 31. Original synthesis of Kerr group *ortho*-HIE catalysts.

In a second objective, complementary to the first, it is desirable that this project explores alteration of the catalyst counterion, hexafluorophosphate, PF₆. Literature precedent in iridium-catalysed hydrogenation suggests that moving to a larger, more weakly-coordinating anion can improve catalyst efficiency and longevity.^{141–144} It is thus hypothesised that moving to larger counterions, such as tetrakis[3,5-

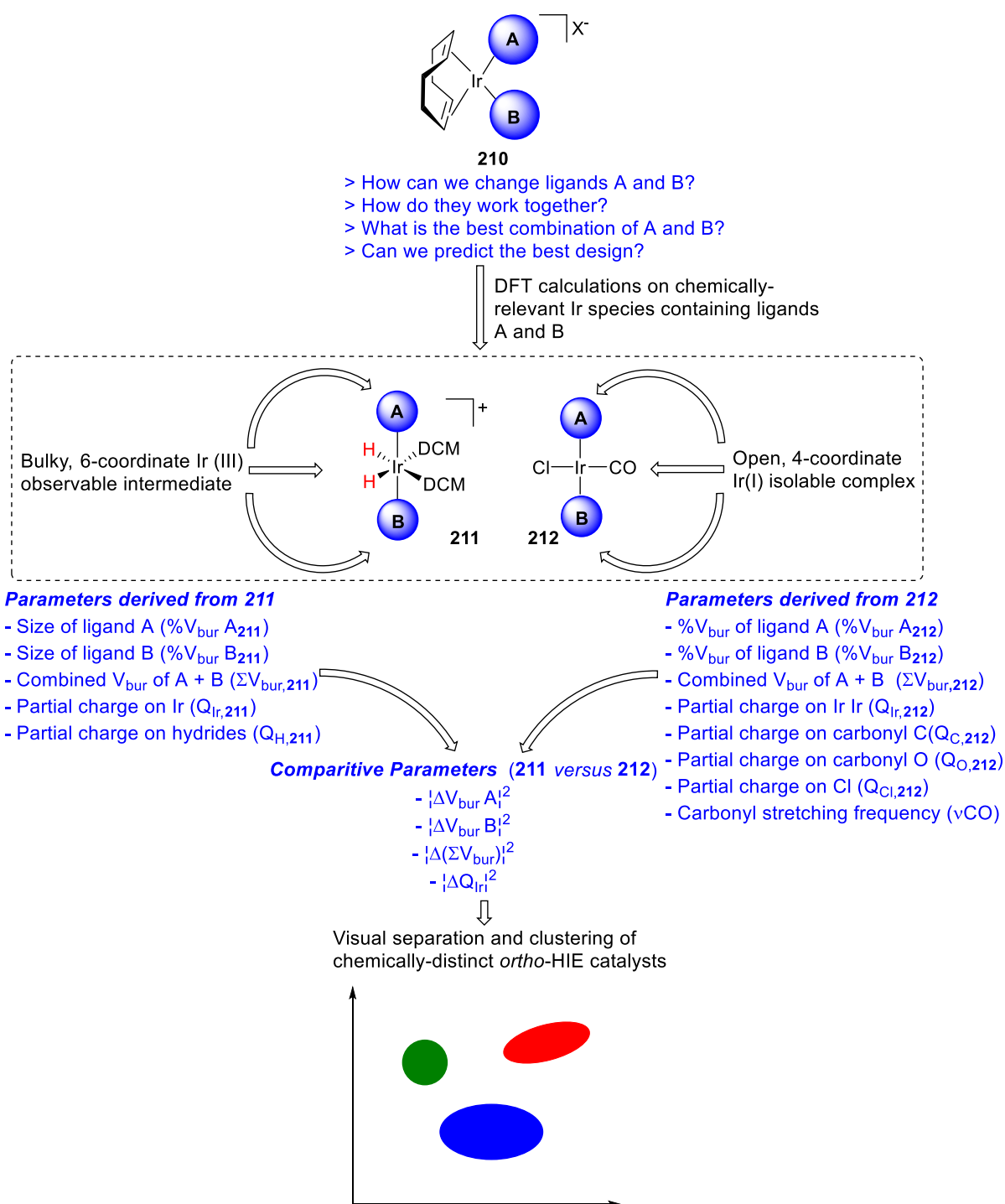
bis(trifluoromethyl)phenyl] borate (BArF), will enhance the activity of the proposed new Ir catalysts at lower catalyst loadings. To substantiate these proposals, it is necessary to study complexes bearing counterions both larger *and* smaller than for catalyst **196a**. To initiate investigations in this area, complexes **208a** – **208c** will be the primary targets (**Scheme 32**). Indeed, Pregosin has shown that these alternative counterions decrease in size BArF, to OTf, to PF₆, to BF₄.¹⁴³ With these complexes in hand, the effect of the outer coordination sphere on the efficacy of HIE processes similar to those already described can be probed quickly. Additionally, it is proposed that these counterion effects may contribute to development of *ortho*-labelling methods for weakly coordinating and highly challenging substrates, such as tetrazoles, **209**, and carboxylic acids, **13**, which may require as-yet unexplored basic reaction conditions.



Scheme 32. Proposed catalyst anion development and applications in *ortho*-HIE of acids and tetrazoles.

In a more wide-reaching aim of this project, it is anticipated that the involvement of complementary computational studies can vastly improve and refine our means of designing novel isotope exchange catalysts.¹⁴⁵ How bulky should our ligand sphere be? Does the carbene size outweigh its electronic contributions? What ligand combinations should we avoid? All these questions and more can be answered by partnering our established experimental measures with carefully selected, computationally-accessed parameters. In an extension of concepts introduced *vide supra* (**Section 1.5**), existing and proposed *ortho*-HIE catalysts will be characterised in terms of the steric and electronic characteristics of the ligand *combination*, rather than assessing the influence of each ancillary ligand separately (**Scheme 33**). By using two electronically and sterically distinct but nonetheless chemically relevant Ir species, useful parameters can be derived to describe ligand combinations of A and B. Ultimately, it is envisaged that the wealth of information available from such calculations

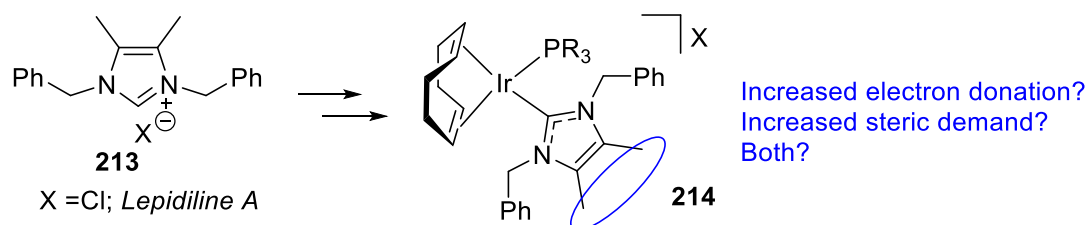
will be distilled *via* statistical methods to provide a user-friendly visual map of different catalyst types.



Scheme 33. Proposed strategy for describing the combined influence of ancillary ligands A and B *via* DFT methods.

To parallel an intensified computational mode of catalyst design, the concepts must be tested experimentally. Thus, it is proposed that these theoretical studies are applied to the investigation of as yet unsolved challenges within HIE chemistry.

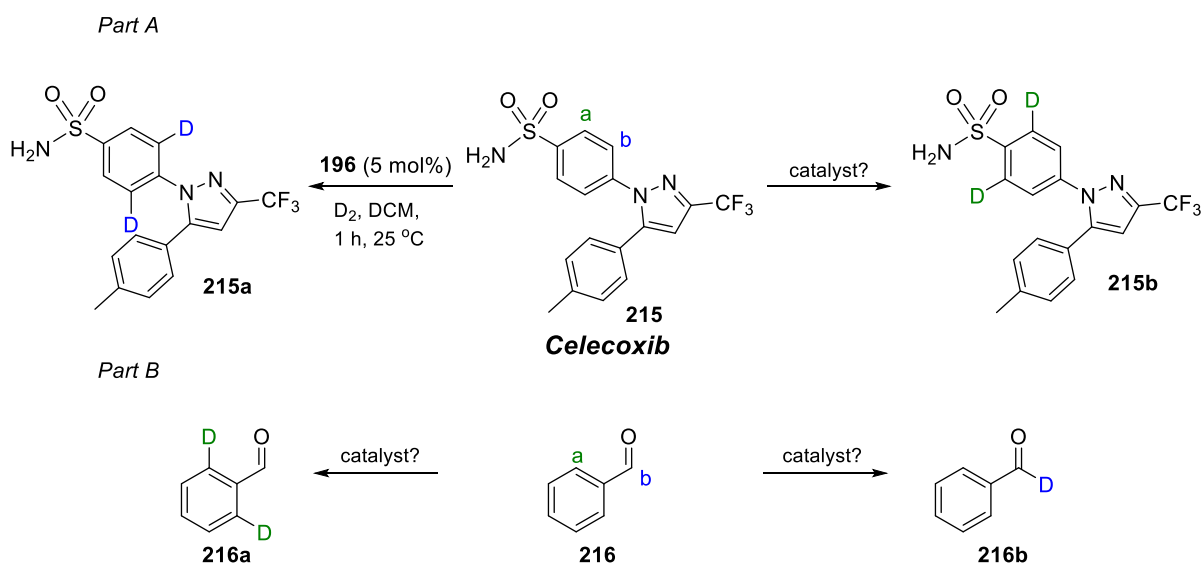
In a further extension to this overall programme of work, we wish to further broaden the scope of our most successful catalysts of type **196**. As well as efforts concentrated on judicious alteration of the catalyst counterion, it is important to continue investigations into the effects of changing the ligands which support the iridium centre. More specifically, there remains scope to explore structural variations in the carbene ligand, probing further the effects of the steric bulk and electron donation imparted by this part of the catalyst. Imidazolium salts derived from **213** will thus be prime synthetic targets in this area of study (**Scheme 34**). In this case study with **213** (where the chloride salt represents natural product *Lepidiline A*),¹⁴⁶ its 4,5-unsubstituted analogue has already been successfully applied to HIE chemistry.¹⁴⁷ It has recently been shown that such additional methyl substitution can increase both the electron-donating capability and steric bulk of NHC ligands;^{148,149} two highly desirable traits in designing effective HIE catalysts.^{113,150} Therefore, a combined experimental and computation assessment of **214** *versus* existing catalysts will be undertaken in order to rationalise the effects of 4,5-dimethyl substitution.



Scheme 34. Proposed NHC variations to investigate experimentally and computationally.

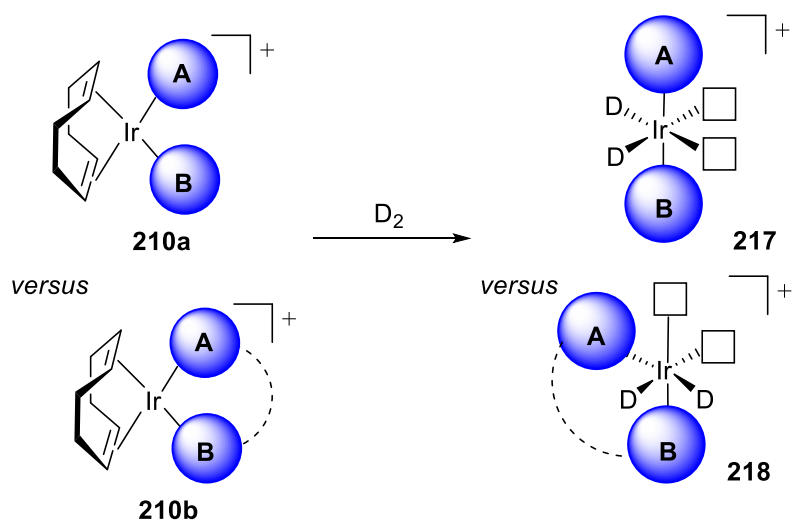
Among other remaining challenges in homogeneous HIE, selective labelling *via* sterically-encumbered primary sulfonamide directing groups remains unsolved.¹¹¹ To address this, the bifunctional drug molecules derived from COX-2 inhibitor Celecoxib, **215**, will be studied in detail. Methods to label *via* the alternative pyrazole directing group are already known (Part A, **Scheme 35**).^{114,147,151} In a related regioselectivity problem, the labelling of aldehydes remains a remarkably under-developed field, despite the widespread use of such compounds as an indispensable building block in organic synthesis. Evolving theoretical understanding of

catalyst design will thus be used in an attempt to find novel and complementary methods for the production of labelled aldehydes, **216a** and **216b** (Part B, **Scheme 35**).



Scheme 35. Unsolved questions in the regioselective labelling of 1° sulfonamides and aldehydes.

In the final aim of this project, it is proposed that the study of novel bidentate rather than monodentate ligand partnerships be initiated. As described in the **Introduction**, bidentate ligands can offer more spatially accessible catalyst coordination spheres relative to monodentate phosphines, providing exploitable opportunities to develop HIE methods for more challenging substrate classes.⁹⁸ Driven by the well-documented success of NHC/phosphine ligand spheres in HIE catalysis, it is proposed that this work be extended to encompass mixed NHC/phosphine bidentate ligands. As such, the steric and electronic properties of the related iridium catalysts will be assessed computationally in order to assess the propensity for such species to deliver new technologies for the HIE community (**210a** versus **210b**, **Scheme 36**).

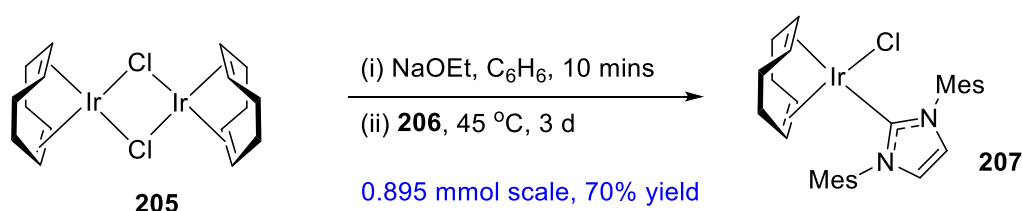


Scheme 36. Proposed assessment of mono- *versus* bidentate NHC/phosphine HIE catalysts.

3. Expanding the Applicability of [(COD)Ir(NHC)(PR₃)]X Complexes in HIE Processes

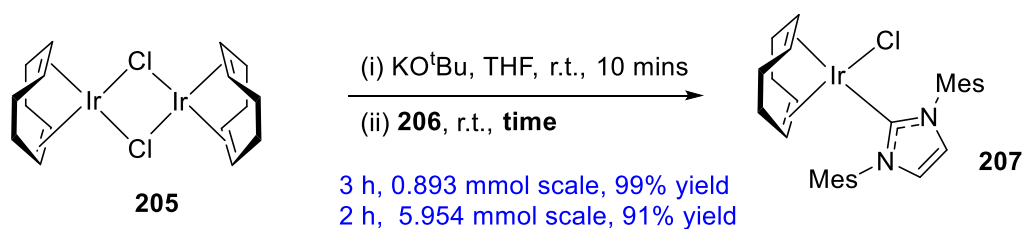
3.1 Alternative Synthetic Route to [(COD)Ir(IMes)(PR₃)]PF₆

It was proposed that a simpler, more scalable and more flexible synthesis of benchmark catalysts **196a** – **196c** would be achieved by isolating large scale, pure quantities of **207**. This would aid in avoiding mechanically-cumbersome solvent changes and additional argon filtration steps that are hurdles to scalable catalyst synthesis. Before embarking on alternative synthetic routes towards **207**, it was deemed necessary to perfect the aforementioned synthetic methodology most traditionally employed within our laboratories.^{112,114,147,151} Using the latest optimised conditions for this particular reaction,¹⁴⁷ **207** could be isolated in good yield, approaching gram-scale quantities of the desired product (**Scheme 37**).



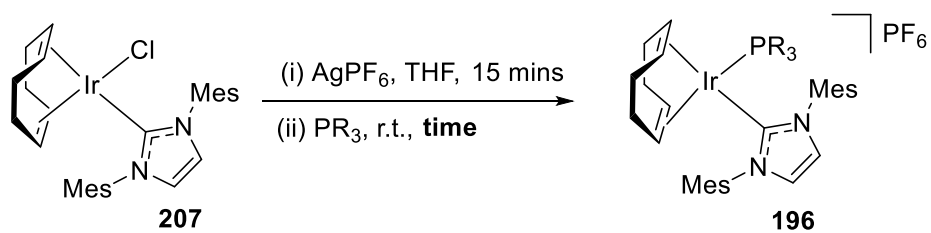
Scheme 37. Synthesis of **207** *via* established methods.

In approaching an alternative synthetic procedure towards complex **207**, promising reports from Plenio¹⁵² and Glorius¹⁴⁸ revealed that it can be readily synthesised from dimer **205**, and IMes salt **206**, using KO^tBu in THF. In combining the best traits from these syntheses of **207**, dimer **205** and KO^tBu were stirred together in dry THF before salt **206** was added to the reaction mixture in one portion, causing an instant dark red to dark yellow colour change. On work up, isolation of the desired product by simple flash column chromatography was readily achieved in good to excellent yields (**Scheme 38**). Reactions of this type are highly efficient at room temperature and proceed to near completion within 2 – 3 h. Under these new conditions, complex **207** can now be synthesised on an unprecedented multi-gram scale, with a significant reduction in reaction time and complete eradication of the need for using benzene or, indeed, metallic sodium.



Scheme 38. Alternative synthesis of **207**.

With a vastly improved route to **207** in place, stock quantities of this complex were available for improving the synthesis of our most successful catalyst range, **196a – 196c**, bearing the PF₆ counterion. It was deemed advantageous to first perfect (and improve) on the standard protocol for synthesising HIE catalysts **196a – 196c**. If any problem could be identified in preparing these catalysts from **207**, it lies not in the reaction itself but in the isolation of the desired catalysts. Traditionally, and according to published procedures,¹¹⁴ these iridium complexes have been purified and isolated *via* recrystallisation from a DCM/Et₂O solvent system. Looking more closely at repeated syntheses of said complexes, it can be seen that this isolation method provides product yields that are highly variable.^{147,153} To investigate these concerns, complex **196a** was synthesised according to this commonly utilised method (see **Table 4, Entry 1** for a representative example carried out on the largest scale to date). The carbene chloride complex, **207**, was dissolved in dry THF and treated with silver hexafluorophosphate, causing immediate precipitation of silver chloride. After filtration of the reaction mixture through celite and addition of PPh₃, a yellow/orange to bright red colour change was observed. Having stirred the reaction mixture for the allotted reaction time, the desired complex was isolated *via* the recrystallisation method described above in moderate yields comparable with those described in the literature. The mixed solvent system used for recrystallisation in this case does purify the complex but undoubtedly possesses the danger of triturating unreacted PPh₃ along with the desired product.¹⁴⁷ To improve the yield and consistency of this synthetic procedure, it was proposed that a mechanically simpler trituration method be identified. To our satisfaction, a simple solvent screen has uncovered EtOAc as the perfect trituration agent, allowing the full catalyst range to be isolated in higher yields and at scales previously unachievable (**Table 4, Entries 2 – 4**). This improved synthetic method has culminated in **196a – 196c** being made commercially available by Strem Chemicals, Ltd.^{154–156}

Table 4. Improved syntheses of complexes **196a** – **196c** from **207**.

Entry	PR ₃	Time (h)	Work-up Procedure	Yield (%) ^a	Lit. Yield(%) ^b
1			DCM/Et ₂ O recryst.	50	
2	PPh ₃	1	EtOAc trit.	80	62
3	PBn ₃	1	EtOAc trit.	77	59
4	PMe ₂ Ph	16	EtOAc trit.	90	71

^a All reactions carried out on a 1.093 mmol scale with respect to **207**.

^b Lit. yields refer to method shown in **Scheme 31**.¹¹³

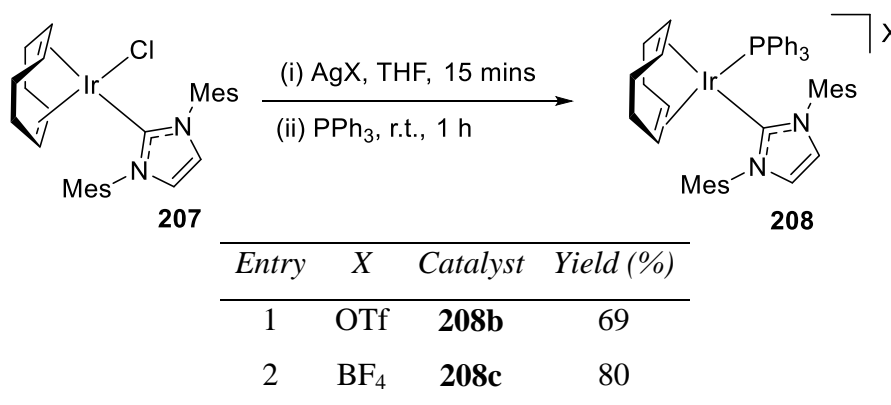
3.2 Anion Effects in Iridium-catalysed Isotope Exchange Processes

Ionic transition metal complexes play a central role in catalysis and organic synthesis. Although it is more common to tune the properties of such catalysts *via* manipulation of the coordinated ligands on the transition metal cation, the past two decades have witnessed a significant increase in studies of the effects of changing the negatively charged counterion.^{157–159} In most cases where the counterion plays a spectator role, moving to larger, more weakly coordinating counterions has evidenced a positive influence on catalyst efficiency across various methodologies, with examples spanning palladium,^{160,161} rhodium,¹⁶² and iridium^{141,144,163,164} catalyses, among others.^{157,158} Having stated this, there also exist some cases in which the ability of the counterion to coordinate to the inner sphere of the transition metal cation is essential for overall structural stability.^{165–168} Furthermore, changing the counterion has also been documented to completely alter reaction pathways in both transition metal complex synthesis^{169,170} and organic synthesis.¹⁷¹

As previously described, our interest in this field stems from the development of cationic complexes of the type **196** for HIE processes. In this contribution, the syntheses and application in HIE of complexes **208a** – **208c**, counterion variations of flagship catalyst **196a** are reported. Furthermore, as wider preparative applications of HIE require catalysts operable in a more expansive array of solvent media,^{66,115,172} it was theorised that the more diffuse counterions would enhance the solvent scope of the catalyst beyond that which we have already reported.

Studies began with the syntheses of novel complexes **208b** and **208c**, using a method similar to that from **Table 4**. Starting from the chloro-carbene complex, **207**, the choice of silver salt used to abstract the chloride ligand simultaneously delivered the counterion of choice (after addition of PPh₃). Both complexes were isolated in acceptable yields by simple trituration from ethyl acetate, as for complexes **196a** – **196c** (**Table 5**).

In turning our attention to the synthesis of complex **208a**, the lack of a commercially available source of AgBARf prompted the search for a silver-free synthetic route. In this regard, it was hypothesised that the chloro-carbene intermediate, **207**, may be circumvented if the parent imidazolium salt required to provide the NHC ligand was

Table 5. General syntheses of novel complexes **208b** and **208c**.

partnered with a large and weakly coordinating counterion such as BArF. Indeed, this approach has promising literature precedent relating to iridium complexes bearing a chelating carbene-phosphine ligand.¹⁷³ Accordingly, and as detailed in **Scheme 39**, this approach was successfully realised for our monodentate NHC-phosphine ligand combination. Firstly, NHC precursor **219** was synthesised by salt metathesis from **206**. Following *in-situ* generation of [(COD)Ir(PPh₃)Cl] from **205** and PPh₃, **219** was added followed by base to yield the desired complex, **208a**, in good yield, and on gram scale. As a brief diversion into studying the mechanistic aspects of this reaction, the suspected intermediate phosphine complex, **220**, was prepared and isolated¹⁷⁴ before subsequently reacting this with NHC salt, **219**, in the presence of KO^tBu (**Scheme 39**, bottom). In agreement with previous observations, a yellow to deep red colour change was observed on addition of the base. The red solid isolated from the reaction mixture was identical in composition to **208a**, indicating that intermediate, **220**, is likely to be formed during the one-pot procedure.

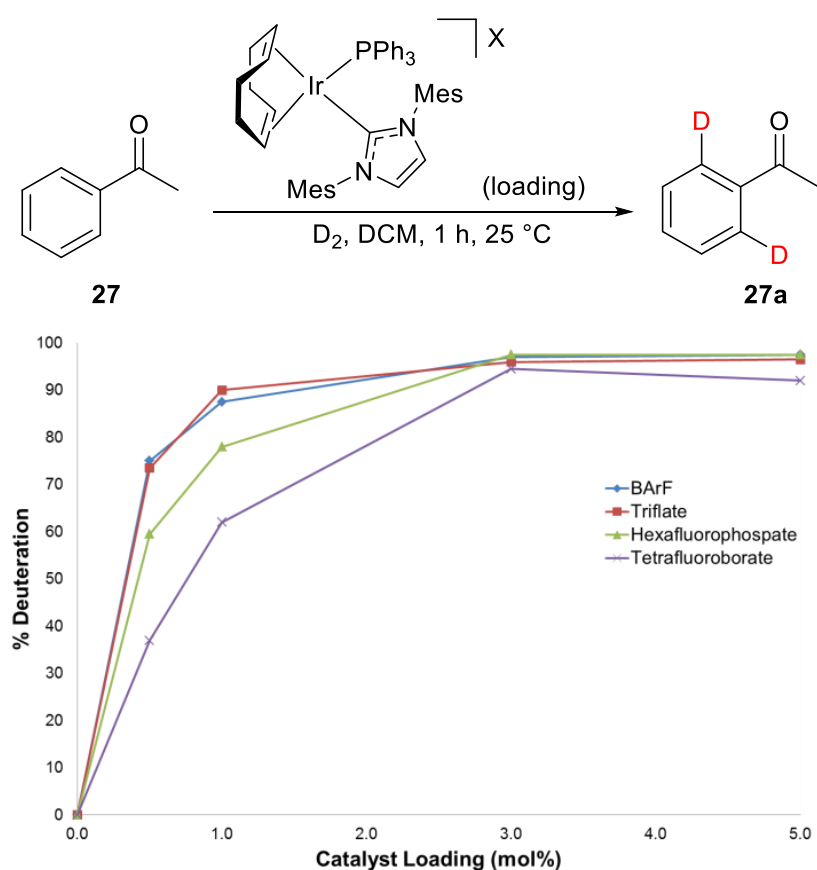
All novel compounds, **208a** – **208c** and **219**, were characterised by NMR (¹H, ¹³C, ³¹P, ¹⁹F, and ¹¹B), IR, melting point, HRMS, and X-ray crystallography. Of particular note is the X-ray structure determination of complex **208a**, which reveals the similar size of the BArF counterion relative to the cationic portion of the complex (**Figure 16**).

To investigate the impact of the series of counterions in iridium-based HIE processes, model reactions employing acetophenone, **27**, as the substrate were undertaken. In particular, the effect of catalyst loading on the labelling efficacy of complexes **208a** – **208c** was scrutinised. As shown in **Scheme 40**, the effect of changing the counterion

was clearly drawn out at the most accessible and commonly applied reaction temperature of 25 °C (but not at 40 °C; see **Experimental** section). As predicted, the relative efficiency of each catalyst increases in order of increasing counterion volume.¹⁴³ Catalysts **208a** and **208b**, bearing the BArF and OTf counterions, respectively, are more active than parent catalyst, **196a**, and the catalyst bearing the small BF₄ counterion, **208c**. Notably, the reactivity of the OTf catalyst, **208b**, contrasts with observations made by Pfaltz and co-workers during their study on the counterion effects in olefin hydrogenation using PHOX-type chelating ligands.¹⁴⁴ Where these previous studies showed complete shutdown of catalytic activity using the triflate species, we have evidenced that both OTf and BArF counterions perform equally well (and, indeed, better than the parent catalyst, **196a**) at 25 °C within HIE processes. Presumably, this difference in the effectiveness of OTf across these two systems is related to the different orientations of the ancillary ligands in the active catalyst forms. For bidentate PHOX ligands, the coordinating groups adopt a *cis* configuration, allowing coordination of the dipolar triflate anion to the iridium centre. In catalyst series **196**, the bulky NHC and phosphine ligands are known to rest *trans* to one another in the active form.¹¹⁴ Therefore, OTf coordination may be blocked by the more effective combined steric bulk of a *trans* NHC-phosphine system relative to the more open *cis*-coordinated PHOX ligands.

Next, we explored the effective solvent scope of the catalysts with different counterions. Previously, we have identified 2-MeTHF, MTBE, and Et₂O as viable alternatives to DCM using catalyst **196a**.^{115,147} Therefore, we compared the applicable solvent scope of **196a** *versus* the most non-polar derivative, **208a**, across a wider range of solvents than previously explored. Using the same reference reaction as shown in **Scheme 40** (5 mol% catalyst, 25 °C, 1 h), a series of ethereal, alcoholic, ester, chlorinated, and aromatic solvents were screened. Firstly, it was encouraging to note that the more soluble catalyst, **208a**, was generally superior to parent catalyst **196a** within HIE for the range of ether and carbonate solvents tested (**Figure 17**). For dioxane, MTBE, Et₂O, and 2-MeTHF both catalysts were shown to perform equally well, with the larger counterion of **208a** offering slight improvements to an already efficient deuteration system. However, more significant improvements were recorded on comparing the activities of **196a** and **208a** in ¹Pr₂O, THF, and the recognised green solvents,¹⁷⁵⁻¹⁷⁷ CPME and dimethyl carbonate.

Alcohol-derived solvents provided a more varied range of reaction efficiencies (**Figure 18**). Notably, in all cases, catalyst **208a** displayed greater levels of activity and was more widely applicable than **196a**. The most significant reactivity from the alcoholic solvents shown was observed in the most sterically shielded (and presumably least coordinating) alcohol, ^tAmOH. A similar pattern of reactivity was observed for ester solvents, and accompanied with higher overall levels of deuterium incorporation. Again, the combination of catalyst **208a** and the most sterically encumbered solvent (ⁱPrOAc over EtOAc) proved most effective.



Scheme 40. Assessment of counterion effects on catalyst efficiency.

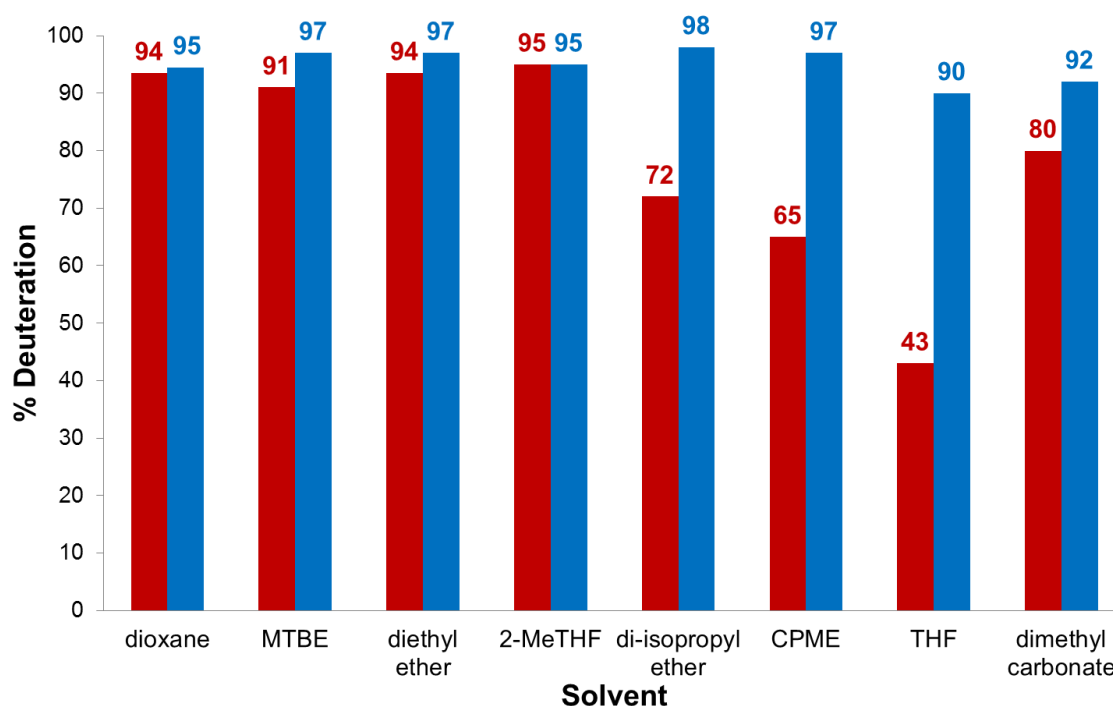


Figure 17. Counterion influence on ether and carbonate solvents using **196a** and **208a** with acetophenone, **27** (red = PF₆; blue = BArF).

Chlorinated solvents DCM and DCE evidenced no difference in catalysts **196a** and **208a**, with both producing almost quantitative D-incorporation. In contrast, a stark difference in deuterium labelling efficiency was recorded when using toluene as the solvent. Again, catalyst **208a** was superior to the less soluble catalyst, **196a**. Finally, it is also worth noting that more polar solvents DMSO and DMF were tested under the same reaction conditions with complex **208a**, however, only very low levels of deuteration in acetophenone were detected (see **Experimental** section).

Having shown that larger counterions are beneficial in *ortho*-HIE processes, the propensity to move beyond BArF to an even more diffuse counterions was investigated. To this end, Krossing's lithium tetrakis(perfluoro-*tert*-butylalkoxy)aluminate (LiPFTB)^{159,178} salt, **222**, was synthesised in modest yield from LiAlH₄ and employed in the synthesis of a fifth counterion derivative of this catalyst class, **208d**, using the same method employed for catalyst **208a** (**Scheme 41**). Using the acetophenone reference reaction (*vide supra*), this latest catalyst was compared to the BArF analogue across a more limited number of alternative reaction solvents

(Figure 19). Interestingly, **208d** proved to offer significantly improved activity in IPA, EtOAc and toluene, but was otherwise comparable with or less effective than **208a**.

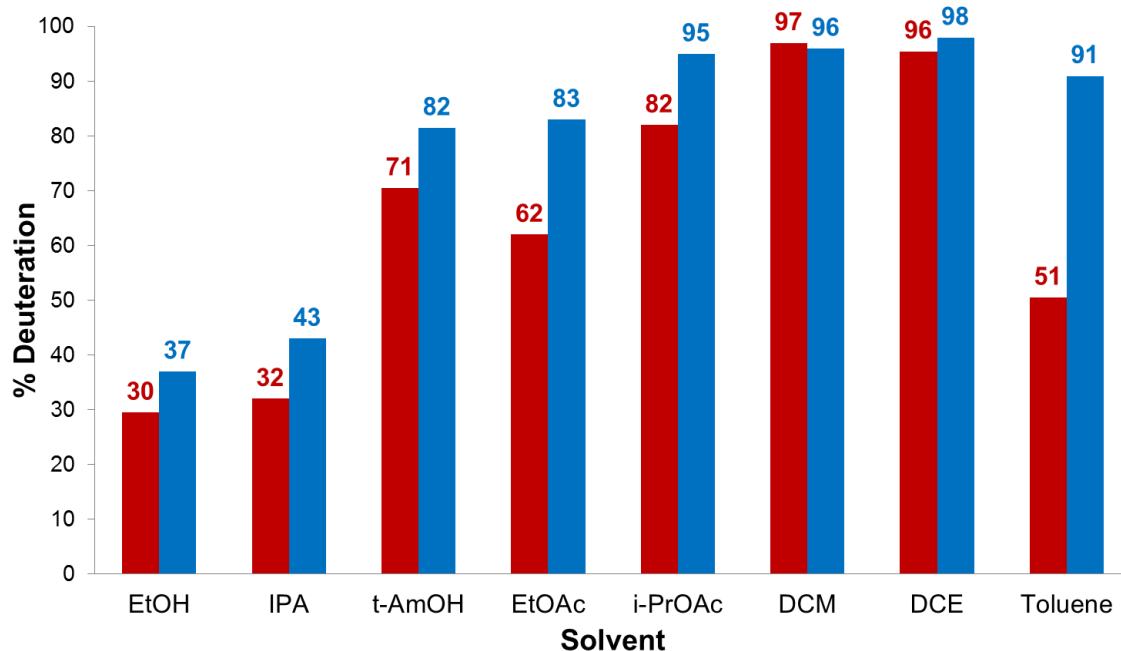
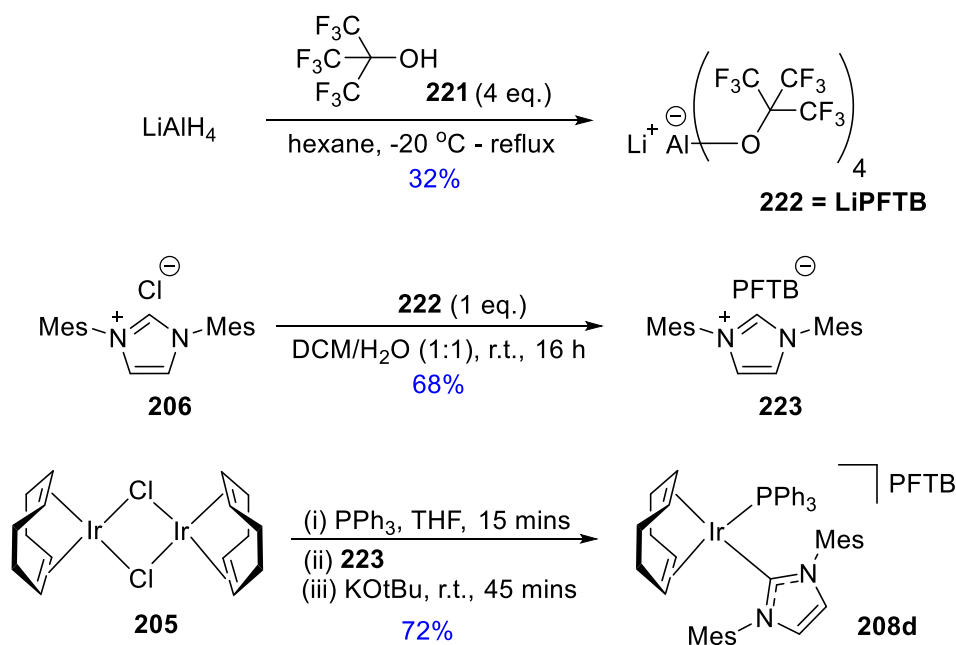


Figure 18. Counterion influence on alcohol, ester, chlorinated, and aromatic solvents (red = PF₆⁻; blue = BArF⁻).



Scheme 41. Synthesis of complex **208d**, bearing the PFTB counterion.

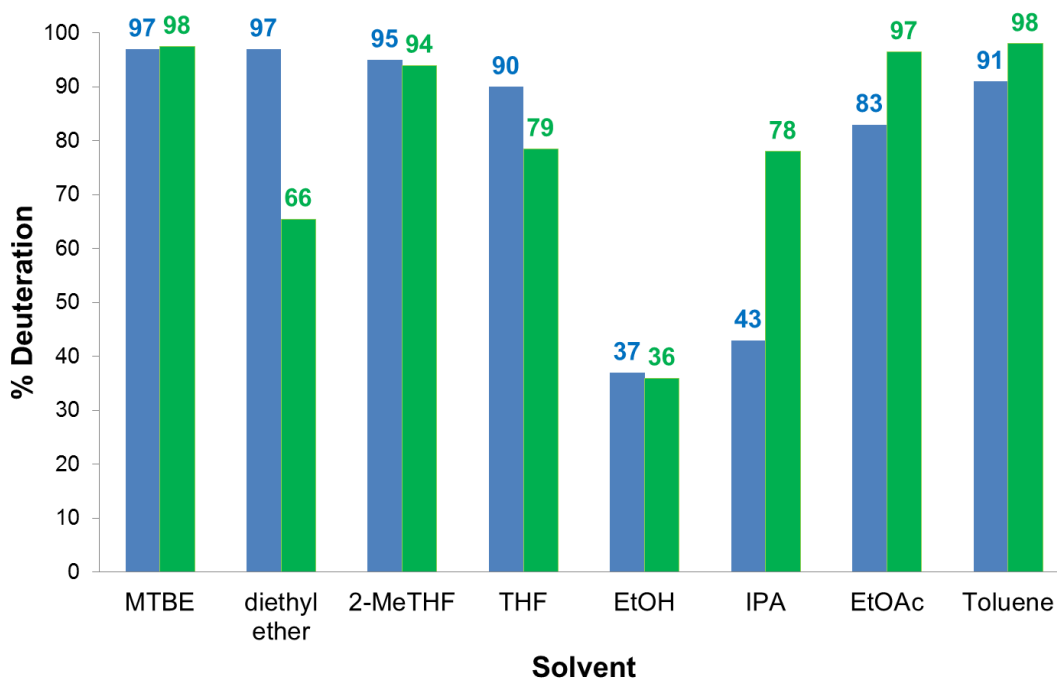


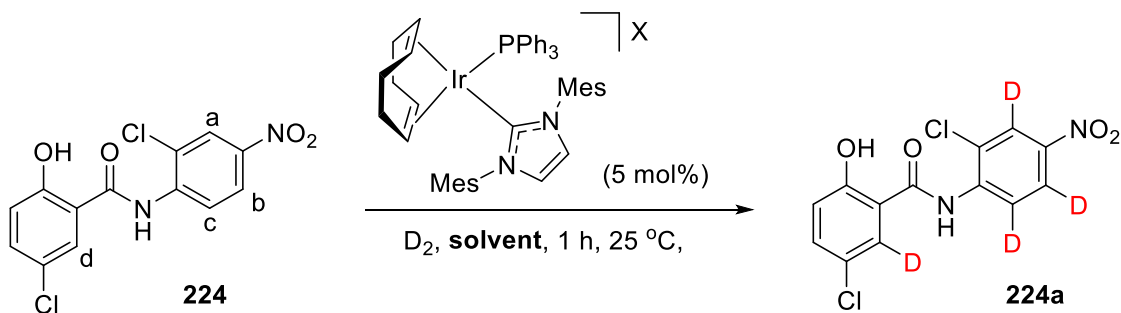
Figure 19. Comparative solvent screen of largest counterion catalysts **208a** (blue) and **208d** (green) with acetophenone, **27**.

Although it must be acknowledged that the use of **208d** may be advantageous in some instances, LiPFTB requires a more specialised synthesis¹⁵⁹ than for NaBARF.¹⁷⁹ As such, no further study was carried out using the PFTB catalyst, **208d**.

Owing to the highly variable solubility profile of different drug classes, HIE processes with drug candidates require a flexible solvent choice. To explore the potential benefits of expanded solvent scope with catalyst **208a** over **196a**, attention was turned to the deuterium labelling of drug molecule, Niclosamide, **224** (Table 6). Using catalyst **196a** or **208a** in DCM, similarly moderate to good deuterium incorporation was achieved across all four possible labelling sites (Table 6, Entries 1 and 2). This is presumed to be due to the relative insolubility of **224** in DCM. On moving to 2-MeTHF as an alternative solvent (able to fully solubilise all reactants), catalyst **196a** showed suppressed deuteration in positions *a-c*, and enhanced deuteration at position *d* (Table 6, Entry 3). The increased selectivity for position *d* when using **196a** in 2-MeTHF may be based on the increased polarity of the solvent relative to DCM and the resultant increase in competition between substrate and solvent for coordination to iridium.¹¹⁵ Coordination of the amide carbonyl and labelling *via* a 5-mm (position *d*) is more facile than *via* the 6-mm (position *c*). Additionally, coordination through

the nitro group (for labelling at *a* and *b*) is presumed to be weaker than for the amide.¹⁸⁰ Pleasingly, and to exemplify the effectiveness of the larger anionic counterion, especially with more demanding pharmaceutically-related substrates, catalyst **208a** in 2-MeTHF showed improved labelling in *all four positions* over all other conditions tested (**Table 6, Entry 4 versus 1-3**).

Table 6. Improved labelling of Niclosamide with **208a**.



Entry	Catalyst	X	Solvent	%D _a	%D _b	%D _c	%D _d
1	196a	PF ₆	DCM	66	53	41	66
2	208a	BArF	DCM	71	57	18	73
3	196a	PF ₆	2-MeTHF	51	11	4	98
4	208a	BArF	2-MeTHF	97	96	65	96

To investigate the protective role played by larger counterions against cluster formation in hydride-mediated iridium catalysis, Diffusion Ordered NMR Spectroscopy (DOSY NMR) can be employed to assess the relative diffusion rates of catalyst cation and anion in solution.^{142,143,158} For **196a** and **208a**, ¹H and ¹⁹F DOSY experiments were conducted to compare cation and anion diffusion, respectively. As illustrated in **Figure 20**, in catalyst **196a**, bearing the PF₆ counterion, the cation and anion move independently through solution. In the other case, although not formally ion-paired, the cation and anion of **208a** move at almost equal rates in solution phase. This suggests that the counterion for catalyst **208a** is more likely to be within the proximity of the reactive cation, and able to play the protective role discussed above.

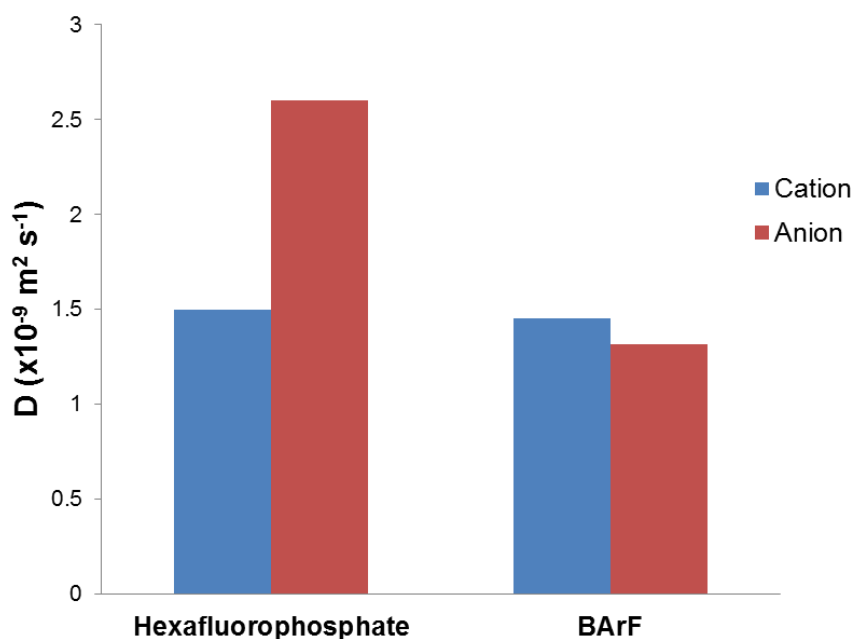


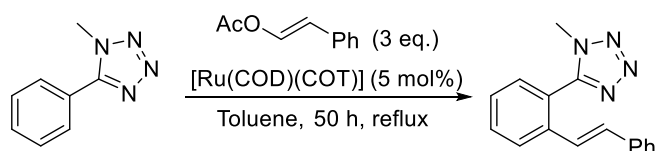
Figure 20. Relative diffusion of cation and anion fragments of catalysts **196a** and **208a**.

In summary, the syntheses of four novel complexes of the type $[(\text{COD})\text{Ir}(\text{IMes})(\text{PPh}_3)]\text{X}$ ($\text{X} = \text{BF}_4$, OTf, BArF, and PFTB) have been accomplished, with the BArF and PFTB complexes having been accessed by a modified and more direct preparative process. Application of these complexes as catalysts in hydrogen isotope exchange has demonstrated improved catalytic activity at lower catalyst loadings in the order $\text{X} = \text{BArF} \approx \text{OTf} > \text{PF}_6 > \text{BF}_4$. Relative to the parent complex (**196a**, $\text{X} = \text{PF}_6$), **208a** ($\text{X} = \text{BArF}$) possesses a superior solubility profile and applicable solvent scope in HIE processes. This finding is of fundamental importance to the delivery of labelled drug candidates for use in ADMET studies. Complex **208d** ($\text{X} = \text{PFTB}$) was compared to **208a** in this way, revealing potential scope for future investigations, should its overall synthesis be improved. Accordingly, the complex **208a** now provides a catalyst system of wider potential applicability and effectiveness, in particular, within pharmaceutical settings. In relation to this point, the utility of improved solvent scope has been demonstrated through improved global deuterium labelling of the drug molecule Niclosamide, **224**, in 2-MeTHF.

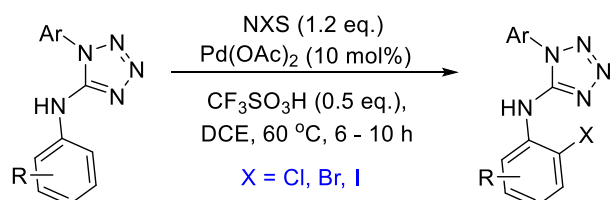
3.3 Base-sensitive HIE: *ortho*-Directed Labelling of Unprotected Tetrazoles

The tetrazole represents an important azacyclic functional group in pharmaceutical science and drug design. As a key bioisostere of the carboxylic acid, this functionality has been employed in with great success within the *sartan* drug class.¹⁸¹ Having said this, methods to *ortho*-functionalise tetrazoles are surprisingly rare, and have tended to involve *N*-protected analogues (**Scheme 42**).^{182–184} Specific to this work, functionalisation protocols employing *unprotected* tetrazoles (a key element of some drug classes) are especially scarce, with only an isolated and inefficient (17%) tritiation example having been reported using the RhCl₃·3H₂O catalyst.⁸ As such, it was proposed to investigate the propensity for the novel *ortho*-HIE Ir catalyst, **208a** (*vide supra*) to mediate the deuteration of such tetrazoles (**Scheme 42**, inset).

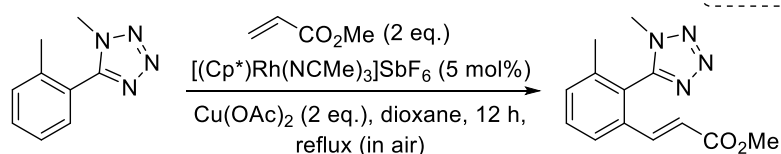
Kakiuchi (2007)



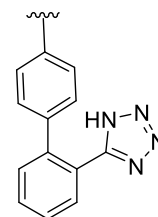
Punniyamurthy (2013)



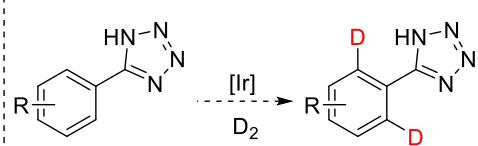
Wang & He (2014)



Common Sartan Substructure



This Work



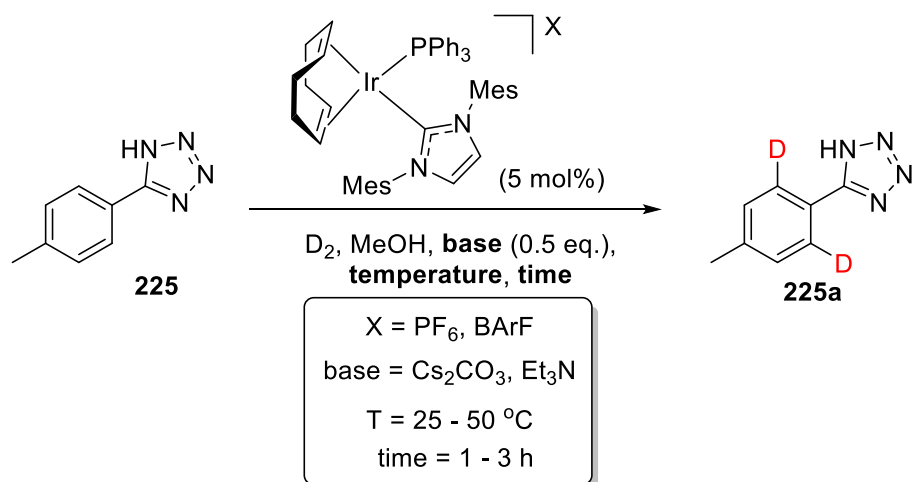
Scheme 42. Tetrazole directing groups in C-H functionalisation.

In approaching the problem, we first recognised that the aforementioned C-H activation protocols all involved the generation of acetate, a potential mediator for *concerted metalation-deprotonation* (CMD),^{47,185} a mechanism distinct from that operative under the normal deuteration conditions for catalyst **208a**.¹¹⁴ Secondly, the bioisosteric carboxylic acid functionality requires high temperature and base-mediated deuteration methods,¹⁸⁶ suggesting

weak coordinating ability of the directing group. This holds true for the tetrazole functionalisations described in **Scheme 42**. Finally, it has been shown by Zhou and co-workers that bis-phosphine hydrogenation catalysts related to **208a** can be employed under basic conditions (Et_3N or Cs_2CO_3 in MeOH) to mediate the carboxylate-directed asymmetric hydrogenation of cinnamic acid derivatives.^{187–190}

Based on the aforementioned literature observations, a *design of experiments* (DoE)^{191–193} approach was used to efficiently explore a range of conditions (base, temperature, and time) in labelling unprotected tetrazole, **225** (**Table 7**). In all cases, lower temperatures and times were insufficient, regardless of catalyst or base used (**Entries 1 – 3**). More encouragingly, increasing the temperature to 37.5 °C with BArF catalyst **208a** in combination with Cs_2CO_3 for 2 h, evidenced a 66% *ortho*-deuteration of **225**, and was superior to the alternative catalyst and base under similar conditions (**Entry 7 versus 4 – 6**). The true superiority of Cs_2CO_3 over Et_3N was drawn out at 50 °C (**Entries 8 and 9**), along with the need for longer reaction times (**Entries 9 and 12 versus 10 and 11**, respectively). Most intriguingly however, the benefit of the larger counterion in catalyst **208a** was no longer apparent at this temperature (**Entry 9 versus 12**), even with the addition of extraneous water (**Entry 9 versus 12**, parenthesised). In line with initial suspicions, base was necessary for catalysis (**Entry 14 versus 12**), while lowering the catalyst loading of **208a** had only a minor deleterious effect. Overall, the conditions from **Entry 12** represented a promising and novel approach to *ortho*-deuteration with this challenging substrate class, and were thus chosen for further study.

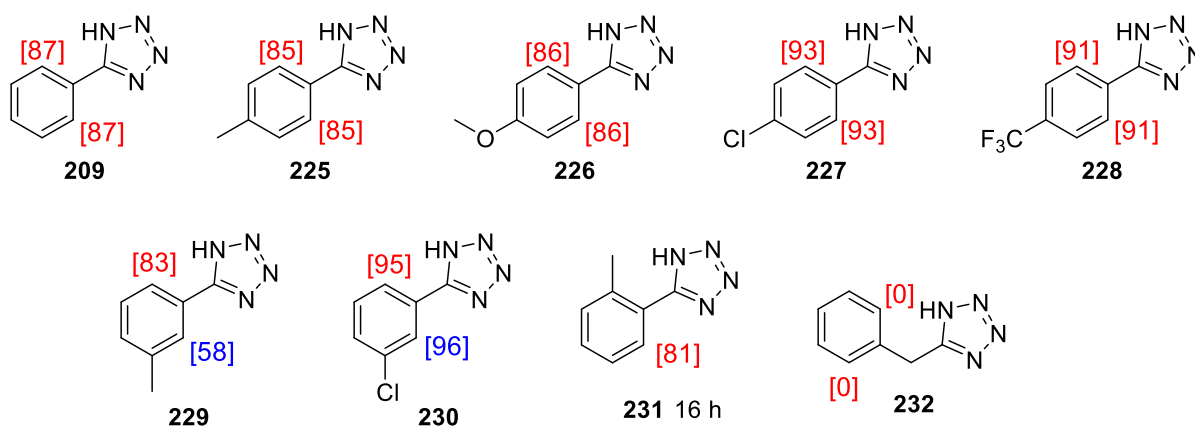
Under the optimised reaction conditions, the scope of applicable tetrazole derivatives was investigated (**Figure 21**). To our satisfaction, a range of electron-donating and electron-withdrawing substituents were tolerated in the *para*-position (**225 – 228**). Various *meta*-substituted derivatives were also successfully applied (**229 and 230**), with the preference to label the least hindered site varying depending on the ability of the substituent to assist labelling in the more hindered *ortho*-site.⁹⁴ Additionally, it was encouraging to note that the most sterically restrictive substrate, **231**, could be labelled with high efficiency, albeit with a longer reaction time. Unfortunately, the 6-mm benzyl tetrazole analogue, **232**, was not compatible with this method, showing evidence of decomposition by LC-MS (see **Experimental** section for full details).

Table 7. Reaction optimisation for *ortho*-HIE with *N*-H tetrazoles.

Entry	Catalyst	X	Base	Time (h)	Temperature ($^\circ\text{C}$)	%D
1	196a	PF ₆	Et ₃ N	1	25	7
2	196a	PF ₆	Cs ₂ CO ₃	1	25	6
3	208a	BArF	Cs ₂ CO ₃	1	25	10
4	196a	PF ₆	Et ₃ N	2	37.5	10
5	196a	PF ₆	Cs ₂ CO ₃	2	37.5	15
6	208a	PF ₆	Et ₃ N	2	37.5	0
7	208a	BArF	Cs ₂ CO ₃	2	37.5	66
8	196a	PF ₆	Et ₃ N	3	50	5
9 ^a	196a	PF ₆	Cs ₂ CO ₃	3	50	83 (83)
10	196a	PF ₆	Cs ₂ CO ₃	1	50	72
11	208a	BArF	Cs ₂ CO ₃	1	50	80
12^a	208a	BArF	Cs₂CO₃	3	50	85 (83)
13 ^b	208a	BArF	Cs ₂ CO ₃	3	50	81
14	208a	BArF	-	3	50	<5
15	196a	PF ₆	Cs ₂ CO ₃	3	50	10

^a Values in parentheses reflect reactions carried out with added H₂O (50 μL , ~3 mol%).

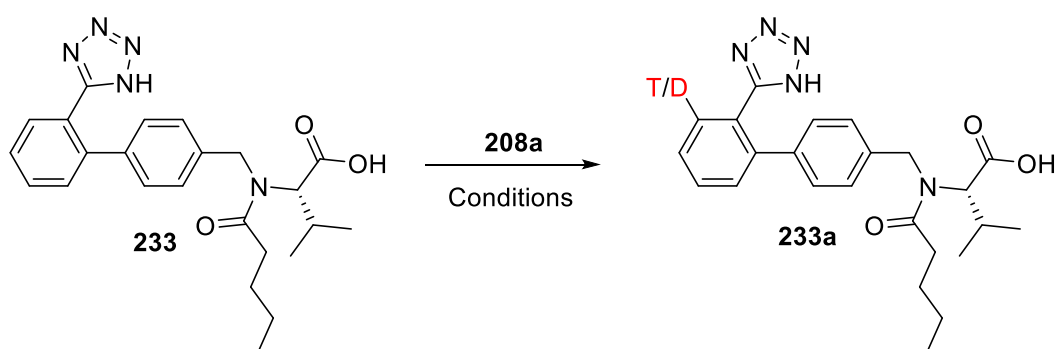
^b Reaction carried out using 2.5 mol% [Ir] instead of 5.0 mol%.



Conditions: substrate (1.0 eq.), **208a** (5 mol%), Cs₂CO₃ (0.5 eq.), MeOH, 3 h, 50 °C

Figure 21. Substrate scope for tetrazole *ortho*-HIE protocol.

Due to the collaborative nature of this particular project, it was deemed important to highlight the applicability of this method to more structurally challenging and pharmaceutically-relevant HIE processes. To this end, we subjected the beta-blocker *Valsartan*, **233**, to modified conditions (accounting for the additional acid site in the molecule). In testament to this new labelling method, the drug molecule was shown to incorporate one deuterium atom, as expected, and at a very high 88% incorporation, showing only minor degradation of the product *via* LC-MS (**Scheme 43**). Crucially, this new method has also been successfully applied to an analogous tritiation of **233**, confirming beyond doubt by ³H NMR that labelling is selective for the desired position only (see **Experimental** section).



Conditions: a) **208a** (5 mol%), D₂ (1 atm), Cs₂CO₃ (1.0 eq.), MeOH, 6 h, 50 °C; **88%D**; b) **208a** (6.7 mol%), T₂ (0.212 - 0.370 atm; 1.5 Ci), Cs₂CO₃ (1.1 eq.), 3.25 h, r.t. - 50 °C, **50%T**, **98.9% radiochemical purity**.

Scheme 43. Iridium-catalysed deuterium and tritium labelling of Valsartan.

This *ortho*-HIE process is not only novel for tetrazole functionalisation, but employment of base also indicates a potentially new mode of reactivity for HIE catalysts such as **208a**. Some initial mechanistic experiments have thus been conducted. Firstly, the optimised reference reaction (**Table 7, Entry 12**) and the unproductive base-free counterpart (**Entry 14**) were repeated, with pH indicator *methyl red* being added after the optimised reaction time.⁷⁵ In the latter case, a red solution resulted, indicating an acidic medium of pH < 4.4. In stark contrast, and perhaps unsurprisingly, the reaction conducted in the presence of Cs₂CO₃ resulted in a yellow solution, indicating a more basic medium of pH > 6.6 (**Figure 22, left**). Therefore, under the operative reaction conditions, the tetrazole substrate (pK_a ≈ 4) is most likely deprotonated. This conjecture was strengthened on analysing the ¹⁹F NMR shifts of substrate **228** under the optimised reaction conditions with and without base (**Figure 22, right**).

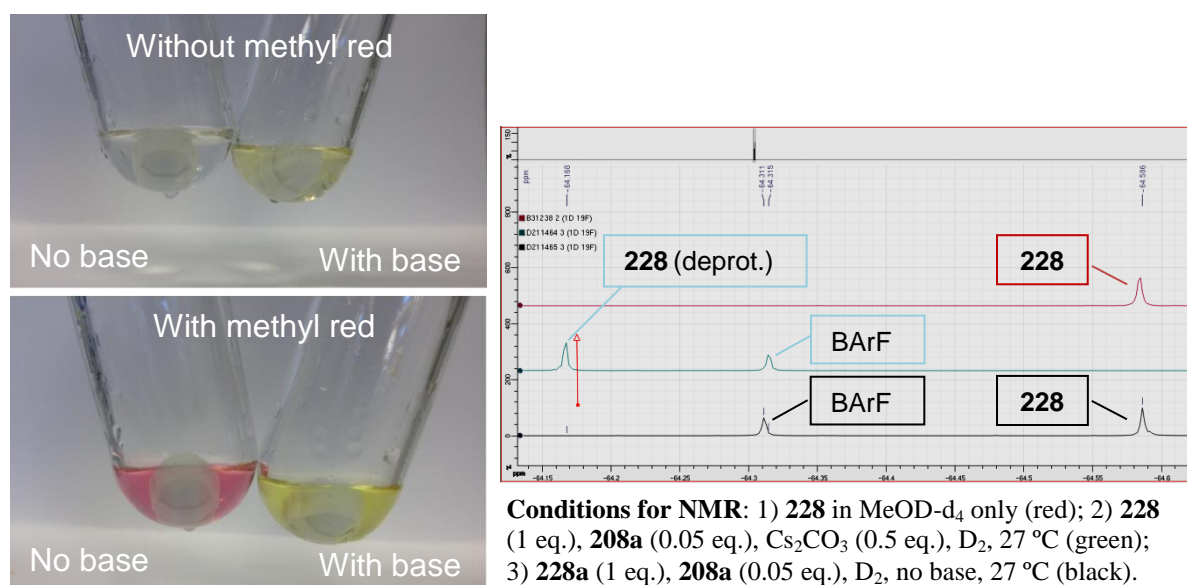
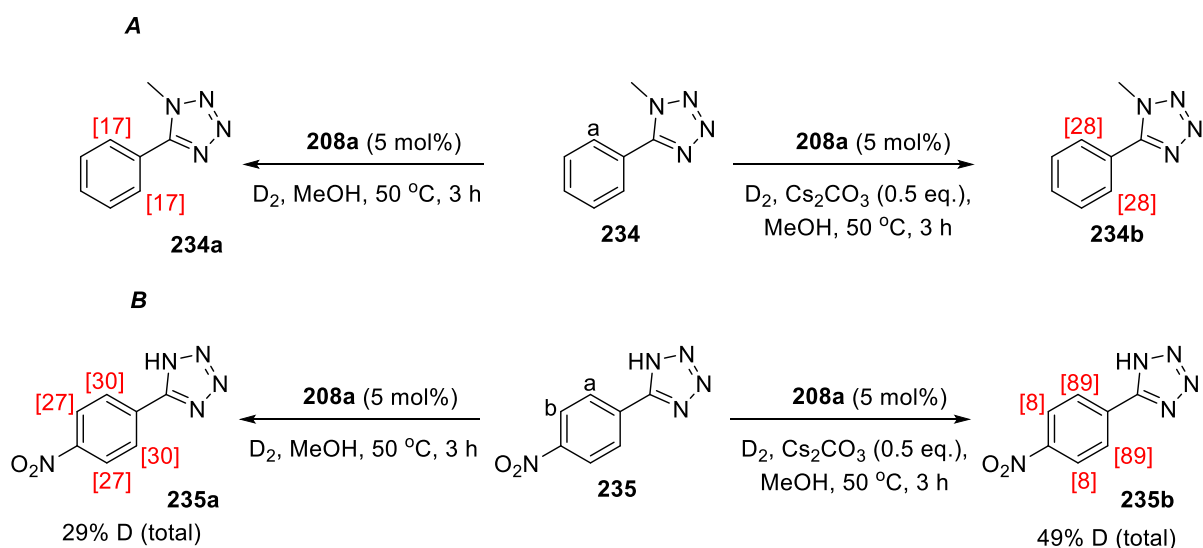


Figure 22. Tetrazole labelling mixtures with and without base.

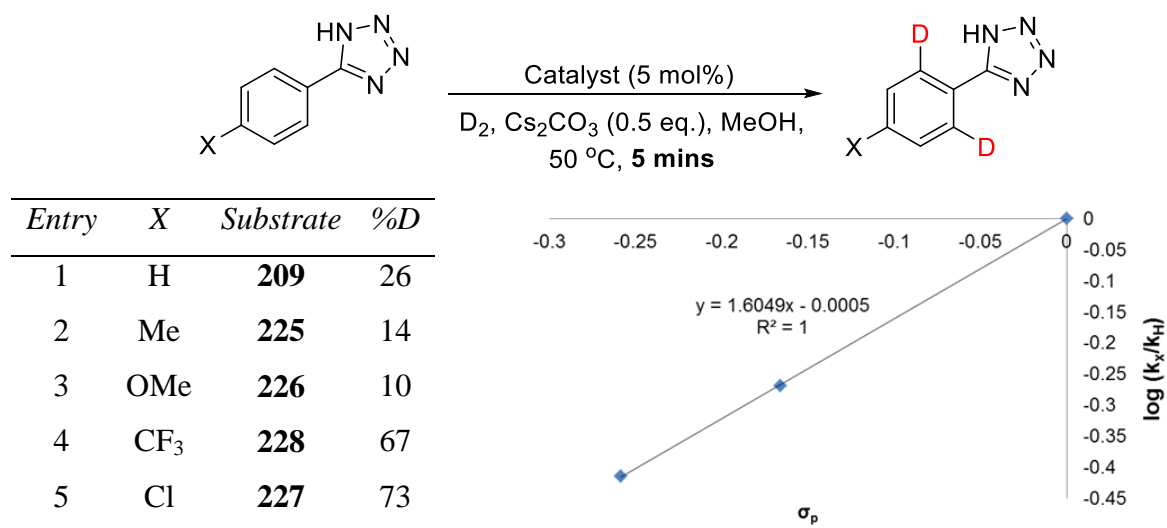
Attempted labelling of *N*-methyl-2-phenyltetrazole, **234**, under either basic or acidic conditions resulted in poor levels of D-incorporation, with presence of base nonetheless proving beneficial to *ortho*-deuteration, and suggesting a change in reaction mechanism (**Scheme 44, Part A**). By a similar method, bifunctional substrate, 2-(4'-nitrophenyl)-1H-tetrazole, **235**, was applied to the reaction conditions with and without base (**Scheme 44, Part B**). In the presence of base, relative data from ¹H NMR, LC-MS and HRMS suggest primary formation of the di-deuterated product in accordance with tetrazole selectivity, and represents yet another viable substrate for this novel labelling method. Alternatively, the absence of base resulted in low conversion and an equal distribution of deuterium, indicating

balanced competition between the neutral tetrazole and nitro directing groups. This indicates that the free *N*-H tetrazole is necessary to allow formation of the anion and more efficient interaction with iridium. Overall, this implied that the pH of the solution changed the active catalyst in the reaction, with optimal conditions being selective for unprotected (rather than *N*-capped) tetrazoles.



Scheme 44. Investigating the importance of *N*-H tetrazoles and changes in the active catalyst.

Under the current reaction set-up, acquisition of rate data was, unfortunately, difficult to achieve. Having said this, halting reactions after 5 mins rather than 3 h offered insight into the relative rates of labelling disparately substituted tetrazoles (**Table 8**). In this way, it was found that overall more electron-withdrawing substituents favoured faster reactions, further strengthening the case for a base-assisted reaction mechanism. Although the rate (even within 5 mins) was too fast for X = CF₃ and Cl to be considered as initial rates, using Swain-Lupton parameters for X = H, Me, and OMe in order to construct a modified Hammett plot yielded a perfect straight line with $\rho = 1.60$ when assuming resonance and field effects were almost equal.¹⁹⁴ This suggests that a partial (but not formal) negative charge builds up on the aromatic ring during the rate-limiting step, and further supports a base-assisted metalation pathway.

Table 8. Investigating substrate electronics in Ir-catalysed tetrazole labelling.

A ³¹P NMR study of the catalyst in MeOD-d₄ under different conditions revealed an intriguing variation in the phosphine-containing species present in solution (**Figure 23**). A single peak at ~16.2 ppm was visible for the precatalyst, **208a**, in the absence of any other reagent. This remained unchanged at 45 °C (see **Experimental** section). Interestingly, whether mixing **208a** and H₂, or **208a** and Cs₂CO₃, a similar red to yellow colour change occurred, resulting in similar and complete conversion to a new peak at ~32.3 ppm. Only when **208a**, base, and H₂ were mixed *together* were the distinct peaks at ~14.2 and ~13.3 ppm observed, with both species persisting in the presence of tetrazole, **228**. Parallel ¹H NMR studies support the presence of at least two mixed NHC/phosphine species, where the NHC is non-innocent (see **Experimental** section). Additional NMR studies with pure triphenylphosphine revealed yet another distinct peak at ~ -5.9 ppm, presenting evidence against phosphine ligand dissociation from the precatalyst under the standard reaction conditions. However, similar measurements using triphenylphosphine oxide revealed that a signal at ~32.1 ppm which, *versus* ~32.3 ppm observed in all other catalyst activation experiments, may indicate oxidative ligand cleavage as a PPh₃ possible side reaction.

It was proposed that the ³¹P NMR species observed at ~32 ppm may represent an inactive iridium species, formed in the absence of base, hydrogen, or tetrazole substrate. This reflects upon an interesting dependence on the order of addition of reaction components to the activity of the catalyst. It was observed that, if the tetrazole, base and solvent were preheated to 50 °C *before* the addition of D₂, no labelling was observed. However, the standard conditions of mixing all reaction components at room temperature prior to heating to 50 °C

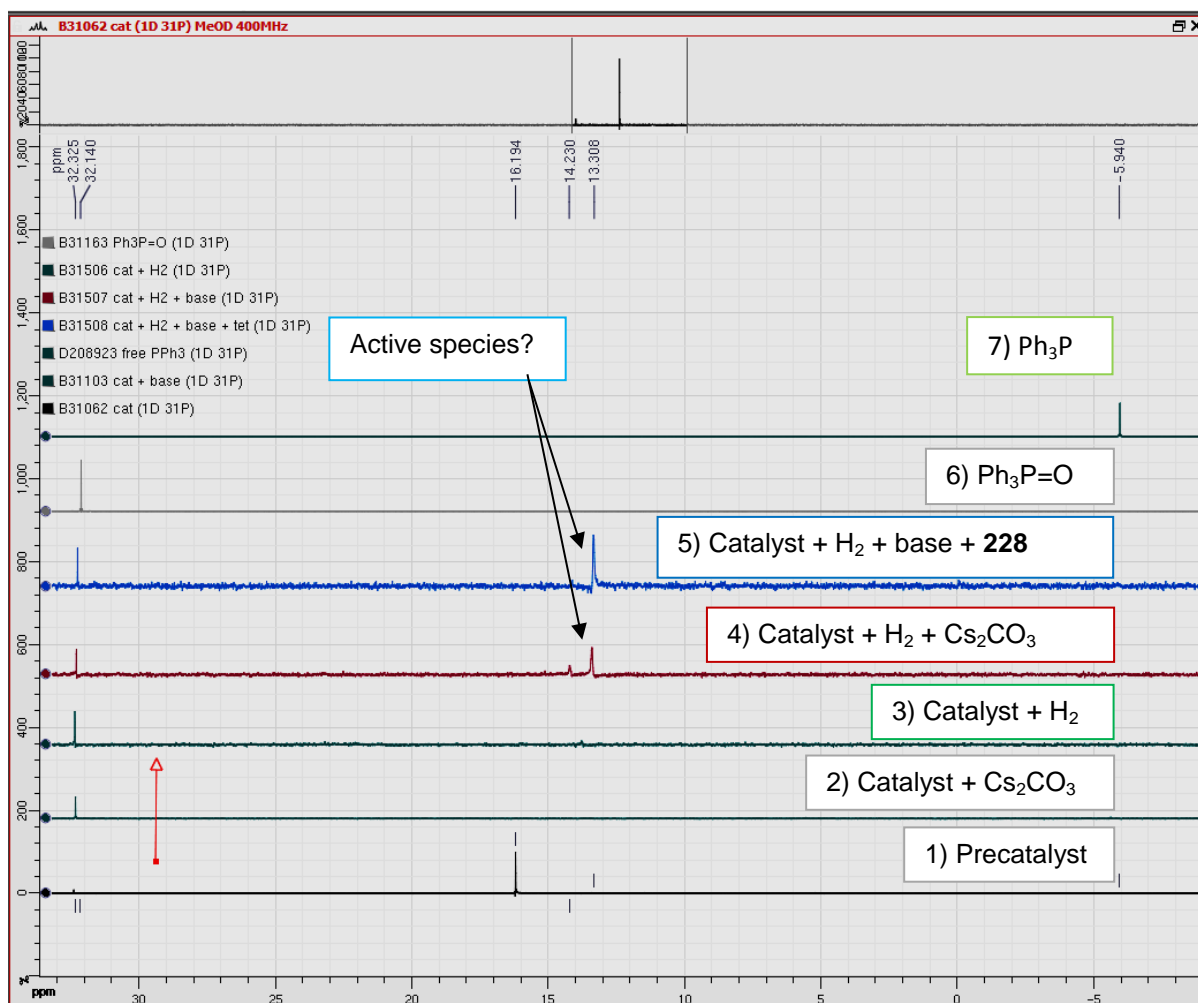
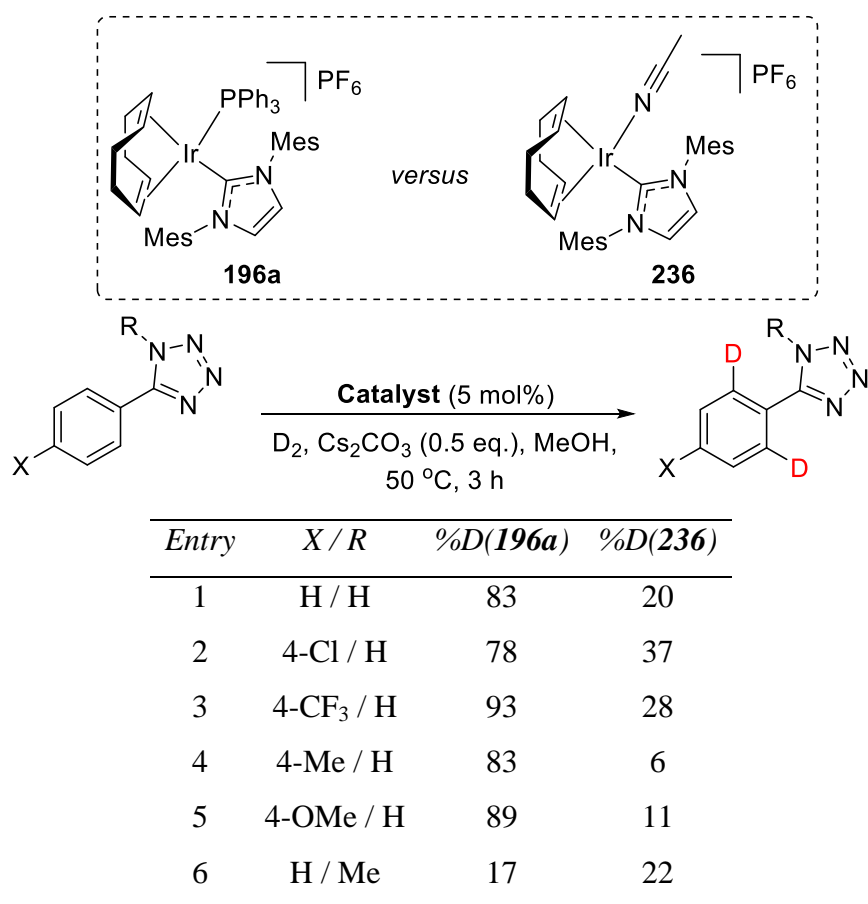


Figure 23. ^{31}P NMR study of the catalyst with various components of the tetrazole labelling method.

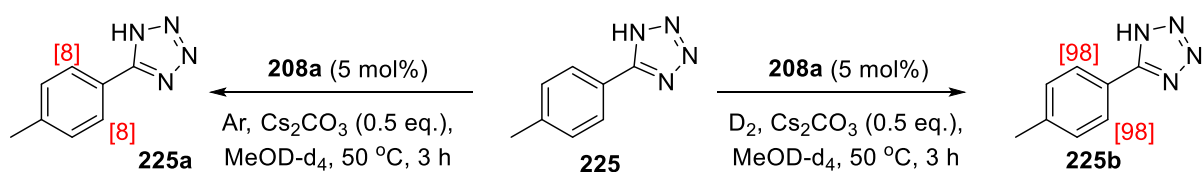
resulted in the optimal catalyst active already discussed (see **Experimental** section for full details).

The case against PPh_3 dissociation during catalyst activation was strengthened when alternative catalyst **196a** was compared to easily-prepared derivative **236** (see Experimental section), bearing a more labile acetonitrile ligand (**Table 9**). For all unprotected tetrazoles (**Entries 1 – 5**), catalyst **196a** proved superior to **236**, indicating the beneficial role of the phosphine in the reaction. Similarly to earlier studies, the *N*-Me tetrazole performed poorly, regardless of reaction conditions (**Entry 6**).

Table 9. Investigating the role of the PPh₃ ligand in Ir-catalysed tetrazole labelling.



In a final mechanistic investigation, the source of deuterium label was probed. By employing MeOD-d₄ as the sole deuterium source to label **225** (under Ar rather than D₂), a low 8% D-incorporation was recorded, indicating the necessity for gaseous D₂ (**Scheme 45**, left). In line with this result, employing D₂ and MeOD-d₄ together was found to improve the D-incorporation to 98%, better than any other result recorded (**Scheme 45**, right). From these results, it appears likely that at least one major and one minor reaction pathway may be operating to deliver the *ortho*-deuterium label to the tetrazole.



Scheme 45. Probing the deuterium source in Ir-catalysed tetrazole labelling.

In summary, complexes **196a** and **208a** have been developed to catalyse the first general method for the *ortho*-deuteration of pharmaceutically-relevant aryl tetrazoles. Furthermore,

this method represents a rare case of selective C-H functionalisation on unprotected tetrazoles. Mechanistic investigations have revealed evidence for the first base-assisted catalysis using **196a** and **208a**, from which the following key points can be drawn:

- 1) The role of the base is not simple substrate deprotonation (Et_3N *versus* Cs_2CO_3).
- 2) The tetrazole is likely to be fully deprotonated (methyl red indicator).
- 3) The active catalyst is only formed in the presence of D_2 and Cs_2CO_3 *together*.
- 4) The phosphine ligand is key to the active catalyst and, based on current evidence, is believed not to dissociate. However, ligation of $\text{Ph}_3\text{P}=\text{O}$ may play a role and remains to be fully explored.
- 5) More electron-poor tetrazoles are labelled fastest, strengthening the proposal of a CMD-type mechanism.
- 6) There is at least one major and one minor pathway by which deuterium can be incorporated into the substrate (D_2 *versus* MeOD-d_4).

Further work in this area will concentrate on fully elucidating the reaction mechanism(s), and expanding the scope of this industry-aligned labelling method to encompass carboxylic acids.

4. Experimental & Theoretical Ligand Design Methods in HIE Processes

The current library of available HIE catalysts is formidable, and has been acknowledged to often render substrate-specific catalyst choice as *trial and error*.⁶⁶ In order to fully exploit their potential, it is essential that *ortho*-HIE catalysts be characterised on a meaningful, quantitative, and predictive footing. Indeed, work of this nature has been undertaken by previous researchers, where the use and application of different phosphines was rationalised based on available *Tolman Cone Angle* and *TEP* data.^{101,151} Whilst this work was able to provide a qualitative means of rationalising the labelling efficacy and selectivity in a limited number of isotopic labelling processes, there have been no attempts to compare NHC and phosphine ligands of HIE catalysts on a comparable and quantifiable basis. Furthermore, it is now proposed that it is not the influence of any one ligand that is important, as previously studied, but instead the *combined* effect of the ligand set on the iridium centre. Herein, experimental and computational methods which differentiate ancillary ligand partnerships in iridium-based HIE catalysts are divulged.

4.1 Experimental Evidence for Observable Ligand Pairing Behaviour

The overall proposal of this work is to provide a computationally-derived visual map of available ligand space. However, it was first deemed necessary to provide evidence that different ligand partnerships could be analysed experimentally and grouped according to their combined influence on specific iridium complexes.

4.1.1 Ir(I) Di- & Tricarbonyl Complexes in the Assessment of Combined Ligand Sterics

Recent work on Ir(I) dicarbonyl complexes has revealed that the configuration of the carbonyl ligands, though preferentially *cis* (as in **237** – **239**, **Figure 24**), is dictated by the ligand size, with larger combinations driving a *trans* dicarbonyl arrangement (**240** – **242**, **Figure 24**).^{120,195,196} This structural promiscuity limits the use of electronic parameters derived from such complexes.¹⁹⁶ The synthesis and X-ray characterisation of further NHC/phosphine derivatives, such as **240**, could, however, be used to define a *steric threshold* – the ligand size at which Ir(I) multi-carbonyl complexes switch from *cis* to *trans*, based on % V_{bur} , even within this one ligand pairing class. This could then be used as a proxy for

cis/trans equilibria of HIE-active Ir(III) dihydride complexes – an important consideration when examining substrate labelling regioselectivity (*vide supra* and *vide infra*).

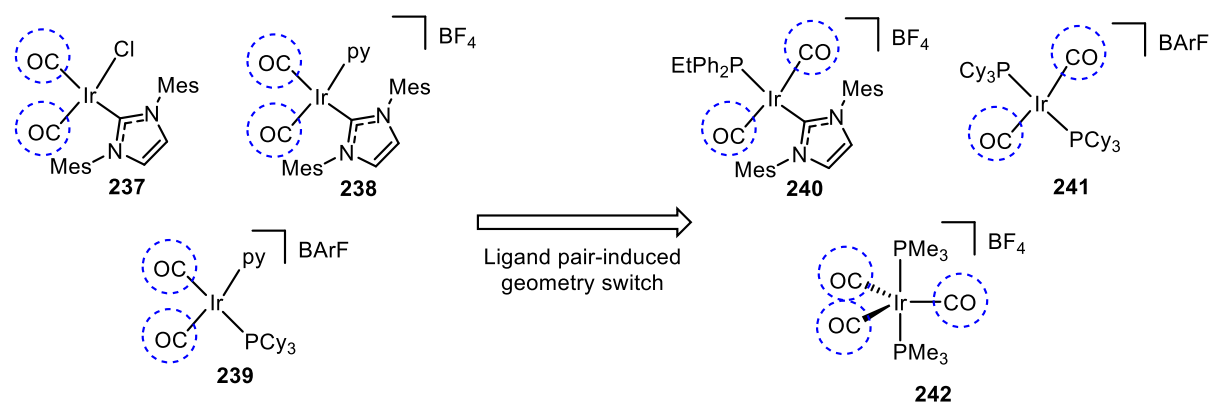


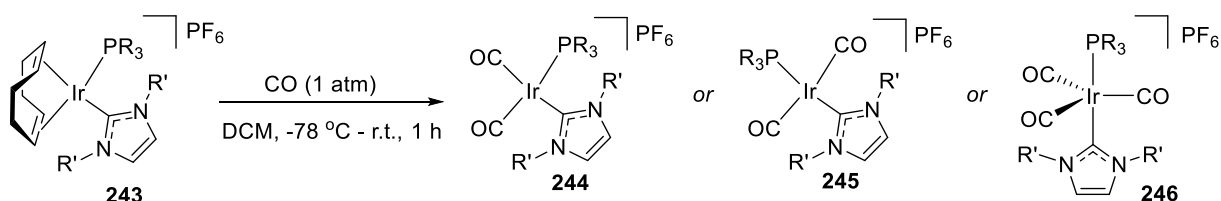
Figure 24. Known Ir(I) dicarbonyl complexes showing sterically-controlled geometry switch.

Using HIE precatalysts from our laboratory, the dicarbonyl derivatives were simply prepared *via* exposure of a DCM solution of the COD-ligated complex, **243**, to an atmosphere of CO, producing the desired dicarbonyl complexes in good yield following work-up (**Table 10**). As hypothesised, smaller NHC/phosphine combinations were shown to form exclusively **244** (*cis*-type complexes), where larger variants produced either the **245** or **246** (*trans*-type complexes). These observations were supported by IR spectroscopy, where complexes derived from **244** produced two clear absorption peaks, representing the symmetric and asymmetric dicarbonyl stretching frequencies. Conversely, complexes derived from **245** and **246** showed broader signals that almost coalesce at lower wavenumbers (**Table 10, Entries 1 – 3 versus Entries 4 – 6**). Subsequent X-ray and $\%V_{bur}$ analyses of each carbonyl complex was more revealing (**Table 11**). Directly comparable dicarbonyl complexes (**Entries 1 – 4**), indeed, show an increased deformation of the ideal 90° (CO)-Ir(CO) bond angle with increasing size of the ligand sphere. Although reasons for forming tri- *versus* di-carbonyl complexes have not yet been delineated (**Entries 5 – 6**), it is interesting to note the exclusive *trans* arrangement of the IMes/phosphine ligand sphere, irrespective of the phosphine.

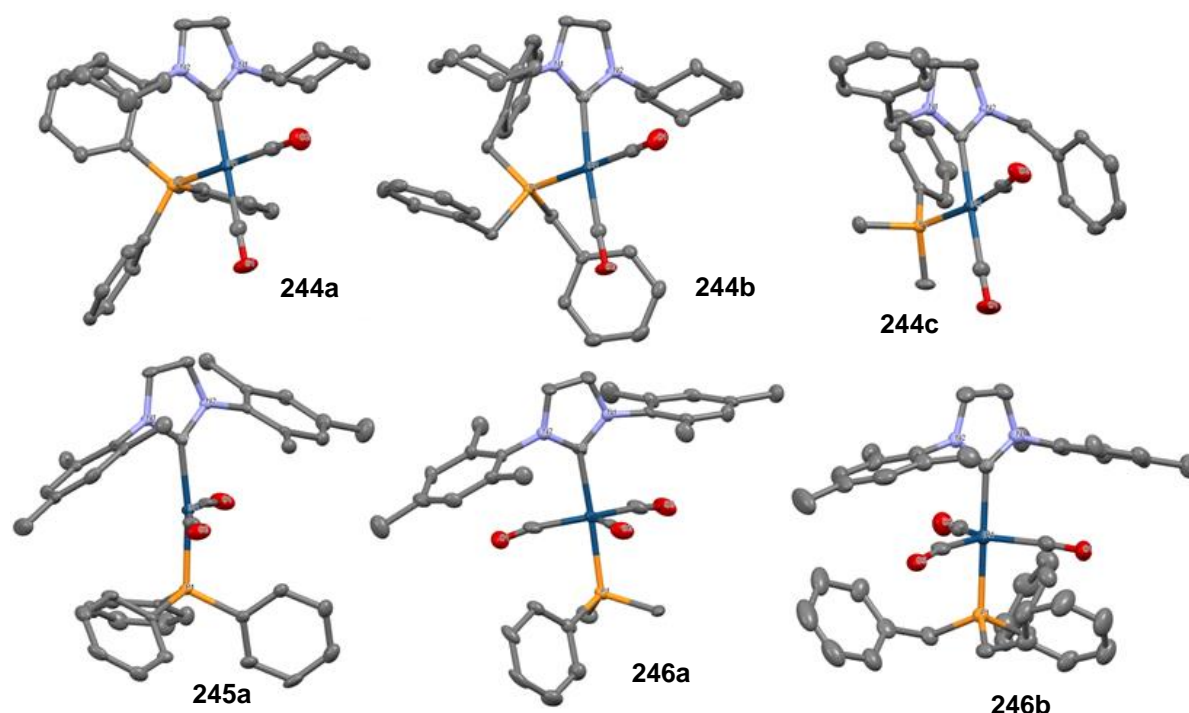
These studies serve to demonstrate that, even within one ligand pairing class (NHC/phosphine), chemical behaviour and relative ligand geometries can be influenced, depending on the exact nature of each ligand, and the relationship between them. Furthermore, it is important to note that the $\%V_{bur}$ method of calculating steric encumbrance

is sensitive enough to record ligand contraction on moving to higher Ir coordination numbers (for example, the IMes ligand in **Table 11, Entry 4 versus 5 and 6**). In combination with the literature examples (**Figure 24**), this is taken as good evidence that modelling related HIE catalysts based on steric parameters could (in part) help explain their catalytic behaviour.

Table 10. Synthesis of Ir(I) NHC/phosphine di- and tri-carbonyl complexes.



Entry	PR_3	R'	Complex	Yield / %	$\nu(CO)_{DCM} / cm^{-1}$
1	PPh_3	Cy	244a	81	2083, 2025
2	PBn_3	Cy	244b	83	2081, 2025
3	PMe_2Ph	Bn	244c	49	2081, 2023
4	PPh_3	Mes	245a	69	2010, 1991
5	PMe_2Ph	Mes	246a	69	2004, 1987
6	PBn_3	Mes	246b	80	2000, 1991

Table 11. Ir(I) di- and tri-carbonyl complexes bearing mixed NHC/phosphine ligand sphere.^a

Entry	Complex	% $V_{bur}(PR_3)$	% $V_{bur}(NHC)$	$\Sigma(\%V_{bur})$	$\theta_{CO-Ir-CO}$ ($^\circ$)
1	244a	27.3	26.6	53.9	90.2
2	244b	30	26.7	56.7	90.7
3	244c	23.3	36.0	59.3	92.7
4	245a	29.3	35.6	64.9	160.0
5 ^b	246a	25	30.6	55.6	127.2, 116.8, 115.2
6 ^b	246b	32.6	31.2	63.8	125.2, 116.4, 117.6

^a H-atoms and PF_6^- anions removed from X-ray structures for clarity.

^b Tricarbonyl complexes possess three distinct (CO)-Ir-(CO) angles.

4.1.2 Ir(I) Chloro-carbonyl Complexes in the Study of Combined Ligand Electronics

Beyond steric encumbrance, it is also important to accrue evidence that ligand partnerships can exert combined *electronic* influence before undertaking expensive computational modelling. In this case, literature examples of Ir(I) chloro-carbonyl complexes - including *Vaska's complex*, **247a** - have demonstrated that the combined influence of various ligand partnerships on the metal's π -donating ability can be measured *via* IR spectroscopy (**247** - **250**, **Figure 25**).¹⁹⁷⁻²⁰⁰

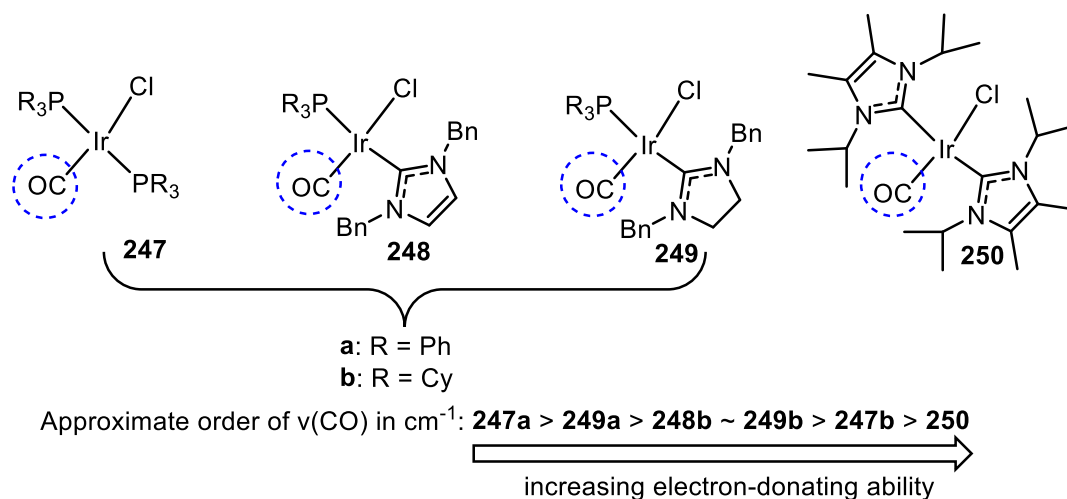
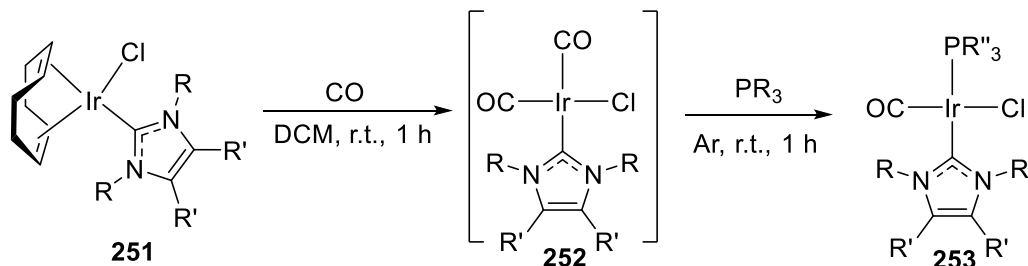


Figure 25. Known Ir(I) chloro-carbonyl complexes.

Herein, further NHC/phosphine examples of interest have been synthesised and compared *via* IR spectroscopy and X-ray crystallography. Importantly, these include NHC/phosphine partnerships previously studied in HIE, as well as novel partnerships examined in more detail below. In this primary study, chloro-carbonyl complexes **253a** – **253e** were synthesised as shown in **Table 12**. Starting from known chloro-carbene complexes of the type **251**, complexes **252** can be formed *in-situ* under an atmosphere of CO before switching to argon, allowing **253** to be formed *via* substitution of one CO ligand by the addition of the chosen phosphine. All novel complexes, **253b** – **253e**, were found to generate more electron-rich iridium centres than the known complex, **253a** (**Entries 1 versus 2 – 5**).¹⁹⁷ Advantageously, this method was sensitive enough to record the increasing electron-donating power of adding methyl substitution to the NHC architecture across complexes **253b** – **253d** (**Entry 2 versus Entry 3 versus Entry 4**). For the same NHC, moving to a more electron-donating (sp^3 -substituted) phosphine increased the electron-rich nature of the final iridium complex (**Entry 3 versus 5**). Crucially, by comparing complexes **253a** and **253e** (**Entry 1 versus Entry 5**), it is clear that this method allows comparison of the electron-donating properties of complexes where *both* ancillary ligands – the NHC and the phosphine - are altered. Finally, X-ray analysis of selected complexes **253b** – **253d** (**Table 13**) revealed the exclusive *trans* geometry of the chloro- carbonyl complexes, in agreement with that already reported for the literature examples in **Figure 25**. Notably, $\%V_{bur}$ analysis of the carbene ligands from **253b** – **253d** revealed a rather counterintuitive order of steric encumbrance (**253b** > **253c** > **253d**), and was coupled with an increasing distortion from the ideal square planar geometry. Interestingly, analysis of CO bond lengths was deemed impossible due to inherent disorder

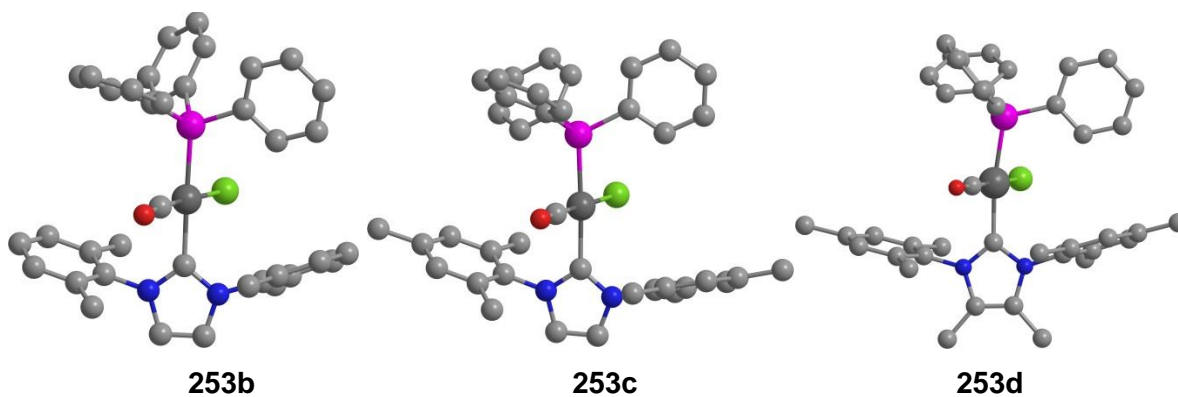
and equal occupancy of the coordination sites occupied by the chloride and carbonyl ligands.²⁰¹

Table 12. Synthesis of Ir(I) chloro-carbonyl complexes.



Entry	Complex	R	R'	PR ₃ ''	Yield / %	$\nu(\text{CO})_{\text{DCM}} / \text{cm}^{-1}$
1	253a	Bn	H	PPh ₃	42	1950
2	253b	2,6-Xy	H	PPh ₃	67	1944
3	253c	Mes	H	PPh ₃	47	1942
4	253d	Mes	Me	PPh ₃	44	1940
5	253e	Mes	H	PMe ₂ Ph	53	1937

Table 13. Molecular structure of chloro-carbonyl complex as determined *via* X-ray analysis.

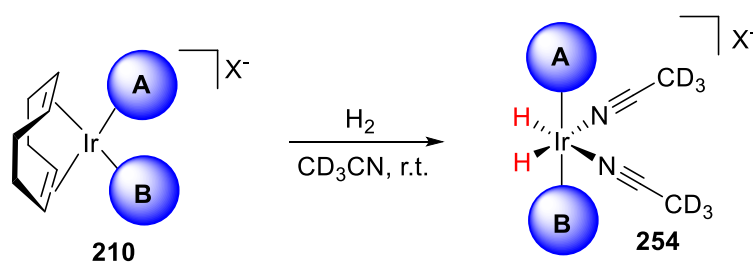


Entry	Complex	% $V_{bur}(\text{NHC})$	$\theta_{\text{C-Ir-P}} (^{\circ})$
1	253b	34.2	178.8
2	253c	33.7	173.4
3	253d	32.9	171.9

4.1.3 Ir(III) Dihydride Complexes in the Study of Combined Ligand Electronics

It has been acknowledged that measurement of $\nu(\text{CO})$ in complexes such as **253** mainly details the π -donating ability of the resultant iridium complexes.¹²¹ Therefore, additional effort was needed to provide experimental evidence that the overall σ -donating ability of a ligand sphere could be measured as a single value. To achieve this, it was hypothesised that NMR measurements of catalytically relevant Ir(III) dihydride structures generated *in situ* (such as complex **254**, **Scheme 25**) would provide a convenient handle, as the hydride ligands are solely σ -bonding in nature. Such complexes are made stable and easy to handle in monomeric form by using MeCN solvent to trap the intermediate of interest.^{10,202} In practice, a small quantity of each precatalyst was dissolved in CD_3CN inside an NMR tube. Bubbling H_2 through the solution activated the complex **210** to generate **254** as the main species *in situ* (**Table 14**). For phosphine-containing examples, the primarily *trans* geometry of the ancillary ligands was confirmed by complementary coupling observed in the ^1H and ^{31}P NMR spectra (see **Experimental** section).

In **Entries 1 – 5** of **Table 14**, the same ligand partnerships employed in synthesising chloro-carbonyl complexes **253a – 253e** were investigated. For four of these five ligand partnerships, similar electron-donating ability was noted as for the carbonyl complexes: **254e** > **254d** > **254c** > **254a**. However, *the order of 254b and 254c in the study of the hydride complexes is reversed relative to the carbonyl complexes*. This provides important evidence that the properties of a given ligand partnership are best described by a multi- rather than a univariate approach in order to capture a more holistic assessment of its properties. The simplicity of the hydride NMR method allowed for a straight forward extension into a comparative study with Crabtree's catalyst (**254f**, **Entry 6**) and the chloro carbene complex of IMes (**254g**, **Entry 7**), both of which were successively more σ -donating than complexes **254a – 254e**.

Table 14. Generation of MeCN-stabilised Ir(III)-dihydride complexes *in-situ*.

Entry	Complex	A	B	X	δ_H /ppm	$\nu(\text{CO})_{\text{DCM}} / \text{cm}^{-1}$ ^a
1	254a	PPh ₃	IBn	PF ₆	-21.33	1950
2	254b	PPh ₃	IXy	PF ₆	-21.59	1944
3	254c	PPh ₃	IMes	PF ₆	-21.56	1942
4	254d	PPh ₃	IMes ^{Me}	PF ₆	-21.60	1940
5	254e	PMe ₂ Ph	IMes	PF ₆	-21.99	1937
6	254f	PCy ₃	py	PF ₆	-22.08	-
7	254g	Cl	IMes	-	-22.70	-

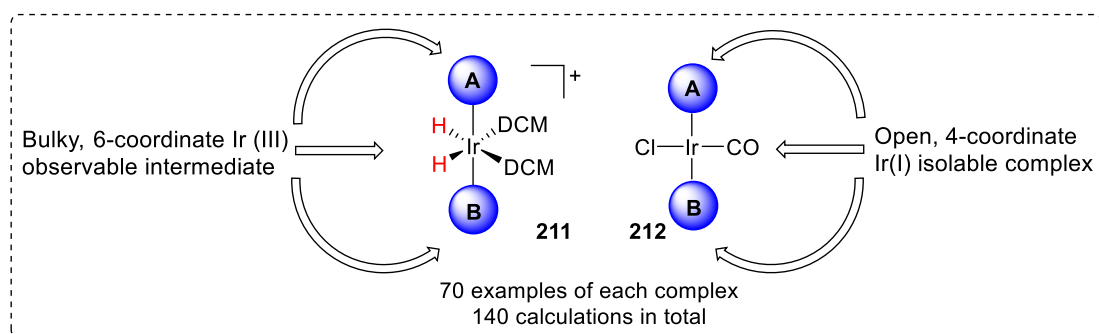
^a $\nu(\text{CO})_{\text{DCM}}$ values duplicated from **Table 12** for convenience.

In summary, three distinct experimental methods have been employed to assess the combined effect of two monodentate ancillary ligands within one Ir-based complex, with particular attention paid to mixed NHC/phosphine systems of interest within our laboratory in the development of HIE catalysts. The ancillary ligands of iridium(I) dicarbonyl complexes undergo a geometry switch from *cis* to *trans* on moving to more encumbered ligand spheres, the effect being captured by IR, X-ray and % V_{bur} calculations. Related iridium(I) chloro-carbonyl complexes have been shown to possess a more exclusive *trans* geometry between ancillary ligands, making the sole CO ligand a suitable IR handle for the study of combined ligand π -donation. This picture is complemented by *in-situ* generation of Ir(III) dihydride complexes from the relevant parent HIE precatalyst, capturing the σ -donation properties of the combined ligand sphere and highlighting the possible re-ordering of comparable ligand partnerships when using different electronic parameters. Together, these data show that, beyond more well-known single ligand descriptors, ligand partnerships can also be experimentally described to capture combined ligand effects on a single metal centre. As such, additional experimental effort may be circumvented by investigating computational combined ligand parameters that help visualise catalyst properties in an informative and predictive manner.

4.2 Theoretical Ligand Design Methods in HIE Processes

With sufficient evidence that combined ligand properties relevant to Ir-based HIE catalysts could be experimentally determined, work could begin on expanding this method towards computational catalyst mapping (**Scheme 33** in the Proposed Work; condensed in **Scheme 46**). Using principal components analysis (PCA)²⁰³ to describe the combined ligand parameters derived from DFT-calculated structures **211** and **212**, 69.5% of the variance in the data could be described with just two principal components, PC1 and PC2. A further 9.4% (78.9% cumulative) variance was captured by a third principal component, PC3 (**Figure 26** and **Figure 27**).

Two points close in PC space represent different ligand pairs that impart similar properties to the resulting Ir complexes, and may be interpreted as breeding catalysts with similar chemical properties.^{140,203–206} In colouring the maps according to each ligand combination class, it is clear that PC1 most obviously separates each class, whereas PC2 and PC3 represent a continuum with more overlap in the properties of each ligand combination. As PCA statistically condenses multi-dimensional parameter space into just two dimensions, chemical interpretation of the data can be difficult. Having stated this, closer scrutiny of the correlations between the PCs and the original DFT parameters suggests that PC1 largely describes the π -donating ability of a particular ligand sphere ($Q_{\text{Ir},211}$, $E_{\text{HOMO},211}$, $E_{\text{HOMO},212}$, $\nu(\text{CO})$, $Q_{\text{O},212}$, and $Q_{\text{Cl},212}$). Alternatively, PC2 captures the steric and σ -donating parameters ($\Sigma V_{\text{bur},211}$, $\Sigma V_{\text{bur},212}$, and $Q_{\text{H},211}$), whilst PC3 is almost solely composed of the ligand flexibility parameter, $[\Delta(\Sigma V_{\text{bur}})]^2$. The details of these correlations and calibration of the various $\%V_{\text{bur}}$ analyses can be found in the **Computational Methods** section.



Parameters derived from 211

- Size of ligand A ($\%V_{\text{bur}} A_{211}$)
- Size of ligand B ($\%V_{\text{bur}} B_{211}$)
- Combined V_{bur} of A + B ($\Sigma V_{\text{bur},211}$)
- Partial charge on Ir ($Q_{\text{Ir},211}$)
- Partial charge on hydrides ($Q_{\text{H},211}$)
- Energy of the HOMO ($E_{\text{HOMO},211}$)

Parameters derived from 212

- $\%V_{\text{bur}}$ of ligand A ($\%V_{\text{bur}} A_{212}$)
- $\%V_{\text{bur}}$ of ligand B ($\%V_{\text{bur}} B_{212}$)
- Combined V_{bur} of A + B ($\Sigma V_{\text{bur},212}$)
- Partial charge on Ir ($Q_{\text{Ir},212}$)
- Partial charge on carbonyl C ($Q_{\text{C},212}$)
- Partial charge on carbonyl O ($Q_{\text{O},212}$)
- Partial charge on Cl ($Q_{\text{Cl},212}$)
- Energy of the HOMO ($E_{\text{HOMO},212}$)
- Carbonyl stretching frequency (ν_{CO})

Comparitive Parameters

- $|\Delta V_{\text{bur}} A_i|^2$
- $|\Delta V_{\text{bur}} B_i|^2$
- $|\Delta(\Sigma V_{\text{bur}})_i|^2$
- $|\Delta Q_{\text{Ir}}|^2$
- $|\Delta E_{\text{HOMO}}|^2$

Scheme 46. Condensed summary of computational parameters derived for ligand mapping.

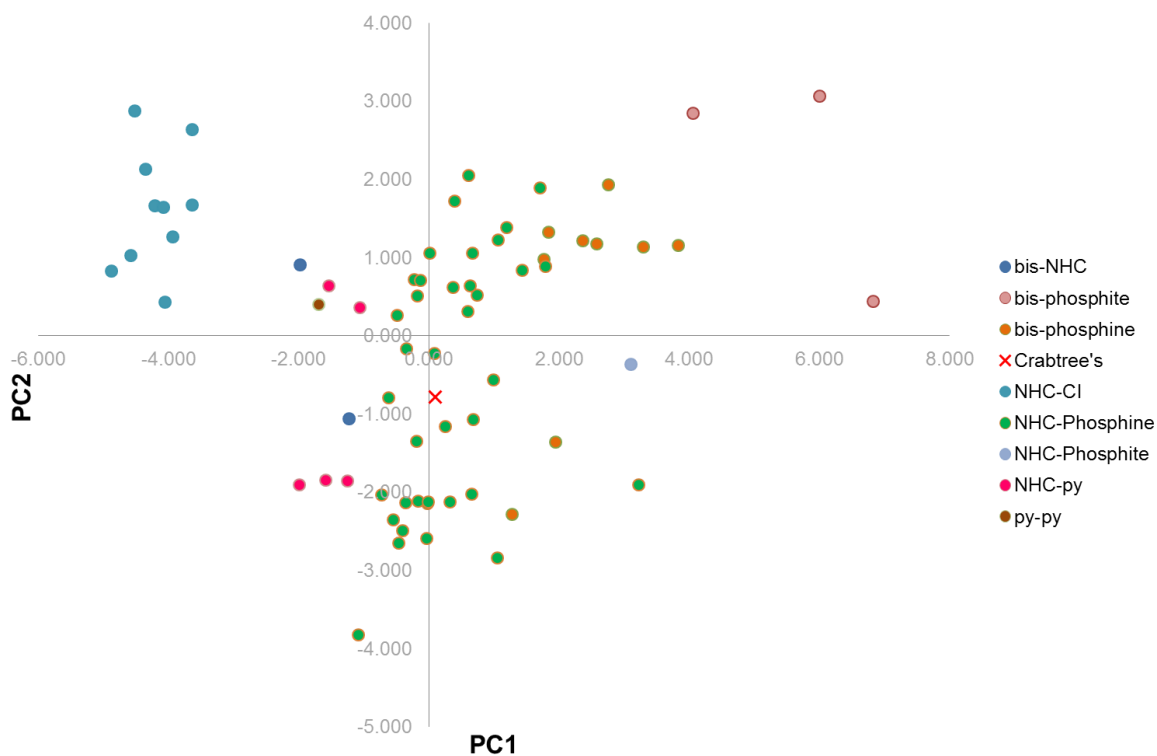


Figure 26. PCA plot for PCs 1 *versus* 2 of combined ligand space (69.5% variance captured).

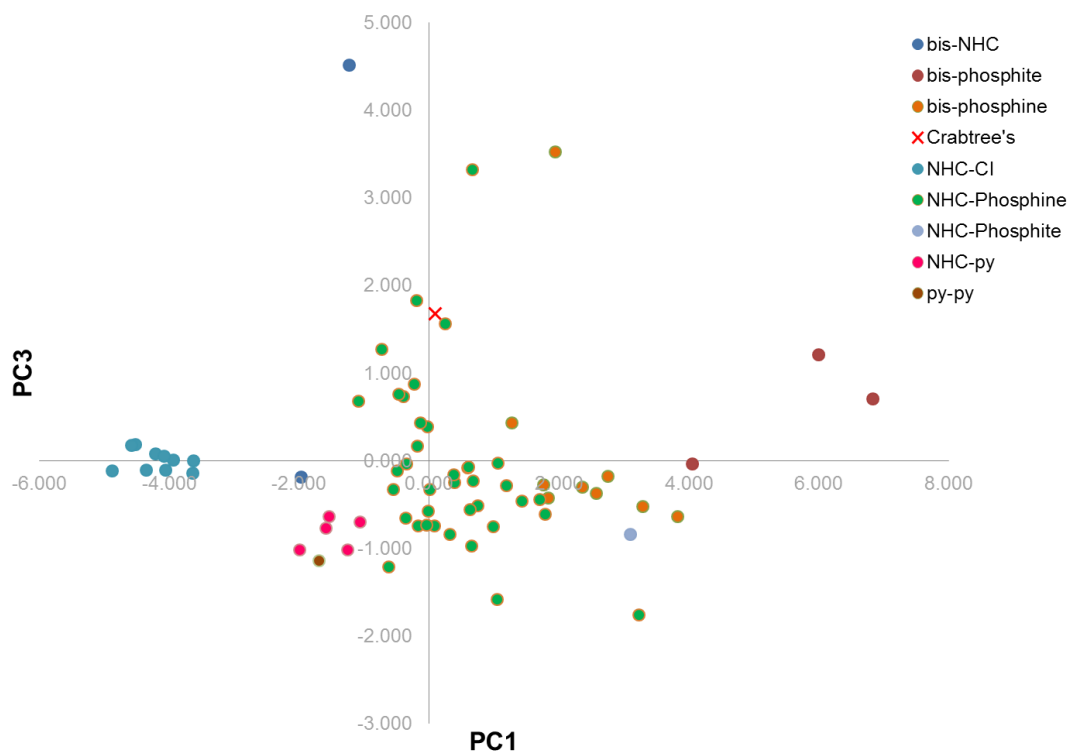


Figure 27. PCA plot for PCs 1 *versus* 3 of combined ligand space (56.2% variance captured).

Beyond the PCA plots themselves, the same analytical tools have revealed some additional, simpler correlations that are of use when considering the DFT parameters in future applications of this work. Firstly, there is a strong positive correlation between the calculated combined volume parameters for complexes of the type **211** and **212** ($\Sigma V_{\text{bur},211}$ *versus* $\Sigma V_{\text{bur},212}$, **Figure 28**). This suggests that either structural scaffold can be employed to adequately describe the combined steric impact of a given ligand pair. Secondly, within complex class **212**, $E_{\text{HOMO},212}$ and $\nu(\text{CO})$ are negatively correlated, as would be expected with increased π -back bonding onto the CO ligand for a more π -rich metal centre (**Figure 29**).³⁰ Finally, although ligand sphere flexibility, $[\Delta(\Sigma V_{\text{bur}})]^2$, was found to have no strong correlations, plotting this parameter against either $\Sigma V_{\text{bur},211}$ or $\Sigma V_{\text{bur},212}$ revealed that ligand flexibility only begins to be important at $\sim \Sigma V_{\text{bur}} > 46\%$ (for example, see **Figure 30**).

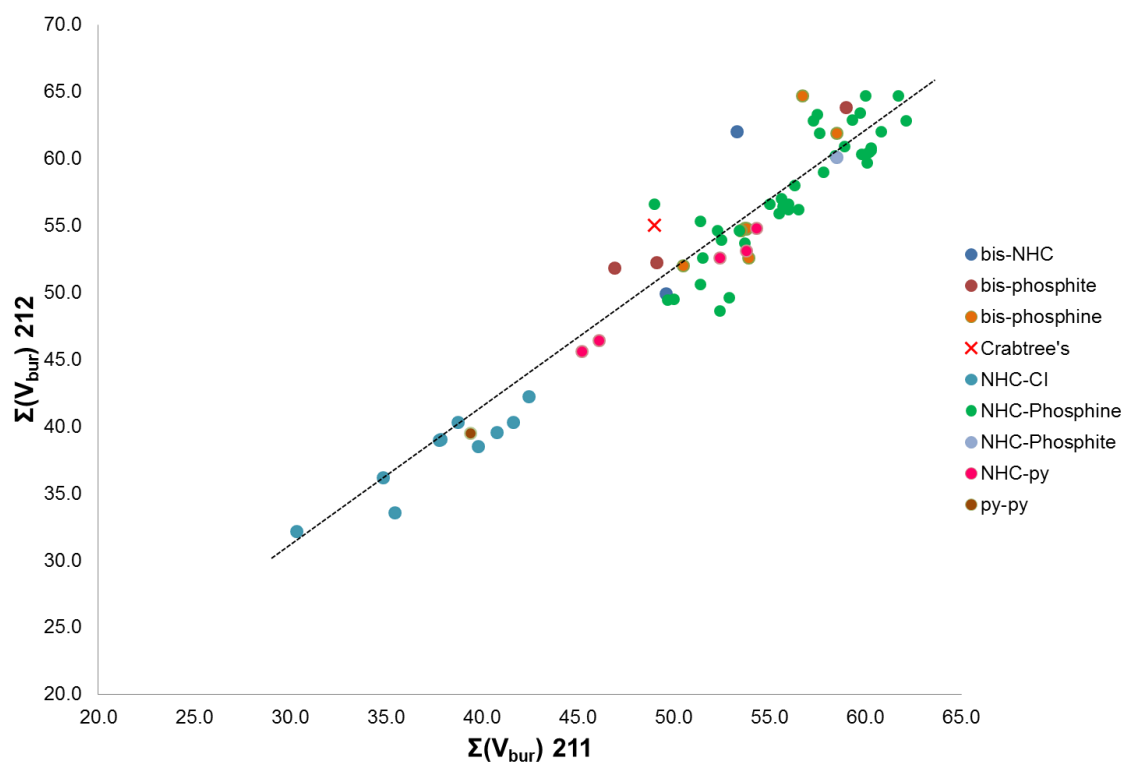


Figure 28. Correlation between Combined Buried Volume values for complex types **211** and **212**.

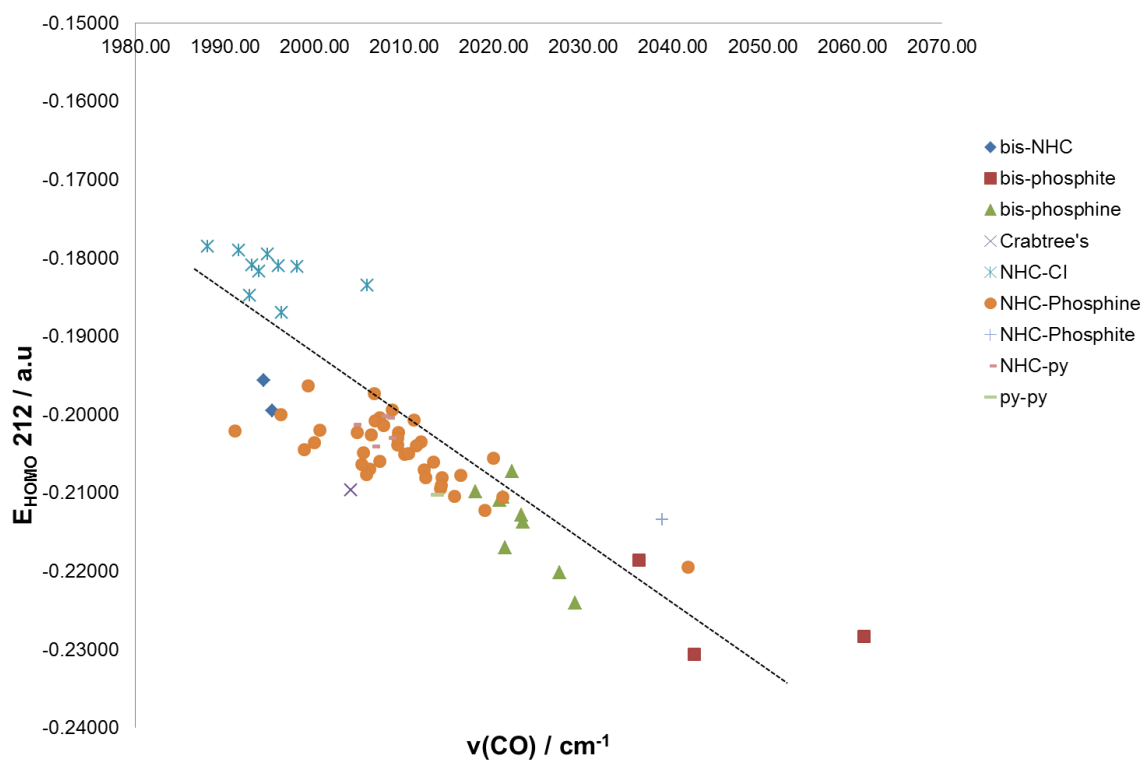


Figure 29. Correlation between $E_{\text{HOMO},212}$ and $\nu(\text{CO})$.

$$\text{Ligand Flexibility Parameter} = [\Delta(\Sigma V_{bur})]^2 = [\Sigma(V_{bur,211}) - \Sigma(V_{bur,212})]^2$$

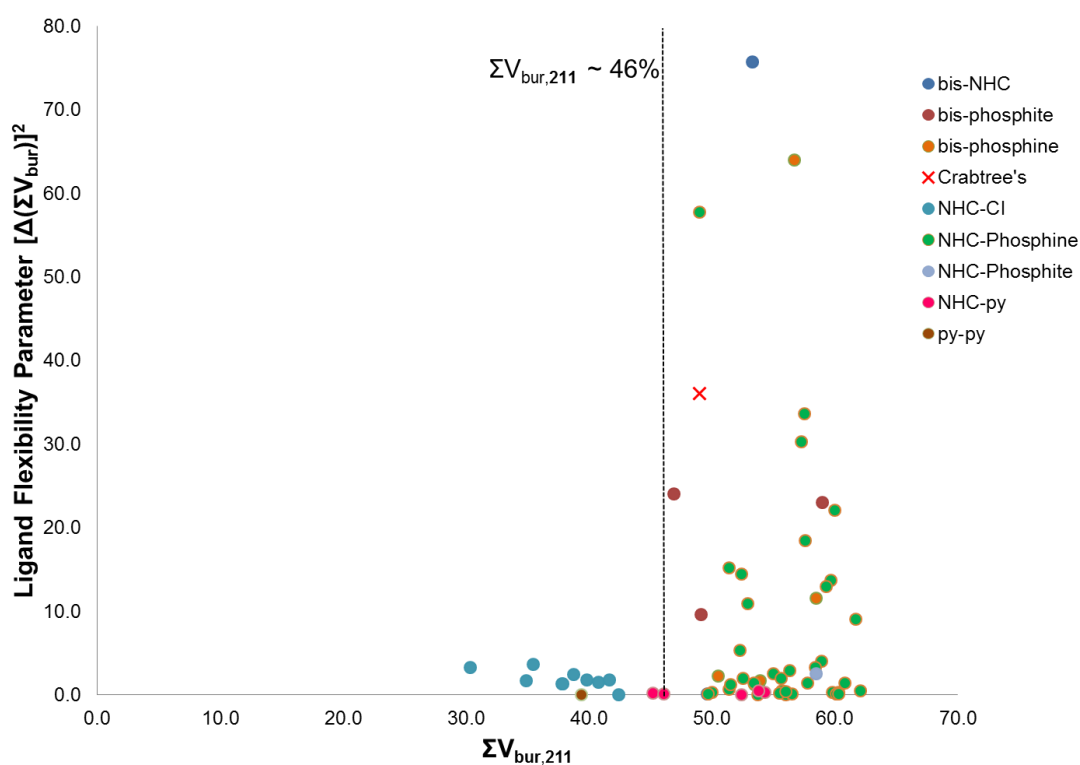


Figure 30. Relationship between ΣV_{bur} and ligand flexibility, $[\Delta(\Sigma V_{bur})]^2$.

The combined DFT and PCA analyses of different ligand spheres supports the experimental conclusion that ligand partnerships rather than single ligands can be described in a quantitative and visual manner. The multivariate data generated and described above is but an overview of the information stored in the graphs thus far shown. Indeed, the true power of such an approach to catalyst design can only be demonstrated *via* its application in unsolved problems in modern homogeneous hydrogen isotope exchange. The remainder of this report is thus dedicated to addressing several such challenges.

5. Combined Experimental & Theoretical Approach to Unsolved Challenges in HIE

5.1 Alternative NHC Ligands in HIE Catalyst Motif [(COD)Ir(NHC)(PR₃)]X

Returning to HIE catalysts sharing the motif, [(COD)Ir(NHC)(PR₃)]X, interest remains in exploring NHC structures alternative and complementary to IMes. As a first combined experimental and computational case study, **214** *versus* known catalyst **255** was investigated; the former envisaged to be a slightly bulkier and more electron-rich progression from the latter (Scheme 34 and Figure 31). It should also be noted that **255**, reported previously,¹⁴⁷ was found to be less active than flagship catalyst **196a** across a range of substrates, however, no detailed explanation of this observation was offered at the time. Therefore, this study aimed to answer several questions: (1) Is **214** an improvement over **255**? (2) Can the differences be described computationally? (3) Can **214** and **255** be compared in a useful manner to **196a**? (4) Can these assessments lead to novel *ortho*-HIE applications?

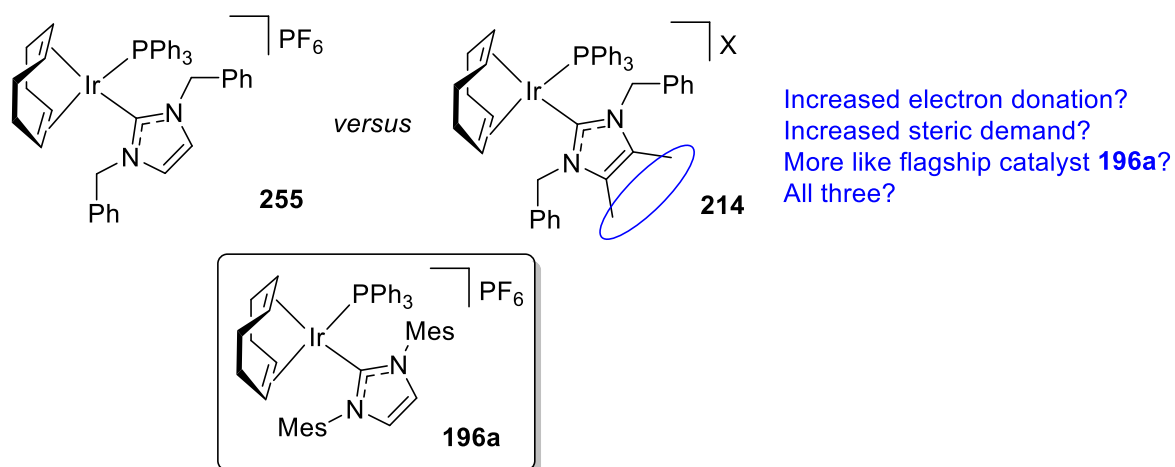


Figure 31. Considerations in designing novel HIE catalysts.

Before embarking on any synthetic studies, the ligand partnerships in **214**, **255**, and **196a** were compared according to the DFT and PCA studies discussed in Section 4.2. Using PC1 *versus* PC2 (and earlier discussion about the relevant parameters contributing to the PCs), it could be immediately inferred that **214** was both slightly larger and more π -donating than parent **255**, but still vastly inferior on both counts compared to flagship catalyst **196a** (Figure 32). Turning to PC1 *versus* PC3, the alternative y-axis (closely linked to ligand sphere flexibility) revealed that **214**, **255** and **196a** possessed similar flexibility, and together are largely inflexible against the spectrum of ligand combinations studied (Figure 33).

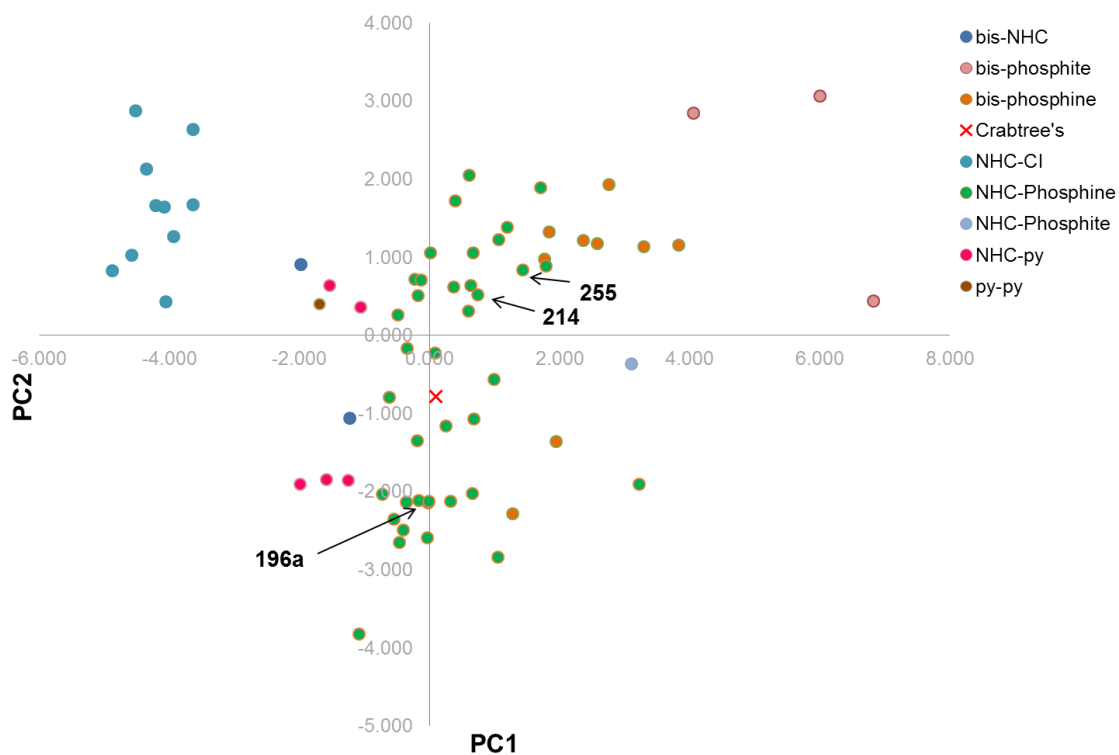


Figure 32. Comparison of catalysts **214**, **255**, and **196a** using PC1 *versus* PC2.

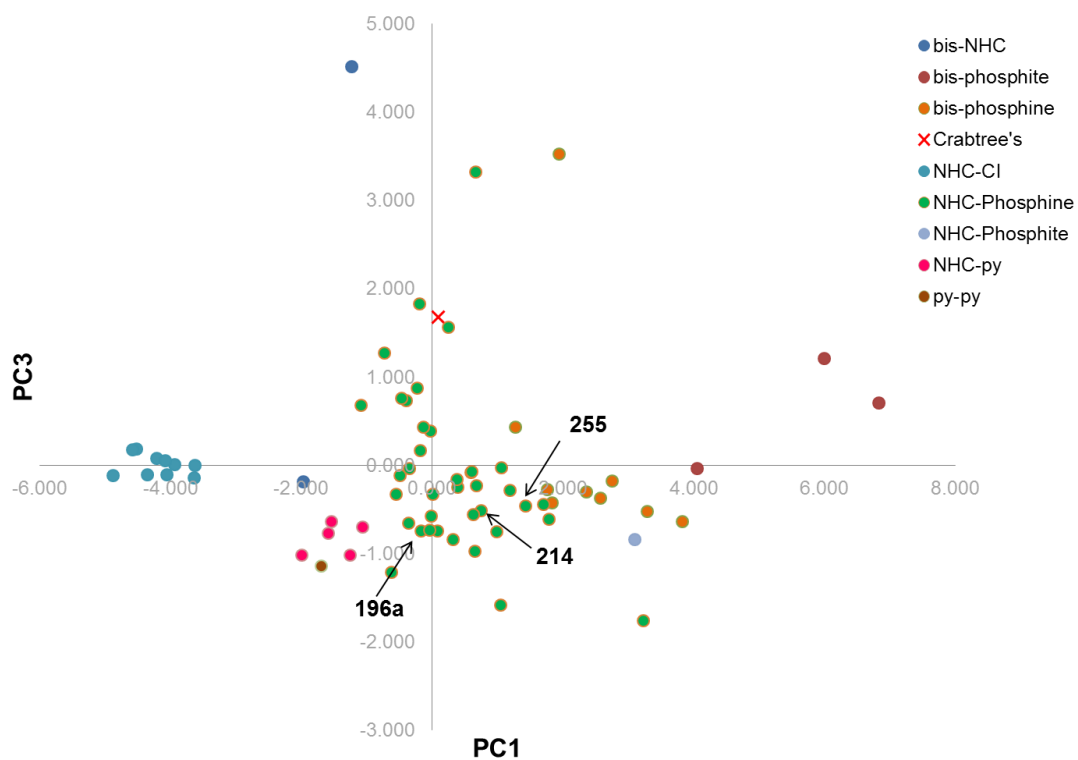
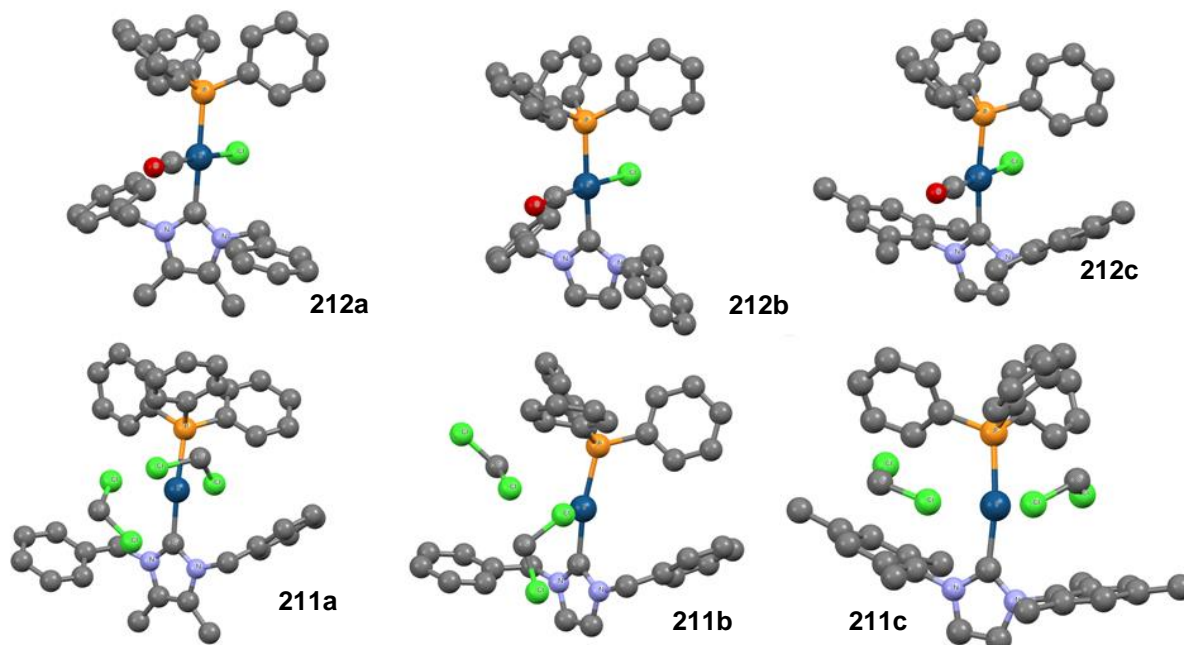


Figure 33. Comparison of catalysts **214**, **255**, and **196a** using PC1 *versus* PC3.

Overall, **214** and **255** can be said to be chemically similar (though not identical), and significantly distinct from **196a**. The exact DFT structures and selected parameters from which these inferences are made are illustrated in **Table 15**.

Table 15. Illustration of DFT structures and key parameters extracted from PCA graphs.



Entry	DFT Complex	A	B	Derived Parameter	Parameter Value
1	212a	PPh ₃	IBn ^{Me}	$\Sigma V_{\text{bur},212}$	55.7%
2	212b	PPh ₃	IBn	$\Sigma V_{\text{bur},212}$	55.5%
3	212c	PPh ₃	IMes	$\Sigma V_{\text{bur},212}$	60.2%
4	211a	PPh ₃	IBn ^{Me}	$\Sigma V_{\text{bur},211}$	56.4%
5	211b	PPh ₃	IBn	$\Sigma V_{\text{bur},211}$	55.9%
6	211c	PPh ₃	IMes	$\Sigma V_{\text{bur},211}$	60.5%
7 ^a	211a, 212a	PPh ₃	IBn ^{Me}	$[\Delta(\Sigma V_{\text{bur}})]^2$	0.5
8 ^a	211b, 212b	PPh ₃	IBn	$[\Delta(\Sigma V_{\text{bur}})]^2$	0.2
9 ^a	211c, 212c	PPh ₃	IMes	$[\Delta(\Sigma V_{\text{bur}})]^2$	0.1
10	212a	PPh ₃	IBn ^{Me}	$\nu(\text{CO})$	2014 cm ⁻¹
11	212b	PPh ₃	IBn	$\nu(\text{CO})$	2016 cm ⁻¹
12	212c	PPh ₃	IMes	$\nu(\text{CO})$	2009 cm ⁻¹

^a As a point of reference, for ligand sphere of catalyst **159** (A = PCy₃, B = py), $[\Delta(\Sigma V_{\text{bur}})]^2 = 35.0$. For the largest recorded flexibility in this study (A = B = IBn), $[\Delta(\Sigma V_{\text{bur}})]^2 = 75.0$.

Through this case study, the analysis of *combined* ligand size and *combined* ligand flexibility rather than individual ligand analysis deserves further discussion. If the benzyl NHC ligands IBn and IBn^{Me} are compared *via* geometry optimisation of the free ligand, subsequent %V_{bur} analysis with set metal-ligand distance predicts (as hypothesised) that the latter ligand is the larger (**Table 16, Entry 1**). This is the common method for comparing such ligands.¹²⁸ However, if we compare the ligand sizes according to their complex-driven geometries, their sizes are almost identical (**Table 16, Entries 2 and 3**). Therefore, it is pertinent that ligand comparisons only be made in the context of the fuller chemical environment they are likely to occupy. The care taken in defining ligand size can be extended to the discussion of ligand flexibility, $[\Delta(\Sigma V_{bur})]^2$, and is the main reason that this parameter is calculated by accounting for ligand size across two distinct complex environments (**Scheme 46**). In line with literature precedent, Cavallo has previously considered NHC flexibility using %V_{bur} methods in conjunction with molecular dynamics simulations.²⁰⁷

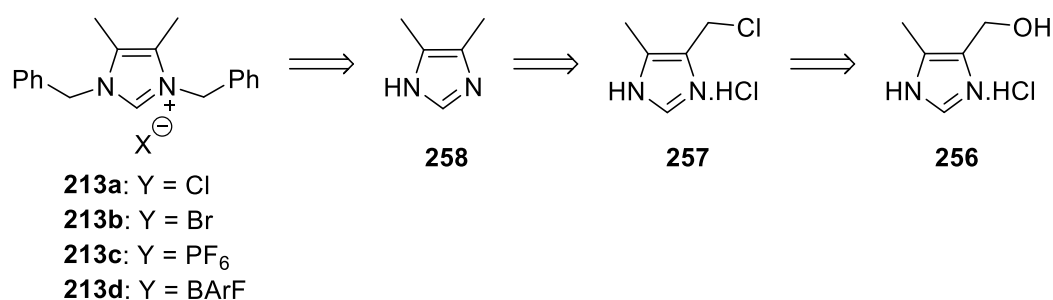
Table 16. Comparison of %V_{bur} methods for IBn *versus* IBn^{Me}

Entry	DFT Calculation	%V _{bur} (IMes)	%V _{bur} (IBn)	%V _{bur} (IBn ^{Me})	Delta ^b
1	free ligand ^a	35.5	29.6	31.4	1.8
2	255	32.4	28.7	28.7	0.0
3	214	32.8	28.4	29.0	0.6

^a Metal-ligand distance set to 2.06 Å, based on available X-ray structural data.

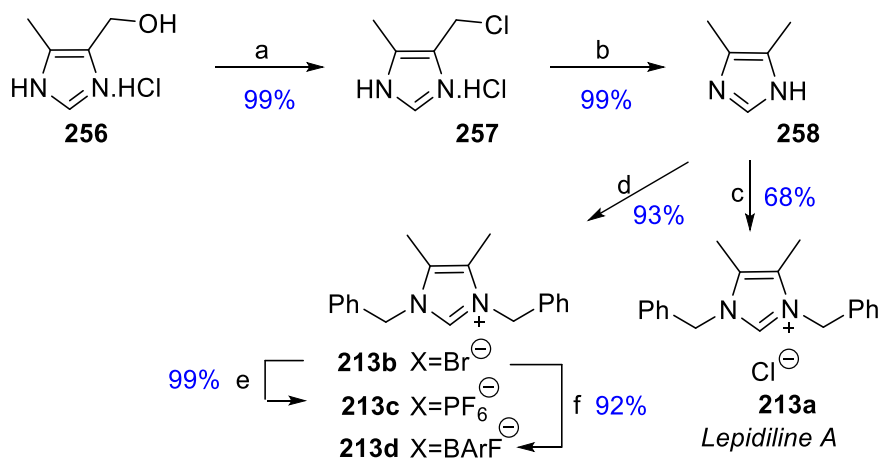
^b Difference between benzyl ligands only. IMes values are supplied only as a reference for the reader.

With computational assessment of **214**, **255** and **196a** in place, work began on the synthesis of the proposed HIE catalyst series, **214**. Access to the requisite ligand was proposed to be most readily achieved by doubly alkylating 4,5-dimethylimidazole, **258**. This key intermediate is known to be derived from hydrogenation of chloride **257**, which in turn can be sourced from commercially available hydrochloride salt **256** (**Scheme 47**).²⁰⁸ The ambiguity surrounding the anionic portion of the desired product stems from the fact that, depending on the anion chosen, different routes to novel iridium-based HIE catalysts can be applied. Nonetheless, incentive was added to first target the chloride salt, **213a**, owing to that fact that this represents the structure of *Lepidiline A*, a naturally occurring imidazolium salt for which no synthetic preparation has been reported.¹⁴⁶



Scheme 47. Retrosynthetic analysis of *Lepidiline A* and related anion derivatives.

As summarised in **Scheme 48**, chlorination of starting material **256** in neat thionyl chloride was easily achieved in excellent yields on a multi-gram scale to deliver **257**. Reduction and basification of **257** yielded the free 4,5-dimethylimidazole, **258**, in excellent yield. Subsequently, double-alkylation of **258** under basic conditions could be achieved using benzyl chloride to give *Lepidiline A*, **213a**, in good yield, or with benzyl bromide to give **213b** in excellent yield. Either **213a** or **213b** could be used in subsequent salt metathesis steps to give PF₆ and BArF salts **213c** and **213d**, respectively, though this is illustrated in the context of the bromide only.



Conditions: (a) SOCl₂ (neat), 0 °C - r.t., 4 h; (b) H₂ (5 atm), Pd/C (10% w/w), EtOH, 3 d, then K₂CO₃; (c) NaH (1 eq.), BnCl (2.0 eq.), THF, reflux (80 °C), 48 h; (d) NaH (1 eq.), BnBr (2.2 eq.), THF, reflux (80 °C), 4 h; (e) NH₄PF₆ (1 eq.), MeOH/H₂O (1:1), r.t., 16 h; (f) NaBArF (1 eq.), DCM/H₂O (1:1), r.t., 16 h.

Scheme 48. Forward synthesis of *Lepidiline A* and its anion derivatives.

With the successful preparation of *Lepidiline A* and its derivatives, X-ray quality crystals were grown and the structure solved to reveal a molecular footprint in direct agreement with

the available evidence and with the reported natural product structure (**Figure 34**, left).¹⁴⁶ The crystal structure was found to be a solvate containing one molecule of water – disorder in the water and chloride atoms has been removed for clarity. The same cationic footprint was found in the X-ray structure determination of **213c**, which possesses a dimeric unit cell with two crystallographically distinct salt units (**Figure 34**, right).

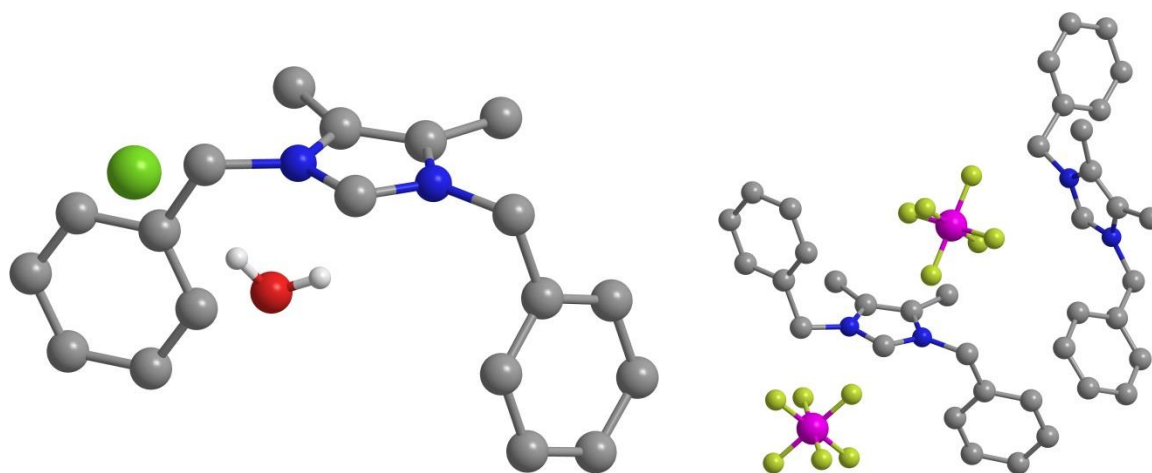
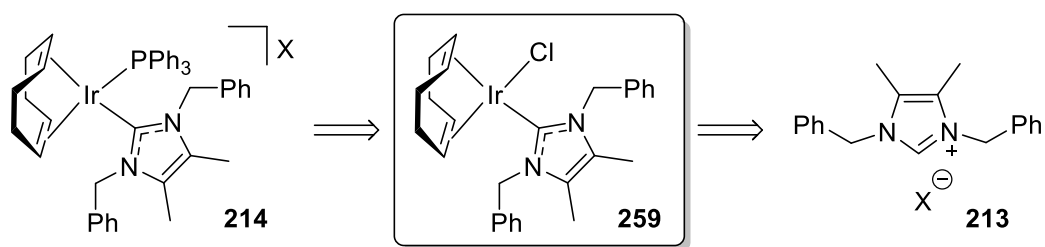


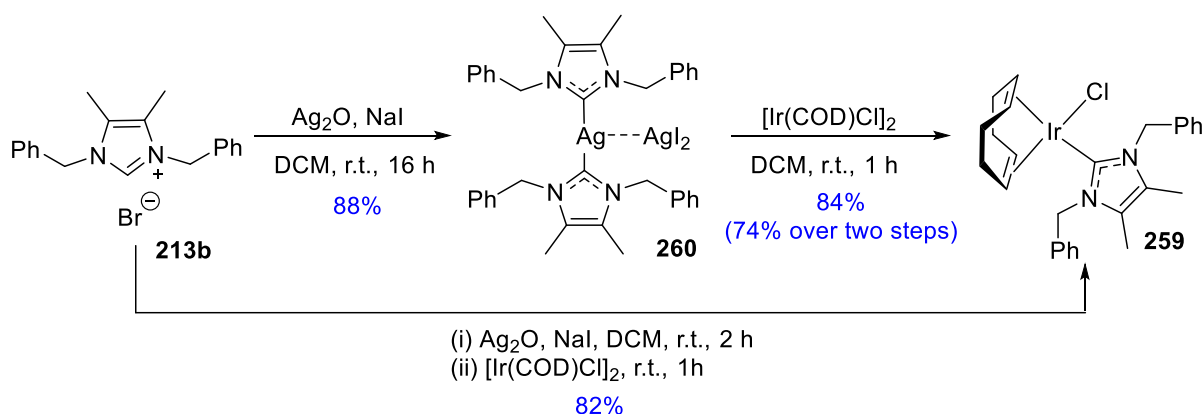
Figure 34. X-ray structure of *Lepidiline A* (left) and its PF₆ derivative (right).

Having established efficient synthetic routes to all desired imidazolium salts, the NHC precursors were now readily available to investigate their potential in forming new iridium-based HIE catalyst, **214**. It was deemed suitable to first target the synthesis of carbene chloride complex, **259**, akin to **207**, isolated whilst employing IMes (*vide supra*). As initially demonstrated in **Section 3.1**, isolation of this key intermediate iridium complex allows for facile divergence in subsequent catalyst design (**Scheme 49**). More specifically, isolation of the carbene chloride complex allows for easy variation in the final catalyst structure with regards to the choice of both the phosphine and counterion employed.



Scheme 49. Synthetic strategy for the synthesis of proposed HIE catalyst, **214**.

Based on work by Lin²⁰⁹ and Liu,¹⁹⁷ the iridium complex of the type desired can be synthesised *via* a transmetallation procedure after first making the related silver bis-carbene complex, **260**. Employing specifically the bromide salt, **213b**, of the imidazolium species in question, mixing silver(I) oxide and sodium iodide in DCM gave isolable complex **260** in excellent yield (**Scheme 50**). The natural product, **213a**, can also be employed (results not shown) but **213b** is used on account of its greater ease of synthesis. This intermediate could be taken forward into a transmetallation procedure under similar conditions to yield the desired chloro-carbene complex, **259**, in excellent yield and in a short reaction time. Alternatively, it was later found that isolation of **260** could be circumvented *via* direct addition of $[\text{Ir}(\text{COD})\text{Cl}]_2$ following *in situ* formation of the necessary silver species, forming **259** in a further improved overall yield. Additionally, with this high-yielding method in place, X-ray quality crystals of **259** could be grown to confirm the proposed structure (**Figure 35**).



Scheme 50. Synthesis of Ir chloro-carbene complex, **259**, *via* Ag(I) transmetallation procedure.

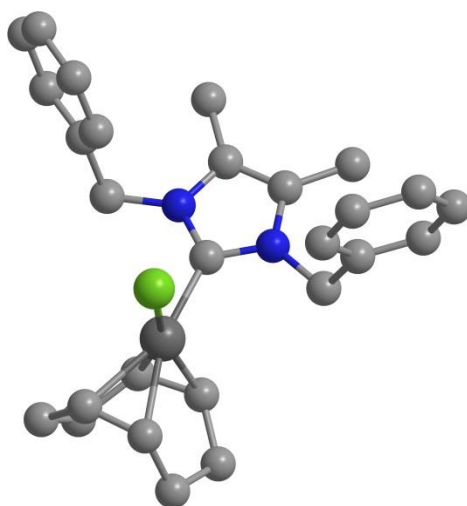
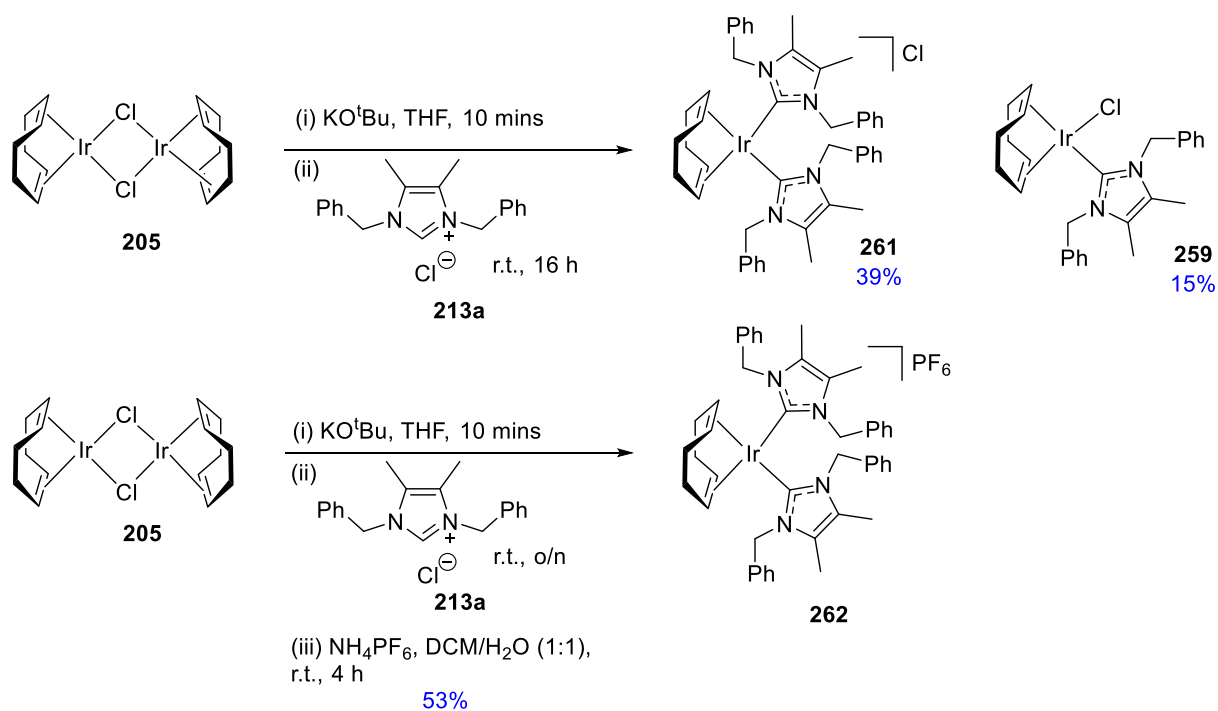


Figure 35. Molecular structure of **259** as determined *via* X-ray crystallography.

As an interesting and informative aside, it was discovered that **259** could not be synthesised in an efficient manner employing the same method used to make IMes derivative, **207**. Instead, the major product of this reaction was the bis-carbene salt, **261**, formed by displacement of the chloride ligand by a second carbene molecule (**Scheme 51**, top). A more stable variant, **262**, was later synthesised deliberately in a similar synthetic procedure, this time employing two additional equivalents of the carbene salt, **213a**, in order to favour the formation of this undesired complex (**Scheme 51**, bottom). The spectroscopic and crystallographic analyses of **261** and **262** confirmed the suspected cationic structure (**Figure 36**).

The discovery of the bis-carbene by-product, **261**, highlights an added value in modelling ligand pairs *via* DFT/PCA techniques. More specifically, the PCA maps shown previously in **Figures 26** and **27** may also be viewed from the perspective of grouping catalysts in terms of the varying synthetic strategies required for their syntheses.



Scheme 51. Bis-carbene COD complex of Ir formed as major product under basic conditions.

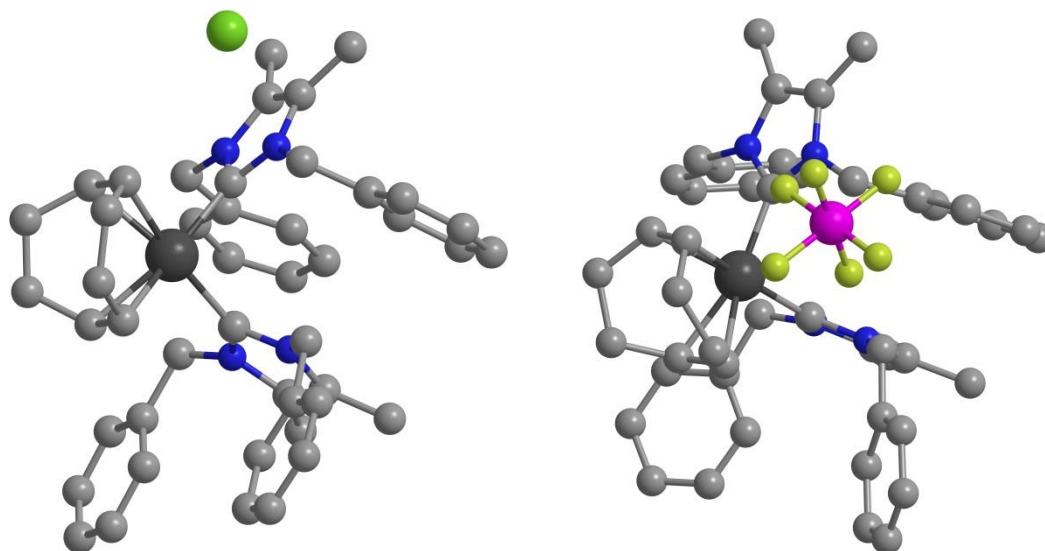


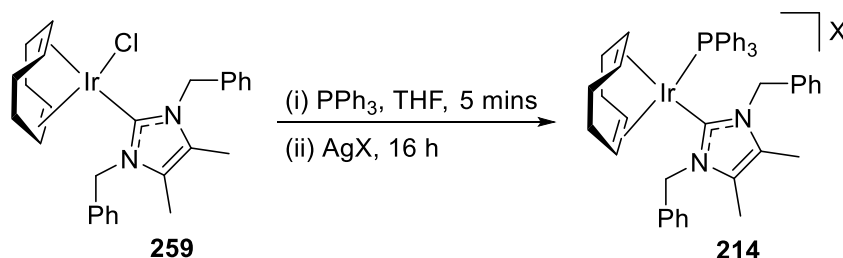
Figure 36. X-ray determined structure of bis-carbene complexes **261** and **262** derived from *Lepidiline A*.

With the key iridium complex, **259**, now available in abundance, attention could now be turned to the most highly anticipated series of reactions – forming novel $[(\text{COD})\text{Ir}(\text{NHC})(\text{PR}_3)]\text{X}$ architectures for use as HIE catalysts. To do so, reactions of the type shown in **Table 17** were to be investigated employing the IMes NHC alternative present in **259**. A crucial advantage of the smaller NHC in **259** is that it allows the desired catalyst motif

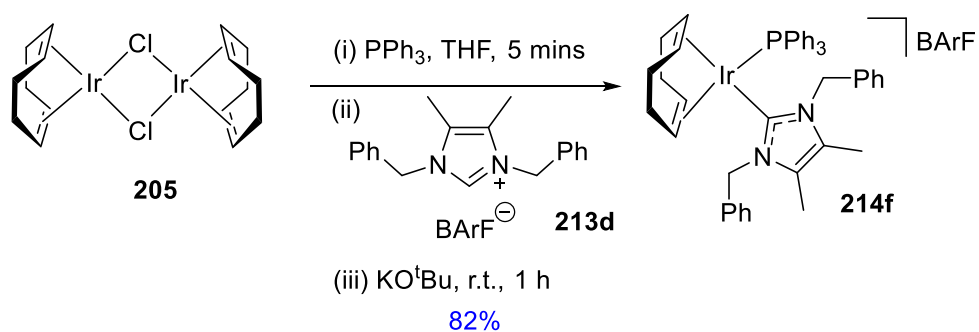
to be prepared in one pot, with no necessity for filtration of an unsaturated iridium species through celite *prior* to addition of the desired phosphine ligand. In clarification, the use of such alternative, smaller NHCs allows for mechanically simpler (and faster) preparation of HIE catalysts. To illustrate this point, it has now been shown that carbene chloride **259**, when stirred in THF in the presence of PPh₃, undergoes a yellow to bright red colour change on addition of a silver salt. Pleasingly, this synthetic procedure appears to be general and high-yielding across a range of silver salts chosen (**214a-214e**, **Table 17**), highlighting the possibility of studying such complexes further in relation to any reactivity discrepancies that may centre on differences in the counterion chosen.

Following on from novel complexes **214a-214e**, and in testament to the one-pot procedure developed in **Section 3.2**, the synthesis of the BARf derivative, **214f**, was realised in excellent yield by employing *Lepidiline A* derivative **213d** (**Scheme 52**). The series of six counterion derivatives of the novel NHC/phosphine ligand sphere were fully characterised, including by X-ray analysis, as exemplified for complex **214b** in **Figure 37**.

Table 17. Generalised synthesis of potential HIE catalysts based on *Lepidiline A*.



Entry	Complex	X	Yield (%)
1	214a	BF ₄	92
2	214b	PF ₆	75
3	214c	SbF ₆	85
4	214d	OTf	99
5	214e	BPh ₄	82



Scheme 52. One-pot synthesis of BArF-containing HIE catalyst derived from *Lepidiline A*.

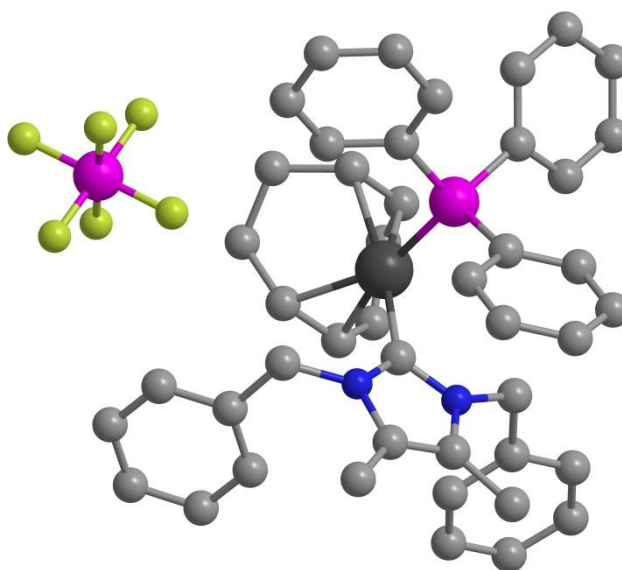
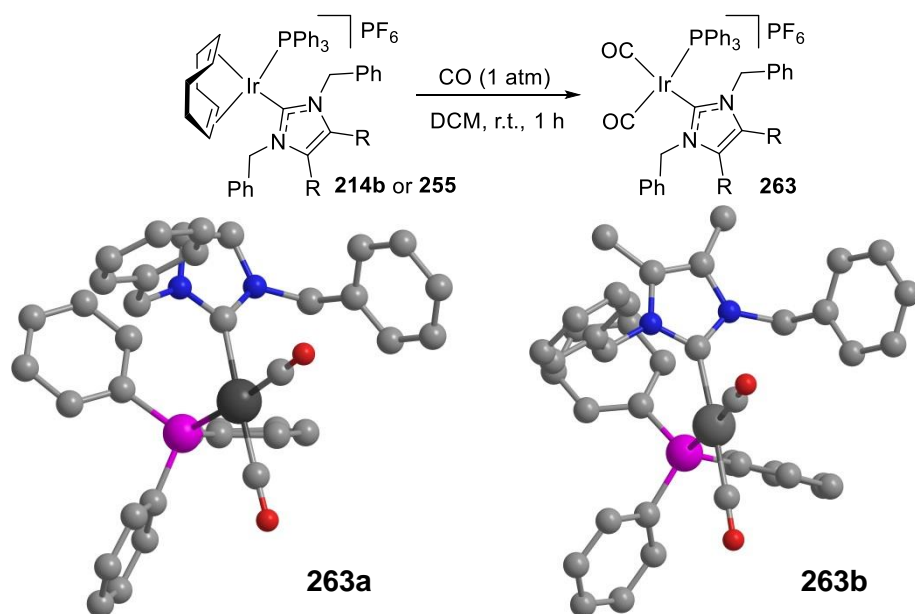


Figure 37. X-ray structure of complex **214b** bearing the PF₆ counterion.

Having successfully produced the desired Ir complexes, attention now turned to sampling and comparing the reactivity of this novel ligand sphere *versus* the alternative ligand spheres in **255** and **196a**. As discussed previously, DFT/PCA mapping of the ligand properties suggests that IBn^{Me}/PPh₃ should be similar (but not identical) to IBn/PPh₃, and more significantly distinct from IMes/PPh₃. Firstly, in line with methods and results from **Section 4.1**, the carbonyl complexes of the IBn/PPh₃ and IBn^{Me}/PPh₃ were synthesised (**Table 18**). Direct exposure of the HIE precatalyst structures to an atmosphere of CO resulted in a *cis*-orientated ligand sphere in both cases, with similar ΣV_{bur} values as determined by X-ray crystallography. As predicted, these complexes are distinct in size and geometry from the IMes/PPh₃ analogue, **245a**.

Table 18. Synthesis of Ir(I) NHC/phosphine di- and tri-carbonyl complexes.

Entry	Complex	R	Yield (%)	% V_{bur} (PPh ₃)	% V_{bur} (NHC)	Σ (% V_{bur})	θ (°) ^a
1	263a	H	49	27.8	29.8	57.6	93.2
2 ^{b,c}	263b	Me	52	27.2	30.9	58.1	89.4
				27.8	30.5	58.3	92.6

^a θ represents the angle $CO-Ir-CO$

^b Complex **263b** crystallised with two independent salt pairs in the unit cell.

^c The relevant IMes/PPh₃ values from dicarbonyl complex, **245a**, are $\Sigma(\%V_{bur}) = 64.9$; $\theta_{CO-Ir-CO} = 160.0^\circ$.

Again, using similar methods from **Section 4.1**, the electronic characteristics of the IBn^{Me} partnership were explored by synthesising the chloro-carbonyl complex, **253f**, and the *in situ* generated dihydride, **254h** (see **Experimental** section for details). As shown in **Figure 38**, IBn^{Me}/PPh₃ (red) was found to be slightly more electron-rich than IBn/PPh₃ (blue) and more significantly less electron-rich than IMes/PPh₃ (green).

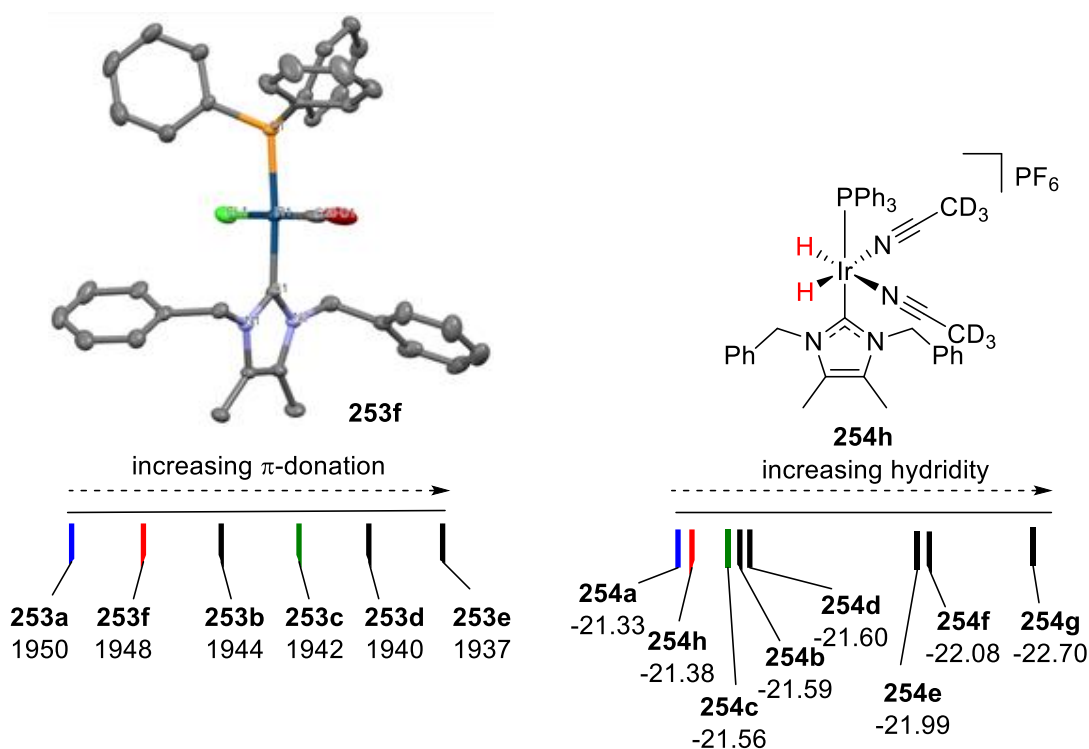
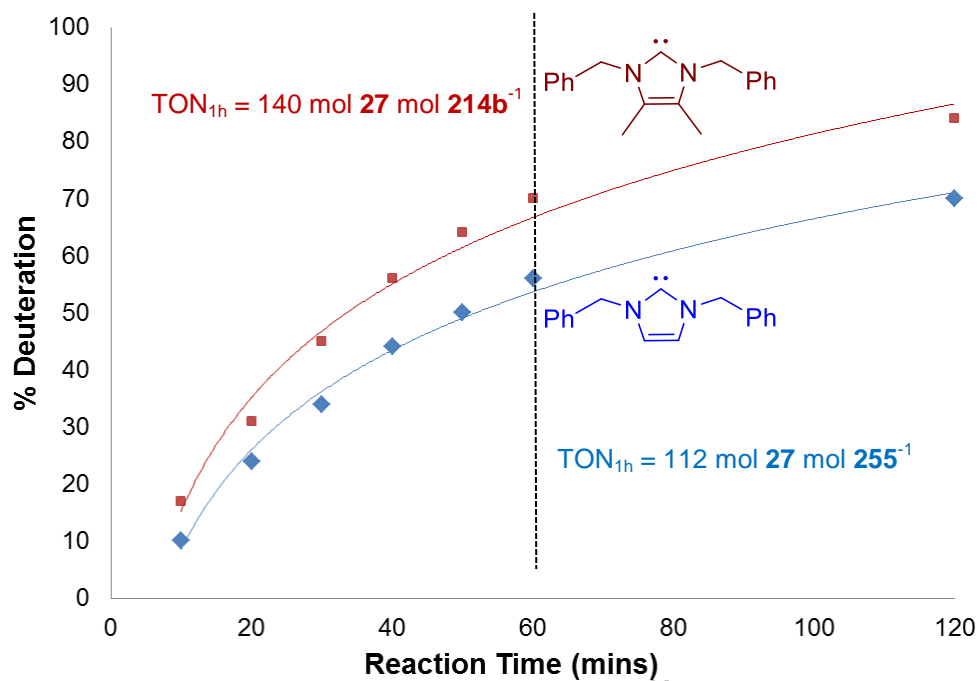
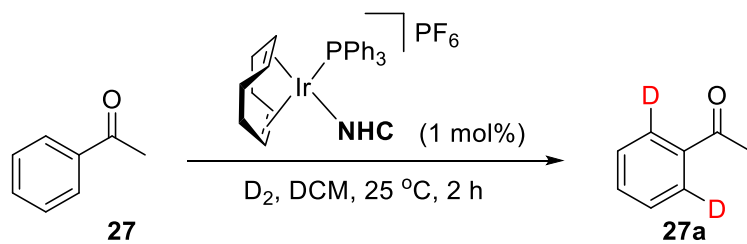
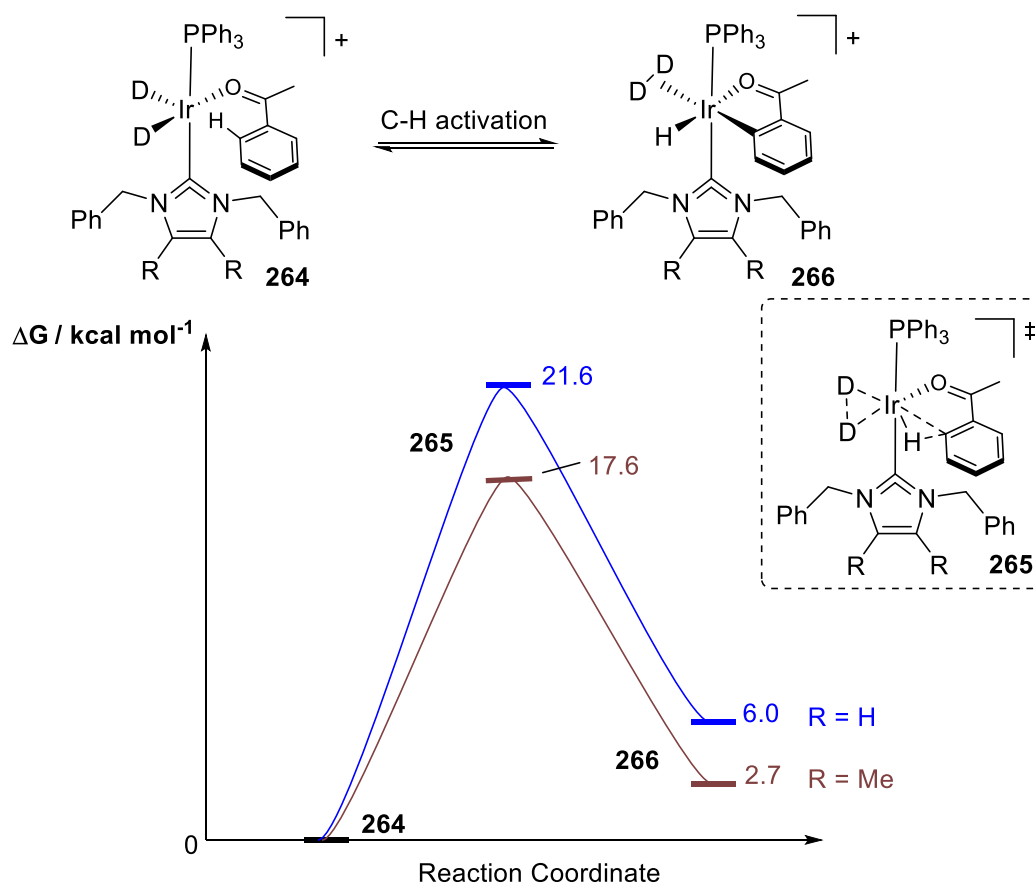


Figure 38. Comparative experimental electron donating ability for $\text{IBn}^{\text{Me}}/\text{PPh}_3$ (red).

With specific focus on the close relationship between IBn/PPh_3 and $\text{IBn}^{\text{Me}}/\text{PPh}_3$, the relevant HIE precatalysts were compared *via* kinetic analysis of the simple reference labelling reaction with acetophenone, **27** (Scheme 53). Catalyst **214b**, derived from *Lepidiline A*, was clearly faster reacting, possessing a pseudo first order rate constant, $k_{\text{obs}}(\mathbf{214b}) = 0.0224 \text{ s}^{-1}$ versus $k_{\text{obs}}(\mathbf{255}) = 0.0145 \text{ s}^{-1}$ (see **Experimental** section for details). This result was supported by DFT modelling of the turnover-limiting¹¹⁴ C-H activation step (**264**→**266**, Scheme 54). With the aid of the PCA model developed above, the greater reactivity of catalyst **214b** can be rationalised on the basis of the increased π -donating ability of the Ir centre, and not on any steric difference between the two catalysts. The transient Ir(V)-like structure, **265**, shows D-D bond forming as well as C-H breaking on the imaginary frequency, suggesting a σ -complex-assisted metathesis mechanism,²¹⁰ rather than formal oxidative addition, as had been previously conjectured.⁹⁸



Scheme 53. Measured TON and TOF of IBn^{Me} versus IBn/PPh₃.



Scheme 54. DFT-calculated PES for C-H activation of **27** with IBn/PPh₃ and IBn^{Me}/PPh₃.

The variation in reactivity between the IBn^{Me}/PPh₃ ligand sphere in **214** and IMes/PPh₃ in **196a** was most interestingly drawn out in studying the counterion dependence on catalyst reactivity. Even at a relatively high and unoptimised catalyst loading of 5 mol%, larger and more weakly coordinating substrates **27**, **160**, and **267** perform poorly when catalyst **214d**, bearing the OTf counterion, is used in the HIE reaction (**Figure 39**). Alternatively, the more basic substrate, **94**, is unaffected, and the order of reactivity reflects that garnered for IMes/PPh₃ (see **Section 3.2**). Presumably, the smaller size of the IBn^{Me}/PPh₃ system suffers from competitive coordination of the triflate to the metal centre.¹⁴⁴ Most curiously, the catalyst series **214** is ineffective at labelling the weakly coordinating substrate, nitrobenzene, **268**, whereas the flagship IMes/PPh₃ system, **196a**, labels the compounds to ca. 95% D under similar conditions.¹¹³ This may be due to differences in available intermolecular (for example π - π) interactions of the substrate to the different catalyst systems upon binding. Nonetheless, such effects may be exploited favourably to induce directing group chemoselectivity in labelling multifunctional molecules.

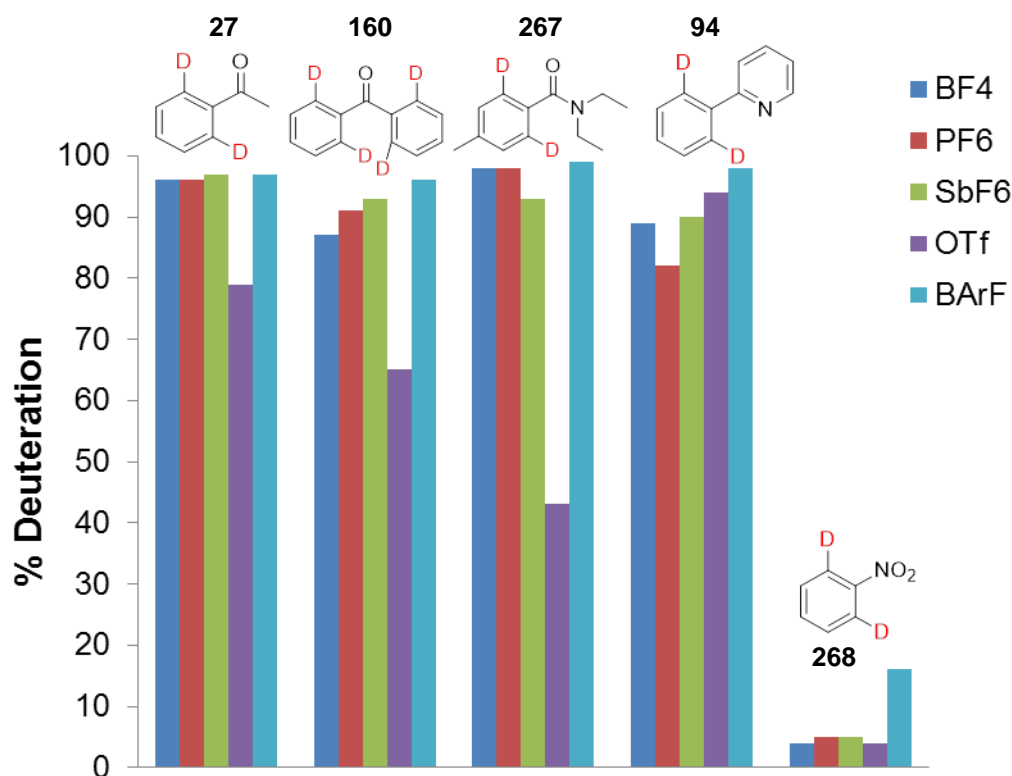


Figure 39. Attenuated reactivity of $\text{IBn}^{\text{Me}}/\text{PPh}_3$ in the presence of OTf counterion.

Interestingly, attempts to assess the labelling efficiency of bis-carbene complex **262** under similar conditions resulted in no observable labelling. Indeed, the precatalyst was found to be unreactive towards D_2 and was recovered unchanged at the end of the reaction (see **Experimental** section for full details). This highlights the importance of the NHC/phosphine partnership and is in line with similar studies on related bis-carbene complexes of iridium.¹⁹⁸

In summary, the first synthesis of the simple imidazolium-based natural product, *Lepidiline* A, **213a**, has been reported, along with Br, PF_6 , and BArF derivatives **213b** - **213d**, respectively. This has been followed by the development of novel HIE catalysts and the inception of a mechanically simple, silver-based approach to HIE catalyst synthesis. Detailed and combined experimental/computational analysis of resulting HIE catalysts derived from the natural product has led to quantitative insight into parameters responsible for observed differences in resulting catalyst reactivity *versus* lesser substituted analogue, **255**, and existing flagship HIE catalyst, **196a**. Overall, dimethyl substitution on the backbone of the novel NHC was found to impart an electronic influence with minimal impact to sterics. The

reactivity differences between the catalysts studied are now being exploited in labelling regioselectivity studies which will be reported in due course.

5.2 *ortho*-Deuteration of 1° Sulfonamides – An Experimental & Computational Study

Regardless of the many accomplishments of iridium-based HIE, a key challenge for which no general solution has been presented is C-H activation adjacent to primary sulfonamides. Related to this, the *sulfa drugs* derived from sulfonamides represent a significant milestone in pharmaceutical science, and, since their emergence in 1935, have been developed to produce various antibiotics, diuretics, hypoglycemic agents, and anti-hypertensive treatments.^{211,212} To our knowledge, primary sulfonamide substrates remain largely unexplored in C-H activation processes in a general sense. Further, only a handful of limited examples of *ortho*-directed deuterium labelling of primary sulfonamides have been reported (**Figure 40**). Through independent studies, Hesk,¹⁷² and later Herbert,¹⁰⁴ applied commercially available Crabtree's catalyst, **159**, to this problem. Despite these studies spanning catalyst loadings of 5 to 100 mol%, respectively, a maximum of only 15% D in benzenesulfonamide was achieved in the latter study. More successfully, Lockley applied iridium 1,3-dionate **187** to achieve 66% D in 4-methylbenzenesulfonamide, albeit at the high temperature of 130 °C and with a relatively elevated catalyst loading of 24 mol%.¹⁰⁸ Perhaps most notably to date, Herbert applied the *in situ*-generated complex **269** to the labelling of benzenesulfonamide, achieving 85% D at room temperature, but with a substantial 52 mol% catalyst loading.¹⁰⁰

Based on the DFT/PCA model described in **Section 4.2**, it could be reasoned that, owing to the tetrahedral geometry of the sulfonamide group, and the fact that such HIE processes are believed to proceed *via* concerted C-H activation,¹¹⁴ *a sterically less encumbered and more electron-rich ligand sphere would enhance the efficiency of the sulfonamide coordination and subsequent ortho-deuteration processes*. In this light, it was hypothesized that flagship HIE catalyst **196a** would not be an effective mediator of the desired process, due mainly to its combined ligand volume. In contrast, however, a complex of the class exemplified by **207**, the precursor of **196a**, fits both the steric and electronic ligand profiles proposed above for successful deuteration of primary aryl sulfonamides (**Scheme 55**). Furthermore, viewing the PCA model (**Figure 26**), these complexes hold a privileged position in ligand space, suggestive of unique reactivity compared to other possible catalyst structures.

We initiated our studies by testing the ability of sterically distinct catalysts **196a** and **207** to mediate the *ortho*-deuteration of 4-methylbenzenesulfonamide, under our standard labelling conditions. In agreement with our initial hypothesis, the latter system delivered far superior

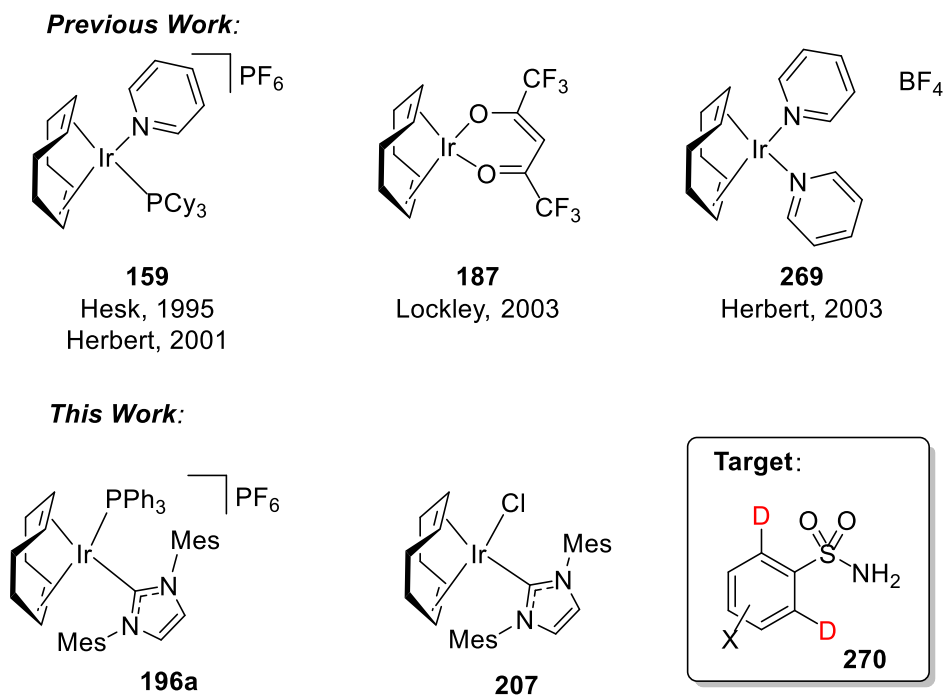
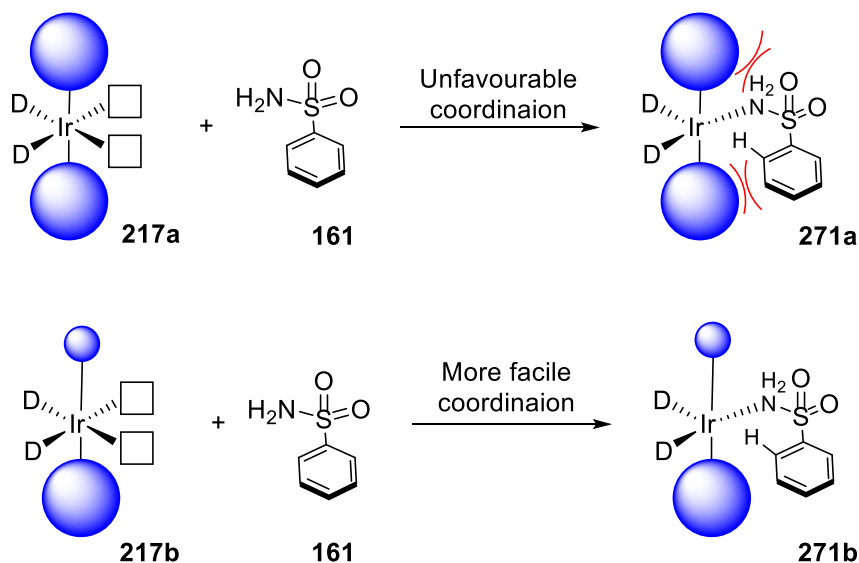
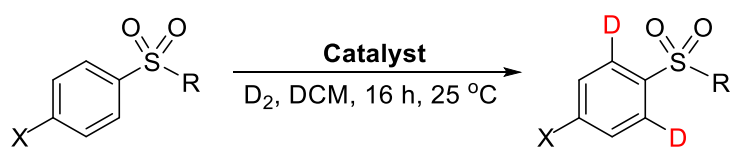


Figure 40. Proposed and existing HIE catalysts for *ortho*-deuteration of 1° sulfonamides.

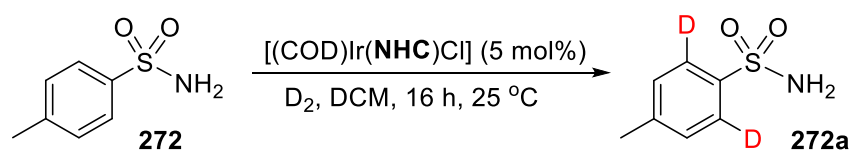


deuterium incorporation, and at levels currently unprecedented in the literature (**Table 19, Entry 1 versus Entry 4**). In labelling the related substrates, methyl phenyl sulfone and *N*,4-dimethylbenzenesulfonamide, catalyst **196a** remained inactive (**Entry 1 vs. 2 and 3**) whilst the activity of **207** fell markedly (**Entry 4 versus Entries 5 and 6**). Thus, catalyst **207** shows exploitable chemoselectivity for coordination of primary sulfonamides over secondary sulfonamides and sulfones.

Table 19. Catalyst discovery for *o*-deuteration of primary sulfonamides.

Entry	X/R	Catalyst	% D
1	Me/NH ₂	196a	12
2	H/Me	196a	9
3	Me/NHMe	196a	7
4	Me/NH ₂	207	90
5	H/Me	207	17
6	Me/NHMe	207	8

Having identified **207** as a viable catalyst motif for labelling primary sulfonamides, analogues of this system were screened, varying the steric bulk and electron-releasing capabilities of the pendant NHC ligand (**Table 20**). Using *Percent Buried Volume* ($\%V_{bur}$) and modified $\nu(\text{CO})$ analyses extracted from earlier DFT/PCA calculations, two inferences can be drawn from this catalyst screen. Firstly, catalytic activity is negligible when $\%V_{bur}(\text{NHC})$ falls below $\sim 32\%$ (**Entries 1 and 2 versus 3 – 7**). Presumably, this is as a result of the necessity for larger ligands in order to encourage reductive elimination, releasing the labelled substrate from the active catalyst. Secondly, for NHCs of similar size, those bearing more electron-donating substituents increase catalyst activity, supporting a more facile C-H activation across the *ortho* C-H bonds of the substrate (for example, **Entry 3 versus 4**). Overall, complex **273f**,¹⁴⁸ the most electron-rich of all complexes tested, warranted further study. The reaction conditions were further optimized to assess the potential for labelling primary sulfonamides in reduced reaction times, whilst maintaining relatively low catalyst loadings and ambient reaction temperature. This was achieved using a full factorial design of experiments (DoE),^{191–193} scrutinizing reaction time, catalyst loading, and solvent volume. Pleasingly, after only 11 experiments, it was found that a small increase in catalyst loading from 5 to 6.5 mol%, and employed under more dilute solvation, permitted a reduction in reaction time from 16 h to just 2 h (see **Experimental** section for full details).

Table 20. Catalyst screening for *ortho*-deuteration of 4-methylbenzenesulfonamide.

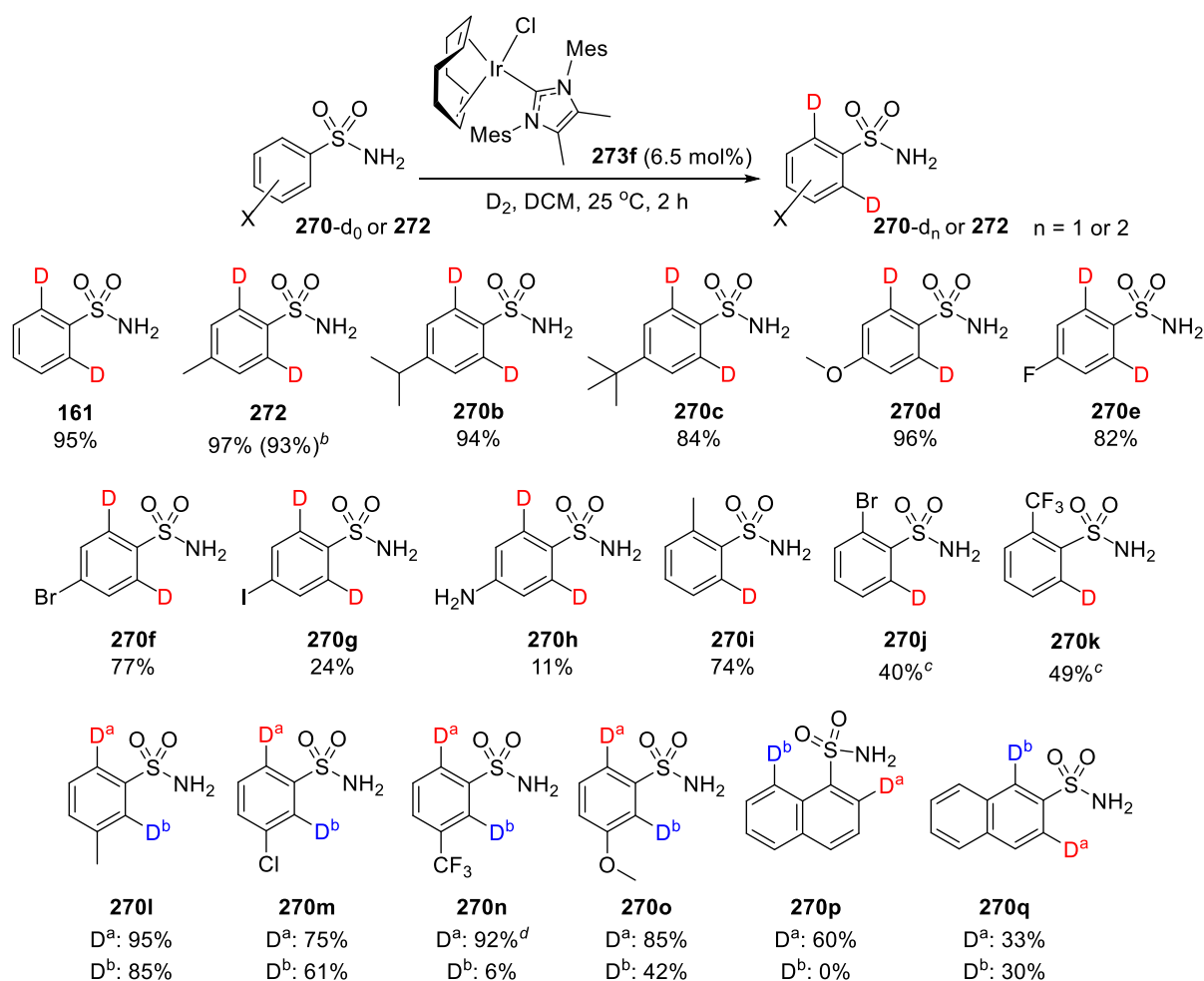
Entry	NHC	Catalyst	% V_{bur} ^a	$\nu(\text{CO})$ ^b	% D
1		273a	25.0	1993	2
2		273b	30.0	1996	3
3		273c	32.5	1994	75
4		273d	32.4	1993	90
5		273e	33.4	1998	95
6		273f	34.4	1992	96
7		273g	35.4	1996	93

^a Values taken from DFT calculated dihydride structures of the type **211**, proposed to be key intermediates in the catalytic cycle, and used in the PCA model, *vide supra*.

^b Values taken from DFT calculated carbonyl complex of the type **212**, used in the PCA model, *vide supra*.

To examine the general efficacy of this methodology, the optimised reaction conditions were applied to the *ortho*-deuteration of various primary sulfonamides (**Table 21**). For the parent substrate, benzenesulfonamide, **161**, an impressive and encouraging 95% D-incorporation was achieved. Similarly, *para*-alkyl and methoxy-benzenesulfonamides, **272** and **270b** – **270d**, gave excellent levels of deuteration, whereas only the *p*-*tert*-butyl analogue, **270c**, labelled below 90% D. This suggests that the steric influence of the NHC ligand on the catalyst is felt even by substituent groups at such a remote position relative to the ligating center of the substrate. To demonstrate the practicality of the HIE procedure, deuteration of **272** was repeated using a five-fold increase in reaction scale, with only 4% loss in catalyst efficiency. On studying *para*-halogenated substrates, very good deuteration efficiency was

achieved for fluoro- and bromo-compounds **270e** and **270f**, respectively, whereas the iodo-derivative, **270g**, gave much lower deuterium incorporation. The most likely explanation for these marked differences lie in the relative insolubility of **270g** in DCM. By a similar argument, a poor 11% D was achieved when labelling the simple sulfa drug, *Sulfanilamide*,²¹³ **270h**, making any rationalization based on competitive coordination of the *p*-amino group unclear. The labelling of more challenging *ortho*-substituted sulfonamides was also investigated. Whereas the methyl substituent in substrate **270i** only moderately affected the efficiency of the labelling process, introduction of a bromide or trifluoromethyl group (**270j** and **270k**, respectively) meant that gentle heating to 40 °C was required to achieve acceptable levels of deuteration. In such cases, lone pairs on the heteroatoms may impede the substrate coordination to the iridium center. Finally, a series of primary sulfonamides containing two distinct sites of potential deuteration *through the same sulfonamide directing group* was studied. For *meta*-substituted benzenesulfonamides, **270l** – **270o**, labelling was favoured at the least hindered C-6 position. Most notably, for the largest *meta*-substituent, present in **270n**, labelling occurred almost exclusively at the C-6 position. Moving to naphthalene-1-sulfonamide **270p**, despite the potential for labelling *via* both 5- and 6-membered metallocycles, deuteration occurred exclusively *via* the former, and is in line with our previous observations.¹¹⁴ In the isomeric substrate, **270q**, no discrimination was observed in labelling at positions C-1 and C-3, both proceeding through 5-membered metallocycles. However, as with substrates **270g** and **270h**, **270q** suffers from low solubility in DCM, leading to only moderate levels of deuteration overall.

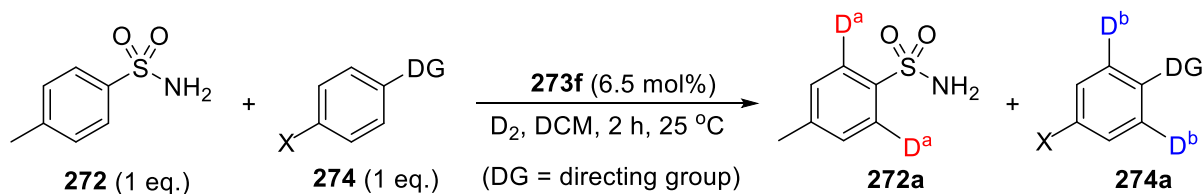
Table 21. Substrate Scope for *o*-Deuteration of Primary Sulfonamides^a

^a Conditions: **270-d₀** or **272** (0.215 mmol), **273f** (6.5 mol%), D₂ (balloon), DCM, 2 h, 25 °C. %D based on ¹H NMR. ^b Value in parenthesis is indicative of large scale reaction employing 1.075 mmol of **272**. ^c Values indicate level of deuterium incorporation at 40 °C. ^d Ratio estimated by HRMS.

The true value of any catalyst system can be more fully assessed by determining its robustness in the face of additives that may act as a catalyst poison.²¹⁴ Thus, it was important to assess not only the activity of catalyst **273f** but its ability to label primary sulfonamides in the presence of other potential directing groups. **Table 22** summarises a series of competition experiments where **272** was deuterated under the optimised reaction conditions in the presence of an equimolar quantity of a given additive. Only two of eight additives tested hindered the sulfonamide labelling process. Evidently, *N*-heterocyclic directing groups (**Entries 1** and **2**) compete for coordination to iridium, whereas carbonyl-based directing groups (**Entries 3 – 7**) and the nitro functionality (**Entry 8**) do not compete as readily with **272**. However, it should be clarified that, due to the relatively small size of each substrate, these studies mainly reflect competing directing group electronic characteristics. These

studies are not believed to be representative of the steric impact of having the sulfonamide and the competing functionality *in the same molecule*.

Table 22. Competition studies to assess robustness and chemoselectivity of catalyst system.

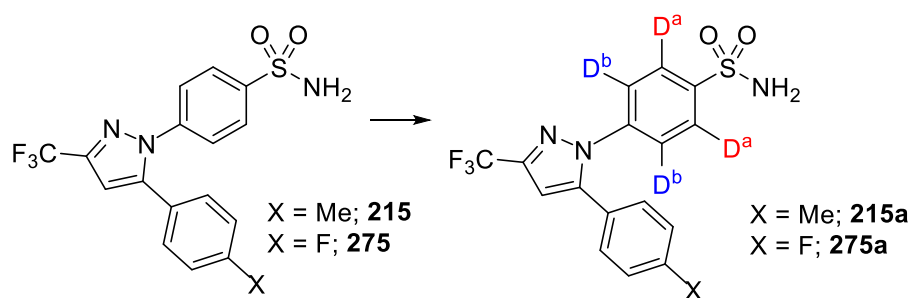


Entry	DG	X	%D(a)	%D(b)
1		H	7	47
2		H	7	19
3		Me	94	54
4		Me	95	11
5		Me	93	26
6		Me	97	10
7		Me	93	1
8		H	97	4

In a further assessment of the present *ortho*-deuteration protocol, we investigated its utility in labelling the more complex drug molecules, *Celecoxib*, **215**, and *Mavacoxib*, **275**, COX-2 inhibitors first commercialized by Pfizer.²¹⁵ Unlike the other substrates in this study, *Celecoxib* possesses two potential sites of labelling *via* two distinct directing groups: a primary sulfonamide and a pyrazole ring. Employing the optimised conditions described above, we compared catalysts **273f** and **196a** in their ability to mediate the C-H activation and deuterium labelling of **215** and **275** (Table 23). Rather unsurprisingly, the more encumbered complex **196a** showed unquestionable chemoselectivity for C-H activation

adjacent to the pyrazole rather than the sulfonamide (**Table 23, Entries 1 and 3**). This inactivity of **196a** toward the sulfonamide moiety is in agreement with earlier studies (**Table 19, Entry 1**). However, employment of catalyst **273f** evidenced a *complete switch in the chemoselectivity of ortho-deuteration* in labelling drug molecules **215** and **275** (**Table 23, Entries 2 and 4**). Indeed, these results are in direct contrast to that shown in the competition study involving **272** and *N*-phenylpyrazole (**Table 22, Entry 1**), where the pyrazole outcompeted the sulfonamide in coordinating and reacting at the iridium centre of **273f**. Accordingly, such marked results called for a deeper understanding of the catalysis mechanism and, hence, the origin of the contrasting chemoselectivity of *ortho*-deuteration when using sterically distinct catalysts to label such multifunctional molecules as employed in this study.

Table 23. Chemoselective deuterium labeling of Celecoxib and Mavacoxib.

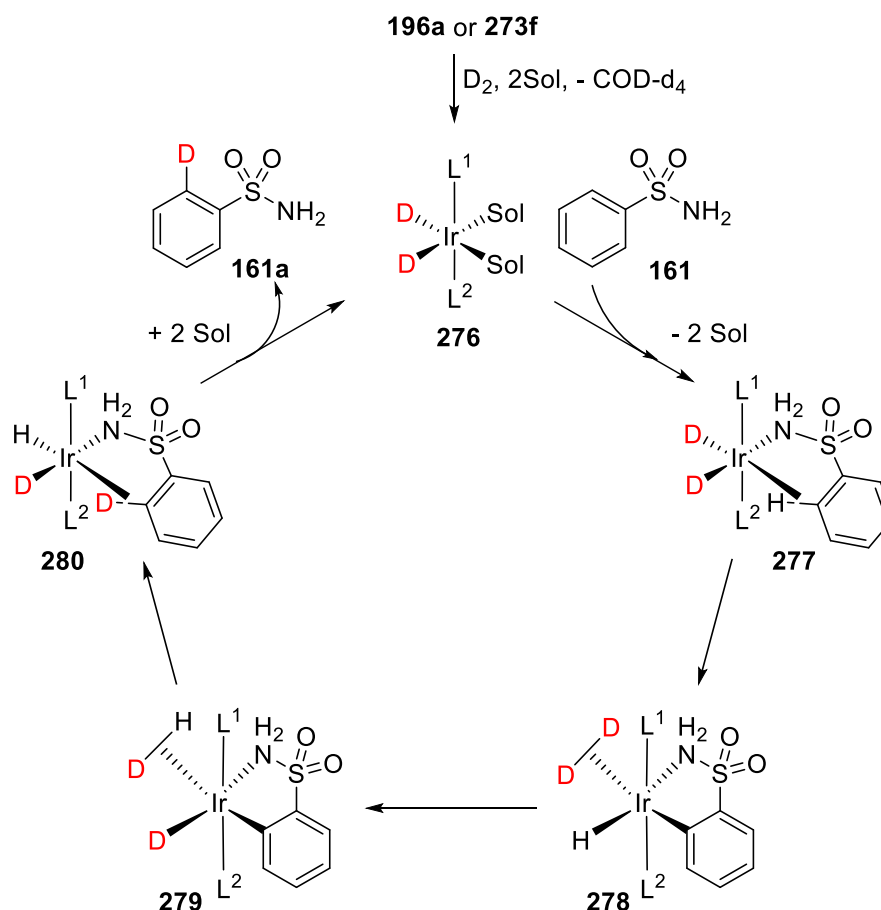


Entry	Catalyst	X	%D(a)	%D(b)
1	196a	Me	16	95
2	273f	Me	97	11
3	196a	F	7	89
4	273f	F	98	11

Based on the range of studies with various HIE catalysts, and on recent experimental and computational studies from our own laboratories, there exists an escalating body of insight surrounding the proposed mechanism for Ir-catalysed *ortho*-deuteration processes.¹¹⁴ As depicted in **Scheme 56** for sulfonamides, this is similar to details discussed earlier (**Scheme 25**) but additionally assumes the basic sulfonamide nitrogen to be most heavily involved in binding.

Attempts to probe the reaction mechanism began by measuring the kinetic isotope effect (KIE) of the C-H activation step.¹¹⁷ Thus, exposing substrate **272a** to the reverse reaction, employing H₂ in place of D₂, revealed a primary KIE value of approximately 3.2, indicating

that C-H activation of the *ortho*-C-H bonds is involved in the rate-limiting step (**Scheme 57**). Indeed, this is similar in value to that obtained from studies of HIE with catalyst **196a** and deuterated acetophenone, **197**,¹¹⁴ suggesting that both reactions proceed *via* a similar mechanistic process. Additionally, no depletion in the activity of catalyst **273f** in the deuteration of **272** was observed when the reaction was run in the presence of Hg(0).²¹⁶ This supports the view that the labelling process operates under homogeneous catalysis.

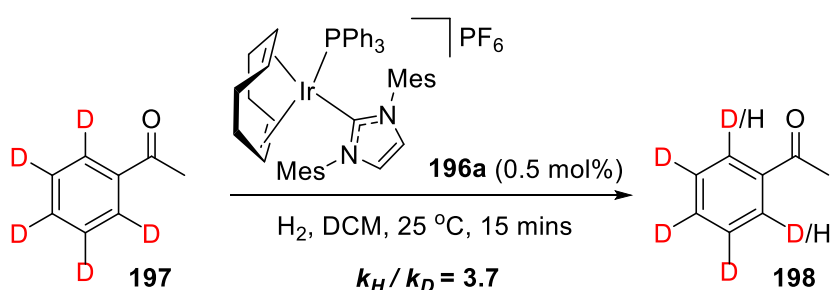


Scheme 56. Proposed mechanism for Ir-catalysed ortho-deuteration of 1° sulfonamides.

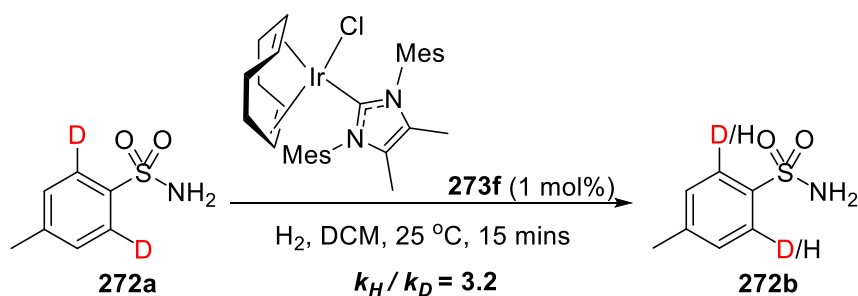
From the outcomes accumulated to this stage, experimental studies were combined with a complementary theoretical analysis of the operative reaction mechanism (see **Computational Details** section for full details). The first task was to strengthen our original hypothesis for the catalyst design, aiming to show that catalysts such as **273f** (or **207**), with a relatively small coordination sphere, can bind and react with the large sulfonamide directing group more readily than encumbered catalysts such as **196a**. To this end, we assessed the sulfonamide binding and C-H activation enthalpies of representative catalysts **273f** and **196a** (*cf.* processes **276**→**277**, and **277**→**278**, **Scheme 56**). Interestingly, on assessing the substrate

binding energies to the appropriate analogues of **281**, it was established that complexation of benzenesulfonamide, **161**, to the activated form of **196a** was more exothermic than to the equivalent activated form of **273f** (**281**→**282**, **Scheme 58**). However, and in contrast, the rate-limiting C-H activation process is less endothermic when the smaller catalyst is employed (**282**→**283**, **Scheme 58**). This is in qualitative agreement with our experimental findings (**Table 19**, **Entries 1** and **4**) and infers that the reduced steric encumbrance of catalyst **273f** relative to **196a** is essential for efficient catalytic reactivity with sulfonamide substrates.

Previous studies:



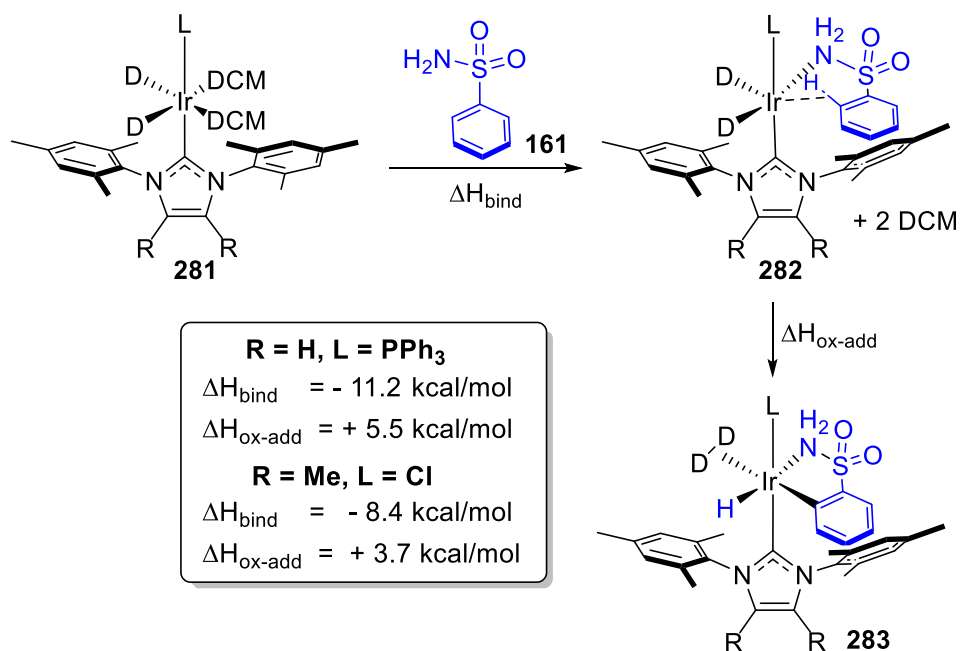
This work:



Scheme 57. Investigating kinetic isotope effects in Ir-catalysed *ortho*-HIE.

Concentrating on catalyst **273f**, the full PES of the labelling reaction with **272** was then calculated. In line with our KIE studies, C-H activation was shown to be the most energetically demanding, and thus rate-limiting, step (**284**→**286**, **Figure 41**). Furthermore, we calculated a theoretical KIE of 3.9 for this step, showing very good agreement with experimental observation. As with our previous studies, the initial C-H activation step is endergonic. Comparatively, hydride fluxionality (**286**→**288**) is energetically neutral on the

PES. Finally, the second C-H activation step (288→290) almost mirrors the first, and is exergonic in nature.



Scheme 58. Calculated energies for binding of benzenesulfonamide and C-H activation with sterically distinct catalysts.

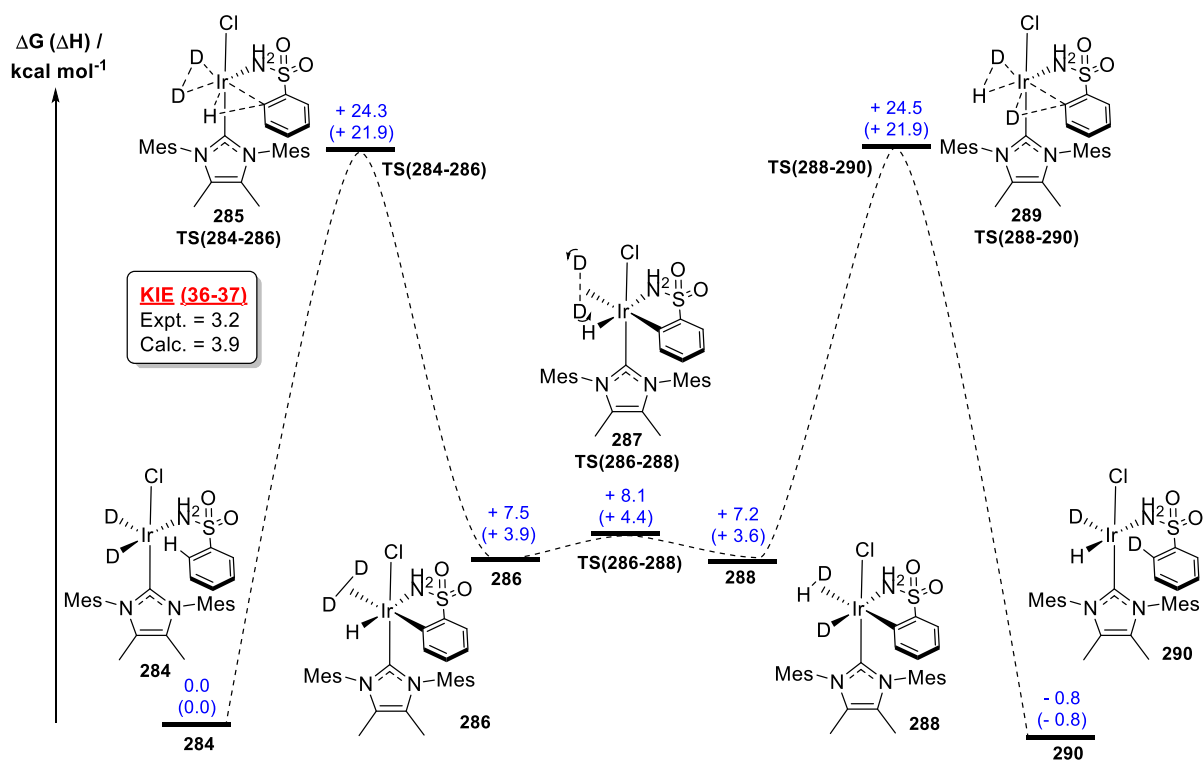


Figure 41. PES for *ortho*-deuteration of benzenesulfonamide with catalyst **273f**, scaled according to free energy, ΔG .

With the above insights in place, attention turned to explaining the origins of labelling chemoselectivity. Previously, our group studied the regioselectivity of labelling benzanilide which, through a *single coordinating group*, can undergo HIE through a 5- or a 6-membered iridacycle.^{113,114} In that case, a preference to label through the smaller 5-membered iridacycle was shown to originate from energetic differences in the C-H activation step,¹¹⁴ with the initial binding of the substrate proving to be insignificant. Conversely, the situation with sulfa-drugs **215** and **275** is more complex. Specifically, there are now two structurally different coordinating groups, both directing *ortho*-deuteration through a 5-membered iridacycle. As such, it cannot be assumed that the observed labelling selectivity using catalysts **273f** and **196a** is resultant of the oxidative addition *or* the initial binding step. A detailed study of the overall substrate complexation *and* C-H activation pathways of Celecoxib, **215**, with catalysts **273f** and **196a** was thus undertaken.

Firstly, the binding interactions and C-H activation of **215** with the larger catalyst, **196a**, was scrutinized (**Figure 42**). From the appropriate analogue of **281** (**Scheme 58**), solvated explicitly with two DCM molecules, subsequent complexation of **215** and release of solvent proved entropically favourable and enthalpically neutral for substrate binding modes **291** and **292**. However, both the complexation and subsequent C-H activation step are significantly lower in energy when proceeding through **292**, leading to *ortho*-deuteration *via* the pyrazole. This is in agreement with the experimentally observed labelling chemoselectivity (**Table 23, Entry 1**). Additionally, it is important to note that the energy difference in the binding modes ($\Delta\Delta G_{\text{bind}} = 13.1 \text{ kcal mol}^{-1}$) is much larger than the energy difference in the C-H activation transition states ($\Delta\Delta G_{\text{trans}} = 0.6 \text{ kcal mol}^{-1}$). We can therefore infer that the observed pyrazole chemoselectivity in labelling **215** with catalyst **196a** originates from the complexation event more so than the subsequent C-H activation process.

The change in labelling chemoselectivity observed upon switching from encumbered catalyst, **196a**, to the smaller catalyst, **273f** (**Table 23, Entry 2**), was subsequently explored. Similarly to **Figure 42**, complexation and C-H activation of **215** with catalyst **273f** were modelled computationally (**Figure 43**). Now, substrate complexation is calculated to be enthalpically disfavoured, presumably in connection with the lower electrophilicity of catalyst **273f** relative to **196a**. Nonetheless, there is once again a clear energetic bias for complexation and subsequent C-H activation through one directing group: the sulfonamide now being preferred over the pyrazole. In this case, discrimination between the binding modes **293** and **294**

($\Delta\Delta G_{\text{bind}} = 3.7 \text{ kcal mol}^{-1}$) is more similar in magnitude to the energy difference in the subsequent C-H activation pathways ($\Delta\Delta G_{\text{trans}} = 0.7 \text{ kcal mol}^{-1}$). Thus, it is theorised that chemoselective binding and labelling adjacent to the sulfonamide using the chloro-carbene catalysts is dictated by the combined influence of substrate binding and C-H activation transition state energies. The selective binding of the sulfonamide functionality in **215** by catalyst **273f** is worthy of further discussion. Whereas benzenesulfonamide, **161**, was predicted to bind to **273f** via the nitrogen lone pair (**Scheme 58**), Celecoxib, **215**, binds preferentially through an oxygen lone pair, supplemented by a hydrogen bond between the amino group of the substrate and the chloride ligand of the catalyst. This highlights the flexible nature of the sulfonamide directing group, with the nitrogen or oxygen groups able to actively participate, depending on the structure of both the substrate and the catalyst.

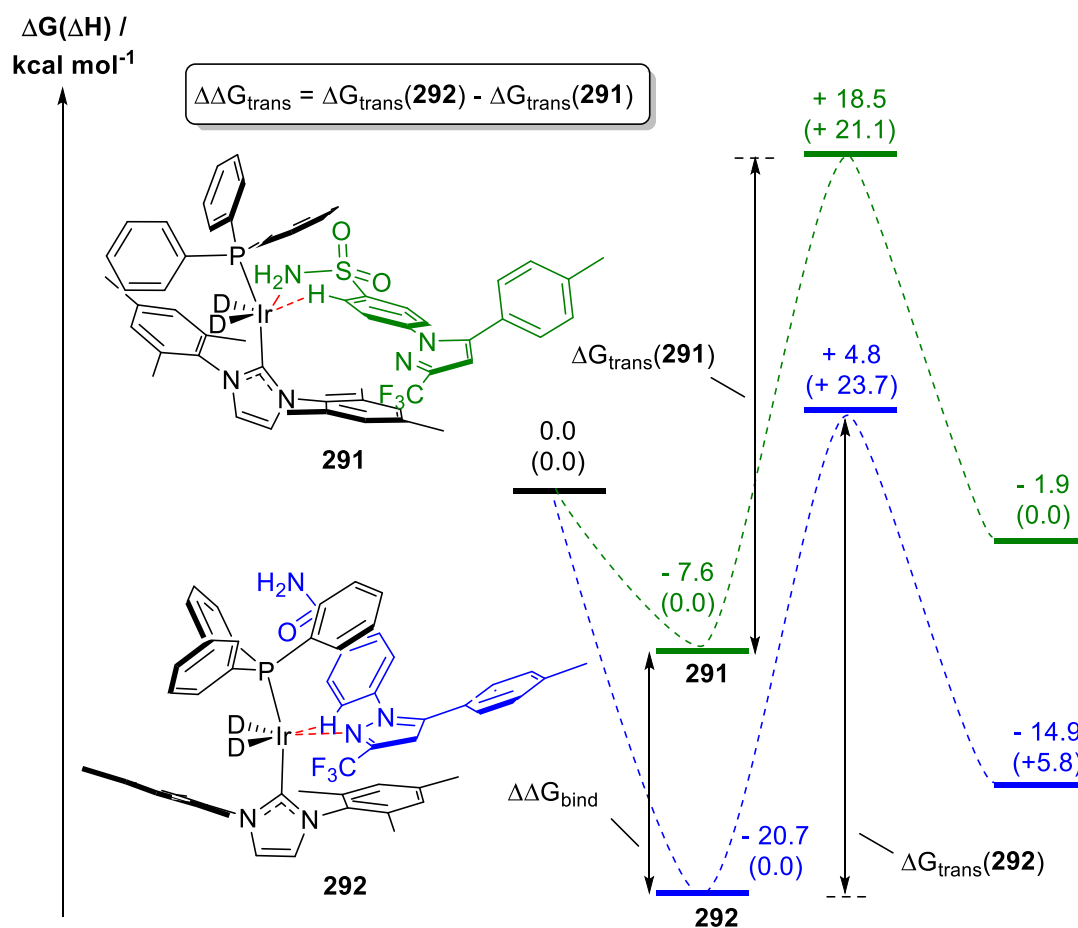


Figure 42. PES for the complexation and C-H activation of Celecoxib, **215**, with catalyst **196a**.

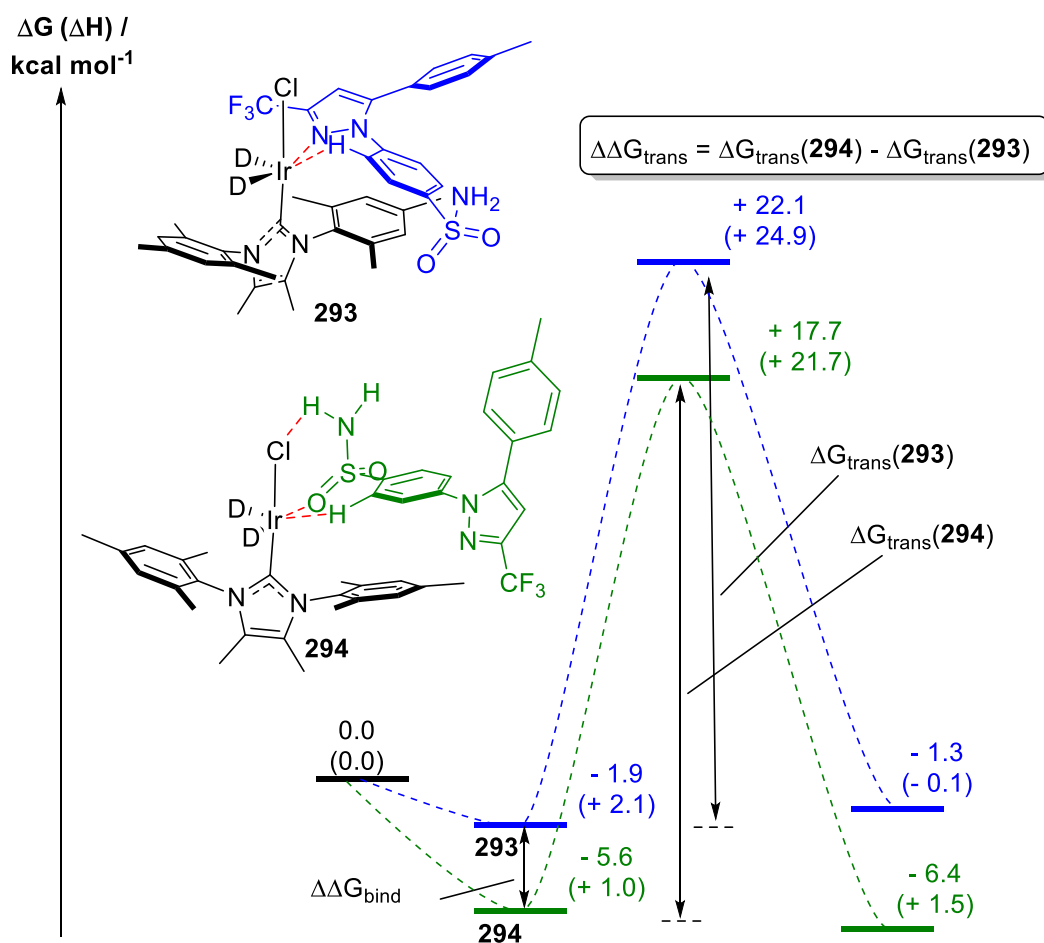


Figure 43. PES for the complexation and C-H activation of Celecoxib, **215**, with catalyst **273f**.

Computational analysis of chemoselective substrate binding (and thus regioselective D-labelling) has revealed that the energies of the initial binding conformers are *product determining* whilst subsequent C-H activation is *rate determining*. To test this concept further, two *Celecoxib* derivatives, **295** and **296**, have been synthesised (details in **Experimental** section) and tested with catalysts, **273f** and **196a**, in triplicate. Here, two questions were posed: (i) Can the observed labelling selectivity be predicted on the basis of binding energy calculations only, and (ii) What is the effect of the bulky CF₃ group in aiding selectivity for sulfonamide binding when using catalyst **273f**? As depicted in **Figure 44**, consideration of the lowest energy sulfonamide and pyrazole binding energies was sufficient to predict the direction and magnitude of observed labelling selectivity. Most remarkably, this held true for substrate **296**, where swapping CF₃ for the smaller CF₂H unit eroded the previously observed selectivity for labelling the sulfonamide over the pyrazole using catalyst **273f** (*vide supra*), and was reversed to show slight selectivity for the pyrazole. All labelling

results were determined by ^1H NMR and the distribution of isotopomers later verified by HRMS.

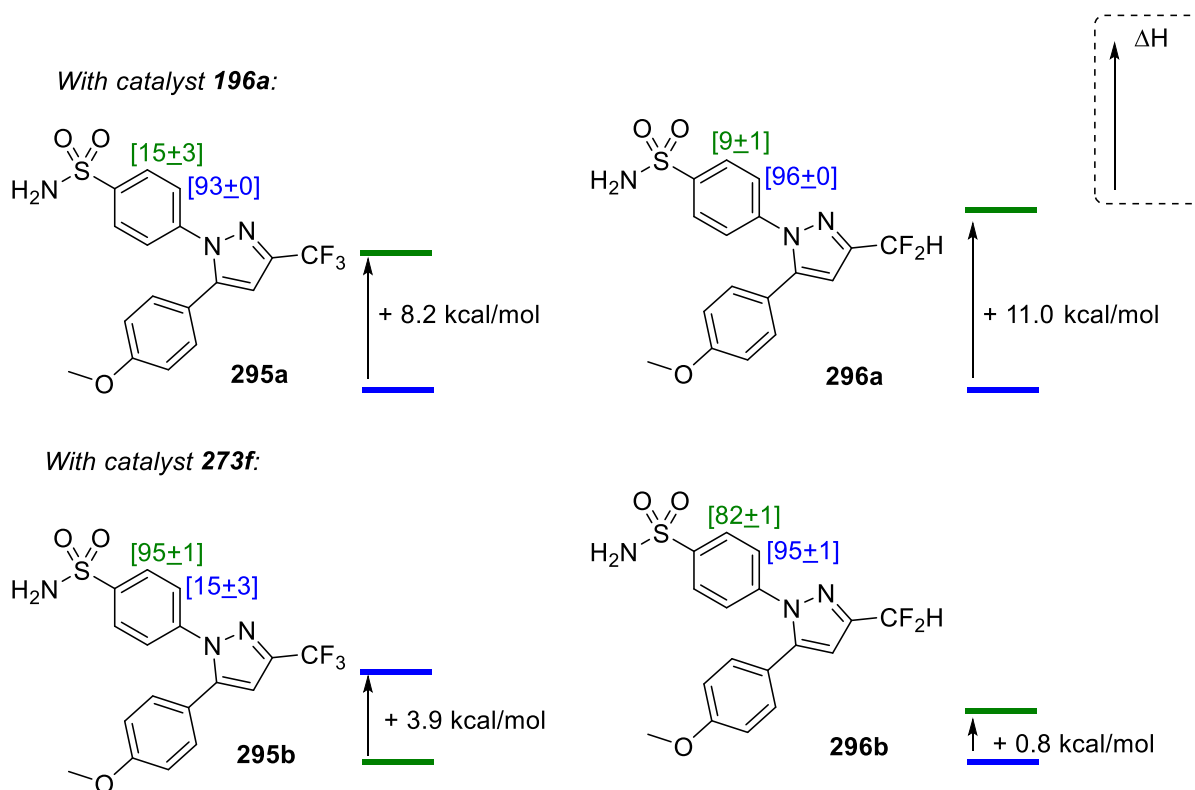
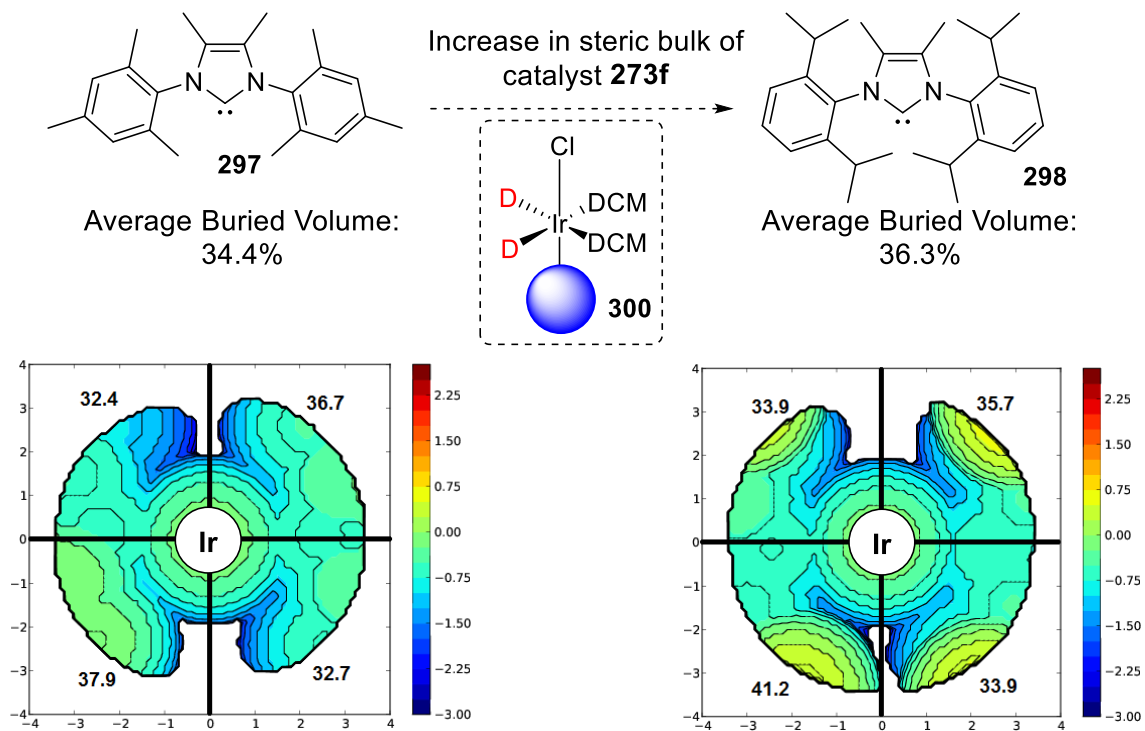


Figure 44. Calculated binding energies *versus* experimental labelling selectivities.

The additional comparison of theoretical binding energy *versus* labelling selectivity highlighted both the predictive power of the DFT calculations and, from a practical stance, the necessity to redesign catalyst **273f** to allow for high sulfonamide binding selectivity, even in the face of stronger competitors. On the basis of more sophisticated $\%V_{bur}$ calculations,²¹⁷ it was predicted that a sterically more hindered analogue of catalyst **273f**, catalyst **273h**, would provide the necessary steric clash with the CF_2H substituent to block labelling *via* the pyrazole unit (**Scheme 59**).

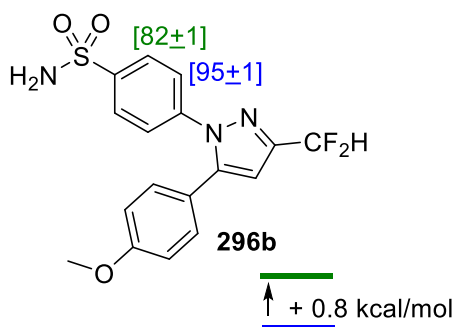
On comparing predicted binding energies and observed labelling selectivity, the desired restoration of sulfonamide selectivity was observed, albeit with some variation in the level of pyrazole labelling (**Scheme 60**, top). The predesigned steric clash between the NHC ligand of the 2nd generation catalyst and the CF_2H group of the substrate can be seen in the resultant DFT structures (**Scheme 60**, bottom). From this encouraging result, and with no requirement

for further binding energy calculations, a third generation catalyst based on NHC **303** was synthesised and applied with great success, fully restoring the desired selectivity and reducing all noise in the results (**Scheme 61**).

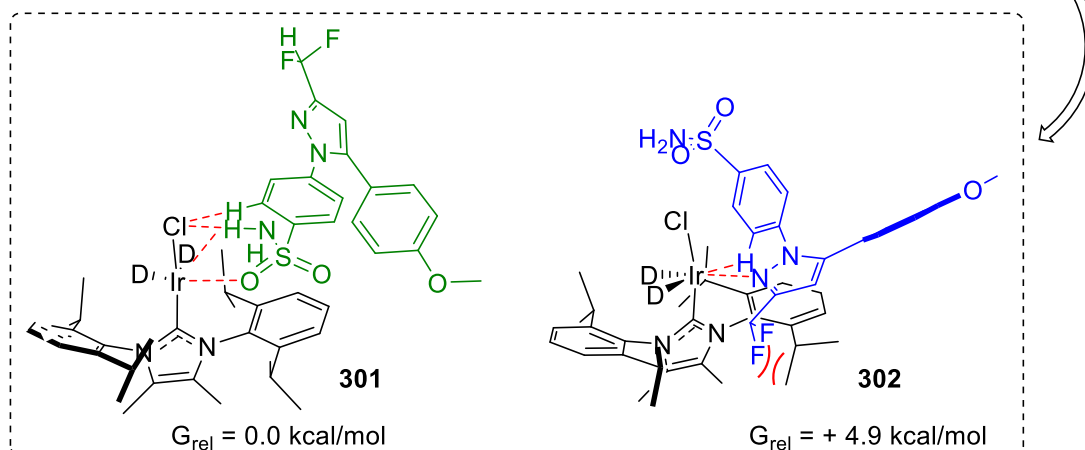
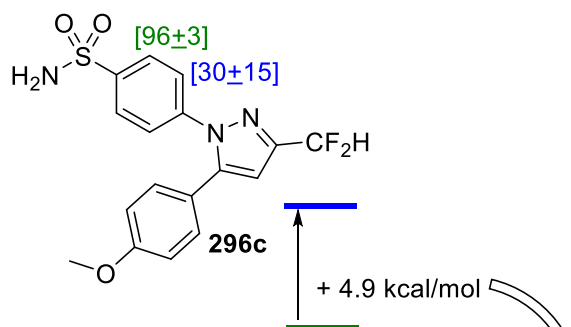


Scheme 59. Calculated steric maps for 1st and 2nd generation sulfonamide labelling catalysts.

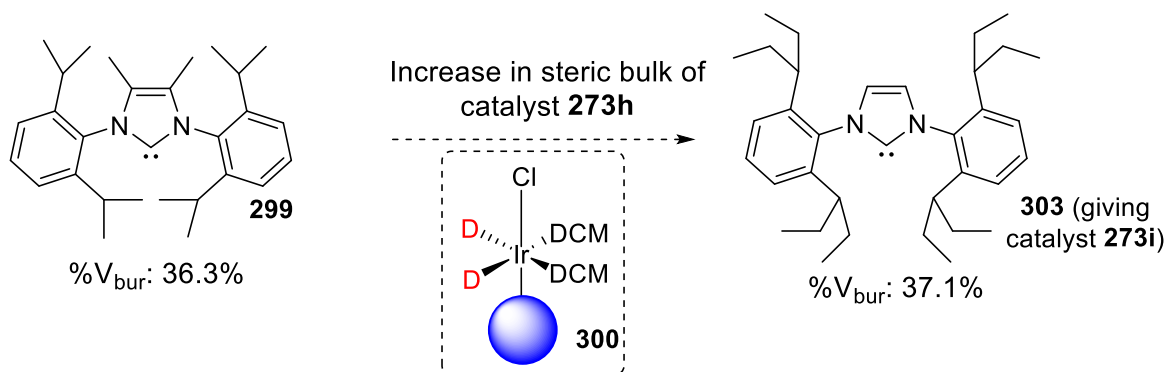
With catalyst **273f**:



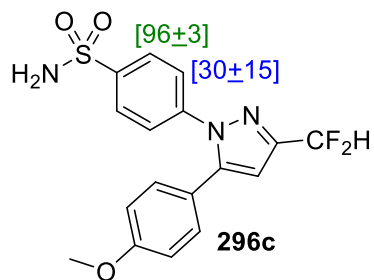
With catalyst **273h**:



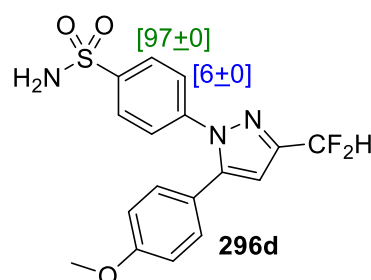
Scheme 60. Improved sulfonamide selectivity *via* predictive catalyst design.



With catalyst **273h**:

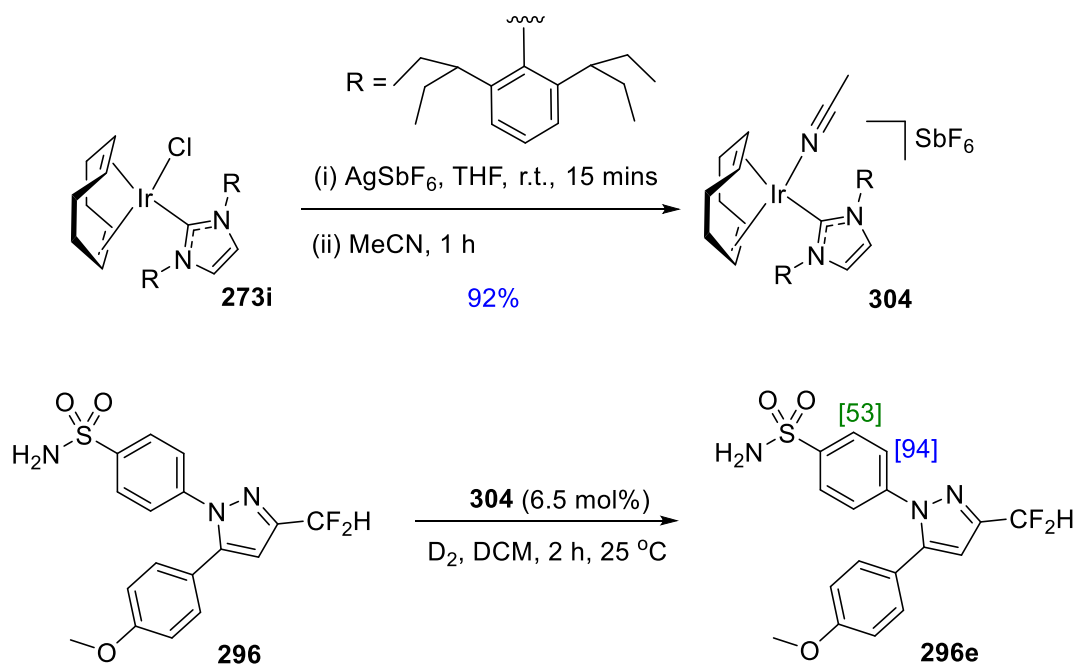


With catalyst **273i**:



Scheme 61. Third generation sulfonamide labelling catalyst.

In a final test of latest catalyst **273i**, the chloride ligand was replaced with a more weakly ligating acetonitrile ligand, to give **304** (Scheme 62). This cationic catalyst was applied under the optimal reaction conditions to reveal a radically different labelling pattern relative to **273i**. This further supports the experimental evidence accumulated to date emphasising the importance of the chloride ligand in the optimal catalyst systems.



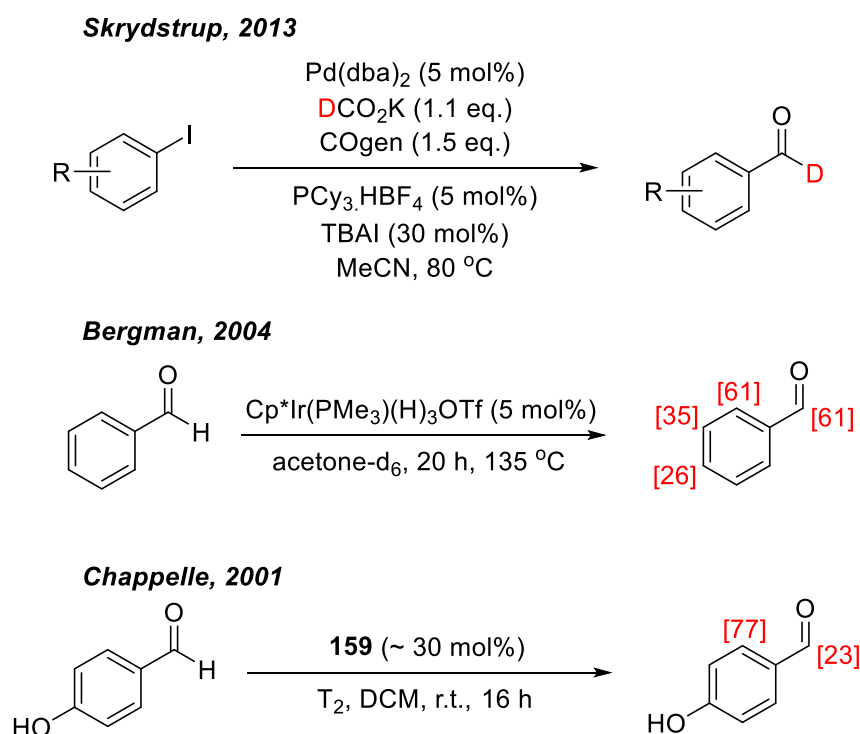
Scheme 62. Investigating the effect of the chloride ligand in 1° sulfonamide labelling.

In summary, a novel and efficient catalyst for the selective *ortho*-deuteration of primary sulfonamides has been discovered on the basis of earlier DFT/PCA calculations. Original catalyst **273f** was shown to be applicable across a range of substituted benzenesulfonamides, including several drug molecules. Subsequent mechanistic studies led to the discovery that substrate binding energies are product-determining (but not rate-limiting) in multifunctional drug systems. This theoretical model was applied to the development of second and third generation catalysts, **273h** and **273i**, respectively, which demonstrated improved levels of sulfonamide selectivity in the face of more challenging and competitive directing groups.

5.3 Regioselective Control in the Deuteration of Aromatic Aldehydes – An Experimental & Computational Study

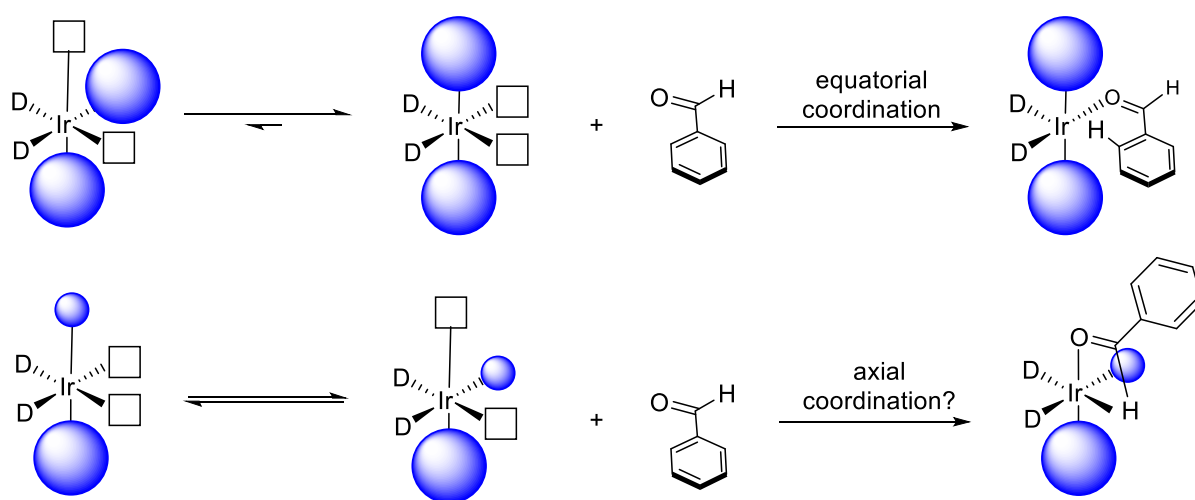
Beyond labelling of drug molecules, the supply of isotopically-labelled molecules has a sustained importance in the study of preparative chemistry and reaction mechanisms.^{19,20,117,218–222} Therefore, exploration into methods for the delivery of deuterated chemical feedstocks is important to the chemical industry in the widest possible sense.

The versatile nature of aldehydes as a synthetic intermediate in organic chemistry has resulted, unsurprisingly, in some research attention being directed at methods of labelling this functional group (**Scheme 63**).^{69,223–229} However, despite the possible distinction between aromatic and formyl labelling, little effort has been made to achieve such selectivity in a mild (room temperature), predictive, and switchable manner, *direct from the aldehyde*. With particular interest in Chappelle's method²²⁶ using Crabtree's catalyst, **159**, the complementary theoretical and experimental expertise on Ir-catalysed HIE developed earlier in this report was thus applied to the problem.



Scheme 63. Selected literature examples of homogeneous HIE with aldehydes.

To achieve classical *ortho*-directed labelling with aldehydes, available evidence suggests that a large ancillary ligand pair bonded mutually *trans* to the metal centre is necessary to induce equatorial aldehyde binding (**Scheme 64**, top). Conversely, from decarbonylation^{199,230–235} and hydroacylation^{236–244} literature, a bidentate ligand or smaller ligand pair is required to enforce the necessary *cis*-geometry for selective axial aldehyde binding and subsequent formyl C-H activation. As such, selective formyl labelling was hypothesised to require a smaller ligand sphere able to establish a *cis/trans* isomer equilibrium (**Scheme 64**, bottom).



Scheme 64. Conceptual model for catalyst design toward switchable aldehyde labelling.

To test this hypothesis, 2-naphthaldehyde, **305** (bearing three distinct labelling sites), was employed as a reference substrate under our standard catalytic labelling conditions. Similarly to Chappelle's tritiation efforts, **159** was shown to deuterate both aromatic labelling sites and the formyl position, and with an overall 1:1 selectivity under these conditions (**Table 24**, **Entry 1**). Moving to the NHC/phosphine ligand pairing, larger and more electron-rich variants resulted in an increasing selectivity for aromatic labelling, especially in the more electron-poor C1-position of the substrate (**Table 24**, **Entries 2 - 4**). Some parameters included in the overall PCA map have been included in **Table 24** for clarity.

Screening the larger ligand partnerships has served to strengthen the first part of the original hypothesis – larger ligands force a more rigid *trans* ancillary ligand geometry, favouring aldehyde binding on the equatorial plane and, ultimately, aromatic labelling. This has led to an efficient method for selective aryl labelling of 2-naphthaldehyde with minimal reaction optimisation. Due to the strong precedent for this reaction, no further studies were conducted

with catalyst **196b**. Instead, all further efforts were focused on confronting the more challenging problem of exclusive formyl labelling direct from the aldehyde.

Table 24. Hypothesis testing for selective labelling of aromatic aldehydes.

Entry	Catalyst	$\Sigma V_{bur,211}$	$\nu(CO)/cm^{-1}$	%D(a)	%D(b)	% D(c)
1	159	49.0	2004	45	45	95
2	214b	55.7	2014	1	2	2
3	196a	60.2	2009	71	43	8
4	196b	61.7	1999	94	32	9

In approaching the catalyst design for selective formyl labelling, the aforementioned results were viewed from the perspective of the PCA model (**Figure 45**), where the evolution of an aryl selective labelling catalyst followed a clear trajectory. To achieve the desired orthogonal reactivity, the chloro-carbene class of Ir complexes once again appeared to occupy a unique area of ligand space such that distinct reactivity may be expected. Going further, their potential to solve the current selectivity problem can be reinforced several-fold by the following points: (i) they possess the smallest ΣV_{bur} values of all ligand pairings, and may thus allow for the hypothesised *cis* ligand geometry for formyl C-H activation, (ii) unlike the

bis-phosphites (an alternative catalyst choice, top right of **Figure 45**), the chloro-carbene catalysts are small and electron-rich, and (iii) these smaller structures have already proven invaluable in solving the 1° sulfonamide labelling problem, and are thus known to be active HIE catalysts.

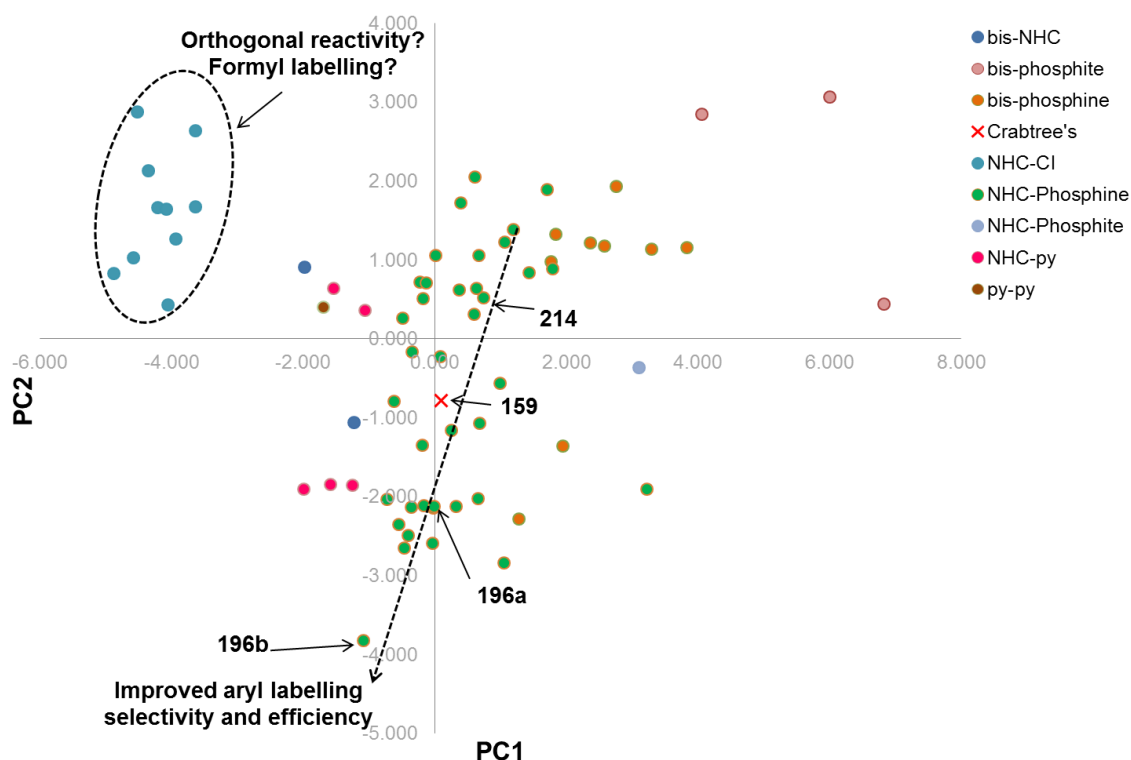
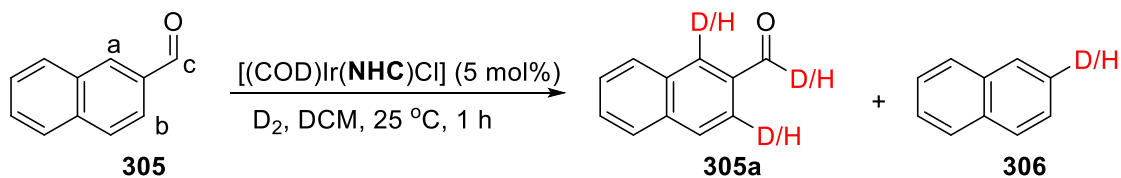


Figure 45. Aryl labelling catalysts and hypothesised formyl labelling catalysts as depicted in PC1 versus PC2.

Upon screening chloro-carbene catalysts in the labelling of **305**, the smallest of all those tested proved catalytically inactive, as with sulfonamide labelling, *vide supra* (**Table 25**, **Entries 1** and **2**). However, increasing the size and electron-donating ability of the NHC (**Entries 3 – 8**) delivered unprecedented levels of formyl labelling selectivity. Catalyst **273h** (**Entry 8**, 2nd generation sulfonamide labelling catalyst) proved most promising. Although other catalysts were seemingly just as active, only optimal catalyst, **273h**, maximised labelling whilst suppressing any observable decarbonylative by-products (**Entry 6 versus 8**, for example). In agreement with the initial hypothesis, moving to more extreme sizes of NHC ligand decreased the overall reactivity (**Entry 9**) and, in the case of Nolan's IPr*^{OMe} ligand,²⁴⁵ the selectivity is reversed back in the direction of aryl labelling (**Entry 10**). Further optimisation of the reaction conditions allowed the optimal catalyst to be employed at

loadings of just 1 – 2 mol% by simply running the reaction for 3 h rather than 1 h (see **Experimental** section for full details).

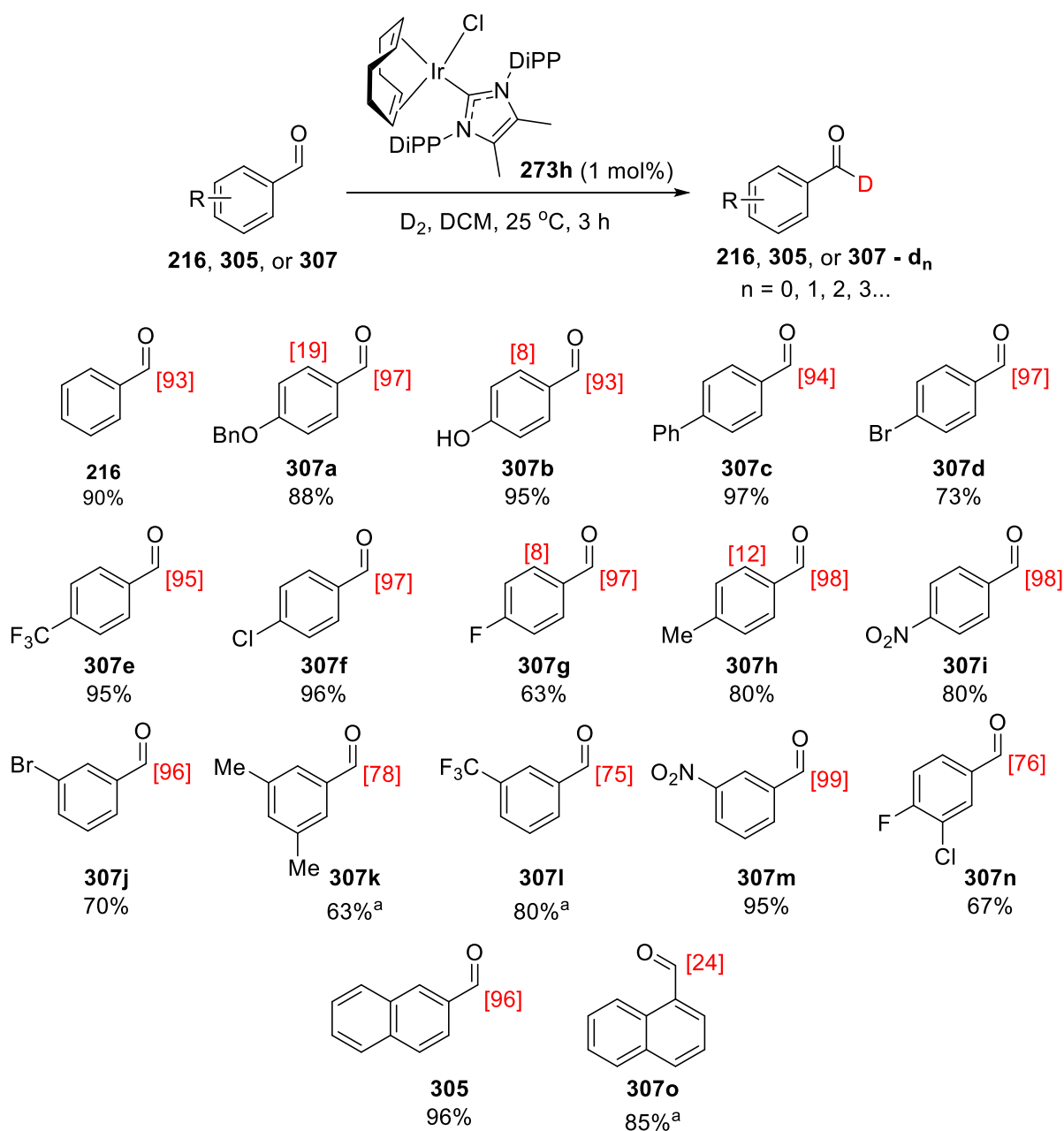
Table 25. Catalyst discovery and optimisation for formyl-selective aldehyde labelling.



Entry	NHC	Catalyst	%D(a)	%D(b)	%D(c)	%306 _{NMR} ^a
1		273a	2	3	0	0
2		273b	1	1	1	0
3		273c	3	7	42	0
4		273d	0	0	49	2
5		273e	0	1	82	5
6		273f	4	3	97	2
7		273g	4	3	93	0
8		273h	8	5	98	0
9		273i	9	6	90	0
10		273j	19	32	10	0

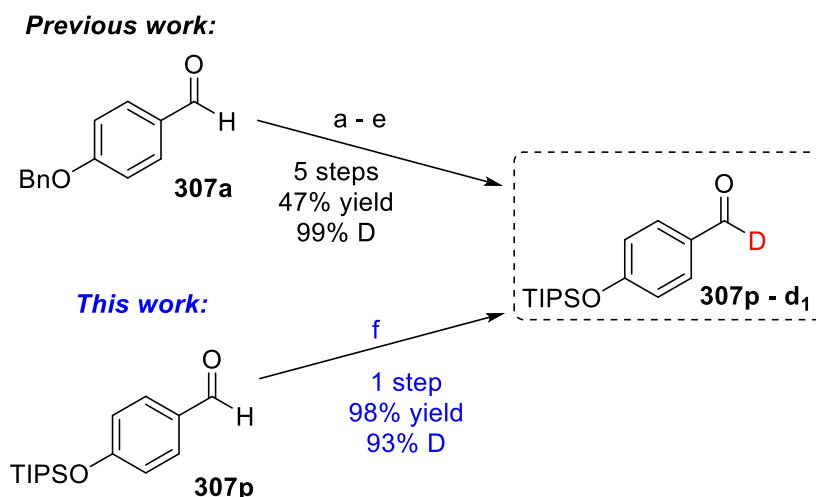
Under the optimised reaction conditions, a range of aromatic aldehydes were successfully labelled, isolated, and analysed (^1H and ^{13}C NMR, IR, HRMS). As depicted in **Table 26**, unsubstituted and *para*-substituted substrates (**216**, and **307a** – **307i**) were labelled with good to excellent regioselectivity and isolated yields. Small levels of aryl labelling were detectable in (π)-electron-rich examples only. A series of *meta*-substituted examples (**307j** – **307n**) were also well-tolerated and only the more encumbered aldehydes, such as 1-naphthaldehyde (**307o**), remain challenging.

Table 26. Substrate scope of formyl-selective aldehyde labelling method.



^a Reaction carried out at 2 mol% [Ir].

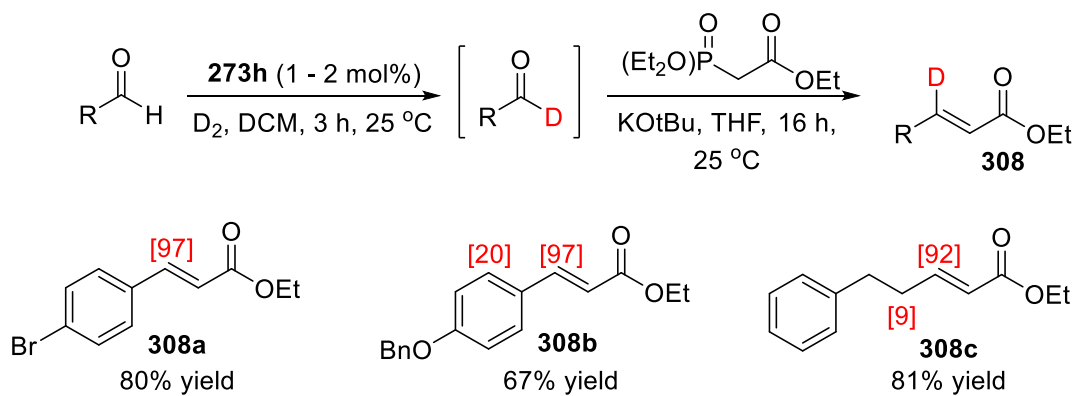
To further demonstrate the utility of this catalytic formyl labelling method, it was possible to demonstrate that silyl-protected phenol, **307p**, used in the synthesis of enantiopure d_1 -benzyl alcohols,²²⁴ could be successfully labelled in one high-yielding step and with high deuterium incorporation (**Scheme 65**). This method is competitive with a previously published route to the same aldehyde, which required five stoichiometric steps starting from an alternative aldehyde.



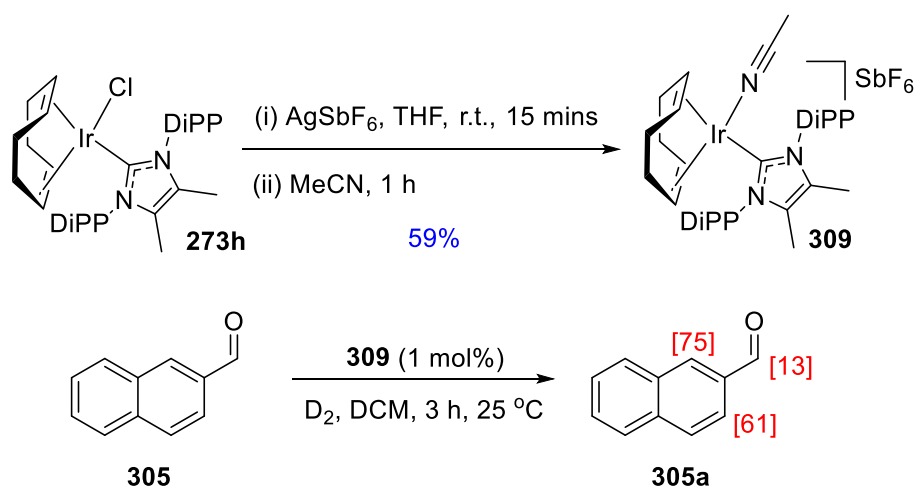
Scheme 65. Improved synthesis of d_1 -aldehyde **307p**.

In a further extension of work, it has been demonstrated that potentially air sensitive d_1 -aldehydes need not be isolated, but instead can be further derivatised in one pot (**Scheme 66**). Most notably, this allowed the method to be extended to the labelling of aliphatic aldehydes such as in derivative **308c**, with only minor D-incorporation at the enolisable sites. Such labelling cannot be achieved when using ethyl cinnamate directly.²⁴⁶

The initial success and novelty of this method, in line with the initial hypothesis, has prompted preliminary mechanistic investigations, with the ultimate aim of allowing future work to expand the mechanistic evidence and existing substrate scope. Firstly, as with sulfonamide labelling, the presence of the chloride ligand in the optimal catalyst was crucial, as its replacement with acetonitrile gave an alteration in the labelling selectivity (**Scheme 67**).



Scheme 66. One pot labelling and HWE derivatisation of d_1 -aldehydes.



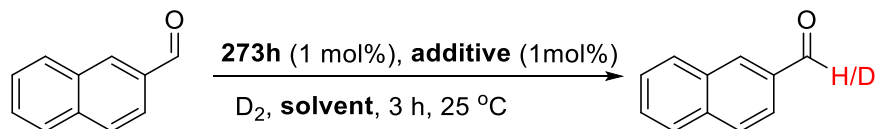
Scheme 67. Investigating the effect of the chloride ligand in formyl-selective aldehyde labelling.

Building on the test for the chloride ligand, similar experiments using various silver-based chloride abstraction additives witnessed a complete suppression of the catalysis (**Table 27, Entries 1 - 3**). Beyond this, an additive-free variation in the solvent highlighted an interesting reliance of the labelling method on DCM, and may be as a result of unique catalyst speciation (**Entries 4 - 15**). Most interestingly, even dichloroethane (**Entry 8**) – a higher boiling homologue of DCM – reduced catalyst efficiency by 49% relative to the optimal conditions. This may reflect the chelating ability and more entropically favoured coordination of DCE *versus* DCM, making it a more potent catalyst poison.

To investigate reaction intermediates, benzyl alcohol, **310**, was subjected to the optimised conditions, swapping D_2 for H_2 in order to detect any aldehyde formation. In this case, <2%

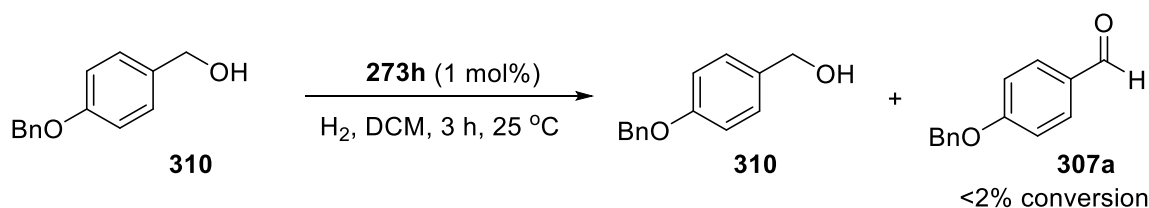
conversion of the alcohol to the corresponding aldehyde was observed, suggesting that a *hydrogen borrowing*²⁴⁷ mechanism plays only a minor role (**Scheme 68**).

Table 27. Additive and solvent effects in formyl-selective aldehyde labelling.



Entry	Solvent	Additive	% D ^a
1	DCM	AgOTf	0
2	DCM	AgSbF ₆	0
3	DCM	AgNO ₃	0
4	THF	-	0
5	2-MeTHF	-	2
6	dioxane	-	2
7	MTBE	-	2
8	DCE	-	51
9	DMC	-	0
10	DEC	-	1
11	Toluene	-	1
13	PhCl	-	4
14	PhCF ₃	-	11
15	^t AmOH	-	13

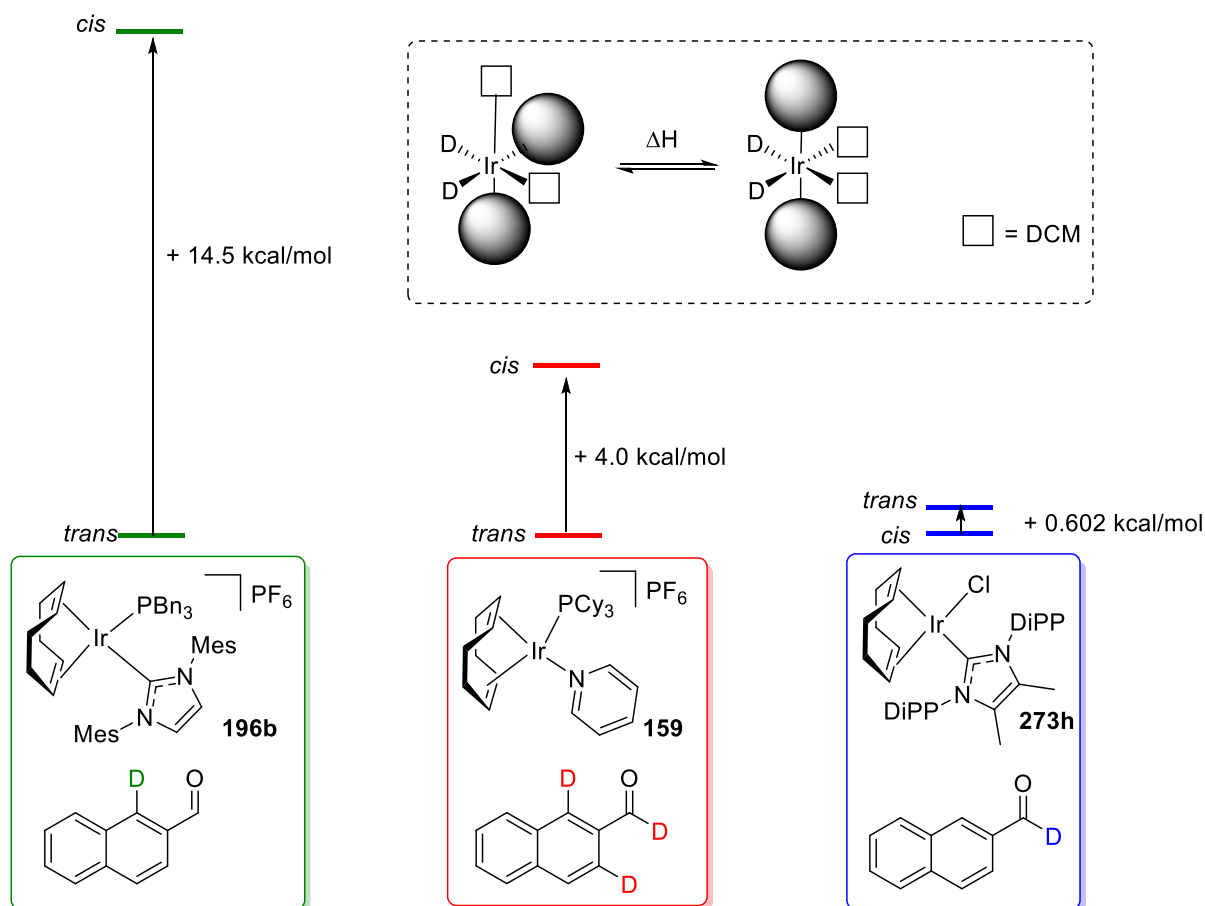
^a Formyl labelling only. No aryl labelling observed.



Scheme 68. Evidence against hydrogen borrowing in formyl-selective aldehyde labelling.

Although a comprehensive body of kinetic data is the subject of future work in this area, computational support has been used to model a proposed mechanism consistent with the initial hypothesis and all available experimental evidence. To begin, the enthalpy differences in the *cis* and *trans* isomers of representative activated catalysts were assessed (**Scheme 69**).

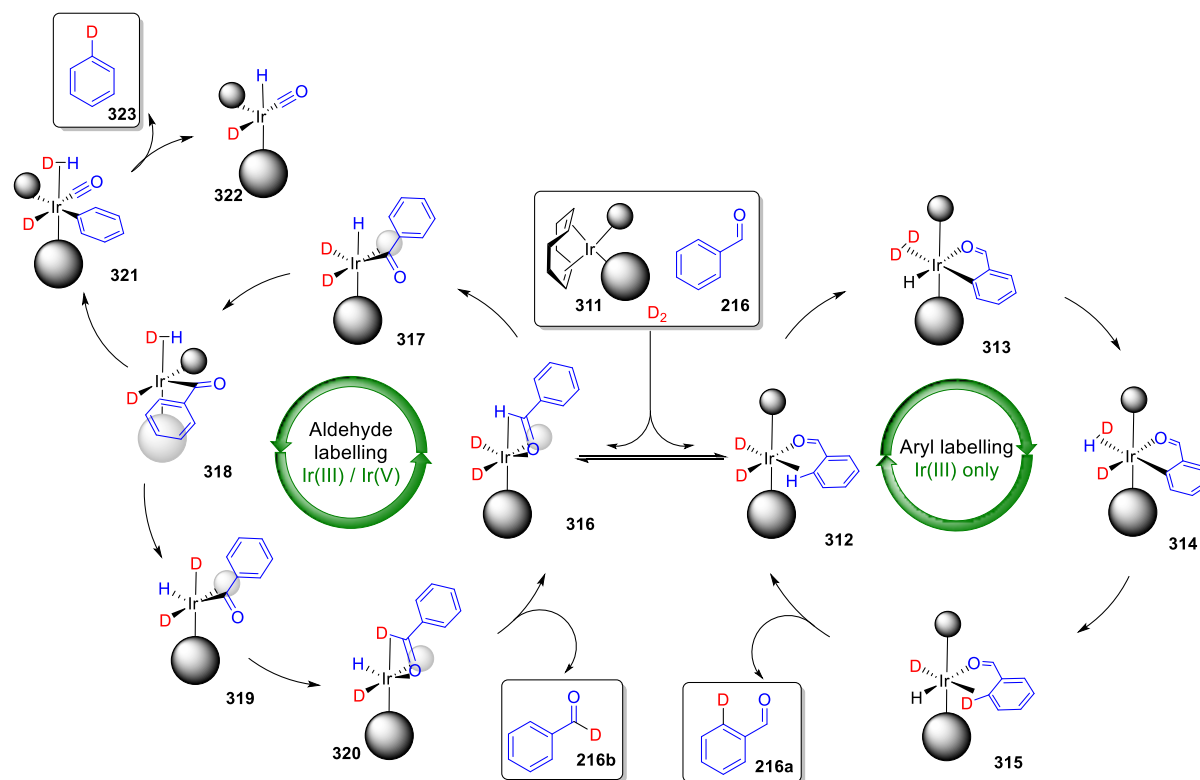
In the progression towards formyl selective labelling catalysts, the *trans/cis* energy gap diminishes. Notably, the order of *cis* and *trans* is reversed on moving to the formyl selective labelling catalyst, **273h**, with the overall energy gap being the smallest of all three catalysts.



Scheme 69. Comparison of *cis* and *trans* geometric energies for active catalysts **196b**, **159** and **273j** proposed to deliver the experimental labelling selectivities shown.

Moving forward, mechanistic processes for catalyst **273h** were investigated. Overall, three competing processes are proposed to explain the three observed products: aryl labelling, formyl labelling, and decarbonylation (**Scheme 70**). The first of these pathways proceeds *via* an all-Ir(III) cycle with *trans* ancillary ligands (**312** – **315**), as discussed extensively in earlier sections of this report. After catalyst activation, *cis* ancillary ligand geometry in **316** allows axial coordination of the aldehyde and subsequent formyl activation to give Ir(V) intermediate, **317**. Reductive elimination across two of the three hydrides gives dihydrogen complex **318**. This can return to Ir(V) *via* oxidative addition to bring a deuteride *cis* to the acyl ligand, **319**, allowing reductive elimination to give the labelled and bound aldehyde, **320**. This is the microscopic reverse of the initial activation step (**316**→**317**). At Ir(III)

intermediate **318** along the formyl labelling pathway, the productive cycle may partition to decarbonylate the acyl ligand *via* migratory insertion (**318**→**321**). Reductive elimination from **321** would yield decarbonylation by-product **323**.



Scheme 70. Proposed competing mechanisms for aryl labelling, formyl labelling, and decarbonylation.

Following extensive binding conformer comparison, the lowest energy pathways for aryl, formyl, and decarbonylative labelling are summarised on **Figure 46**. Overall, formyl labelling represents the lowest energy pathway, despite the starting intermediate, **316a**, being significantly destabilised relative to that for aryl labelling, **312**. The formyl C-H activation (**316a**→**317**) is predicted to be enthalpically flat on the PES with the Ir(V) – Ir(III) reductive elimination (**317**→**318**) being rate-limiting. Using intrinsic reaction coordinate calculations, the formyl activation step is seen to be coupled with a rotation of one *iso*-propyl group on the ligand to accommodate the substrate (**317** in **Figure 46**). Conversely, the barrier to the classical *ortho*-labelling process from **318** is unproductively high relative to formyl labelling. Finally, the partition towards decarbonylation represents the most energetically unfavourable of all these processes at the catalytically-relevant temperature (298.15 K), and is in qualitative agreement with only trace observation of such products when using catalyst **273h**.

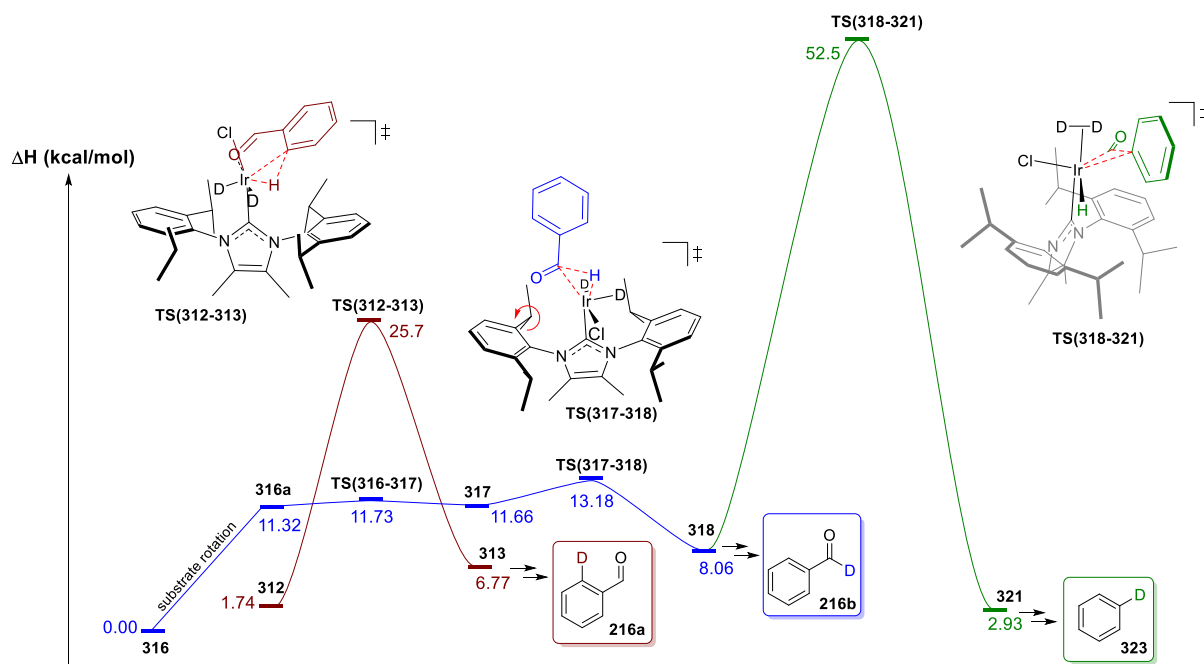


Figure 46. Informative sample of relative PESs for formyl (blue), aryl (red), and decarbonylative labelling (green).

The model for selective aldehyde labelling can also help rationalise other observed phenomena. The degree of aryl labelling in **307a** is higher than in any other substrate, whilst formyl labelling remains near quantitative. On comparing the energetics of aryl activation for benzaldehyde and *p*-hydroxybenzaldehyde, **307b** (a computationally cheaper analogue of **307a**), both possessed almost identical enthalpy of activation but the latter was less endothermic and less reversible (**Figure 47**).

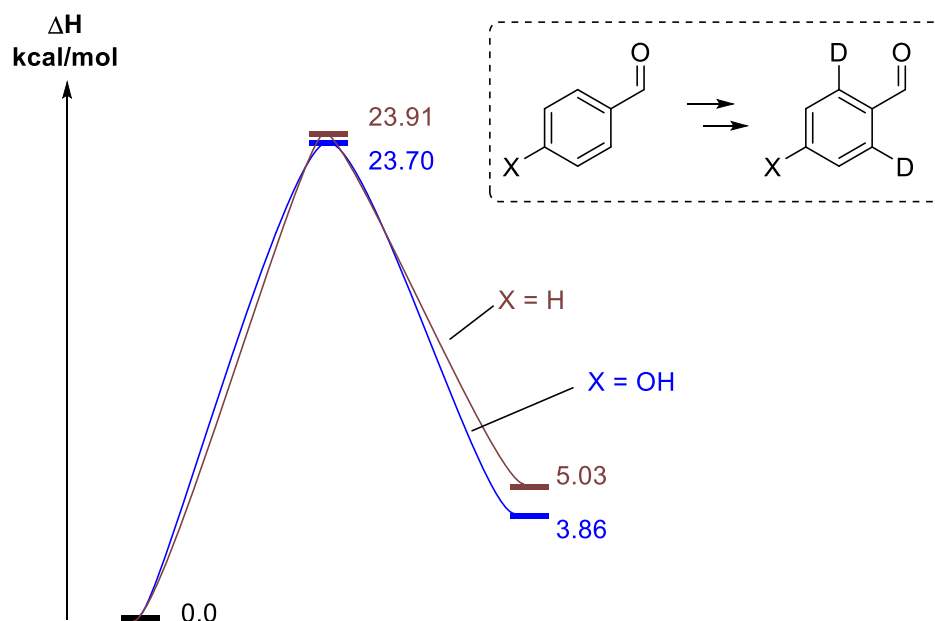


Figure 47. Differences in aryl activation PES for electron-rich aldehydes.

The model proposed can also be used to explain the higher degree of decarbonylation observed when using catalysts smaller than **273h**. As part of the design of **273h**, the large NHC (IPr^{Me}) serves to destabilise the barrier to decarbonylation, which requires an increase in Ir coordination number from 5 to 6 (**318**→**321**). On modelling this step, the smaller catalyst, **273f**, was found to proceed through a lower energy transition state and thus a more stable decarbonylated intermediate (**Figure 48**). This is in agreement with experimental observation (*vide supra*).

In summary, computational ligand design has been used in combination with experiment to produce a novel, mild, and highly selective method for formyl labelling of aldehydes. This method has been deployed to improve the synthetic route towards valuable aldehyde **307p**, and can be employed as a one-pot process in further derivatisation of the aldehyde moiety. Computational analysis supports a competition between an Ir(III) catalytic cycle for aryl labelling, and Ir(III)/Ir(V) cycles for formyl labelling and decarbonylation. Future work will focus on strengthening the kinetic understanding of formyl labelling such that the substrate scope can be extended to *ortho*-substituted and heteroaromatic aldehydes.

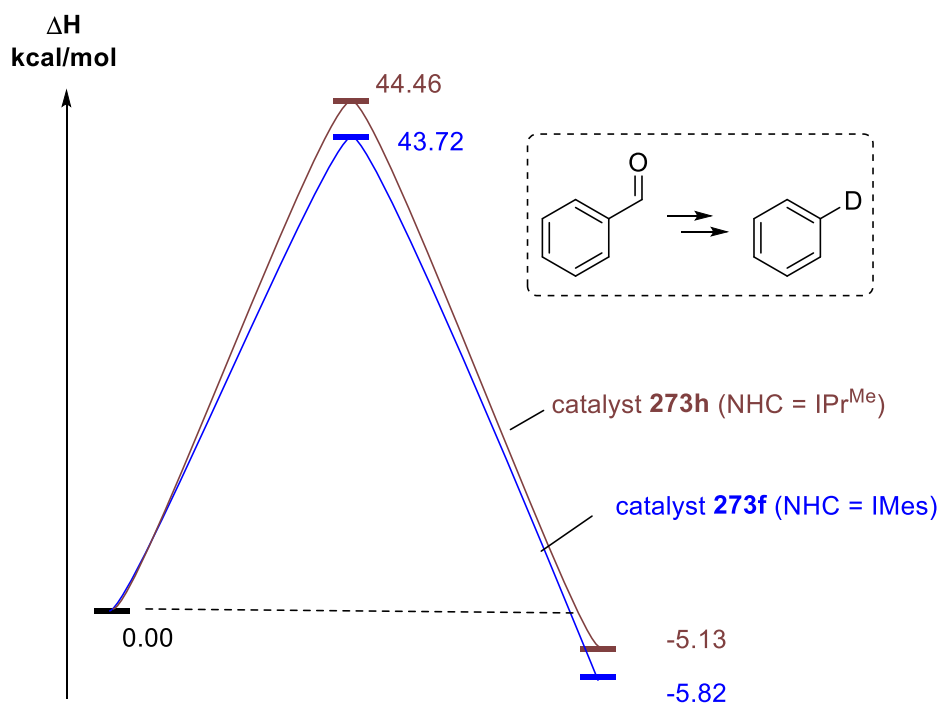
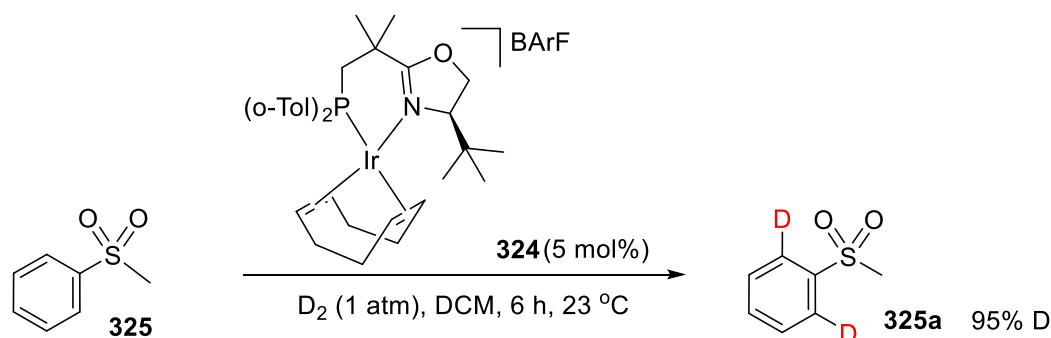


Figure 48. Lower energy decarbonylation pathway for a smaller chloro-carbene catalyst.

5.4 On the Fundamentals of Chelating Ligand Design Towards Novel HIE Technologies

Chelating, bidentate ligands are ubiquitous in organometallic chemistry, with their importance to Ir-catalysed HIE having already been made clear through catalysts such as **163** (*vide supra*).^{66,98,102} Interest in this ligand class within HIE was recently revalidated by Muri and Pfaltz, who serendipitously discovered that catalyst **324** was highly efficient in *ortho*-labelling the otherwise elusive aryl sulfone moiety, **325** (**Scheme 71**).¹¹⁸ As yet, no explanation has been offered to rationalise the catalyst performance/design or, indeed, how it compares to other such ligands. Given our interest in mixed NHC/phosphine ligation, some bidentate NHC/phosphine variants of interest are shown in **Figure 49**.



Scheme 71. Muri and Pfaltz's system for efficient labelling of the weakly-coordinating sulfone directing group.

Building on catalyst design by comparative ligand parameterisation, it was hypothesised that methylphenylsulfone, **325**, could be used as a *probe molecule* in binding energy calculations aimed at assessing chelating ligands *via* one, quantitative descriptor (**Figure 50**). Using the counterpoise method,²⁴⁸ the binding descriptor (ΔE_{bind}) would capture favourable interactions of the substrate stabilising the catalyst, and destabilising deformations of substrate/ligand structure caused by steric clashes. Based on the findings from **Figure 42**, **Figure 43**, and **Figure 46**, more favourable binding energies are assumed to be a suitable proxy for lower energy C-H activation pathways, even if the pre-activated complex is not the most stable available conformer. This offers a new paradigm for ligand description, such that mono- and bidentate ligand spheres may be compared *on the same basis*.

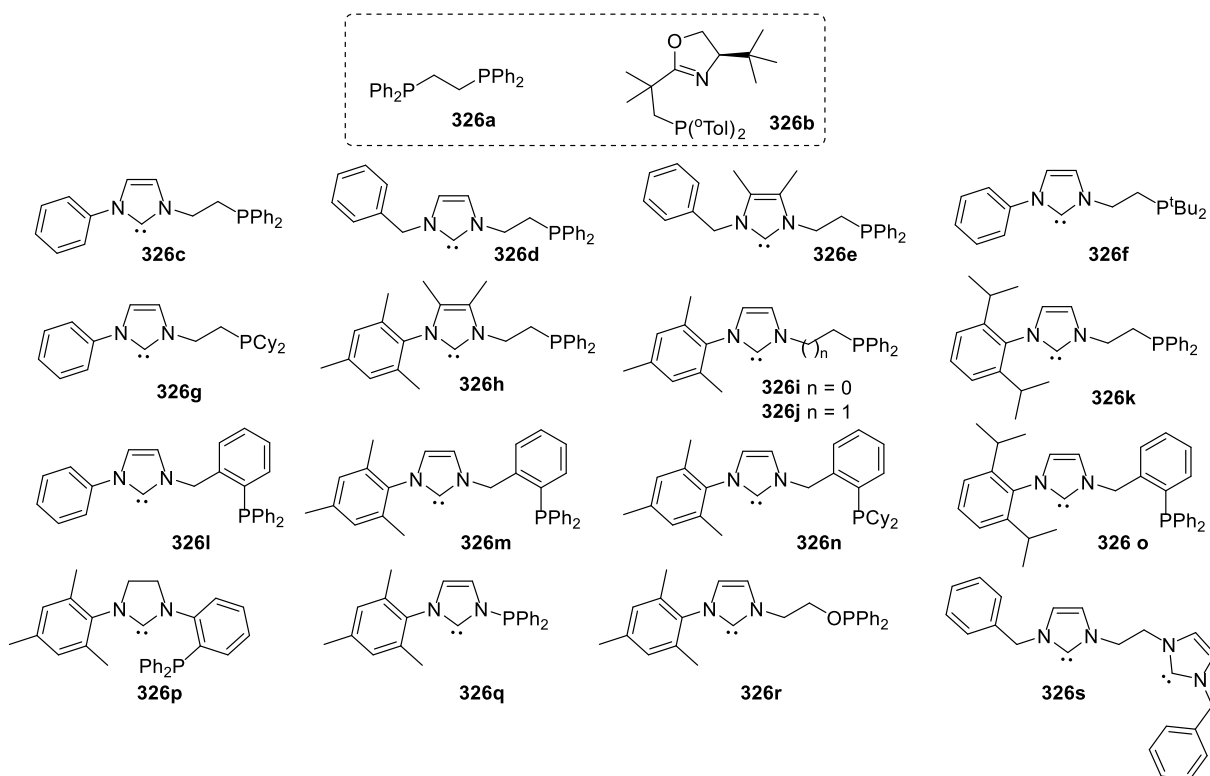


Figure 49. Chelating ligands discussed in this report.

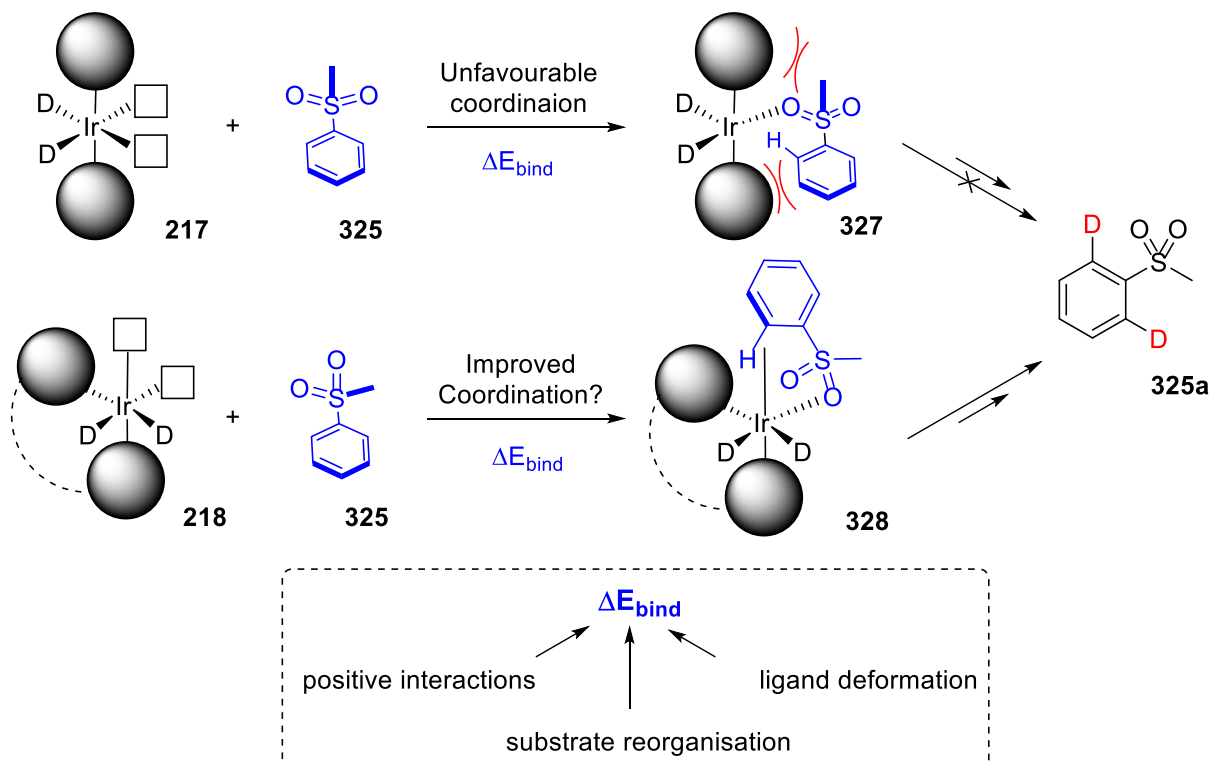


Figure 50. Using a probe molecule to deliver a combined model for mono- and bidentate ligands in Ir-catalysed HIE.

The overall result of this approach is summarised in **Figure 51** for all ligands described in **Figure 49**. As points of reference, these results include the binding energies of acetophenone and methylphenylsulfone to benchmark IMes/PPh₃ catalyst **196a** (**326t** and **326u**, respectively), as well as the binding of methylphenylsulfone to the IMes/Cl catalyst, **326v**. This highlights the added depth to this new theoretical approach. Not only can mono- and bidentate catalysts be easily compared on the same basis, but different *substrates* (and their ability to bind to different catalysts) can also be assessed.

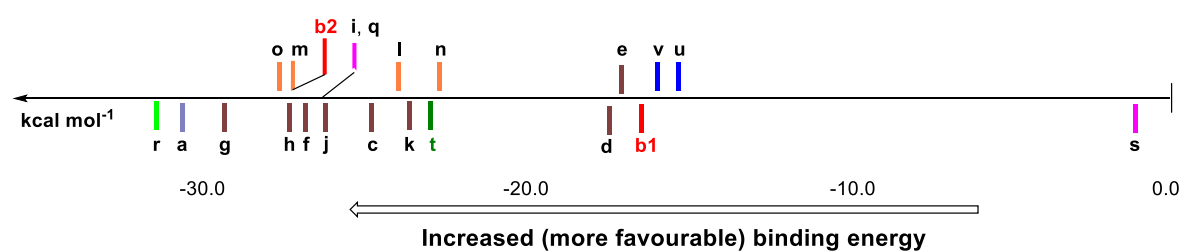
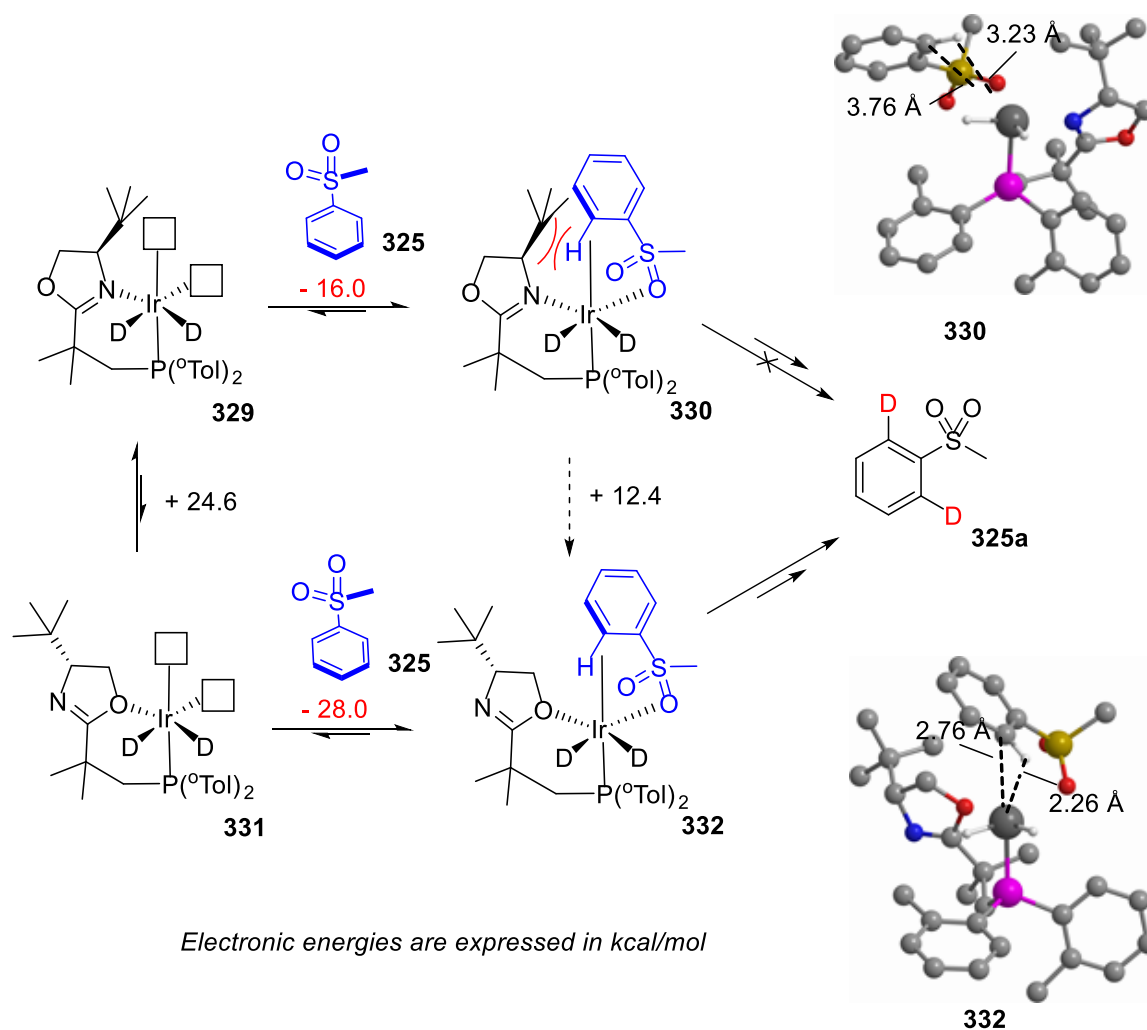


Figure 51. Scale of ΔE_{bind} for methylphenylsulfone binding to chelating catalyst based on ligand class **326**.

As a first consideration from the ΔE_{bind} calculations, a hypothesis for the origins of efficiency in the Muri/Pfaltz system can be offered (**Scheme 72**). Within the oxazoline portion of the ligand bound to iridium *via* the more energetically favourable nitrogen atom (**b1** in **Figure 51**), sulfone **325** binds to **329** yielding **330** with a favourable $\Delta E_{\text{bind}} = -16.0$ kcal/mol. Alternatively, it is envisaged that the oxazoline may undergo a *N/O*-isomerisation to give less stable isomer **331** (**b2** in **Figure 51**), which binds **325** with a far more significant $\Delta E_{\text{bind}} = -28.0$ kcal/mol. Furthermore, although pre-activated complex **332** is still energetically less stable than **330**, the sulfone is more favourably positioned for subsequent C-H activation (compare DFT representations of **330** *versus* **332**). This is supported by the fact that the C-H bond to be activated is lengthened in isomer **332** (1.10Å) relative to isomer **330** (1.09Å). Therefore, this inceptive example is believed to strengthen the case for ΔE_{bind} being an informative parameter in assessing the propensity for a given ligand sphere to support C-H activation of a weakly coordinating substrate such as **325**.



Scheme 72. Proposed ligand isomerisation mechanism for the Muri/Pfaltz sulfone labelling catalyst with key ΔE_{bind} values in red.

Starting from ΔE_{bind} values, other interesting ligand comparisons can be drawn. Firstly, the worst predicted sulfone binding energies relate to the catalyst from bis-carbene ligand, **326s** ($\Delta E_{\text{bind}} = -1.0$ kcal/mol). In this case, the poor sulfone binding can be attributed to the relative stability of the unbound dihydride catalyst, **218**, where coordination is blocked due to the π -complexation of the benzyl side arms (**Figure 52**, top). This is made clearer by comparison with more efficient binding catalysts derived from ligands **326j** and **326k** (**Figure 52**, middle and bottom, $\Delta E_{\text{bind}} = -23.7$ and -27.0 kcal/mol, respectively).

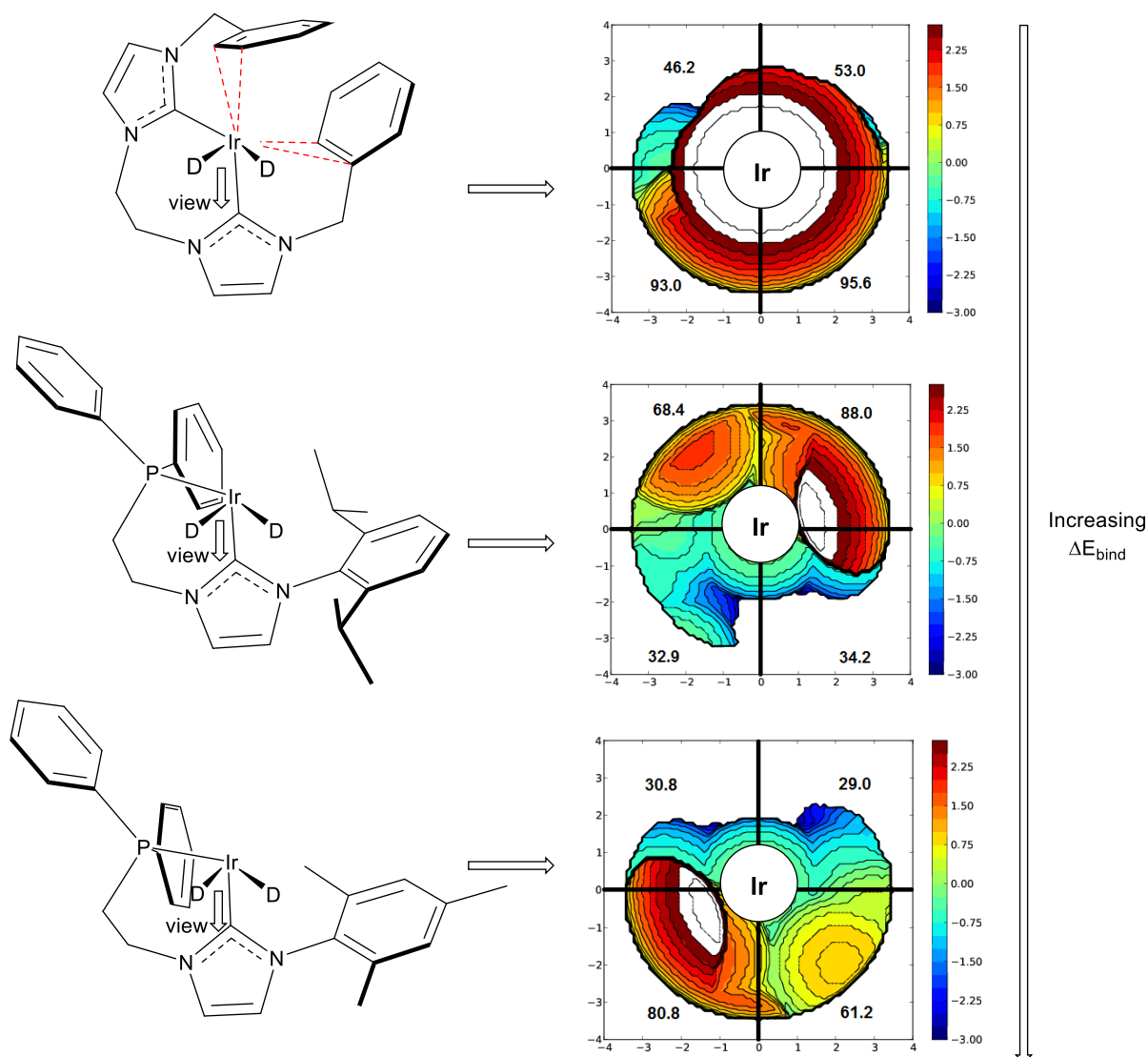
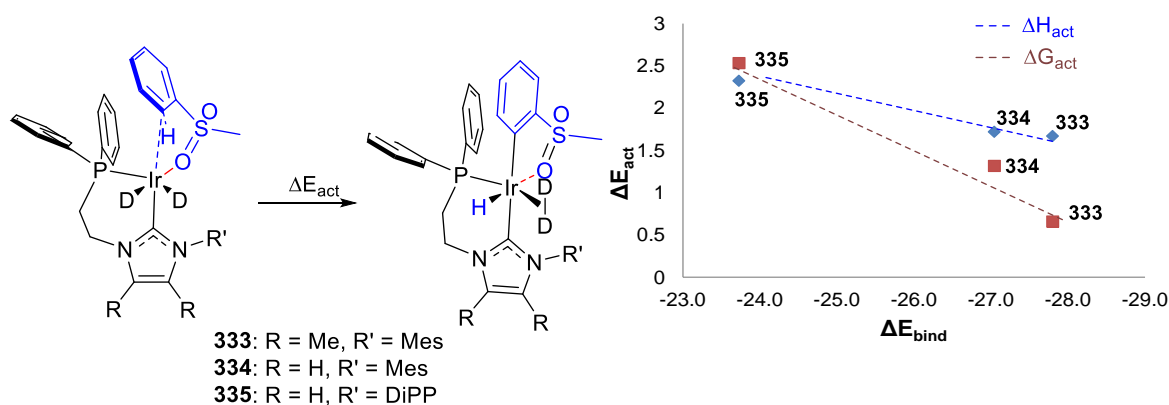


Figure 52. Tuning steric bulk to achieve better substrate binding.

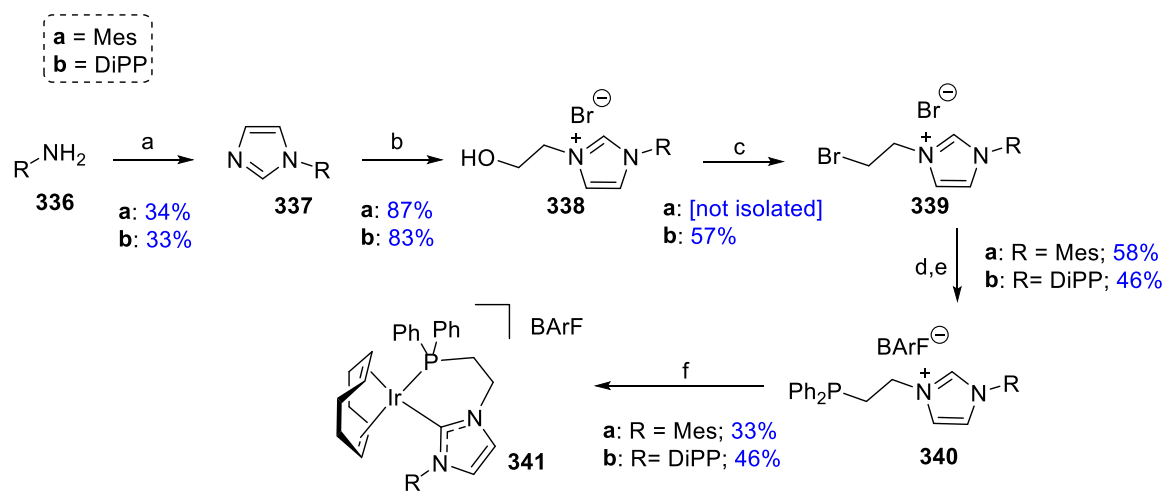
For a select number of cases, ΔE_{bind} was compared to the change in energy, ΔH , following sulfone C-H activation (**Scheme 73**). As hypothesised, efficient binding appears to be a suitable proxy for the overall efficiency of the C-H activation step en route to deuterium labelling.



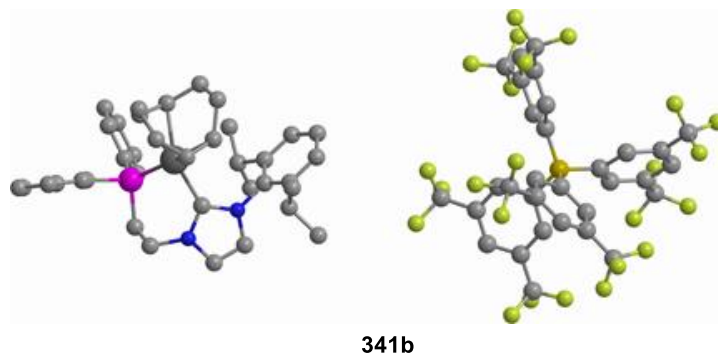
Scheme 73. Correlation between ΔE_{bind} and energy of C-H activation.

As a more rigorous proof-of-concept, catalysts based on NHC/phosphine bidentate ligands **326j** and **326k** were targeted. These examples represent ligands borne from the same substructure but which possess distinct ΔE_{bind} values, as previously calculated (*vide supra*). Steps a – c for the syntheses depicted in **Scheme 74** are derived from literature procedures,²⁴⁹ whilst the combined phosphide displacement/salt metathesis (steps d and e), and final catalyst synthesis (step f) were novel (see **Experimental** section for full details). In the case of catalyst **341b**, the expected monometallic chelated NHC/phosphine structure was confirmed unequivocally by X-ray crystallography.

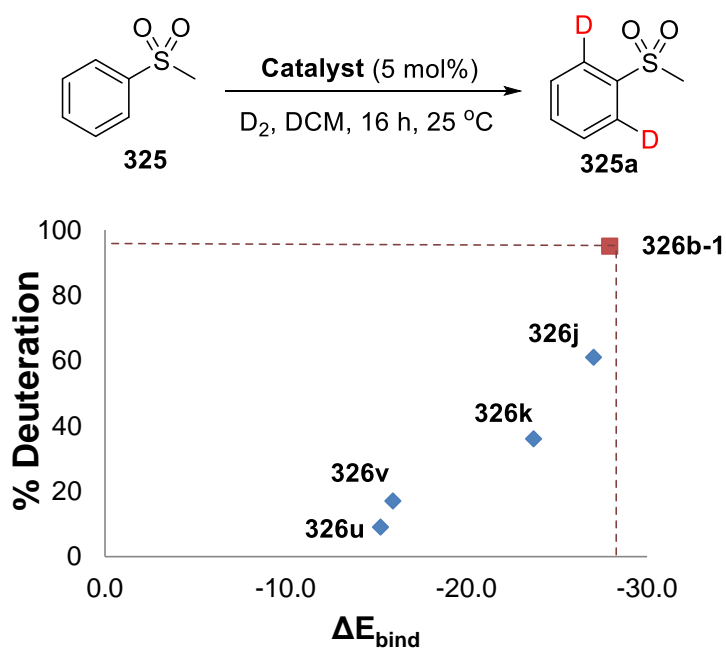
With novel chelated Ir complexes **341a** and **341b** in hand, their efficiency in the labelling of methylphenylsulfone was compared, both against one another (see **326k** *versus* **326j**) and against previously utilised monodentate catalysts, **196a** and **207** (**326u** and **326v**, **Scheme 75**). Encouragingly, catalyst efficiency was seen to improve markedly with ΔE_{bind} value, with catalyst **346** showing the most dramatic improvement over monodentate analogue **196a** (61% D *versus* 9% D, respectively), and the Muri/Pfaltz system remaining the most efficient overall. Indeed, novel catalyst, **346**, could instil an excellent 83% D in **325** when the same reaction was run at 35 °C (see **Experimental** section). Future work can now focus on targeting those NHC/phosphine systems predicted to deliver even better ΔE_{bind} values, with the ultimate aim of delivering a more easily synthesised and mechanistically better understood catalyst than the current Muri/Pfaltz system.



Conditions: (a) formaldehyde (37% w/w in H₂O), glyoxal (40% w/w H₂O), NH₄OAc, AcOH, 70 °C, 16 h; (b) Br(CH₂)₂OH, toluene, 110 °C, 16 h; (c) PBr₃, DCM, 0 °C - r.t., 16 h; (d) Ph₂PH, KOtBu, DMSO, r.t., 1 h; (e) NaBArF, DCM/H₂O (1:1), r.t., 16 h; (f) [Ir(COD)Cl]₂, KOtBu, THF, r.t., 1 h.

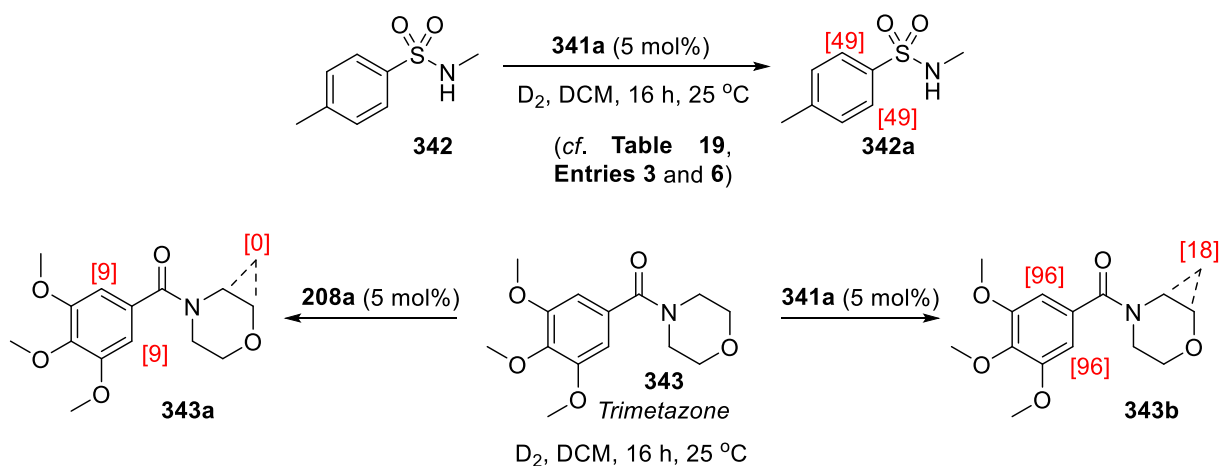


Scheme 74. Synthesis of novel chelating ligand catalysts **341a** and **341b**, with X-ray confirmed structure of **341b**.



Scheme 75. Proof-of-concept reactions for labelling methylphenylsulfone based on ΔE_{bind} design of ligand group **326**.

As mentioned above, the ΔE_{bind} method uses methylphenylsulfone as a *probe molecule* – a difficult-to-label species that serves as a computational means of comparison between mono- and bidentate catalysts. In extension, this parameter is designed to direct catalyst design beyond labelling sulfones. Pleasingly, this has been demonstrated effectively by employing novel catalyst **341a** in other unexplored *ortho*-labelling challenges. For the first time with NHC/phosphine based HIE catalysts, appreciable levels of D-incorporation in a secondary sulfonamide, **342**, have been recorded at room temperature (**Scheme 76**, top). Further still, novel catalyst **341a** has been employed as a highly efficient catalyst in labelling sterically hindered amide drug molecule, *Trimetazone*, **343**, where the monodentate catalyst, **208a**, proved ineffective (**Scheme 76**, bottom).



Scheme 76. Novel reactivity for bidentate catalysts beyond sulfone predictions.

In summary, a novel approach to comparative modelling of mono- *versus* bidentate ligands has been revealed. Using a challenging probe molecule, counterpoise-corrected binding energy calculations have guided the understanding of the existing Muri/Pfaltz sulfone labelling catalyst, **324**, and how it compares to novel bidentate NHC/phosphine ligands of interest within our group. This concept has been demonstrated *via* the synthesis and testing of two novel chelating HIE catalysts, **341a** and **341b**, in the labelling of **325**. In line with theoretical predictions, these systems represent the most efficient NHC/phosphine based room-temperature HIE catalysts to date. Additionally, probe molecule binding energy calculations have proven to be an excellent proxy for the discovery of new labelling reactivities distinct from the more thoroughly explored monodentate catalysts. Namely,

routes to efficient room-temperature labelling of secondary sulfonamides and sterically hindered amides have been identified, and will be the subject of intense future work.

6. Conclusions

In this report, a range of experimental and theoretical techniques have been introduced (and used in tandem) to facilitate a broader understanding and predictive power of catalyst design in *ortho*-directed hydrogen isotope exchange processes.

For the purposes of scale up and commercialisation, benchmark catalysts **196a** – **196c** have been synthesised by a higher yielding and scalable route²⁵⁰ to that already published (**Scheme 38, Table 4**).¹¹⁴ This has resulted in the ongoing commercial access to these globally-utilised catalysts in collaboration with Strem Chemicals, Ltd (**Figure 53**).

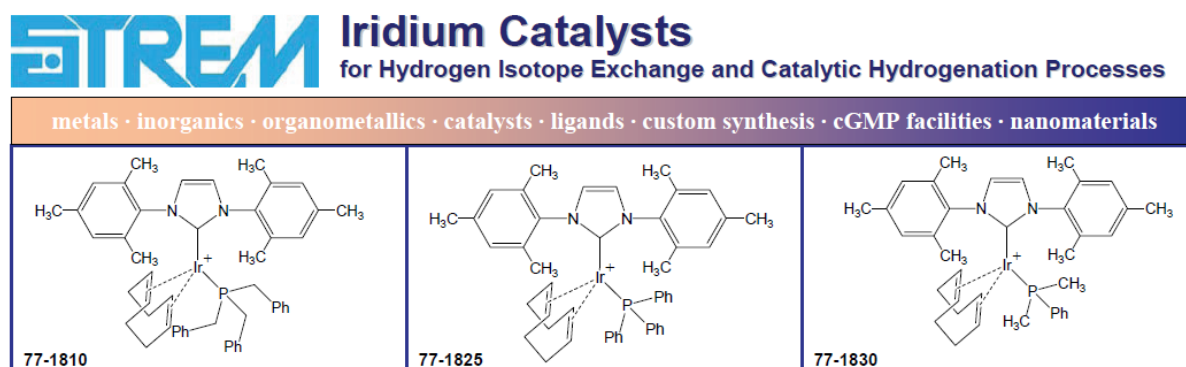


Figure 53. Commercial advertisement for catalysts **196a** – **196c**.

An improved perspective on catalyst synthesis has led to successful exploration of counterion effects in HIE catalysis. Crucially, this is now allowing such catalysts to be employed at reduced catalyst loadings, and across a significantly broader scope of industrially and environmentally acceptable solvents (**Figure 54**). The preliminary findings from this work have now been published in the primary literature.²⁵¹

Capitalising on the improved solvent dependence of novel catalyst **208a**, a base-mediated method for the *ortho*-deuteration of unprotected tetrazoles has been realised (**Scheme 77**). This method represents a rare example of C-H activation with unprotected tetrazoles. It has been applied to both simple and more complex drug-like substrates, and represents a new mode of reactivity for HIE catalysts beyond simple D₂ activation.

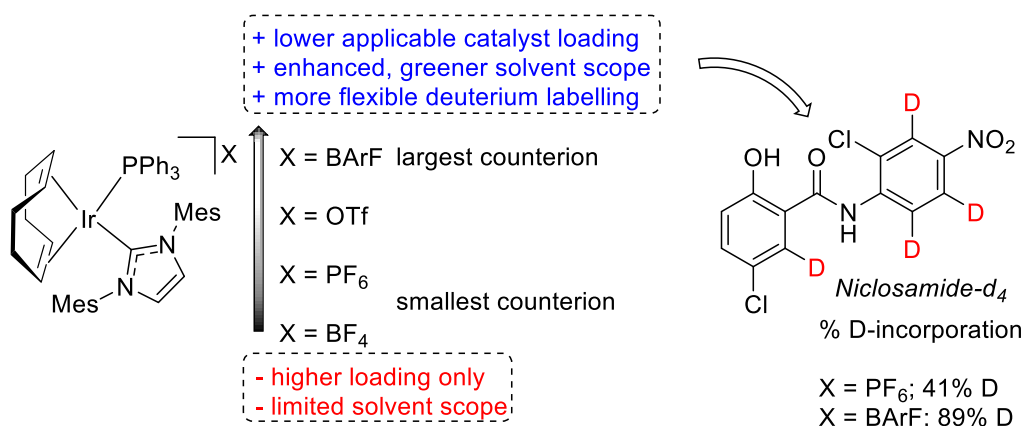
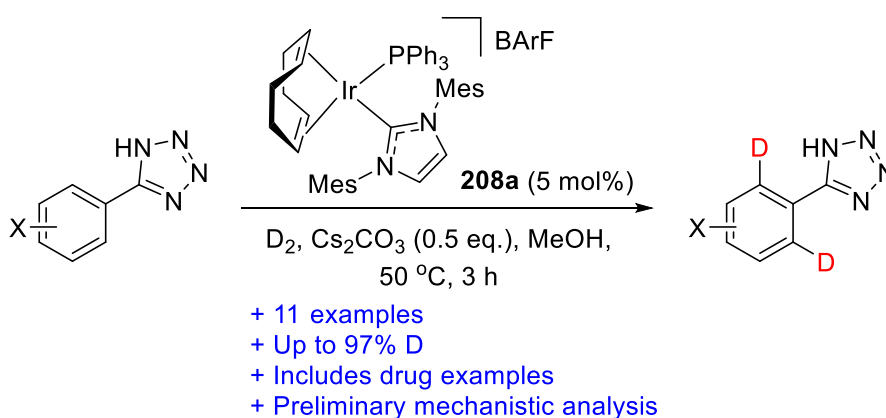


Figure 54. Summary of published aspects of project on anion effects in HIE.



Scheme 77. Summarised outcomes of project on Ir-catalysed *ortho*-deuteration of unprotected tetrazoles.

Establishing the wide-reaching theme of this report, experimental and computational (DFT) methods have been used to offer methods of assessing the *combined* influence of two ancillary ligands, rather than assessing each ligand individually (**Figure 55**). Carbonyl and hydride complexes of iridium provided experimental verification for the subsequent development of a combined ligand map, derived from *principal components analysis* (**Figure 26** and **Figure 27**).

Based on the aforementioned ligand parameterisation and mapping efforts, several challenges in Ir-catalysed HIE have been assessed *via* rational catalyst design. As part of a broader exploration into novel catalyst architectures, the first total synthesis of the simple, imidazolium-based natural product, *Lepidiline A* was realised. Using this compound as an NHC precursor, a series of six novel HIE catalysts was synthesised, using a silver-mediated, operationally simple synthetic route developed herein. Through this work, the PCA model

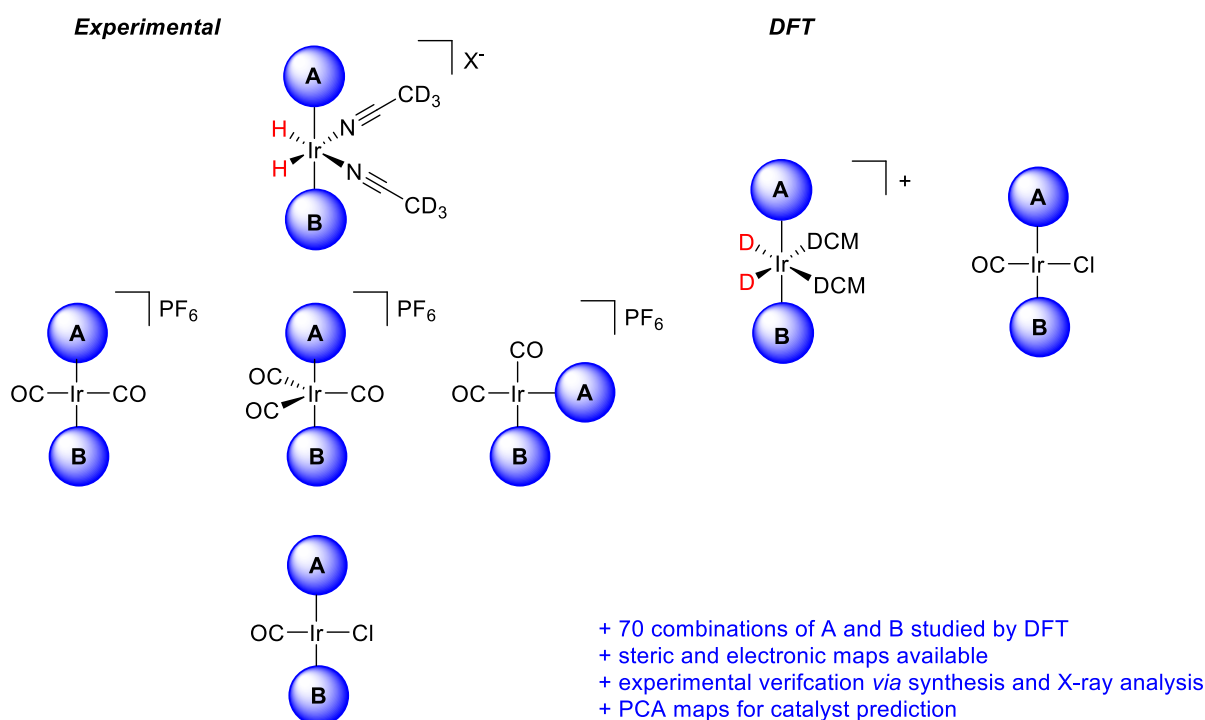
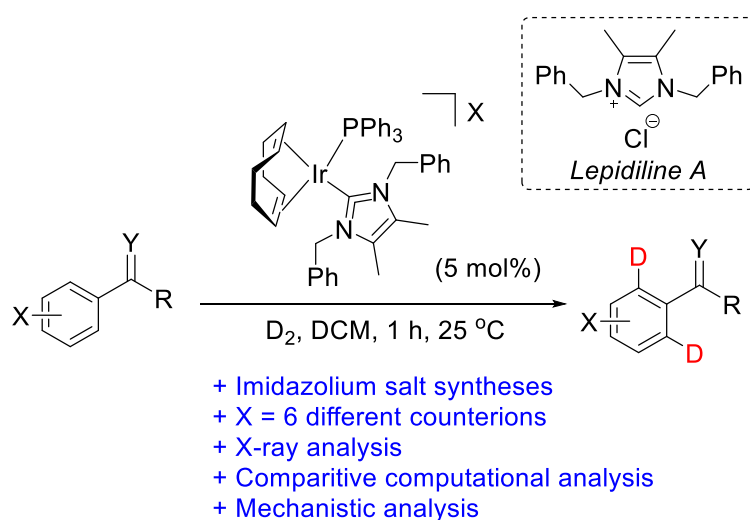


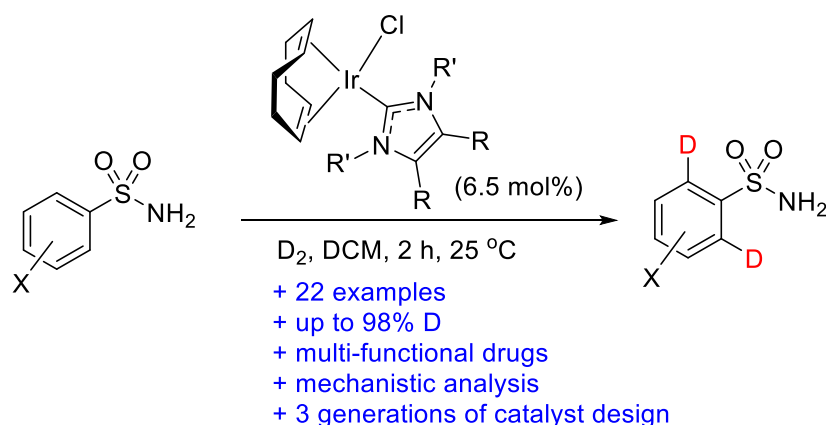
Figure 55. Experimental and DFT structure exploration in assessing combined ligand effects.

was used to decipher the importance of the 4,5-dimethyl substitution in the NHC ligand. Where it was originally hypothesised that extra methyl groups would increase both the size ($\%V_{bur}$) and electron-rich nature (νCO) of the resultant iridium catalyst, our combined experimental and theoretical outlook revealed that only the latter parameter was influenced (**Scheme 78**).



Scheme 78. A case study in catalyst design using data from PCA model.

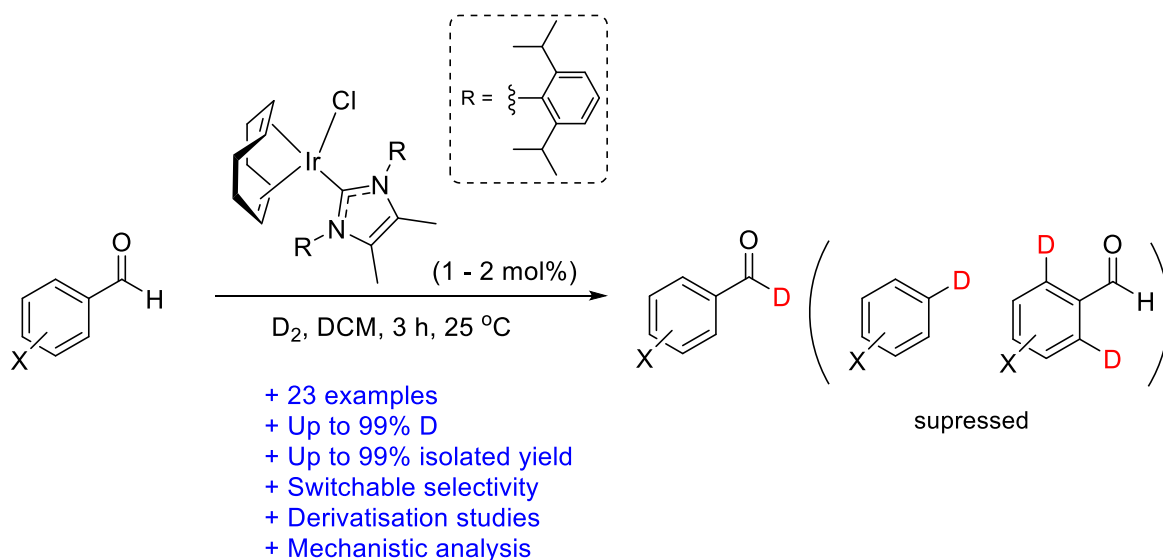
In another successful exploitation of the ligand mapping explored in this report, the first mild catalytic method for the labelling of primary sulfonamides has been developed. In depth mechanistic analysis of labelling multifunctional sulfonamide drugs has led to a vastly improved understanding of labelling chemo- and regioselectivity, where substrate binding has been invoked as a key, product-determining step (**Scheme 79**). The initial method development has now been published,²⁵⁰ with later catalyst redesign studies to follow.



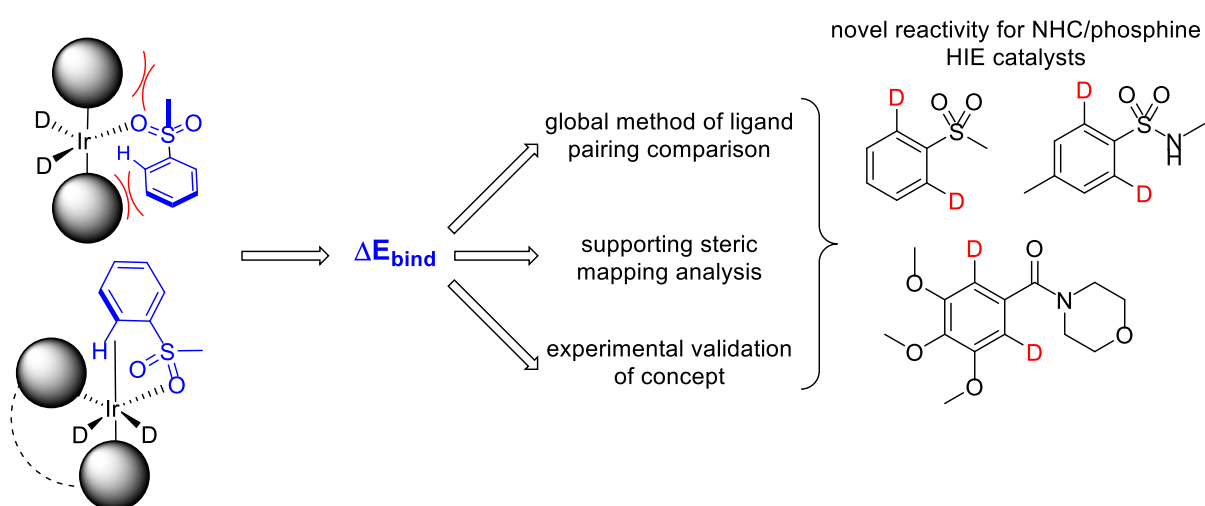
Scheme 79. Summarised outputs from method development for labelling 1° sulfonamides.

In a similar vein to sulfonamides, rational catalyst design has led to the first study on switchable selectivity in labelling aromatic aldehydes (**Scheme 80**). With particular focus on formyl selectivity, this work represents the first direct, mild, and formyl-selective aldehyde labelling method. Unlike labelling sulfonamides, this project explored labelling selectivity originating from different mechanisms, rather than different binding patterns within the same mechanism.

Finally, preliminary studies have established probe molecule binding energy calculations as a new method of comparing mono- and bidentate ligand partnerships within one analytical regime (**Scheme 81**). This method has been used to offer a theoretical explanation of an existing sulfone labelling catalyst, and in the accelerated discovery of previously unattainable reaction modes for NHC/phosphine HIE catalysts.



Scheme 80. Summarised outputs from method development for formyl-selective aldehyde labelling.



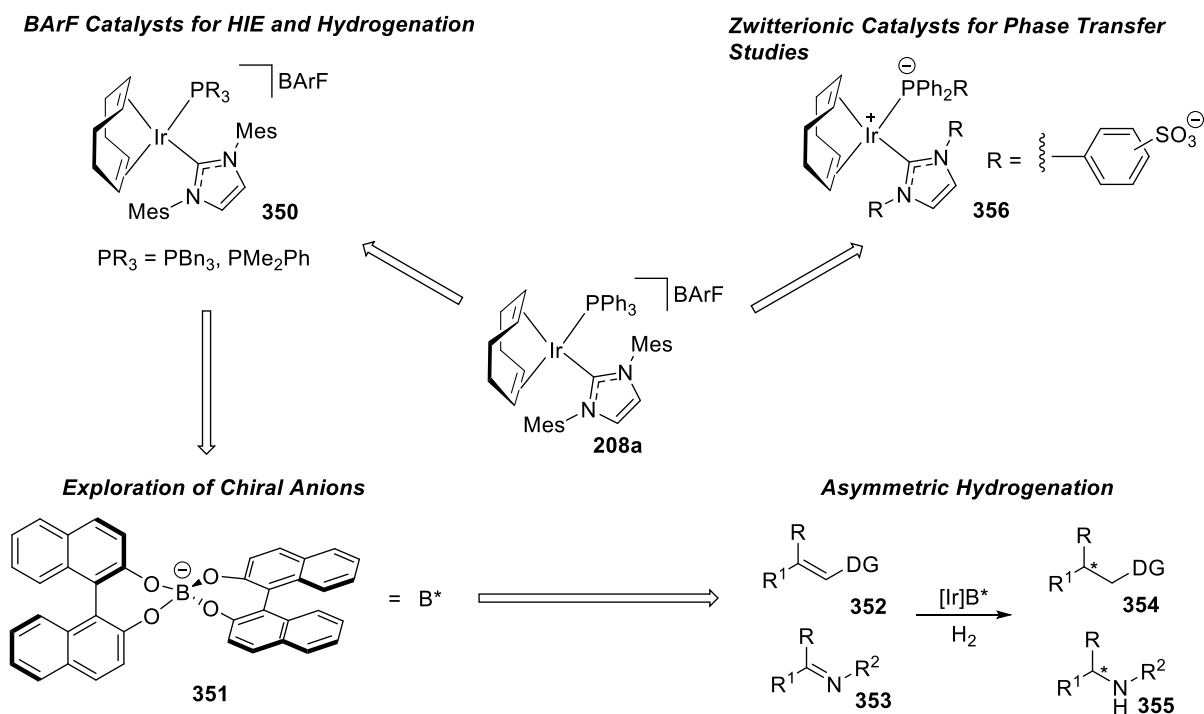
Scheme 81. Summarised proof-of-concept studies for using ΔE_{bind} as a theoretical precursor to reaction discovery.

7. Future Work

This report has served to demonstrate that reaction development can benefit tremendously from being coupled to mechanistic and computational studies. As such, it is proposed that this method of enquiry be carried forward into future developments within the field. To this end, possible future projects are detailed below and, where appropriate, proof-of-concept results are provided (full details under the **Future Work** subheading in the **Experimental** section).

Having established the anion effects relative to Ir-catalysed HIE using catalyst **208a**, BArF analogues other existing PF₆ catalysts should be explored, namely **350** in the first instance. Beyond HIE, it is envisaged that such complexes can improve on existing efforts in related hydrogenation chemistries (**Scheme 82**).⁷⁷ Further to this, chiral derivatives of the BArF anion should be explored in studies towards asymmetric hydrogenation catalysts bearing non-chiral ligands. In a final extension to the anion work presented herein, ligands bearing charged tags may be explored such that an inner sphere ligand also plays the role of catalyst ‘anion’, forming formally zwitterionic iridium complexes. This is now being pursued *via* phosphine ligands, such as in **356**. Such complexes may also offer a functional handle with which to deliver catalysts functional under phase transfer conditions.

In line with studies on *Lepidiline A*, it is proposed that the *N,N'*-diphenylmethyl substitution pattern will provide an interesting line of enquiry for HIE and related studies. The NHC produced from the chloride analogue of salt **357** has been utilised in previous studies within the Kerr group but without the successful preparation of any complexes of type **358**.¹⁴⁷ In more recent times, this author has developed a counterion-flexible synthetic route to such complexes.¹⁵³ Initial experimental and PCA analysis of the PPh₃ coupled complex suggests a uniquely electron-poor system relative to other HIE catalysts (see, for example, **Table 28**).

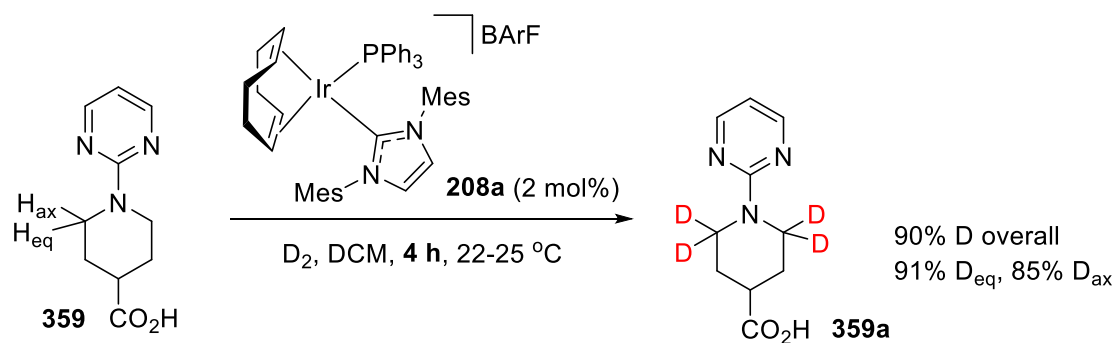


Scheme 82. Proposed future work on exploration of anion effects in Ir-catalysed reactions.

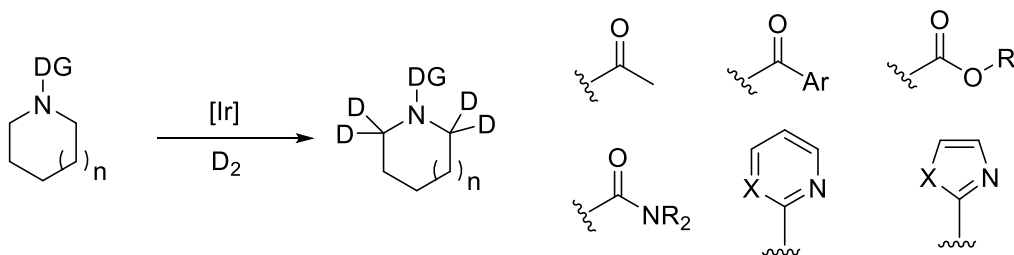
Table 28. Proposed study of electron-poor IDiphen complexes.

Entry	Complex	$\Sigma V_{bur,211}$	$\nu(\text{CO})$	$\Delta(\Sigma V_{bur})^2$
1	358	57.8	2019.89	1.4
2	214	55.7	2014.02	0.5
3	196a	60.2	2009.26	0.1

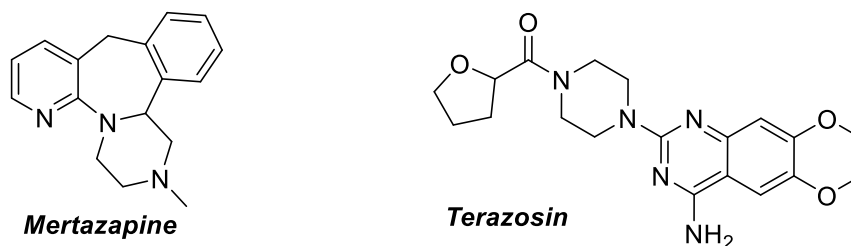
In a direct extension of the improved scope of catalyst **208a**, it has recently been discovered that such complexes effectively catalyse sp^3 -deuteration under unprecedentedly mild conditions (**Scheme 83**).¹⁰⁵ Consequently, the applicable scope of this reactivity should be explored towards the ultimate aim of labelling drug molecules such as **359**. In a still wider reaching arm of this study, the observed (albeit minor) selectivity for equatorial over axial labelling should be explored in order to develop a so-called *enantiolabelling* strategy.



Alternative Directing Group Exploration

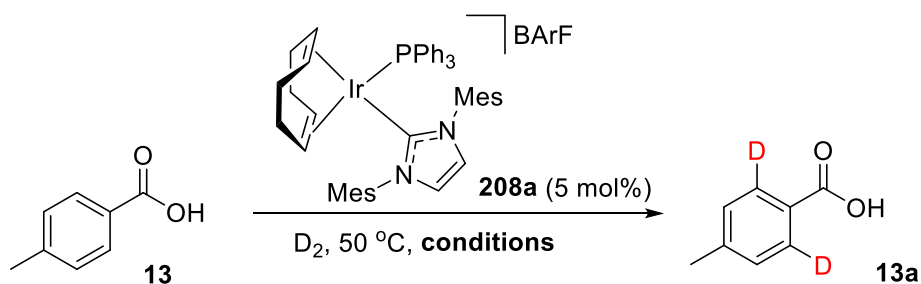


sp³ labelling of drugs



Scheme 83. Future working in sp³-labelling chemistry.

With a view to establishing new modes of precatalyst activation for **208a**, full mechanistic analysis should be pursued for the tetrazole labelling methodology. Indeed, it has already been shown that the optimised conditions do *not* readily extend to carboxylic acid derivatives, where in fact newly optimised conditions have begun to be explored (**Scheme 84**). Beyond mechanistic curiosity, understanding the role of precatalyst **208a** under basic conditions in protic solvent will aid in uncovering the ability of these catalysts to extend to use in transfer hydrogenation chemistries.^{247,252}



Condition A: MeOH, Cs₂CO₃ (0.5 eq.), 3 h; 37%D

Condition B: MTBE, DIPEA (0.5 eq.), 16 h; 89%D

Scheme 84. Low reactivity of carboxylic acids under tetrazole labelling conditions and current progress towards reoptimisation.

In relation to holistic modelling and PCA data, the predictive power of such techniques can be increased by the overlay of an experimentally-derived *catalyst scoring system*. It is hereby proposed that this may be achieved *via* a mechanically simple and easy-to-analyse parallel synthesis technique (carousel coupled with ¹H NMR). ‘Cherry-picked’ catalysts presenting different areas of the presented PCA maps would be subjected to labelling a finite number of representative substrates under the most testing conditions possible (low catalyst loading, short reaction time). Ultimately, the resulting ‘score’ for each catalyst may be represented in the form of a classical Nightingale Rose diagram (**Figure 56**). This directional plot can be used to overlay the results from distinct catalysts, allowing complementary modes of substrate reactivity to be made more visually apparent. The examples provided below would show that **Catalyst 1** is selective for substrate types *a* and *b*, whereas **Catalyst 2** is better for labelling substrate types *d* and *e*. Alternatively, **Catalyst 3** is unselective but globally applicable. This system is currently being piloted with further catalyst derivatives of *Lepidiline A*.

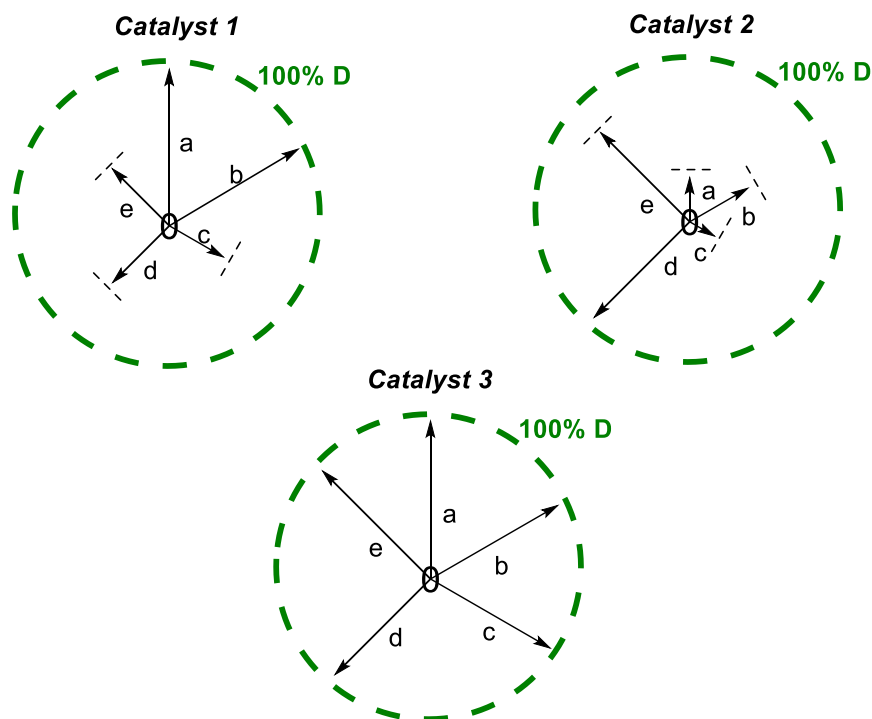


Figure 56. Generalised representation of proposed catalyst scoring system.

Moving to the chloro-carbene catalysed reactions, it has been noted that the labelling of primary sulfonamides and aldehydes is extremely sensitive to changes in solvent, where only DCM is currently applicable (see **Table 27**, for example). Efforts should thus be made to understand the role of the solvent in these reactions, building first on our published understanding.¹¹⁵

Unique aspects of the chloride ligand in the aforementioned catalysts have been explored in two different reactions. As has also been reported in the literature, simple halide ligands are often non-innocent, and significantly alter the size and electronic characteristics of a given complex.^{200,253,254} The effect of altering the halogen ligand on catalysts such as **207** should therefore be explored in order to assess the propensity for such species to broaden the scope of substrates (sulfonamides and aldehydes) currently tolerated, and as part of understanding the operative labelling mechanisms in each case (**Figure 57**).

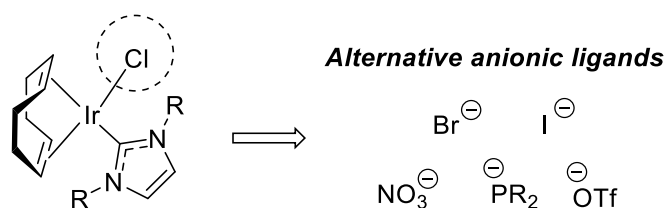
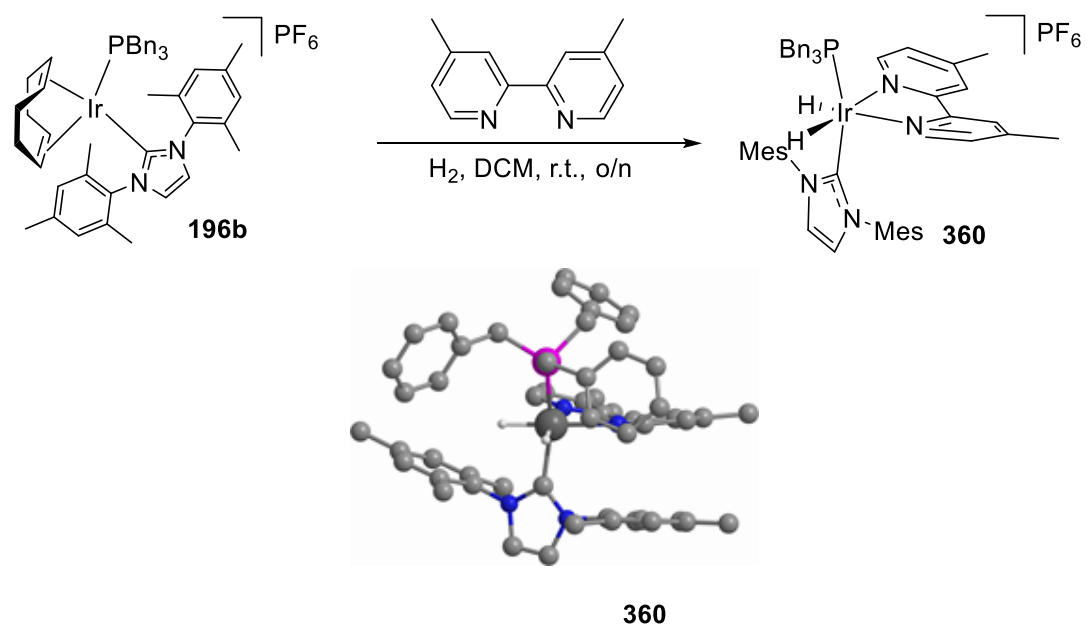


Figure 57. Possible structure variations in the further exploration of halo-carbene Ir catalysts.

In moving towards the most globally accessible model for describing ligand partnerships, the emerging ΔE_{bind} descriptor should be explored in terms of a broader scope of mono- and bidentate ligand partnerships, including more chiral derivatives of the latter. As has been shown, the new bidentate labelling catalysts derived from these studies are able to instil modes of reactivity previously unattainable in *ortho*-HIE methodology. The applicable limit of labelling protected sulfonamides and sterically-challenging amides should be fully exploited in the first instance.

Finally, experimental characterisation of HIE catalyst derivatives has inspired the idea of *catch and release catalysis*. More specifically, reduced catalyst loading represents a main driver in Ir-based HIE, due (in part) to the expense of the metal. However, this could be reduced in importance if the catalyst could be ‘captured’ and stored *after* the reaction, and later *released* again once required. One strategy for achieving this would be to form isolable dihydride complexes, displacing weakly bound substrates and solvents with, for example, acetonitrile or bipyridine derivatives. This author has initiated this line of enquiry with the isolation and X-ray characterisation of several Ir-hydride complexes (see, for example, **Scheme 85**).



Scheme 85. One potential ‘caught’ form of catalyst **196b**.

8. Experimental

8.1 General Considerations

All reagents were obtained from commercial suppliers (Aldrich, Alfa Aesar or Strem) and used without further purification, unless otherwise stated. Purification was carried out according to standard laboratory methods.²⁵⁵

- Benzene was dried by heating to reflux over sodium wire, and then distilled over argon.
- Tetrahydrofuran and 1,4-dioxane were dried by heating to reflux over sodium wire, using benzophenone ketyl as an indicator, and then distilled under nitrogen.
- Diethyl ether and toluene were obtained from a PureSolv SPS-400-5 Solvent Purification System, and deoxygenated by bubbling argon through for a minimum of thirty minutes.
- Methanol, ethanol, isopropyl acetate, diisopropyl ether, and cyclopentyl methyl ether were dried by heating to reflux over calcium chloride, and then distilled under argon.
- *Tert*-butyl methyl ether, dimethylformamide, and dimethyl carbonate were dried by heating to reflux over calcium sulfate, and then distilled under argon.
- Isopropyl alcohol and *tert*-amyl alcohol were dried by heating to reflux over calcium oxide, and then distilled under argon.
- Dimethylsulfoxide, 2-methyltetrahydrofuran, ethyl acetate, and dichloromethane were dried by heating to reflux over calcium hydride, and then distilled under argon.
- All distilled solvents were stored under an argon atmosphere over molecular sieves (Å).
- Acetanilide, benzamide, benzanilide and triphenylphosphine were purified by recrystallisation from ethanol.
- *N,N'*-Diethyl-*p*-toluoylamide was readily available within the laboratory having been synthesised during previous studies in HIE chemistry.¹⁵¹

Thin layer chromatography was carried out using Camlab silica plates coated with fluorescent indicator UV₂₅₄. This was analysed using a Mineralight UVGL-25 lamp or developed using vanillin solution.

Flash column chromatography was carried out using Prolabo silica gel (230-400 mesh).

IR spectra were obtained on a Shimadzu IRAffinity-1 Spectrophotometer machine.

^1H , ^{13}C , ^{11}B , ^{19}F , and ^{31}P spectra were recorded on a Bruker DPX 400 spectrometer at 400 MHz (unless otherwise stated), 100 MHz, 128 MHz, 376 MHz, and 162 MHz, respectively. Chemical shifts are reported in ppm. Coupling constants are reported in Hz and refer to H-H couplings, unless otherwise stated. Written accounts of ^{13}C DEPT-90° NMR spectra list CH carbons only. Similarly, for ^{13}C DEPT-135° spectra, only negative (i.e. CH_2) carbon signals are detailed. For ^{13}C DEPT-135°q spectra, quaternary carbon atoms are negative and also reported. For ^{13}C JMOD NMR, inverted signals are labelled specifically and assigned where necessary.

On collaborative projects with Sanofi (Frankfurt, Germany), the distribution of hydrogen isotopes in the products was determined by one of two liquid chromatography-mass spectrometry (LC-MS) systems.

System 1 - with a Symmetry Shield RP18 column, 3.9 x 150 mm² with gradient program. LC column conditions were as follows:

mobile phase A: water (900 mL), acetonitrile (100 mL), TFA (1 mL)

mobile phase B: water (100 mL), acetonitrile (900 mL), TFA (0.75 mL)

Flow rate: 0.6 mL/min

Detection: UV 254 nm and UV 210 nm.

System 2 – with a Dionex Summit LC System with a DAD detector, coupled to a Thermo MSQ+ single quad MS; the LC column used was a Phenomenex Luna C18(2), 3 μm, 100A, 4.6x150 mm².

mobile phase A: water (900 mL), acetonitrile (100 mL), formic acid (1 mL)

mobile phase B: water (100 mL), acetonitrile (900 mL), formic acid (0.75 mL)

Flow rate: 0.6 mL/min

Detection: UV 254 nm and UV 210 nm.

Prior to mass detection, eluted samples were mixed with a 2.5% (v/v) solution of aqueous ammonia in order to form anionic entrants to the MS system.

High resolution mass spectrometry (HRMS) data were acquired at the EPSRC UK National Mass Spectrometry Facility at Swansea University unless stated otherwise. Ionisation methods are stated for each example.

Alternatively, collaborative projects with Sanofi (Frankfurt, Germany) provided HRMS *via* a Bruker micro-TOF-QII in positive ESI mode. Calibration was achieved against an injection of a sodium formate. The sample was loaded at a flowrate of 0.5 mL/min of 0.044 % TFA in 50% acetonitrile (aq.). No LC column was used. A Dionex Ultimate 3000 RSLC system was used as an inlet to the MS. Use of this system is stated where necessary, and no predicted ion is given.

Crystallographic measurements were typically made at low temperature using Oxford Diffraction diffractometers equipped with CCD detectors. Data for all samples were measured by the UK National Crystallography Service (NCS) at the University of Southampton.²⁵⁶ All structures were refined against F^2 to convergence using all unique reflections and programmes from the SHELX suit.²⁵⁷ In samples with solvent that was too disordered to model, the solvent was removed from these models using the SQUEEZE routine contained within PLATON.²⁵⁸ Selected crystallographic and refinement parameters, along with the .res files (opened in Mercury) associated with X-ray crystal structures are provided separately from the current document and are available in **Appendix A**.

8.2 General Procedures

General Procedure A – Preparation of Iridium(I) Complexes of the Type (COD)Ir(NHC)Cl
113

A stock solution of 1 M sodium ethoxide was prepared by dissolving sodium metal (0.25 g) in ethanol (10 mL).

A solution of η^4 -cycloocta-1,5-dieneiridium(I) chloride dimer, **205**, in dry benzene (10 mL) was prepared in a flame-dried Schlenk tube. To the benzene solution was added 1 M sodium

ethoxide, resulting in a red to yellow colour change. After stirring the solution for 10 min at r.t., the imidazolium salt was added in one portion. The solution was stirred for 3 d at 45 °C under Ar, resulting in a gradual colour change from yellow to orange. The solvent was subsequently removed *in vacuo* and the residue purified *via* flash column chromatography, eluting the yellow fraction with a 1:1 mixture EtOAc and petroleum ether. The combined yellow fractions were combined and concentrated under reduced pressure. The desired yellow, crystalline solid precipitated from the resultant oil on addition of petroleum ether.

General Procedure B – Preparation of Iridium(I) Complexes of the Type (COD)Ir(NHC)Cl^{148,152}

To a flame-dried Schlenk tube was added η^4 -cycloocta-1,5-dieneiridium(I) chloride dimer, **205**, and KO^tBu. After stirring the solid mixture under high vacuum for 10 mins, dry THF was added under an Ar atmosphere, and the resultant red-black solution stirred at r.t. for a further 10 mins. Subsequently, the imidazolium salt was added in one portion, causing a dark red to dark yellow colour change, and the reaction mixture stirred for the allotted time. The THF was then removed *in vacuo* and the residue purified by flash column chromatography, eluting the yellow fraction with a 1:1 mixture EtOAc and petroleum ether.

General Procedure C – Preparation of Iridium (I) Complexes of the Type [(COD)Ir(IMes)(L)]X where X = BF₄, PF₆, or OTf, and L = PR₃ or MeCN

The yellow complex (COD)Ir(IMes)Cl, **207**, was dissolved in dry THF in a previously flame-dried round bottom flask, fitted with stopcock sidearm. After all solids had dissolved, the desired silver salt, AgX, was added, affording a yellow to opaque orange colour change on formation of a precipitate. The reaction mixture was stirred for 15 mins at r.t. before carrying out filtration through celite under Ar using the necessary flame-dried glassware. Addition of phosphine or acetonitrile to the clear orange solution resulted in the immediate appearance of a bright red colour. Finally, after stirring the solution for the allotted reaction time at r.t., the solvent was expelled under reduced pressure and the product recrystallised as specified for each specific complex.

*General Procedure D – Preparation of Imidazolium BArF Salts via Imidazolium Halides*¹⁷³

The imidazolium halide and NaBArF were added to a 50 mL round bottom flask and dissolved in a 1:1 mixture of DCM and H₂O (5 mL:5 mL). The reaction mixture was stirred overnight, ensuring that the organic and aqueous phases stirred without a visual bilayer. The reaction mixture was subsequently transferred to a separating funnel and diluted with DCM (5 mL). The aqueous phase was washed with DCM (5 mL) and the combined organic phase washed with water (10 mL) then brine (10 mL). After drying the DCM layer over anhydrous sodium sulfate and filtering through a Büchner funnel, the solvent was removed *in vacuo* and the residue purified through a short plug of silica, eluting with DCM. Removal of the solvent *in vacuo* once more gave the desired product as a white solid.

General Procedure E – Preparation of [(COD)Ir(NHC)(PR₃)]BArF via Imidazolium BArF

173

To a flame-dried round bottom flask fitted with stopcock sidearm was added η^4 -cycloocta-1,5-dieneiridium(I) chloride dimer, **205**, and dry THF (5 mL). After all solids had dissolved, the phosphine was added in one portion, sparking an orange to yellow colour change. Having allowed the reaction mixture to stir at r.t. for 15 mins, the imidazolium BArF salt was added in one portion and allowed to dissolve completely. After a further 5 mins stirring, KO^tBu was added in one portion, causing an immediate yellow to bright red, then black, colour change. The reaction mixture was stirred for the allotted time at r.t. before the THF was removed *in vacuo*. The red-black residue was dissolved in DCM and purified directly through a short plug of silica, eluting the bright red fraction with DCM. The combined fractions were concentrated under reduced pressure to reveal a red, oily solid which was recrystallised by various methods depending on the exact structure of the complex.

General Procedure F – Standard Deuteration of Substrates Using Iridium(I) Complexes

A three-necked round bottom flask was fitted with two stopcock side arms and a suba seal and flame-dried. To this flask was added the iridium(I) complex and substrate of choice. The solvent (2.5 mL, unless stated otherwise) was added, rinsing the inner walls of the flask, and the suba seal was replaced with a Teflon-sleeved glass stopper. The solution was quickly placed under an atmosphere of Ar and stirred whilst being cooled to -78 °C in a dry

ice/acetone slurry. The flask was twice evacuated and flushed with Ar. Upon a third evacuation, an atmosphere of deuterium gas was introduced to the flask. After sealing the flask, the cold bath was removed and the flask heated in a water bath to the desired temperature. **NOTE** – the glass stopper was physically restrained in case of pressure build up during the reaction. The reaction mixture was stirred for the allotted reaction time before removing excess deuterium and replacing with air. The yellow solution was washed with DCM and transferred to a single necked flask before removing the solvent under reduced pressure. The catalyst was triturated from the remaining residue by addition of diethyl ether (3 x 5 mL). The solution was filtered through a short plug of silica before the solvent was, again, evacuated.

The level of deuterium incorporation in the substrate was determined by ¹H NMR. The integrals were calibrated against a peak corresponding to a position not expected to be labelled. **Equation 1** was then used to calculate the extent of labelling:

$$\% \text{ Deuteration} = 100 - \left[\left(\frac{\text{residual integral}}{\text{number of labelling sites}} \right) \times 100 \right]$$

Equation 1

General Procedure G – Alternative Deuteration Procedure Using Carousel

All such reactions were carried out using a Radley's 12-chamber carousel.

The water inlet for the carousel reflux system was turned on prior to any further reaction set up. To a 25 mL oven-dried carousel tube was added the substrate of choice (0.086 mmol, unless otherwise stated) and iridium(I) catalyst (0.0043 mmol, 5 mol%, unless otherwise stated) under air. The desired solvent (1 mL, unless otherwise stated) was added, rinsing the inner walls of the tube. The tube was then sealed at the screw cap (with gas inlet left open) and reconnected to the carousel rack. After charging all necessary carousel tubes with reactants, the air in the tubes was replaced with argon before cooling the base of the tubes of the rack to 0 °C in the cooling basin. Separately, the carousel heating block was set to the desired reaction temperature. The cooled flasks on the carousel rack were twice evacuated and flushed with deuterium *via* a balloon. The carousel tube gas inlets were then closed,

creating a sealed atmosphere of deuterium. After sealing the flasks, the rack was transferred to the heating block and the reaction timer was started. The reaction mixture was stirred for the allotted time before removing excess deuterium and replacing with air. The solution was then washed with DCM and transferred to a single necked flask before removing the solvent under reduced pressure. The residue was worked up differently for particular reactions (*vide infra*). The residue isolated after work-up was analysed by ^1H NMR. The level and regioselectivity of deuterium incorporation in the substrate was determined by ^1H NMR and, where stated, compared with LC-MS. The integrals were calibrated against a peak corresponding to a position not expected to be labelled.

*General Procedure H – Preparation of N,N'-Dibenzyl-4,5-dimethylimidazolium halides via 4,5-dimethyl imidazole*²⁵⁹

To a flame-dried round bottom flask was added 4,5-dimethylimidazole, **258**, and dry THF. Once all solids had dissolved, sodium hydride was added portion-wise to control the rate of effervescence. Following this, the appropriate benzyl halide was added to the reaction mixture dropwise with stirring. The flask was then fitted with a reflux condenser and heated to the desired temperature before leaving the reaction mixture to stir for the allotted time. On cooling, the solvent was removed *in vacuo* and the residue diluted with DCM (20 mL). This DCM mixture was filtered through celite and concentrated under reduced pressure to reveal an off white solid. The solid was collected by filtration and washed with acetone to reveal the desired product as a bright white solid.

General Procedure I – One Pot Preparation of Iridium (I) Complexes of the Type [(COD)Ir(NHC)(PR₃)]X where X = BF₄, PF₆, SbF₆, OTf, or BPh₄

To a flame-dried round bottom flask fitted with stopcock sidearm was added (COD)Ir(NHC)Cl, phosphine, and dry THF (5 mL). On formation of a homogeneous yellow solution after 5 mins stirring, AgX was added to the reaction vessel in one portion, causing a yellow to opaque red colour change. After stirring the reaction mixture at r.t. for approximately 16 h, the reaction mixture was directly filtered through celite in air, rinsing the celite with DCM before concentrating the filtrate *in vacuo*. The resulting red solid was triturated by various means depending on the exact nature of the complex.

General Procedure J – Preparation of Iridium(I) Di- and Tricarbonyl Complexes

Similarly to *General Procedure G*, reactions were carried out in a Radley's carousel. Precatalysts of the type $[(\text{COD})\text{Ir}(\text{NHC})(\text{PR}_3)]\text{PF}_6$ were dissolved in DCM (5 mL) inside an oven-dried carousel tube. Under an argon atmosphere, the stirred reaction mixture was cooled to $-78\text{ }^\circ\text{C}$ placing the tube under vacuum and backfilling with CO gas *via* a balloon. The carousel was transferred to the heating block and stirred at r.t. for 1 h. In this time, a red to yellow (or orange) colour change was observed. To isolate the products, the reaction volume was reduced by half before adding dry Et_2O dropwise ($\sim 5\text{ mL}$) to triturated the product from DCM, yielding bright yellow or colourless solids after collection by filtration. X-ray quality crystals were obtained *via* slow diffusion of Et_2O in a saturated DCM solution of the product at r.t.

General Procedure K – Preparation of Iridium(I) Complexes of the Type $[(\text{OC})\text{Ir}(\text{NHC})(\text{PR}_3)\text{Cl}]$

Ir complexes of the type $[(\text{COD})\text{Ir}(\text{NHC})\text{Cl}]$ were added to a flame-dried Schlenk tube under an argon atmosphere then dissolved in dry DCM (5 mL). At r.t., the flask was placed under a light vacuum before sealing the system. The argon/vacuum line was replaced by a CO balloon before re-opening the Schlenk valve. Stirring at r.t. for 1 h, the reaction mixture turned from dark to light yellow. After this time, the flask was replaced under an argon atmosphere and phosphine (1 eq.) added slowly in one portion. This caused some effervescence due to the substitution of a CO ligand by phosphine. After a further 1 h stirring, the volume of DCM was reduced by half before triturating the product as a yellow solid using dry Et_2O . X-ray quality crystals were obtained *via* slow diffusion of Et_2O in a saturated DCM solution of the product at r.t.

General Procedure L – Synthesis of Primary Aromatic Sulfonamides

To a stirred solution ($\sim 50\text{ mL}$) of ammonium hydroxide (30% aqueous solution) at r.t., the necessary sulfonyl chloride or benzoyl chloride was added portion-wise (if solid) or dropwise (if liquid). The reaction mixture was stirred at r.t. for 16 h, after which time the product had formed as a white solid precipitate, unless otherwise stated. The solid was collected by filtration, and washed with cold, deionised water ($3 \times 10\text{ mL}$). Subsequently, the product was

recrystallised from ethyl acetate/hexanes and then dried in the vacuum oven (0 bar, 40 °C) overnight.

Following *General Procedure L*, results are reported as: a) amount of sulfonyl chloride or benzoyl chloride, and b) product yield.

General Procedure M – Synthesis of Celecoxib Drug Derivatives

To an oven-dried 100 mL round bottom flask fitted with reflux condenser was added the relevant β -hydroxyenone (1 eq.), 4-sulfonamidophenylhydrazine hydrochloride (1 eq.), and ethanol (20 mL). The slurry was stirred under reflux for 16 h. After cooling to room temperature, ethanol was removed *in vacuo* and the remaining residue purified by silica column chromatography (eluting with ethyl acetate/hexanes, 1:2). The product was isolated as a white solid and recrystallised from DCM/petroleum ether.

Following *General Procedure M*, results are reported as: a) amount of β -hydroxyenone, b) amount of 4-sulfonamidophenylhydrazine hydrochloride, and c) yield.

Throughout the **Experimental** section, where possible, reaction parameters (stoichiometries, time, temperature, yield, etc.) are identified according to the relevant Scheme, Table, or Figure from the **Results** section. Where multiple results require comparison, these are tabulated, otherwise, results appear in a linear, non-tabulated format.

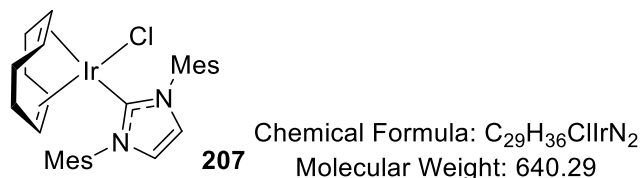
8.3 Alternative Synthetic Route to [(COD)Ir(IMes)(PR₃)PF₆]

Preparation of Chloro(η^4 -Cycloocta-1,5-diene)(1,3-dimesityl-2-ylidene) iridium(I), 207

Following *General Procedure A*, results are reported as a) amount of **205**, b) amount of NaOEt, c) amount of imidazolium salt, and d) product yield.

Scheme 37

a) 0.600 g, 0.895 mmol, b) 1.8 mL, 1.8 mmol, c) 1,3-dimesitylimidazolium chloride **206**, 0.406 g, 1.191 mmol, and d) 0.801 g, 70%.



Appearance: yellow, microcrystalline solid.

m.p. (°C): decomposes at > 200 °C.

FTIR (neat): 3092, 3009, 2916, 2876, 1609, 1485 cm⁻¹.

¹H NMR (400 MHz, CDCl₃): δ 6.99-6.96 (2 x bs, 4H, ArH), 6.93 (s, 2H, olefinic CH), 4.14-4.10 (m, 2H, COD olefinic CH), 2.96-2.94 (m, 2H, COD olefinic CH), 2.34 (s, 12H, ArCH₃), 2.14 (s, 6H, ArCH₃), 1.74-1.59 (m, 4H, COD CH₂), 1.33-1.21 (m, 4H, COD CH₂)

¹³C NMR (100 MHz, CDCl₃): δ 181.0, 138.8, 137.6, 136.3, 134.6, 133.0, 129.7, 128.3, 123.5, 82.8, 66.1, 51.6, 33.7, 29.2, 21.4, 19.9, 15.5.

Alternative Preparation of Chloro(η⁴-Cycloocta-1,5-diene)(1,3-dimesityl-2-ylidene)iridium(I), 207^{148,152}

Following *General Procedure B*, results are reported as follows:

From Scheme 38:

Entry	205 (g, mmol)	<i>KOtBu</i> (g, mmol)	<i>THF</i> (mL)	206 (g, mmol)	Time	Yield (g, %)
1	0.600, 0.893	0.200, 1.786	15	0.609, 1.786	3 h	1.132, 99
2	4.000, 5.954	1.337, 11.910	100	4.060, 11.910	2 h	6.919, 91

The analytical data was consistent with that reported above.

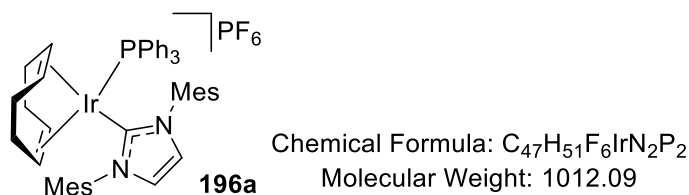
*Preparation of η⁴-Cycloocta-1,5-diene(1,3-dimesitylimidazoline-2-ylidene)(triphenylphosphine)iridium(I) hexafluorophosphate, 196a*¹¹³

Following *General Procedure C*, results are reported as follows:

From Table 4:

Entry	207 (g, mmol)	AgPF ₆ (g, mmol)	THF (mL)	PPh ₃ (g, mmol)	Time (h)	Yield (g, %)
1 ^a	0.700, 1.093	0.276, 1.093	15	0.287, 1.093	1	0.553, 50
2 ^b	0.700, 1.093	0.276, 1.093	15	0.287, 1.093	1	0.885, 80

^a Product was isolated *via* recrystallization from DCM/Et₂O.
^b Product was isolated *via* trituration from EtOAc.



Appearance: red, microcrystalline solid.

FTIR (CH₂Cl₂): 3040, 2995, 2319, 1631, 1495 cm⁻¹.

¹H NMR (400 MHz, CDCl₃): δ 7.49-7.45 (m, 5H, ArH), 7.34-7.30 (m, 6H, ArH), 7.16-7.12 (m, 6H, ArH), 7.05 (s, 2H, ArH), 6.67 (s, 2H, olefinic CH), 4.41-4.40 (m, 2H, olefinic COD CH), 3.33-3.31 (m, 2H, COD CH), 2.37 (s, 6H, ArCH₃), 2.13 (s, 6H, ArCH₃), 1.78 (s, 6H, ArCH₃), 1.63-1.51 (m, 6H, COD CH₂), 1.49 (m, 2H, COD CH₂).

¹³C NMR (100 MHz, CDCl₃): δ 176.5 (d, ³J_{C-P} = 8.0 Hz), 139.2, 135.7, 135.2, 135.1, 134.6, 131.2, 130.7, 130.2, 129.7, 128.5, 126.4, 80.9, 80.0, 77.4, 31.4, 30.4, 21.2, 20.9, 18.9.

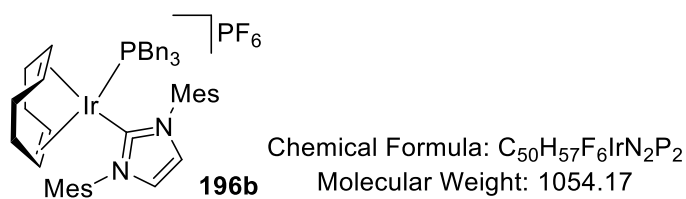
³¹P NMR (162 MHz, CDCl₃): δ 16.3 (PPh₃), -144.3 (PF₆).

Preparation of η⁴-Cycloocta-1,5-diene(1,3-dimesitylimidazoline-2-ylidene) (tribenzylphosphine)iridium(I) hexafluorophosphate, **196b**¹¹³

Following *General Procedure C*, results are reported as a) amount of **207**, b) volume of THF, c) amount of AgPF₆, d) amount of phosphine, e) reaction time, f) product yield, and g) purification technique.

From Table 4:

a) 0.700 g, 1.093 mmol, b) 15 mL, c) 0.276 g, 1.093 mmol, d) PBn₃, 0.333 g, 1.093 mmol, e) 1 h, f) 0.888 g, 77%, and g) trituration from EtOAc.



Appearance: red, microcrystalline solid.

FTIR (CH_2Cl_2): 3040, 2995, 2319, 1631, 1495 cm^{-1} .

1H NMR (400 MHz, $CDCl_3$): δ 7.79 (s, 2H, NCH=CHN), 7.41 (s, 2H, ArH), 7.34 (s, 2H, ArH), 7.30-7.28 (m, 9H, ArH), 6.99-6.97 (m, 6H, ArH), 4.72-4.70 (m, 2H, COD CH), 3.27-3.26 (m, 2H, COD CH), 3.02 (d, $^2J_{P-H} = 8.8$ Hz, 6H, PCH₂Ar), 2.57 (s, 6H, ArCH₃), 2.47 (s, 6H, ArCH₃), 2.39 (s, 6H, ArCH₃), 1.83-1.77 (m, 2H, COD CH₂), 1.60-1.48 (m, 4H, COD CH₂), 1.37-1.30 (m, 2H, COD CH₂).

^{13}C NMR (100 MHz, $CDCl_3$): δ ~175.0 (unable to observe C-P coupling), 141.1, 137.4, 137.0, 136.3, 134.4, 131.0, 130.7, 129.6, 128.8, 128.0, 127.9, 87.2, 75.8, 32.5, 31.2, 31.1, 21.1, 20.6, 20.0.

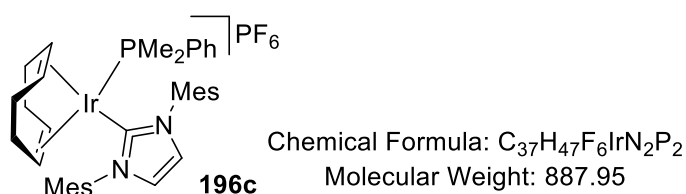
^{31}P NMR (162 MHz, $CDCl_3$): δ -7.0 (Pn₃), -144.2 (PF₆).

*Preparation of η^4 -Cycloocta-1,5-diene(1,3-dimesitylimidazoline-2-ylidene) (dimethylphenylphosphine)iridium(I) hexafluorophosphate, 196c*¹¹³

Following *General Procedure C*, results are reported as a) amount of **207**, b) volume of THF, c) amount of AgPF₆, d) amount of phosphine, e) reaction time, f) product yield, and g) purification technique.

From Table 4:

a) 0.700 g, 1.093 mmol, b) 20 mL, c) 0.276 g, 1.093 mmol, d) PMe₂Ph, 0.151 g, 1.093 mmol, e) 16 h, f) 0.872 g, 90%, and g) trituration from EtOAc.



Appearance: red, microcrystalline solid.

FTIR (neat): 3040, 2995, 2319, 1631, 1495 cm^{-1} .

¹H NMR (400 MHz, CDCl₃): δ 7.40-7.37 (m, 3H, ArH), 7.32-7.29 (m, 4H, ArH and olefinic CH), 7.07 (s, 2H, ArH), 6.94 (s, 2H, ArH), 4.32-4.29 (m, 2H, COD CH), 3.48-3.46 (m, 2H, COD CH), 2.40 (s, 6H, ArCH₃), 2.23 (s, 6H, ArCH₃), 2.16, (s, 6H, ArCH₃), 1.77-1.50 (m, 8H, COD CH₂), 1.51 (d, ²J_{P-H} = 8.4 Hz, 6H, CH₃).

¹³C NMR (100 MHz, CDCl₃): δ 177.05, 139.4, 135.0, 134.3, 131.3, 130.9, 129.5, 129.2, 128.1, 125.3, 83.5, 82.8, 76.2, 75.3, 30.9, 29.9, 21.1, 20.4, 18.6, 16.6, 15.6.

³¹P NMR (162 MHz, CDCl₃): δ -14.06 (PMe₂Ph), -144.35 (PF₆).

8.4 Anion Effects in Iridium-catalysed Isotope Exchange Processes

The main findings from this section have now been published and can be found at the reference provided.²⁵¹

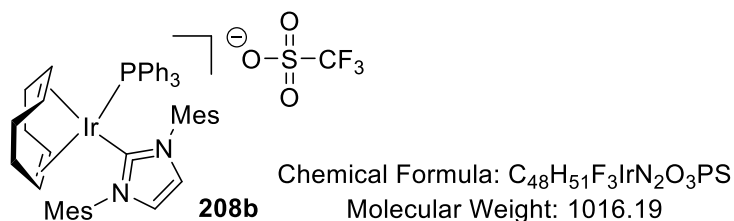
Preparation of η⁴-Cycloocta-1,5-diene(1,3-dimesitylimidazoline-2-ylidene)(triphenylphosphine)iridium(I) trifluoromethylsulfonate, 208b

Following *General Procedure C*, results are reported as a) amount of **207**, b) volume of THF, c) amount of AgOTf, d) amount of phosphine, e) reaction time, f) product yield, and g) purification technique.

From Table 5:

a) 0.500 g, 0.781 mmol, b) 20 mL, c) 0.201 g, 0.781 mmol, d) PPh₃, 0.204 g, 0.781 mmol, e) 16 h, f) 0.545 g, 69%, and g) trituration from EtOAc.

X-ray quality crystals were prepared by allowing diethyl ether to diffuse into a saturated DCM solution of the product at 4 °C overnight.



Appearance: red, microcrystalline solid.

m.p.: Decomposes >170 °C.

FTIR (neat): 3174, 2951, 2924, 2887, 1477, 1437, 1381, 1267, 1140, 1032 cm^{-1} .

^1H NMR (400 MHz, CDCl_3): δ 7.50 (s, 2H, NCH=CHN), 7.49-7.45 (m, 3H, ArH), 7.34-7.28 (m, 6H, ArH), 7.16-7.11 (m, 6H, ArH), 7.05 (s, 2H, ArH), 6.67 (s, 2H, ArH), 4.31-4.38 (m, 2H, COD CH), 3.34-3.32 (m, 2H, COD CH), 2.37 (s, 6H, ArCH₃), 2.13 (s, 6H, ArCH₃), 1.77 (s, 6H, ArCH₃), 1.70-1.50 (m, 6H, COD CH₂), 1.33-1.25 (m, 2H, COD CH₂).

^{13}C NMR (100 MHz, CDCl_3): δ 176.2 (d, $^3J_{\text{C-P}} = 8.0$ Hz), 139.2, 135.2, 135.1, 134.7, 134.3, 134.2, 130.8, 130.2, 129.8, 129.2, 128.1, 128.0, 126.4, 80.0, 79.9, 77.5, 31.4, 29.7, 20.8, 20.4, 18.6.

^{13}C DEPT-135° NMR (100 MHz, CDCl_3): δ 31.9, 30.2.

^{31}P NMR (162 MHz, CDCl_3): δ 16.3 (PPh₃).

^{19}F NMR (376 MHz, CDCl_3): δ -78.0 (SO₃CF₃).

HRMS (positive ESI): m/z calc'd for C₂₉H₃₂¹⁹¹IrN₂ [M-SO₃CF₃-PPh₃-4H]⁺: 599.2166; found: 599.2169. No mass ion observed.

HRMS (negative ESI): m/z calc'd for [SO₃CF₃]⁻: 148.9526; found: 148.9528.

X-Ray: see Appendix A.

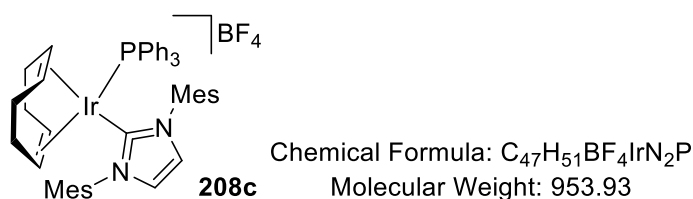
Preparation of η^4 -Cycloocta-1,5-diene(1,3-dimesitylimidazoline-2-ylidene) (triphenylphosphine)iridium(I) tetrafluoroborate, 208c

Following *General Procedure C*, results are reported as a) amount of **207**, b) volume of THF, c) amount of AgBF₄, d) amount of phosphine, e) reaction time, f) product yield, and g) purification technique.

From Table 5:

a) 0.250 g, 0.390 mmol, b) 15 mL, c) 0.076 g, 0.390 mmol, d) PPh₃, 0.099 g, 0.390 mmol, e) 1 h, f) 0.298 g, 80%, and g) trituration from EtOAc.

X-ray quality crystals were prepared by layering diethyl ether on top of a saturated DCM solution of the product, allowing the biphasic solvent system to mix for four days at r.t.



Appearance: dark red, microcrystalline solid.

m.p.: Decomposes > 160 °C.

FTIR (neat): 3043, 2920, 2364, 1606, 1585, 1566, 1477, 1435, 1049 cm^{-1} .

1H NMR (400 MHz, $CDCl_3$): δ 7.50 (s, 2H, NCH=CHN), 7.48-7.44 (m, 3H, ArH), 7.34-7.29 (td, $J = 7.8, 2.5$ Hz, 6H, ArH), 7.15-7.10 (m, 6H, ArH), 7.04 (s, 2H, ArH), 6.66 (s, 2H, ArH), 4.40-4.38 (m, 2H, COD CH), 3.33-3.31 (m, 2H, COD CH), 2.36 (s, 6H, ArCH₃), 2.12 (s, 6H, ArCH₃), 1.77 (s, 6H, ArCH₃), 1.68-1.49 (m, 6H, COD CH₂), 1.32-1.27 (m, 2H, COD CH₂).

^{13}C NMR (100 MHz, $CDCl_3$): δ 176.1 (d, $^2J_{C-P} = 8.0$ Hz), 139.1, 135.2, 135.1, 134.7, 134.3, 134.2, 130.7, 130.3, 129.8, 129.2, 128.1, 128.0, 126.4, 79.9, 79.8, 77.5, 31.4, 29.7, 20.7, 20.4, 18.5.

^{13}C DEPT-90° NMR (100 MHz, $CDCl_3$): δ 134.8, 134.7, 131.2, 130.3, 129.7, 128.6, 128.5, 126.9, 80.4, 80.3, 78.0.

^{13}C DEPT-135° NMR (100 MHz, $CDCl_3$): δ 31.9, 30.2.

^{31}P NMR (162 MHz, $CDCl_3$): δ 16.3 (PPh₃).

^{11}B NMR (128 MHz): δ -0.9 (BF₄).

^{19}F NMR (376 MHz, $CDCl_3$): δ -153.8 (BF₄).

HRMS (positive ESI): m/z calc'd for $C_{29}H_{31}^{191}IrN_2 [M-BF_4-PPh_3-5H]^+$: 599.2166; found: 599.2168. No mass ion observed.

HRMS (negative ESI): m/z calc'd for [BF₄]⁻: 87.0000; found: 87.0042.

X-Ray: see Appendix A.

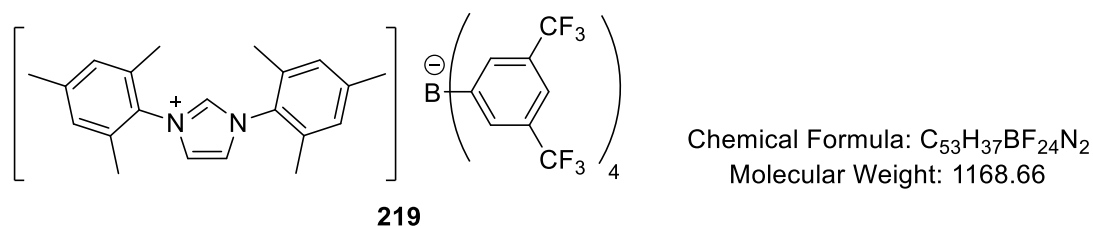
Preparation of N,N'- Dimesitylimidazolium tetrakis[(3,5-trifluoromethylphenyl)]borate, 219

Following *General Procedure D*, results are reported as a) amount of **206**, b) amount of NaBARF, and c) product yield.

From Scheme 39:

a) 0.269 g, 0.789 mmol, b) 0.700 g, 0.789 mmol, and c) 0.840 g, 92%.

X-ray quality crystals were grown by solution evaporation of a DCM solution of **220** at r.t. overnight.



m.p.: 135-136 °C.

FTIR (neat): 3156, 2994, 2968, 2928, 1609, 1545, 1479, 1352, 1273, 1115 cm⁻¹.

¹H NMR (400 MHz, CDCl₃): δ 8.11 (t, ⁴J = 1.6 Hz, 1H, NCHN), 7.70-7.68 (m, 8H, ArH_{BArF}), 7.50 (s, 4H, ArH_{BArF}), 7.40 (d, ⁴J = 1.6 Hz, 2H, NCH=CHN), 7.08 (s, 4H, ArH), 2.37 (s, 6H, ArCH₃), 2.04 (s, 12H, ArCH₃).

¹³C NMR (100 MHz, CDCl₃): δ 161.8 (q, ¹J_{C-B} = 49.5 Hz), 143.1, 135.3, 134.8, 133.4, 130.4, 129.4-128.4 (unidentified multiplet), 125.0, 124.6 (q, ¹J_{C-F} = 270.7 Hz), 117.4, 21.0, 16.9.

¹¹B NMR (128 MHz, CDCl₃): δ -6.7 (BArF B(Ar)₄).

¹⁹F NMR (376 MHz, CDCl₃): -62.4 (BArF ArCF₃)

HRMS (positive ESI): m/z calc'd for C₂₁H₂₅N₂ [M-BArF]⁺: 305.2012; found: 305.2012 [M-BArF]⁺.

HRMS (negative ESI): m/z calc'd for [C₃₂H₁₂BF₂₄, BArF]⁻: 863.0660; found: 863.0621.

X-Ray: see Appendix A.

Preparation of η⁴-Cycloocta-1,5-diene(1,3-dimesitylimidazolium-2-ylidene) (triphenylphosphine)iridium(I) tetrakis[(3,5-trifluoromethylphenyl)]borate, 208a

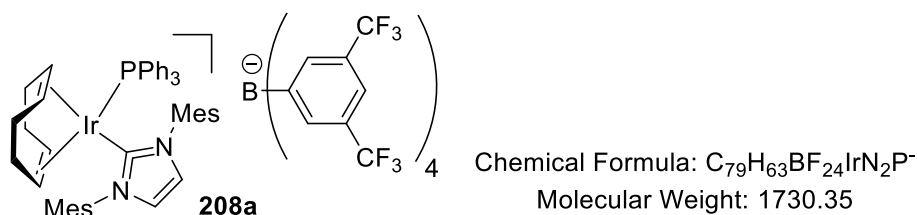
Following *General Procedure E*, results are reported as a) amount of **205**, b) amount of PPh₃, c) amount of **219**, d) amount of KO^tBu, e) reaction time, and f) product yield.

From Scheme 39:

a) 0.544 g, 0.810 mmol, b) 0.426 g, 1.620 mmol, c) 1.894 g, 1.62 mmol, d) 0.273 g, 2.43 mmol, e) 1 h, and f) 1.860 g, 67%.

The product was isolated as a red solid by layering petroleum ether on top of the oily solid obtained after column chromatography, and standing at r.t. overnight. X-ray quality crystals

were prepared by layering hexane on top of a saturated THF solution of the product, allowing the biphasic solvent system to mix for one week at r.t.



Appearance: dark red, granny solid.

m.p.: Decomposes >156 °C.

FTIR (neat): 3024, 2978, 1610, 1539, 1479, 1467, 1426, 1352, 1271, 1187 cm^{-1} .

1H NMR (400 MHz, $CDCl_3$): δ 7.74-7.73 (m, 8H, ArH_{BArF}), 7.53 (bs, 4H, ArH_{BArF}), 7.46-7.42 (m, 3H, ArH), 7.32-7.27 (overlapping s and m, 8H, ArH + NCH=CHN), 7.16-7.11 (m, 6H, ArH), 7.05 (s, 2H, ArH), 6.69 (s, 2H, ArH), 4.40-4.37 (m, 2H, COD CH), 3.38-3.36 (m, 2H, COD CH), 2.36 (s, 6H, $ArCH_3$), 2.11 (s, 6H, $ArCH_3$), 1.77 (s, 6H, $ArCH_3$), 1.71-1.48 (m, 6H, COD CH_2), 1.33-1.27 (m, 2H, COD CH_2).

^{13}C NMR (100 MHz, $CDCl_3$): δ 178.0 (d, $^3J_{C-P} = 10.0$ Hz), 161.8 (q, $^1J_{C-B} = 50.0$ Hz), 140.1, 135.4, 135.1, 134.8, 134.7, 131.3, 131.2, 130.7, 130.4, 129.8, 129.0, 128.7, 128.5, 124.5 (q, $^1J_{C-F} = 270.0$ Hz), 117.4, 80.5, 80.4, 78.5, 31.8, 21.1, 20.7, 18.9.

^{13}C DEPT-135° NMR (100 MHz, $CDCl_3$): δ 31.8, 30.1.

^{31}P NMR (162 MHz, $CDCl_3$): δ 16.4 (PPh_3).

^{19}F NMR (376 MHz, $CDCl_3$): δ -62.5 ($BArF$ $ArCF_3$).

^{11}B NMR (128 MHz, $CDCl_3$): δ -6.60 ($BArF$ $B(Ar_4)$).

HRMS (positive ESI): m/z calc'd for $C_{29}H_{32}^{191}IrN_2$ [$M-BArF-PPh_3-4H$] $^+$: 599.2166; found: 599.2168. No mass ion observed.

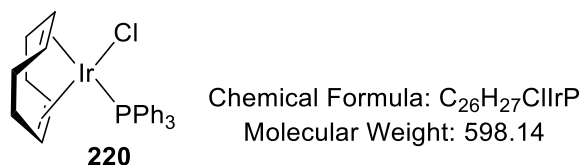
HRMS (negative ESI): m/z calc'd for [$C_{32}H_{12}BF_{24}$, $BArF$] $^-$: 863.0660; found: 863.0632.

X-Ray: see Appendix A.

*Preparation of Chloro(η^4 -cycloocta-1,5-diene)(triphenylphosphine) iridium(I), **220**²⁶⁰*

To a flame-dried 100 mL round bottom flask fitted with a stopcock sidearm was added **205** (0.300 g, 0.447 mmol) and dry DCM (10 mL). Once all solids had dissolved, triphenylphosphine (0.234 g, 0.894 mmol) was added in one portion causing a red to orange-yellow colour change. The reaction mixture was stirred at r.t. for 30 mins before dry EtOH

(20 mL) was added, causing a yellow to red colour change. At this time, the flask was placed under high vacuum with continuous stirring until a bright yellow precipitate formed. The product was collected by filtration and washed with cold EtOH (5 mL), to deliver the desired product as a yellow solid (**Scheme 39**; 0.368 g, 69%).



Appearance: yellow powder.

m.p. (°C): 175-177 (Lit. = 175-178).

FTIR (neat): 3051, 2955, 2878, 1479, 1433 cm⁻¹.

¹H NMR (400 MHz, CDCl₃): δ 7.70-7.65 (m, 6H, ArH), 7.42-7.35 (m, 9H, ArH), 5.18-5.15 (m, 2H, COD CH), 2.73-2.70 (m, 2H, COD CH), 2.29-2.11 (m, 4H, COD CH₂), 1.88-1.82 (m, 2H, COD CH₂), 1.61-1.54 (m, 2H, COD CH₂).

¹³C NMR (100 MHz, CDCl₃): δ ppm 135.3, 135.1, 131.3, 130.8, 130.6, 128.3, 128.2, 94.3, 94.1, 53.8, 33.7, 29.7.

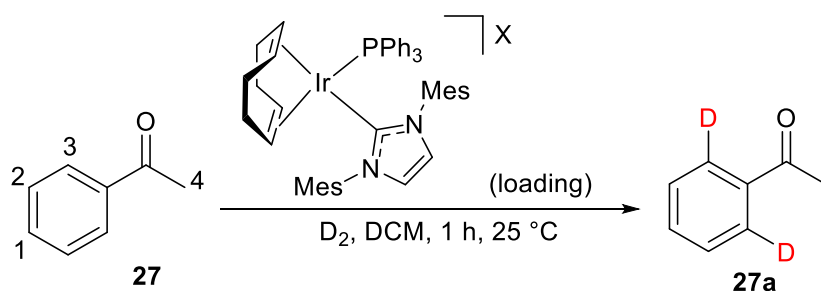
³¹P NMR (162 MHz, CDCl₃): δ 21.9 (PPh₃).

Preparation of η⁴-Cycloocta-1,5-diene(1,3-dimesitylimidazoline-2-ylidene) (triphenylphosphine)iridium(I) tetrakis[(3,5-trifluoromethylphenyl)]borate, 208a, from 220

To a flame-dried 50 mL round bottom flask fitted with stopcock sidearm was added **220** (0.031 g, 0.052 mmol), **219** (0.061 g, 0.052 mmol), and dry THF (2.2 mL). After a homogeneous, yellow solution was formed and, after 5 mins stirring, KO^tBu (0.009 g, 0.078 mmol) was added in one portion, causing a yellow to deep red colour change. After stirring the resultant reaction mixture at r.t. for 2 d, the solvent was removed *in vacuo* and the residue purified through a short plug of silica, eluting with DCM, as per *General Procedure E*. The combined red fractions were concentrated under reduced pressure to reveal the product as a red oil. Purification was achieved by pouring petroleum ether over the oil, allowing the complex to crystallise as a deep red solid (**Scheme 39**; 0.038 g, 42%).

Data are consistent with that reported above for **208a**.

Assessment of Counterion Effects on Catalyst Efficiency (from Scheme 40)



Data for unlabeled acetophenone, 27:

¹H NMR (400 MHz, CDCl₃): δ 7.95 (d, ³J = 7.5 Hz, 2H, ArH³), 7.47 (t, ³J = 7.4 Hz, 1H, ArH¹), 7.35 (t, ³J = 7.4 Hz, 2H, ArH²), 2.62 (s, 3H, CH₃⁴).

Incorporation expected at δ 7.95. Determined against integral at δ 2.62.

Scheme 40 represents assessment of five different catalyst loadings (0.0, 0.5, 1.0, 3.0, and 5.0 mol%) at 25 °C. Each point on a graph is representative of an average of two independent runs for that particular set of reaction conditions. Following *General Procedure F*, all reactions were carried out using **27** (0.028 mL, 0.215 mmol). Results are delineated in the following table.

<i>Entry</i>	<i>X</i>	<i>Loading (mg, mol%)</i>	<i>%D (run 1)</i>	<i>%D (run 2)</i>
1	-	-	0	0
2	BF ₄	1.0, 0.5	36	38
3	BF ₄	2.0, 1.0	58	66
4	BF ₄	6.2, 3.0	92	97
5	BF ₄	9.5, 5.0	87	97
6	PF ₆	1.1, 0.5	60	59
7	PF ₆	2.2, 1.0	77	79
8	PF ₆	6.5, 3.0	97	98
9	PF ₆	10.8, 5.0	97	98
10	OTf	1.1, 0.5	68	79
11	OTf	2.2, 1.0	86	94
12	OTf	6.6, 3.0	96	96
13	OTf	10.9, 5.0	96	97
14	BArF	1.9, 0.5	71	79
15	BArF	3.7, 1.0	89	86
16	BArF	11.1, 3.0	98	96
17	BArF	18.3, 5.0	97	98

All reactions carried out at 25 °C.

The same set of experiments was also run at 40 °C. These are mentioned in the results section but not included. These additional experiments are tabulated below:

<i>Entry</i>	<i>X</i>	<i>Loading (mg, mol%)</i>	<i>%D(run 1)</i>	<i>%D(run 2)</i>
1	-	-	0	0
2	BF ₄	1.0, 0.5	90	89
3	BF ₄	2.0, 1.0	96	98
4	BF ₄	6.2, 3.0	96	98
5	BF ₄	9.5, 5.0	97	98
6	PF ₆	1.1, 0.5	92	96
7	PF ₆	2.2, 1.0	96	98
8	PF ₆	6.5, 3.0	97	97
9	PF ₆	10.8, 5.0	97	96
10	OTf	1.1, 0.5	97	94
11	OTf	2.2, 1.0	93	95
12	OTf	6.6, 3.0	96	96
13	OTf	10.9, 5.0	95	96
14	BArF	1.9, 0.5	96	94
15	BArF	3.7, 1.0	95	97
16	BArF	11.1, 3.0	95	97
17	BArF	18.3, 5.0	97	96

All reactions carried out at 40 °C.

Counterion Influence on Ether and Carbonate Solvent Scope

Figure 17 represents assessment of catalysts **196a** and **208a** in various ether and carbonate solvents. Each bar on a graph is representative of an average of two independent runs for that particular set of reaction conditions. Reactions were run using *General Procedure F*, and all were carried out using **27** (0.028 mL, 0.215 mmol). The results are shown in the table below.

Entry ^a	Solvent	Catalyst ^b	% Deuteration		Average % D
			Run 1	Run 2	
1	dioxane	196a	93	94	94
2	dioxane	208a	94	95	95
3	MTBE	196a	90	92	91
4	MTBE	208a	97	97	97
5	Et ₂ O	196a	94	93	94
6	Et ₂ O	208a	96	98	97
7	2-MeTHF	196a	95	94	95
8	2-MeTHF	208a	96	94	95
9	ⁱ Pr ₂ O	196a	78	66	72
10	ⁱ Pr ₂ O	208a	98	98	98
11	CPME	196a	66	64	65
12	CPME	208a	96	98	97
13	THF	196a	38	48	43
14	THF	208a	92	88	90
15	dimethyl carbonate	196a	72	88	80
16	dimethyl carbonate	208a	92	92	92

^aConditions: 2.5mL solvent, 0.215 mmol **27**, 1 h, 25 °C, 5 mol% [Ir]
^bMass of **196a** per reaction = 10.8 mg; mass of **208a** per reaction = 18.3 mg

Counterion Influence on Alcohol, Ester, Chlorinated, and Aromatic Solvent Scope

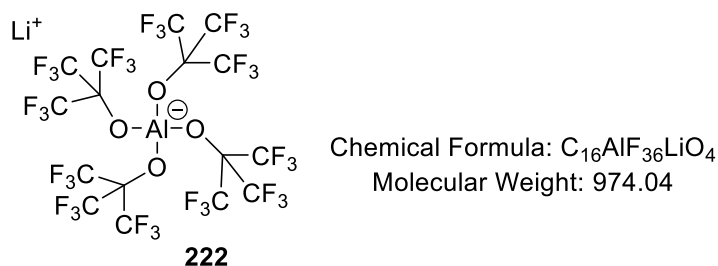
Figure 18 represents assessment of catalysts **196a** and **208a** in various additional solvents. Each bar on a graph is representative of an average of two independent runs for that particular set of reaction conditions. Following *General Procedure F*, all reactions were carried out using **27** (0.028 mL, 0.215 mmol). Results are delineated in the following table. This also includes results of labelling reactions using DMSO and DMF as the solvent (not shown in **Section 3**). For these two solvents, reactions were run with catalyst **208a** only.

Entry ^a	Solvent	Catalyst ^b	% Deuteration		Average % Deuteration
			Run 1	Run 2	
1	EtOH	196a	31	28	30
2	EtOH	208a	37	37	37
3	IPA	196a	28	36	32
4	IPA	208a	40	46	43
5	^t AmOH	196a	65	76	71
6	^t AmOH	208a	88	75	82
7	EtOAc	196a	56	68	62
8	EtOAc	208a	86	80	83
9	ⁱ PrOAc	196a	84	80	82
10	ⁱ PrOAc	208a	97	93	95
11	DCM	196a	97	97	97
12	DCM	208a	96	96	96
13	DCE	196a	95	97	96
14	DCE	208a	99	97	98
15	Toluene	196a	57	44	51
16	Toluene	208a	90	92	91
17	DMSO	196a	-	-	-
18	DMSO	208a	4	8	6
19	DMF	196a	-	-	-
20	DMF	208a	3	0	2

^aConditions: 2.5mL solvent, 0.215 mmol **27**, 1 h, 25°C, 5 mol% [Ir]
^bMass of **196a** per reaction = 10.8 mg; mass of **208a** per reaction = 18.3 mg

Synthesis of Lithium tetrakis(perfluoro-tert-butyl)aluminate, **222**¹⁵⁹

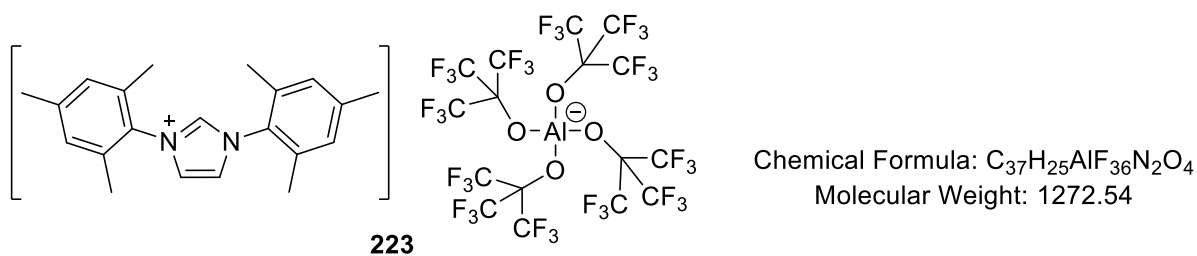
To a flame-dried Schlenk flask under argon, LiAlH₄ (0.200 g, 5.3 mmol) was suspended in hexane (12 mL), which was cooled to -20 °C and nonafluoro-*tert*-butyl alcohol, **221** (3.1 mL, 22.3 mmol), added drop wise. After the mixture stirred for 45 mins, the suba seal was swapped for a cold finger condenser before heating the reaction mixture to reflux overnight at 80 °C. The solution was then allowed to cool to r.t. before being passed through filter paper, the grey residue washed with DCM. The filtrate was collected and the solvent removed *in vacuo* to give the product as a white solid (**Scheme 41**, 1.62 g, 32% yield).



^{19}F NMR (376 MHz, $CDCl_3$): δ - 75.5 (CF_3).

Synthesis of 1,3-dimesitylimidazolium tetrakis(perfluoro-tert-butyl)aluminate, 223

Imidazolium salt **206** (0.210 g, 0.620 mmol) and **222** (0.600 g, 0.620 mmol) were added to a 50 mL round bottom flask and dissolved in a 1:1 mixture of DCM and H_2O (5 mL:5 mL). The reaction mixture was stirred overnight, ensuring that the organic and aqueous phases stirred without a visual bilayer. The reaction mixture was subsequently transferred to a separating funnel and diluted with DCM (5 mL). The aqueous phase was washed with DCM (5 mL) and the combined organic phase washed with water (10 mL) then brine (10 mL). After drying the DCM layer over anhydrous sodium sulfate and filtering through a Büchner funnel, the solvent was removed *in vacuo* and the residue purified through a short plug of silica, eluting with DCM. Removal of the solvent *in vacuo* once more gave the desired product as a white solid (0.533 g, 68% yield).



Appearance: colourless, crystalline solid.

1H NMR (400 MHz, $CDCl_3$): δ 8.08 (t, $^4J = 1.5$ Hz, 1H, NCHN), 7.38 (d, $^4J = 1.6$ Hz, 2H, NCH=CHN), 7.05 (s, 4H, ArH), 2.34 (s, 6H, ArCH₃), 2.01 (s, 12H, ArCH₃).

^{13}C NMR (100 MHz, $CDCl_3$): δ 142.5, 134.9, 133.0, 129.9, 129.0, 124.5, 120.7 (q, $^1J_{C-F} = 291.7$ Hz), 20.5, 16.3. The quaternary carbon adjacent to the oxygen in the anion could not be observed.

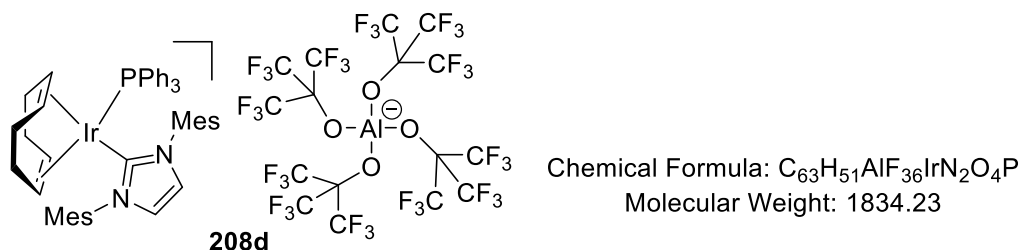
^{19}F NMR (376MHz, $CDCl_3$): δ -75.5 (CF_3).

HRMS (positive ESI): m/z calc'd for C₂₁H₂₅N₂ [M-PFTB]⁺: 305.2012; found: 305.2012.

HRMS (negative ESI): m/z calc'd for [C₁₆AlO₄F₃₆, PFTB]⁻: 966.9043; found: 966.9026.

Preparation of η^4 -Cycloocta-1,5-diene(1,3-dimesitylimidazoline-2-ylidene) (triphenylphosphine)iridium(I) tetrakis(perfluoro-tert-butyl)aluminate, **208d**

To a flame-dried round bottom flask fitted with stopcock sidearm was added η^4 -cycloocta-1,5-dieneiridium(I) chloride dimer, **205** (0.161 g, 0.240 mmol), and dry THF (5 mL). After all solids had dissolved, the phosphine (0.124 g, 0.480 mmol) was added in one portion, sparking an orange to yellow colour change. Having allowed the reaction mixture to stir at r.t. for 15 mins, **223** (0.599 g, 0.480 mmol) was added in one portion and allowed to dissolve completely. After a further 5 mins stirring, KO^tBu (0.080 g, 0.710 mmol) was added in one portion, causing an immediate yellow to bright red, then black, colour change. The reaction mixture was stirred for the allotted time at r.t. before the THF was removed *in vacuo*. The red-black residue was dissolved in DCM and purified directly through a short plug of silica, eluting the bright red fraction with DCM. The combined fractions were concentrated under reduced pressure to reveal a red, oily solid which was triturated with petroleum ether to give the product as a red solid (0.623 g, 72% yield).



Appearance: red, microcrystalline solid.

¹H NMR (400 MHz, CDCl₃): 7.38-7.34 (m, 3H, ArH), 7.23-7.19 (overlapping s and m, 10H, ArH + NCH=CHN), 7.17-7.13 (m, 6H, ArH), 6.60 (s, 4H, ArH), 4.31-4.28 (m, 2H, COD CH), 3.30-3.28 (m, 2H, COD CH), 2.28 (s, 6H, ArCH₃), 2.02 (s, 6H, ArCH₃), 1.69 (s, 6H, ArCH₃), 1.61-1.40 (m, 6H, COD CH₂), 1.25-1.19 (m, 2H, COD CH₂).

¹³C NMR (100 MHz, CDCl₃): δ 177.9 (d, ²J_{C-P} = 8.2 Hz), 140.1, 135.7, 135.2, 135.1, 134.6, 131.2, 130.7, 130.2, 129.7, 128.5, 126.4, 121.3 (q, ¹J_{C-F} = 291.7 Hz), 80.5, 80.4, 78.5, 31.4, 30.4, 21.1, 20.7, 18.9, 16.8.

³¹P NMR (162 MHz, CDCl₃): δ 16.4 (PPh₃).

^{19}F NMR (376MHz, CDCl_3): δ -75.5 (CF_3).

HRMS (positive ESI): No fragment ions yet observed.

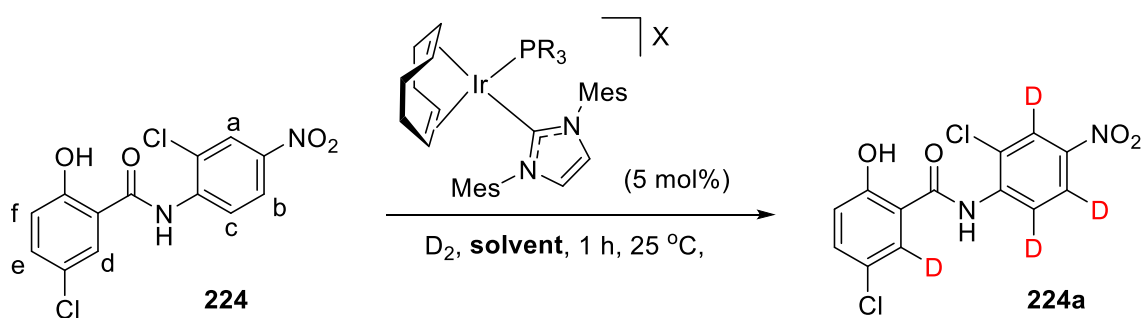
Comparative Solvent Screen of Largest Counterion Catalysts, 208a and 208d

Figure 19 describes similar experiments for catalyst **208d** as described for Figure 17 and Figure 18 for other catalysts. As the BArF results have already been tabulated (*vide supra*), the table below shows the results for catalyst **208d** only.

Entry ^a	Solvent	Catalyst ^b	% Deuteration		Average % D
			Run 1	Run 2	
1	MTBE	208d	97	98	98
2	Et ₂ O	208d	65	66	66
3	2-MeTHF	208d	94	94	94
4	THF	208d	76	82	79
5	EtOH	208d	38	34	36
6	IPA	208d	78	77	78
7	EtOAc	208d	96	98	97
8	Toluene	208d	97	98	98

^aConditions: 2.5mL solvent, 0.215 mmol **27**, 1 h, 25°C, 5 mol% [Ir]
^bMass of **208d** per reaction = 19.7 mg

Improved Labelling of Niclosamide:



Data for unlabeled Niclosamide, **224**:

^1H NMR (400 MHz, DMSO): δ 11.47 (s, 1H, OH), 8.82 (d, $^3J = 9.2$ Hz, 1H, CH^c), 8.43 (d, $^4J = 2.8$ Hz, 1H, CH^a), 8.30 (dd, $J = 9.2$ Hz, $^4J = 2.7$ Hz, 1H, CH^b), 7.97 (d, $^4J = 2.8$ Hz, 1H, CH^d), 7.55 (dd, $^3J = 8.7$ Hz, $^4J = 2.8$ Hz, 1H, CH^e), 7.10 (d, $^3J = 8.7$ Hz, 1H, CH^f).

Incorporation expected at δ 8.82, 8.43, 8.30 and 7.97. Determined against integral at δ 7.55.

NOTE: The reactions involving Niclosamide were run in accordance with *General Procedure F* but with a modified work-up. On completion, the reaction mixture was concentrated *in vacuo* and the product triturated with acetone. The product was collected as a white solid *via* filtration. Deuterium incorporations are delineated below.

Entry ^a	Solvent	Catalyst ^b	% D											
			Run 1				Run 2				Average % D			
1	DCM	196a	a:	b:	c:	d:	a:	b:	c:	d:	a:	b:	c:	d:
			67	50	30	70	65	55	52	62	66	53	41	66
2	DCM	208a	a:	b:	c:	d:	a:	b:	c:	d:	a:	b:	c:	d:
			68	53	17	70	74	60	19	76	71	57	18	73
3	2-MeTHF	196a	a:	b:	c:	d:	a:	b:	c:	d:	a:	b:	c:	d:
			48	9	4	98	53	13	4	97	51	11	4	98
4	2-MeTHF	208a	a:	b:	c:	d:	a:	b:	c:	d:	a:	b:	c:	d:
			96	97	73	96	97	95	56	96	97	96	65	96

^aConditions: 1.25 mL solvent, 0.1075 mmol **224**, 1 h, 25 °C, 5 mol% [Ir]

^bMass of **196a** per reaction = 5.4 mg; mass of **208a** per reaction = 9.1 mg; mass of **224** per reaction = 34.0 mg

*Relative Diffusion of Cation and Anion Fragments of Catalysts 196a and 208a*¹⁴³

DOSY NMR experiments were performed with ¹H NMR for cations and ¹⁹F NMR for anions in CD₂Cl₂ at 300 K, according to reported procedures,¹⁴³ using the synthesised precatalysts only. No measurements were taken with activated intermediates. The raw values for relative diffusion rates are detailed below:

Entry	Complex	$D_{\text{cation}} (x10^{-9} m^2 s^{-1})$	$D_{\text{anion}} (x10^{-9} m^2 s^{-1})$
1	196a	1.496	2.604
2	208a	1.453	1.315

8.5 Base-sensitive HIE: *ortho*-Directed Labelling of Unprotected Tetrazoles

All tetrazole substrates were provided by Sanofi and acquired in-house during this collaborative project.

Following *General Procedure G*, the tetrazole (0.086 mmol, 1.0 eq.), base (0.043 mmol, 0.5 eq.), and catalyst (0.05 eq., 5 mol%, unless otherwise stated), were dissolved in MeOH (1.0 mL). At the end of each reaction (and after taking a 2 μ L LC-MS sample), the solvent was removed *in vacuo* and the remaining residue partitioned between water (5 mL) and 2-MeTHF (5 mL) in a separated funnel. The organic phase was washed with 0.1 M HCl (5 mL), then dried over anhydrous Na₂SO₄ before filtering and concentrating *in vacuo*. The product was then analysed directly *via* ¹H NMR. Deviations from the tetrazole labelling procedure are indicated where necessary.

NOTE: in accordance with the general procedure, it is imperative in this case that the reaction mixture be cooled *prior* to the introduction of deuterium. Heating the basified reaction mixture was found to degrade the catalyst before the reaction began.

Reaction Optimisation for ortho-HIE with N-H Tetrazoles

The table provide below provides additional details not shown in

Table 7. Relevant spectroscopic and spectrometric data are provided in the substrate scope section (*vide infra*).

Entry ^a	Catalyst	X	Base	Time (h)	Temperature (°C)	%D
1	196a	PF ₆	Et ₃ N	1	25	7
2	196a	PF ₆	Cs ₂ CO ₃	1	25	6
3	208a	BArF	Cs ₂ CO ₃	1	25	10
4	196a	PF ₆	Et ₃ N	2	37.5	10
5	196a	PF ₆	Cs ₂ CO ₃	2	37.5	15
6	208a	PF ₆	Et ₃ N	2	37.5	0
7	208a	BArF	Cs ₂ CO ₃	2	37.5	66
8	196a	PF ₆	Et ₃ N	3	50	5
9 ^b	196a	PF ₆	Cs ₂ CO ₃	3	50	83 (83)
10	196a	PF ₆	Cs ₂ CO ₃	1	50	72
11	208a	BArF	Cs ₂ CO ₃	1	50	80
12^b	208a	BArF	Cs₂CO₃	3	50	85 (83)
13 ^c	208a	BArF	Cs ₂ CO ₃	3	50	81
14	208a	BArF	-	3	50	<5
15	196a	PF ₆	Cs ₂ CO ₃	3	50	10

^a Standard reagent quantities: **225** (0.086 mmol, 13.8 mg), Cs₂CO₃ (0.043 mmol, 14.0 mg), or Et₃N (0.006 mL), **208a** (5 mol%, 7.4 mg), or **196a** (5 mol%, 4.4 mg).

^b Values in parentheses reflect reactions carried out with added H₂O (50 μL, ~3 mol%).

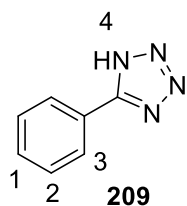
^c Reaction carried out using 2.5 mol% **208a** (3.7 mg) instead of 5.0 mol%.

Substrate Scope for Tetrazole ortho-HIE Protocol (Figure 21)

In the spectroscopic data reported for tetrazoles, *N*-H protons are not visible and not reported.

In all reactions, catalyst **208a** (7.4 mg, 0.0043 mmol, 5 mol%) was employed. All reactions used 1 mL from a stock supply of 0.043 mM Cs₂CO₃ in MeOH as the source of solvent and base combined, and all employed a reaction temperature of 50 °C. Following *General Procedure G*, and notes at the start of **Section 8.5**, results are reported as a) amount of substrate, b) reaction time, and c) level of incorporation.

4-phenyl-1H-tetrazole, 209



Chemical Formula: C₇H₆N₄
Molecular Weight: 146.15

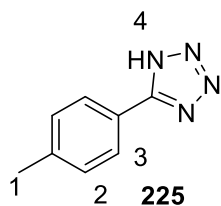
¹H NMR (300 MHz, DMSO): δ 8.05 – 8.02 (m, 2H, ArH³), 7.63 – 7.58 (m, 3H, ArH¹ + ArH²).

Incorporation expected at δ 8.05 – 8.02. Determined against integral at δ 7.63 – 7.58.

a) 12.6 mg, 0.086 mmol, b) 3 h and c) 87% D.

Sanofi HRMS (positive ESI): m/z observed for C₇H₅D₂N₄⁺, [M_{d2} + H]⁺: 149.0791.

5-(4-methylphenyl)-1H-tetrazole, 225



Chemical Formula: C₈H₈N₄
Molecular Weight: 160.18

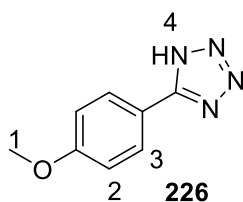
¹H NMR (300 MHz, DMSO): δ 7.92 (d, 2H, ³J = 8.1 Hz, ArH³), 7.40 (d, 2H, ³J = 8.1 Hz, ArH²), 2.38 (s, 3H, ArCH₃).

Incorporation expected at δ 7.92. Determined against integral at δ 2.38.

a) 13.8 mg, 0.086 mmol, b) 3 h, and c) 85% D.

HRMS (positive ESI): m/z calc'd for C₈H₇D₂N₄⁺, [M_{d2} + H]⁺: 163.0947; observed: 163.0946.

5-(4-methoxyphenyl)-1H-tetrazole, 226



Chemical Formula: C₈H₈N₄O
Molecular Weight: 176.1790

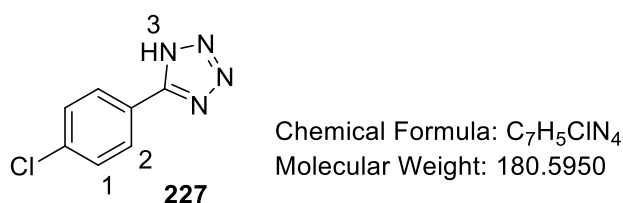
¹H NMR (300 MHz, DMSO): δ 7.97 (d, 2H, ³J = 12.0 Hz, ArH³), 7.15 (d, 2H, ³J = 12.0 Hz, ArH²), 3.83 (s, 3H, OCH₃).

Incorporation expected at δ 7.97. Determined against integral at δ 3.83.

a) 15.2 mg, 0.086 mmol, b) 3 h, and c) 86% D.

Sanofi HRMS (positive ESI): m/z observed for C₈H₇D₂N₄O⁺, [M_{d2} + H]⁺: 178.0893.

5-(4-chlorophenyl)-1H-tetrazole, 227



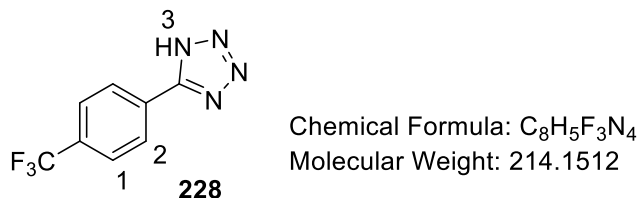
¹H NMR (300 MHz, DMSO): δ 8.04 (d, 2H, ³J = 11.6 Hz, ArH²), 7.68 (d, 2H, ³J = 11.6 Hz, ArH¹).

Incorporation expected at δ 8.04. Determined against integral at δ 7.68.

a) 15.5 mg, 0.086 mmol, b) 3 h, and c) 93% D.

Sanofi HRMS (positive ESI): m/z observed for C₇H₄D₂ClN₄⁺, [M_{d2} + H]⁺: 183.0398 and 185.0372, according to ~4:1 natural abundance of ³⁵Cl versus ³⁷Cl.

5-(4-trifluoromethylphenyl)-1H-tetrazole, 228



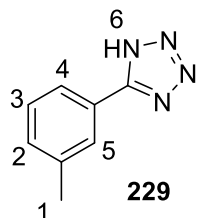
¹H NMR (300 MHz, DMSO): δ 8.25 (d, 2H, ³J = 8.3 Hz, ArH²), 7.98 (d, 2H, ³J = 8.3 Hz, ArH¹).

Incorporation expected at δ 8.25. Determined against integral at δ 7.98.

a) 18.4 mg, 0.086 mmol, b) 3 h, and c) 91% D.

Sanofi HRMS (positive ESI): m/z observed for $C_8H_4D_2F_3N_4^+$, $[M_{d2} + H]^+$: 217.0665.

5-(3-methylphenyl)-1H-tetrazole, 229



Chemical Formula: $C_8H_8N_4$
Molecular Weight: 160.18

1H NMR (300 MHz, DMSO): δ 7.86 (s, 1H, ArH⁵), 7.82 (d, 1H, $^3J = 10.4$ Hz, ArH⁴), 7.48 (t, 1H, $^3J = 10.4$ Hz, ArH³), 7.41 – 7.39 (m, 1H, ArH²), 2.40 (s, 3H, ArCH₃).

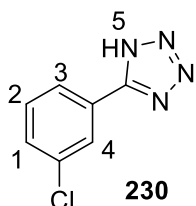
Incorporation expected at δ 7.86 and 7.82. Determined against integral at δ 2.40.

a) 13.8 mg, 0.086 mmol, b) 3 h, and c) 83% D (ArH⁴), 58% D (ArH⁵).

HRMS (positive ESI): m/z calc'd for $C_8H_7D_2N_4^+$, $[M_{d2} + H]^+$: 163.0947; observed: 163.0946.

HRMS (positive ESI): m/z calc'd for $C_8H_8D_1N_4^+$, $[M_{d1} + H]^+$: 162.0884; observed: 162.0884.

5-(3-chlorophenyl)-1H-tetrazole, 230



Chemical Formula: $C_7H_5ClN_4$
Molecular Weight: 180.60

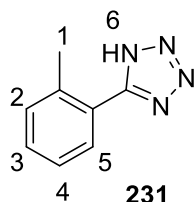
1H NMR (300 MHz, DMSO): δ 8.07 – 8.06 (m, 1H, ArH³), 8.02 – 7.98 (m, 1H, ArH⁴), 7.68 – 7.60 (m, 2H, ArH¹ + ArH²).

Incorporation expected at δ 8.07 – 8.06 and 8.02 – 7.98. Determined against integral at δ 7.68 – 7.60.

a) 15.5 mg, 0.086 mmol, b) 3 h, and c) 95% D (ArH³), 96% D (ArH⁴).

Sanofi HRMS (positive ESI): m/z observed for $C_7H_4D_2ClN_4^+$, $[M_{d2} + H]^+$: 183.0403 and 185.0372, , according to ~4:1 natural abundance of ^{35}Cl versus ^{37}Cl .

5-(2-methylphenyl)-1H-tetrazole, 231



Chemical Formula: $C_8H_8N_4$
Molecular Weight: 160.18

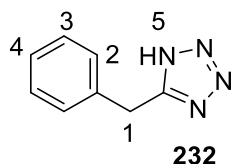
1H NMR (300 MHz, DMSO): δ 7.92 (d, 1H, $^3J = 9.2$ Hz, ArH⁵), 7.50 – 7.36 (m, 3H, ArH² – ArH⁴), 2.43 (s, 3H, ArCH₃).

Incorporation expected at δ 7.92. Determined against integral at δ 2.43.

a) 13.8 mg, 0.086 mmol, b) 16 h, and c) 81% D.

Sanofi HRMS (positive ESI): m/z observed for $C_8H_8D_1N_4^+$, $[M_{d1} + H]^+$: 162.0884.

5-benzyl-1H-tetrazole, 232

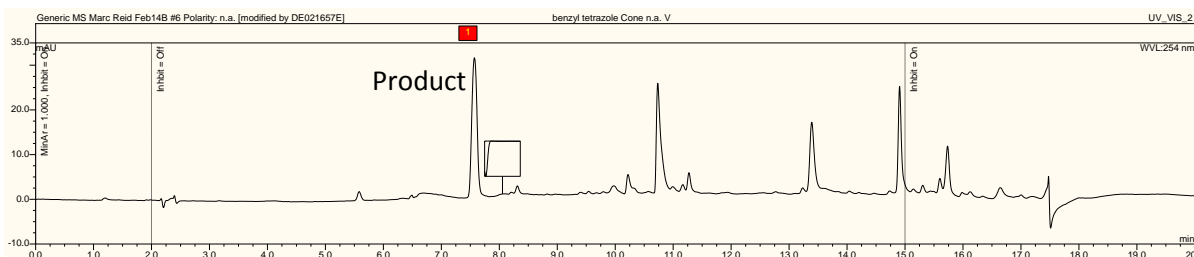


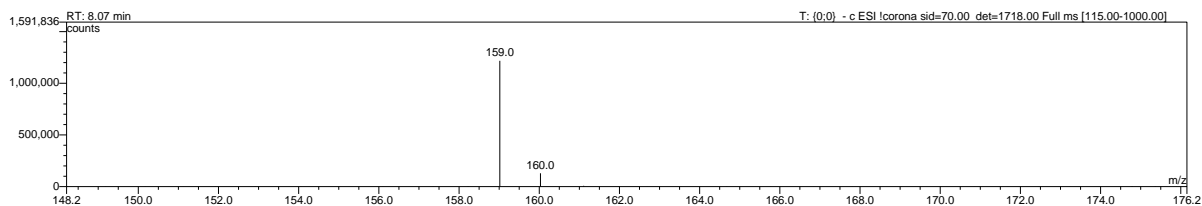
Chemical Formula: $C_8H_8N_4$
Molecular Weight: 160.18

1H NMR (300 MHz, DMSO): δ 7.35 – 7.25 (m, 5H, ArH² – ArH⁴), 4.28 (s, 2H, PhCH₂¹)

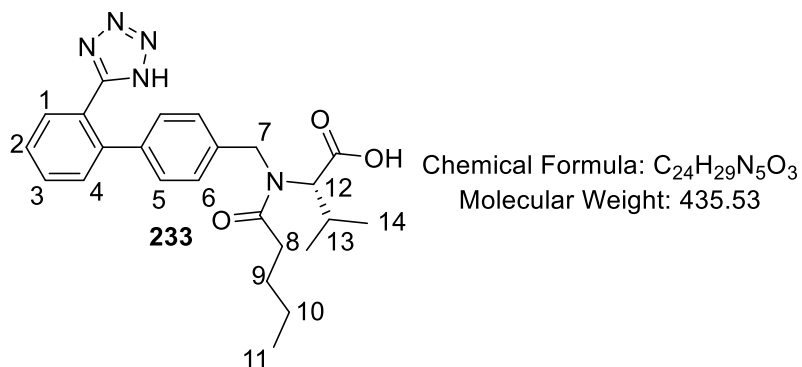
Incorporation expected at δ 7.35 – 7.25. Determined against integral at δ 4.28.

No detailed analysis was carried out on substrate **232** after observation of only non-deuterated $[M - H]^-$ and degradation *via* LC-MS (see below).





Valsartan, **233** (Scheme 43)



The deuterium labelling reaction was carried out in a Heidolph Synthesis 1 Liquid 16 device (see below):



Following *General Procedure G*, no work-up of the sample was attempted. Results are reported as: a) amount of **233**, b) amount of **208a**, c) amount of Cs₂CO₃, d) amount of MeOH, e) reaction temperature, f) reaction time, and g) %D.

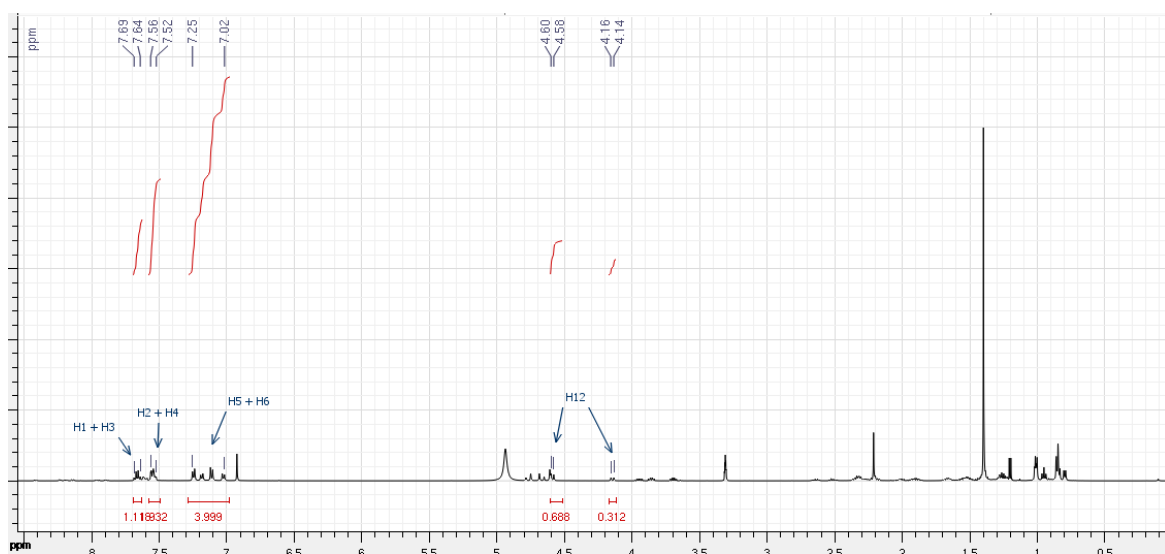
It has been reported in the literature that Valsartan, **233**, exists in solution as a pair of conformers due to *cis/trans* isomerisation of the amide bond.²⁶¹ In light of these complications, full ¹H NMR analysis of **233** is not provided. Instead, partial analysis of the aromatic and stereogenic protons is given, along with the consistent LC-MS trace showing primarily **233-d**₁.

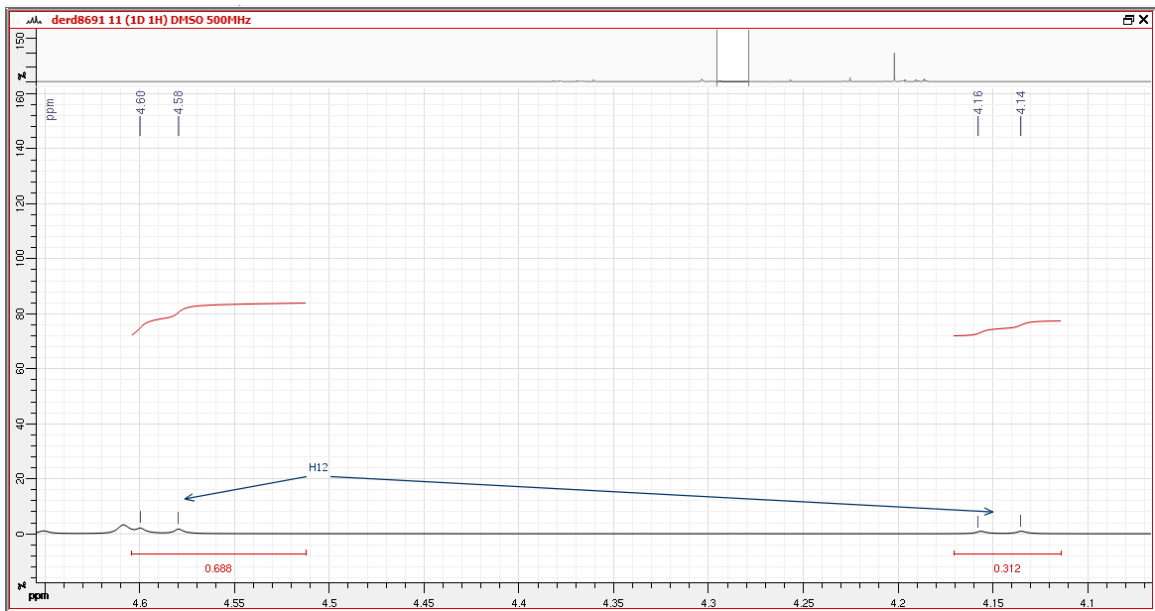
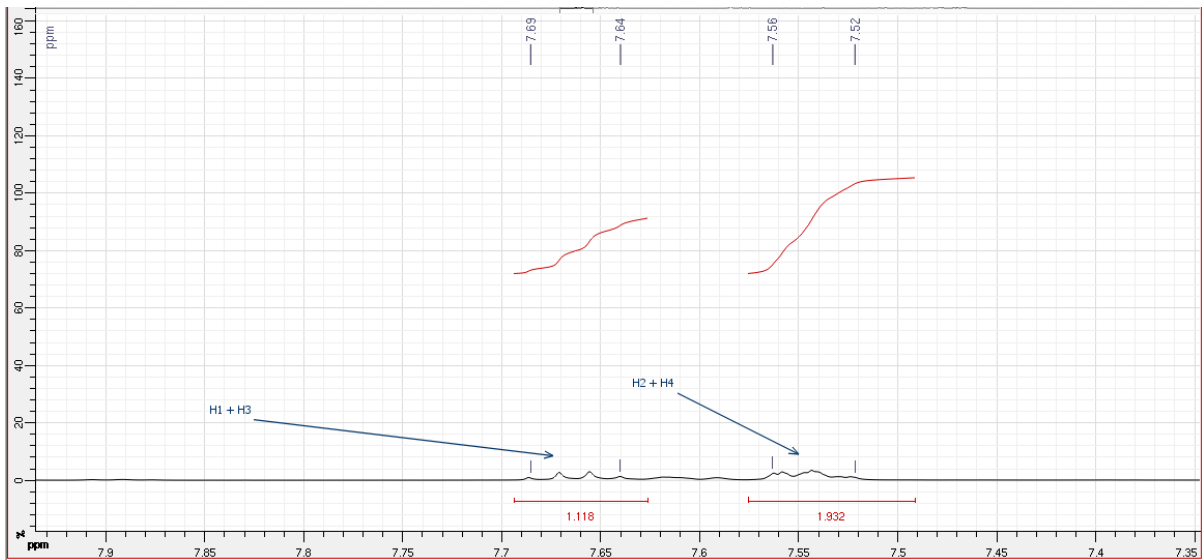
¹H NMR (500 MHz, DMSO): δ 7.69 – 7.64 (m, 2H, ArH¹ + ArH³), 7.56 – 7.52 (m, 2H, ArH² + ArH⁴), 7.25 – 7.02 (2 x d, with each d split into a ~66.6 : 33.3 mixture according to the presence of two rotamers, 4H in total, all d's share ³J = 8.3 Hz, ArH⁵ + ArH⁶), 4.59 and 4.15 (1 x d split into a ~66.6 : 33.3 mixture according to the presence of two rotamers, 1H in total, both d's share ³J = 10.6 Hz, CH¹²).

Incorporation expected at δ 7.96 - 7.64. Determined against integral at δ 7.25 – 7.02.

a) 18.5 mg, 0.043 mmol, b) 3.7 mg, 0.002 mmol, 5 mol%, c) 14.0 mg, 0.043 mmol, d) 1 mL, e) 50 °C, f) 6 h, and g) 88% D.

In lieu of full spectroscopic analysis, spectrum screenshots are shown below. From this, it can be seen that the stereogenic proton, H¹², remains largely untouched, with an estimated total integration of ~1H:

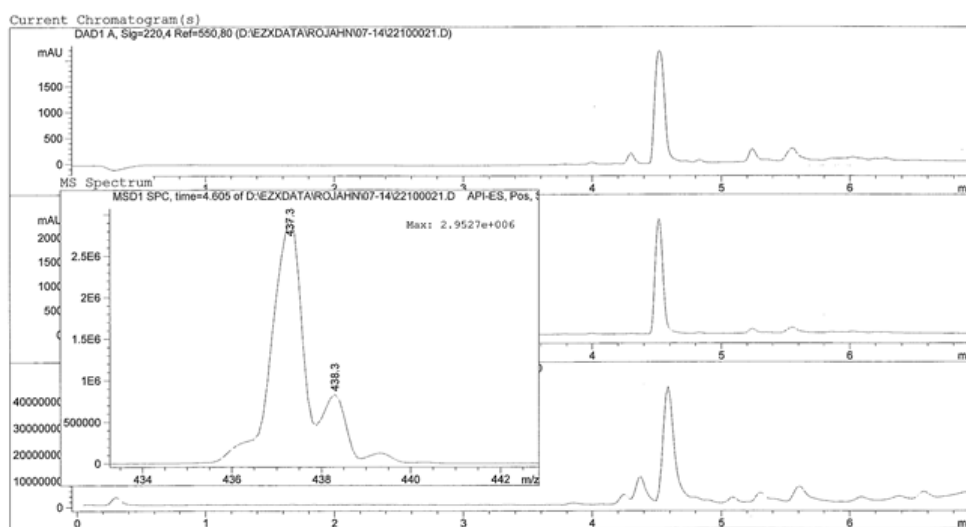




Low resolution LC-MS supports the presence of majority **233-d₁**:

Print of all graphic windows
Valsartan, 6h
Agilent Easy-Access Method: 'M2M.M'
*** No target masses specified ***

=====
Injection Date : 22.07.2014 15:56:29 Location : Vial 84
Sample Name : PR36.2 A4 Inj : 1
Acq. Operator : P.Rojahn Inj Volume : 2 µl
Acq. Instrument : INSTRUMENT1
Acq. Method : C:\HPCHEM\1\METHODS\M2M.M
Last changed : 22.07.2014 15:55:19 by P.Rojahn
(modified after loading)
Analysis Method : C:\HPCHEM\1\METHODS\LCMSKURZ.M
Last changed : 30.11.2012 13:20:14 by G.Scholz



INSTRUMENT1 05.08.2014 09:05:27 P.Rojahn

Page 1 of 1

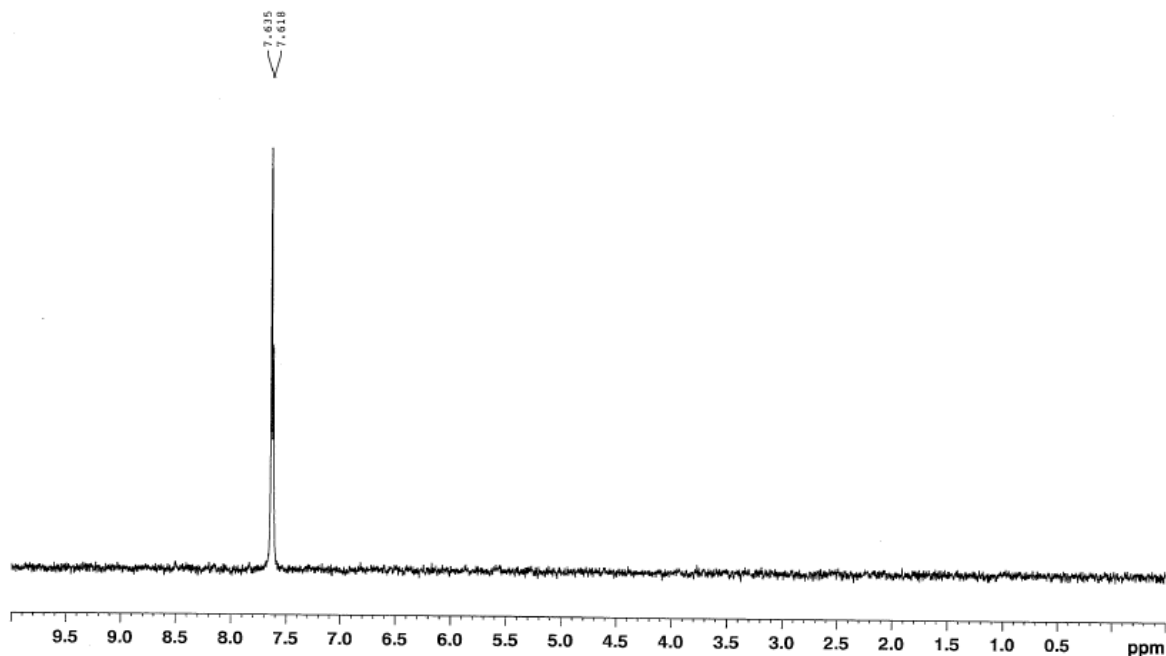
Sanofi HRMS (positive ESI): m/z observed for $C_{24}H_{29}D_1N_5O_3^+$, $[M_{d1} + H]^+$: 437.2406.

The tritiation of **233** was carried out at Sanofi (Frankfurt) using a standard Tritec tritium manifold. A solution of **233** (3.5 mg, 8.0 µmol), Cs_2CO_3 (2.62 mg, 8.0 µmol, 1.1 eq.), and **208a** (0.7 mg, 0.4 8.0 µmol, 6.7 mol%) were dissolved in MeOH (0.7 mL) in a 1.0 mL reaction flask before being secured to the manifold. The solution was frozen in liquid nitrogen, evacuated and charged with tritium (3.2 eq., 0.153 mg, 1.5 Ci, 40 mbar). The reaction mixture was then allowed to warm to room temperature over 15 mins before stirring at r.t. for a further 30 mins (212 mbar pressure). The reaction mixture was then heated to 50 °C (370 mbar) and stirred for 45 mins before cooling again to r.t. and stirring for a final 2 h. Purification and isolation *via* HPLC gave the tritiated product (0.91 mg, **233-T₁**, 50% T, 98.9% radiochemical purity).

Sanofi HRMS (positive ESI): m/z observed for $C_{24}H_{29}T_1N_5O_3^+$, $[M_{t1} + H]^+$: 438.2502.

Please see below for a screen shot of the ^3H NMR, showing tritium incorporation *ortho* to the tetrazole only:

533MHz $^3\text{H}/\text{T}$ Dr.De Valsartan-T FFC.URA.055.1 0.05mg ; DMSO-d6
zg3h1Hig



Investigating the pH of Reaction and Likely State of the Tetrazole (Figure 22)

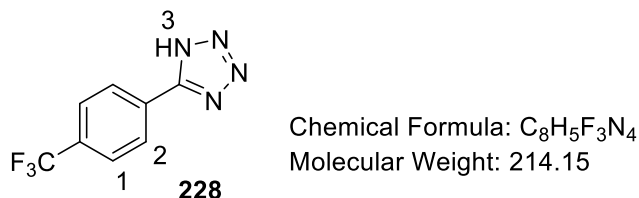
Methyl red indicator test

As described in the results section, substrate **228** was used in repeat experiments of those conditions from

Table 7 (Entries 12 and 14). In the first instance, these two reactions were compared visually without the addition of indicator. Separately, two more reactions were carried out, and a similar visual comparison made *after* the addition of a spatula-tip of methyl red into each carousel flask. No further analyses of these reactions were carried out beyond what is shown in **Figure 22**.

¹⁹F NMR studies of substrate **228**

The relevant data for substrate **228** in MeOD-d₄ (condition 1 from **Figure 22**) are provided below:



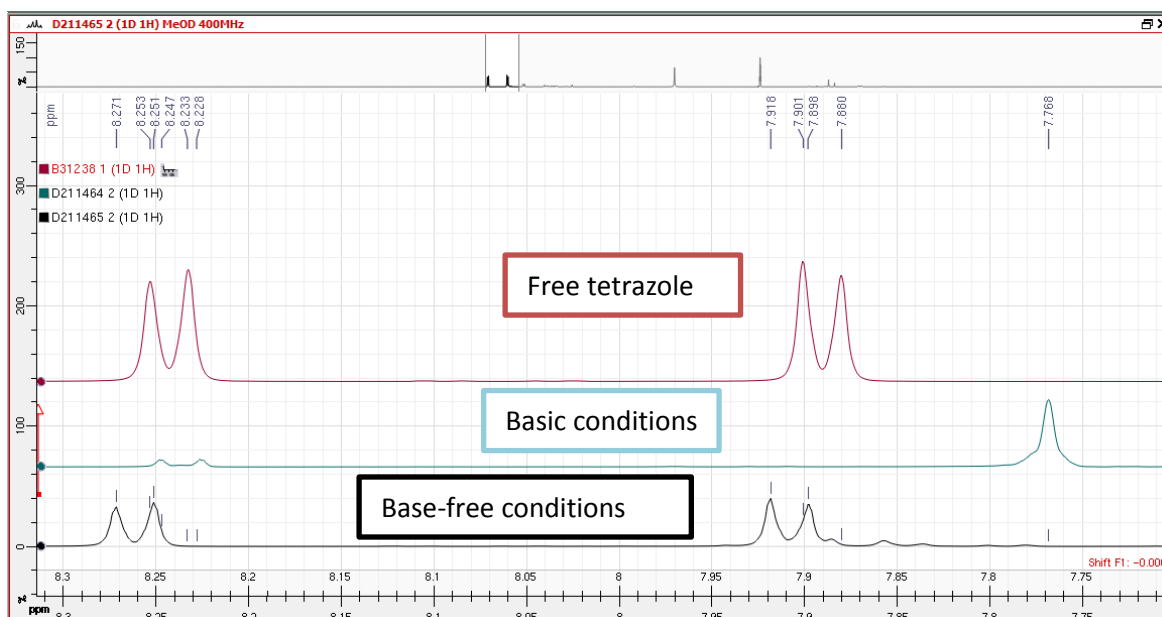
¹H NMR (400 MHz, MeOD-d₄): δ 8.24 (d, 2H, ³J = 8.6 Hz, ArH²), 7.89 (d, 2H, ³J = 8.6 Hz, ArH¹).

¹⁹F NMR (376 MHz, MeOD-d₄): δ - 64.6 (CF₃).

To assess the effects of the optimised (basic) reaction conditions on tetrazole **228**, the substrate (18.4 mg, 0.086 mmol), catalyst **208a** (7.4 mg, 0.0043 mmol), and Cs₂CO₃ (14.0 mg, 0.043 mg) were dissolved in MeOD-d₄ (1 mL) and added to an oven-dried NMR tube. After sealing the tube with a rubber septum, D₂ was bubbled through the tube for 30 mins prior to NMR analysis (300 K).

Similarly for assessing the base-free conditions, the same preparations were made in a separate NMR tube, *minus* the addition of Cs₂CO₃.

Comparative ¹H NMR resonances (not shown in the **Results** section) are shown below. In addition, all peak positions and relevant integrations are listed in the table below the spectra.



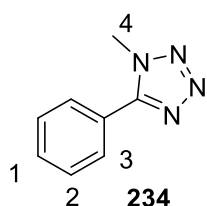
Entry	Condition	^{19}F NMR (ppm)	^1H NMR (ppm) ^a	Integral ratio (ArH ¹ :ArH ²)
1	Free tetrazole	-64.6	8.24, 7.89	2.0 : 2.0
2 ^b	Basic	-64.2	8.24, 7.77	2.0 : 0.3
3	Base-free	-64.6	8.26, 7.91	2.0 : 1.8

^a Position of each resonance stated only.
^b Significant deuterium labelling observed.

Investigating the Importance of N-H Tetrazoles and Changes in the Active Catalyst (Scheme 44)

In all reactions, substrate (0.086 mmol) was employed with catalyst **208a** (7.4 mg, 0.0043 mmol, 5 mol%). All reactions employing base used 1 mL from a stock supply of 0.043 mM Cs₂CO₃ in MeOH as the source of solvent and base combined, and all employed a temperature of 50 °C over a 3 h reaction time. Base-free reactions used 1 mL pure MeOH as the solvent rather than the basified stock solution. *General Procedure G* was followed otherwise, and no work-up was used before analysis.

5-phenyl-*N*-methyltetrazole, **234**



Chemical Formula: C₈H₈N₄
Molecular Weight: 160.18

¹H NMR (300 MHz, MeOD-*d*₄): δ 7.85 – 7.82 (m, 2H, ArH³), 7.68 – 7.61 (m, 3H, ArH¹ + ArH²), 4.21 (s, 3H, NCH₃).

Incorporation expected at δ 7.85 – 7.82. Determined against integral at δ 4.21.

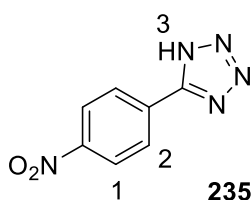
Reactions monitored *via* ¹H NMR only.

From Scheme 44, Part A

Entry	Conditions	% D
1 ^a	basic	28
2 ^b	base-free	17

^aConditions: **234** (13.8 mg), Cs₂CO₃ (1 mL from 0.043 mM solution in MeOH), **208a** (5 mol%).
^bConditions: **234** (13.8 mg), MeOH (1 mL), **208a** (5 mol%)

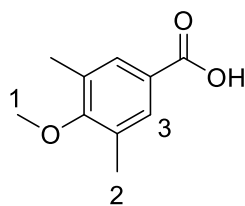
5-(4-nitrophenyl)-1*H*-tetrazole, **235**



Chemical Formula: C₇H₅N₅O₂
Molecular Weight: 191.15

¹H NMR (300 MHz, DMSO): δ 8.42 (d, 2H, ³J = 8.8 Hz, ArH¹), 8.29 (d, 2H, ³J = 8.8 Hz, ArH²).

Incorporation expected at all positions. For the base-free reaction, incorporation in positions ArH¹ and ArH² was measured against an equimolar quantity of the following internal standard (15.5 mg, 0.086 mmol):



Chemical Formula: C₁₀H₁₂O₃

Molecular Weight: 180.20

¹H NMR (300 MHz, DMSO): δ 7.61 (s, 2H, ArH³), 3.67 (s, 3H, ArOCH₃¹), 2.23 (s, 6H, ArCH₃²). Signal at δ 3.67 used to calibrate substrate **235** signals.

For the base-mediated reaction, the ratio of ¹H NMR signals in the product was compared to HRMS data in order to estimate %D adjacent to each directing group. Specifically, an NMR peak ratio of 1: 0.095 (b : a) favouring tetrazole labelling was compared to HRMS peaks [M(*n*D) +H]⁺ (*n* = 1, 2, 3) in the ratio 7.4 : 85.0 : 7.6 (d₁ : d₂ : d₃). This translates to approximately 89% D_a and 8% D_b.

Reactions in base and base-free conditions for substrate **235** (16.4 mg, 0.086 mmol) and were carried out in a similar fashion to those described for **Scheme 44, Part A**. Results are summarised in the table below.

Entry	Conditions	% D _a	%D _b
1 ^a	basic	89	8
2 ^b	base-free	30	27

^aConditions: **235** (16.4 mg), Cs₂CO₃ (1 mL from 0.043 mM solution in MeOH), **208a** (5 mol%), 3 h, 50 °C.
^bConditions: **235** (16.4 mg), MeOH (1 mL), **208a** (5 mol%), 3 h, 50 °C.

Investigating Substrate Electronics in Ir-catalysed Tetrazole Labelling (Table 8)

Following *General Procedure G* and notes on at the start of **Section 8.5**, tetrazoles **209** and **225 – 228** were subjected to identical labelling conditions as reported *vide supra* for the reaction scope. The only change was in the time (now 5 mins rather than 3 h). For brevity, readers are directed to the spectroscopic data and reagent stoichiometries reported in the *Substrate Scope* subsection. For construction of the Hammett plot, %D values for substrates

manifesting <30% D (X = H, Me, and OMe) were used as reaction rate surrogates. These values were then manipulated as shown in the table below.

Entry	X	Substrate	%D	%D _X /%D _H	log ₁₀ (%D _{X/H})	F ^b	R ^b	σ _P ^c
1	H	209	26	1.00	0.00	0.00	0.00	0.00
2	Me	225	14	0.54	-0.27	0.01	-0.18	-0.17
3	OMe	226	10	0.38	-0.41	0.29	-0.56	-0.26
4 ^a	CF ₃	228	67	2.58	-	-	-	-
5 ^a	Cl	227	73	2.81	-	-	-	-

^a Not considered in Hammett analysis.

^b Field (F) and resonance (R) values collected from the literature.¹⁹⁴

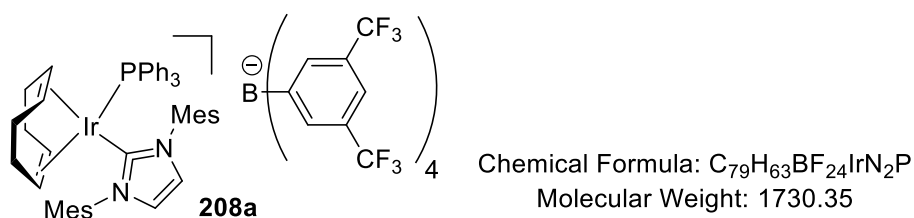
^c σ_P = a.F + b.R such that σ_P produces a straight line of R² = 1 when plotted against log₁₀(%D_{X/H}). Here, a = 1.00, b = 0.98. In other words, field and resonance effects are almost balanced.

³¹P NMR Study of the Catalyst with various Components of the Tetrazole Labelling Method (Figure 23)

The relevant spectroscopic analyses of the precatalyst in MeOD-d₄ are given below. **NOTE:** the precatalyst is only sparingly soluble in MeOD-d₄ and has to be shaken vigorously to create a red solution.

η⁴-Cycloocta-1,5-diene(1,3-dimesitylimidazoline-2-ylidene)

(triphenylphosphine)iridium(I) tetrakis[(3,5-trifluoromethylphenyl)]borate, **208a**



¹H NMR (400 MHz, MeOD-d₄): δ 7.74 (s, 2H, NCH=CHN), 7.61 – 7.59 (m, 12H, ArH_{BArF}), 7.52-7.48 (m, 3H, ArH), 7.38-7.33 (m, 6H, ArH), 7.24-7.19 (m, 6H, ArH), 7.13 (s, 2H, ArH),

6.76 (s, 2H, ArH), 4.48-4.45 (m, 2H, COD CH), 3.39-3.36 (m, 2H, COD CH), 2.37 (s, 6H, ArCH₃), 2.17 (s, 6H, ArCH₃), 1.83 (s, 6H, ArCH₃), 1.76-1.52 (m, 6H, COD CH₂), 1.34-1.29 (m, 2H, COD CH₂).

³¹P NMR (162 MHz, MeOD-d₄): δ 16.2 (PPh₃).

¹⁹F NMR (376 MHz, MeOD-d₄): δ -64.3 (BArF ArCF₃).

These spectral details were largely unchanged between 300 and 318 K.

Triphenylphosphine

³¹P NMR (162 MHz, MeOD-d₄): δ -5.94 (PPh₃).

Triphenylphosphine oxide

³¹P NMR (162 MHz, MeOD-d₄): δ 32.1 (POPh₃).

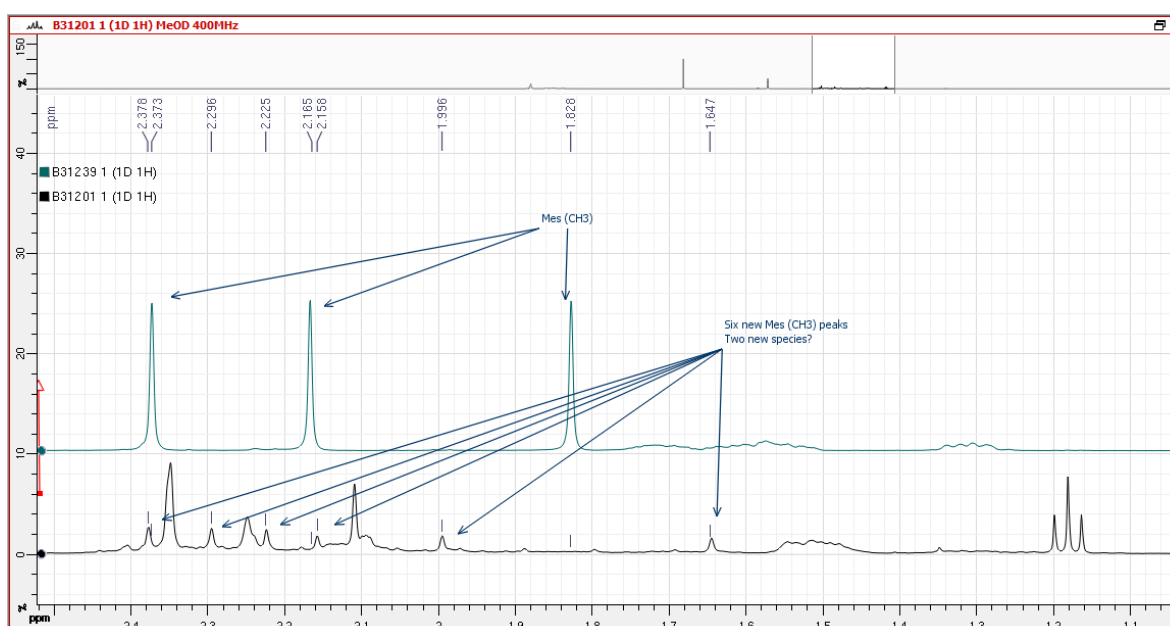
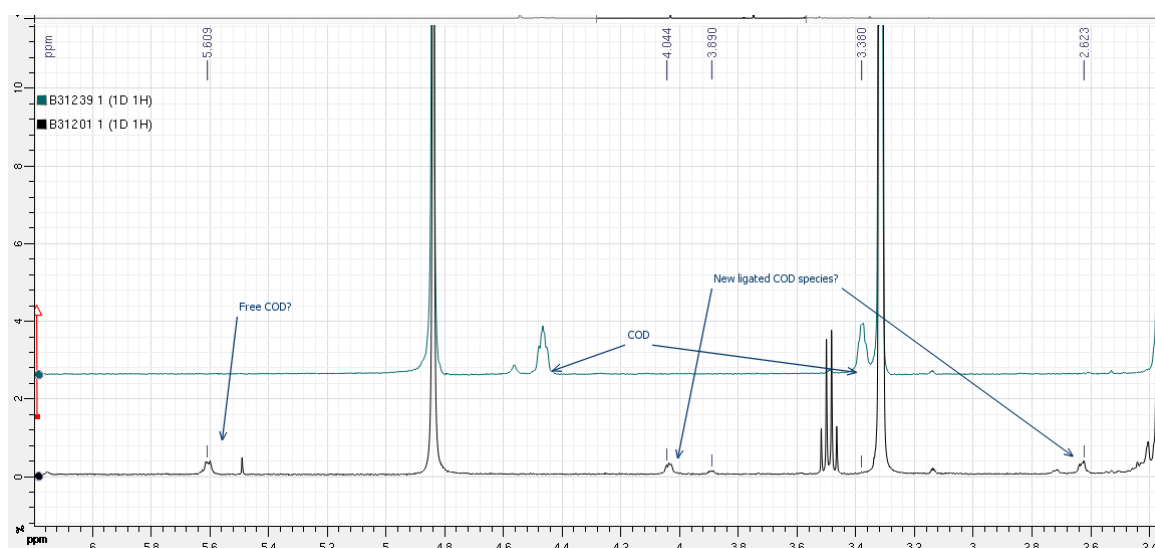
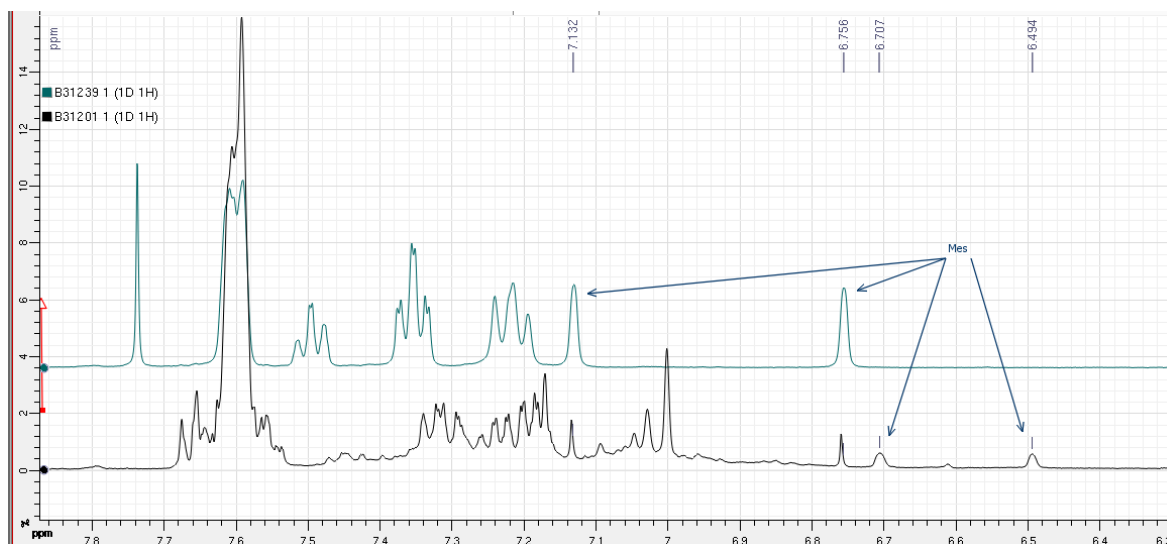
Analysis of Catalyst 208a + Cs₂CO₃

208a (7.4 mg, 0.0043 mmol) and Cs₂CO₃ (2.8 mg, 0.0086 mmol, ~ 2.0 eq.) were dissolved in MeOD-d₄ (1 mL) and sealed in an NMR tube under an argon atmosphere. The contents of the tube were shaken vigorously for 10 mins, causing a red to yellow colour change. In relation to the results in **Figure 23**, NMR analysis of the sample at 300K is provided (primarily ³¹P). Additional spectral overlays are provided for ¹H NMR data (relative to another species) where formal peak assignment is not yet possible.

³¹P NMR (162 MHz, MeOD-d₄): δ 32.3 (unknown).

¹⁹F NMR (376 MHz, MeOD-d₄): δ -64.3 (BArF ArCF₃).

¹H NMR (400 MHz, MeOD-d₄): Overlaid with precatalyst (green).



Similar results were achieved when applying **208a** (7.4 mg, 0.0043 mmol) and Cs_2CO_3 (14.0 mg, 0.043 mmol).

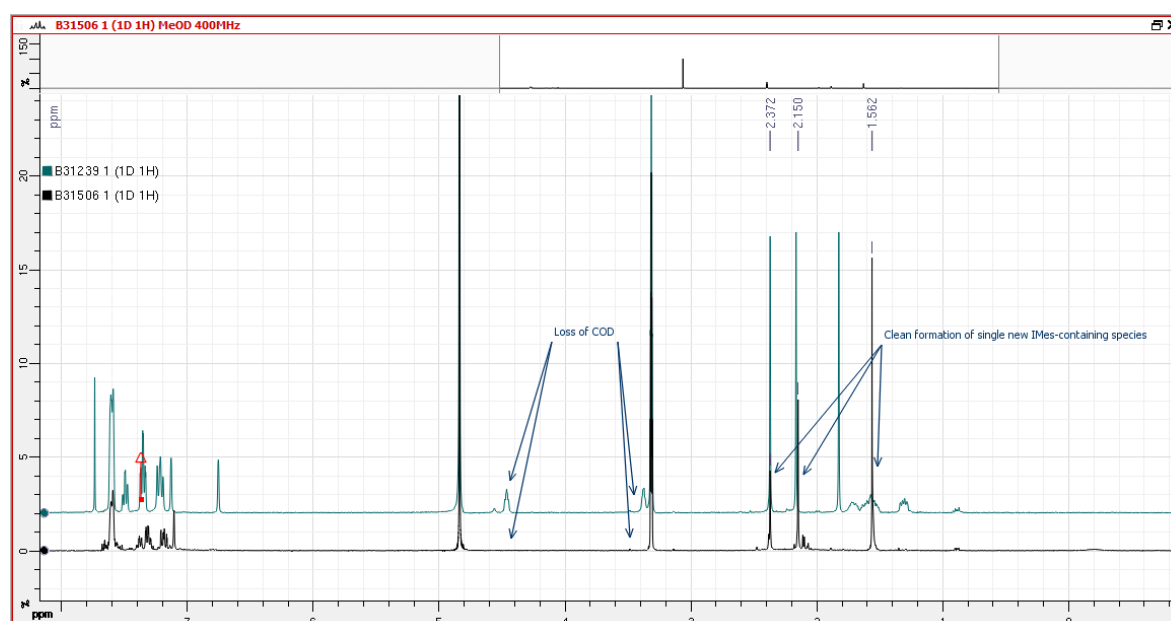
Analysis of Catalyst **208a** + H₂

208a (7.4 mg, 0.0043 mmol) was placed in MeOD-d₄ (1 mL) and sealed in an NMR tube using a rubber septum. Hydrogen gas was bubbled through the mixture with shaking, dissolving the precatalyst and giving a clear yellow solution.

³¹P NMR (162 MHz, MeOD-d₄): δ 32.4 (unknown).

¹⁹F NMR (376 MHz, MeOD-d₄): δ -64.3 (BArF ArCF₃).

¹H NMR (400 MHz, MeOD-d₄): Overlaid with precatalyst (green).



No hydride signals ($\delta < 0$ ppm) were observed.

Analysis of Catalyst **208a** + H₂ + Cs₂CO₃

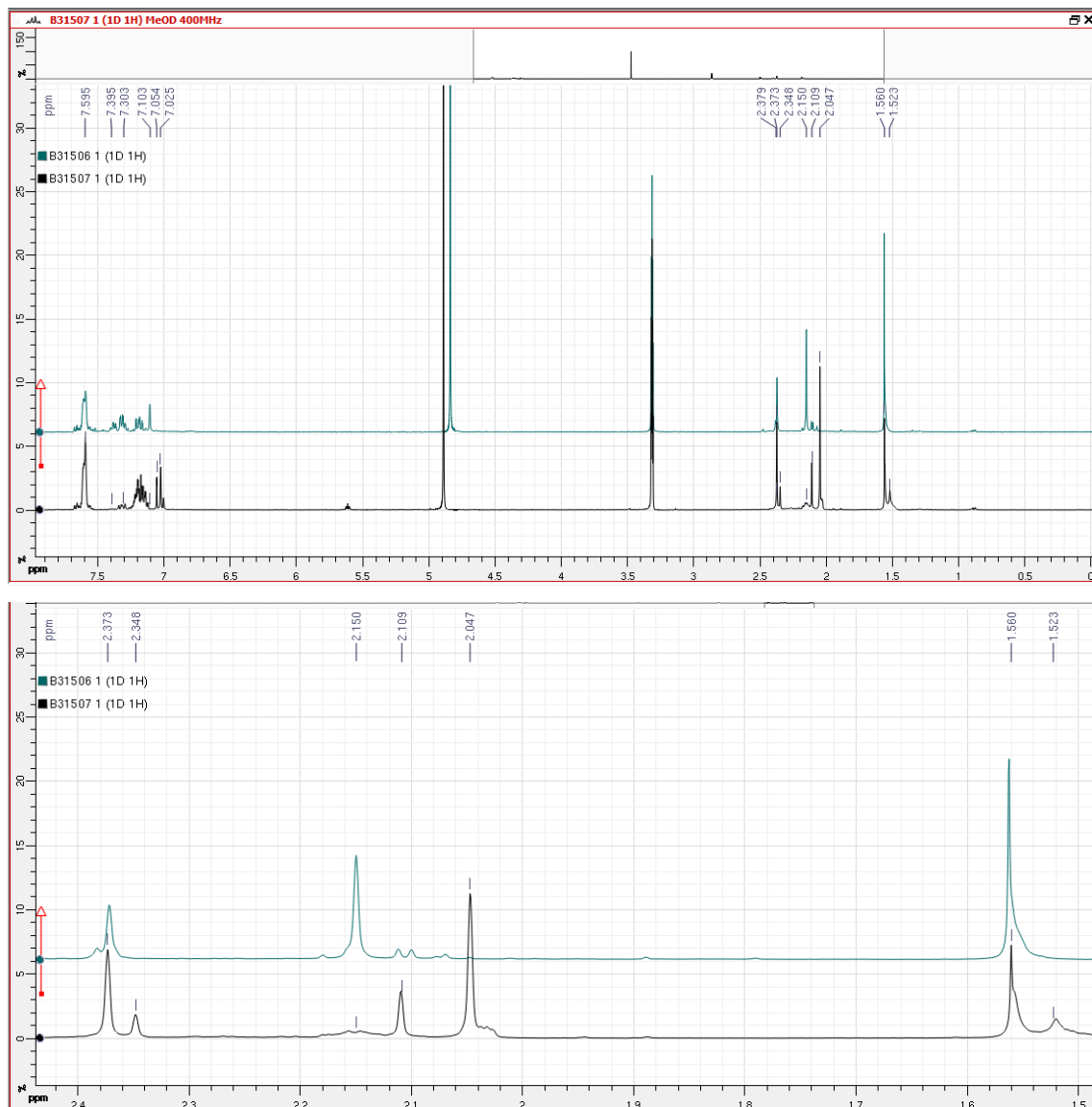
208a (7.4 mg, 0.0043 mmol) and Cs₂CO₃ (14.0 mg, 0.043 mmol) were dissolved in MeOD-d₄ (1 mL) and sealed in an NMR tube using a rubber septum. Hydrogen gas was bubbled through the mixture, producing a clear yellow solution.

³¹P NMR (162 MHz, MeOD-d₄): δ 32.3, 14.2, 13.3 (unknown).

¹⁹F NMR (376 MHz, MeOD-d₄): δ -64.3 (BArF ArCF₃).

¹H NMR (400 MHz, MeOD-d₄): The overlap provided shows the current experiment (black) versus the previous experiment (green) where only H₂ was used. The zoom in of the aliphatic

region shows the formation of (at least) two distinct patterns of mesityl substitution. Analysis of the hydride region allowed observation of a trace doublet (-9.7 ppm) with a suspected $^3J_{H-P} = 13.8$ Hz, consistent with a *cis*-ligated phosphine relative to (at least) one hydride.



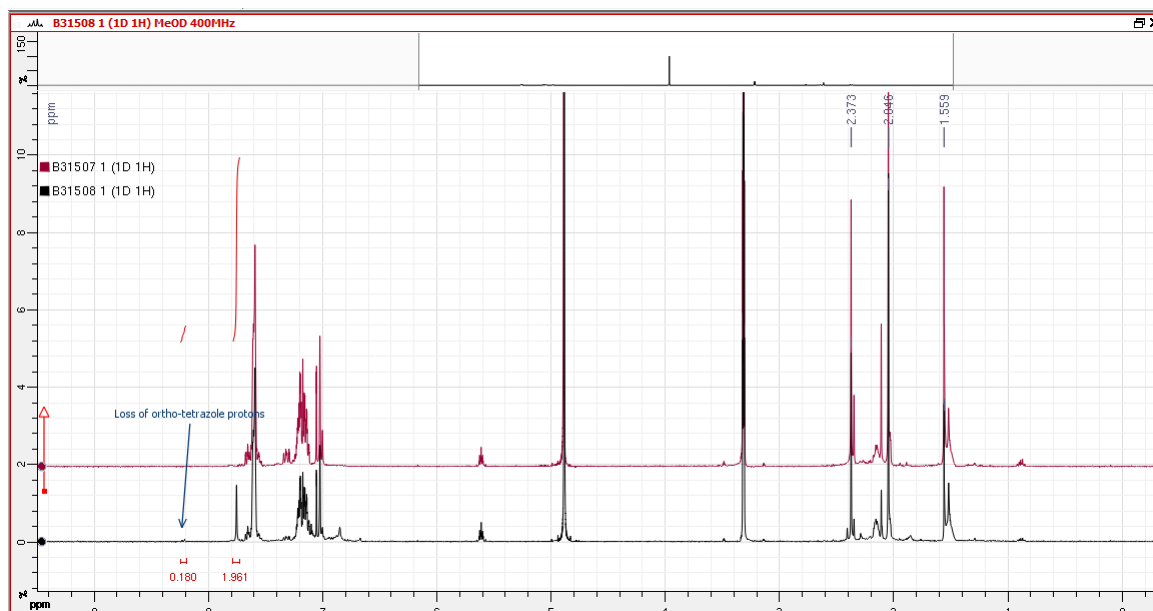
Analysis of Catalyst **208a** + H_2 + Cs_2CO_3 + tetrazole **228**

208a (7.4 mg, 0.0043 mmol), Cs_2CO_3 (14.0 mg, 0.043 mmol) and **228** (1.1 mg, 0.0051 mmol) were dissolved in MeOD-d_4 (1 mL) and sealed in an NMR tube using a rubber septum. Hydrogen gas was bubbled through the mixture, producing a clear yellow solution.

^{31}P NMR (162 MHz, MeOD-d_4): δ 32.3, 14.3 (trace), 13.5 (unknown).

^{19}F NMR (376 MHz, MeOD- d_4): δ -64.3 (BArF ArCF $_3$), -64.2 (tetrazole CF $_3$).

^1H NMR (400 MHz, MeOD- d_4): The overlay provided shows the current experiment (black) *versus* the previous experiment (red) where no tetrazole was present. Firstly, it appears that similar species are formed in solution in the presence or absence of tetrazole **228**. Most interestingly however, complete exchange of the *ortho*-protons was observed, despite the fact that H $_2$ has been used in place of D $_2$. The use of a 1:1.2 mixture of **208a** : **228** is not representative of the true reaction stoichiometry and thus does not allow strong inferences to be made. Nonetheless, this may indicate a favourable exchange between H and D, mediated by iridium. Analysis of the hydride region allowed observation of the same trace doublet (-9.7 ppm) with a suspected $^3J_{\text{H-P}} = 12.8$ Hz, consistent with a *cis*-ligated phosphine relative to (at least) one hydride.

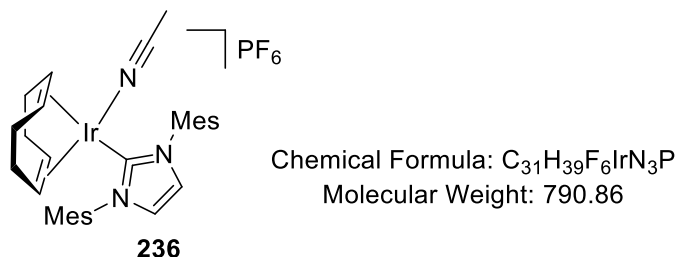


Investigating the Role of the PPh $_3$ Ligand in Ir-catalysed Tetrazole Labelling (Table 9)

Synthesis of η^4 -Cycloocta-1,5-diene(1,3-dimesitylimidazol-2-ylidene) (acetonitrile)iridium(I) hexafluorophosphate, 236

Following *General Procedure C*, results are reported as a) amount of **207**, b) volume of THF, c) amount of AgPF $_6$, d) amount of MeCN, e) reaction time, f) product yield, and g) purification technique.

a) 0.250 g, 0.389 mmol, b) 10 mL, c) 0.098 g, 0.389 mmol, d) 0.016 g, 0.389 mmol, e) 16 h, f) 0.241 g, 78% yield, and g) the THF solution was evacuated to quarter-volume and the product triturated using cold hexane.



Appearance: orange/yellow solid.

m.p.: Decomposes >175 °C.

FTIR (neat): 2980, 2935, 2920, 2885, 1607, 1495, 1335, 1240 cm^{-1} .

1H NMR (400 MHz, $CDCl_3$): δ 7.10 (s, 2H, NCH=CHN), 7.08 (bs, 4H, ArH), 4.03-4.01 (m, 2H, COD CH), 3.46-3.44 (m, 2H, COD CH), 2.48 (s, 3H, CH_3CN), 2.41 (s, 6H, $ArCH_3$), 2.18 (s, 12H, $ArCH_3$), 1.89-1.82 (m, 2H, COD CH_2), 1.75-1.66 (m, 2H, COD CH_2), 1.61-1.51 (m, 4H, COD CH_2).

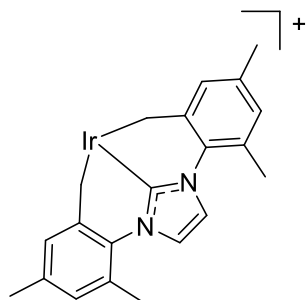
^{13}C NMR (100 MHz, $CDCl_3$): δ 173.9, 140.0, 135.0, 134.9, 129.3, 125.1, 124.2, 82.7, 65.8, 32.8, 29.0, 21.1, 18.3, 3.44.

^{13}C JMOD NMR (100 MHz, $CDCl_3$): δ 140.0 ($CH_3\text{C}\underline{N}$, inverted), 135.0 (inverted), 134.9 (inverted), 129.3, 125.1 (inverted), 124.2, 82.7 (inverted), 65.8 (inverted), 32.8 (inverted), 29.0 (inverted), 21.1, 18.3, 3.44 ($\underline{C}H_3CN$, inverted).

^{31}P NMR (162 MHz, $CDCl_3$): δ -144.4 (septet, $^1J_{P-F} = 711.8$ Hz, PF_6).

^{19}F NMR (376 MHz, $CDCl_3$): δ -73.2 (d, $^1J_{P-F} = 711.8$ Hz, PF_6).

HRMS (positive ESI): No mass ion observed and is expected based on literature precedent.²⁶² Suspected fragment (below) for $[M - PF_6 - COD - MeCN - 2H]^+$ at $m/z = 495.1402$.



Application of Alternative Catalyst, 236, in Tetrazole Labelling

Following *General Procedure G* and notes on at the start of **Section 8.5**, tetrazoles **209**, **234**, and **225** – **228** were subjected to identical labelling conditions as reported *vide supra* for the reaction scope. The only change was in the catalyst (**196a** and **236** rather than **208a**). The comparison of catalysts here was chosen in order to maintain the same counterion throughout. For brevity, readers are directed to the spectroscopic data and reagent stoichiometries reported earlier in this section regarding the substrates tested. These values were then manipulated as shown in the table below.

Entry	X	Substrate	%D(196a) ^a	%D(236) ^b
1	H	209	83	20
2	Cl	227	78	37
3	4-CF ₃	228	93	28
4	4-Me	225	83	6
5	4-OMe	226	89	11
6	N-Me	234	17	22

^aConditions: Substrate (0.086 mmol), Cs₂CO₃ (1 mL from 0.043 mM solution in MeOH), **196a** (4.3 mg, 0.0043 mmol, 5 mol%).
^b Conditions: As in *a*, except using **236** (3.4 mg, 0.0043 mmol, 5 mol%)

Probing the Deuterium Source in Ir-catalysed Tetrazole Labelling (Scheme 44)

Labelling of Substrate 225 in MeOD-d₄ in the Absence of D₂

Following *General Procedure G*, **225** (13.8 mg, 0.086 mmol), Cs₂CO₃ (14.0 mg, 0.043 mmol), and **208a** (7.4 mg, 0.0043 mmol) were dissolved in MeOD-d₄ (1 mL) and added to the oven-dried carousel tube under an argon atmosphere. Here, no cooling was carried out as no D₂ was introduced to the system. The reaction tube was heated to 50 °C (as before) and stirred for 3 h. The solvent was removed *in vacuo* and the product analysed directly via ¹H NMR (8% D). See above for the spectroscopic data relating to **225**.

Labelling of Substrate **225** in MeOD-*d*₄ in the Presence of D₂

Following *General Procedure G* and notes at the start of **Section 8.5**, tetrazole **225** was subjected to identical labelling conditions as reported *vide supra* for the reaction scope, replacing MeOH with MeOD-*d*₄. The evacuated reaction mixture was analysed directly *via* ¹H NMR (98% D).

8.6 Experimental & Theoretical Ligand Design Methods in HIE Processes

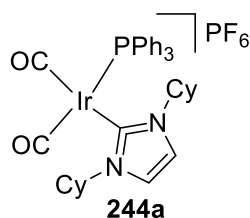
Ir(I) Di- and Tricarbonyl Complexes in the Assessment of Combined Ligand Sterics

Following *General Procedure J*, results are reported as a) amount of [(COD)Ir(NHC)(PR₃)]PF₆, and b) product yield.

In all cases, clear ¹³C NMR spectra could not be acquired and are thus not reported. This has been noted previously for similar complexes by Hope *et al.*¹⁹⁵ For starting chloro/carbene complexes that are not described elsewhere in this section, readers are directed to the references provided, or to **Section 8.6**, where the catalytic properties of such complexes bear most relevance.^{112,147,151}

*Preparation of Dicarbonyl(dicyclohexylimidaz-2-ylidene)(triphenylphosphine)iridium(I) hexafluorophosphate, **244a***

a) [(COD)Ir(ICy)(PPh₃)]PF₆ (0.200 g, 0.213 mmol), and b) 0.153 g, 81% yield.



Chemical Formula: C₃₅H₃₉F₆IrN₂O₂P₂
Molecular Weight: 887.86

Appearance: bright yellow solid.

m.p.: Decomposes >188 °C.

FTIR (CH₂Cl₂): 2941, 2083, 2025, 1436, 1098, 847cm⁻¹.

FTIR (neat): 2938, 1864, 2075, 2018, 1481, 1435, 1242, 1099, 1831 cm⁻¹.

¹H NMR (400 MHz, CDCl₃): δ 7.62 – 7.58 (m, 3H, ArH), 7.53 – 7.49 (m, 6H, ArH), 7.26 (s partially hidden under CHCl₃, 2H, NCH=CHN), 7.23 – 7.17 (m, 6H, ArH), 4.08 (tt, 2H, ³J_{ax-ax} = 12.2 Hz, ³J_{ax-eq} = 3.7 Hz), 2.00 – 1.89 (m, 4H, CH₂), 1.67 – 1.32 (m, 12H, CH₂), 1.21 – 1.11 (m, 2H, CH₂), 0.59 – 0.56 (m, 2H, CH₂).

³¹P NMR (162 MHz, CDCl₃): δ 15.6 (PPh₃), -144.3 (septet, ¹J_{P-F} = 711.8 Hz, PF₆).

¹⁹F NMR (376 MHz, CDCl₃): δ -72.3 (d, ¹J_{P-F} = 711.8 Hz, PF₆).

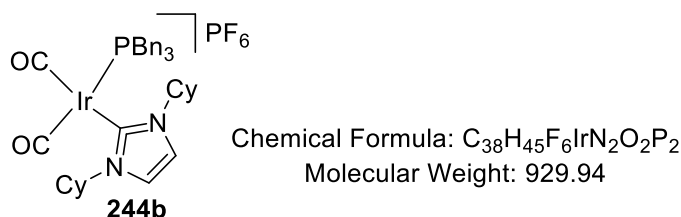
HRMS (positive ESI): m/z calc'd for C₃₄H₃₇¹⁹¹IrN₂OP [M-PF₆-CO-2H]⁺: 713.2269; found: 713.2264. No mass ion observed.

HRMS (negative ESI): m/z calc'd for PF₆ [M]⁻: 144.9647; found: 144.9638.

X-Ray: see Appendix A.

Preparation of Dicarbonyl(dicyclohexylimidaz-2-ylidene)(tribenzylphosphine)iridium(I) hexafluorophosphate, 244b

a) [(COD)Ir(ICy)(PBn₃)]PF₆ (0.196 g, 0.200 mmol), and b) 0.154 g, 83% yield.



Appearance: bright yellow solid.

m.p.: 171 - 172 °C.

FTIR (CH₂Cl₂): 2941, 2860, 2081, 2025, 1601, 1495, 1454, 1273, 847 cm⁻¹.

FTIR (neat): 2938, 2079, 2014, 1497, 1450, 1427, 1409, 1196, 837 cm⁻¹.

¹H NMR (400 MHz, CDCl₃): δ 7.46 (s, 2H, NCH=CHN), 7.44 – 7.36 (m, 9H, ArH), 7.28 – 7.26 (m, 6H, ArH), 4.23 (tt, 2H, ³J_{ax-ax} = 11.9 Hz, ³J_{ax-eq} = 3.5 Hz), 3.17 (d, 6H, ³J_{P-H} = 9.6 Hz), 2.00 – 1.63 (m, 14H, CH₂), 1.43 – 1.28 (m, 4H, CH₂), 1.15 – 1.09 (m, 2H, CH₂).

³¹P NMR (162 MHz, CDCl₃): δ 6.43 (PBn₃), -144.2 (septet, ¹J_{P-F} = 711.8 Hz, PF₆).

¹⁹F NMR (376 MHz, CDCl₃): δ -72.3 (d, ¹J_{P-F} = 711.8 Hz, PF₆).

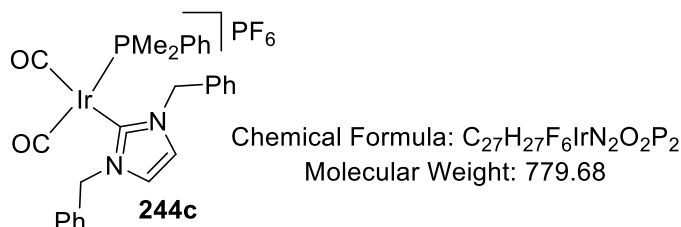
HRMS (positive ESI): m/z calc'd for C₃₈H₄₅¹⁹¹IrN₂O₂P [M-PF₆]⁺: 783.2819; found: 783.2819.

HRMS (negative ESI): m/z calc'd for PF₆ [M]⁻: 144.9647; found: 144.9647.

X-Ray: see Appendix A.

Preparation of Dicarbonyl(dicyclohexylimidaz-2-ylidene)(dimethylphenylphosphine)iridium(I) hexafluorophosphate, **244c**

a) [(COD)Ir(IBn)(PMe₂Ph)]PF₆ (0.060 g, 0.068 mmol), and b) 0.026 g, 49% yield.



Appearance: bright yellow solid.

m.p.: 136 – 137 °C.

FTIR (CH₂Cl₂): 2081, 2023, 847 cm⁻¹.

FTIR (neat): 2980, 2068, 2019, 1494, 1456, 878, 831 cm⁻¹.

¹H NMR (400 MHz, CDCl₃): δ 7.58 – 7.53 (m, 5H, ArH), 7.39 – 7.34 (m, 6H, ArH), 7.21 (s, 2H, NCH=CHN), 7.15 – 7.12 (m, 4H, ArH), 5.16 (d, 2H, ²J = 14.9 Hz, ArCH₂), 4.89 (d, 2H, ²J = 14.9 Hz, ArCH₂), 1.87 (d, 6H, ³J_{H-P} = 10.0 Hz, P(CH₃)₂Ph).

³¹P NMR (162 MHz, CDCl₃): δ 11.7 (PMe₂Ph), -144.2 (septet, ¹J_{P-F} = 711.8 Hz, PF₆).

¹⁹F NMR (376 MHz, CDCl₃): δ -72.3 (d, ¹J_{P-F} = 711.8 Hz, PF₆).

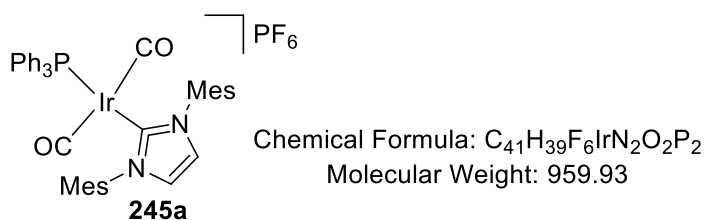
HRMS (positive ESI): m/z calc'd for C₂₆H₂₇¹⁹¹IrN₂OP [M - CO - PF₆]⁺: 607.1486; found: 607.1481.

HRMS (negative ESI): m/z calc'd for PF₆ [M]⁻: 144.9647; found: 144.9647.

X-Ray: see Appendix A.

Preparation of Dicarbonyl(dimesitylimidaz-2-ylidene)(triphenylphosphine)iridium(I) hexafluorophosphate, **245a**

a) [(COD)Ir(IMes)(PPh₃)]PF₆ (0.200 g, 0.198 mmol), and b) 0.130 g, 69% yield.



Appearance: bright orange solid.

m.p.: decomposes > 195 °C.

FTIR (CH₂Cl₂): 3169, 3140, 3072, 2924, 2010, 1991, 1609, 1483, 1436, 1234, 847 cm⁻¹.

FTIR (neat): 2980, 2052, 1994, 1981, 1483, 1435, 1030, 833 cm⁻¹.

¹H NMR (400 MHz, CDCl₃): δ 7.56 – 7.53 (m, 3H, ArH), 7.50 (s, 2H, NCH=CHN), 7.46 – 7.42 (m, 6H, ArH), 7.15 – 7.10 (m, 10H, ArH), 2.40 (s, 6H, ArCH₃), 2.09 (s, 12H, ArCH₃).

³¹P NMR (162 MHz, CDCl₃): δ -4.2 (bs), -7.7 (sharp s), -144.4 (septet, ¹J_{P-F} = 711.8 Hz, PF₆).

¹⁹F NMR (376 MHz, CDCl₃): δ -73.7 (d, ¹J_{P-F} = 711.8 Hz, PF₆).

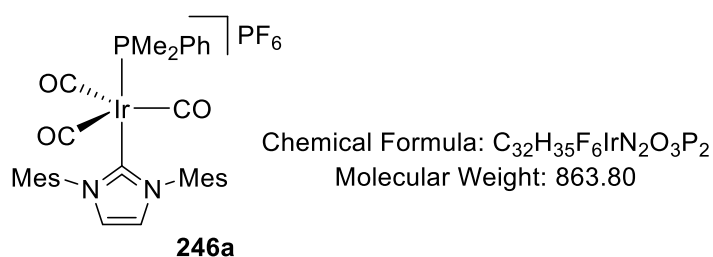
HRMS (positive ESI): m/z calc'd for C₄₀H₃₉¹⁹¹IrN₂OP [M – CO – PF₆ – H]⁺: 787.2426; found: 787.2423.

HRMS (negative ESI): m/z calc'd for PF₆ [M]: 144.9647; found: 144.9649.

X-Ray: see Appendix A.

Preparation of Tricarbonyl(dimesitylimidaz-2-ylidene)(dimethylphenylphosphine)iridium(I) hexafluorophosphate, 246a

a) [(COD)Ir(IMes)(PMe₂Ph)]PF₆ (0.220 g, 0.248 mmol), and b) 0.148 g, 69% yield.



Appearance: colourless solid.

m.p.: 151 – 152 °C.

FTIR (CH₂Cl₂): 2924, 2004, 1987, 1609, 1485, 1410, 1323, 1105, 951, 918, 847 cm⁻¹.

FTIR (neat): 2922, 2064, 2002, 1607, 1485, 1439, 1283, 1232, 1103, 831 cm⁻¹.

¹H NMR (400 MHz, CDCl₃): δ 7.50 – 7.42 (m, 5H, ArH), 7.40 (s, 2H, NCH=CHN), 7.09 (s, 4H, ArH), 2.41 (s, 6H, ArH), 2.09 – 2.06 (overlapping s and d, 18H, ArCH₃ and P(CH₃)₂Ph).

³¹P NMR (162 MHz, CDCl₃): δ -22.5 (sharp s), -36.4 (bs), -144.3 (septet, ¹J_{P-F} = 711.8 Hz, PF₆).

¹⁹F NMR (376 MHz, CDCl₃): δ -73.4 (d, ¹J_{P-F} = 711.8 Hz, PF₆).

HRMS (positive ESI): m/z calc'd for C₃₀H₃₅¹⁹¹IrN₂OP [M – 2CO – PF₆]⁺: 633.2112; found: 663.2120.

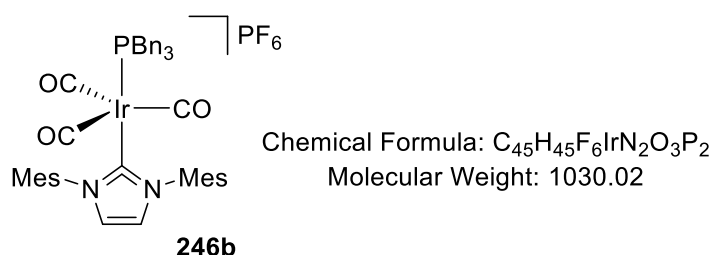
m/z calc'd for $C_{29}H_{33}^{191}IrN_2P [M - 3CO - PF_6 - 2H]^+$: 633.2006; found: 633.2012.

HRMS (negative ESI): m/z calc'd for $PF_6 [M]$: 144.9647; found: 144.9649.

X-Ray: see **Appendix A**.

Preparation of Tricarbonyl(dimesitylimidaz-2-ylidene)(dtribenzylphosphine)iridium(I) hexafluorophosphate, 246b

a) $[(COD)Ir(IMes)(PBN_3)]PF_6$ (0.196 g, 0.186 mmol), and b) 0.153 g, 80% yield.



Appearance: colourless solid.

m.p.: 226 °C.

FTIR (CH₂Cl₂): 2058, 2000, 1991 cm^{-1} .

FTIR (neat): 2922, 2064, 2002, 1607, 1485, 1439, 1283, 1232, 1103, 831 cm^{-1} .

¹H NMR (400 MHz, CDCl₃): δ 7.30 – 7.20 (m, 11H, ArH), 7.07 – 7.03 (overlapping s and m, 10H, NCH=CHN), 3.59 (d, 6H, $^3J_{P-H} = 11.3$ Hz, ArCH₂), 2.42 (s, 6H, ArCH₃), 1.96 (s, 12H, ArCH₃).

³¹P NMR (162 MHz, CDCl₃): δ 0.5, -144.1 (septet, $^1J_{P-F} = 711.8$ Hz, PF₆).

¹⁹F NMR (376 MHz, CDCl₃): δ -72.0 (d, $^1J_{P-F} = 711.8$ Hz, PF₆).

HRMS (positive ESI): m/z calc'd for $C_{43}H_{45}^{191}IrN_2OP [M - 2CO - PF_6]^+$: 829.2894; found: 829.2898.

X-Ray: see **Appendix A**.

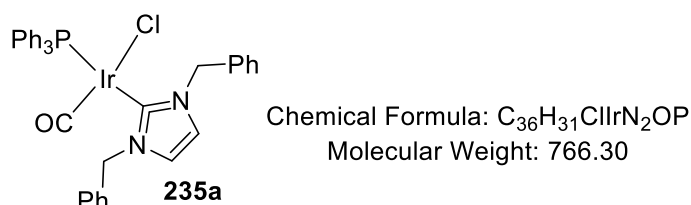
Ir(I) Chloro-carbonyl Complexes in the Study of Combined Ligand Electronics

Following *General Procedure K*, results are reported as a) amount of $[(COD)Ir(NHC)(Cl)]$, b) amount of phosphine, and c) product yield.

For known starting complexes that are not elsewhere described in this report, readers are directed to the references provided.^{120,152,250,263}

Preparation of *Chloro(carbonyl)(dibenzylimidazol-2-ylidene)(triphenylphosphine)iridium(I)*¹⁹⁷, **253a**

a) [(COD)Ir(IBn)Cl], 0.206 g, 0.353 mmol, b) PPh₃, 0.092 mg, 0.353 mmol, and c) 0.114 g, 42% yield.



Appearance: yellow solid.

FTIR (CH₂Cl₂): 3049, 1950, 1497, 1481, 1454, 1435, 1406, 1271, 1260, 1096, 756, 731, 702 cm⁻¹.

FTIR (neat): 3100, 1942, 1604, 1585, 1570, 1495, 1479, 1408, 1207, 1096, 692 cm⁻¹.

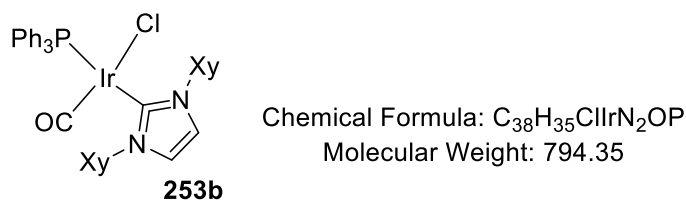
¹H NMR (400 MHz, CDCl₃): δ 7.75 – 7.70 (m, 6H, ArH), 7.47 – 7.45 (m, 4H, ArH), 7.40 – 7.33 (m, 15H, ArH), 6.82 (s, 2H, NCH=CHN), 5.93 (d, 2H, ²J = 14.7 Hz, ArCH₂), 5.67 (d, 2H, ²J = 14.7 Hz, ArCH₂).

¹³C NMR (100 MHz, CDCl₃): δ 176.6 (d, ³J_{C-P} = 114.9), 170.5 (d, ³J_{C-P} = 10.2 Hz), 136.4, 134.8, 134.7, 134.1, 133.6, 129.8, 128.8, 128.6, 128.1, 127.9, 127.8, 120.7, 55.0.

³¹P NMR (162 MHz, CDCl₃): δ 23.3 (PPh₃).

Preparation of *Chloro(carbonyl)(bis[2,6-xylyl]imidazol-2-ylidene)(triphenylphosphine)iridium(I)*, **253b**

a) [(COD)Ir(IXy)Cl], 0.205 g, 0.335 mmol, b) PPh₃, 0.088 mg, 0.335 mmol, and c) 0.179 g, 67% yield.



Appearance: yellow solid.

m.p.: 266 – 268 °C.

FTIR (CH₂Cl₂): 3074, 3045, 2924, 1944, 1479, 1435, 1332, 1096, 777 cm⁻¹.

FTIR (neat): 1942, 1479, 1435, 1096, 777 cm⁻¹.

¹H NMR (400 MHz, CDCl₃): δ 7.41 – 7.36 (m, 8H, ArH), 7.32 – 7.28 (m, 3H, ArH), 7.25 – 7.21 (m, 10H, ArH), 7.17 (apparent d, 2H, ³J = 0.4 Hz, NCH=CHN), 2.36 (s, 12H, ArCH₃).

¹³C NMR (100 MHz, CDCl₃): δ 179.0 (d, ³J_{C-P} = 119.1 Hz), 171.1 (d, ³J_{C-P} = 10.7 Hz), 138.1, 138.0, 137.6, 136.8, 135.8, 134.4, 134.3, 134.1, 133.4, 132.9, 129.9, 128.9, 128.7, 128.2, 127.7, 127.3, 127.2, 127.0, 126.9, 122.03, 122.01, 18.5.

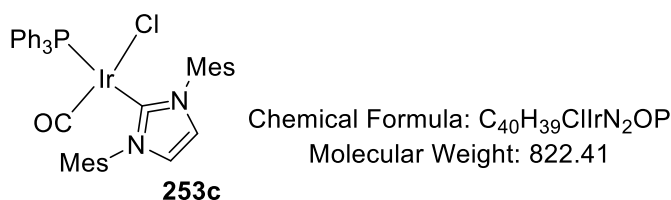
³¹P NMR (162 MHz, CDCl₃): δ 23.5 (PPh₃).

HRMS (positive ESI): m/z calc'd for C₃₂H₃₅¹⁹¹IrN₂OP [M – Cl]⁺: 759.2113; found: 759.2113.

X-Ray: see Appendix A.

Preparation of Chloro(carbonyl)(dimesitylimidazol-2-ylidene)(triphenylphosphine)iridium(I), 253c

a) [(COD)Ir(IMes)Cl], 0.200 g, 0.312 mmol, b) PPh₃, 0.082 mg, 0.312 mmol, and c) 0.120 g, 47% yield.



Appearance: bright yellow solid.

m.p.: decomposes > 195 °C.

FTIR (CH₂Cl₂): 3057, 2991, 2920, 1942, 1607, 1481, 1435, 1255, 708 cm⁻¹.

FTIR (neat): 2980, 2907, 1928, 1479, 1433, 1404, 1379, 1332, 1095, 847 cm⁻¹.

¹H NMR (400 MHz, CDCl₃): δ 7.41 – 7.36 (m, 6H, ArH), 7.31 – 7.27 (m, 3H, ArH), 7.24 – 7.20 (m, 6H, ArH), 7.10 (s, 2H, NCH=CHN), 7.02 (s, 4H, ArH), 2.42 (s, 6H, ArCH₃), 2.29 (s, 12H, ArCH₃).

¹³C NMR (100 MHz, CDCl₃): δ 179.5 (d, ²J_{C-P} = 116.4 Hz), 171.6 (d, ²J_{C-P} = 11.7 Hz), 138.2, 136.2, 135.9, 134.9, 134.8, 134.0, 133.5, 129.4, 128.9, 127.5, 127.4, 122.7, 122.6, 21.3, 18.9.

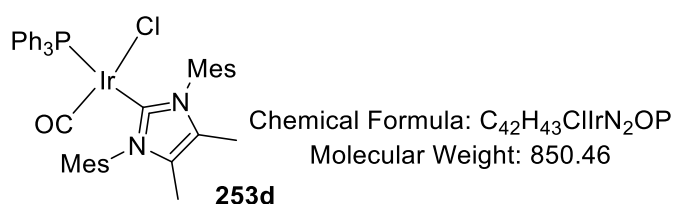
³¹P NMR (162 MHz, CDCl₃): δ 23.6 (PPh₃).

HRMS (positive ESI): m/z calc'd for $C_{32}H_{35}^{191}IrN_2OP$ $[M - Cl]^+$: 787.2426; found: 787.2429.

X-Ray: see Appendix A.

Preparation of Chloro(carbonyl)(dimesityl-4,5-dimethyl-imidazol-2-ylidene)(triphenylphosphine)iridium(I), 253d

a) $[(COD)Ir(IMesMe_2)Cl]$, 0.100 g, 0.150 mmol, b) PPh_3 , 0.039 mg, 0.150 mmol, and c) 0.056 g, 44% yield.



Appearance: bright yellow solid.

m.p.: decomposes > 210 °C.

FTIR (CH_2Cl_2): 2924, 1940, 1481, 1435, 1377, 1325, 1096, 856 cm^{-1} .

FTIR (neat): 2980, 2970, 1946, 1608, 1481, 1435, 1377, 1325, 1095, 940, 690 cm^{-1} .

1H NMR (400 MHz, $CDCl_3$): δ 7.40 – 7.35 (m, 6H, ArH), 7.31 – 7.26 (m, 3H, ArH), 7.24 – 7.19 (m, 6H, ArH), 7.03 (s, 4H, ArH), 2.44 (s, 6H, ArCH₃), 2.22 (s, 12H, ArCH₃), 1.95 (s, 6H, ArCH₃).

^{13}C NMR (100 MHz, $CDCl_3$): δ 176.1 (d, $^2J_{C-P} = 177.7$), 171.5 (d, $^2J_{C-P} = 10.7$ Hz), 138.4, 137.6, 137.4, 136.7, 134.5, 134.4, 134.3, 134.2, 134.1, 133.8, 133.3, 129.7, 128.8, 128.3, 128.0, 127.9, 127.2, 127.1, 126.9, 126.8, 125.0(3), 125.0(0), 20.8, 18.3, 18.0, 14.8, 8.9, 8.7.

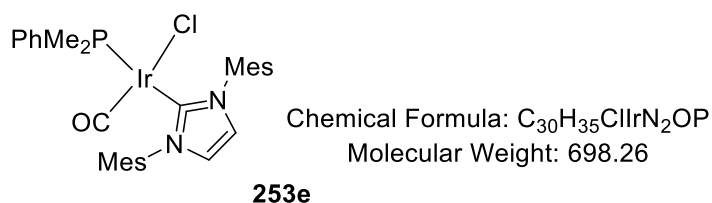
^{31}P NMR (162 MHz, $CDCl_3$): δ 23.5 (PPh_3).

HRMS (positive ESI): m/z calc'd for $C_{42}H_{43}^{191}IrN_2OP$ $[M - Cl]^+$: 815.2739; found: 815.2736.

X-Ray: see Appendix A.

Preparation of Chloro(carbonyl)(dimesitylimidazol-2-ylidene)(dimethylphenylphosphine)iridium(I), **253e**

a) [(COD)Ir(IMes)Cl], 0.100 g, 0.150 mmol, b) PPh₃, 0.039 mg, 0.150 mmol, and c) 0.056 g, 53% yield.



Appearance: yellow solid.

m.p.: 198 – 200 °C.

FTIR (CH₂Cl₂): 2924, 1940, 1481, 1435, 1377, 1325, 1096, 856 cm⁻¹.

FTIR (neat): 2980, 2970, 1946, 1608, 1481, 1435, 1377, 1325, 1095, 940, 690 cm⁻¹.

¹H NMR (400 MHz, CDCl₃): δ 7.53 – 7.49 (m, 3H, ArH), 7.21 – 7.18 (m, 2H, ArH), 7.10 (s, 2H, NCH=CHN), 7.02 (s, 4H, ArH), 2.40 (s, 6H, ArCH₃), 2.27 (s, 12H, ArCH₃), 1.63 (d, 6H, ²J_{H-P} = 8.8 Hz, P(CH₃)₂Ph).

¹³C NMR (100 MHz, CDCl₃): δ 181.4 (d, ²J_{C-P} = 177.7), 172.1 (d, ²J_{C-P} = 11.7 Hz), 138.3, 135.8, 133.0, 132.8, 129.4, 128.9, 128.5, 127.6, 127.5, 122.6, 21.2, 18.7, 14.6 (d, ¹J_{C-P} = 34.9 Hz).

³¹P NMR (162 MHz, CDCl₃): δ -10.5 (PMe₂Ph).

HRMS (positive ESI): m/z calc'd for C₄₂H₄₃¹⁹¹IrN₂OP [M – Cl]⁺: 663.2112; found: 663.2116.

X-Ray: see Appendix A.

Generation of MeCN-stabilised Ir(III)-dihydride Complexes in-situ (Table 14)

The complex of interest (~10 mg) was dissolved in 0.6 mL MeCN-d₃ and transferred to an oven-dried NMR tube which was then sealed with a rubber septum. Hydrogen gas was bubbled through the solution carefully for 30 mins, taking care not to force the solution from the tube. **NOTE:** chloro-carbene complexes often take longer to activate and may be left for up to 1 h with hydrogen bubbling. After this time, the sample was analysed directly by NMR spectroscopy at 300 K.

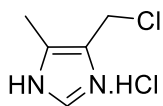
In line with the ‘quick screen’ nature of this method, full analysis of ^1H and ^{13}C NMR is not provided for each derivative studied. However, in all cases, a clear loss of the COD olefinic proton signals was observed, in line with literature precedent.^{114,202} For ease of comparison, ^1H NMR hydride signals reported in the results are tabulated alongside the major ^{31}P NMR triplet shift, concentrating on ligated phosphine shifts/coupling constants and omitting counterions.

<i>Entry</i> ^a	<i>Complex</i>	<i>A</i>	<i>B</i>	$\delta_{\text{H}}/\text{ppm}$	$\delta_{\text{P}}/\text{ppm}$	$^3J_{\text{P-H}}$ (Hz)
1	254a	PPh ₃	IBn	-21.33	16.7 (t)	16.0
2	254b	PPh ₃	IXy	-21.59	18.6 (t)	16.1
3	254c	PPh ₃	IMes	-21.56	18.6 (t)	16.1
4	254d	PPh ₃	IMes ^{Me}	-21.60	18.7 (t)	16.0
5	254e	PMe ₂ Ph	Mes	-21.99	-26.0 (t)	17.4
6	254f	PCy ₃	py	-22.08	18.7 (t)	17.8
7	254g	Cl	IMes	-22.70	-	-

Alternative NHC Ligands in HIE Catalyst Motif [(COD)Ir(NHC)(PR₃)]X

*Preparation of 5-(Chloromethyl)-4-methyl-1H-imidazole hydrochloride, 257*²⁰⁸

A 250 mL round bottom flask was charged with thionyl chloride (~50 mL, excess) and a stirrer bar then cooled to 0 °C using an ice bath. Subsequently, (4-methyl-1H-imidazol-5-yl)methanol hydrochloride (10.0 g, 68.0 mmol), **256**, was added portion wise, taking care in controlling the rate of effervescence. Once all of **256** had been added, cooling was removed and the reaction mixture stirred at r.t. for 4 h. Following this, chloroform (50 mL) was added to the reaction mixture, the precipitate was collected by filtration and washed with cold chloroform (20 mL). The product was dried in a vacuum oven (0 mbar, 40 °C) overnight, to yield a bright white solid (11.56 g, 99%).



Chemical Formula: C₅H₈Cl₂N₂
Molecular Weight: 167.03

257

Appearance: bright white solid.

m.p.: 274-275 °C (Lit. = 277 °C).

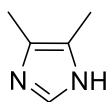
FTIR (neat): 3086, 2988, 2826, 2736, 2646, 1638, 1530, 1481, 1443, 833 cm⁻¹.

¹H NMR (400 MHz, DMSO-d₆): δ 14.52 (bs, ~2H, CH=N⁺H), 8.93 (s, 1H, ArH), 5.54 (bs, 1H, NH), 4.46 (s, 2H, ArCH₂Cl), 2.25 (s, 3H, ArCH₃).

¹³C NMR (100 MHz, DMSO-d₆): δ 134.0, 128.5, 125.2, 34.3, 9.0.

*Preparation of 4,5-Dimethyl-1H-imidazole, 258*²⁰⁸

5-(Chloromethyl)-4-methyl-1H-imidazole hydrochloride, **257** (8.0 g, 48.0 mmol) was dissolved in ethanol (125 mL) inside a reinforced hydrogenation vessel. Subsequently, palladium on charcoal (0.8 g, 10% w/w) was added, ensuring no dry powder remained on the sides of the vessel. The reaction vessel was sealed and placed under a hydrogen atmosphere (5 atm) in a Cook hydrogenator. After agitating the reaction mixture overnight, the hydrogen atmosphere was replenished inside the vessel and the reaction mixture agitated for a further 2 d. After removal of the vessel from the hydrogenation apparatus, the reaction mixture was passed through celite; ensuring ethanol was used to rinse the glassware, keeping the palladium residues wet. The filtrate was concentrated under reduced pressure then mixed with saturated K₂CO₃ (100 mL). **NOTE** – palladium residues on celite were quenched separately by soaking with saturated aqueous K₂CO₃. The basified reaction mixture was placed in a separating funnel and extracted using diethyl ether (4 x 50 mL). The combined organic layers were dried over anhydrous Na₂SO₄, filtered and concentrated *in vacuo* to reveal the desired product as an off-white solid (4.023 g, 99%).



Chemical Formula: C₅H₈N₂
Molecular Weight: 96.13

258

Appearance: bright white solid.

m.p.: 101-102 °C (Lit. = 102 °C).

FTIR (neat): 3123, 2918, 1657, 1607, 1449 cm⁻¹.

$^1\text{H NMR}$ (400 MHz, CDCl_3): δ 7.39 (s, 1H, ArH), 2.14 (s, 6H, ArCH_3).

$^{13}\text{C NMR}$ (100 MHz, CDCl_3): δ 132.4, 126.6, 10.7.

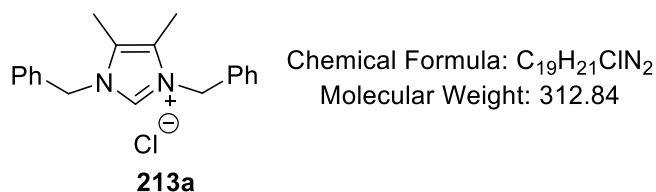
Preparation of N,N'-Dibenzyl-4,5-dimethylimidazolium chloride (Lepidiline A), 213a

Following *General Procedure H*, results are reported as a) amount of **258**, b) volume of THF, c) amount of sodium hydride, d) amount of benzyl chloride, e) temperature, f) reaction time, and g) product yield.

From Scheme 48:

a) 2.000 g, 21.0 mmol, b) 20 mL, c) 0.499 g, 21.0 mmol, d) 5.270 g, 42.0 mmol, e) 80 °C, f) 48 h, and g) 4.397 g, 68%.

X-ray quality crystals were prepared by allowing diethyl ether to diffuse into a saturated DCM solution of the product at 4 °C overnight.



Appearance: bright white solid.

m.p.: 245-247 °C.

FTIR (neat): 3375, 3111, 3030, 2956, 1628, 1551, 1497, 1454 cm^{-1} .

$^1\text{H NMR}$ (400 MHz, DMSO-d_6): δ 9.41 (s, 1H, NCHN), 7.45-7.43 (m, 4H, ArH), 7.40-7.37 (m, 2H, ArH), 7.34-7.32 (m, 4H, ArH), 5.44 (s, 4H, CH_2Ar), 2.12 (s, 6H, CH_3).

$^{13}\text{C NMR}$ (100 MHz, DMSO-d_6): δ 135.4, 134.3, 129.0, 128.5, 127.7, 127.1, 49.6, 8.1.

HRMS (positive NSI): m/z calc'd for $\text{C}_{19}\text{H}_{21}\text{N}_2$ $[\text{M}]^+$: 277.1699; found: 277.1699.

HRMS (negative NSI): peaks observed at m/z 34.8 and 36.8 in a 3:1 ratio of abundance, consistent with a chloride anion.

X-ray data: See Appendix A.

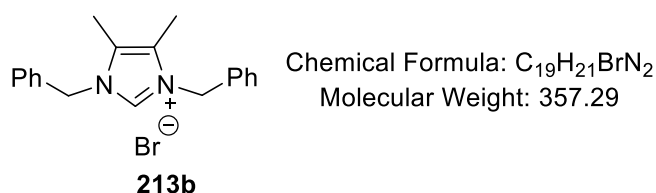
Preparation of N,N'-Dibenzyl-4,5-dimethylimidazolium bromide, 213b

Following *General Procedure H*, results are reported as a) amount of **258**, b) volume of THF, c) amount of sodium hydride, d) amount of benzyl bromide, e) temperature, f) reaction time, and g) product yield.

From Scheme 48:

a) 1.000 g, 10.0 mmol, b) 10 mL, c) 0.240 g, 10 mmol, d) 3.740 g, 22.2 mmol, e) 80 °C, f) 4 h, and g) 6.462 g, 93%.

X-ray quality crystals were prepared by allowing diethyl ether to diffuse into a saturated DCM solution of the product at 4 °C overnight.



Appearance: bright white solid.

m.p.: 240-241 °C.

FTIR (neat): 3028, 2910, 2752, 1761, 1628, 1558, 1495, 1452 cm⁻¹.

¹H NMR (400 MHz, DMSO-d₆): δ 9.33 (s, 1H, NCHN), 7.46-7.32 (m, 10H, ArH), 5.45 (s, 4H, CH₂Ar), 2.13 (s, 6H, CH₃).

¹³C NMR (100 MHz, DMSO-d₆): δ ppm 135.3, 134.2, 129.0, 128.5, 127.7, 127.1, 49.6, 8.0.

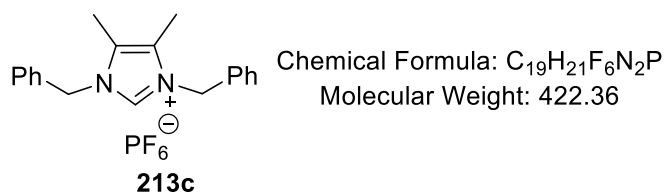
HRMS (positive NSI): m/z calc'd for C₁₉H₂₁N₂ [M]⁺: 277.1699; found: 277.1699.

HRMS (negative NSI): peaks observed at m/z 78.9 and 80.9 in a 1:1 ratio of abundance, consistent with a bromide anion.

Preparation of N,N'-Dibenzyl-4,5-dimethylimidazolium hexafluorophosphate, 213c

213b (1.0 g, 2.8 mmol) was dissolved in a methanol/water mixture (5 mL: 5 mL) and stirred vigorously before the addition of ammonium hexafluorophosphate (0.548 g, 3.350 mmol) to the reaction vessel in one portion, causing immediate precipitation of a bright white solid. After stirring overnight at r.t., the solid was collected by filtration, washed with diethyl ether

then dried in a vacuum oven (40 °C) overnight (1.180 g, 99% yield). X-ray quality crystals were grown by recrystallisation of the white solid from hot chloroform.



Appearance: colourless, crystalline solid.

m.p.: 139-140 °C.

FTIR (neat): 3159, 3105, 2752, 1973, 1638, 1564, 1497, 1452, 1352, 1213, 1184 cm⁻¹.

¹H NMR (400 MHz, CDCl₃): δ 9.24 (s, 1H, NCHN), 7.48-7.38 (m, 6H, ArH), 7.34-7.32 (m, 4H, ArH), 5.43 (s, 4H, CH₂Ar), 2.14 (s, 6H, CH₃).

¹³C NMR (100 MHz, CDCl₃): δ 135.3, 134.2, 129.1, 128.5, 127.7, 127.2, 49.7, 8.0.

³¹P NMR (162 MHz, CDCl₃): δ -144.2 (septet, ¹J_{P-F} = 711.8 Hz, PF₆).

HRMS (positive NSI): m/z calc'd for C₁₉H₂₁N₂ [M]⁺: 277.1699; found: 277.1699.

HRMS (negative NSI): m/z found for [PF₆]⁻: 144.9167. No theoretical mass supplied.

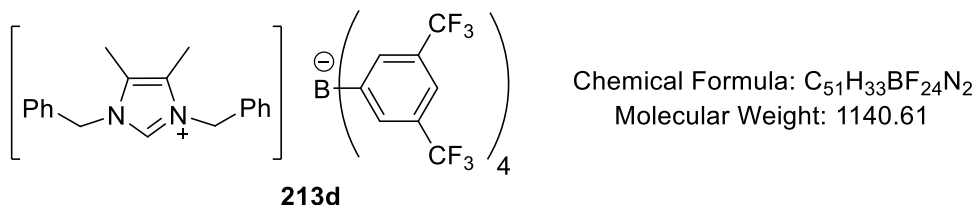
X-ray data: See Appendix A.

Preparation of N,N'-Dibenzyl-4,5-dimethylimidazolium tetrakis[(3,5-trifluoromethylphenyl)]borate, 213d

Following *General Procedure D*, results are reported as a) amount of imidazolium halide, b) amount of NaBArF, and c) product yield.

From Scheme 48:

a) **213b**, 0.040 g, 0.113 mmol, b) 0.100 g, 0.113 mmol, and c) 0.118 g, 92%.



Appearance: bright white solid.

m.p.: 92 - 94 °C

FTIR (neat): 2959, 1609, 1562, 1458, 1437, 1352, 1273, 1123 cm^{-1} .

^1H NMR (400 MHz, CDCl_3): δ 7.70 (m, 8H, ArH_{BArF}), 7.52 (s, 1H, NCHN), 7.48 (bs, 4H, ArH_{BArF}), 7.39-7.31 (m, 6H, ArH), 7.03-7.01 (m, 4H, ArH), 4.97 (s, 4H, CH_2Ar), 2.10 (s, 6H, CH_3).

^{13}C NMR (100 MHz, CDCl_3): δ 161.2 (q, $^1J_{\text{C-B}} = 49.5$ Hz), 135.0, 132.0, 130.6, 130.3, 129.7-128.7 (m), 124.1 (q, $^1J_{\text{C-F}} = 270.3$ Hz), 120.6, 117.7, 51.9, 8.6.

^{11}B NMR (128 MHz, CDCl_3): δ -6.64 [$\text{BArF B}(\text{Ar}_4)$].

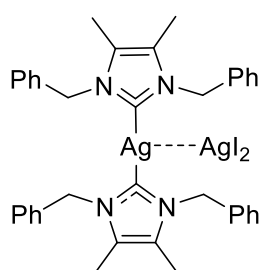
^{19}F NMR (365 MHz, CDCl_3): δ -62.39 (BArF CF_3).

HRMS (positive ESI): m/z calc'd for $\text{C}_{19}\text{H}_{21}\text{N}_2$ [M-BArF] $^+$: 277.1699; found: 277.1703 [M-BArF] $^+$.

HRMS (negative ESI): m/z calc'd for $\text{C}_{32}\text{H}_{12}\text{BF}_{24}$ [BArF] $^-$: 863.0660; found: 863.0623.

Preparation^{197,209} of *bis(N,N'-dibenzyl-4,5-dimethylimidazol-2-ylidene)silver(I) silver diiodide, 260*

In a modification of published procedures,^{197,209} a flame-dried round-bottom flask fitted with one stopcock sidearm was charged with silver(I) oxide (0.065 g, 0.280 mmol), sodium iodide (0.084 g, 0.559 mmol), and **213b** (0.200 g, 0.599 mmol). Dry DCM (5 mL) was added to the solid mixture with stirring, with the resulting coal black mixture being stirred under an argon atmosphere for 16 h. During the course of the reaction, the coal black colour of the reaction mixture turned clear, leaving a grey-white precipitate. The reaction mixture was diluted with DCM and filtered through celite to produce a colourless solution. Addition of hexane (5 - 10 mL) and removal of half the solvent mixture under reduced pressure led to the precipitation of the product as a bright white solid (0.252 g, 88%).



260

Chemical Formula: $\text{C}_{38}\text{H}_{40}\text{Ag}_2\text{I}_2\text{N}_4$
Molecular Weight: 1022.31

Appearance: bright white solid.

m.p.: Decomposes > 200 $^\circ\text{C}$.

FTIR (neat): 3063, 3028, 2999, 2949, 1645, 1494, 1454, 1389 cm^{-1} .

^1H NMR (400 MHz, CDCl_3): δ 7.28-7.27 (m, 12H, ArH), 7.14-7.13 (m, 8H, ArH), 5.34 (s, 8H, CH_2Ar), 1.98 (s, 12H, CH_3).

^{13}C NMR (100 MHz, CDCl_3): δ 182.1, 135.8, 128.4, 127.4, 126.2, 125.6, 52.7, 8.8.

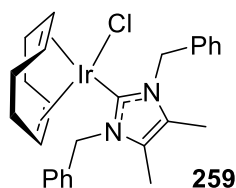
HRMS (positive NSI): m/z calc'd for $\text{C}_{38}\text{H}_{40}\text{AgN}_4$ $[\text{M}-\text{AgI}_2]^+$: 859.2298; found: 859.2297.

HRMS (negative NSI): the anion, $[\text{AgI}_2]^-$, could not be detected.

*Preparation*¹⁹⁷ of Chloro(η^4 -cycloocta-1,5-diene)(1,3-dibenzyl-4,5-dimethylimidazol-2-ylidene) iridium(I), **259**, via **260**

To a flame-dried round bottom flask fitted with one stopcock sidearm was added η^4 -cycloocta-1,5-dieneiridium(I) chloride dimer, **205** (0.131 g, 0.196 mmol), and dry DCM (20 mL). To this stirred, orange solution was added **260** (0.200 g, 0.196 mmol) in one portion, causing the immediate formation of a bright yellow, opaque reaction mixture. After stirring the contents of the flask for 1 h, the mixture was filtered through celite and the filtrate concentrated *in vacuo*. Subsequent dilution of the crude product with diethyl ether and scratching the inside of the glassware with a spatula initiated immediate crystallisation of the desired product. The product was collected by filtration and washed with cold diethyl ether (5 mL) to yield a yellow, crystalline solid (0.212 g, 84%).

X-ray quality crystals were grown *via* slow diffusion of diethyl ether into a DCM solution of the product at 4 $^\circ\text{C}$ overnight.



Chemical Formula: $\text{C}_{27}\text{H}_{32}\text{ClIrN}_2$
Molecular Weight: 612.23

Appearance: bright yellow solid.

m.p.: 224-226 $^\circ\text{C}$

FTIR (neat): 3051, 2951, 2924, 2872, 2826, 1655, 1602, 1497, 1452, 1391 cm^{-1} .

^1H NMR (400 MHz, CDCl_3): δ 7.35-7.32 (m, 4H, ArH), 7.28-7.23 (m, 6H, ArH), 5.83 (d, $^2J = 16.1$ Hz, 2H, CH_2Ar), 5.69 (d, $^2J = 16.1$ Hz, 2H, CH_2Ar), 4.54-4.53 (m, 2H, COD CH), 2.85-2.84 (m, 2H, COD CH), 2.12-2.02 (m, 2H, COD CH_2), 1.91-1.77 (overlapping m and s, 8H, COD CH_2 , CH_3), 1.63-1.55 (m, 2H, COD CH_2), 1.42-1.34 (m, 2H, COD CH_2).

^{13}C NMR (100 MHz, CDCl_3): δ 176.4, 136.7, 129.3, 128.0, 126.9, 125.3, 84.4, 52.6, 52.3, 33.6, 29.5, 9.6.

HRMS (positive NSI): m/z calc'd for $\text{C}_{27}\text{H}_{32}^{191}\text{IrN}_2$ $[\text{M}-\text{Cl}]^+$: 469.1251; found: 469.1246.

X-ray Data: See Appendix A.

Preparation of Chloro(η^4 -cycloocta-1,5-diene)(1,3-dibenzyl-4,5-dimethylimidazol-2-ylidene) iridium(I), 259, via 260 in One Pot

A flame-dried round-bottom flask fitted with one stopcock sidearm was charged with silver(I) oxide (0.227 g, 0.979 mmol), sodium iodide (0.293 g, 1.960 mmol), and **213b** (0.200 g, 0.599 mmol). Dry DCM (5 mL) was added to the solid mixture with stirring, with the resulting coal black mixture being stirred under an argon atmosphere for 2 h. On observing the black to clear colour change (indicating the formation of **260**), η^4 -cycloocta-1,5-dieneiridium(I) chloride dimer, **205** (0.700 g, 1.960 mmol), was added to the reaction vessel in one portion, causing the same clear to bright yellow colour change. After 1 h stirring at r.t., the mixture was filtered through celite and the filtrate concentrated *in vacuo*. Subsequent dilution of the crude product with diethyl ether and scratching the inside of the glassware with a spatula initiated immediate crystallisation of the desired product. The product was collected by filtration and washed with cold diethyl ether (5 mL) to yield a yellow, crystalline solid (**Scheme 50**, 1.032 g, 82%).

Data are consistent with those reported above.

Attempted Alternative Preparation of Chloro(η^4 -cycloocta-1,5-diene)(1,3-dibenzyl-4,5-dimethylimidazol-2-ylidene) iridium(I), 259

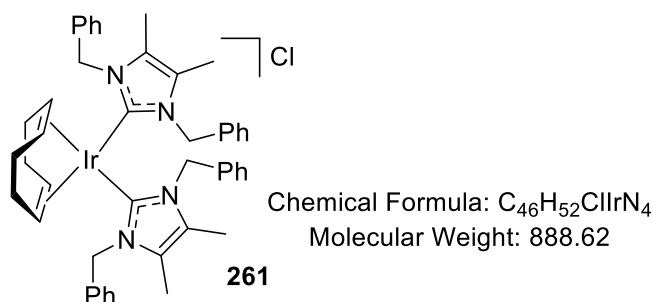
Following *General Procedure B*, results are reported as a) amount of **205**, b) amount of KO^tBu , c) amount of imidazolium salt, d) reaction time, e) volume of THF, and f) product yield.

From Scheme 51:

a) 0.200 g, 0.298 mmol, b) 0.073 g, 0.595 mmol, c) **213a**, 0.186 g, 0.595 mmol, d) 16 h, e) 10 mL, and f) 0.055 g, 15%.

Isolation of by-product, **261**

From **Scheme 51**, by-product, **261**, was isolated *via* elution from silica using MeOH/DCM (1:1), collecting the red fraction. The red solution was concentrated *in vacuo* to reveal the by-product as a red solid (0.051 g, 39% yield). X-ray quality crystals were grown by layering hexane on top of a THF solution of the product, allowing the bilayer to mix for 1 week.



Appearance: deep red crystals.

m.p.: Decomposes > 155 °C.

FTIR (neat): 3032, 2920, 2876, 2826, 1657, 1605, 1495, 1452, 1391 cm⁻¹.

¹H NMR (400 MHz, CDCl₃): δ 7.35-7.26 (m, 12H, ArH), 6.81-6.79 (m, 8H, ArH), 5.74 (d, ²J = 16.7 Hz, 4H, CH₂Ar), 4.97 (d, ²J = 16.7 Hz, 4H, CH₂Ar), 3.70 (bs, 4H, COD CH), 1.81-1.76 (m, 4H, COD CH₂), 1.71 (s, 12H, CH₃), 1.60-1.57 (m, 4H, COD CH₂).

¹³C NMR (100 MHz, CDCl₃): δ 175.8, 136.0, 128.6, 127.4, 126.3, 124.6, 51.0, 30.6, 8.7.

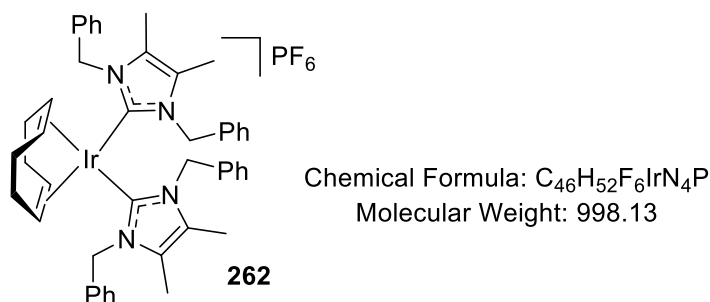
HRMS (positive NSI): m/z calc'd for C₄₆H₅₂¹⁹¹IrN₄ [M-Cl]⁺: 853.3819; found: 853.3810.

X-ray data: See **Appendix A**.

Preparation of η⁴-Cycloocta-1,5-diene-bis(1,3-dibenzyl-4,5-dimethylimidazol-2-ylidene) iridium(I) hexafluorophosphate, **262**

To a flame-dried Schlenk tube was added **205** (0.200 g, 0.298 mmol) and KO^tBu (0.146 g, 1.300 mmol), the mixture being stirred under high vacuum for 5 mins before being placed back under argon atmosphere. Dry THF (20 mL) was then added, creating a black red reaction mixture, and stirred for 10 mins. Subsequently, **213a** (0.373 g, 1.190 mmol) was added in one portion, causing an immediate back to bright red colour change. After stirring the reaction mixture at r.t. overnight, the THF was removed *in vacuo*, leaving a bright red residue which was dissolved in DCM (10 mL). Following this, NH₄PF₆ (0.195 g, 1.190 mmol) and water (10 mL) were added to the DCM solution, and the biphasic mixture stirred

vigorously for 4 h. The mixture was then transferred to a separating funnel and the DCM layer isolated. The aqueous layer was washed with DCM (2 x 10 mL) and the combined organic fractions dried over anhydrous sodium sulfate. Finally, the DCM solution was filtered and concentrated under reduced pressure to yield the desired product as a bright red solid. X-ray quality crystals were grown by slow diffusion of diethyl ether into a saturated DCM solution of the product (**Scheme 51**, 0.0635 g, 53%).



Appearance: red/orange crystals.

m.p.: Decomposes > 242 °C

FTIR (neat): 3030, 2920, 2853, 1663, 1605, 1497, 1452, 1393, 1350 cm⁻¹.

¹H NMR (400 MHz, CDCl₃): δ 7.34-7.24 (m, 12H, ArH), 6.83-6.81 (m, 8H, ArH), 5.78 (d, ²J = 16.8 Hz, 4H, CH₂Ar), 5.00 (d, ²J = 16.8 Hz, 4H, CH₂Ar), 3.70 (bs, 4H, COD CH), 1.79-1.76 (m, 4H, COD CH₂), 1.71 (s, 12H, CH₃), 1.57-1.53 (m, 4H, COD CH₂).

¹³C NMR (100 MHz, CDCl₃): δ 175.7, 136.2, 128.6, 127.2, 126.2, 124.7, 51.0, 30.6, 8.7.

³¹P (162 MHz, CDCl₃): δ -144.2 (septet, ¹J_{P-F} = 711.8 Hz, PF₆).

HRMS (positive NSI): m/z calc'd for C₄₆H₅₂¹⁹¹IrN₄ [M-PF₆]⁺: 853.3819; found: 853.3812.

X-ray data: See Appendix A.

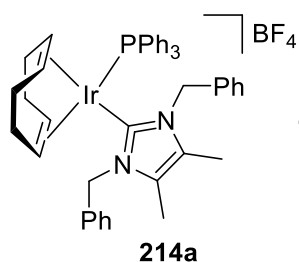
Preparation of η⁴-Cycloocta-1,5-diene(1,3-dibenzyl-4,5-dimethylimidazol-2-ylidene)(triphenylphosphine)iridium(I) tetrafluoroborate, 214

Following *General Procedure I*, results are reported as a) amount of **259**, b) amount of phosphine, c) amount of AgBF₄ d) product yield, and e) purification technique.

X-ray quality crystals were grown *via* slow diffusion of diethyl ether into a saturated DCM solution of the product at 4 °C over 2 d.

From Table 17, Entry 1:

a) 0.100 g, 0.163 mmol, b) PPh₃, 0.043 g, 0.163 mmol c) 0.032 g, 0.163 mmol, d) 0.132 g, 92%, and e) trituration from DCM/EtOH solution using petroleum ether.



Chemical Formula: C₄₅H₄₇BF₄IrN₂P
Molecular Weight: 925.88

Appearance: red, microcrystalline solid.

m.p.: Decomposes > 221 °C.

FTIR (neat): 3075, 2957, 2886, 2357, 1609, 1564, 1479, 1435, 1352, 1273 cm⁻¹.

¹H NMR (400 MHz, CDCl₃): δ 7.52-7.42 (m, 15H, ArH), 7.38-7.35 (m, 4H, ArH), 7.31-7.27 (m, 2H, ArH), 6.99-6.97 (m, 4H, ArH), 5.91 (d, ²J = 16.7 Hz, 2H, CH₂Ar), 4.53 (d, ²J = 16.7 Hz, 2H, CH₂Ar), 4.19-4.18 (m, 2H, COD CH), 3.69-3.67 (m, 2H, COD CH), 2.08-2.00 (m, 2H, COD CH₂), 1.80-1.74 (overlapping m and s, 8H, COD CH₂, and CH₃), 1.66-1.58 (m, 4H, COD CH₂).

¹³C NMR (100 MHz, CDCl₃): δ 172.9, 136.1, 133.9, 133.8, 131.3, 130.7, 130.2, 129.3, 129.0, 128.8, 127.9, 127.8, 125.2, 87.4, 87.2, 79.6, 51.9, 30.8, 30.3, 9.2.

³¹P NMR (162 MHz, CDCl₃): δ 16.0 (PPh₃).

¹⁹F NMR (376 MHz, CDCl₃): δ -153.4 (BF₄).

¹¹B NMR (128 MHz, CDCl₃): δ -0.7 (BF₄).

HRMS (positive NSI): m/z calc'd for C₄₅H₄₇¹⁹¹IrN₂P [M-BF₄]⁺: 839.3102; found: 839.3103.

Presence of the BF₄ counterion could not be confirmed by HRMS.

X-ray data: See Appendix A.

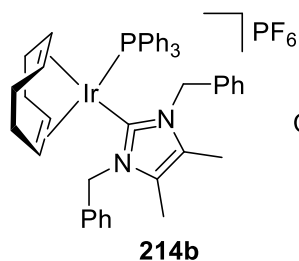
Preparation of η⁴-Cycloocta-1,5-diene(1,3-dibenzyl-4,5-dimethylimidazol-2-ylidene) (triphenylphosphine)iridium(I) hexafluorophosphate, 214b

Following *General Procedure I*, results are reported as a) amount of **259**, b) amount of phosphine, c) amount of AgPF₆ d) product yield, and e) purification technique.

X-ray quality crystals were grown *via* slow evaporation of a CDCl₃ solution of the product at r.t. over 2 weeks.

From Table 17, Entry 2:

a) 0.100 g, 0.163 mmol, b) PPh₃, 0.043 g, 0.163 mmol c) 0.041 g, 0.163 mmol, d) 0.121 g, 75%, and e) trituration from Et₂O using EtOH.



Chemical Formula: C₄₅H₄₇F₆IrN₂P₂
Molecular Weight: 984.04

214b

Appearance: red, microcrystalline solid.

m.p.: Decomposes > 228 °C.

FTIR (neat): 2959, 2932, 1497, 1477, 1435, 1094 cm⁻¹.

¹H NMR (400 MHz, CDCl₃): δ 7.56-7.45 (m, 15H, ArH), 7.43-7.39 (m, 4H, ArH), 7.35-7.31 (m, 2H, ArH), 7.03-7.01 (m, 4H, ArH), 5.93 (d, ²J = 16.7 Hz, 2H, CH₂Ar), 4.55 (d, ²J = 16.7 Hz, 2H, CH₂Ar), 4.23-4.22 (m, 2H, COD CH), 3.73-3.71 (m, 2H, COD CH), 2.14-2.05 (m, 2H, COD CH₂), 1.84-1.77 (overlapping m and s, 8H, COD CH₂, and CH₃), 1.71-1.61 (m, 4H, COD CH₂).

¹³C NMR (100 MHz, CDCl₃): δ 172.4, 135.5, 133.3, 133.2, 130.8, 130.1, 129.6, 128.8, 128.5, 128.4, 127.4, 127.3, 124.7, 87.9, 87.0, 79.0, 51.4, 30.3, 29.8, 8.7.

³¹P NMR (162 MHz, CDCl₃): δ 16.0 (PPh₃), -144.2 (septet, ¹J_{P-F} = 711.8 Hz, PF₆).

HRMS (positive NSI): m/z calc'd for C₄₅H₄₇¹⁹¹IrN₂P [M-PF₆]⁺: 839.3102; found: 839.3099.

HRMS (positive NSI): m/z calc'd for [PF₆]⁻: 144.9647; found: 144.9649.

X-ray data: See **Appendix A**.

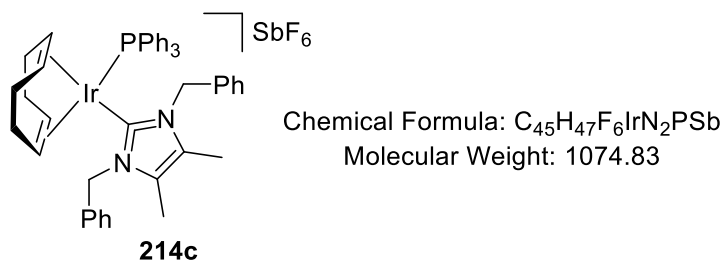
Preparation of η⁴-Cycloocta-1,5-diene(1,3-dibenzyl-4,5-dimethylimidazol-2-ylidene) (triphenylphosphine)iridium(I) hexafluoroantimonate, 214c

Following *General Procedure I* results are reported as a) amount of **259**, b) amount of phosphine, c) amount of AgSbF₆ d) product yield, and e) purification technique.

X-ray quality crystals were grown by layering diethyl ether on top of a CDCl₃ solution of the product. The bilayer was allowed to mix for approximately 1 week.

Table 17, Entry 3

a) 0.100 g, 0.163 mmol, b) PPh₃, 0.043 g, 0.163 mmol c) 0.056 g, 0.163 mmol, d) 0.142 g, 85%, and e) trituration from crude using petroleum ether.



Appearance: red, microcrystalline solid.

m.p.: Decomposes > 224 °C.

FTIR (neat): 3053, 2909, 2878, 1607, 1497, 1433 cm⁻¹.

¹H NMR (400 MHz, CDCl₃): δ 7.53-7.38 (m, 19H, ArH), 7.33-7.30 (m, 2H, ArH), 7.01-6.99 (m, 4H, ArH), 5.92 (d, ²J = 16.6 Hz, 2H, CH₂Ar), 4.52 (d, ²J = 16.7 Hz, 2H, CH₂Ar), 4.21-4.20 (m, 2H, COD CH), 3.72-3.71 (m, 2H, COD CH), 2.12-2.04 (m, 2H, COD CH₂), 1.83-1.77 (overlapping m and s, 8H, COD CH₂, and CH₃), 1.70-1.64 (m, 4H, COD CH₂).

¹³C NMR (100 MHz, CDCl₃): δ 172.8, 136.0, 133.8, 133.7, 131.3, 130.6, 130.1, 129.3, 128.9, 128.8, 127.9, 127.8, 125.2, 87.5, 87.4, 79.6, 51.9, 30.8, 30.3, 9.2.

³¹P NMR (162 MHz, CDCl₃): δ 16.1 (PPh₃).

HRMS (positive NSI): m/z calc'd for C₄₅H₄₇¹⁹¹IrN₂P [M-SbF₆]⁺: 839.3102; found: 839.3097.

HRMS (positive NSI): m/z calc'd for ¹²¹SbF₆ [SbF₆]⁻: 234.8948; found: 234.8942.

X-ray data: See Appendix A.

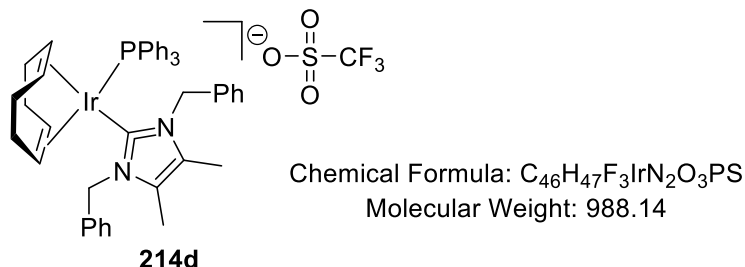
Preparation of η⁴-Cycloocta-1,5-diene(1,3-dibenzyl-4,5-dimethylimidazol-2-ylidene) (triphenylphosphine)iridium(I) trifluoromethanesulfonate, 214d

Following *General Procedure I*, results are reported as a) amount of **259**, b) amount of phosphine, c) amount of AgOTf, d) product yield, and e) purification technique.

X-ray quality crystals were grown *via* slow diffusion of diethyl ether into a saturated DCM solution of the product at 4 °C overnight.

Table 17, Entry 4

a) 0.100 g, 0.163 mmol, b) PPh₃, 0.043 g, 0.163 mmol c) 0.056 g, 0.163 mmol, d) 0.142 g, 99%, and e) trituration from crude using petroleum ether.



Appearance: red, microcrystalline solid.

m.p.: Decomposes > 224 °C.

FTIR (neat): 3061, 2949, 2922, 1657, 1497, 1433, 1395, 1220 cm⁻¹.

¹H NMR (400 MHz, CDCl₃): δ 7.56-7.38 (m, 19H, ArH), 7.34-7.31 (m, 2H, ArH), 7.00-6.99 (m, 4H, ArH), 5.92 (d, ²J = 16.6 Hz, 2H, CH₂Ar), 4.54 (d, ²J = 16.6 Hz, 2H, CH₂Ar), 4.22-4.21 (m, 2H, COD CH), 3.72-3.71 (m, 2H, COD CH), 2.12-2.01 (m, 2H, COD CH₂), 1.83-1.77 (overlapping m and s, 8H, COD CH₂, and CH₃), 1.71-1.61 (m, 4H, COD CH₂).

¹³C NMR (100 MHz, CDCl₃): δ 171.9, 134.9, 132.8, 132.7, 130.4, 129.6, 129.1, 128.3, 128.0, 127.9, 127.0, 126.8, 124.2, 86.5, 86.4, 78.6, 50.9, 29.8, 29.3, 8.3.

³¹P NMR (162 MHz, CDCl₃): δ 16.18 (PPh₃).

¹⁹F NMR (376 MHz, CDCl₃): δ -77.94 (OTf).

HRMS (positive NSI): m/z calc'd for C₄₅H₄₇¹⁹¹IrN₂P: 839.3103; found: 839.3097.

HRMS (positive NSI): m/z calc'd for [CF₃SO₃]⁻: 148.9526; found: 148.9528.

X-ray data: See Appendix A.

Preparation of η⁴-Cycloocta-1,5-diene(1,3-dibenzyl-4,5-dimethylimidazol-2-ylidene) (triphenylphosphine)iridium(I) tetraphenylborate, 214e

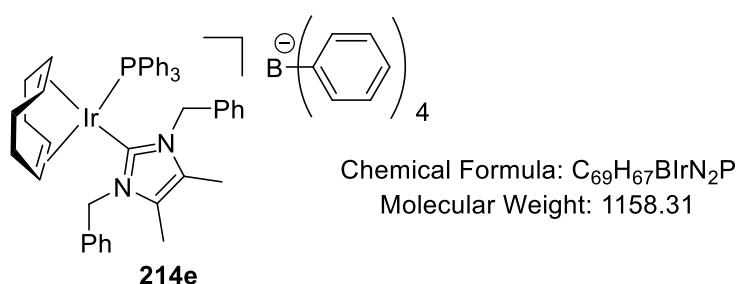
Prior to the reaction, a small batch of the relevant silver tetraphenyl borate was synthesised. As such, sodium tetraphenylborate (0.250 g, 0.731 mmol) and silver nitrate (0.124 g, 0.731 mmol) were dissolved in a minimal quantity of water, and in separate two dram vials. Subsequently, the aqueous solution of the former was added dropwise to the latter, causing immediate formation of a bright white precipitate. The vial was sealed and shaken vigorously for 2 mins. The white solid was collected by filtration and dried in a vacuum oven (1 mbar,

40 °C) for 1 h prior to use. No detailed analysis was carried out on this salt, and its structure is inferred from its reactivity and product analyses described below.

Following *General Procedure I*, results are reported as a) amount of **259** b) amount of phosphine, c) amount of AgBPh₄, d) product yield, and e) purification technique.

Table 17, Entry 5

a) 0.100 g, 0.163 mmol, b) PPh₃, 0.043 g, 0.163 mmol c) 0.070 g, 0.163 mmol, d) 0.142 g, 82%, and e) trituration from crude using petroleum ether.



Appearance: red, microcrystalline solid.

m.p.: Decomposes > 204 °C

FTIR (neat): 3051, 3032, 2978, 1607, 1578, 1433, 1352, 1271, 1115, 1092 cm⁻¹.

¹H NMR (400 MHz, CDCl₃): δ 7.52-7.33 (m, 30H, ArH), 7.05-7.01 (m, 8H, ArH), 6.92-6.86 (m, 7H, ArH), 5.86 (d, ²J = 16.5 Hz, 2H, CH₂Ar), 4.38 (d, ²J = 16.4 Hz, 2H, CH₂Ar), 4.22-4.21 (m, 2H, COD CH), 3.72-3.70 (m, 2H, COD CH), 2.10-2.00 (m, 2H, COD CH₂), 1.85-1.60 (overlapping m and s, 12H, COD CH₂, and CH₃).

¹³C NMR (100 MHz, CDCl₃): δ ppm 172.3, 164.3 (q, ¹J_{C-B} = 49.5 Hz), 136.4, 135.6, 133.7, 133.6, 131.5, 130.5, 129.5, 129.0, 128.9, 128.7, 128.4, 128.3, 127.9, 125.4, 125.1, 121.5, 87.7, 87.6, 79.9, 51.9, 30.8, 30.3, 9.3.

³¹P NMR (162 MHz, CDCl₃): δ 16.6 (PPh₃).

¹¹B NMR (128 MHz, CDCl₃): δ -6.5 (BPh₄).

HRMS (positive NSI): m/z calc'd for C₄₅H₄₇¹⁹¹IrN₂P [M-BPh₄]⁺: 839.3103; found: 839.3099.

HRMS (positive NSI): m/z calc'd for [BC₂₄H₂₀]⁻: 319.1664; found: 319.1652.

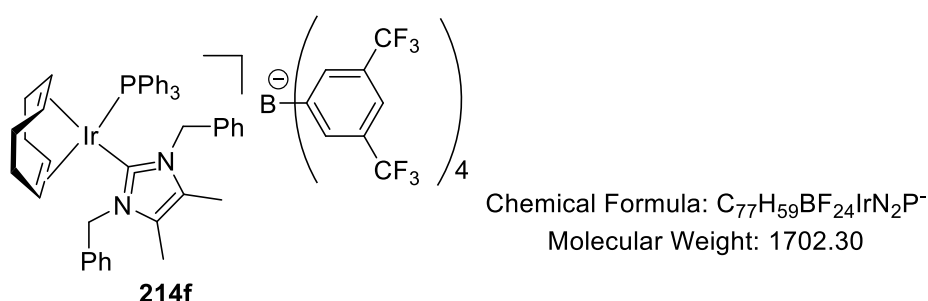
X-ray data: See Appendix A.

Preparation of η^4 -Cycloocta-1,5-diene(1,3-dibenzyl-4,5-dimethylimidazol-2-ylidene) (triphenylphosphine)iridium(I) tetrakis(3,5-trifluoromethylphenyl)borate, **214f**

Following *General Procedure E*, results are reported as a) amount of **205**, b) amount of phosphine, c) amount of **213d**, d) amount of KO^tBu, e) reaction time, f) product yield, and g) purification technique.

From *Scheme 52*:

a) 0.015 g, 0.022 mmol, b) PPh₃, 0.0114 g, 0.044 mmol, c) 0.050 g, 0.044 mmol, d) 0.008 g, 0.066 mmol, e) 1 h, f) 0.062 g, 82%, and g) recrystallisation from EtOH/H₂O.



Appearance: red, microcrystalline solid.

m.p.: 158-160 °C.

FTIR (neat): 3080, 2928, 1608, 1499, 1435, 1352 cm⁻¹.

¹H NMR (400 MHz, CDCl₃): δ 7.80-7.79 (m, 8H, ArH_{BArF}), 7.49-7.28 (m, 25H, ArH_{BArF} + ArH), 6.91-6.89 (m, 4H, ArH), 6.12 (d, ²J = 16.7 Hz, 2H, CH₂Ar), 4.85 (d, ²J = 16.6 Hz, 2H, CH₂Ar), 4.34-4.33 (m, 2H, COD CH), 3.75-3.74 (m, 2H, COD CH), 2.18-2.09 (m, 2H, COD CH₂), 1.85-1.79 (overlapping m and s, 8H, COD CH₂, and CH₃), 1.75-1.64 (m, 4H, COD CH₂).

¹³C NMR (100 MHz, CDCl₃): δ 173.1, 161.5 (q, ¹J_{C-B} = 49.5 Hz), 135.4, 134.8, 133.7, 133.6, 131.4, 130.6, 130.1, 129.4, 129.1, 129.0, 128.9, 128.8, 128.7, 128.3, 124.6 (q, ¹J_{C-F} = 270.7 Hz), 117.4, 87.8, 87.7, 80.1, 52.0, 30.7, 30.3, 9.1.

³¹P NMR (162 MHz, CDCl₃): δ 16.75 (PPh₃).

¹¹B NMR (128 MHz, CDCl₃): δ -6.62 (BArF).

HRMS (positive NSI): m/z calc'd for C₄₅H₄₇¹⁹¹IrN₂P [M-BArF]⁺: 839.3103; found: 839.3089.

HRMS (positive NSI): m/z calc'd for [C₃₂H₁₂BF₂₄]⁻: 863.0660; found: 863.0639.

X-ray: see **Appendix A**.

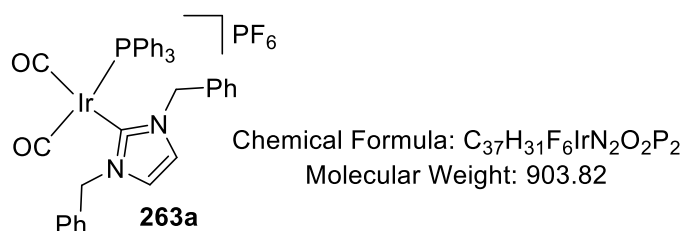
Preparation of Dicarbonyl(dibenzylimidaz-2-ylidene)(triphenylphosphine)iridium(I) hexafluorophosphate, 263a

Following *General Procedure J*, results are reported as a) amount of [(COD)Ir(NHC)(PR₃)]PF₆, and b) product yield.

From Table 18, Entry 1:

(a) [(COD)Ir(PhN)(PPh₃)]PF₆, 0.065 g, 0.068 mmol, and b) 0.030 g, 49%.

.



Appearance: bright yellow solid.

m.p.: 155 - 157 °C.

FTIR (neat): 3161, 3134, 2922, 2852, 2054, 1973, 1687, 1591, 1552, 1472, 1404, 1379, 1367, 1223, 1165, 1111, 1034, 945, 773 cm⁻¹.

¹H NMR (400 MHz, CDCl₃): δ 7.67 – 7.63 (m, 3H, ArH), 7.59 – 7.54 (m, 6H, ArH), 7.41 – 7.32 (m, 12H, ArH), 7.10 – 7.07 (overlapping s and m, 6H, NCH=CHN + ArH), 5.01 – 4.95 (m, 2H, ArCH₂), 4.54 – 4.48 (m, 2H, ArCH₂).

³¹P NMR (162 MHz, CDCl₃): δ 20.0 (sharp s), 16.5 (bs, unknown), -144.2 (septet, ¹J_{P-F} = 711.8 Hz, PF₆).

¹⁹F NMR (376 MHz, CDCl₃): δ -72.1 (d, ¹J_{P-F} = 711.8 Hz, PF₆).

HRMS (positive ESD): m/z calc'd for C₃₇H₃₃¹⁹¹IrN₂O₂P [M - PF₆]⁺: 761.1905; found: 761.1904.

X-Ray: see **Appendix A**.

Preparation of Dicarbonyl(dibenzylimidaz-2-ylidene)(triphenylphosphine)iridium(I) hexafluorophosphate, 263b

Following *General Procedure J*, results are reported as a) amount of [(COD)Ir(NHC)(PR₃)]PF₆, and b) product yield.

FTIR (CH₂Cl₂): 3053, 1948, 1497, 1435, 1096, 746 cm⁻¹.

FTIR (neat): 3055, 1944, 1603, 1587, 1495, 1433, 1394, 1116, 858, 742 cm⁻¹.

¹H NMR (400 MHz, CDCl₃): δ 7.66 – 7.62 (m, 5H, ArH), 7.59 – 7.55 (m, 6H, ArH), 7.51 – 7.46 (m, 6H, ArH), 7.40 – 7.31 (m, 6H, ArH), 7.00 – 6.98 (m, 2H, ArH), 5.27 (d, 2H ²J = 16.0 Hz, ArCH₂), 4.53 (d, 2H ²J = 16.0 Hz, ArCH₂), 1.88 (s, 6H, ArCH₃).

¹³C NMR (100 MHz, CDCl₃): unable to obtain clear resonances to carbene and CO signals.

³¹P NMR (162 MHz, CDCl₃): δ 16.0 (PPh₃), -144.3 (septet, ¹J_{P-F} = 711.8 Hz, PF₆).

¹⁹F NMR (376 MHz, CDCl₃): δ -73.2 (d, ¹J_{P-F} = 711.8 Hz, PF₆).

HRMS (positive ESI): m/z calc'd for C₂₆H₂₇¹⁹¹IrN₂OP [M – CO – PF₆]⁺: 789.2219; found: 789.2215.

X-Ray: see **Appendix A**.

Rate Monitoring for the Deuteration of Acetophenone with Catalysts 214 and 255 (Scheme 53)

A three-necked round bottom flask fitted with one stopcock side arm and two suba seals (as shown in the picture below) was flame-dried. To this flask was added the iridium(I) complex, **214b** (21.2 mg, 0.0215 mmol, 1 mol%) or **255** (20.5 mg, 0.0215 mmol, 1 mol%), and **27** (0.28 mL, 2.150 mmol). The solvent, DCM (25mL) was added, rinsing the inner walls of the flask, and one suba seal was replaced with a greased glass stopper. The solution was placed under an atmosphere of Ar and stirred whilst being cooled to -78 °C in a dry ice/acetone slurry. The flask was twice evacuated and flushed with Ar. Upon a third evacuation, an atmosphere of deuterium gas was introduced to the flask. The deuterium balloon was left in place for the duration of the reaction to ensure a continuous supply of D₂. The cold bath was removed and the flask heated in oil bath to the desired temperature. The reaction mixture was stirred for 2 h. An aliquot (0.2 mL) of the reaction mixture was removed at intervals of 10, 20, 30, 40, 50, 60, and 120 mins). Each aliquot was transferred to a vial containing diethyl ether. After removal of solvent *in vacuo*, the residue was analysed *via* ¹H NMR. The extent of labelling was determined using **Equation 1** and as described earlier for substrate **27**.



The raw data pertaining to **Scheme 53**, is detailed below:

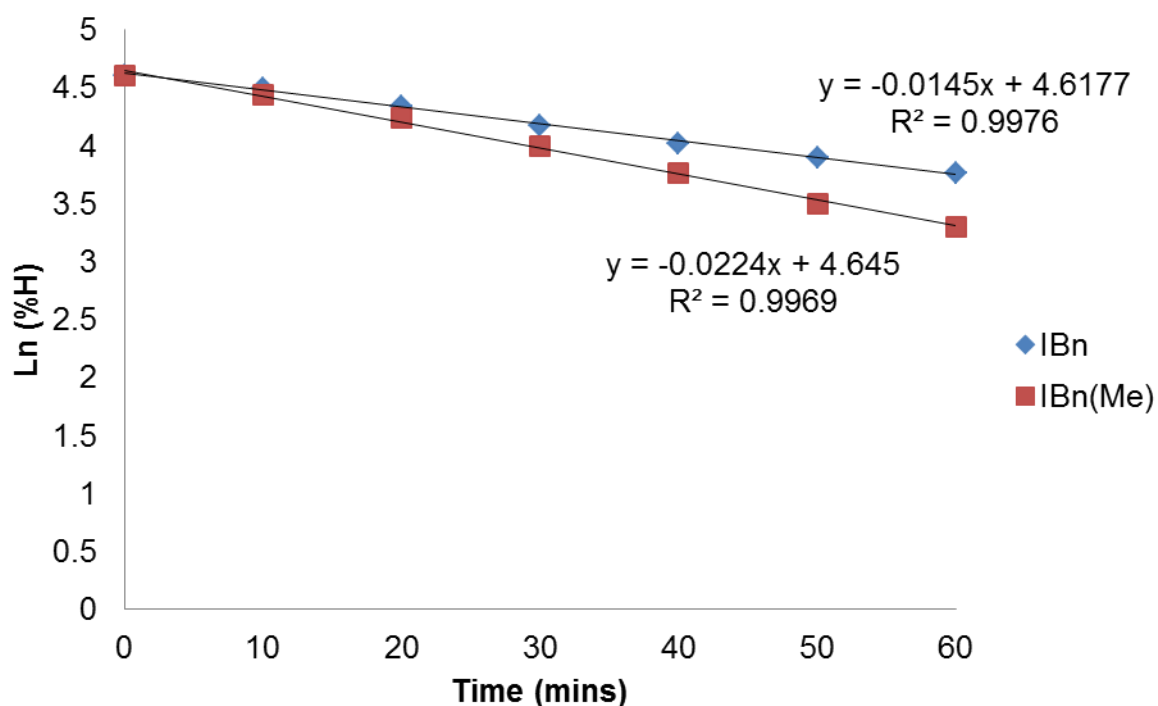
<i>Entry^a</i>	<i>Time (mins)</i>	<i>%D (255)</i>	<i>%D (214b)</i>
1	10	10	17
2	20	24	31
3	30	34	45
4	40	44	56
5	50	50	64
6	60	56	70
7	120	70	84

The turnover frequencies (TOFs) reported in the main text were calculated on the basis of the number of moles of C-H positions converted per mole of substrate per mole of catalyst per hour, *not* per mole of substrate outright. The calculation is as described in **Equation 2** below. Here, F stands for the fraction conversion (e.g. 70% D implies F = 0.7).

$$TOF = F \cdot \frac{\text{No. Moles substrate} \times \text{No. C - H Positions}}{\text{No. Moles catalyst} \times t}$$

Equation 2

As these reaction were carried out with a vast excess of substrate and D_2 versus catalyst, the conditions can be described as pseudo first order in catalyst. Therefore, a plot of $\ln(\%H)$ versus time gives a straight line representing first order decay of substrate with a gradient of $-k_{obs}$. The positive value of this gradient is the value quoted in the main text. See a graphical illustration below:



Attenuated Reactivity of IBn^{Me}/PPh_3 in the Presence of OTf Counterion (Figure 39)

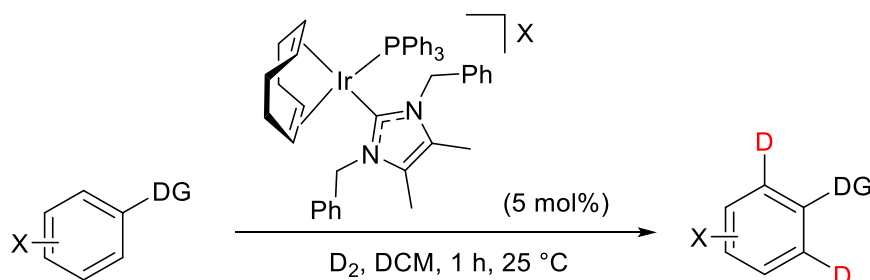
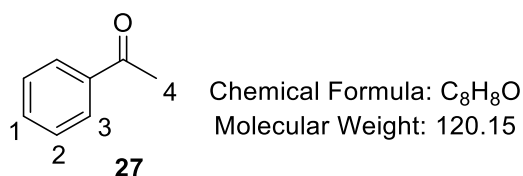


Figure 39 represents the assessment of five different catalysts ($X = BF_4, PF_6, SbF_6, OTf,$ and $BARf$) at $25\text{ }^\circ\text{C}$, applying substrates **27**, **160**, **267**, **94**, and **268**. Each coloured column is representative of one run for that particular set of reaction conditions. Following *General Procedure B*, all reactions were carried out using substrate (0.215 mmol), catalyst (0.01075

mmol, 5 mol%), and DCM (2.5 mL). Spectroscopic details of each substrate are detailed below, and labelling results are summarised in the table immediately following.

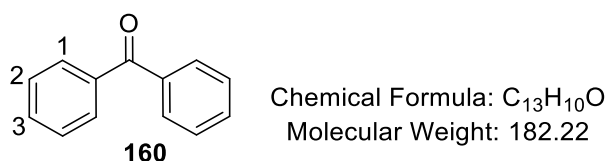
Data for unlabelled acetophenone, **27**:



¹H NMR (400 MHz, CDCl₃): δ 7.95 (d, ³J = 7.5 Hz, 2H, ArH³), 7.47 (t, ³J = 7.4 Hz, 1H, ArH¹), 7.35 (t, ³J = 7.4 Hz, 2H, ArH²), 2.62 (s, 3H, CH₃⁴).

Incorporation expected at δ 7.95. Determined against integral at δ 2.62.

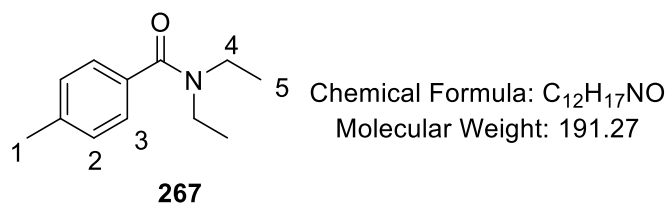
Data for unlabeled benzophenone, **160**



¹H NMR (400 MHz, CDCl₃): δ 7.81 (d, ³J = 8.0 Hz, 4H, ArH¹), 7.59 (t, ³J = 8.0 Hz, 2H, ArH³), 7.49 (t, ³J = 7.9 Hz, 4H, ArH²).

Incorporation expected at δ 7.81. Determined against integral at δ 7.59.

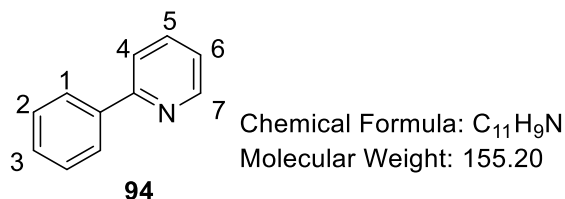
Data for unlabelled *N,N*-Diethyltoluamide, **267**



¹H NMR (400 MHz, d₆-acetone): δ 7.27 - 7.21 (m, 4H, ArH² + ArH³), 3.54 - 3.31 (m, 4H, NCH₂⁴), 2.35 (s, 3H, ArCH₃¹), 1.13 (br s, 6H, NCH₂CH₃⁵).

Incorporation expected at δ 7.27 - 7.21, and determined against integral at δ 2.35.

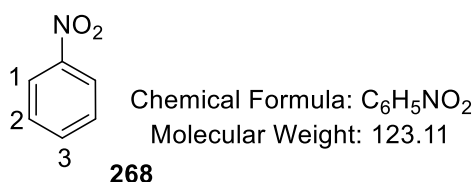
Data for unlabelled 2-Phenylpyridine, **94**



¹H NMR (400 MHz, CDCl₃): δ 8.71 (d, ³J = 4.7 Hz, 1H, ArH⁷), 8.00 (d, ³J = 7.1 Hz, 2H, ArH¹), 7.79-7.73 (m, 2H, ArH⁵ + ArH⁶), 7.52-7.41 (m, 3H, ArH² + ArH³), 7.26-7.23 (m, 1H, ArH⁴).

Incorporation expected at δ 8.00. Determined against integral at δ 7.79-7.73.

Data for unlabelled nitrobenzene, **268**



¹H NMR (400 MHz, CDCl₃): δ 8.25 (dd, ³J = 7.7 Hz, ⁴J = 1.1 Hz, 2H, ArH¹), 7.71 (tt, ³J = 7.4 Hz, ⁴J = 1.1 Hz, 1H, ArH³), 7.56 (t, ³J = 7.4 Hz, 2H, ArH²).

Incorporation expected at δ 8.25. Determined against integral at δ 7.71.

Entry	Substrate	%D (214a) ^f	%D (214b) ^g	%D (214c) ^h	%D (214d) ⁱ	%D (214f) ^j
1	27 ^a	96	96	97	79	97
2	160 ^b	87	91	93	65	98
3	267 ^c	98	98	93	43	99
4	94 ^d	89	82	90	94	98
5	268 ^e	4	5	5	4	16

Substrate quantities per reaction: ^a 26.0 mg; ^b 33.0 mg; ^c 39.0 mg; ^d 41.0 mg; ^e 26.0 mg.
Catalyst quantities per reaction: ^f 10.0 mg, ^g 10.6 mg, ^h 11.6 mg, ⁱ 10.6 mg, ^j 18.3 mg.

Attempted Labelling of 27 Using Bis-carbene Complex, 262

Following *General Procedure B*, results are reported as: a) amount of **27**, b) amount of **262**, c) volume of DCM, d) reaction time, and e) %D.

a) 26 mg, 0.215 mmol, b) 10.7 mg, 0.01075 mmol, 5 mol%, c) 2.5 mL, d) 1h, and e) 0% D.

Upon introducing D₂ to the reaction, it was noticed that no colour change took place. The reaction mixture remained orange rather than turning yellow, as would normally be expected. At the end of the reaction, trituration with Et₂O caused formation of a bright orange solid which, once isolated by filtration, was analysed by NMR, showing identical spectral details to those for complex **262**, detailed above. The filtrate was concentrated *in vacuo* and analysed via ¹H NMR as substrate **27**. Separate attempts to form the iridium dihydride complex of **262** in MeCN-d₆ by bubbling H₂ through a solution in an NMR tube also failed, even when left bubbling for > 2h. The low reactivity of bis-carbene Ir(I) complexes towards H₂ has been observed elsewhere in the literature.¹⁹⁸

8.6 *ortho*-Deuteration of 1° Sulfonamides – An Experimental & Computational Study

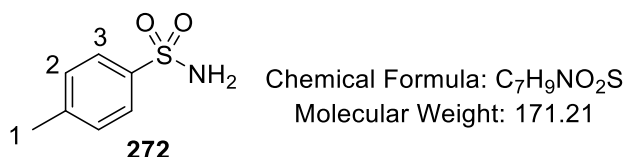
As described in the main text, much of the preliminary findings from this section have now been published, and additional details can be found at the reference provided.²⁵⁰

Synthesis of Substrates

Substrates not detailed here were acquired from commercial suppliers.

Synthesis of 4-methylbenzenesulfonamide, 272²⁶⁴

Following *General Procedure L*: a) 4-methylbenzenesulfonyl chloride, 1.0 g, 5.245 mmol, and b) 0.805 g, 83%.



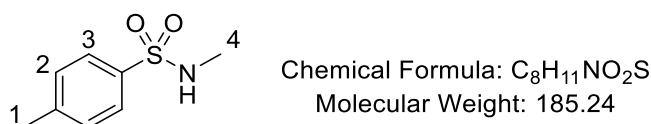
FTIR (neat): 3323, 3233, 3123, 1597, 1572, 1321, 1148 cm⁻¹.

¹H NMR (400 MHz, DMSO-d₆): δ 7.71 (d, 2H, ³J = 8.2 Hz, ArH³), 7.36 (d, 2H, ³J = 8.2 Hz, ArH²), 7.25 (bs, 2H, SO₂NH₂), 2.37 (s, 3H, ArCH₃).

¹³C NMR (100 MHz, DMSO-d₆): δ 141.8, 141.4, 129.3, 125.6, 20.9.

*Synthesis of N,4-dimethylbenzenesulfonamide*²⁶⁵

To a 100 mL round bottom flask was added aqueous methylamine (40% w/w, 40 mL) and 4-methylbenzenesulfonyl chloride (1.0 g, 5.245 mmol). The reaction mixture was stirred at r.t. for 1 h before transferring the reaction mixture to a separating funnel. The product was extracted with diethyl ether (3 x 50 mL). The combined organic phase was washed with aqueous HCl (2 M, 2 x 100 mL) to remove excess methylamine and then dried over anhydrous Na₂SO₄. The solvent was then reduced *in vacuo* to reveal the product as a white solid (0.805 g, 83% yield).



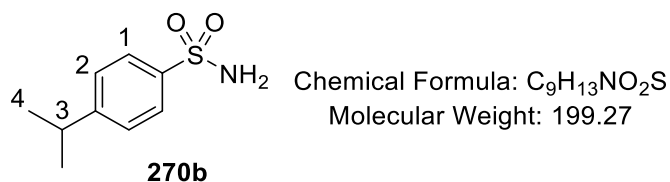
FTIR (neat): 3267, 3064, 2980, 2928, 1595, 1452, 1408, 1306, 1153 cm⁻¹.

¹H NMR (400 MHz, CDCl₃): δ 7.75 (d, 2H, ³J = 8.3 Hz, ArH³), 7.31 (d, 2H, ³J = 8.3 Hz, ArH²), 4.61-4.56 (m, 1H, NH), 2.63 (d, 3H, ³J = 5.4 Hz, NCH₃⁴), 2.43 (s, 3H, ArCH₃¹).

¹³C NMR (100 MHz, DMSO-d₆): δ 143.0, 135.3, 129.2, 126.8, 28.8, 21.0.

*Synthesis of 4-(iso-propyl)-benzenesulfonamide, 270b*²⁶⁶

Following *General Procedure L*: a) 4-iso-propylbenzenesulfonyl chloride, 0.54 mL, 3.0 mmol, and b) 0.436 g, 73%.



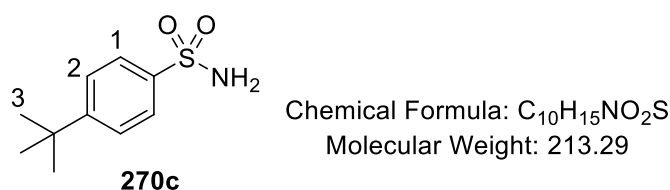
FTIR (neat): 3343, 3262, 2963, 2932, 2868, 1537, 1458, 1325, 1175 cm⁻¹.

¹H NMR (400 MHz, DMSO-d₆): δ 7.74 (d, 2H, ³J = 8.3 Hz, ArH¹), 7.43 (d, 2H, ³J = 8.3 Hz, ArH²), 7.24 (bs, 2H, NH₂), 2.97 (septet, 1H, ³J = 6.9 Hz, CH³), 1.22 (d, 6H, ³J = 6.9 Hz, CH₃⁴).

¹³C NMR (100 MHz, DMSO-d₆): δ 152.5, 141.7, 126.8, 125.8, 33.3, 23.5.

*Synthesis of 4-(tert-butyl)benzenesulfonamide, 270c*²⁶⁷

Following *General Procedure L*: a) 4-tert-butylbenzenesulfonyl chloride, 0.698 g, 3.0 mmol, and b) 0.519 g, 81%.



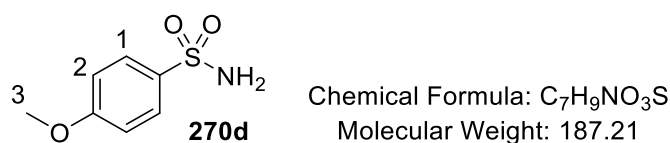
FTIR (neat): 3358, 3264, 2963, 1566, 1319, 1163 cm⁻¹.

¹H NMR (400 MHz, DMSO-d₆): δ 7.75 (d, 2H, ³J = 8.4 Hz, ArH¹), 7.58 (d, 2H, ³J = 8.4 Hz, ArH²), 7.25 (bs, 2H, NH₂), 1.30 (s, 9H, CH₃³).

¹³C NMR (100 MHz, DMSO-d₆): δ 154.7, 141.3, 125.7, 125.5, 34.7, 30.8.

*Synthesis of 4-methoxybenzenesulfonamide, 270d*²⁶⁸

Following *General Procedure L*: a) 4-methoxybenzenesulfonyl chloride, 3.9 g, 18.9 mmol, and b) 2.840 g, 65%.



FTIR (neat): 3343, 3265, 2982, 1595, 1574, 1499, 1300, 1153 cm⁻¹.

¹H NMR (400 MHz, DMSO-*d*₆): δ 7.75 (d, 2H, ³*J* = 8.9 Hz, ArH¹), 7.20 (s, 2H, NH₂), 7.08 (d, 2H, ³*J* = 8.9 Hz, ArH²), 3.82 (s, 3H, CH₃O).

¹³C NMR (100 MHz, DMSO-*d*₆): δ 161.6, 136.2, 127.6, 114.0, 55.6.

*Synthesis of 4-fluorobenzenesulfonamide, 270e*²⁶⁹

Following *General Procedure L*: a) 4-fluorobenzenesulfonyl chloride, 4.0 g, 20.6 mmol, and b) 1.820 g, 51%.



Chemical Formula: C₆H₆FNO₂S
Molecular Weight: 175.18

FTIR (neat): 3356, 3258, 3109, 1585, 1329, 1148 cm⁻¹.

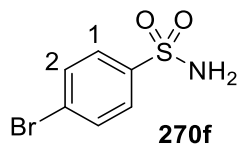
¹H NMR (400 MHz, DMSO-*d*₆): δ 7.90-7.86 (m, 2H, ArH¹), 7.42-7.38 (m, 4H, ArH² and SO₂NH₂).

¹³C NMR (100 MHz, DMSO-*d*₆): δ 163.7 (d, ¹*J*_{C-F} = 247.3 Hz), 140.6, 128.5 (d, ³*J*_{C-F} = 8.6 Hz), 115.9 (d, ²*J*_{C-F} = 11.6 Hz).

¹⁹F NMR (376 MHz, DMSO-*d*₆): -108.1 (*p*-F).

*Synthesis of 4-bromobenzenesulfonamide, 270f*²⁶⁹

Following *General Procedure L*: a) 4-bromobenzenesulfonyl chloride, 5.0 g, 19.6 mmol, and b) 3.640 g, 79%.



Chemical Formula: C₆H₆BrNO₂S
Molecular Weight: 236.08

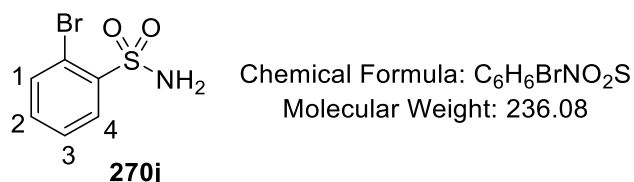
FTIR (neat): 3323, 3235, 3115, 1574, 1323, 1144 cm⁻¹.

¹H NMR (400 MHz, DMSO-*d*₆): δ 7.79 (d, 2H, ³*J* = 8.8 Hz, ArH²), 7.75 (d, 2H, ³*J* = 8.8 Hz, ArH¹), 7.46 (bs, NH₂).

¹³C NMR (100 MHz, DMSO-*d*₆): δ 143.4, 132.0, 127.7, 125.4.

Synthesis of 2-bromobenzenesulfonamide, **270j**²⁷⁰

Following *General Procedure L*: a) 2-bromobenzenesulfonyl chloride, 0.980 g, 19.6 mmol, and b) 0.739 g, 82%.



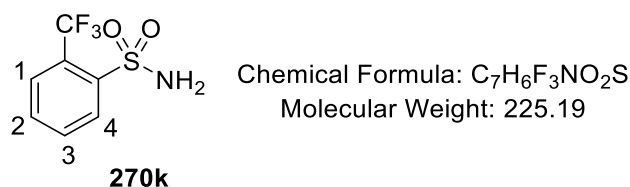
FTIR (neat): 3358, 3258, 3094, 1553, 1329, 1153 cm⁻¹.

¹H NMR (400 MHz, DMSO-d₆): δ 8.01 (dd, 1H, ³J = 7.8 Hz, ⁴J = 1.8 Hz, ArH⁴), 7.81 (dd, 1H, ³J = 7.8 Hz, ⁴J = 1.8 Hz, ArH¹), 7.58-7.54 (m, 3H, ArH² and SO₂NH₂), 7.49 (td, 1H, ³J = 7.6 Hz, ⁴J = 1.8 Hz, ArH³).

¹³C NMR (100 MHz, DMSO-d₆): δ 142.7, 135.0, 133.3, 129.1, 127.9, 118.1.

Synthesis of 2-(trifluoromethyl)benzenesulfonamide, **270k**²⁷¹

Following *General Procedure L*: a) 2-trifluoromethylbenzenesulfonyl chloride, 0.3 mL, 1.9 mmol, and b) 0.293 g, 67%.



FTIR (neat): 3370, 3262, 3115, 1564, 1342, 1304, 1157, 1134, 1119 cm⁻¹.

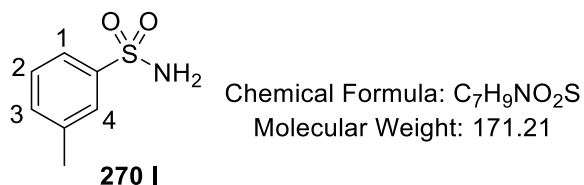
¹H NMR (400 MHz, DMSO-d₆): δ 8.18 (d, 1H, ³J = 7.9 Hz, ArH⁴), 7.94 (d, 1H, ³J = 7.9 Hz, ArH¹), 7.89 (t, 1H, ³J = 7.9 Hz, ArH²), 7.80 (t, 1H, ³J = 7.9 Hz, ArH³), 7.71 (bs, 2H, NH₂).

¹³C NMR (100 MHz, DMSO-d₆): δ 142.4, 133.1, 132.3, 129.4, 127.9 (q, ³J_{C-F} = 7.3 Hz), 125.5 (q, ²J_{C-F} = 270.7 Hz), 123.0 (q, ¹J_{C-F} = 272.1 Hz).

¹⁹F NMR (376 MHz, DMSO-d₆): - 56.1 (*o*-CF₃).

*Synthesis of 3-methylbenzenesulfonamide, 270l*²⁷²

Following *General Procedure L*: a) 3-methylbenzenesulfonyl chloride, 1.31 mL, 9.0 mmol, and b) 0.667 g, 57%.



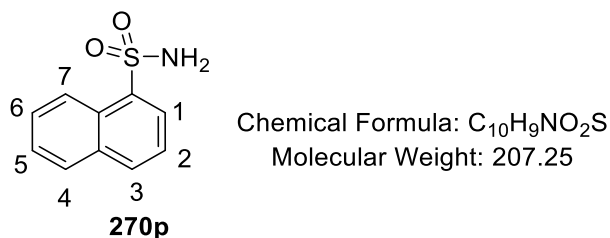
FTIR (neat): 3319, 3235, 3100, 2980, 1558, 1481, 1327, 1153 cm⁻¹.

¹H NMR (400 MHz, DMSO-d₆): δ 7.65-7.64 (m, 1H, ArH⁴), 7.63-7.61 (m, 1H, ArH¹), 7.46-7.41 (m, 2H, ArH² and ArH³), 7.28 (s, 2H, NH₂), 2.38 (s, 3H, ArCH₃).

¹³C NMR (100 MHz, DMSO-d₆): δ 144.0, 138.5, 132.3, 128.8, 125.8, 122.7.

*Synthesis of naphthalene-1-sulfonamide, 270 p*²⁷³

Following *General Procedure L*: a) naphthalene-1-sulfonamide chloride, 1.0 g, 4.4 mmol, and b) 0.734 g, 80%.



FTIR (neat): 3379, 3277, 3098, 1566, 1506, 1323, 1159, 1130 cm⁻¹.

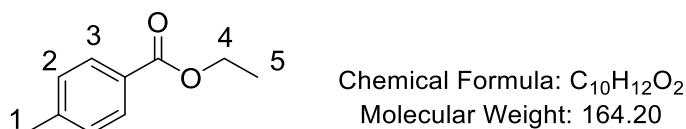
¹H NMR (400 MHz, DMSO-d₆): δ 8.68 (d, 1H, ³J = 8.8 Hz, ArH⁷), 8.19-8.14 (m, 2H, ArH¹ and ArH), 8.10-8.07 (m, 1H, ArH), 7.74-7.63 (m, 5H, ArH and NH₂).

¹³C NMR (100 MHz, DMSO-d₆): δ 139.2, 133.7, 133.0, 128.8, 127.5, 127.4, 126.7, 126.4, 125.1, 124.4.

*Synthesis of ethyl 4-methylbenzoate*²⁷⁴

To an oven dried three-neck round bottom flask were added ethanol (~50 mL) and triethylamine (1.7 mL, 12.2 mmol). The resulting solution was stirred while being cooled in

an ice bath. Subsequently, 4-methylbenzoyl chloride (1.9 g, 12.2 mmol) was then added dropwise. The flask was removed from the ice bath and heated at reflux for 16 h. Excess ethanol was removed under partial pressure and the ester was extracted with diethyl ether, with the ether layer being subsequently dried over anhydrous sodium sulfate. Finally, the product was purified by flash column chromatography, eluting with ethyl acetate/hexanes (1:10). The product was isolated as a clear oil (1.25 g, 63% yield).



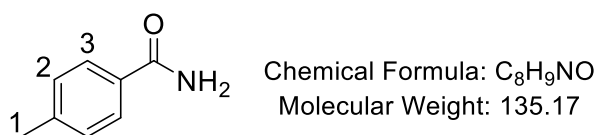
FTIR (neat): 2980, 1713, 1512 cm⁻¹.

¹H NMR (400 MHz, CDCl₃): δ 7.91 (d, ³J = 7.9 Hz, 2H, ArH³), 7.21 (d, 2H, ³J = 7.9 Hz, ArH²), 4.34 (q, 2H, ³J = 7.1 Hz, CH₂⁴), 2.38 (s, 3H, ArCH₃¹), 1.36 (t, 3H, ³J = 7.1 Hz, CH₃⁵).

¹³C NMR (100MHz, CDCl₃): δ 166.6, 143.5, 129.8, 129.3, 127.6, 60.7, 21.5, 14.4.

*Synthesis of 4-Methylbenzamide*²⁷⁵

Following *General Procedure L*: a) 4-methylbenzoyl chloride (1.17 g, 7.60 mmol), and b) 0.871 g, 85%.



FTIR (neat): 3339, 3157, 1666, 1568, 1410 cm⁻¹.

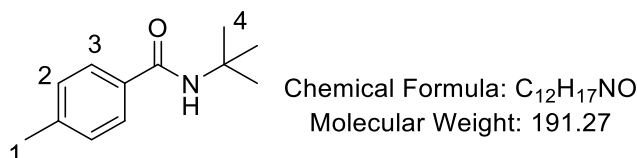
¹H NMR (400 MHz, CDCl₃): δ 7.88 (bs, 1H, NH), 7.77 (d, 2H, ³J = 8.2 Hz, ArH³), 7.24-7.22 (m, 3H, ArH² and NH), 2.33 (s, 3H, ArCH₃).

¹³C NMR (100MHz, CDCl₃): δ 167.8, 141.0, 131.5, 128.7, 127.5, 20.9.

*Synthesis of N-tert-butyl-p-toluoylamide*²⁷⁶

To a 100 mL two-necked round-bottomed flask with a suba seal attached to the main neck was added DCM (50 mL) and *p*-toluoyl chloride (1.7 mL, 12.9 mmol). The solution was cooled in an ice-bath to 0 °C before *tert*-butylamine (1.38 g, 19 mmol), was added dropwise,

resulting in gaseous HCl effervescing from the reaction vessel. After stirring the reaction mixture for 4 h, no starting material remained as shown by TLC analysis (eluent: 50% Et₂O/petrol). The contents of the flask were transferred to a separating funnel and washed with 3 M HCl (3 x 100 mL) and saturated NaHCO₃ (100 mL) before drying the DCM layer over anhydrous Na₂SO₄. The filtered solution had the solvent removed under reduced pressure to afford the desired product as a white solid (1.12 g, 96% yield).

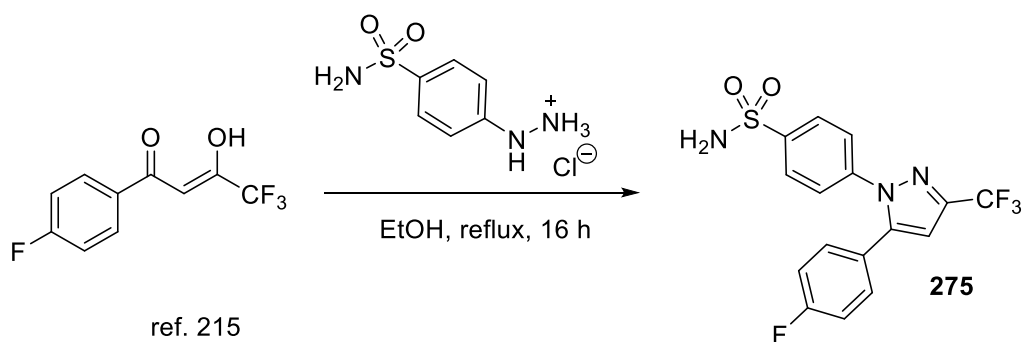


FTIR (CH₂Cl₂): 3443, 3050, 2969, 2927, 2872, 1661, 1523, 1498 cm⁻¹.

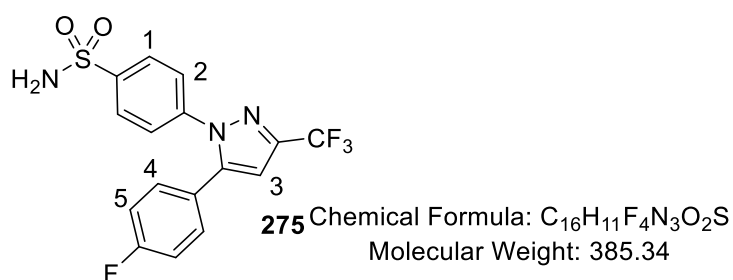
¹H NMR (400 MHz, CDCl₃): δ 7.61 (d, ³J = 8.0 Hz, 2H, ArH³), 7.20 (d, ³J = 8.0 Hz, 2H, ArH²) 5.90 (bs, 1H, NH), 2.38 (s, 3H, ArCH₃), 1.47 (s, 9H, CCH₃).

¹³C NMR (100 MHz, CDCl₃): 166.3, 140.8, 132.6, 128.5, 126.2, 51.0, 28.4, 20.8.

Synthesis of Mavacoxib, **275**²¹⁵



Following *General Procedure M*: a) 4,4,4-trifluoro-1-(4-fluorophenyl)-3-hydroxybut-2-en-1-one, 0.400 g, 1.708 mmol, b) 0.382 g, 1.708 mmol, and c) 0.674 g, 99% yield.



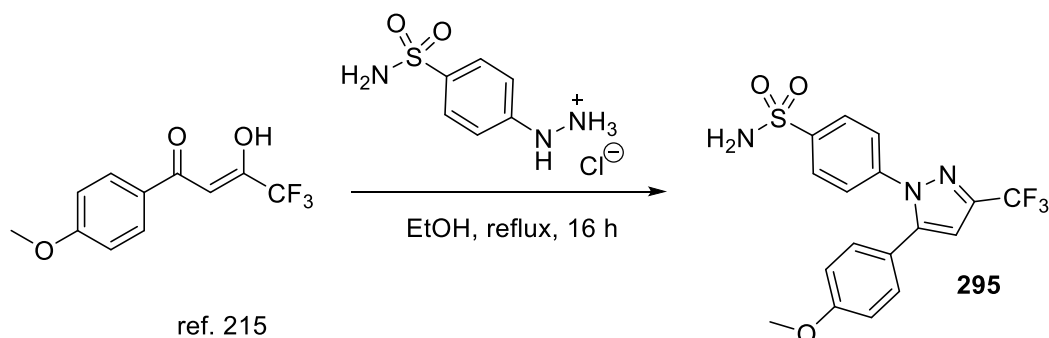
FTIR (CH₂Cl₂): 3356, 3281, 3076, 1331, 1159, 1134 cm⁻¹.

¹H NMR (400 MHz, CD₃OD): δ 7.14 (d, 2H, ³J = 8.7 Hz, ArH¹), 6.69 (d, 2H, ³J = 8.7 Hz, ArH²), 6.53 (dd, 2H, ³J = 8.6 Hz, ⁴J_{H-F} = 5.2 Hz, ArH⁴), 6.32 (apparent t, 2H, ³J = 8.6 Hz, ArH⁵), 6.15 (s, 1H, ArH³).

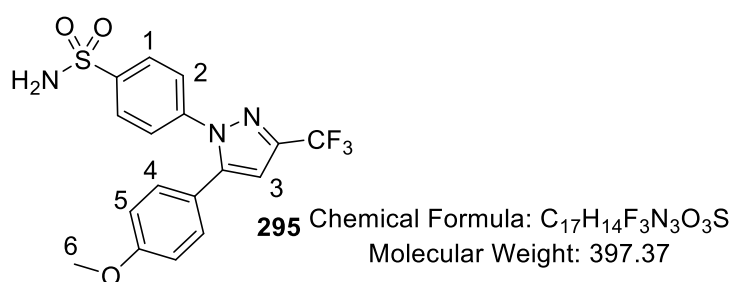
¹³C NMR (100 MHz, CD₃OD): 162.9 (d, ¹J_{C-F} = 251.6 Hz), 144.1, 143.4, 141.1, 130.6, 130.5, 126.5, 125.2, 124.5, 115.2, 115.0, 105.4. Overlapping signals meant that coupling constant and signal for CF₃ could not be defined. See ¹⁹F NMR for CF₃ characterisation.

¹⁹F NMR (376 MHz, CD₃OD): -63.9 (CF₃), -113.2 (*p*-F).

Synthesis of **295**²¹⁵



Following *General Procedure M*: a) 4,4,4-trifluoro-1-(4-methoxyphenyl)-3-hydroxybut-2-en-1-one, 0.300 g, 1.219 mmol, b) 0.273 g, 1.219 mmol, and c) 0.478 g, 99% yield.



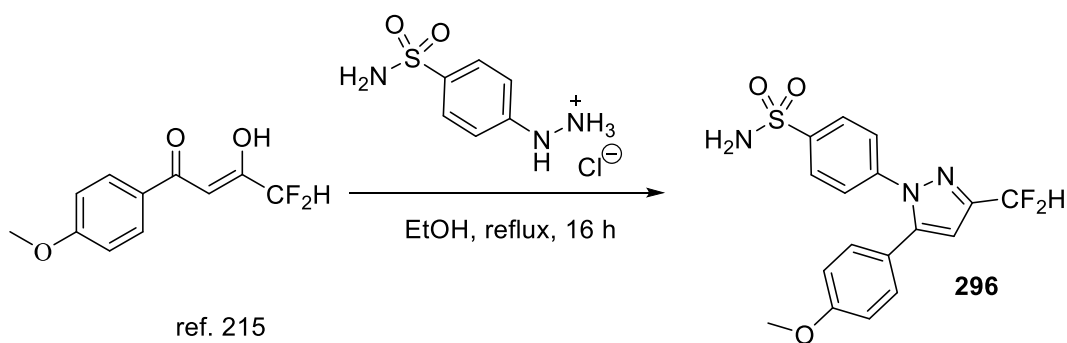
FTIR (CH₂Cl₂): 3970, 3264, 3086, 2980, 2839, 1614, 1595, 1471, 1339, 1157, 1124 cm⁻¹.

¹H NMR (400 MHz, CD₃OD): δ 7.96 (d, 2H, ³J = 8.7 Hz, ArH¹), 7.52 (d, 2H, ³J = 8.7 Hz, ArH²), 7.23 (d, 2H, ³J = 8.8 Hz, ArH⁴), 6.94 (d, 2H, ³J = 8.8 Hz, ArH⁵), 6.89 (s, 1H, ArH³), 3.82 (s, 3H, OCH₃⁶).

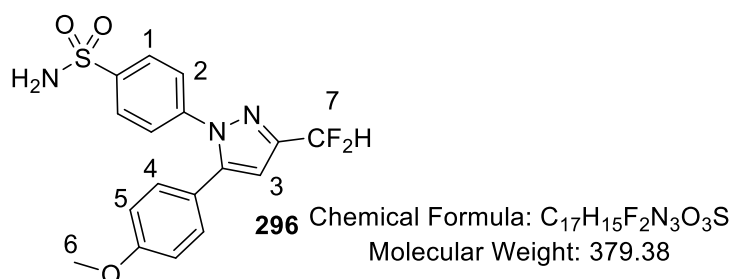
¹³C NMR (100 MHz, CD₃OD): 160.2, 145.1, 143.2, 142.7, 141.4, 129.7, 126.4, 125.1, 120.3, 113.5, 104.7, 54.0.

¹⁹F NMR (376 MHz, CD₃OD): -63.9 (CF₃).

Synthesis of **296**²¹⁵



Following *General Procedure M*: a) 4,4-difluoro-1-(4-methoxyphenyl)-3-hydroxybut-2-en-1-one, 0.350 g, 1.534 mmol, b) 0.343 g, 1.534 mmol, and c) 0.431 g, 74% yield.



FTIR (CH₂Cl₂): 3318, 3188, 3150, 3086, 1595, 1458, 1342, 1157 cm⁻¹.

¹H NMR (400 MHz, CD₃OD): δ 7.94 (d, 2H, ³J = 8.7 Hz, ArH¹), 7.49 (d, 2H, ³J = 8.7 Hz, ArH²), 7.22 (d, 2H, ³J = 8.8 Hz, ArH⁴), 6.94 (d, 2H, ³J = 8.8 Hz, ArH⁵), 6.85 (d, ²J_{H-F} = 31.6 Hz, 1H, CF₂H⁷), 6.77 (s or unresolved triplet, 1H, ArH³), 3.82 (s, 3H, OCH₃⁶).

¹³C NMR (100 MHz, CD₃OD): 158.6, 146.2, 143.3, 141.2, 140.3, 128.1, 124.9, 123.4, 119.4, 112.0, 109.2 (t, ¹J_{C-F} = 226.0 Hz), 102.5, 52.4.

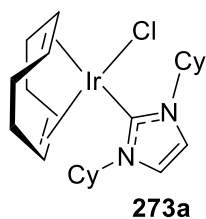
¹⁹F NMR (376 MHz, CD₃OD): -114.1 (CF₂H).

Celecoxib was provided by Astrazeneca.

Synthesis of Catalysts

Chloro(η⁴-cycloocta-1,5-diene)(1,3-dicyclohexylimidazoline-2-ylidene) iridium(I), **273a**¹²⁰

Following *General Procedure A*: a) 0.400 g, 0.595 mmol, b) 1.2 ml, 1.2 mmol, c) 1,3-dicyclohexylimidazolium chloride, 0.320 g, 1.191 mmol, and d) 0.602 g, 91%.



Chemical Formula: $C_{23}H_{36}ClIrN_2$
Molecular Weight: 568.22

273a

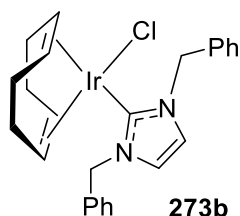
FTIR (CH_2Cl_2): 2932, 2846, 1567, 1426 cm^{-1}

1H NMR (400 MHz, $CDCl_3$): δ 6.84 (s, 2H, ArH), 5.14-5.16 (m, 2H, CH), 4.57-4.59 (m, 2H, COD CH), 2.94-2.95 (m, 2H, COD CH), 2.17-2.29 (m, 6H, CH_2), 2.02 (d, $^3J = 12.0$ Hz, 2H, CH_2), 1.95 (dd, $^3J = 13.1$ Hz, $^4J = 2.1$ Hz, 2H, CH_2), 1.85 (dd, $J = 13.4$ Hz, $^4J = 2.2$ Hz, 2H, CH_2), 1.72-1.78 (m, 4H, CH_2), 1.57-1.66 (m, 4H, COD CH_2), 1.46-1.55 (m, 4H, COD CH_2), 1.18-1.39 (m, 4H, CH_2).

^{13}C NMR (100 MHz, $CDCl_3$): δ 177.4, 116.4, 82.8, 59.4, 50.3, 33.8, 33.7, 33.3, 29.2, 25.6, 25.3, 24.9.

Chloro(η^4 -cycloocta-1,5-diene)(1,3-dibenzylimidazoline-2-ylidene) iridium(I), **273b**^{147,197}

Following *General Procedure A*: a) 0.4 g, 0.595 mmol, b) 1.2 ml, 1.2 mmol, c) 1,3-dibenzylimidazolium chloride, 0.339 g, 1.191 mmol, and d) 0.553 g, 80%.



Chemical Formula: $C_{25}H_{28}ClIrN_2$
Molecular Weight: 584.18

273b

m.p.: decomposes at > 195 $^{\circ}C$.

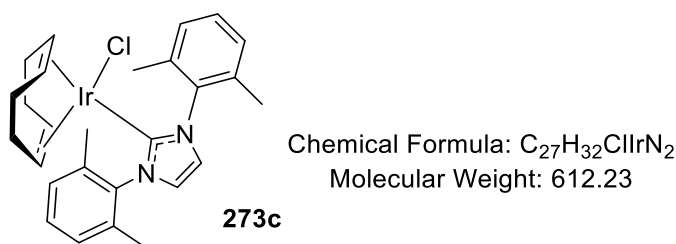
FTIR (neat): 3171, 3111, 2951, 1569, 1500 cm^{-1} .

1H NMR (400 MHz, $CDCl_3$): δ 7.39-7.32 (m, 10H, ArH), 6.77 (s, 2H, NCH=CHN), 5.78 (d, $^3J = 14.8$ Hz, 2H, Ar CH_2), 5.62 (d, $^3J = 14.8$ Hz, 2H, Ar CH_2), 4.67 (m, 2H, COD CH), 2.98 (m, 2H, COD CH), 2.11-2.22 (m, 4H, COD CH_2), 1.76-1.71 (m, 2H, COD CH_2), 1.61-1.56 (m, 2H, COD CH_2).

^{13}C NMR (100 MHz, $CDCl_3$): δ 180.5, 135.8, 128.4, 127.7, 127.6, 120.0, 84.6, 53.9, 51.4, 33.1, 29.0.

*Chloro(η^4 -cycloocta-1,5-diene)(1,3-bis[2,6-dimethylphenyl]-imidazol-2-ylidene) iridium(I), 273c*¹⁵²

Following *General Procedure B*: a) 0.322 g, 0.480 mmol, b) 0.108 g, 0.959 mmol, c) 1,3-bis[*meta*-xylyl]-imidazolium chloride, 0.300 g, 0.959 mmol, and d) 0.534 g, 91%.

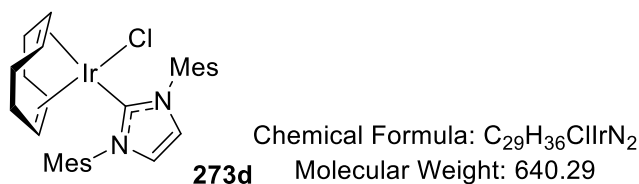


FTIR (neat): 3169, 3140, 3019, 2924, 2974, 2826, 1470 cm⁻¹.

¹H NMR (400 MHz, CDCl₃): δ 7.30 (t, 2H, ³*J* = 7.5 Hz, ArH), 7.21 – 7.17 (m, 4H, ArH), 7.01 (s, 2H, NCH=CHN), 4.18-4.13 (m, 2H, COD olefinic CH), 2.98-2.93 (m, 2H, COD olefinic CH), 2.41 (s, 6H, ArCH₃), 2.22 (s, 6H, ArCH₃), 1.75-1.59 (m, 4H, COD CH₂), 1.38-1.31 (m, 2H, COD CH₂), 1.27-1.21 (m, 2H, COD CH₂).

¹³C NMR (100 MHz, CDCl₃): δ 179.6, 137.4, 136.8, 133.8, 128.0, 127.8, 126.5, 122.2, 81.9, 50.5, 32.5, 27.9, 18.8, 17.3.

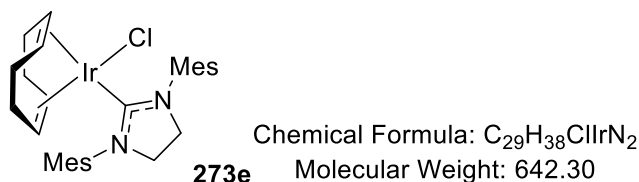
*Chloro(η^4 -cycloocta-1,5-diene)(1,3-dimesitylimidazol-2-ylidene) iridium(I), 273d*¹²⁰



See **Section 8.3**, under **207**.

*Chloro(η^4 -cycloocta-1,5-diene)(1,3-dimesitylimidazol-2-ylidene) iridium(I), 273e*¹²⁰

Following *General Procedure B*: a) 0.400 g, 0.595 mmol, b) 0.133 g, 1.191 mmol, c) 1,3-dimesitylimidazolium chloride, 0.408 g, 1.191 mmol, and d) 0.672 g, 88%.



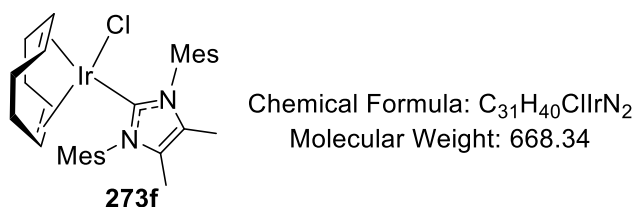
FTIR (neat): 2999, 2908, 2878, 2832, 1476, 1416 cm⁻¹.

¹H NMR (400 MHz, CDCl₃): δ 7.98 (s, 2H, ArH), 6.94 (s, 2H, ArH), 4.11-4.09 (m, 2H, COD olefinic CH), 3.92-3.88 (m, 4H, N(CH₂)₂N), 3.10-3.05 (m, 2H, COD olefinic CH), 2.55 (s, 6H, ArCH₃), 2.35 (s, 6H, ArCH₃), 2.32 (s, 6H, ArCH₃), 1.69-1.57 (m, 4H, COD CH₂), 1.35-1.19 (m, 4H, COD CH₂).

¹³C NMR (100 MHz, CDCl₃): δ 206.3, 137.0, 136.8, 135.2, 134.2, 128.8, 127.3, 82.7, 50.8, 50.4, 32.4, 27.4, 20.0, 18.8, 17.4.

Chloro(η⁴-cycloocta-1,5-diene)(4,5-dimethyl-1,3-dimesitylimidazol-2-ylidene) iridium(I),
273f¹⁴⁸

Following *General Procedure B*: a) 0.910 g, 1.355 mmol, b) 0.304 g, 2.710 mmol, c) 1,3-dimesityl-4,5-dimethylimidazolium chloride, 1.000 g, 2.710 mmol, and d) 1.393 g, 77%.



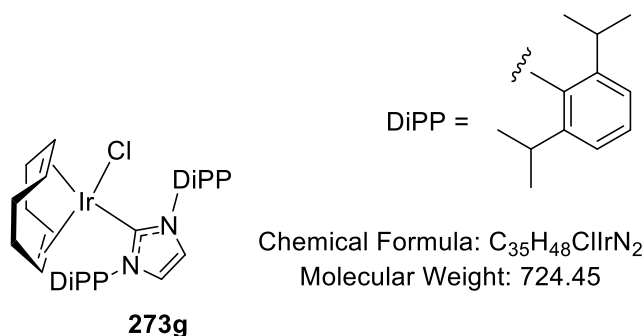
FTIR (neat): 3005, 2916, 2876, 2828, 1483, 1445 cm⁻¹.

¹H NMR (400 MHz, CDCl₃): δ 7.01 (s, 2H, ArH), 6.97 (s, 2H, ArH), 4.07-4.01 (m, 2H, COD olefinic CH), 3.05-3.00 (m, 2H, COD olefinic CH), 2.35 (s, 6H, ArCH₃), 2.29 (s, 6H, ArCH₃), 2.04 (s, 6H, ArCH₃), 1.81 (s, 6H, ArCH₃), 1.65-1.54 (m, 4H, COD CH₂), 1.30-1.18 (m, 4H, COD CH₂).

¹³C NMR (100 MHz, CDCl₃): δ 178.3, 137.8, 134.3, 133.8, 129.1, 127.5, 125.4, 80.6, 50.2, 33.0, 28.4, 20.6, 19.2, 17.7, 8.7.

*Chloro(η^4 -cycloocta-1,5-diene)(1,3-bis(2,6-diisopropylphenyl)imidazol-2-ylidene) iridium(I), 273g*¹²⁰

Following *General Procedure B*: a) 0.400 g, 0.595 mmol, b) 0.134 g, 1.190 mmol, c) 1,3-bis[2,6-diisopropylphenyl]-imidazolium chloride, 0.506 g, 1.190 mmol, and d) 0.355 g, 82%.



FTIR (CH₂Cl₂): 2963, 2928, 2866, 2824, 1591, 1566, 1445 cm⁻¹.

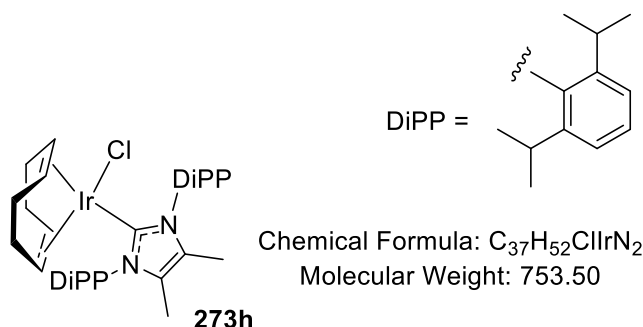
¹H NMR (400 MHz, CDCl₃): δ 7.45 (t, ³J = 7.7 Hz, 2H, ArH), 7.36-7.29 (m, 4H, ArH), 7.00 (s, 2H, ArH), 4.19-4.16 (m, 2H, COD CH), 3.47-3.37 (m, 2H, CH(CH₃)₂), 2.88-2.86 (m, 2H, COD CH), 2.73-2.64 (m, 2H, CH(CH₃)₂), 1.71-1.62 (m, 2H, COD CH₂), 1.54-1.11 (m, 16H, COD CH₂ and CH(CH₃)₂), 1.08 (d, ³J = 6.7 Hz, 12H, CH(CH₃)₂), 0.93-0.81 (m, 2H, COD CH₂).

¹³C NMR (100 MHz, CDCl₃): δ 181.9, 135.7, 129.2, 123.8, 122.4, 82.3, 50.9, 33.0, 28.4, 28.2, 25.9, 22.7, 22.0.

*Chloro(η^4 -cycloocta-1,5-diene)(1,3-bis(2,6-diisopropylphenyl)-4,5-dimethylimidazol-2-ylidene) iridium(I), 273h*²⁷⁷

In a modification to *General Procedure B*, 1,3-bis[2,6-diisopropylphenyl]-4,5-dimethylimidazolium chloride (0.340 g, 0.750 mmol) was added to a flame-dried Schlenk flask under an argon atmosphere. Dry THF (7.5 mL) was added with stirring, forming a slurry. Fresh potassium *tert*-butoxide (0.101 g, 0.900 mmol) was added to the flask in a single portion, causing gradual dissolution of the imidazolium salt and carbene formation. Stirring was continued at r.t. for 30 mins before adding [Ir(COD)Cl]₂. An instant clear to bright yellow colour change occurred, slowly turning to dark yellow over the course of 16 h. Removal of the solvent *in vacuo* followed by purification through a short plug of silica

(eluting with 1:1 petroleum ether/Et₂O) gave the product as a bright yellow solid (0.227 g, 40%).



FTIR (CH₂Cl₂): 3063, 2961, 2923, 2870, 2825, 1460, 1443, 1341, 1307, 806 cm⁻¹.

¹H NMR (400 MHz, toluene-d₈, 353 K): In accordance with the published data, NMR spectra were collected at 80 °C to account for rotameric effects associated with the C-N bonds. Due to the broadness of the signals collected, exact structural assignments are not provided for all positions.

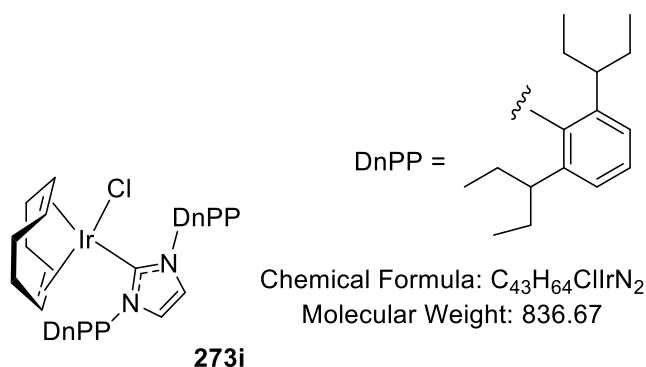
δ 7.30 (t, ³J = 7.6 Hz, 2H, ArH), 7.21 (d, 4H, ³J = 7.6 Hz, ArH), 4.55-4.53 (m, 2H, COD CH), 3.30-3.08 (m, 5H, COD CH + CH(CH₃)₂), 1.74- 1.55 (m, 10H, ArCH₃ + COD CH₂), 1.45 (d, 12H, ³J = 6.4 Hz, CH(CH₃)₂), 1.37-1.20 (m, 5H, COD CH₂), 1.08 (d, ³J = 6.4 Hz, 12H, CH(CH₃)₂).

¹³C NMR (100 MHz, CDCl₃): δ 184.3, 134.8, 130.0, remaining aromatic peaks obscured by toluene*, 81.9, 50.4, 34.2, 29.2, 28.8, 25.6, 25.4, 10.5.

Chloro(η⁴-cycloocta-1,5-diene)(1,3-bis(2,6-neopentylphenyl)-imidazol-2-ylidene) iridium(I), 273i

Following the same procedure as reported above for catalyst **273h**, results are reported as: a) amount of imidazolium salt, b) amount of KO^tBu, c) amount of [Ir(COD)Cl]₂, and d) product yield.

a) 0.500 g, 0.931 mmol, b) 0.115 g, 1.024 mmol, c) 0.313 g, 0.465 mmol, and d) 0.370 g,



m.p.: 175 – 176 °C (Lit. = 169 – 170 °C).

1H NMR (400 MHz, $CDCl_3$): δ As in the published data, much of the alkyl region is comprised of broad signals. As such, specific structural assignments are not provided for all peaks.

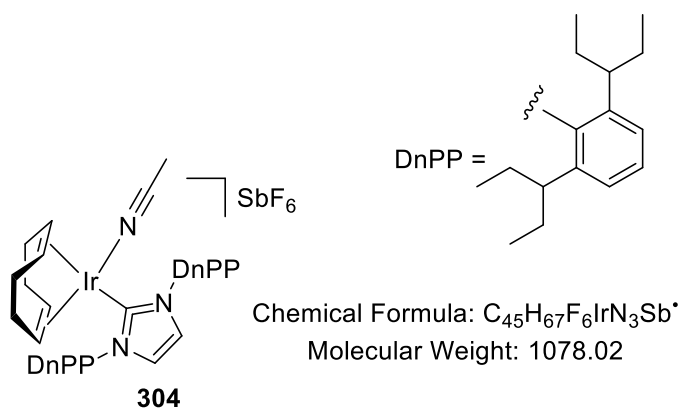
7.41 (t, $^3J = 8.0$ Hz, 2H, ArH), 7.20 (d, 4H, $^3J = 8.0$ Hz, ArH), 6.97 (s, 2H, ArH), 4.19-4.17 (m, 2H, COD CH), 2.96 – 2.94 (m, 2H, COD CH), 2.67 (bs, 4H), 2.04 – 1.87 (m, 10H), 1.66 – 1.47 (m, 10H), 1.40 – 1.32 (m, 2H), 1.20 – 1.12 (m, 2H), 1.05 (t, 12H, $^3J = 7.0$ Hz, CH_2CH_3), 0.75 (t, 12H, $^3J = 7.0$ Hz, CH_2CH_3).

^{13}C NMR (100 MHz, $CDCl_3$): δ 179.8, 144.2, 137.6, 128.6, 125.0, 124.5, 122.4, 82.7, 51.4, 41.2, 33.3, 28.8, 28.2, 26.6, 12.6, 10.9.

Synthesis of η^4 -Cycloocta-1,5-diene(1,3-bis(dineopentylphenyl)imidazol-2-ylidene)(acetonitrile)iridium(I) hexafluoroantimonate, 304

Following *General Procedure B*, results are reported as a) amount of **207**, b) volume of THF, c) amount of $AgSbF_6$, d) amount of MeCN, e) reaction time, f) product yield, and g) purification technique.

a) 0.100 g, 0.120 mmol, b) 10 mL, c) 0.041 g, 0.120 mmol, d) 0.005 g, 0.120 mmol, e) 4 h, f) 0.118 g, 92% yield, and g) the THF solution was reduced to quarter-volume and the product triturated using cold hexane. After collection by filtration, the product was washed with cold Et_2O and dried under vacuum for 16 h.



Appearance: orange solid.

m.p.: Decomposes >160 °C.

FTIR (neat): 3615, 3533, 2965, 1616, 1452, 1398, 1381, 1314, 1201, 652 cm^{-1} .

1H NMR (400 MHz, $CDCl_3$): δ 7.56 (t, 2H, $^3J = 8.1$ Hz, ArH), 7.30 (d, 4H, $^3J = 8.1$ Hz, ArH), 7.12 (s, 2H, NCH=CHN), 3.98 – 3.96 (m, 2H, COD CH), 3.38 – 3.36 (m, 2H, COD CH), 4.10 (m, 4H, $CH(Et)_2$), 2.21 (s, 3H, CH_3CN), 2.07 – 1.47 (m, 24H, COD CH_2 + $CH(CH_2CH_3)_2$), 1.05 (t, 12H, $^3J = 7.4$ Hz, $CH(CH_2CH_3)_3$), 0.76 (t, 12H, $^3J = 7.4$ Hz, $CH(CH_2CH_3)_3$).

^{13}C NMR (100 MHz, $CDCl_3$): δ 171.0, 143.1, 136.5, 129.8, 125.9, 125.2, 125.1, 82.9, 64.7, 41.6, 32.1 28.3, 27.6, 27.3, 12.1, 11.0, 3.9.

^{13}C DEPT-135° NMR (100 MHz, $CDCl_3$): δ 32.1 28.3, 27.6, 27.3.

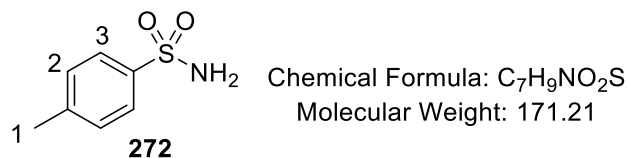
HRMS (positive NSI): m/z calc'd for $C_{43}H_{62}^{191}IrN_2 [M - MeCN - SbF_6]^+$: 799.4539; found: 799.4542.

Low resolution-MS (negative NSI): m/z calc'd for $^{123}SbF_6 [SbF_6]^-$: 236.9; found: 236.9.

Deuterium Labelling Experiments for Catalyst Discovery and Screening (Table 19)

Following *General Procedure F* results are reported as: a) amount of catalyst, b) amount of substrate, c) volume of solvent, d) reaction temperature, e) reaction time, and f) % D in labelled substrate. 1H NMR is reprinted for all starting materials, accompanied by details of where deuterium incorporation is expected and what signal is used as an internal reference.

Table 19, Entry 1

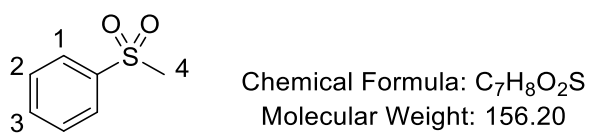


¹H NMR (400 MHz, DMSO-*d*₆): δ 7.71 (d, 2H, ³*J* = 8.2 Hz, ArH³), 7.36 (d, 2H, ³*J* = 8.2 Hz, ArH²), 7.25 (bs, 2H, SO₂NH₂), 2.37 (s, 3H, ArCH₃).

Incorporation expected at δ 7.71. Determined against integral at δ 2.37.

a) **196a** (10.9 mg, 0.01075 mmol, 5 mol%), b) 4-methylbenzenesulfonamide (36.8 mg, 0.215 mmol) c) DCM (2.5 mL), d) 25 °C, e) 16 h, and f) 12% D.

Table 19, Entry 2

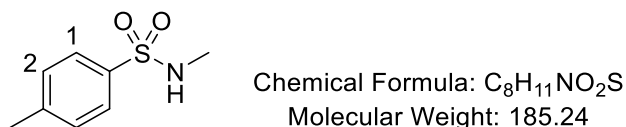


¹H NMR (400 MHz, DMSO-*d*₆): δ 7.94 (d, 2H, ³*J* = 8.4 Hz, ArH¹), 7.65 (tt, 1H, ³*J* = 7.2 Hz, ⁴*J* = 2.4 Hz, ArH³), 7.57 (t, 2H, ³*J* = 7.2 Hz, ArH²), 3.05 (s, 3H, SO₂CH₃).

Incorporation expected at δ 7.94. Determined against integral at δ 3.05.

a) **196a** (10.9 mg, 0.01075 mmol, 5 mol%), b) methylphenylsulfone (33.0 mg, 0.215 mmol), c) DCM (2.5 mL), d) 25 °C, e) 16 h, and f) 9% D.

Table 19, Entry 3

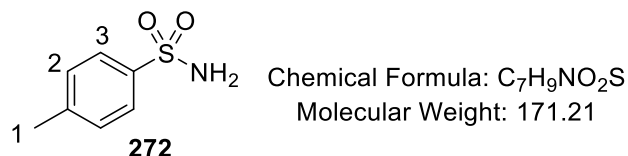


¹H NMR (400 MHz, CDCl₃): δ 7.75 (d, 2H, ³*J* = 8.3 Hz, ArH¹), 7.31 (d, 2H, ³*J* = 8.3 Hz, ArH²), 4.61-4.56 (m, 1H, SO₂N(CH₃)H), 2.63 (d, 3H, ³*J* = 5.4 Hz, N(CH₃)H), 2.43 (s, 3H, ArCH₃).

Incorporation expected at δ 7.75. Determined against integral at δ 2.43.

a) **196a** (10.9 mg, 0.01075 mmol, 5 mol%), b) *N*,4-dimethylbenzenesulfonamide (39.8 mg, 0.215 mmol), c) DCM (2.5 mL), d) 25 °C, e) 16 h, and f) 7% D.

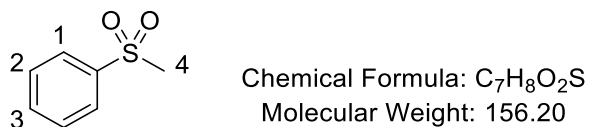
Table 19, Entry 4



For spectral details, see above.

a) **207** (6.9 mg, 0.01075 mmol, 5 mol%), b) 4-methylbenzenesulfonamide (36.8 mg, 0.215 mmol), c) DCM (2.5 mL), d) 25 °C, e) 16 h, and f) 90% D.

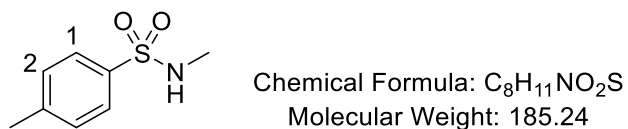
Table 19, Entry 5



For spectral details, see above.

a) **207** (6.9 mg, 0.01075 mmol, 5 mol%), b) methylphenylsulfone (33.0 mg, 0.215 mmol), c) DCM (2.5 mL), d) 25 °C, e) 16 h, and f) 17% D.

Table 19, Entry 6

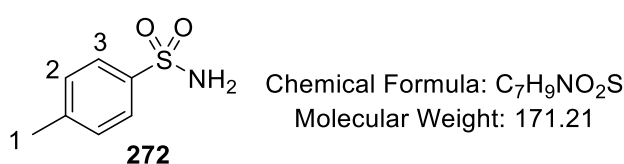


For spectral details, see above.

a) **207** (6.9 mg, 0.01075 mmol, 5 mol%), b) *N*,4-dimethylbenzenesulfonamide (39.8 mg, 0.215 mmol), c) DCM (2.5 mL), d) 25 °C, e) 16 h, and f) 8% D.

Catalyst Screening for o-Deuteration of 4-methylbenzenesulfonamide (Table 20)

All reactions from **Table 20** were carried out using *General Procedure F*, and the same conditions, labelling **272** (36.8 mg, 0.215 mmol) with catalyst (0.01075 mmol, 5 mol%) in DCM (2.5 mL) at 25 °C for 16 h. As only the mass quantity of the particular catalyst changed between experiments, these are summarised in the table below.



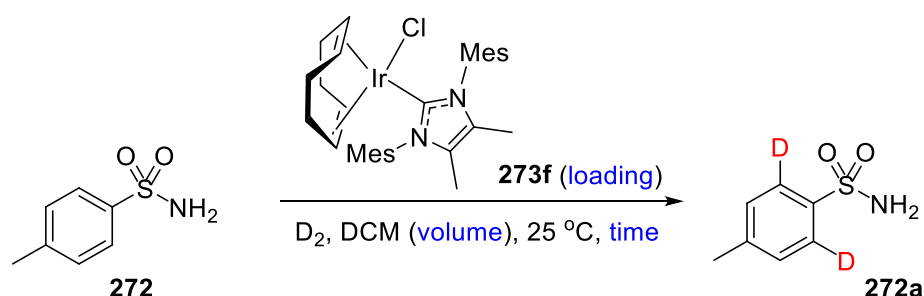
For spectral details, see above.

<i>Entry</i>	<i>Catalyst (mg)</i>	<i>%D (272)</i>
1	273a (6.1)	2
2	273b (6.2)	3
3	273c (6.6)	75
4	273d (6.1)	90
5	273e (7.2)	95
6	273f (6.9)	96
7	273g (6.1)	93

Notes on Reaction Optimisation via Experimental Design

Experimental design was used to assess the effect of varying catalyst loading, reaction time, and solvent volume. As such, ‘high’ and ‘low’ values for each of these three variables were chosen. To generate a series of experiments to study optimal conditions within the variable ranges chosen, Design Expert™ software v8.0 (Stat-Ease Inc., Minneapolis, MN) was used. This generated a 2 level, 3 factorial design containing three centre points, giving 11

experiments in total. The % D incorporation in 4-methylbenzenesulfonamide was used as the response (see below).



Spectral details for substrate **272** for the assessment of % D by ^1H NMR are available above.

<i>Run</i> ^a	<i>Variable A:</i> Time (h)	<i>Variable B:</i> Cat. Loading (mol%)	<i>Variable C:</i> Solvent Volume (mL)	<i>Response:</i> % D
1 (-++)	1.0	10.0	10.0	96
2 (--+)	1.0	10.0	2.0	93
3 (---)	1.0	3.0	2.0	86
4 (++-)	3.0	10.0	2.0	93
5 (+--)	3.0	3.0	2.0	91
6 (+++)	3.0	3.0	10.0	92
7 (--+)	1.0	3.0	10.0	86
8 (000)[‡]	2.0	6.5	6.0	97
9 (-++)	3.0	10.0	10.0	97
10 (000)[‡]	2.0	6.5	6.0	97
11 (000)[‡]	2.0	6.5	6.0	97

^a(+) = high value, (-) = low value, and (0) = centre point value of a variable. (+--) = combination of high A, low B, and low C

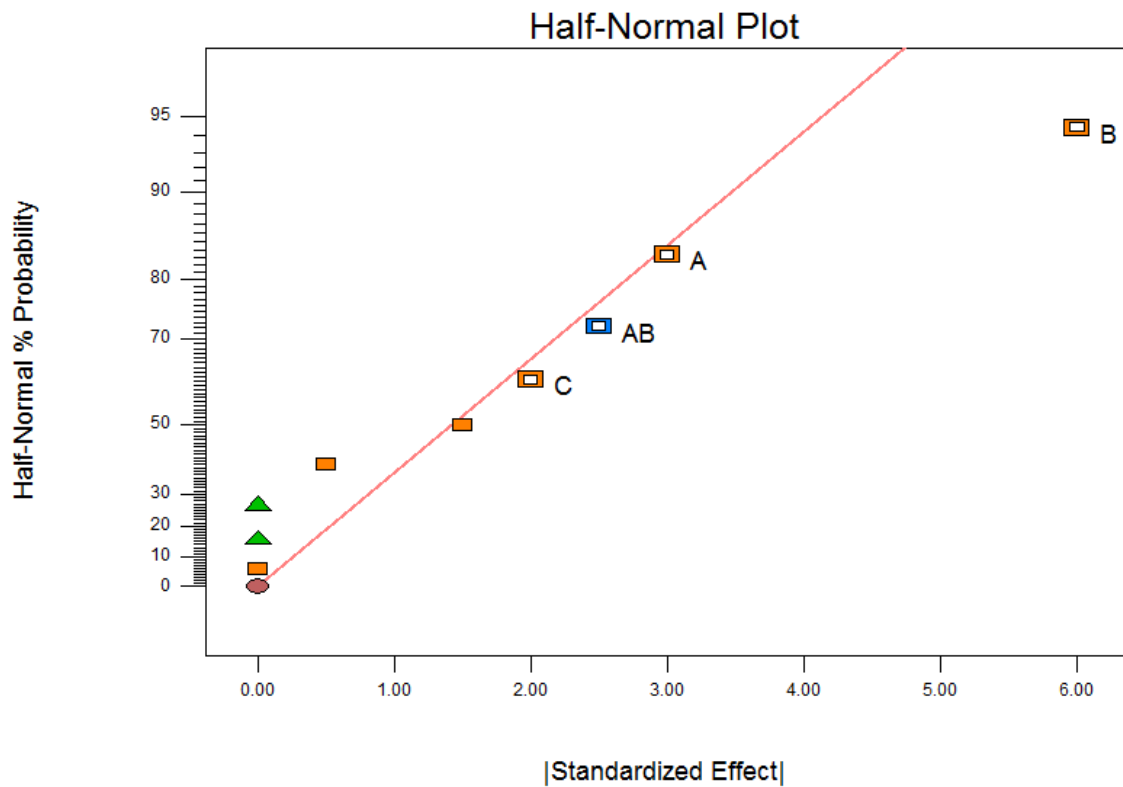
[‡]Entries highlighted in blue represent centre points and the chosen optimal conditions for assessment of substrate scope.

Entries 8, 10, and 11 represent the centre points of the design. These were employed in order to:

- (i) Assess any curvature in the response of % D to changes in the variables, and
- (ii) Assess repeatability of the deuteration experiment.

A response surface was created in the same design program. This generated a half normal plot (see below), inferring that catalyst loading had the most significant impact on the efficacy of the deuteration protocol. Without further optimisation, the centre point conditions (Entries 8, 10, and 11) were chosen as the new optimum conditions for assessing substrate scope.

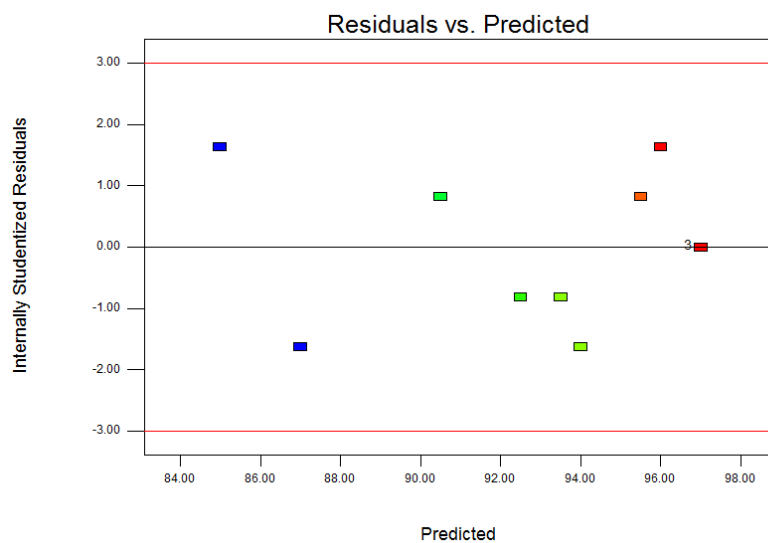
Half Normal Plot for assessment of the impact of variables A-C on % D.



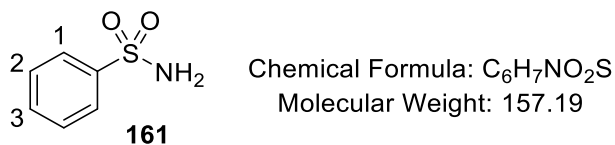
Finally, provided below is a graph of *Residuals versus Predicted* plot. This is a plot of the residuals versus the ascending predicted response values (lower % D to higher % D). It tests the assumption of constant variance in the data. As desired, the plot is a random scatter, and a constant range of residuals across the graph is therefore assumed (see below).

Residuals versus Predicted plot for the full factorial experimental design response

Design-Expert® Software
 %D
 (adjusted for curvature)
 Color points by value of
 %D:
 97
 86



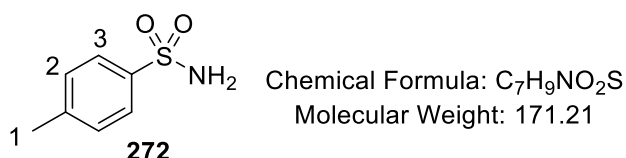
Substrate Scope for *o*-Deuteration of Primary Sulfonamides (Table 21)



¹H NMR (400 MHz, DMSO-*d*₆): δ 7.86-7.83 (m, 2H, ArH¹), 7.63-7.55 (m, 3H, ArH² and ArH³), 7.35 (bs, 2H, NH₂).

Incorporation expected at δ 7.86-7.83. Determined against integral at δ 7.63-7.55.

a) **273f** (9.3 mg, 0.01398 mmol, 6.5 mol%), b) benzenesulfonamide (33.8 mg, 0.215 mmol),
c) DCM (6.0 mL), d) 25 °C, e) 2 h, and f) 95% D.



For spectral details, see above.

Normal scale reaction:

a) **273k** (9.3 mg, 0.01398 mmol, 6.5 mol%), b) 4-methylbenzenesulfonamide (36.8 mg, 0.215 mmol) c) DCM (6.0 mL), d) 25 °C, e) 2 h, and f) 97% D.

Mercury test reaction:

The normal scale reaction was run exactly as shown above but with the addition of one pipette droplet of Hg(0). A result of 96% D was observed.²¹⁶

Large scale reaction:

NOTE: Reaction carried out in 250 mL rather than a 100 mL flask. A higher concentration of 0.072 M was employed rather than the 0.036 M used in normal scale optimised reactions.

To demonstrate the practicality of the reaction, an isolated yield of the labelled compound from the large scale reaction was assessed as follows:

After the 2 h reaction time, the flask was opened to air and petroleum ether (40-60) was added (~50 mL). The product precipitated from solution, whilst the catalyst remained dissolved. The product was isolated by Buchner filtration, washed with petroleum ether and dried in a vacuum oven (40 °C, 0 mbar) overnight (156 mg, 84% yield). The yield was calculated based on the % D incorporation by ¹H NMR, assuming that the product mixture is composed of **272** and **272a** only.

a) **273f** (46.5 mg, 0.06988 mmol, 6.5 mol%), b) 4-methylbenzenesulfonamide (184 mg, 1.075 mmol), c) DCM (15 mL), d) 25 °C, e) 2 h, and f) 93% D.

To assess the accuracy of % D incorporation calculated from ¹H NMR, HRMS was obtained on the isolated compound **272a** (93% D) from the large scale reaction. Mass ions were detected for **272-d**₁ and **272-d**₂. The % D incorporation was calculated from the relative ratio of these two ions.

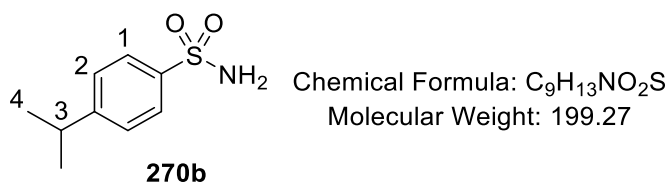
HRMS (positive NSI, DCM + MeOH + NH₄OAc):

[M(d₂) + NH₄]⁺; expected = 191.0818, observed = 191.0818.

[M(d₁) + NH₄]⁺; expected = 190.0755, observed = 190.0756.

Ratio of ion intensities = (**272-d**₂) : (**272-d**₁) = 6.1734 : 1.

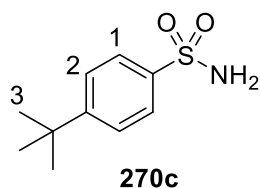
% Deuterium Incorporation = 93%



¹H NMR (400 MHz, DMSO-*d*₆): δ 7.74 (d, 2H, ³J = 8.3 Hz, ArH¹), 7.43 (d, 2H, ³J = 8.3 Hz, ArH²), 7.24 (bs, 2H, NH₂), 2.97 (septet, 1H, ³J = 6.9 Hz, H³), 1.22 (d, 6H, ³J = 6.9 Hz, H⁴).

Incorporation expected at δ_H 7.74. Determined against integral at δ_H 2.97.

a) **273f** (9.3 mg, 0.01398 mmol, 6.5 mol%), b) 4-*iso*-propylbenzenesulfonamide (42.8 mg, 0.215 mmol), c) DCM (6.0 mL), d) 25 °C, e) 2 h, and f) 94% D.

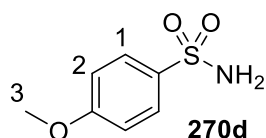


Chemical Formula: C₁₀H₁₅NO₂S
Molecular Weight: 213.29

¹H NMR (400 MHz, DMSO-d₆): δ 7.75 (d, 2H, ³J = 8.4 Hz, ArH¹), 7.58 (d, 2H, ³J = 8.4 Hz, ArH²), 7.25 (bs, 2H, NH₂), 1.30 (s, 9H, H³).

Incorporation expected at δ_H 7.75. Determined against integral at δ_H 1.30.

a) **273f** (9.3 mg, 0.01398 mmol, 6.5 mol%), b) 4-*tert*-butylbenzenesulfonamide (45.9 mg, 0.215 mmol), c) DCM (6.0 mL), d) 25 °C, e) 2 h, and f) 84% D.



Chemical Formula: C₇H₉NO₃S
Molecular Weight: 187.21

¹H NMR (400 MHz, DMSO-d₆): δ 7.75 (d, 2H, ³J = 8.9 Hz, ArH¹), 7.20 (s, 2H, NH₂), 7.08 (d, 2H, ³J = 8.9 Hz, ArH²), 3.82 (s, 3H, CH₃O).

Incorporation expected at δ_H 7.75. Determined against integral at δ_H 3.82.

a) **273f** (9.3 mg, 0.01398 mmol, 6.5 mol%), b) 4-methoxybenzenesulfonamide (40.0 mg, 0.215 mmol), c) DCM (6.0 mL), d) 25 °C, e) 2 h, and f) 96% D.

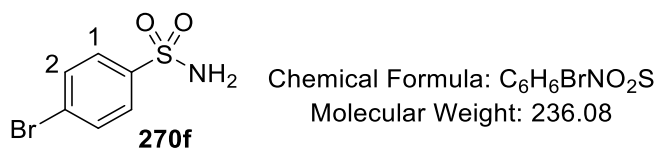


Chemical Formula: C₆H₆FNO₂S
Molecular Weight: 175.18

¹H NMR (400 MHz, DMSO-d₆): δ 7.90-7.86 (m, 2H, ArH¹), 7.42-7.38 (m, 4H, ArH² and NH₂).

Incorporation expected at δ 7.90-7.86. Determined against integral at δ 7.42-7.38.

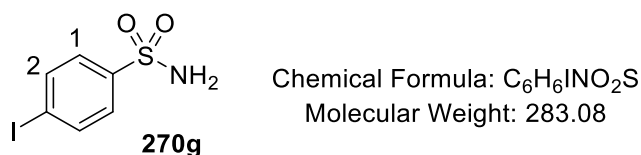
a) **273f** (9.3 mg, 0.01398 mmol, 6.5 mol%), b) 4-fluorobenzenesulfonamide (37.7 mg, 0.215 mmol), c) DCM (6.0 mL), d) 25 °C, e) 2 h, and f) 82% D.



¹H NMR (400 MHz, DMSO-*d*₆): δ 7.79 (d, 2H, ³*J* = 8.8 Hz, ArH²), 7.75 (d, 2H, ³*J* = 8.8 Hz, ArH¹), 7.46 (bs, NH₂).

Incorporation expected at δ 7.75. Determined against integral at δ 7.79.

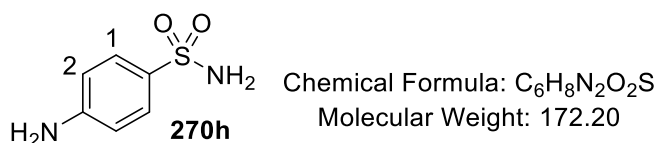
a) **273f** (9.3 mg, 0.01398 mmol, 6.5 mol%), b) 4-bromobenzenesulfonamide (50.8 mg, 0.215 mmol), c) DCM (6.0 mL), d) 25 °C, e) 2 h, and f) 77% D.



¹H NMR (400 MHz, DMSO-*d*₆): δ 7.97 (d, 2H, ³*J* = 8.8 Hz, ArH²), 7.59 (d, 2H, ³*J* = 8.8 Hz, ArH¹), 7.43 (bs, NH₂).

Incorporation expected at δ 7.59. Determined against integral at δ 7.97.

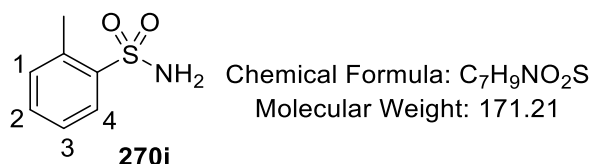
a) **273f** (9.3 mg, 0.01398 mmol, 6.5 mol%), b) 4-iodobenzenesulfonamide (60.9 mg, 0.215 mmol), c) DCM (6.0 mL), d) 25 °C, e) 2 h, and f) 24% D.



¹H NMR (400 MHz, DMSO-*d*₆): δ 7.45 (d, 2H, ³*J* = 8.8 Hz, ArH¹), 6.87 (bs, SO₂NH₂), 6.59 (d, 2H, ³*J* = 8.8 Hz, ArH²), 5.78 (bs, ArNH₂),

Incorporation expected at δ 7.45. Determined against integral at δ 6.59.

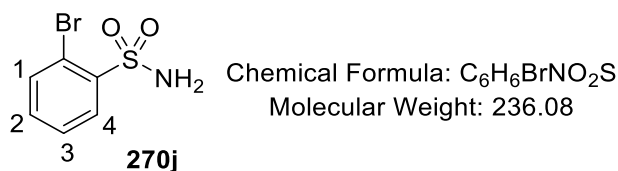
a) **273f** (9.3 mg, 0.01398 mmol, 6.5 mol%), b) 4-aminobenzenesulfonamide, Sulfanilamide (37.0 mg, 0.215 mmol), c) DCM (6.0 mL), d) 25 °C, e) 2 h, and f) 11% D.



¹H NMR (400 MHz, DMSO-*d*₆): δ 7.87-7.85 (m, 1H, ArH⁴), 7.50-7.46 (m, 1H, ArH²), 7.38-7.34 (m, 4H, ArH¹, ArH³, and SO₂NH₂), 2.60 (s, 3H, ArCH₃).

Incorporation expected at δ 7.87-7.85. Determined against integral at δ 2.60.

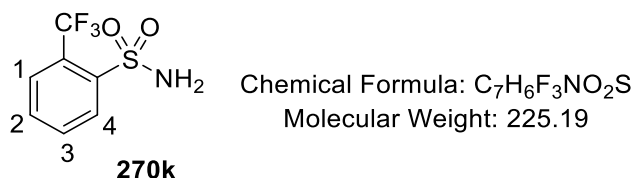
a) **273f** (9.3 mg, 0.01398 mmol, 6.5 mol%), b) 2-methylbenzenesulfonamide (36.8 mg, 0.215 mmol), c) DCM (6.0 mL), d) 25 °C, e) 2 h, and f) 74% D.



¹H NMR (400 MHz, DMSO-*d*₆): δ 8.01 (dd, 1H, ³J = 7.8 Hz, ⁴J = 1.8 Hz, ArH⁴), 7.81 (dd, 1H, ³J = 7.8 Hz, ⁴J = 1.8 Hz, ArH¹), 7.58-7.54 (m, 3H, ArH² and SO₂NH₂), 7.49 (td, 1H, ³J = 7.6 Hz, ⁴J = 1.8 Hz, ArH³).

Incorporation expected at δ 8.01. Determined against integral at δ 7.81.

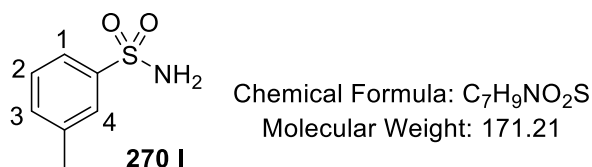
a) **273f** (9.3 mg, 0.01398 mmol, 6.5 mol%), b) 2-bromobenzenesulfonamide (50.6 mg, 0.215 mmol), c) DCM (6.0 mL), d) 40 °C, e) 2 h, and f) 40% D.



¹H NMR (400 MHz, DMSO-*d*₆): δ 8.18 (d, 1H, ³J = 7.9 Hz, ArH⁴), 7.94 (d, 1H, ³J = 7.9 Hz, ArH¹), 7.89 (t, 1H, ³J = 7.9 Hz, ArH²), 7.80 (t, 1H, ³J = 7.9 Hz, ArH³), 7.71 (bs, 2H, NH₂).

Incorporation expected at δ 8.18. Determined against integral at δ 7.80.

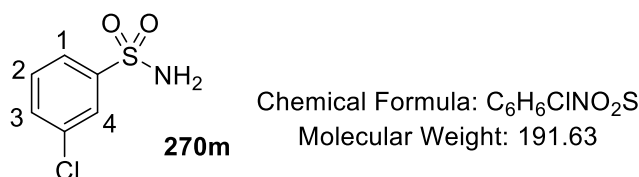
a) **273f** (9.3 mg, 0.01398 mmol, 6.5 mol%), b) 2-(trifluoromethyl)benzenesulfonamide (48.4 mg, 0.215 mmol), c) DCM (6.0 mL), d) 40 °C, e) 2 h, and f) 49% D.



¹H NMR (400 MHz, DMSO-*d*₆): δ 7.65-7.64 (m, 1H, ArH⁴), 7.63-7.61 (m, 1H, ArH¹), 7.46-7.41 (m, 2H, ArH² and ArH³), 7.28 (s, 2H, NH₂), 2.38 (s, 3H, ArCH₃).

Incorporation expected at δ 7.65-7.64 and 7.63-7.61. Determined against integral at δ 2.38.

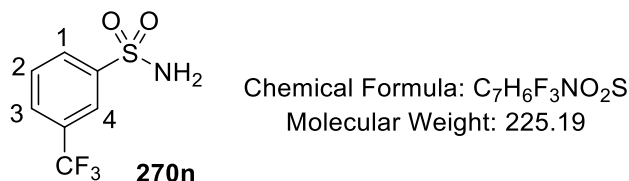
a) **270 l** (9.3 mg, 0.01398 mmol, 6.5 mol%), b) 3-methylbenzenesulfonamide (36.8 mg, 0.215 mmol), c) DCM (6.0 mL), d) 25 °C, e) 2 h, and f) 95% D^a (H¹), 85% D^b (H⁴).



¹H NMR (400 MHz, DMSO-*d*₆): δ 7.84 (t, 1H, ⁴J = 1.8 Hz, ArH⁴), 7.78 (dt, 1H, ³J = 7.6 Hz, ⁴J = 1.6 Hz, ArH¹), 7.70-7.67 (m, 1H, ArH³), 7.61 (apparent t, 1H, ³J = 7.6 Hz, ArH²), 7.50 (bs, 2H, NH₂).

Incorporation expected at δ 7.84 and 7.78. Determined against integral at δ 7.70-7.67.

a) **273f** (9.3 mg, 0.01398 mmol, 6.5 mol%), b) 3-chlorobenzenesulfonamide (41.2 mg, 0.215 mmol), c) DCM (6.0 mL), d) 25 °C, e) 2 h, and f) 75% D^a (H¹), 61% D^b (H⁴).



¹H NMR (400 MHz, DMSO-*d*₆): δ 8.13-8.11 (m, 2H, ArH¹ and ArH⁴), 8.00 (apparent d, 1H, ³J = 8.0 Hz, ArH³), 7.84 (apparent t, 1H, ³J = 8.0 Hz, ArH²), 7.58 (bs, 2H SO₂NH₂).

Incorporation expected at δ 8.13-8.11. Determined against integral at δ 7.84.

a) **273f** (9.3 mg, 0.01398 mmol, 6.5 mol%), b) 3-(trifluoromethyl)-benzenesulfonamide (48.4 mg, 0.215 mmol), c) DCM (6.0 mL), d) 25 °C, e) 2 h, and f) 92% D^a (H¹), 6% D^b (H⁴).

As the regioselectivity of deuteration could not be assessed by ¹H NMR, HRMS was obtained on the isolated compound **270n** (52% D overall from ¹H NMR). Mass ions were detected for **270n-d**₀, **270n-d**₁, and **270n-d**₂. The % D incorporation was calculated from the relative ratio of these three ions.

HRMS (positive NSI, DCM + MeOH + NH₄OAc):

[M(d₀) + NH₄]⁺; expected = 243.0410, observed = 243.0411.

[M(d₁) + NH₄]⁺; expected = 244.0472, observed = 244.0475.

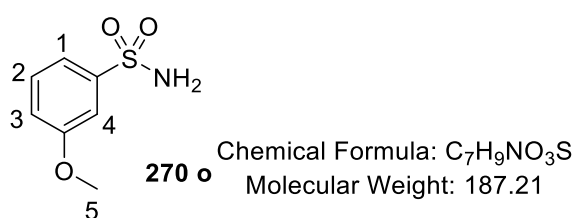
[M(d₂) + NH₄]⁺; expected = 245.0535, observed = 245.0536.

Ratio of ion intensities = (**270n-d**₂) : (**270n-d**₁) : (**270n** : d₀) = 3.360667 : 49.98262 : 1.

%Overall Deuterium Incorporation from HRMS = 52%

Ratio of % D^a (H¹): % D^b (H⁴) = 92% : 6%.

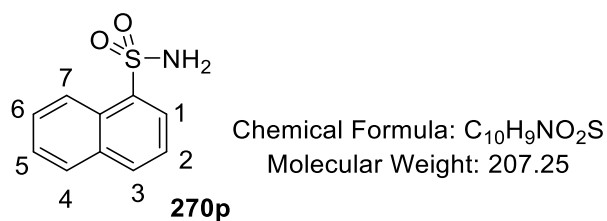
NOTE: From the ¹H NMR data related to **270n**, and the regioselectivity in labelling of *m*-substituted benzenesulfonamides **270 l**, **270m**, and **270o**, it is assumed that the majority of the mass ion for **270n-d**₁ relates to the product labelled at position 'a' only.



¹H NMR (400 MHz, DMSO-d₆): δ 7.48 (t, 1H, ³J = 8.0 Hz, ArH²), 7.40 (dt, 1H, ³J = 8.0 Hz, ⁴J = 1.2 Hz, ArH¹), 7.36 (t, 1H, ⁴J = 2.2 Hz, ArH⁴), 7.16 (ddd, 1H, ³J = 8.0 Hz, ⁴J = 2.2 Hz, ⁴J = 1.2 Hz, ArH³).

Incorporation expected at δ 7.40 and 7.36. Determined against integral at δ 7.48.

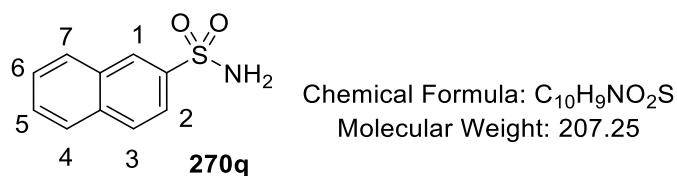
a) **273f** (9.3 mg, 0.01398 mmol, 6.5 mol%), b) 3-methoxybenzenesulfonamide (40.0 mg, 0.215 mmol), c) DCM (6.0 mL), d) 25 °C, e) 2 h, and f) 85% D^a (H¹), 42% D^b (H⁴).



¹H NMR (400 MHz, DMSO-d₆): δ 8.68 (d, 1H, ³J = 8.8 Hz, ArH⁷), 8.19-8.14 (m, 2H, ArH¹ and ArH), 8.10-8.07 (m, 1H, ArH), 7.74-7.63 (m, 5H, ArH and NH₂).

Incorporation expected at δ 8.68 and 8.19 - 8.14. Determined against integral at δ 8.10 - 8.07.

a) **273f** (9.3 mg, 0.01398 mmol, 6.5 mol%), b) 1-sulfonamidonaphthalene (44.6 mg, 0.215 mmol), c) DCM (6.0 mL), d) 25 °C, e) 2 h, and f) 60% D^a (H¹), 0% D^b (H⁷).

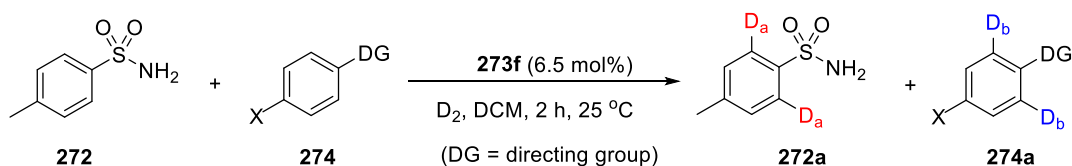


¹H NMR (400 MHz, DMSO-d₆): δ 8.44 - 8.43 (m, 1H, ArH¹), 8.15 - 8.11 (m, 2H, ArH⁴ and ArH⁷), 8.04 - 8.02 (m, 1H, ArH³), 7.89 (dd, 1H, ³J = 8.6 Hz, ⁴J = 1.9 Hz, ArH²), 7.71 - 7.63 (m, 2H, ArH⁵ and ArH⁶), 7.45 (s, 2H, NH₂).

Incorporation expected at δ 8.44-8.43 and 7.89. Determined against integral at δ 7.71-7.63.

a) **273f** (9.3 mg, 0.01398 mmol, 6.5 mol%), b) 2-sulfonamidonaphthalene (44.6 mg, 0.215 mmol), c) DCM (6.0 mL), d) 25 °C, e) 2 h, and f) 33% D^a (H²), 30% D^b (H¹).

Competition Studies to Assess Robustness and Chemoselectivity of Catalyst – Table 22



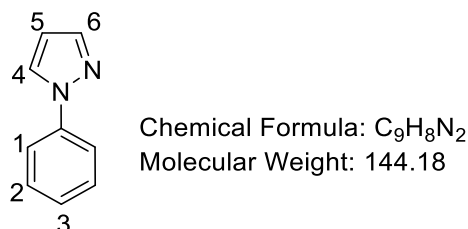
In a modification to *General Procedure F*, sulfonamide **272** (36.8 mg, 0.215 mmol) and competitive substrate **274** (0.215 mmol) were added to the same deuteration flask along with catalyst **273f** (18.7 mg, 0.02795 mmol, 6.5 mol% with respect to the combined total of **272** +

274). The substrates were dissolved in dry DCM (12.0 mL) under an argon atmosphere and the reaction run according to *General Procedure F*. At the end of the reaction, the solvent was removed *in vacuo*. The residue was then purified *via* silica column chromatography. Isolated compounds **272a** and **274a** were analysed separately by ^1H NMR to assess the % deuteration in each compound.

Results for each competition experiment are reported as: a) amount of substrate **274**, b) column separation conditions, and c) % D in labelled substrates.

Spectroscopic details for substrate **272** are available above.

Table 22, Entry 1

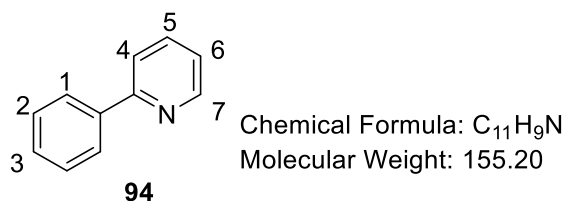


^1H NMR (400 MHz, CDCl_3): δ 7.93 (d, $^3J = 7.5$ Hz, 1H, ArH⁴), 7.74-7.66 (m, 3H, ArH¹ and ArH⁶), 7.46 (t, $^3J = 7.4$ Hz, 2H, ArH²), 7.29 (t, $^3J = 7.4$ Hz, 1H, ArH³), 6.46 (t, $^3J = 2.0$ Hz, 1H, ArH⁵).

Incorporation expected at δ 7.74-7.66. Determined against integral at δ 6.46.

a) 1-Phenylpyrazole, 0.215 mmol, 0.028 mL, b) Diethyl ether/petroleum ether (1:4 \rightarrow 1:1 \rightarrow 1:0), and c) 7% D^a (**272**), 47% D^b (**274**, H¹).

Table 22, Entry 2

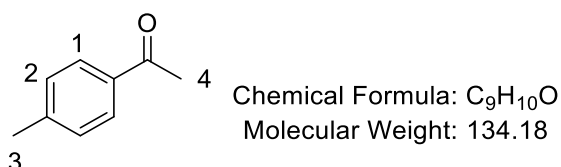


^1H NMR (400 MHz, CDCl_3): δ 8.71 (d, $^3J = 4.7$ Hz, 1H, ArH⁷), 8.00 (d, $^3J = 7.1$ Hz, 2H, ArH¹), 7.79-7.73 (m, 2H, ArH⁵ and ArH⁶), 7.52-7.41 (m, 3H, ArH² and ArH³), 7.26-7.23 (m, 1H, ArH⁴).

Incorporation expected at δ 8.00. Determined against integral at δ 7.79 - 7.73.

a) 2-Phenylpyridine, 0.215 mmol, 0.031 mL, b) Diethyl ether/petroleum ether (1:1 \rightarrow 1:0), and c) 7% D^a (**272**), 19% D^b (**274**, H¹).

Table 22, Entry 3

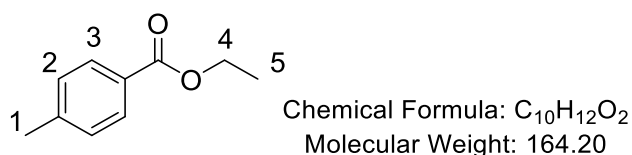


¹H NMR (400 MHz, CDCl₃): δ 7.88 (d, 2H, ³J = 8.4 Hz, ArH¹), 7.27 (d, 2H, ³J = 8.4 Hz, ArH²), 2.59 (s, 3H, ⁴C(O)H₃), 2.43 (s, 3H, ArCH₃).

Incorporation expected at δ 7.88. Determined against integral at δ 2.43.

a) 4-Methylacetophenone, 0.215 mmol, 0.029 mL, b) Diethyl ether/petroleum ether (1:4 \rightarrow 1:1 \rightarrow 1:0), and c) 94% D^a (**272**), 54% D^b (**274**, H¹).

Table 22, Entry 4

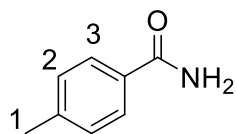


¹H NMR (400 MHz, CDCl₃): δ 7.91 (d, J = 7.9 Hz, 2H, ArH³), 7.21 (d, ³J = 7.9 Hz, 2H, ArH²), 4.34 (q, ³J_{H-H} = 7.1 Hz, 2H, CH₂⁴), 2.38 (s, 3H, ArCH₃¹), 1.36 (t, ³J = 7.1 Hz, 3H, CH₃⁵).

Incorporation expected at δ 7.91. Determined against integral at δ 2.38.

a) Ethyl 4-methylbenzoate, 0.215 mmol, 35.3 mg, b) Diethyl ether/petroleum ether (1:4 \rightarrow 1:1 \rightarrow 1:0), and c) 95% D^a (**272**), 11% D^b (**274**, H³).

Table 22, Entry 5



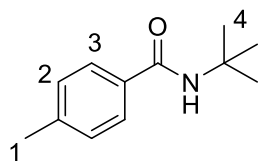
Chemical Formula: C₈H₉NO
Molecular Weight: 135.17

¹H NMR (400 MHz, CDCl₃): δ 7.88 (bs, 1H, NH), 7.77 (d, 2H, ³J = 8.2 Hz, ArH³), 7.24-7.22 (m, 3H, ArH² and NH), 2.33 (s, 3H, ArCH₃).

Incorporation expected at δ 7.77. Determined against integral at δ 2.33.

a) 4-methylbenzamide, 0.215 mmol, 29.1 mg, b) Diethyl ether/petroleum ether (1:1 → 1:0), and c) 93% D^a (**272**), 26% D^b (**274**, H³).

Table 22, Entry 6



Chemical Formula: C₁₂H₁₇NO
Molecular Weight: 191.27

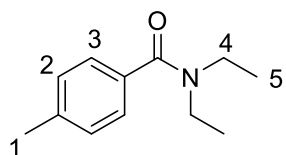
¹H NMR (400 MHz, CDCl₃): δ 7.61 (d, 2H, ³J = 8.0 Hz, ArH³), 7.20 (d, ³J = 8.0 Hz, 2H, ArH²), 5.90 (bs, 1H, NH), 2.38 (s, 3H, ArCH₃), 1.47 (s, 9H, CCH₃).

Incorporation expected at δ 7.61. Determined against integral at δ 2.38.

a) *N*,4-Dimethylbenzamide, 0.215 mmol, 41.1 mg, b) Diethyl ether/petroleum ether (1:1 → 1:0), and c) 97% D^a (**272**), 10% D^b (**274**, H³).

Table 22, Entry 7

NOTE: in this example, both substrates co-eluted. It was possible to determine % deuteration in each substrate from the ¹H NMR of the crude product mixture (see spectrum below).



Chemical Formula: C₁₂H₁₇NO

Molecular Weight: 191.27

¹H NMR (400 MHz, DMSO-d₆): δ 7.24-7.23 (m, 4H, ArH² and ArH³), 3.37-3.20 (m, 4H, NCH₂⁴), 2.34 (s, 3H, ArCH₃¹), 1.10 (br s, 6H, NCH₂CH₃⁵).

Incorporation expected at δ 7.24 - 7.23. Determined against integral at δ 1.10.

a) 4-Methyl-*N,N*-diethylbenzamide, 0.215 mmol, 41.1 mg, b) Diethyl ether/petroleum ether (1:1 → 1:0), and c) 93% D^a (**272**), 1% D^b (**274**, H³).

¹H NMR for crude reaction mixture in DMSO-d₆.

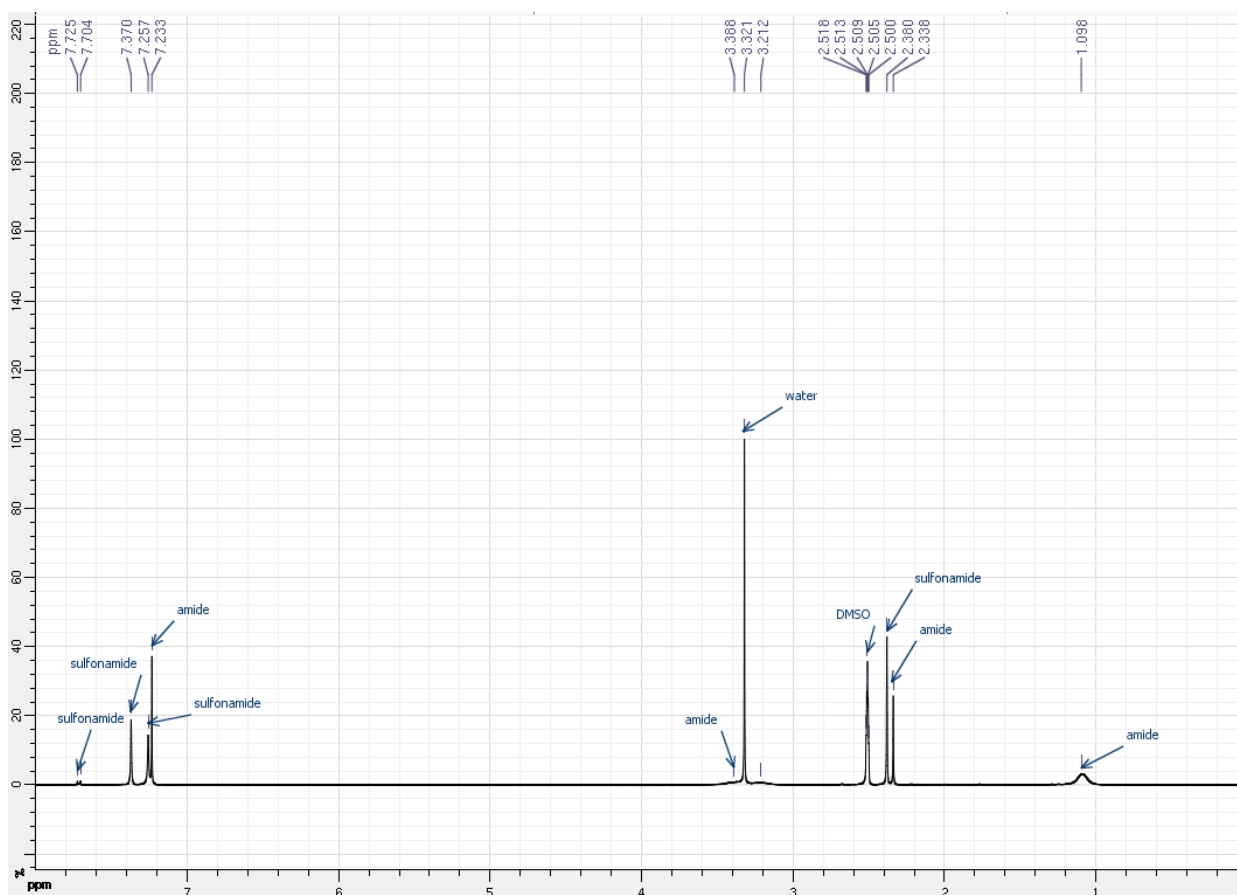
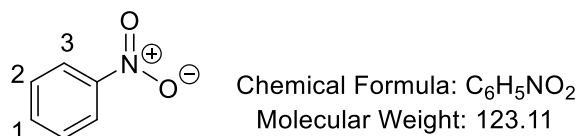


Table 22, Entry 8



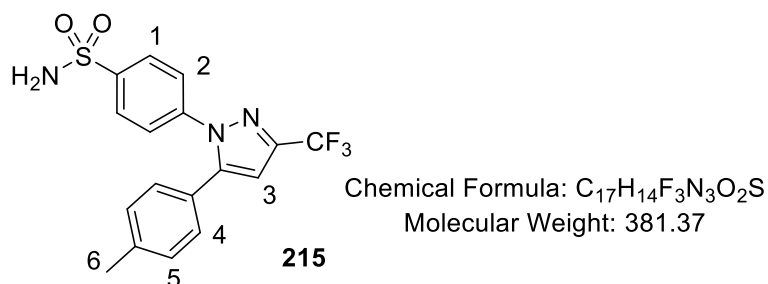
¹H NMR (400 MHz, CDCl₃): δ 8.26 (d, 2H, ³J = 7.6 Hz, ArH³), 7.73 (tt, ³J = 7.3 Hz, ⁴J = 0.8 Hz, 1H, ArH¹), 7.58 (m, 2H, ArH²).

Incorporation expected at δ 8.26. Determined against integral at 7.73.

a) Nitrobenzene, 0.215 mmol, 0.021 mL, b) Diethyl ether/petroleum ether (1:1 → 1:0), and c) 97% D^a (**272**), 4% D^b (**274**, H³).

Deuterium Labelling Experiments for Chemoselectivity Studies with Celecoxib and Mavacoxib (Table 23)

Table 23, Entry 1

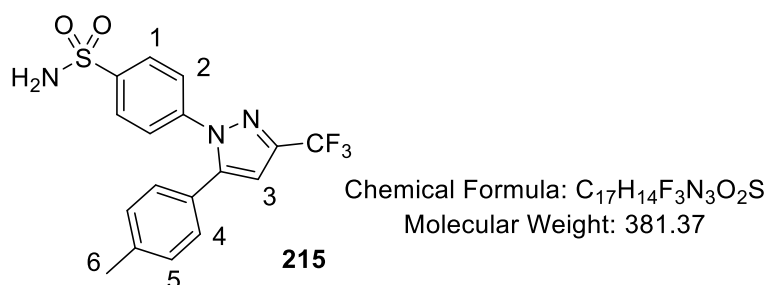


¹H NMR (400 MHz, CD₃OD): δ 7.94 (d, ³J = 8.7 Hz, 2H, ArH¹), 7.50 (d, ³J = 8.7 Hz, 2H, ArH²), 7.22-7.16 (m, 4H, ArH⁴ and ArH⁵), 6.91 (s, 1H, ArH³), 2.36 (s, 3H, ArCH₃⁶).

Incorporation expected at δ 7.94 and 7.50. Determined against integral at δ 2.36.

a) **273f** (1.2 mg, 0.00122 mmol, 6.5 mol%), b) Celecoxib, **215** (6 mg, 0.019 mmol), c) DCM (0.5 mL), d) 25 °C, e) 2 h, and f) 16% D^a (H¹), 95% D^b (H²).

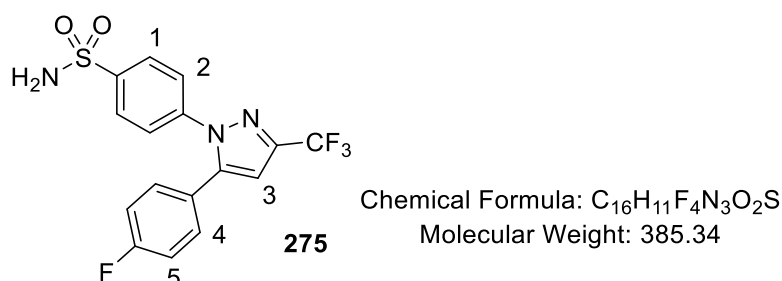
Table 23, Entry 2



Spectroscopic data can be found above.

a) **196a** (2.2 mg, 0.00324 mmol, 6.5 mol%), b) Celecoxib, **215** (19 mg, 0.050 mmol), c) DCM (1.4 mL), d) 25 °C, e) 2 h, and f) 97% D^a (H¹), 11% D^b (H²).

Table 23, Entry 3

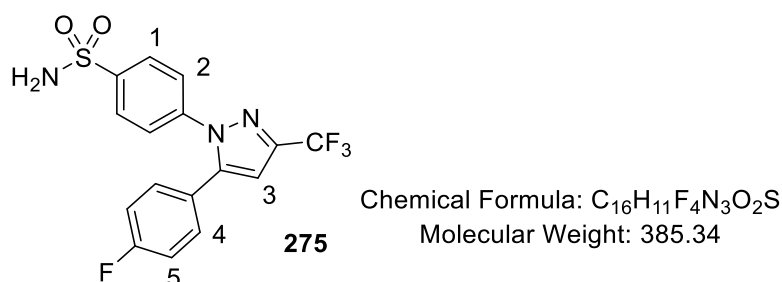


¹H NMR (400 MHz, MeOD): δ 7.14 (d, ³J = 8.7 Hz, 2H, ArH¹), 6.69 (d, ³J = 8.7 Hz, 2H, ArH²), 6.53 (dd, ³J = 8.6 Hz, ⁴J_{H-F} = 5.2 Hz, 2H, ArH⁴), 6.32 (apparent t, ³J = 8.6 Hz, 2H, ArH⁵), 6.15 (s, 1H, ArH³).

Incorporation expected at δ 7.14 and 6.69. Determined against integral at δ 6.32.

a) **196a** (3.3 mg, 0.00325 mmol, 6.5 mol%), b) Mavacoxib, **275** (19.3 mg, 0.019 mmol), c) DCM (1.4 mL), d) 25 °C, e) 2 h, and f) 7% D^a (H¹), 89% D^b (H²).

Table 23, Entry 4



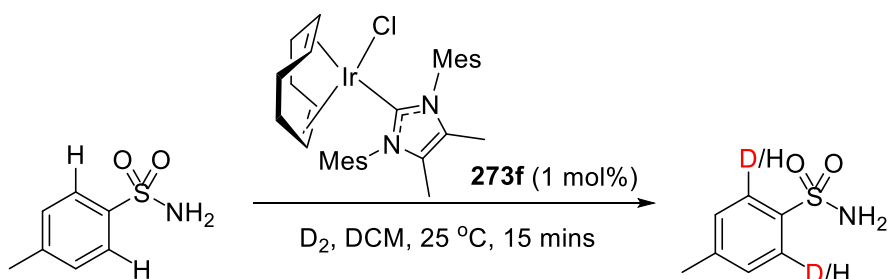
Spectroscopic data can be found above.

a) **273f** (2.2 mg, 0.00324 mmol, 6.5 mol%), b) Mavacoxib, **275** (19.3 mg, 0.050 mmol), c) DCM (1.4 mL), d) 25 °C, e) 2 h, and f) 98% D^a (H¹), 11% D^b (H²).

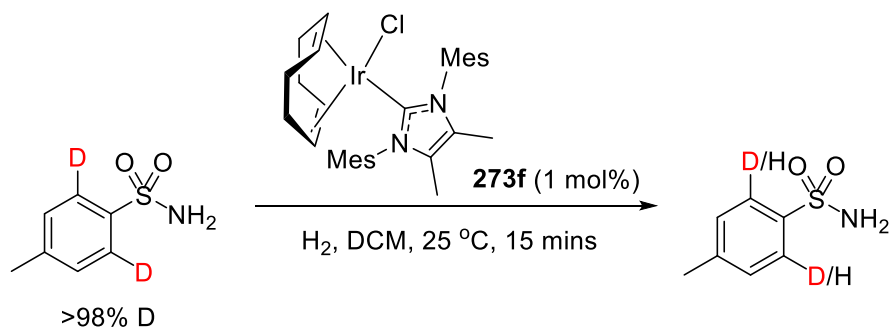
Investigation of Kinetic Isotope Effects (Scheme 57)

Necessary reactions for KIE measurement.

Forward Reaction:



Backward Reaction:



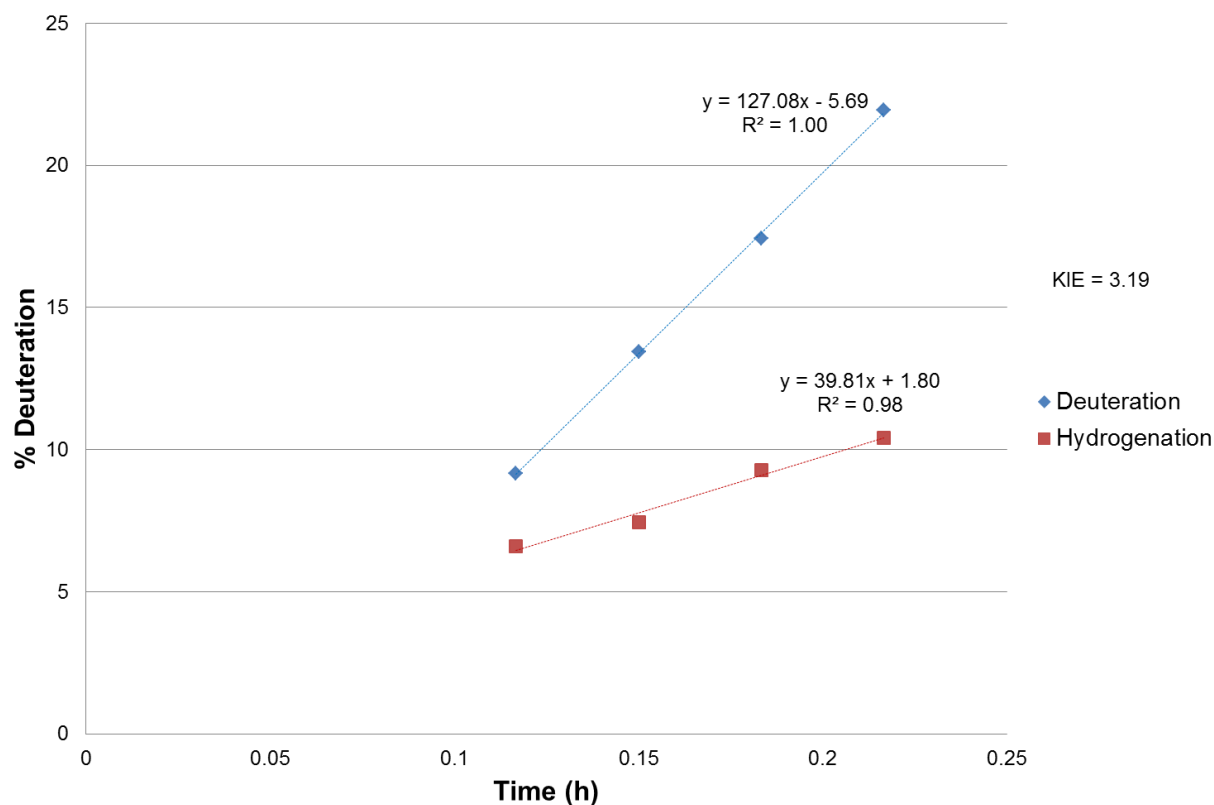
A flame-dried and nitrogen cooled 250 mL 3-neck round-bottom flask, equipped with a stopcock valve and two suba seals (see figure below), was charged with the iridium complex **273f** (3.9 mg, 1.0 mol%) and dry DCM (16.3 mL), followed by the substrate (0.584 mmol, non-deuterated 4-methylbenzenesulfonamide for the forward reaction, or 4-methylbenzenesulfonamide-D₂ for the reverse reaction, see photo). The top suba seal was replaced by a greased glass stopper and the reaction vessel was cooled to -78 °C in a dry ice/acetone bath, prior to being purged twice with nitrogen. The flask was then evacuated and filled with a deuterium gas for the forward reaction, or hydrogen for the reverse reaction, *via* balloon. The flask was removed from the slurry and allowed to warm to room temperature in

an oil bath set to 25 °C – the timer was started as soon as the flask was placed in the oil bath. (NOTE: as a precaution, the glass stopper is physically restrained as the reaction mixture warms to room temperature). The reaction mixture was then allowed to stir vigorously (860 rpm) at 25 °C for 5 mins, allowing for catalyst activation and temperature equilibrium. At 7 mins, 9 mins, 11 mins, and 13 mins, 0.2 mL aliquots were extracted from the reaction mixture *via* syringe and ejected into vials containing diethyl ether (2 mL). The contents of each vial were concentrated *in vacuo* and the level of deuterium incorporation (forward reaction) or hydrogen incorporation (reverse reaction) into the substrate determined by ^1H NMR analysis of the reaction products. As such, the residual proton signal from the site of incorporation was compared against that of a site where incorporation was not expected. To determine the kinetic isotope effect (k_H/k_D), the rate of reaction was determined by plotting reaction progress *versus* time, dividing the rate of the forward reaction, k_H , by the rate of the reverse reaction, k_D (see graph, below).

Reaction set-up for KIE measurement.

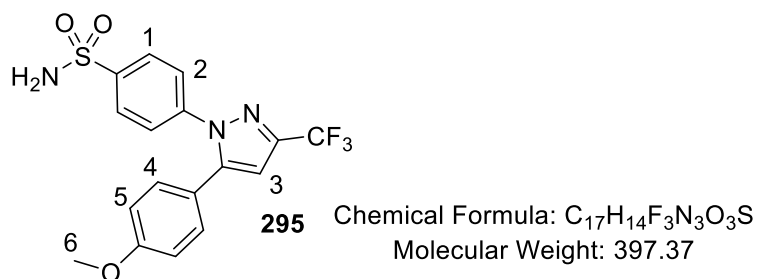


Results of KIE rate studies.



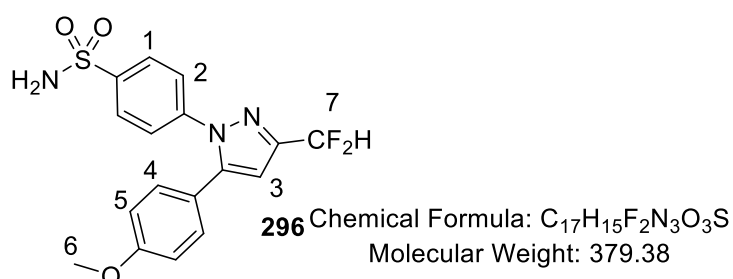
Experimental Labelling Selectivities on Additional Drug-like Structures 295 and 296 (Figure 44)

Following *General Procedure C*, substrate **295** (19.6 mg, 0.05 mmol) or **296** (19.0 mg, 0.05 mmol) was labelled using a choice of catalyst **196a** (3.3 mg, 0.00325 mmol, 6.5 mol%), **273f** (2.2 mg, 0.00325 mmol, 6.5 mol%), **273h** (2.4 mg, 0.00325 mmol, 6.5 mol%) or **273i** (2.7 mg, 0.00325 mmol, 6.5 mol%) under the previously optimised sulfonamide labelling conditions (6 mL DCM, 2 h, 25 °C). Each reaction was run in triplicate, with **Figure 44**, **Scheme 60**, and **Scheme 61** all quoting the average and standard deviation of each condition. The raw data (collected to 3 significant figures) associated with all these experiments is summarised in the table below the spectroscopic data.



¹H NMR (400 MHz, CD₃OD): δ 7.96 (d, 2H, ³J = 8.7 Hz, ArH¹), 7.52 (d, 2H, ³J = 8.7 Hz, ArH²), 7.23 (d, 2H, ³J = 8.8 Hz, ArH⁴), 6.94 (d, 2H, ³J = 8.8 Hz, ArH⁵), 6.89 (s, 1H, ArH³), 3.82 (s, 3H, OCH₃⁶).

Incorporation expected at δ 7.96 and 7.52. Determined against integral at δ 3.82.



¹H NMR (400 MHz, CD₃OD): δ 7.94 (d, 2H, ³J = 8.7 Hz, ArH¹), 7.49 (d, 2H, ³J = 8.7 Hz, ArH²), 7.22 (d, 2H, ³J = 8.8 Hz, ArH⁴), 6.94 (d, 2H, ³J = 8.8 Hz, ArH⁵), 6.85 (d, ²J_{H-F}, 1H, CF₂H⁷), 6.77 (s or unresolved triplet, 1H, ArH³), 3.82 (s, 3H, OCH₃⁶).

Incorporation expected at δ 7.94 and 7.49. Determined against integral at δ 3.82.

<i>Entry</i>	<i>Substrate</i>	<i>Catalyst</i>	<i>%D^a</i>	<i>%D^b</i>
1			14.050	93.125
2	295a	196a	12.215	93.830
3			18.725	93.520
4			94.950	14.170
5	295b	273f	96.575	18.315
6			94.565	12.220
7			9.675	95.720
8	296a	196a	8.295	95.330
9			9.930	95.960
10			83.450	96.605
11	296b	273f	80.735	94.605
12			81.700	94.515
13			98.505	39.390
14	296c	273h	92.405	13.240
15			97.955	38.250
16			96.96	5.43
17	296d	273i	97.03	5.39
18			96.915	6.095

^a Adjacent to sulfonamide; ^b Adjacent to pyrazole.

Investigating the Effect of the Chloride Ligand in 1° Sulfonamide Labelling (Scheme 62)

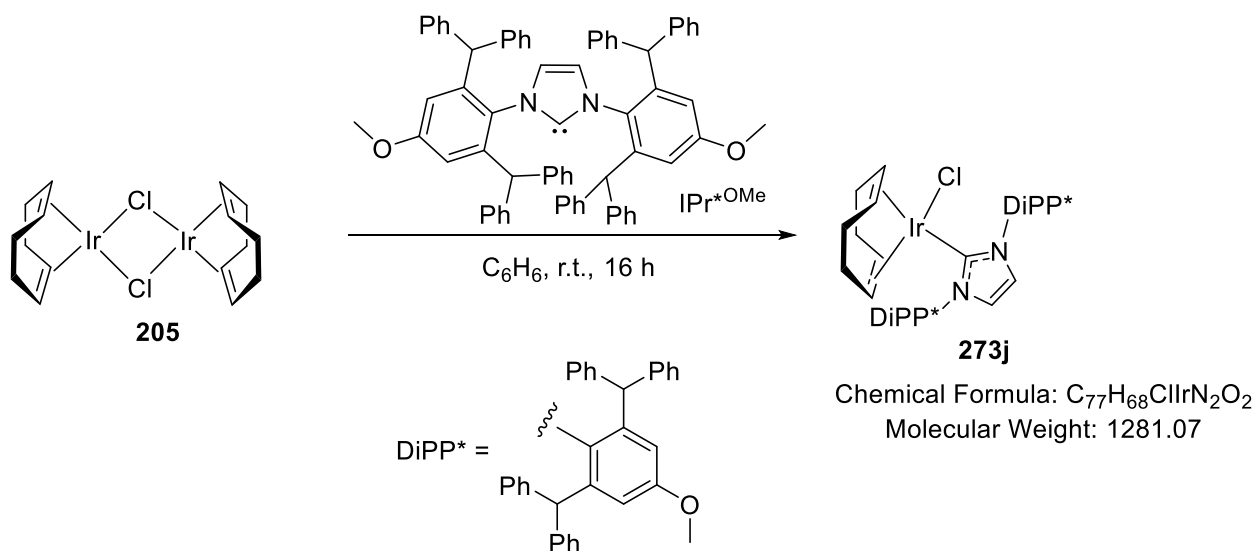
Following *General Procedure C*, results are reported as: a) amount of catalyst, b) amount of substrate, c) volume of solvent, d) reaction temperature, e) reaction time, and f) % D in labelled substrate.

a) **304**, 3.5 mg, 0.00325 mmol, 6.5 mol%, b) **296**, (19.0 mg, 0.05 mmol), c) 6.0 mL, d) 25 °C, e) 2 h, and f) 53% a; 94% b.

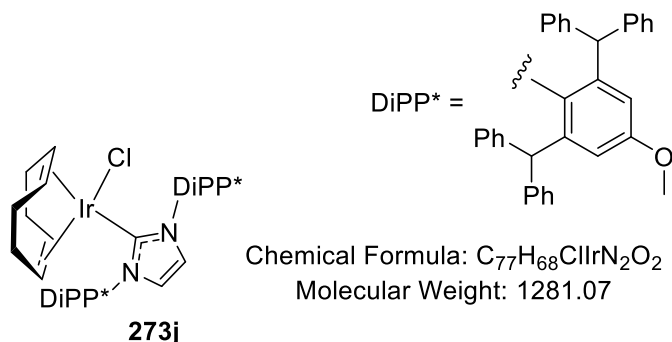
8.7 Regioselective Control in the Deuteration of Aromatic Aldehydes – An Experimental & Computational Study

Synthesis of Additional Catalysts

Catalyst **273j**²⁴⁵



205 (0.088 g, 0.131 mmol) was dissolved in dry benzene (10 mL) in a flame-dried Schlenk flask under an argon atmosphere. Following complete dissolution of **205**, the commercially sourced carbene (0.250 g, 0.262 mmol, see above figure) was added to the flask in one portion, causing a light orange to dark yellow colour change. After stirring at r.t. for 16 h, the solvent was removed *in vacuo* and the remaining residue purified *via* silica column chromatography, eluting with petroleum ether/ Et_2O (1 : 1). The product was isolated as a bright yellow solid (0.118 g, 32%).



FTIR (CH₂Cl₂): 3059, 3022, 2953, 2837, 1597, 1493, 1462, 1447, 1310, 1300, 1049, 700 cm⁻¹.

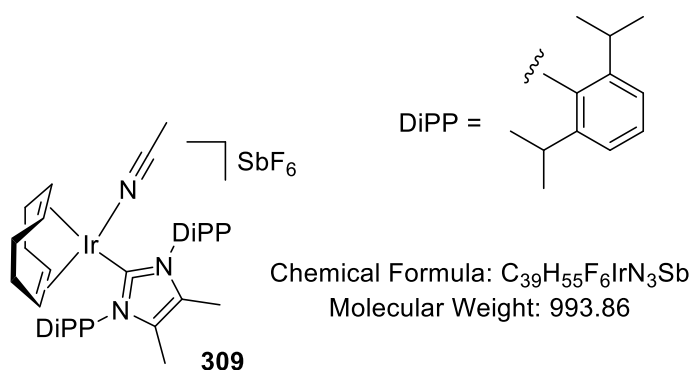
¹H NMR (400 MHz, CDCl₃): δ 7.49 – 6.54 (m, 44H, ArH), 6.46 (s, 2H, CHPh₂), 5.55 (s, 2H, CHPh₂), 4.81 (s, 2H, NCH=CHN), 4.69 – 4.67 (m, 2H, COD CH), 3.58 (s, 6H, OCH₃), 3.28 – 3.26 (m, 2H, COD CH), 2.11 – 2.00 (m, 2H, COD CH₂), 1.72 – 1.61 (m, 2H, COD CH₂), 1.60 – 1.51 (m, 2H, COD CH₂), 1.30 – 1.20 (m, 2H, COD CH₂).

¹³C NMR (100 MHz, CDCl₃): δ 179.6, 158.8, 145.3, 144.0, 143.7, 143.3, 142.3, 131.9, 130.9, 130.1, 129.5, 129.1, 128.2, 128.0(4), 128.0(0), 127.8, 126.6, 126.5, 126.1, 125.9, 123.6, 115.3, 114.5, 83.6, 55.1, 53.0, 51.6, 51.2, 33.4, 28.9.

Synthesis of η⁴-Cycloocta-1,5-diene(1,3-bis(2,6-diisopropylphenyl)-4,5-dimethylimidazol-2-ylidene)(acetonitrile)iridium(I) hexafluoroantimonate, 309

Following *General Procedure C*, results are reported as a) amount of **273h**, b) volume of THF, c) amount of AgSbF₆, d) amount of MeCN, e) reaction time, f) product yield, and g) purification technique.

a) 0.040 g, 0.053 mmol, b) 5 mL, c) 0.020 g, 0.058 mmol, d) 0.0022 g, 0.053 mmol, e) 16 h, f) 0.031 g, 59% yield, and g) the THF solution was reduced to quarter-volume and the product triturated using cold hexane. After collection by filtration, the product was washed with cold Et₂O and dried under vacuum for 16 h.



Appearance: light orange solid.

m.p.: 189 - 190 °C.

FTIR (neat): 2980, 1653, 1472, 1449, 1348, 640 cm⁻¹.

¹H NMR (400 MHz, CDCl₃): δ 7.58 (t, 2H, ³J = 7.8 Hz, ArH), 7.40 (d, 4H, ³J = 7.8 Hz, ArH), 4.00 – 3.98 (m, 2H, COD CH), 3.61 – 3.59 (m, 2H, COD CH), 2.67 (septet, 4H, ³J = 6.9 Hz, CH(CH₃)₂), 2.20 (s, 3H, CH₃CN), 2.00 (s, 6H, ArCH₃), 1.85 – 1.69 (m, 6H, COD CH₂), 1.55 – 1.47 (m, 2H, COD CH₂), 1.35 (d, 12H, ³J = 6.7 Hz, CH(CH₃)₂), 1.19 (d, 12H, ³J = 6.7 Hz, CH(CH₃)₂).

¹³C NMR (100 MHz, CDCl₃): δ 173.6, 146.6, 132.9, 130.7, 129.9, 124.8, 82.0, 65.9, 32.6, 28.9, 28.6, 25.4, 24.4, 10.3, 4.2, 2.2.

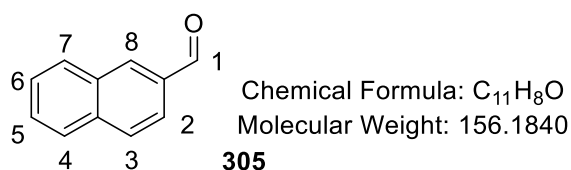
¹³C DEPT-135° NMR (100 MHz, CDCl₃): δ 32.6, 28.9.

HRMS (positive NSI): due to extensive degradation, no mass fragments yet identified.

Low resolution-MS (negative NSI): m/z calc'd for ¹²³SbF₆ [SbF₆]⁻: 236.9; found: 236.9.

Hypothesis Testing for Selective Labelling of Aromatic Aldehydes (Table 24)

Following *General Procedure F*, 2-naphthaldehyde, **305** (33.6 mg, 0.215 mmol) was labelled using various catalysts (0.01075 mmol, 5 mol%) at 25 °C, over 1 h in DCM (2.5 mL). At the end of the reaction, the solvent was removed *in vacuo* and catalyst residues triturated with Et₂O. Upon filtration through a short plug of silica and removal of the solvent, the product was analysed directly *via* ¹H NMR. The relevant catalyst quantities are summarised in the table below the spectral details of **305**.



¹H NMR (400 MHz, CDCl₃): δ 10.16 (s, 1H, CHO), 8.33 (s, 1H, ArH⁸), 8.01 – 7.90 (m, 4H, ArH² + ArH³ + ArH⁴ + ArH⁷), 7.67 – 7.57 (m, 2H, ArH⁵ + ArH⁶).

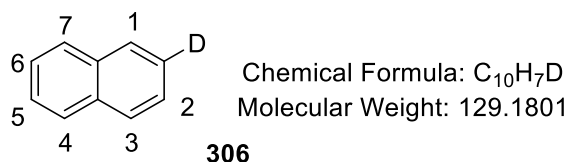
Incorporation expected at δ 10.16, 8.33, and 8.01 – 7.90. Determined against integral at δ 7.67 – 7.57.

Entry	Catalyst (mg)	%D (a)	%D(b)	%D(c)
1	159 (8.7)	45	45	95
2	214b (10.4)	1	2	2
3	196a (10.9)	71	43	8
4	196b (11.3)	94	32	9

Catalyst Discovery and Optimisation for Formyl-selective Aldehyde Labelling (Table 25)

Similarly to the screening experiments from **Table 24**, all reaction followed *General Procedure F*, with **305** (33.6 mg, 0.215 mmol) and various catalysts (0.01075 mmol, 5 mol%). At the end of each reaction, the solvent was removed *in vacuo* and the sample analysed directly by ^1H NMR spectroscopy. Beyond analysis of the expected product, trace quantities of decarbonylated product, **306**, are considered. Spectral details of this product are provided, and HRMS analysis to confirm its presence.

The masses of catalyst used are quantified in the table below.



^1H NMR (400 MHz, CDCl₃ – in a mixture with **305a**): δ 7.86 – 7.81 (m, 4H, ArH¹ + ArH³ + ArH⁴ + ArH⁷), 7.51 – 7.46 (m, 3H, ArH² + ArH⁵ + ArH⁶).

HRMS (positive APCI): m/z calc'd for C₁₀H₇DH [M + H]⁺: 130.0762; found: 130.0760.

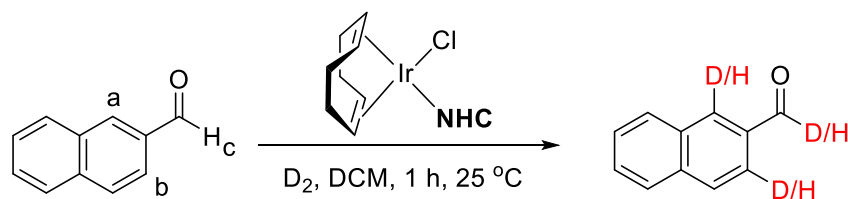
Percentage conversion to by-product **306** was based on δ 7.86 – 7.81 and measured against δ 7.67 – 7.57 in desired product **305a**.

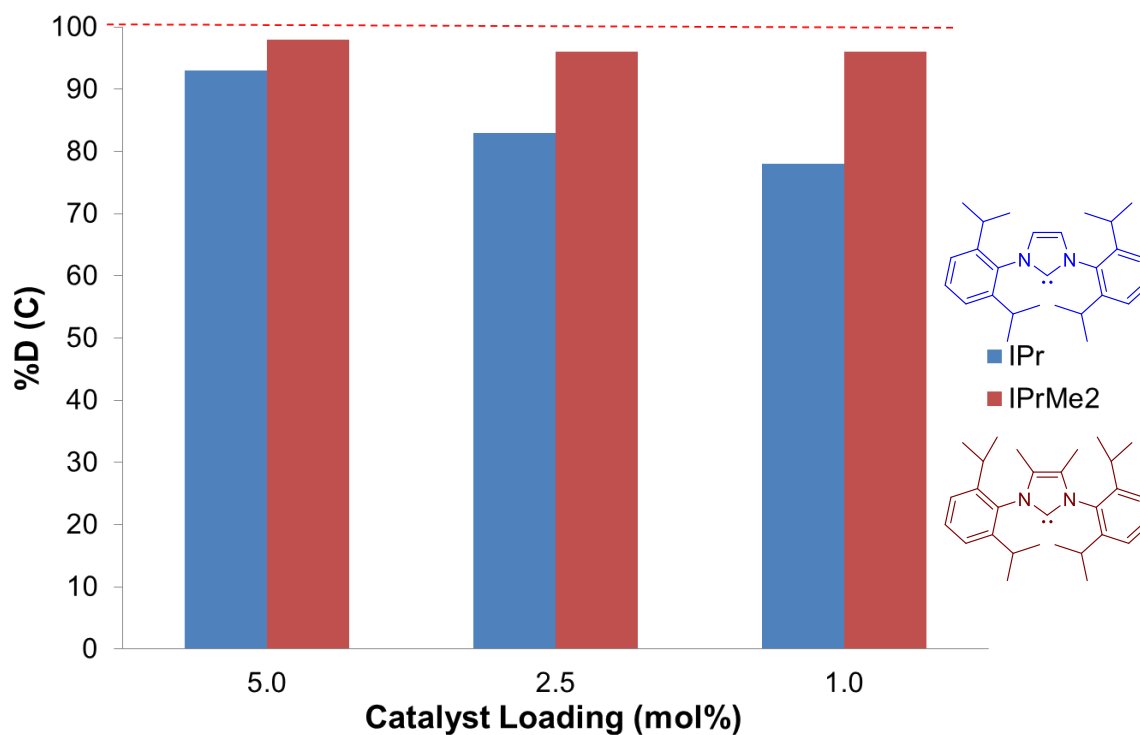
Entry	Catalyst (mg)	%D (a)	%D(b)	%D(c)	% 306 _{NMR}
1	273a (6.1)	2	3	0	0
2	273b (6.2)	1	1	1	0
3	273c (6.6)	3	7	42	0
4	273d (6.9)	0	0	49	2
5	273e (6.9)	0	1	82	5
6	273f (7.2)	4	3	97	2
7	273g (7.8)	4	3	93	0
8	273h (8.1)	8	5	98	0
9	273i (9.0)	9	6	90	0
10	273j (13.8)	19	32	10	0

Further Optimisation of Formyl-selective Aldehyde Labelling Conditions

These results are not presented in the main text. All experiments follow *General Procedure C*, as for those above.

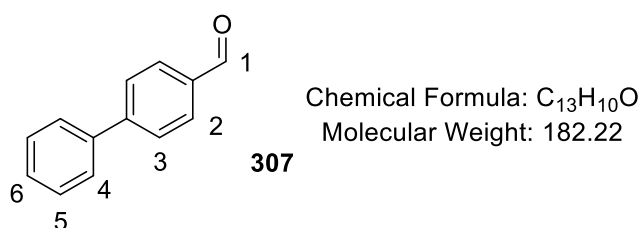
Having identified catalyst **273h** as the most promising candidate, the significance of the 4,5-dimethyl substitution on the NHC was investigated by lowering the catalyst loading below 5 mol%, comparing the results to those obtained with catalyst **273g** (with no 4,5-dimethyl substitution). It was found that the optimum catalyst remained active down to 1 mol%





Entry	Catalyst	Amount (mol%, mg)	%D(a)	%D(b)	%D(c)
1	273h	5, 7.8	98	8	5
2	273h	2.5, 3.9	96	4	1
3	273h	1, 1.6	96	4	1
4	273g	5, 8.1	98	4	3
5	273g	2.5, 4.1	83	4	2
6	273g	1, 1.6	78	4	3

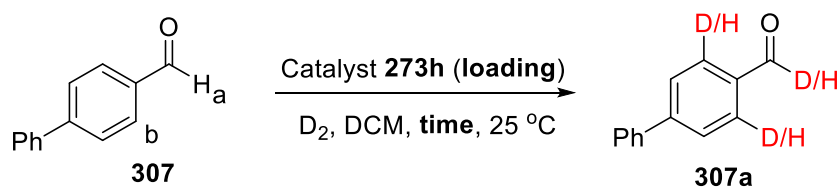
Attempts to label more challenging aldehyde, **307**, under the new optimum conditions (1 mol% **273h**, 1 h), it was quickly discovered that longer reactions times were required to generalise the applicability of such low catalyst loadings. See the results below.



$^1\text{H NMR}$ (400 MHz, CDCl_3): δ 10.07 (s, 1H, CHO), 7.97 (d, 2H, $^3J = 8.2$ Hz, ArH^2), 7.76 (d, d, 2H, $^3J = 8.2$ Hz, ArH^3), 7.65 (dd, 2H, $^3J = 8.1$ Hz, $^4J = 1.5$ Hz, ArH^4), 7.50 (apparent t, 2H, $^3J = 7.4$ Hz, ArH^5), 7.43 (apparent t, 1H, $^3J = 7.2$ Hz, ArH^6).

Incorporation expected at δ 10.07 and 7.97. Determined against integral at δ 7.43.

Each of the following reactions employed *General Procedure F*, using **307** (39.2 mg, 0.215 mmol), DCM (2.5 mL), and a reaction temperature of 25 °C. Again, reactions were analysed directly after removal of the solvent. The supporting table thus lists the catalyst loadings and labelling results.



Entry	Amount (mol%, mg)	Time (h)	%D(a)	%D(b)
1	2.5, 4.0	1	80	4
2	1.0, 1.6	1	55	3
3	2.5, 4.0	3	97	1
4	1.0, 1.6	3	94	3

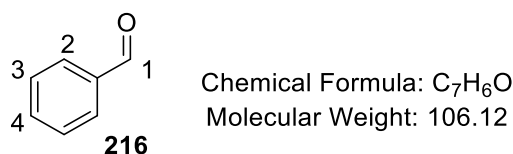
From these data, it was concluded that a catalyst loading of 1 mol% could be exploited by using a 3 h reaction time.

Substrate Scope for Formyl-selective Aldehyde Labelling (Table 26)

Employing *General Procedure F*, results are reported as: a) amount of catalyst, b) amount of substrate, c) %D in labelled substrate, and d) isolated product yield.

At the end of each reaction, the solvent was removed *in vacuo* and the residue redissolved in a minimal quantity of EtOAc. The product was purified *via* silica column chromatography, eluting with petroleum ether/ EtOAc. To ensure separation from the non-polar catalyst residues, the gradient of eluent began at 20:1 and never exceeded 10:1.

As well as ^1H NMR spectroscopy, each deuterated aldehyde was characterised by at least one other method (^{13}C NMR, IR, or HRMS) where possible in order to confirm the presence of deuterium and the maintenance of the aldehyde carbonyl unit. These additional data are presented for the labelled products only, and not for the unlabelled starting compounds.



a) **273h** (3.2 mg, 0.0043 mmol, 1.0 mol%), b) benzaldehyde (45.6 mg, 0.430 mmol), c) 93% D^1 only, and d) 41.0 mg, 90% yield. **NOTE:** double normal reaction scale for ease of product isolation.

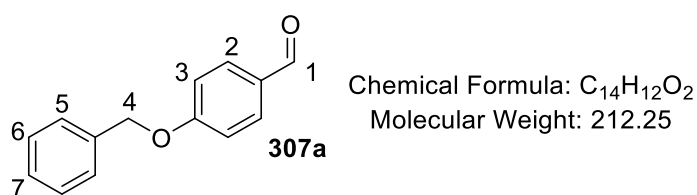
^1H NMR (400 MHz, CDCl_3): δ 10.05 (s, 1H, CHO), 7.91 (dd, 2H, $^3J = 7.9$ Hz, $^4J = 1.5$ Hz, ArH^2), 7.66 (tt, 1H, $^3J = 7.4$ Hz, $^4J = 1.5$ Hz, ArH^4), 7.56 (apparent t, 2H, $^3J = 7.4$ Hz, ArH^3).

Incorporation expected at δ 10.05 and 7.91. Determined against integral at δ 7.79.

^{13}C NMR (100 MHz, CDCl_3): δ 191.5 (t, $^1J_{\text{C-D}} = 26.8$ Hz), 135.9, 134.0, 129.2, 128.5.

FTIR (neat): 3063, 2104, 2050, 1682, 1597, 1584 cm^{-1} .

HRMS (APCI): Unavailable. Analysis revealed that **216** had fully oxidised to the carboxylic acid (presumably in transit to the EPSRC MS facility in Swansea).



a) **273h** (1.6 mg, 0.00215 mmol, 1.0 mol%), b) *p*-benzyloxybenzaldehyde (45.6 mg, 0.215 mmol), c) 97% D^1 ; 19% D^2 , and d) 40.1 mg, 88% yield.

^1H NMR (400 MHz, CDCl_3): δ 9.90 (s, 1H, CHO), 7.85 (d, 2H, $^3J = 8.8$ Hz, ArH^2), 7.46 – 7.35 (m, 5H, $\text{ArH}^5 - \text{ArH}^7$), 7.09 (d, 2H, $^3J = 8.8$ Hz, ArH^3), 5.17 (s, 2H, OCH_2^4).

Incorporation expected at δ 9.90 and 7.85. Determined against integral at δ 5.17.

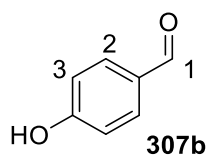
^{13}C NMR (100 MHz, CDCl_3): δ 190.5 (t, $^1J_{\text{C-D}} = 26.8$ Hz), 163.8, 136.0, 132.0, 130.1, 128.7, 128.3, 127.5, 115.2, 70.3

FTIR (neat): 3057, 3036, 2104, 2056, 1670, 1593, 1572, 1509, 1491, 1452 cm^{-1} .

HRMS (APCI): m/z calc'd for $\text{C}_{14}\text{H}_{12}\text{O}_2\text{D}$ [$\text{M}_{\text{d}1} + \text{H}$] $^+$: 214.0973; found: 214.0969.

m/z calc'd for $\text{C}_{14}\text{H}_{11}\text{O}_2\text{D}_2$ [$\text{M}_{\text{d}2} + \text{H}$] $^+$: 215.1036; found: 215.1024.

No d_3 isotopomer was detected, further supporting aromatic labelling a minor by-product to formyl labelling.



Chemical Formula: $\text{C}_7\text{H}_6\text{O}_2$

Molecular Weight: 122.12

a) **273h** (1.6 mg, 0.00215 mmol, 1.0 mol%), b) *p*-hydroxybenzaldehyde (26.3 mg, 0.215 mmol), c) 93% D^1 ; 8% D^2 , and d) 25.0 mg, 95% yield.

^1H NMR (400 MHz, CDCl_3): δ 9.88 (s, 1H, CHO), 7.84 (d, 2H, $^3J = 8.6$ Hz, ArH^2), 7.00 (d, 2H, $^3J = 8.6$ Hz, ArH^3), 6.61 (bs, 1H, OH).

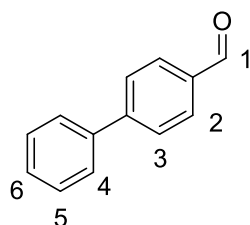
Incorporation expected at δ 9.88 and 7.84. Determined against integral at δ 7.00.

FTIR (neat): 2970, 2860, 2361, 2341, 2253, 1686, 1599, 1483, 1468 cm^{-1} .

HRMS (APCI): m/z calc'd for $\text{C}_7\text{H}_6\text{O}_2\text{D}$ [$\text{M}_{\text{d}1} + \text{H}$] $^+$: 124.0503; found: 124.0501.

m/z calc'd for $\text{C}_7\text{H}_5\text{O}_2\text{D}_2$: 125.0566; found: 125.0561.

No d_3 isotopomer was detected.



Chemical Formula: $\text{C}_{13}\text{H}_{10}\text{O}$

Molecular Weight: 182.22

a) **273h** (1.6 mg, 0.00215 mmol, 1.0 mol%), b) *p*-phenylbenzaldehyde (39.2 mg, 0.215 mmol), c) 94% D^1 only, and d) 38.0 mg, 97% yield.

¹H NMR (400 MHz, CDCl₃): δ 10.07 (s, 1H, CHO), 7.97 (d, 2H, ³J = 8.2 Hz, ArH²), 7.76 (d, d, 2H, ³J = 8.2 Hz, ArH³), 7.65 (dd, 2H, ³J = 8.1 Hz, ⁴J = 1.5 Hz, ArH⁴), 7.50 (apparent t, 2H, ³J = 7.4 Hz, ArH⁵), 7.43 (apparent t, 1H, ³J = 7.2 Hz, ArH⁶).

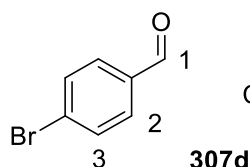
Incorporation expected at δ 10.07 and 7.97. Determined against integral at δ 7.43.

¹³C NMR (100 MHz, CDCl₃): δ 191.1 (t, ¹J_{C-D} = 25.4 Hz), 146.7, 139.2, 134.7, 129.8, 128.6, 128.0, 127.2, 126.9.

FTIR (neat): 3057, 3030, 2961, 2104, 2066, 2040, 1676, 1602, 1564 cm⁻¹.

HRMS (APCI): m/z calc'd for C₁₃H₁₀OD [M_{d1} + H]⁺: 184.0867; found: 184.0865.

No higher isotopomers detected.



a) **273h** (1.6 mg, 0.00215 mmol, 1.0 mol%), b) *p*-bromobenzaldehyde (39.8 mg, 0.215 mmol), c) 97% D¹ only, and d) 29.1 mg, 73% yield.

¹H NMR (400 MHz, CDCl₃): δ 9.98 (s, 1H, CHO), 7.76 (d, 2H, ³J = 8.6 Hz, ArH²), 7.69(d, 2H, ³J = 8.6 Hz, ArH³).

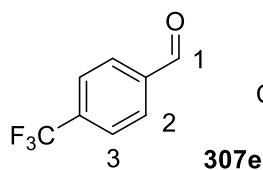
Incorporation expected at δ 9.98 and 7.76. Determined against integral at δ 7.69.

¹³C NMR (100 MHz, CDCl₃): δ 189.7(t, ¹J_{C-D} = 27.7 Hz), 134.0, 131.4, 129.9, 128.8.

FTIR (neat): 3084, 2963, 2131, 2073, 1683, 1634, 1587, 1570 cm⁻¹.

HRMS (APCI): m/z calc'd for C₇H₅⁷⁹BrOD [M_{d1} + H]⁺: 185.9659; found: 185.9657.

m/z calc'd for for C₇H₄⁷⁹BrOD₂ [M_{d2} + H]⁺: 186.9722; found: 186.9716 (trace).



a) **273h** (1.6 mg, 0.00215 mmol, 1.0 mol%), b) *p*-trifluoromethylbenzaldehyde (37.4 mg, 0.215 mmol), c) 95% D¹ only, and d) 35.5 mg, 95% yield.

¹H NMR (400 MHz, CDCl₃): δ 9.99 (s, 1H, CHO), 7.77 (d, 2H, ³J = 8.3 Hz, ArH²), 7.70 (d, 2H, ³J = 8.3 Hz, ArH³).

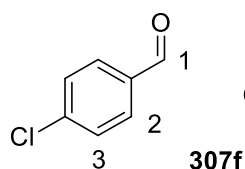
Incorporation expected at δ 9.99 and 7.77. Determined against integral at δ 7.70.

¹³C NMR (100 MHz, CDCl₃): δ 190.2 (t, ¹J_{C-D} = 28.1 Hz), 134.5, 131.9, 130.5, 129.3.
Unable to clearly define CF₃.

FTIR (neat): 2963, 2360, 2344, 2113, 1687, 1585, 1512, 1321 cm⁻¹.

HRMS (APCI): m/z calc'd for C₈H₅FOD [M_{d1} + H]⁺: 176.0428; found: 176.0425.

No other isotopomers detected.



Chemical Formula: C₇H₅ClO
Molecular Weight: 140.57

a) **273h** (1.6 mg, 0.00215 mmol, 1.0 mol%), b) *p*-chlorobenzaldehyde (30.2 mg, 0.215 mmol), c) 97% D¹ only, and d) 29.0 mg, 96% yield.

¹H NMR (400 MHz, CDCl₃): δ 10.00 (s, 1H, CHO), 7.85 (d, 2H, ³J = 8.5 Hz, ArH²), 7.53 (d, 2H, ³J = 8.5 Hz, ArH³).

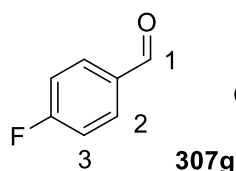
Incorporation expected at δ 10.00 and 7.85. Determined against integral at δ 7.53.

¹³C NMR (100 MHz, CDCl₃): δ 190.0 (t, ¹J_{C-D} = 28.1 Hz), 140.5, 134.2, 130.4, 129.0.

FTIR (neat): 3088, 2963, 2129, 2073, 1691, 1597, 1574, 1463 cm⁻¹.

HRMS (APCI): m/z calc'd for C₇H₅³⁵ClOD [M_{d1} + H]⁺: 142.0164; found: 142.0160.

No higher isotopomers found.



Chemical Formula: C₇H₅FO
Molecular Weight: 124.11

a) **273h** (1.6 mg, 0.00215 mmol, 1.0 mol%), b) *p*-fluorobenzaldehyde (26.7 mg, 0.215 mmol), c) 97% D¹; 8% D² and d) 16.8 mg, 63% yield.

¹H NMR (400 MHz, CDCl₃): δ 10.00 (s, 1H, CHO), 7.94 (dd, 2H, ³J = 8.5 Hz, ³J_{H-F} = 5.4 Hz ArH²), 7.24 (apparent t, 2H, ³J = 8.5 Hz, ArH³).

Incorporation expected at δ 10.00 and 7.94. Determined against integral at δ 7.24.

¹³C NMR (100 MHz, CDCl₃): δ 189.7 (t, ¹J_{C-D} = 28.1 Hz), 166.1 (d, ¹J_{C-F} = 252.9 Hz), 132.4, 131.7 (d, ³J_{C-F} = 9.4 Hz), 115.9 (d, ²J_{C-F} = 21.5 Hz).

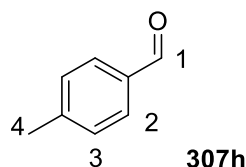
¹⁹F NMR (376 MHz, CDCl₃): δ - 102.4.

FTIR (neat): 2963, 2255, 2108, 2058, 1682, 1597, 1506, 1237 cm⁻¹.

HRMS (APCI): m/z calc'd for C₇H₅FOD [M_{d1} + H]⁺: 124.0460; found: 124.0456.

m/z calc'd for C₇H₄FOD [M_{d2} + H]⁺: 127.0523; found: 127.0517.

No higher isotopomers found.



Chemical Formula: C₈H₈O
Molecular Weight: 120.15

a) **273h** (1.6 mg, 0.0043 mmol, 1.0 mol%), b) *p*-methylbenzaldehyde (51.6 mg, 0.430 mmol),
c) 98% D¹; 12% D² and d) 41.0 mg, 80% yield.

¹H NMR (400 MHz, CDCl₃): δ 9.98 (s, 1H, CHO), 7.79 (d, 2H, ³J = 8.1 Hz, ArH²), 7.34 (d, 2H, ³J = 8.1 Hz, ArH³), 2.45 (s, 3H, ArCH₃⁴).

Incorporation expected at δ 9.98 and 7.79. Determined against integral at δ 2.45.

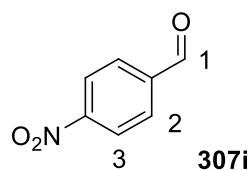
¹³C NMR (100 MHz, CDCl₃): δ 191.2 (t, ¹J_{C-D} = 26.8 Hz), 144.0, 133.6, 129.3, 129.2.

FTIR (neat): 3029, 2922, 2104, 2040, 1684, 1602, 1575, 1489, 1410 cm⁻¹.

HRMS (APCI): m/z calc'd for C₈H₈OD [M_{d1} + H]⁺: 122.0711; found: 122.0708.

m/z calc'd for C₈H₇OD₂ [M_{d2} + H]⁺: 123.0773; found: 123.0768.

No higher isotopomers found.



Chemical Formula: C₇H₅NO₃
Molecular Weight: 151.12

a) **273h** (1.6 mg, 0.001075 mmol, 1.0 mol%), b) *p*-nitrobenzaldehyde (32.5 mg, 0.215 mmol), c) 98% D¹ only, and d) 26.0 mg, 80% yield.

¹H NMR (400 MHz, CDCl₃): δ 10.16 (s, 1H, CHO), 8.39 (d, 2H, ³*J* = 8.5 Hz, ArH³), 8.08 (d, 2H, ³*J* = 8.1 Hz, ArH²).

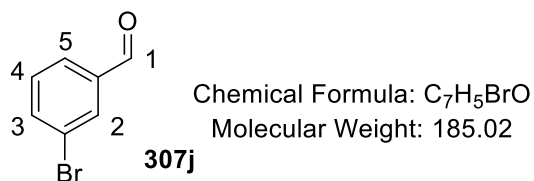
Incorporation expected at δ 10.16 and 8.08. Determined against integral at δ 8.39.

¹³C NMR (100 MHz, CDCl₃): δ 189.0 (t, ¹*J*_{C-D} = 27.7 Hz), 150.1, 129.5, 123.3.

FTIR (neat): 3107, 2963, 2131, 2070, 1684, 1604, 1531, 1344, 1213 cm⁻¹.

HRMS (APCI): *m/z* calc'd for C₇H₅NO₃D [M_{d1} + H]⁺: 153.0405; found: 153.0401.

No higher isotopomers found.



a) **273h** (1.6 mg, 0.001075 mmol, 1.0 mol%), b) *m*-bromobenzaldehyde (39.8 mg, 0.215 mmol), c) 96% D¹ only, and d) 28.0 mg, 70% yield.

¹H NMR (400 MHz, CDCl₃): δ 9.98 (s, 1H, CHO), 8.03 (t, 1H, ⁴*J* = 1.9 Hz, ArH²), 7.83 (dt, 1H, ³*J* = 7.6 Hz, ⁴*J* = 1.5 Hz, ArH⁵), 7.77 (ddd, 1H, ³*J* = 8.0 Hz, ⁴*J* = 2.1, 1.1 Hz, ArH³), 7.44 (t, 1H, ³*J* = 7.8 Hz, ArH⁴).

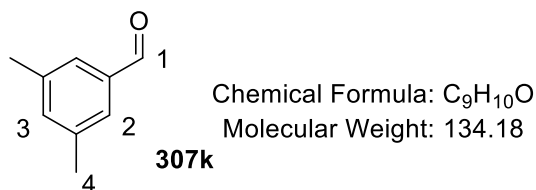
Incorporation expected at δ 9.98, 8.03, and 7.83 Determined against integral at δ 7.44.

¹³C NMR (100 MHz, CDCl₃): δ 189.9 (t, ¹*J*_{C-D} = 28.1 Hz), 139.4 (t, ²*J*_{C-D} = 4.0 Hz), 136.8, 131.8, 130.1, 127.9, 122.9. **NOTE:** The small C-D splitting observed is unresolved in other examples.

FTIR (neat): 3061, 2980, 2110, 2061, 1676, 1568, 1463 cm⁻¹.

HRMS (APCI): *m/z* calc'd for C₇H₅⁷⁹BrOD [M_{d1} + H]⁺: 185.9659; found: 185.9655.

No higher isotopomers found.



a) **273h** (3.2 mg, 0.0043 mmol, 2.0 mol%), b) *m,m'*-dimethylbenzaldehyde (28.8 mg, 0.215 mmol), c) 78% D¹ only, and d) 18.1 mg, 63% yield.

¹H NMR (400 MHz, CDCl₃): δ 9.97 (s, 1H, CHO), 7.52 (s, 2H, ArH²), 7.28 (s, 1H, ArH³), 2.42 (s, 6H, ArCH₃⁴).

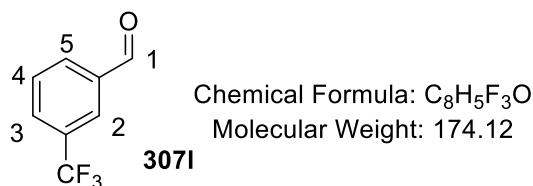
Incorporation expected at δ 9.97 and 7.52. Determined against integral at δ 2.42.

¹³C NMR (100 MHz, CDCl₃): δ 192.0 (t, ¹J_{C-D} = 27.6 Hz), 138.3, 136.0, 135.7, 127.1, 20.6.

FTIR (neat): 2920, 2727, 2361, 2331, 2083, 2054, 1680, 1608, 1597, 1460 cm⁻¹.

HRMS (APCI): m/z calc'd for C₉H₁₀OD [M_{d1} + H]⁺: 136.0864; found: 136.0863.

No higher isotopomers found.



a) **273h** (3.2 mg, 0.0043 mmol, 2.0 mol%), b) *m*-trifluoromethylbenzaldehyde (37.4 mg, 0.215 mmol), c) 75% D¹ only, and d) 23.0 mg, 80% yield.

¹H NMR (400 MHz, CDCl₃): δ 10.09 (s, 1H, CHO), 8.16 (t, 1H, ⁴J = 1.8 Hz, ArH²), 8.10 (dt, 1H, ³J = 7.7 Hz, ⁴J = 1.8 Hz, ArH⁵), 7.90 (dt, 1H, ³J = 7.7 Hz, ⁴J = 1.8 Hz, ArH³), 7.71 (t, 1H, ³J = 7.7 Hz, ArH⁴).

Incorporation expected at δ 10.09, 8.16, and 8.10. Determined against integral at δ 7.71.

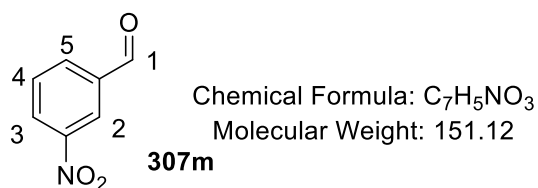
¹³C NMR (100 MHz, CDCl₃): δ 189.4 (t, ¹J_{C-D} = 26.2 Hz), 135.7, 131.6, 130.8 (q, ²J_{C-F} = 34.9 Hz), 129.8, 128.7, 125.4, 122.5 (q, ¹J_{C-F} = 270.7 Hz).

¹⁹F NMR (376 MHz, CDCl₃): δ -63.0.

FTIR (neat): 3069, 2932, 2852, 2118, 1682, 1611, 1439, 1331, 1123 cm⁻¹.

HRMS (APCI): m/z calc'd for $C_8H_5F_3OD [M_{d1} + H]^+$: 176.0427; found: 176.0428.

No higher isotopomers found.



a) **273h** (1.6 mg, 0.00215 mmol, 1.0 mol%), b) *m*-nitrobenzaldehyde (32.5 mg, 0.215 mmol), c) 99% D^1 only, and d) 31.0 mg, 95% yield.

1H NMR (400 MHz, $CDCl_3$): δ 10.14 (s, 1H, CHO), 8.73 (dd, 1H, $^4J = 2.3, 1.2$ Hz, ArH^2), 8.50 (ddd, 1H, $^3J = 8.1$ Hz, $^4J = 2.3, 1.2$ Hz, ArH^3), 8.26 (dt, 1H, $^3J = 7.6$ Hz, $^4J = 1.5$ Hz, ArH^5), 7.79 (t, 1H, $^3J = 7.6$ Hz, ArH^4).

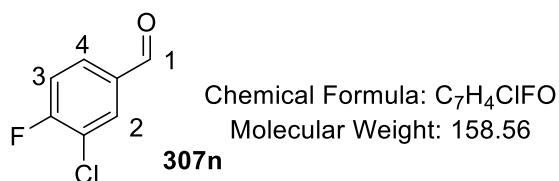
Incorporation expected at δ 10.14, 8.73, and 8.26. Determined against integral at δ 7.79.

^{13}C NMR (100 MHz, $CDCl_3$): δ 188.9 (t, $^1J_{C-D} = 26.7$ Hz), 136.8 (t, $^2J_{C-D} = 4.0$ Hz), 134.1, 129.9, 128.1, 123.9.

FTIR (neat): 3098, 3067, 2156, 2127, 1686, 1531, 1348 cm^{-1} .

HRMS (APCI): m/z calc'd for $C_7H_5NO_3D [M_{d1} + H]^+$: 153.0405; found: 153.0403.

No higher isotopomers found.



a) **273h** (1.6 mg, 0.00215 mmol, 1.0 mol%), b) *m*-chloro-*p*-fluorobenzaldehyde (34.1 mg, 0.215 mmol), c) 76% D^1 only, and d) 23.0 mg, 67% yield.

1H NMR (400 MHz, $CDCl_3$): δ 9.96 (s, 1H, CHO), 7.99 (dd, 1H, $^3J = 7.1$ Hz, $^4J = 2.1$ Hz, ArH^2), 7.83 (ddd, 1H, $^3J = 8.4$ Hz, $^3J_{C-F} = 4.6$ Hz, $^4J = 2.1$ Hz, ArH^4), 7.34 (t, 1H, $^3J = 8.4$ Hz, ArH^3).

Incorporation expected at δ 9.96, 7.99, and 7.83. Determined against integral at δ 7.34.

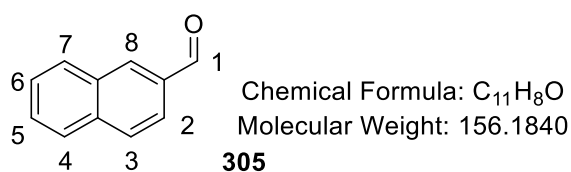
¹³C NMR (100 MHz, CDCl₃): Unable to obtain acceptable signal intensities.

¹⁹F NMR (376 MHz, CDCl₃): δ -104.7.

FTIR (neat): 3547, 3474, 2955, 2866, 2116, 2066, 1690, 1591, 1493, 1252, 1190 cm⁻¹.

HRMS (APCI): m/z calc'd for C₇H₄³⁵ClFOD [M_{d1} + H]⁺: 160.0070; found: 160.0067.

No higher isotopomers found.



a) **273h** (1.6 mg, 0.00215 mmol, 1.0 mol%), b) 2-naphthaldehyde (33.6 mg, 0.215 mmol), c) 96% D¹ only, and d) 30.2 mg, 96% yield.

¹H NMR (400 MHz, CDCl₃): δ 10.16 (s, 1H, CHO), 8.33 (s, 1H, ArH⁸), 8.01 – 7.90 (m, 4H, ArH² + ArH³ + ArH⁴ + ArH⁷), 7.67 – 7.57 (m, 2H, ArH⁵ + ArH⁶).

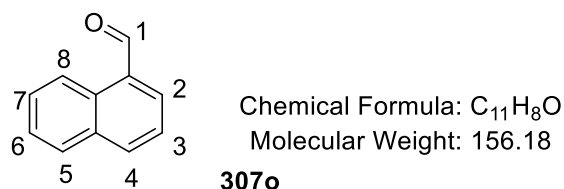
Incorporation expected at δ 10.16, 8.33, and 8.01 – 7.90. Determined against integral at δ 7.67 – 7.57.

¹³C NMR (100 MHz, CDCl₃): δ 190.9 (t, ¹J_{C-D} = 27.6 Hz), 135.4, 133.5, 133.0, 131.6, 128.5, 128.1, 127.1, 126.1, 121.7.

FTIR (neat): 3063, 2847, 2116, 2072, 1670, 1595 cm⁻¹.

HRMS (APCI): m/z calc'd for C₁₁H₈OD [M_{d1} + H]⁺: 158.0711; found: 158.0708.

No higher isotopomers found.



a) **273h** (1.6 mg, 0.00215 mmol, 1.0 mol%), b) 1-naphthaldehyde (33.6 mg, 0.215 mmol), c) 24% D¹ only, and d) 28.6 mg, 85% yield.

¹H NMR (400 MHz, CDCl₃): δ 10.41 (s, 1H, CHO), 9.27 (d, 1H, ³J = 8.7 Hz, ArH⁸), 8.10 (d, 1H, ³J = 8.2 Hz, ArH²), 7.99 (d, 1H, ³J = 7.0 Hz, ArH⁴), 7.93 (d, 1H, ³J = 8.0 Hz, ArH⁵), 7.72, 7.59 (m, 3H, ArH³ + ArH⁶ + ArH⁷).

Incorporation expected at δ 10.41, 9.27, and 8.10. Determined against integral at δ 7.99.

^{13}C NMR (100 MHz, CDCl_3): δ 192.2 (t, $^1J_{\text{C-D}} = 26.2$ Hz), 135.6, 135.5, 134.2, 132.7, 130.4, 129.5, 128.0, 127.4, 125.9, 123.8.

FTIR (neat): 3049, 2965, 2833, 2725, 2060 (other half of typical aldehyde doublet obscured by noise), 1684, 1508 cm^{-1} .

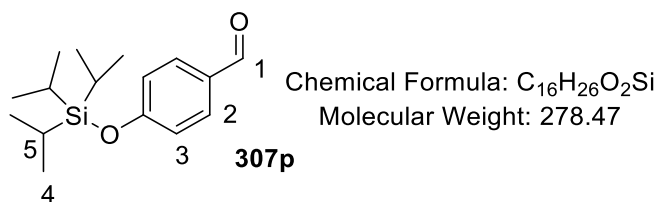
HRMS (APCI): m/z calc'd for $\text{C}_{11}\text{H}_8\text{OD}$ [$\text{M}_{\text{d}1} + \text{H}$] $^+$: 158.0711; found: 158.0705.

No higher isotopomers found.

Improved Synthesis of d_1 -Aldehyde, 307p (Scheme 65)

Employing *General Procedure F*, results are reported as: a) amount of catalyst, b) amount of substrate, c) reaction time, d) %D in labelled substrate, and e) isolated product yield.

At the end of the reaction, the solvent was removed *in vacuo* and the residue redissolved in a minimal quantity of EtOAc. The product was purified *via* silica column chromatography, eluting with petroleum ether/ EtOAc. To ensure separation from the non-polar catalyst residues, the gradient of eluent began at 20:1 and never exceeded 10:1.



a) **273h** (1.6 mg, 0.00215 mmol, 1.0 mol%), b) *p*-tri-isopropyl-siloxybenzaldehyde (59.9 mg, 0.215 mmol), c) 6 h, d) 93% D^1 only e) 58.7 mg, 98% yield.

^1H NMR (400 MHz, CDCl_3): δ 9.90 (s, 1H, CHO), 7.80 (d, 2H, $^3J = 8.6$ Hz, ArH^2), 7.00 (d, 2H, $^3J = 8.6$ Hz, ArH^3), 1.37 – 1.23 (m, 3H, $\text{CH}(\text{CH}_3)_2$), 1.14 – 1.12 (overlapping s, 18H, $\text{CH}(\text{CH}_3^4)$).

^{13}C NMR (100 MHz, CDCl_3): δ 190.0 (t, $^1J_{\text{C-D}} = 26.8$ Hz), 161.4, 131.4, 129.7, 119.6, 17.3, 12.2.

Incorporation expected at δ 9.90 and 7.80. Determined against integral at δ 1.14 – 1.12.

FTIR (neat): 2945, 2843, 2866, 2097, 2052, 1678, 1595, 1595, 1574, 1506, 1462, 1273, 817 cm^{-1} .

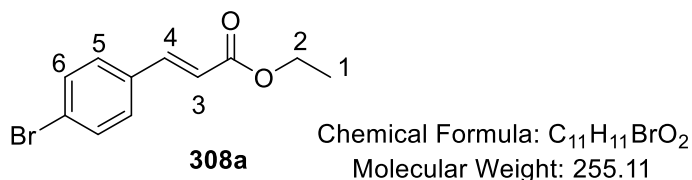
HRMS (APCI): m/z calc'd for $\text{C}_{16}\text{H}_{26}\text{O}_2\text{SiD}$ [$\text{M}_{\text{d}1} + \text{H}$] $^+$: 280.1838; found: 280.1837.

No higher isotopomers detected.

One Pot Labelling and HWE Derivatisation of d_1 -aldehydes (Scheme 66)

The selected aldehyde (0.215 mmol) was labelled using **273h** (1.6 mg, 0.00215 mmol, 1 mol%) in DCM (2.5 mL) at 25 °C for 3 h, according to *General Procedure F*. At the end of the labelling reaction, D_2 and solvent were removed from the flask *in vacuo*. The residue was re-dissolved in dry THF (1 mL) with stirring under an argon atmosphere. Sequentially, the HWE reagent (0.053 mg, 0.2305 mmol) and potassium *tert*-butoxide (0.027 mg, 0.2305 mmol) were then added to the flask which was then left stirring at r.t. for 16 h. The THF solvent was removed *in vacuo* and the remaining residue purified directly *via* silica column chromatography, eluting with petroleum ether/ EtOAc (10:1 to 4:1).

For each example, results are reported as: a) amount of aldehyde, b) %D in labelled product, and c) isolated product yield.



a) *p*-bromobenzaldehyde (39.8 mg, 0.215 mmol), b) 97% D^4 only, and c) 44.0 mg, 80% yield.

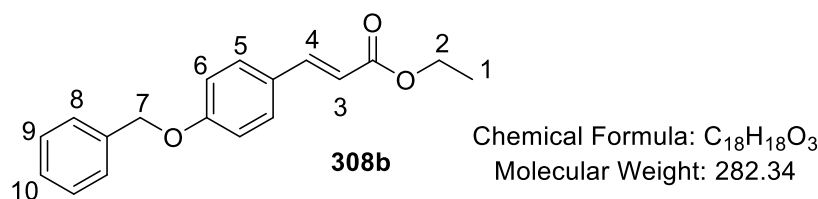
^1H NMR (400 MHz, CDCl_3): δ 7.63 (d, 1H, $^3J = 15.6$ Hz, H^4), 7.53 (d, 2H, $^3J = 8.0$ Hz, ArH^5), 7.39 (d, 2H, $^3J = 8.0$ Hz, ArH^5), 6.43 (d, 1H, $^3J = 15.6$ Hz, H^3), 4.28 (q, 2H, $^3J = 7.1$ Hz, CH_2CH_3), 1.35 (t, 3H, $^3J = 7.1$ Hz, CH_2CH_3).

Incorporation expected at δ 7.63 and 7.53. Determined against integral at δ 1.35.

^{13}C NMR (100 MHz, CDCl_3): δ 166.2, 142.3 (t, $^1J_{\text{C-D}} = 24.1$ Hz), 132.8, 131.6, 128.9, 124.0, 118.4, 60.1, 13.8.

FTIR (neat): 2980, 2160, 1975, 1965, 1708, 1622, 1587, 1487 cm^{-1} .

HRMS (APCI): m/z calc'd for $C_{11}H_{11}^{79}BrO_2D [M_{d1} + H]^+$: 256.0078; found: 256.0076.



a) *p*-benzyloxybenzaldehyde (45.6 mg, 0.215 mmol), b) 97% D^4 ; 20% D^5 , and c) 41.0 mg, 67% yield.

1H NMR (400 MHz, $CDCl_3$): δ 7.66 (d, 1H, $^3J = 16.1$ Hz, H^4), 7.48 (d, 2H, $^3J = 8.0$ Hz, ArH^5), 7.45 – 7.33 (m, 5H, $ArH^8 - ArH^{10}$), 6.99 (d, 2H, $^3J = 8.0$ Hz, ArH^6), 6.32 (d, 1H, $^3J = 16.1$ Hz, H^3), 5.10 (s, 2H, H^7), 4.27 (q, 2H, $^3J = 7.1$ Hz, CH_2CH_3), 1.35 (t, 3H, $^3J = 7.1$ Hz, CH_2CH_3).

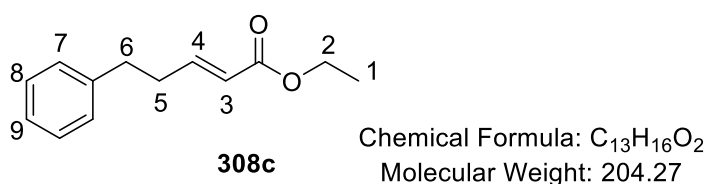
Incorporation expected at δ 7.66 and 7.48. Determined against integral at δ 1.35.

^{13}C NMR (100 MHz, $CDCl_3$): δ 166.3, 159.5, 142.8 (t, $^1J_{C-D} = 23.2$ Hz), 135.5, 128.6, 127.6, 127.1, 126.6, 114.8, 114.2, 114.1, 69.1, 59.3, 13.3.

FTIR (neat): 3011, 2990, 2941, 2860, 2358, 2339, 1780, 1600, 1508, 1456, 1180 cm^{-1} .

HRMS (APCI): m/z calc'd for $C_{18}H_{18}O_3D [M_{d1} + H]^+$: 284.1391; found: 284.1391.

m/z calc'd for $C_{18}H_{17}O_3D_2 [M_{d2} + H]^+$: 285.1454; found: 285.1441.



a) 3-phenylpropionaldehyde (28.8 mg, 0.215 mmol), b) 92% D^4 ; apparent 9% D^5 , and c) 23.3 mg, 81% yield.

1H NMR (400 MHz, $CDCl_3$): δ 7.34 – 7.20 (m, 5H, $ArH^7 - ArH^9$), 7.03 (dt, 1H, $^3J = 15.7$, 6.8 Hz, H^4), 5.87 (dt, 1H, $^3J = 15.7$ Hz, $^4J = 1.6$ Hz, H^3), 4.21 (q, 2H, $^3J = 7.1$ Hz, CH_2CH_3), 2.57 – 2.53 (m, 2H, $CH_2CH_2^5$), 2.83 – 2.79 (m, 2H, $CH_2CH_2^6$), 1.31 (t, 3H, $^3J = 7.1$ Hz, CH_2CH_3).

Incorporation expected at δ 7.03 and 2.57 – 2.53. Determined against integral at δ 1.31.

^{13}C NMR (100 MHz, CDCl_3): δ 166.1, 147.2(t, $^1J_{\text{C-D}} = 24.1$ Hz), 140.3, 128.0, 127.8, 125.7, 121.3, 59.7, 33.8, 33.3, 13.8.

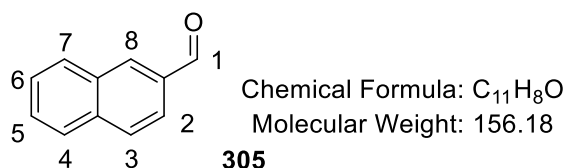
FTIR (neat): 3063, 3026, 2980, 2932, 1717, 1639, 1496, 1454, 1186 cm^{-1} .

HRMS (APCI): m/z calc'd for $\text{C}_{13}\text{H}_{16}\text{O}_2\text{D}$ [$\text{M}_{\text{dl}} + \text{H}$] $^+$: 206.1286; found: 206.1282.

No higher isotopomers detected, despite apparent H^5 labelling calculated *via* ^1H NMR.

Investigating the Effect of the Chloride Ligand in Formyl-selective Aldehyde Labelling (Scheme 67)

Following *General Procedure F*, results are reported as: a) amount of catalyst, b) amount of substrate, c) volume of solvent, d) reaction temperature, e) reaction time, and f) % D in labelled substrate.



a) **309**, 2.1 mg, 0.00215 mmol, 1 mol%, b) **305**, 33.6 mg, 0.215 mmol, c) 2.5 mL, d) 25 $^\circ\text{C}$, e) 3 h, and f) 13% D^1 ; 75% D^2 ; 61% D^8 .

^1H NMR (400 MHz, CDCl_3): δ 10.16 (s, 1H, CHO), 8.33 (s, 1H, ArH^8), 8.01 – 7.90 (m, 4H, $\text{ArH}^2 + \text{ArH}^3 + \text{ArH}^4 + \text{ArH}^7$), 7.67 – 7.57 (m, 2H, $\text{ArH}^5 + \text{ArH}^6$).

Incorporation expected at δ 10.16, 8.33, and 8.01 – 7.90. Determined against integral at δ 7.67 – 7.57.

Additive and Solvent Effects in Formyl-selective Aldehyde Labelling (Table 27)

Following *General Procedure G*, all reactions in this table were run under the optimised conditions scaled to carousel level. As such, **273h** (0.6 mg, 0.0086 mmol, 1 mol%), **305** (13.4 mg, 0.086 mmol), solvent (1 mL), and (where appropriate) the additive (0.00086 mmol, 1 mol%), were used. The additives were used in the following quantities:

AgOTf (0.2 mg)

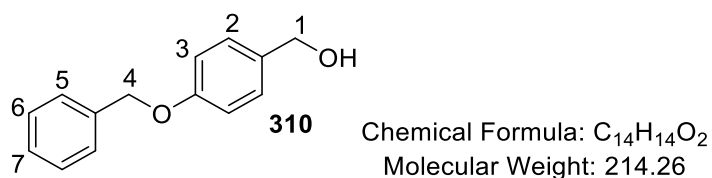
AgSbF₆ (0.3 mg)

AgNO₃ (0.1 mg)

Spectroscopic data for **305** are as reported above. Results are as already stated in **Table 27** and are not printed again in this section.

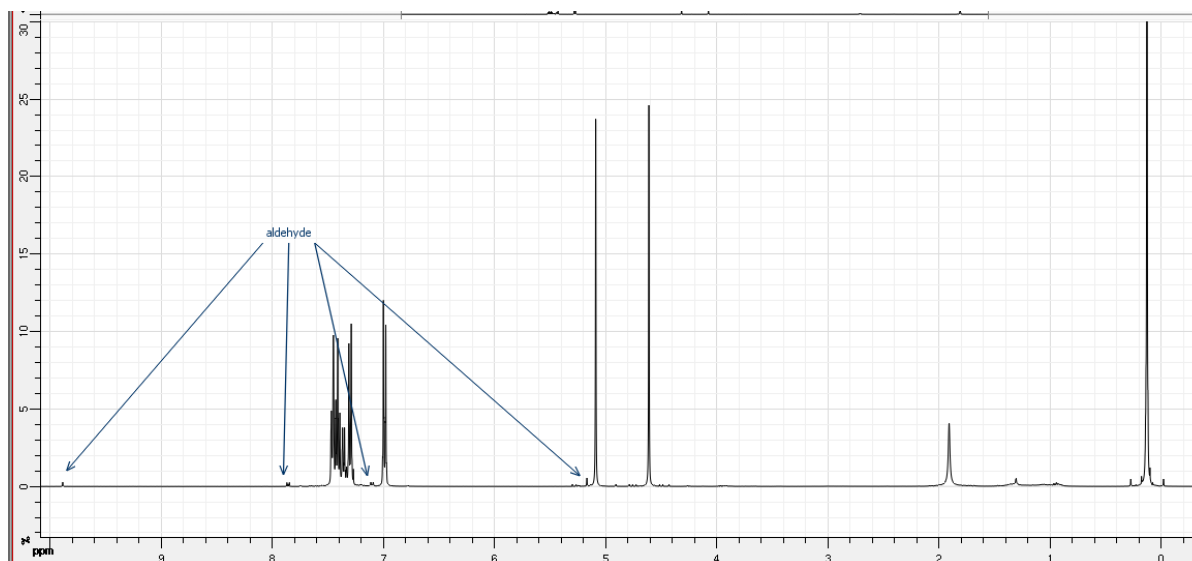
Evidence against Hydrogen Borrowing in Formyl-selective Aldehyde Labelling (Scheme 68)

Following *General Procedure F*, *p*-benzyloxybenzyl alcohol, **310** (46.0 mg, 0.215 mmol) was exposed to the optimised labelling conditions, using H₂ in place of D₂.



¹H NMR (400 MHz, CDCl₃): δ 7.47 – 7.27 (m, 7H, ArH³ – ArH⁷), 6.99 (d, 2H, ³J = 8.4 Hz, ArH²).

No change expected. Trace quantities of oxidized aldehyde, **307a** are highlighted in the screen shot below. Detailed spectroscopic data for **307a** are as reported above:



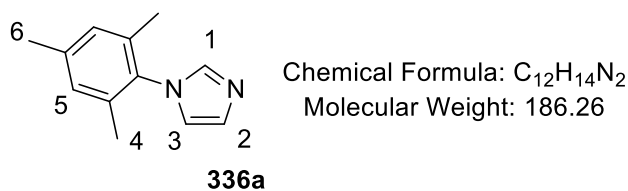
8.8 On the Fundamentals of Chelating Ligand Design Towards Novel HIE Technologies

Synthesis of Novel Chelating Ligand Catalysts (Scheme 74)

NOTE: Reported compound preparations of many runs. The scales provided represent relative stoichiometries as an example. However, these reactions are now being pursued on much larger scales.

*Synthesis of *N*-mesitylimidazole, **337a**²⁷⁸*

In a 500 mL round bottom flask, glacial acetic acid (17.5 mL, 305 mmol), aqueous formaldehyde (37% w/v in aqueous solution, 5.4 mL, 71.1 mmol), and aqueous glyoxal (40% w/v in aqueous solution, 8.1 mL, 71.7 mmol) were added. The flask was placed under an argon atmosphere and the contents stirred at 70 °C. In a separate 250 mL flask, glacial acetic acid (17.3 mL, 302 mmol), ammonium acetate (5.47 g, 71 mmol), mesitylamine (9.3 mL, 66 mmol), and water (~20 mL), were vigorously stirred together at room temperature to dissolve all of the ammonium acetate. The contents of this second flask were then added dropwise to the first over 20 mins. In this time, the reaction mixture became brown, dark brown, then black. The reaction mixture was stirred at 70 °C for 16 h before cooling to room temperature. The mixture was then slowly poured into a 1 L round bottom flask containing saturated NaHCO₃ (~400 mL) and stirred vigorously. **NOTE:** this step must be performed carefully and with patience. The neutralisation of excess acid effervesces uncontrollably if too much of the reaction mixture is poured in at one time. After 1 h stirring, the resultant brown precipitate was collected by filtration and washed with water and petroleum ether. The solid was purified *via* silica column chromatography, eluting with petroleum ether, then pure EtOAc (after necessary gradient). The resultant oily solid was heated in a minimal quantity EtOAc to give homogeneous solution which crystallised in the freezer overnight give the desired product as pale brown crystals (4.145 g, 34% yield). **NOTE:** filtration after crystallisation does not collect the entire product yield. The mother liquor has to be re-subjected to the crystallisation process several times.



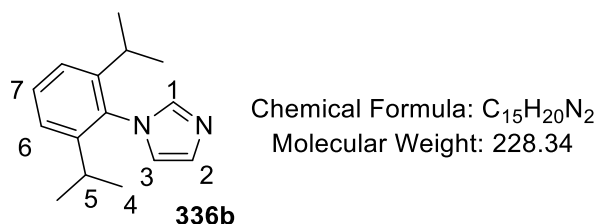
¹H NMR (400 MHz, CDCl₃): δ 7.43 (s, 1H, ArH³), 7.23 (s, 1H, ArH²), 6.96 (s, 2H, ArH⁵), 6.89 (s, 1H, ArH¹), 2.33 (s, 3H, ArCH₃⁶), 1.99 (s, 6H, ArCH₃⁴).

¹³C NMR (100 MHz, CDCl₃): δ 138.8, 137.5, 135.4, 133.4, 129.5, 129.0, 120.0, 21.0, 17.3.

FTIR (neat): 3113, 3094, 2974, 2953, 2922, 1805, 1641, 1598, 1498 cm⁻¹.

*Synthesis of N-2,6-di-iso-propylphenylimidazole, 337b*²⁷⁸

Following an identical procedure to that for the synthesis of **337a**, mesitylamine was replaced with 2,6-di-*iso*-propylaniline (12.4 mL, 66 mmol). The product was isolated as beige crystals (4.941 g, 33% yield).



¹H NMR (400 MHz, CDCl₃): δ 7.46 – 7.41 (m, 2H, ArH), 7.27 – 7.24 (m, 3H, ArH), 6.94 (s, 1H, ArH¹), 2.40 (septet, 2H, ³J = 6.9 Hz, CH(CH₃)₂), 1.13 (d, 12H, ³J = 6.9 Hz, CH(CH₃)₂).

¹³C NMR (100 MHz, CDCl₃): δ 146.5, 138.5, 132.8, 129.8, 129.4, 124.8, 121.5, 28.1, 24.4, 24.3.

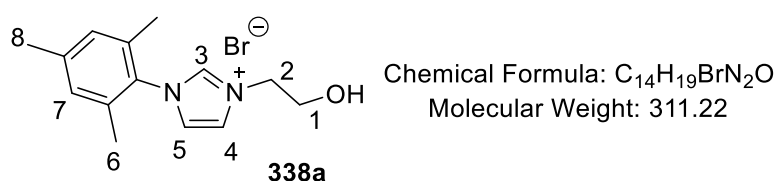
FTIR (neat): 3117, 2965, 2868, 1639, 1589, 1494, 1471, 1458 cm⁻¹.

*Synthesis of 3-(2-hydroxyethyl)-1-mesityl-1H-imidazolium bromide, 338a*²⁴⁹

Mesitylimidazole, **337a** (1.0 g, 5.369 mmol) was added to a dry toluene (~50 mL) solution of 2-bromoethanol (0.42 mL, 5.898 mmol) in an oven dried 250 mL round bottom flask at r.t. under an argon atmosphere. The homogeneous solution was heated to reflux, forming a visible bilayer over 16 h. Upon cooling, toluene (top layer) was decanted out of the flask, leaving a viscous brown oil. Diethyl ether (~100 mL) was added to the flask and, with vigorous stirring over 1 h, a white/brown solid was triturated. The large lumps were broken

down with a spatula and stirring continued until a fine, off-white powder was dispersed in Et₂O. The product was collected by filtration (1.450 g, 87% yield) and washed with Et₂O before stored in the vacuum oven (40 °C).

A small quantity of the white solid was isolated and dried for characterisation purposes. Although the product salt can be isolated, its highly hygroscopic nature means it is easier to store it in full under the blanket of Et₂O until the next synthetic step is set up.



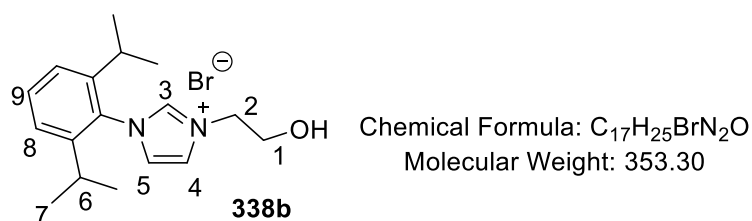
¹H NMR (400 MHz, DMSO-d₆): δ 9.42 (s, 1H, ArH³), 8.06 (s, 1H, ArH⁵), 7.92 (s, 1H, ArH⁴), 7.14 (s, 2H, ArH⁷), 4.34 (t, 2H, ³J = 5.7 Hz, CH₂²CH₂), 3.81 (t, 2H, ³J = 5.7 Hz, CH₂¹CH₂), 2.32 (s, 3H, ArCH₃⁸), 2.02 (s, 6H, ArCH₃⁶).

¹³C NMR (100 MHz, DMSO-d₆): δ 140.2, 137.7, 134.2, 131.2, 129.2, 123.7, 123.3, 59.0, 52.1, 20.5, 16.8.

FTIR (neat): 3306, 3057, 3032, 1607, 1562, 1463, 1446, 1065 cm⁻¹.

*Synthesis of 1-(2,6-diisopropylphenyl)-3-(2-hydroxyethyl)-1H-imidazolium bromide, 338b*²⁷⁹

Following an identical procedure to that for the synthesis of **338a**, mesitylimidazole **337a** was replaced with 2,6-di-*iso*-propylphenylimidazole **337b** (0.600 g, 2.628 mmol), and 2-bromoethanol stoichiometry adjusted (0.20 mL, 2.891 mmol). The product was isolated as a white solid (0.773 g, 83% yield).



¹H NMR (400 MHz, DMSO-d₆): δ 9.59 (t, 1H, ⁴J = 1.6 Hz, ArH³), 8.16 (t, 1H, ⁴J = 1.6 Hz, ArH⁵), 8.09 (t, 1H, ⁴J = 1.6 Hz, ArH⁴), 7.63 (t, 1H, ³J = 7.8 Hz, ArH⁹), 7.46 (d, 2H, ³J = 7.8 Hz, ArH⁸), 4.39 (t, 2H, ³J = 5.0 Hz, CH₂²CH₂), 3.83 (t, 2H, ³J = 5.0 Hz, CH₂¹CH₂), 2.30

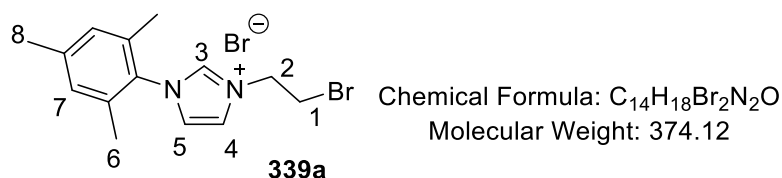
(septet, 2H, $^3J = 7.2$ Hz, $\text{CH}(\text{CH}_3)_3$), 1.15 (d, 12H, $^3J = 7.2$ Hz, $\text{CH}(\text{CH}_3)_3$). No OH peak visible.

^{13}C NMR (100 MHz, DMSO- d_6): δ 145.2, 138.2, 131.4, 130.5, 124.8, 124.4, 123.4, 59.0, 52.0, 28.0, 23.8, 23.7.

FTIR (neat): 3281, 3048, 2963, 2868, 1660, 1543, 1460, 1442 cm^{-1} .

*Synthesis of 3-(2-bromoethyl)-1-mesityl-1H-imidazolium bromide, 339a*²⁴⁹

338a (0.250 g, 0.804 mmol) was dissolved in dry DCM (4.0 mL) in a 100 mL round-bottom flask under an atmosphere of argon. After cooling the solution in an ice bath, PBr_3 (0.076 mL, 0.804 mmol) was added to the flask dropwise. The reaction mixture was stirred and warmed to r.t. over 16 h. At the end of the reaction, the mixture was cooled in an ice bath and quenched with saturated aqueous NaHCO_3 , turning the reaction mixture from brown to colourless. The product was extracted using DCM (2 x 15 mL), dried over anhydrous Na_2SO_4 and concentrated *in vacuo*. Due to the hygroscopic nature of the product, a small quantity was isolated for simple characterisation whilst the remainder was stored under Et_2O under the next reaction. No yield was recorded and was assumed to be 100% in for subsequent synthetic transformations.

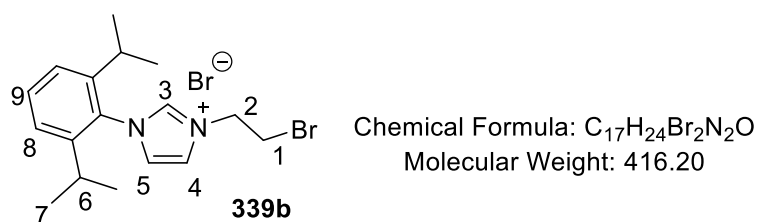


^1H NMR (400 MHz, DMSO- d_6): δ 9.59 (s, 1H, ArH^3), 8.18 (s, 1H, ArH^5), 8.00 (s, 1H, ArH^4), 7.17 (s, 2H, ArH^7), 4.75 (t, 2H, $^3J = 4.0$ Hz, CH_2^2CH_2), 4.10 (t, 2H, $^3J = 4.0$ Hz, CH_2^1CH_2), 2.36 (s, 3H, ArCH_3^8), 2.04 (s, 6H, ArCH_3^6).

FTIR (neat): 3420, 3022, 2970, 1607, 1547, 1485, 1444, 1203 cm^{-1} .

*Synthesis of 3-(2-bromoethyl)-1-(2,6-diisopropylphenyl)-1H-imidazolium bromide, 339b*²⁷⁹

Following an identical procedure to that for the synthesis of **339a**, **338a** was replaced with **338b** (0.400 g, 1.132 mmol), and the PBr_3 stoichiometry adjusted (0.11 mL, 1.132 mmol). In this case, the product was isolated as a white solid after trituration with Et_2O (0.270 g, 57% yield).



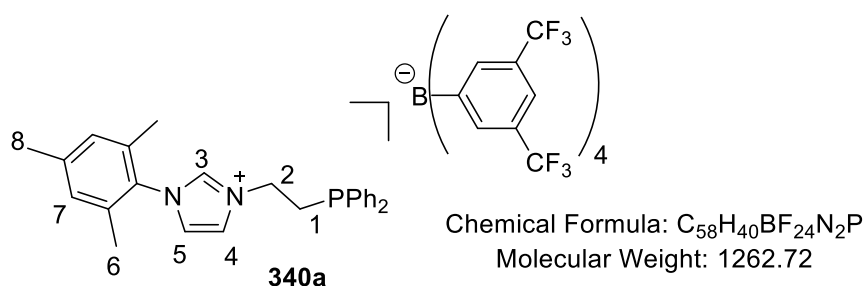
¹H NMR (400 MHz, DMSO-*d*₆): δ 9.70 (t, 1H, ⁴*J* = 1.6 Hz, ArH³), 8.21 (t, 1H, ⁴*J* = 1.6 Hz, ArH⁵), 8.17 (t, 1H, ⁴*J* = 1.6 Hz, ArH⁴), 7.65 (t, 1H, ³*J* = 7.9 Hz, ArH⁹), 7.48 (d, 2H, ³*J* = 7.8 Hz, ArH⁸), 4.75 (t, 2H, ³*J* = 5.5 Hz, CH₂²CH₂), 4.10 (t, 2H, ³*J* = 5.5 Hz, CH₂¹CH₂), 2.31 (septet, 2H, ³*J* = 6.8 Hz, CH(CH₃)₃), 1.16 (d, 12H, ³*J* = 7.2 Hz, CH(CH₃)₃).

FTIR (neat): 3460, 3377, 3063, 2965, 1549, 1468, 1448 cm⁻¹.

Synthesis of 3-(2-diphenylphosphinoethyl)-1-mesityl-1H-imidazolium tetrakis[(3,5-trifluoromethylphenyl)]borate, 340a

339a (1.638 g, 4.378 mmol) was dissolved in DMSO (8.8 mL) under an argon atmosphere in a flame-dried 100 mL round-bottom flask fitted with a stopcock side arm. In a separate flame-dried, 25 mL pear-shaped flask, diphenylphosphine (0.856 g, 4.597 mmol) was dissolved in DMSO (2 mL) and, after adding potassium *tert*-butoxide (0.491 g, 4.378 mmol), a colourless to bright red colour change was observed. After allowing the *in situ* generated KPPh₂ solution to stir for 1 h, it was added dropwise *via* syringe to the main reaction flask. **NOTE:** this reaction is self-indicating – on adding KPPh₂ dropwise, the red colour dispersed and disappeared on reaction with **339a**. Near the end of the addition, it took longer for the colour to disappear. After complete addition, the reaction mixture was left to stir for 1 h at r.t. before added MeOH (~2 mL) in order to quench excess KPPh₂. The reaction mixture was diluted with DCM and water before being added to a separating funnel. The aqueous layer was extracted with DCM. The combined organics were then separately washed with water to remove excess DMSO. The final combined DCM extracts were dried over anhydrous Na₂SO₄, filtered, and concentrated to ~10 mL *in vacuo*. The DCM solution of the reaction mixture was partitioned in a round-bottom flask using an equal volume of water before adding NaBARF (3.880 g, 4.378 mmol). The new mixture was stirred vigorously (to break the bilayer) at r.t. for 16 h. The bilayer was added to a separating funnel and extracted with DCM. The combined extracts were once again dried over anhydrous Na₂SO₄, filtered and concentrated *in vacuo*. The pale yellow oil was dissolved in a minimal quantity of DCM and purified *via* silica column chromatography, eluting with petroleum ether/DCM (1:0 → 2:1).

The product was isolated as a clear oil which crystallised slowly to give a white, mildly air-sensitive solid (3.22 g, 58% yield).



Appearance: white solid.

FTIR (neat): 3123, 3072, 2980, 1610, 1546, 1483, 1435, 1355, 1275, 1121 cm⁻¹.

¹H NMR (400 MHz, DMSO-d₆): δ 9.46 (t, 1H, ⁴J = 1.6 Hz, ArH³), 8.16 (s, 1H, ⁴J = 1.8 Hz, ArH⁵), 7.92 (s, 1H, ⁴J = 1.8 Hz, ArH⁴), 7.69 (s, 4H, BArF ArH), 7.63 (m, 8H, BArF ArH), 7.51 – 7.40 (m, 10H, ArH PPh₂), 7.13 (s, 2H, ArH⁷), 4.39 (m, 2H, CH₂²CH₂PPh₂), 2.89 – 2.85 (m, 2H, CH₂¹CH₂), 2.32 (s, 3H, ArCH₃⁸), 2.02 (s, 6H, ArCH₃⁶).

¹³C NMR (100 MHz, DMSO-d₆): δ 160.9 (q, ²J_{C-F}), 140.2, 137.3, 136.6, 136.5, 134.3, 134.0, 132.6, 132.4, 132.1, 129.2, 128.9, 128.8, 128.7, 128.6, 128.3, 128.0, 125.3, 123.2, 122.6, 119.2, 117.6, 47.0 (d, ¹J_{C-P} = 25.4 Hz), 27.1 (d, ²J_{C-P} = 13.5 Hz), 20.5, 16.9. **NOTE:** in lieu of decoupled spectra, there exists significant overlap with various C-P, C-F, C-¹⁰B and C-¹¹B splitting patterns.

¹³C DEPT-135°q NMR (100 MHz, DMSO-d₆): 140.2, 134.3, 125.3, 123.2, 20.5, 16.9.

¹³C DEPT-90° NMR (100 MHz, DMSO-d₆): 137.3, 134.3, 132.6, 132.4, 129.7, 129.3, 129.2, 123.2, 122.6, 117.6.

³¹P NMR (162 MHz, DMSO-d₆): δ – 22.9 (PPh₂).

¹⁹F NMR (376 MHz, DMSO-d₆): δ – 61.8 (BArF CF₃).

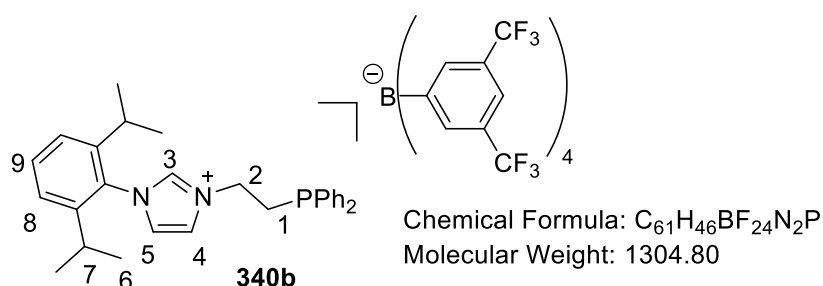
HRMS (positive ESI): m/z calc'd for C₂₆H₂₈N₂P [M-BArF]⁺: 399.1985; found: 399.1990.

HRMS (negative ESI): m/z calc'd for C₃₂H₁₂BF₂₄ [BArF]⁻: 863.0660; found: 863.0623.

Synthesis of 3-(2-diphenylphosphinoethyl)-1-[2,6-diisopropylphenyl]-1H-imidazolium tetrakis[(3,5-trifluoromethylphenyl)]borate, 340b

Following an identical procedure to that for the synthesis of **340a**, **339a** was replaced with **339b** (0.244 g, 0.586 mmol), and the KO^tBu (0.066 g, 0.645 mmol), PPh₂H (0.120 g, 0.645

mmol), and NaBArF (0.571 g, 0.645 mmol) stoichiometries adjusted accordingly. In this case, the product was isolated as a white solid (0.348 g, 46% yield).



Appearance: white solid.

FTIR (neat): 3128, 2976, 1609, 1560, 1544, 1354, 1275, 1109 cm^{-1} .

1H NMR (400 MHz, DMSO- d_6): 8.16 (s, 1H, ArH³), 7.70 (bs, 8H, BArF ArH), 7.61 (t, 1H, $^3J = 7.8$ Hz, ArH⁹), 7.52 (bs, 4H, BArF ArH), 7.42 – 7.33 (m, 13H, ArH⁵ + ArH⁸ + ArH PPh₂), 7.27 (s, 1H, ArH⁴), 4.31 (dt, 2H, $^3J_{H-P} = 12.0$ Hz, $^3J = 6.8$ Hz, CH₂²CH₂PPh₂), 2.62 (t, 2H, $^3J = 6.8$ Hz, CH₂CH₂¹ PPh₂), 2.23 (septet, 2H, $^3J = 6.8$ Hz, CH(CH₃)₃), 1.17 – 1.13 (overlapping d, 12H, $^3J = 6.8$ Hz, CH(CH₃)₃).

^{13}C NMR (100 MHz, DMSO- d_6): δ 161.7 (q, $^2J_{C-F} = 49.5$ Hz), 145.1, 135.0, 134.8, 134.2, 134.1, 132.9, 132.6, 132.4, 130.3, 129.4, 129.3, 129.0, 128.7, 125.9, 125.8, 125.2, 123.2, 122.6, 120.4, 117.5, 48.4 (d, $^1J_{C-P} = 20.0$ Hz), 29.0 (d, $^2J_{C-P} = 16.0$ Hz), 28.8, 24.1, 24.0.

NOTE: in lieu of decoupled spectra, there exists significant overlap with various C-P, C-F, C-¹⁰B and C-¹¹B splitting patterns.

^{13}C DEPT-135° NMR (100 MHz, DMSO- d_6): 48.4, 29.0.

^{31}P NMR (162 MHz, DMSO- d_6): δ – 26.8 (PPh₂).

^{19}F NMR (376 MHz, DMSO- d_6): δ – 62.4 (BArF CF₃).

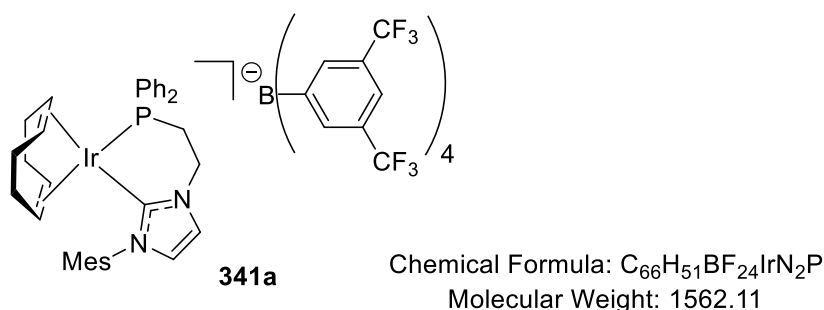
HRMS (positive ESI): m/z calc'd for C₂₉H₃₄N₂P [M-BArF]⁺: 441.2454; found: 441.2453.

m/z calc'd for C₆₁H₄₇BF₂₄N₂P [M+H]⁺: 1305.3186; found: 1305.3193

HRMS (negative ESI): m/z calc'd for C₃₂H₁₂BF₂₄ [BArF]⁻: 863.0660; found: 863.0623.

Synthesis of (Cyclooctadiene) (3-(2-diphenylphosphinoethyl)-1-mesityl-imidazol-2-ylidene) iridium(I) tetrakis[(3,5-trifluoromethylphenyl)]borate, 341a

To a solution of $[\text{Ir}(\text{COD})\text{Cl}]_2$ (0.402 g, 0.599 mmol) in dry THF (12 mL, ~ 0.1 M) was added salt **340a** (1.512 g, 1.197 mmol). After 15 mins stirring at r.t., KO^tBu (0.141 g, 1.257 mmol) was added in one portion, causing a light orange to red to dark red colour change. The reaction mixture was stirred at r.t. for 3 h before the solvent was reduced *in vacuo*. The residue was purified through a plug of silica, eluting with DCM/petroleum ether (2:1), collecting the red band as one fraction. Reducing the solvent *in vacuo* gave the desired product as a dark red solid (0.617 g, 33% yield).



Appearance: deep red solid.

FTIR (neat): 2958, 2928, 2081, 2029, 1611, 1437, 1410, 1354, 1273, 1117, cm^{-1} .

^1H NMR (400 MHz, CDCl_3): δ 7.75 (m, 8H, BArF ArH), 7.54 (bs, 4H, BArF ArH), 7.50 – 7.35 (m, 10H, ArH PPh_2), 7.00 (d, 1H, $^3J = 1.9$ Hz, $\text{NCH}=\text{CHN}$), 6.98 (s, 2H, ArH), 6.79 (d, 1H, $^3J = 1.9$ Hz, $\text{NCH}=\text{CHN}$), 4.60 (d, 2H, $^3J_{\text{C-P}} = 26.0$ Hz, $\text{CH}_2\text{CH}_2\text{PPh}_2$), 4.41 (m, 2H, COD CH), 3.61 (m, 2H, COD CH), 2.51 (m, 2H, $\text{CH}_2\text{CH}_2\text{PPh}_2$), 2.35 (s, 3H, ArCH_3), 1.87 (s, 6H, ArCH_3), 1.59 – 1.16 (m, 8H, COD CH_2).

^{31}P NMR (162 MHz, CDCl_3): δ (PPh_2).

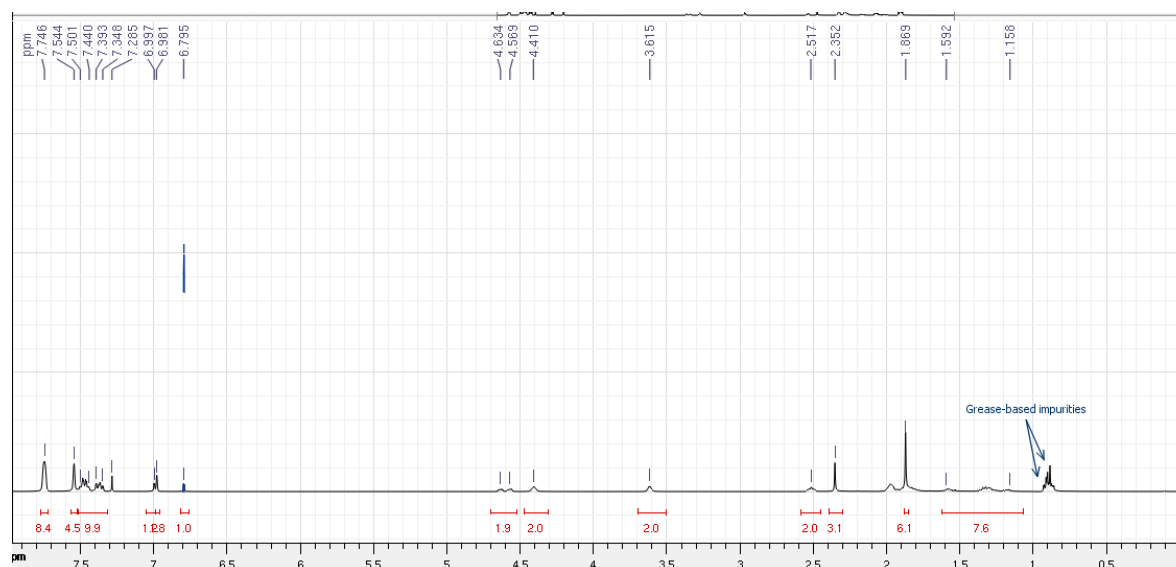
^{19}F NMR (376 MHz, CDCl_3): δ – 62.4 (BArF CF_3).

HRMS (positive ESI): Complete fragmentation of sample observed. A satisfactory method of analysis has not yet been found.

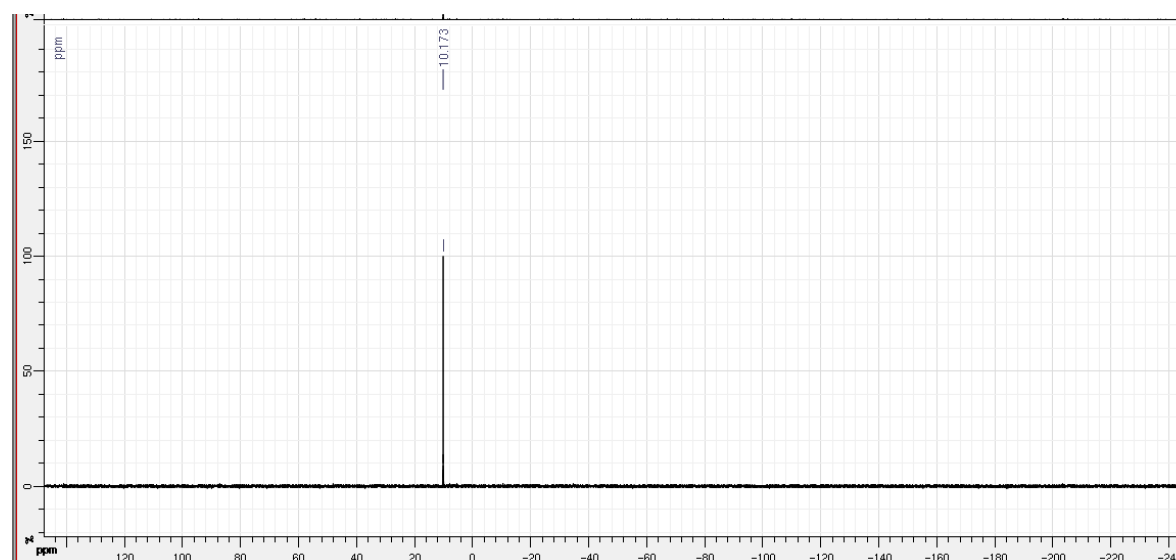
HRMS (negative ESI): m/z calc'd for $\text{C}_{32}\text{H}_{12}\text{BF}_{24}$ [BArF]: 863.0660; found: 863.0623.

In lieu of full analysis, the ^1H , ^{31}P , and ^{19}F NMR spectra for **341a** are provided below:

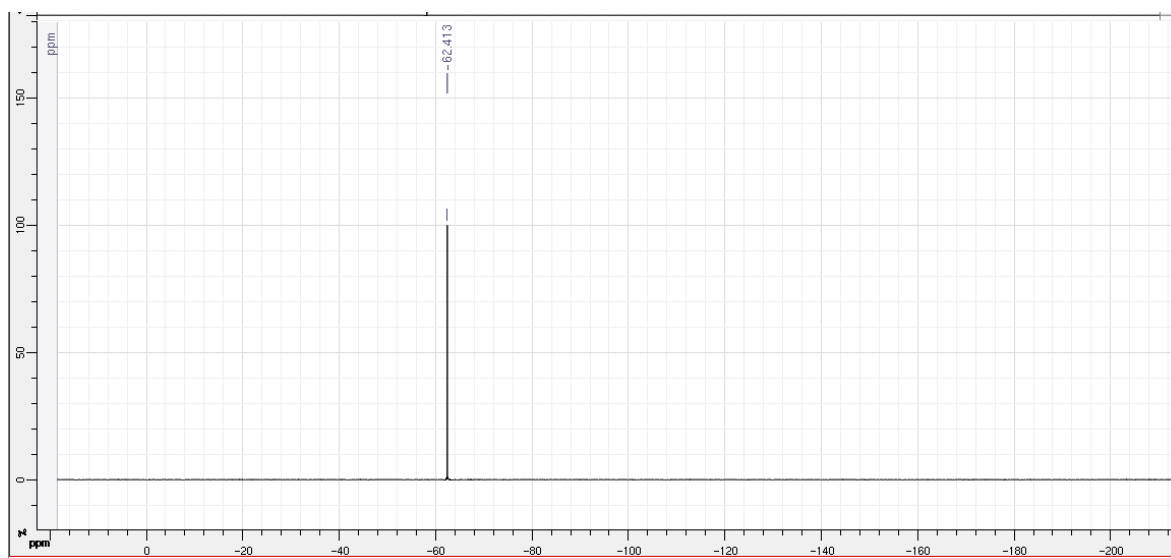
^1H NMR (400 MHz, CDCl_3):



^{31}P NMR (162 MHz, CDCl_3):

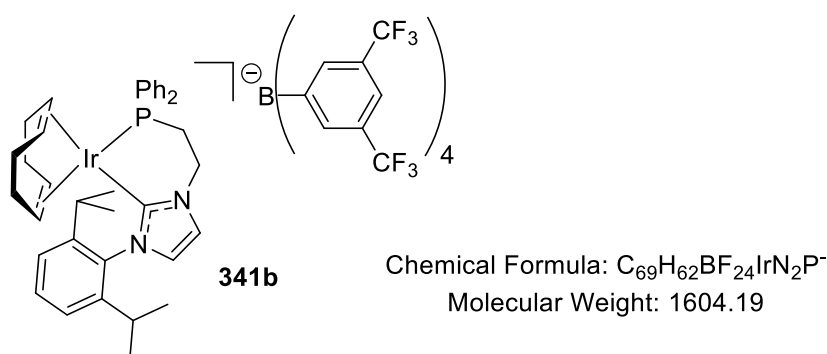


^{19}F NMR (376 MHz, CDCl_3):



*Synthesis of (Cyclooctadiene) (3-(2-diphenylphosphinoethyl)-1-[2,6-diisopropylphenyl]-imidazol-2-ylidene) iridium(I) tetrakis[(3,5-trifluoromethylphenyl)]borate, **341b***

To a solution of $[\text{Ir}(\text{COD})\text{Cl}]_2$ (0.146 g, 0.217 mmol) in dry THF (11 mL, ~ 0.02 M) was added salt **340b** (0.283 g, 0.217 mmol). After 15 mins stirring at r.t., KO^tBu (0.027 g, 0.239 mmol) was added in one portion, causing a light orange to red to dark red colour change. The reaction mixture was stirred at r.t. for 3 h before the solvent was reduced *in vacuo*. The residue was purified through a plug of silica, eluting with DCM/petroleum ether (2:1), collecting the red band as one fraction. Reducing the solvent *in vacuo* gave the desired product as a dark red solid (0.149 g, 43% yield).



Appearance: deep red solid.

m.p.: 159 – 160 $^\circ\text{C}$.

FTIR (neat): 2968, 1611, 1464, 1435, 1354, 1275, 1121 cm^{-1} .

¹H NMR (400 MHz, CDCl₃): δ 7.74 (m, 8H, ArH BArF), 7.55 – 7.47 (overlapping bs and m, 16H, ArH BArF + ArH PPh₂ + ArH), 7.42 – 7.37 (m, 4H, ArH PPh₂), 7.29 (d, 2H, ³J = 8.4 Hz, ArH), 7.02 (d, 1H, ³J = 2.0 Hz, NCH=CHN), 6.91 (d, 1H, ³J = 2.0 Hz, NCH=CHN), 4.54 (dm, 2H, ³J_{C-P} = 24.8 Hz, CH₂CH₂PPh₂), 4.36 (m, 2H, COD CH), 3.79 (m, 2H, COD CH), 2.59 – 2.44 (overlapping septet and m, 4H, ³J = 6.4 Hz, CH(CH₃)₂ + CH₂CH₂PPh₂), 1.98 – 1.77 (m, 8H, COD CH₂), 1.19 (d, 6H, ³J = 6.4 Hz, CH(CH₃)₃), 0.89 (d, 6H, ³J = 6.4 Hz, CH(CH₃)₃).

¹³C NMR (100 MHz, CDCl₃): 161.7 (q, ²J_{C-F} = 49.5 Hz), 144.8, 134.8, 131.7, 131.6, 131.3, 131.2, 130.8, 130.4, 128.9, 128.8, 128.6, 128.3, 128.1, 127.9, 125.8, 125.4, 123.9, 122.7, 120.6, 120.0, 117.0, 86.6 (d, ²J_{C-P} = 13.4 Hz), 79.5, 49.3, 30.8, 30.4, 28.5, 24.7, 22.1,

¹³C DEPT-90° NMR (100 MHz, CDCl₃): 134.8, 131.7, 131.6, 131.2, 130.4, 128.9, 128.8, 125.8, 123.9, 120.6, 117.0, 86.6 (d, ²J_{C-P} = 13.4 Hz), 79.5, 28.5.

³¹P NMR (162 MHz, CDCl₃): δ 9.0 (PPh₂).

¹⁹F NMR (376 MHz, CDCl₃): δ – 62.4 (BArF CF₃).

¹¹B NMR (128 MHz, CDCl₃): δ -6.6 (BArF).

HRMS (positive ESI): m/z calc'd for C₃₇H₄₅IrN₂P [M – BArF]⁺: 741.2946; found: 741.2945.

HRMS (negative ESI): m/z calc'd for C₃₂H₁₂BF₂₄ [BArF]⁻: 863.0660; found: 863.0623.

X-ray data: See Appendix A.

Proof-of-Concept Reactions for Labelling Methylphenylsulfone Based on ΔE_{bind} Design (Scheme 75)

Following *General Procedure G*, all reactions employed methylphenylsulfone (13.4 mg, 0.086 mmol), DCM (1 mL), and a 16 h reaction time. Results are reported as: a) amount of catalyst, b) reaction temperature, and c) %D in labelled substrate.

From Scheme 75:

a) **326u** (catalyst **196a**, 2.8 mg, 0.0043 mmol), b) 25 °C, and c) 9% D.

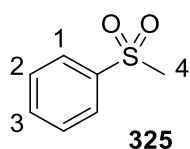
a) **326v** (catalyst **207**, 4.4 mg, 0.0043 mmol), b) 25 °C, and c) 17% D.

a) **326k** (6.9 mg, 0.0043 mmol), b) 25 °C, and c) 37% D.

a) **326j** (6.7 mg, 0.0043 mmol), b) 25 °C, and c) 61% D.

Additional Data:

a) **325** (6.7 mg, 0.0043 mmol), b) 35 °C, and c) 83% D.



Chemical Formula: C₇H₈O₂S
Molecular Weight: 156.20

¹H NMR (400 MHz, DMSO-*d*₆): δ 7.94 (d, 2H, ³J = 8.4 Hz, ArH¹), 7.65 (tt, 1H, ³J = 7.2 Hz, ⁴J = 2.4 Hz, ArH³), 7.57 (t, 2H, ³J = 7.2 Hz, ArH²), 3.05 (s, 3H, SO₂CH₃).

Incorporation expected at δ 7.94. Determined against integral at δ 3.05.

HRMS (APCI): m/z calc'd for C₇H₇O₂SD [M_{d1} + H]⁺: 158.0381; found: 158.0377.

m/z calc'd for C₇H₆O₂SD₂ [M_{d2} + H]⁺: 159.0443; found: 159.0437.

No higher isotopomers found.

Novel Reactivity for Bidentate Catalysts Beyond Sulfone Predictions (Scheme 76)

Following *General Procedure G*, all reactions employed DCM (1 mL), a 16 h reaction time, and 25 °C temperature. Results are reported as: a) amount of catalyst, b) amount of substrate, and c) %D in labelled substrate.

Deuteration of 342 with Complex 341a



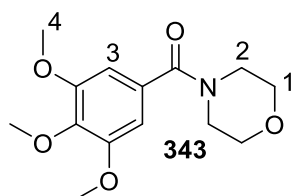
Chemical Formula: C₈H₁₁NO₂S
Molecular Weight: 185.24

¹H NMR (400 MHz, CDCl₃): δ 7.75 (d, 2H, ³J = 8.3 Hz, ArH¹), 7.31 (d, 2H, ³J = 8.3 Hz, ArH²), 4.61-4.56 (m, 1H, SO₂N(CH₃)H), 2.63 (d, 3H, ³J = 5.4 Hz, N(CH₃)H), 2.43 (s, 3H, ArCH₃).

Incorporation expected at δ 7.75. Determined against integral at δ 2.43.

a) **341a** (6.7 mg, 0.0043 mmol), b) **342** (15.9 mg, 0.086 mmol), and c) 49% D.

Deuteration of Trimetazone



Chemical Formula: C₁₄H₁₉NO₅

Molecular Weight: 281.31

¹H NMR (400 MHz, CDCl₃): δ 6.65 (s, 2H, ArH³), 3.89 – 3.88 (overlapping s, 9H, OCH₃⁴), 3.76 - 3.70 (bs, 8H, NCH₂² + OCH₂¹).

Incorporation expected at δ 6.65 and 3.76. Determined against integral at δ 3.89 - 3.88.

NOTE: Positions D¹ and D² are indistinguishable but labelling in these positions is assumed to be primarily D² due to the amide-directed coordination.

a) **208a** (7.4 mg, 0.0043 mmol), b) **343** (24.2 mg, 0.086 mmol), and c) 9% D³; 0% D².

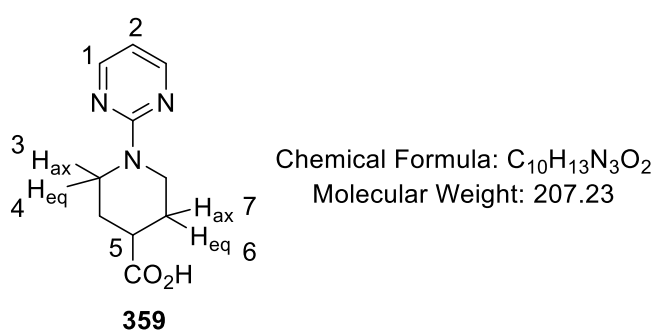
a) **208a** (6.7 mg, 0.0043 mmol), b) **343** (24.2 mg, 0.086 mmol), and c) 96% D³; 18% D².

8.9 Summarised Data Provided on Future Work Elements

The results in this section are deemed to be the minimum necessary to show progress in the suggested lines of enquiry. More detailed analysis of optimisation and substrate studies are available upon request from the author.

Future Work in sp^3 -labelling (Scheme 83)

Following *General Procedure G*, results are reported as: a) amount of catalyst, b) amount of substrate, c) reaction time, d) reaction temperature, and e) %D in labelled substrate.



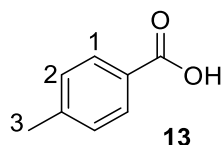
¹H NMR (300 MHz, MeOD-d₄): δ 8.20 (d, 2H, $^3J = 4.8$ Hz, ArH¹), 6.45 (t, 1H, $^3J = 4.8$ Hz, ArH²), 4.50 (dt, 2H, $^3J_{ax-ax} = 13.6$ Hz, $^3J_{ax-eq} = 4.1$ Hz, H_{ax}³), 3.02 – 2.92 (m, 2H, H_{eq}⁴), 2.51 (tt, 1H, $^3J_{ax-ax} = 11.5$ Hz, $^3J_{ax-eq} = 4.3$ Hz, H_{ax}⁵), 1.88 – 1.82 (m, 2H, H_{ax}⁷), 1.58 – 1.45 (m, 2H, H_{eq}⁶). **NOTE:** under these NMR conditions, **359** is observed to exist as the equatorial conformer only, hence the ability to distinguish axial *versus* equatorial labelling.

Incorporation expected at δ 4.50 and 3.02 – 2.92. Determined against integral at δ 2.51.

a) **208a** (1.9 mg, 0.001075 mmol, 2.5 mol%), b) **359** (8.7 mg, 0.043 mmol), c) 4 h, d) 22 – 25 °C, and e) 85% H³; 91% H⁴.

Low Reactivity of Carboxylic Acids Under Tetrazole Labelling Conditions and Current Progress Towards Reoptimisation (Scheme 84)

Following *General Procedure G*, results are reported as: a) amount of catalyst, b) amount of substrate, c) amount of base, d) reaction time, e) reaction temperature, f) solvent, and g) %D in labelled substrate.



Chemical Formula: C₈H₈O₂
Molecular Weight: 136.15

¹H NMR (400 MHz, DMSO-*d*₆): 7.82 (d, 2H, ³*J* = 8.3 Hz, ArH¹), 7.29 (d, 2H, ³*J* = 8.3 Hz, ArH²), 2.36 (s, 3H, ArCH₃³).

Incorporation expected at δ 7.82. Determined against integral at δ 2.36.

a) **208a** (7.4 mg, 0.0043 mmol, 5 mol%), b) **13** (11.7 mg, 0.086 mmol), c) Cs₂CO₃ (14.0 mg, 0.043 mmol), d) 3 h, e) 50 °C, e) MeOH (1 mL), and g) 37% D¹.

a) **208a** (7.4 mg, 0.0043 mmol, 5 mol%), b) **13** (11.7 mg, 0.086 mmol), c) NEt(ⁱPr)₂ (0.018 mL, 0.043 mmol), d) 16 h, e) 50 °C, e) MTBE (1 mL), and g) 89% D¹.

9. Computational Details

In this section, the broad details of how calculations were conducted are detailed. See **Appendix B** for the output structures involved.

9.1 General Considerations

Density functional theory (DFT)²⁸⁰ was employed to calculate the gas-phase electronic structures and energies for all species involved in H/D exchange reactions. All structures have been optimised with the hybrid meta-GGA exchange correlation functional M06.²⁸¹ The M06 density functional was used in conjunction with the 6-31G(*d*)²⁸² basis set for main group non-metal atoms and the Stuttgart RSC²⁸³ effective core potential along with the associated basis set for Ir. Changes to this level of theory are stated where necessary. The participating transition states (TS) are located at the same level of theory. Harmonic vibrational frequencies are calculated (with the inclusion of deuterium isotopes wherever stated) at the same level of theory to characterize respective minima (reactants, intermediates, and products with no imaginary frequency) and first order saddle points (TSs with one imaginary frequency). The validity of using the 6-31G(*d*) basis set for chemical interpretations has been checked by comparative single point energy calculations employing the def2-TZVP^{284,285} basis set for all atoms on similar H/D exchange systems.²⁵⁰ All calculations using the M06 functional have been performed using Gaussian 09 quantum chemistry program package (version A.02).²⁸⁶ All structures considered in the PCA model (details below), the Polarizable Continuum Model (PCM)²⁸⁷ for DCM as the solvent was employed. All structural coordinates are listed in Cartesian format, with charge and multiplicity of each system given at the top of the coordinate list (i.e. 0 1 = neutral singlet; 1 1 = 1+ charged singlet).

9.2 Percent Buried Volume Calculations Using SambVca (Web Application)¹³⁸

The only input data required to run the *SambVca* software are the coordinates of the ligand under investigation, and a putative metal-ligand bond distance, *d*. Mesh spacing and sphere radius were kept constant at 0.05 Å and 3.5 Å, respectively. Additionally, atom radii were described by Bondi radii scaled by 1.17. Hydrogen atoms can be excluded from all %*V_{bur}* values provided. The coordinates of the ligand under scrutiny were acquired from DFT optimised structures ran in *Gaussian 09*, or from molecular geometries solved *via*

experimental X-ray crystallography. The coordinates of the ligand were trimmed from full structures of a given complex and converted to .cif or .xyz format using *Mercury 3.0*.^{288,289} All % V_{bur} calculations were carried out using .cif or .xyz files uploaded to the web application.

9.3 Combined Ligand Volume and Ligand Flexibility Parameters

Using DFT-optimised or X-ray coordinates, the % V_{bur} of each ligand in the catalyst intermediate/complex was analysed in turn, as described in **Section 9.2**. In these examples, the d value (distance from metal) was taken from the optimised coordinates of the catalyst intermediate, or X-ray structure under study. This process was repeated, starting from the full set of optimised coordinates, for the other ligand in the same complex. The *Combined Volume* values were calculated using **Equation 3**.

$$\text{Combined Volume} = \Sigma V_{bur} = \%V_{bur}(L^1) + \%V_{bur}(L^2)$$

Equation 3

Referring specifically to DFT-optimised structure types **211** and **212**, the *Ligand Flexibility Parameter*, $\Delta[\Sigma V_{bur}]^2$ was calculated from ΣV_{bur} values for each complex, calculated as described in **Equation 3**, using **Equation 4**:

$$\text{Ligand Flexibility Parameter} = [\Delta(\Sigma V_{bur})]^2 = [\Sigma(V_{bur,211}) - \Sigma(V_{bur,212})]^2$$

Equation 4

NOTE: the squared term avoids the use of negative numbers and accounts for the fact that a given ligand sphere may have a larger ΣV_{bur} value for complex type **211** or **212**, and not necessarily be the same way round for all combinations considered. Sometimes **211** is larger than **212**, and *vice versa*.

9.4 Calculation of Partial Charges Using Natural Bond Order (NBO) Analysis²⁹⁰

For each structure used in the PCA model (details below), partial charge parameters for Ir, Cl, O, C, and H, were generated using the `pop=(nbo, readradii)` keyword in conjunction with geometry optimisations. A covalent radius of 2.02 Å was employed for Ir. Default values were used for all other atoms. The charge values were extracted from *GaussView*, by mapping the charge values on the atoms of the structure under study. **NOTE:** care must be taken such that the NBO charges are mapped and *not* the Mullikan charges supplied by default.

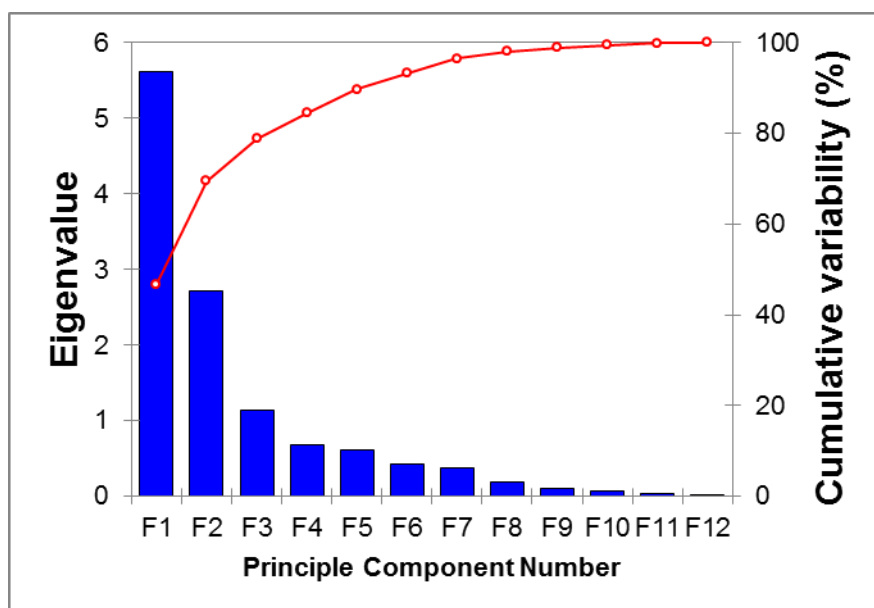
9.5 Generation of Principal Components Analysis Model

Principal Components Analysis (PCA) considers n parameters plotted in n -dimensional space and re-plots the given data in a lower number of dimensions in order to visualise the maximum variance between each data point.²⁰³ In the final model, each axis is labelled as a *Principal Component* (PC1, PC2, PC3, etc.). The lower-numbered PCs represent axes that show a higher degree of spread in the data. For example, PC1 *versus* PC2 will plot the data with the maximum variance available in two dimensions. Plotting PC1 *versus* PC3 may be useful to show variance not captured by PC1 *versus* PC2, however the overall spread will be less than for PC1 *versus* PC2. **NOTE:** each PC represents one axis; however that axis will be representative of a certain combination of the original input variables ($\%V_{bur}$, partial charges, etc.).

Using a selection of those variables described in **Scheme 46**, PCA analysis was performed using the XLSTAT add-in for Microsoft Excel.²⁹¹ The variables used in the final PCA iteration are summarised in the table below. It is important to note that only combined ligand steric parameters are considered in the final model. This avoids ambiguity in defining L^1 and L^2 in each complex.

<i>Variable</i>	<i>Description</i>	<i>Minimum Value</i>	<i>Maximum Value</i>	<i>Standard Deviation</i>
$\Sigma V_{\text{bur},211}$	Combined ligand volume of ligands in 211	30.332	62.100	7.381
$Q_{\text{Ir},211}$	NBO charge on Ir for 211	-1.123	-0.077	0.226
Average $Q_{\text{H},211}$	Average NBO charge for hydrides in 211	0.097	0.180	0.017
$E(\text{HOMO})_{211}$	NBO energy of HOMO in 211	-0.289	-0.210	0.015
$E(\text{HOMO})_{212}$	NBO energy of HOMO in 212	-0.231	-0.179	0.011
$\nu(\text{CO})_{212}$	CO stretching frequency in 212	1988.04	2061.260	13.380
$Q_{\text{C},212}$	NBO charge on carbonyl C in 212	0.586	0.675	0.015
$Q_{\text{O},212}$	NBO charge on carbonyl O in 212	-0.563	-0.451	0.017
$Q_{\text{Ir},212}$	NBO charge on Ir in 212	-0.907	0.547	0.176
$Q_{\text{Cl},212}$	NBO charge on Cl in 212	-0.560	-0.466	0.022
$\Sigma V_{\text{bur},212}$	Combined ligand volume of ligands in 212	32.132	64.700	8.225
$\Delta(\Sigma V_{\text{bur}})^2$	Ligand flexibility parameter	0.000	75.690	15.020

As part of the PCA output, the Scree plot (below) summarises the cumulative variance in the data captured with each successive principle component (PC). The plot uses F rather than PC to mean principle component.



The final table shows the correlations between the original variables and the generated PCs.

<i>Variable</i>	<i>PC1</i>	<i>PC2</i>	<i>PC3</i>
$\Sigma V_{\text{bur},211}$	0.598	-0.716	-0.050
$Q_{\text{Ir},211}$	-0.615	-0.567	-0.252
Average $Q_{\text{H},211}$	0.452	0.814	0.117
$E(\text{HOMO})_{211}$	-0.859	0.144	0.023
$E(\text{HOMO})_{212}$	-0.946	-0.001	0.094
$\nu(\text{CO})_{212}$	0.888	0.098	-0.181
$Q_{\text{C},212}$	0.224	0.725	-0.135
$Q_{\text{O},212}$	0.762	-0.224	-0.188
$Q_{\text{Ir},212}$	-0.566	-0.315	-0.199
$Q_{\text{Cl},212}$	0.947	0.036	-0.096
$\Sigma V_{\text{bur},212}$	0.619	-0.704	0.177
$\Delta(\Sigma V_{\text{bur}})^2$	0.143	-0.147	0.936

9.6 Consideration of Potential Energy Surfaces

In drawing out classical reaction coordinate diagrams from calculated energies, it is imperative that the number of atoms is constant for every structure considered. One structure (often one at the start of the reaction profile) is set to a relative energy of 0 kcal/mol. All other structure energies on the PES are then taken *relative* to the reference structure. Hence, at least one structure on all PES diagrams shown will have a reported relative energy (enthalpy or free energy) of 0 kcal/mol.

9.7 Counterpoise Corrected Binding Energy Calculations

For the purposes of cost-effective bidentate ligand screening *via* ΔE_{bind} , the M06-L functional was used in place of M06.²⁹² Counterpoise corrections and basis set superposition errors were calculated according to published methods.^{248,293} Only the final, *rigorous binding energy* values were extracted from these calculations. No uncorrected terms are reported in

the text. The table below shows the final ΔE_{bind} values for all chelated catalysts considered. All, with the exception of **326t**, have used **325** as the probe molecule. The aforementioned exception uses **27** in place of **325**.

<i>Entry</i>	<i>Ligand</i>	ΔE_{bind} (kcal/mol)
1	326a	-30.8
2	326b-1	-16.0
3	326b-2	-27.9
4	326c	-24.9
5	326d	-17.4
6	326e	-17.1
7	326f	-27.5
8	326g	-29.5
9	326h	-27.8
10	326i	-27.0
11	326j	-24.2
13	326k	-23.7
14	326l	-24.1
15	326m	-27.4
16	326n	-22.8
17	326o	-27.8
18	326p	-27.4
19	326q	-27.1
20	326r	-31.6
21	326s	-27.0
22	326t	-23.1
23	326u	-15.3
24	326v	-15.9

10. References

- (1) Tollefson, J. *Nature* **2011**, 478, 300.
- (2) IMS Health Market Prognosis
http://www.imshealth.com/deployedfiles/imshealth/Global/Content/Corporate/PressRoom/Total_World_Pharma_Market_Topline_metrics_2012-17_regions.pdf (accessed Dec 8, **2014**).
- (3) Alex, A. A.; Storer, R. I. In *Metabolism, Pharmacokinetics and Toxicology of Functional Groups: Impact of Chemical Building Blocks on ADMET*; Smith, D. A., Ed.; Royal Society of Chemistry: Cambridge, **2010**.
- (4) Malik, N. N. *Expert Opin. Drug Discov.* **2009**, 4, 15.
- (5) Lang, L. *Gastroenterology* **2004**, 127, 1026.
- (6) Isin, E. M.; Elmore, C. S.; Nilsson, G. N.; Thompson, R. A.; Weidolf, L. *Chem. Res. Toxicol.* **2012**, 25, 532.
- (7) Ebbing, D. D.; Gammon, S. D. In *General Chemistry*; Houghton Mifflin Company: Boston, **2005**.
- (8) Allen, P. H.; Hickey, M. J.; Kingston, L. P.; Wilkinson, D. J. *J. Label. Compd. Radiopharm.* **2010**, 53, 731.
- (9) Hesk, D.; Lavey, C. F.; McNamara, P. *J. Label. Compd. Radiopharm.* **2010**, 53, 722.
- (10) Heys, J. R. *J. Label. Compd. Radiopharm.* **2007**, 50, 770.
- (11) Lockley, W. J. S.; McEwen, A.; Cooke, R. *J. Label. Compd. Radiopharm.* **2012**, 55, 235.
- (12) Nilsson, G. N.; Kerr, W. J. *J. Label. Compd. Radiopharm.* **2010**, 53, 662.
- (13) Sawama, Y.; Monguchi, Y.; Sajiki, H. *Synlett* **2012**, 23, 959.
- (14) Atzrodt, J.; Derdau, V.; Fey, T.; Zimmermann, J. *Angew. Chem. Int. Ed.* **2007**, 46, 7744.
- (15) Lockley, W. J. S. *J. Label. Compd. Radiopharm.* **2007**, 50, 779.
- (16) Hesk, D.; McNamara, P. *J. Label. Compd. Radiopharm.* **2007**, 50, 875.
- (17) Lin, D.; Chang, W. *J. Anal. Toxicol.* **2000**, 24, 275.
- (18) Atzrodt, J.; Derdau, V. *J. Label. Compd. Radiopharm.* **2010**, 53, 674.
- (19) Parkin, G. *J. Label. Compd. Radiopharm.* **2007**, 50, 1088.

- (20) Heinekey, D. M. *J. Label. Compd. Radiopharm.* **2007**, *50*, 1063.
- (21) Quasdorf, K. W.; Hutters, A. D.; Lodewyk, M. W.; Tantillo, D. J.; Garg, N. K. *J. Am. Chem. Soc.* **2012**, *134*, 1396.
- (22) Jones, J. R.; Lockley, W. J. S.; Lu, S.-Y.; Thompson, S. P. *Tetrahedron Lett.* **2001**, *42*, 331.
- (23) Maegawa, T.; Hirota, K.; Tatematsu, K.; Mori, Y.; Sajiki, H. *J. Org. Chem.* **2005**, *70*, 10581.
- (24) Matsubara, S.; Yokota, Y.; Oshima, K. *Org. Lett.* **2004**, *35*, 2071.
- (25) Matsubara, S.; Yokota, Y.; Oshima, K. *Chem. Lett.* **2004**, *33*, 294.
- (26) Sajiki, H.; Kurita, T.; Esaki, H.; Aoki, F.; Maegawa, T.; Hirota, K. *Org. Lett.* **2004**, *6*, 3521.
- (27) Heys, J. R. *J. Label. Compd. Radiopharm.* **2010**, *53*, 716.
- (28) Lockley, W. J. S.; Hesk, D. *J. Label. Compd. Radiopharm.* **2010**, *53*, 704.
- (29) Winter, M. J. *d-Block Chemistry*; Oxford University Press Inc.: New York, **1994**.
- (30) Crabtree, R. H. *The Organometallic Chemistry of the Transition Metals*; 5th ed.; John Wiley & Sons, Inc.: New Jersey, **2009**.
- (31) Duttwyler, S.; Butterfield, A. M.; Siegel, J. S. *J. Org. Chem.* **2013**, *78*, 2134.
- (32) Garnett, J.; Hodges, R. *J. Am. Chem. Soc.* **1967**, *95*, 4546.
- (33) Emmert, M. H.; Gary, J. B.; Villalobos, J. M.; Sanford, M. S. *Angew. Chem. Int. Ed.* **2010**, *49*, 5884.
- (34) Hickman, A. J.; Cismesia, M. A.; Sanford, M. S. *Organometallics* **2012**, *31*, 1761.
- (35) Blake, M.; Garnett, J.; Gregor, I. *J. Chem. Soc., Chem. Commun.* **1975**, 930.
- (36) Lockley, W. J. S. *Tetrahedron Lett.* **1982**, *23*, 3819.
- (37) Lockley, W. J. S. *J. Label. Compd. Radiopharm.* **1984**, *21*, 45.
- (38) Lockley, W. J. S. *J. Label. Compd. Radiopharm.* **1985**, *22*, 623.
- (39) Hesk, D.; Jones, J. R.; Lockley, W. J. S. *J. Label. Compd. Radiopharm.* **1990**, *28*, 1427.
- (40) Chen, S.; Song, G.; Li, X. *Tetrahedron Lett.* **2008**, *49*, 6929.
- (41) Jones, W. D.; Feher, J. *Organometallics* **1983**, *2*, 562.

- (42) Lenges, C. P.; White, P. S.; Brookhart, M. *J. Am. Chem. Soc.* **1999**, *121*, 4385.
- (43) Milstein, D. *Top. Catal.* **2010**, *53*, 915.
- (44) Campos, J.; Esqueda, A. C.; López-Serrano, J.; Sánchez, L.; Cossio, F. P.; de Cozar, A.; Alvarez, E.; Maya, C.; Carmona, E. *J. Am. Chem. Soc.* **2010**, *132*, 16765.
- (45) Campos, J.; Rubio, M.; Esqueda, A. C.; Carmona, E. *J. Label. Compd. Radiopharm.* **2012**, *55*, 29.
- (46) Rhinehart, J. L.; Manbeck, K. A.; Buzak, S. K.; Lippa, G. M.; Brennessel, W. W.; Goldberg, K. I.; Jones, W. D. *Organometallics* **2012**, *31*, 1943.
- (47) Boutadla, Y.; Davies, D. L.; Macgregor, S. A.; Poblador-Bahamonde, A. I. *Dalton Trans.* **2009**, 5832.
- (48) Di Giuseppe, A.; Castarlenas, R.; Pérez-Torrente, J. J.; Lahoz, F. J.; Polo, V.; Oro, L. A. *Angew. Chem. Int. Ed.* **2011**, *50*, 3938.
- (49) Di Giuseppe, A.; Castarlenas, R.; Pérez-Torrente, J. J.; Lahoz, F. J.; Oro, L. A. *Chem. Eur. J.* **2014**, *20*, 8391.
- (50) Takahashi, M.; Oshima, K.; Matsubara, S. *Chem. Lett.* **2005**, *34*, 192.
- (51) Naota, T.; Takaya, H.; Murahashi, S.-I. *Chem. Rev.* **1998**, *98*, 2599.
- (52) Karvembu, R.; Prabhakaran, R.; Natarajan, K. *Coord. Chem. Rev.* **2005**, *249*, 911.
- (53) Neubert, L.; Michalik, D.; Bähn, S.; Imm, S.; Neumann, H.; Atzrodt, J.; Derdau, V.; Holla, W.; Beller, M. *J. Am. Chem. Soc.* **2012**, *134*, 12239.
- (54) Gröll, B.; Schnürch, M.; Mihovilovic, M. D. *J. Org. Chem.* **2012**, *77*, 4432.
- (55) Azua, A.; Sanz, S.; Peris, E. *Chem. Eur. J.* **2011**, *17*, 3963.
- (56) Piola, L.; Fernández-Salas, J. A.; Manzini, S.; Nolan, S. P. *Org. Biomol. Chem.* **2014**, *12*, 8683.
- (57) Pechtl, M. H. G.; Hölscher, M.; Ben-David, Y.; Theyssen, N.; Loschen, R.; Milstein, D.; Leitner, W. *Angew. Chem. Int. Ed.* **2007**, *46*, 2269.
- (58) Lee, S. H.; Gorelsky, S. I.; Nikonov, G. I. *Organometallics* **2013**, *32*, 6599.
- (59) Leung, C. W.; Zheng, W.; Wang, D.; Ng, S. M.; Yeung, C. H.; Zhou, Z.; Lin, Z.; Lau, C. P. *Organometallics* **2007**, *26*, 1924.
- (60) Young, K. J. H.; Lokare, K. S.; Leung, C. H.; Cheng, M.-J.; Nielsen, R. J.; Petasis, N. A.; Goddard, W. A.; Periana, R. A. *J. Mol. Catal. A* **2011**, *339*, 17.

- (61) Grellier, M.; Mason, S. A.; Albinati, A.; Capelli, S. C.; Rizzato, S.; Bijani, C.; Coppel, Y.; Sabo-Etienne, S. *Inorg. Chem.* **2013**, *52*, 7329.
- (62) Anderson, G.; Saum, S.; Cross, R.; Morris, S. *Organometallics* **1983**, *2*, 780.
- (63) Ryabov, A. D.; Eliseev, A. V.; Yatsimirsky, A. K. *Appl. Organomet. Chem.* **1988**, *2*, 101.
- (64) Ma, S.; Villa, G.; Thuy-Boun, P. S.; Homs, A.; Yu, J.-Q. *Angew. Chem. Int. Ed.* **2014**, *53*, 734.
- (65) Heys, J. R. *J. Label. Compd. Radiopharm.* **2007**, *50*, 770.
- (66) Salter, R. *J. Label. Compd. Radiopharm.* **2010**, *53*, 645.
- (67) Herbert, J. M. *J. Label. Compd. Radiopharm.* **2010**, *53*, 658.
- (68) Lockley, W. J. S. *J. Label. Compd. Radiopharm.* **2010**, *53*, 668.
- (69) Filer, C. N. *J. Label. Compd. Radiopharm.* **2010**, *53*, 739.
- (70) Crabtree, R. H.; Felkin, H.; Morris, G. E. *J. Organomet. Chem.* **1977**, *141*, 205.
- (71) Crabtree, R. H. *Acc. Chem. Res.* **1979**, *12*, 331.
- (72) Lee, H. M.; Jiang, T.; Stevens, E. D.; Nolan, S. P. *Organometallics* **2001**, *20*, 1255.
- (73) Perry, M. C.; Burgess, K. *Tetrahedron Asymm.* **2003**, *14*, 951.
- (74) Smidt, S. P.; Pfaltz, A.; Martínez-Viviente, E.; Pregosin, P. S.; Albinati, A. *Organometallics* **2003**, *22*, 1000.
- (75) Zhu, Y.; Fan, Y.; Burgess, K. *J. Am. Chem. Soc.* **2010**, *132*, 6249.
- (76) Dobereiner, G.; Nova, A. *J. Am. Chem. Soc.* **2011**, *133*, 7547.
- (77) Bennie, L. S.; Fraser, C. J.; Irvine, S.; Kerr, W. J.; Andersson, S.; Nilsson, G. N. *Chem. Commun.* **2011**, *47*, 11653.
- (78) Semeniuchenko, V.; Exner, T. E.; Khilya, V.; Groth, U. *Appl. Organomet. Chem.* **2011**, *25*, 804.
- (79) Hopmann, K. H.; Bayer, A. *Organometallics* **2011**, *30*, 2483.
- (80) Bert, K.; Noël, T.; Kimpe, W.; Goeman, J. L.; Van der Eycken, J. *Org. Biomol. Chem.* **2012**, *10*, 8539.
- (81) Maurer, F.; Huch, V.; Ullrich, A.; Kazmaier, U. *J. Org. Chem.* **2012**, *77*, 5139.
- (82) Gruber, S.; Neuburger, M.; Pfaltz, A. *Organometallics* **2013**, *32*, 4702.

- (83) Kolychev, E. L.; Kronig, S.; Brandhorst, K.; Freytag, M.; Jones, P. G.; Tamm, M. *J. Am. Chem. Soc.* **2013**, *135*, 12448.
- (84) Verendel, J. J.; Pàmies, O.; Diéguez, M.; Andersson, P. G. *Chem. Rev.* **2014**, *114*, 2130.
- (85) Polo, V.; Al-Saadi, A. A.; Oro, L. A. *Organometallics* **2014**, *33*, 5156.
- (86) Liu, Y.; Gridnev, I. D.; Zhang, W. *Angew. Chem. Int. Ed.* **2014**, *53*, 1901.
- (87) Fortman, G. C.; Jacobsen, H.; Cavallo, L.; Nolan, S. P. *Chem. Commun.* **2011**, *47*, 9723.
- (88) Nelson, D. J.; Egbert, J. D.; Nolan, S. P. *Dalt. Trans.* **2013**, *42*, 4105.
- (89) Zhou, J.; Hartwig, J. F. *Angew. Chem. Int. Ed.* **2008**, *47*, 5783.
- (90) Feng, Y.; Jiang, B.; Boyle, P. A.; Ison, E. A. *Organometallics* **2010**, *29*, 2857.
- (91) Lehman, M.; Gary, J.; Boyle, P. *ACS Catal.* **2013**, *3*, 2304.
- (92) Shapley, J. R.; Schrock, R. R.; Osborn, J. A. *J. Am. Chem. Soc.* **1969**, *91*, 2816.
- (93) Heys, J. R. *J. Chem. Soc., Chem. Commun.* **1992**, 680.
- (94) Heys, J. R.; Elmore, C. S. *J. Label. Compd. Radiopharm.* **2009**, *52*, 189.
- (95) Heys, J. R.; Shu, A. Y. L.; Senderoff, S. G.; Phillips, N. M. *J. Label. Compd. Radiopharm.* **1993**, *33*, 431.
- (96) Gusev, D. G.; Berke, H. *Chem. Ber.* **1996**, *129*, 1143.
- (97) Hesk, D.; Das, P. R. *J. Label. Compd. Radiopharm.* **1995**, *36*, 497.
- (98) Shu, A. Y. L.; Chen, W.; Heys, J. R. *J. Organomet. Chem.* **1996**, *524*, 87.
- (99) Ellames, G. J.; Gibson, J. S.; Herbert, J. M.; Kerr, W. J.; McNeill, A. H. *Tetrahedron Lett.* **2001**, *42*, 6413.
- (100) Cross, P. W. C.; Ellames, G. J.; Gibson, J. S.; Herbert, J. M.; Kerr, W. J.; McNeill, A. H.; Mathers, T. W. *Tetrahedron* **2003**, *59*, 3349.
- (101) Ellames, G. J.; Gibson, J. S.; Herbert, J. M.; Kerr, W. J.; McNeill, A. H. *J. Label. Compd. Radiopharm.* **2004**, *47*, 1.
- (102) Herbert, J. M.; Kohler, A. D.; McNeill, A. H. *J. Label. Compd. Radiopharm.* **2005**, *48*, 285.
- (103) Hickey, M. L. J.; Kingston, L. P.; Lockley, W. J. S.; Allen, P.; Mather, A.; Wilkinson, D. J. *J. Label. Compd. Radiopharm.* **2007**, *50*, 286.

- (104) Ellames, G.; Gibson, J.; Herbert, J.; McNeill, A. *Tetrahedron* **2001**, *57*, 9487.
- (105) Bushby, N.; Killick, D. A. *J. Label. Compd. Radiopharm.* **2007**, *50*, 519.
- (106) Vliegen, M.; Haspeslagh, P.; Verluyten, W. *J. Label. Compd. Radiopharm.* **2012**, *55*, 155.
- (107) Kingston, L. P.; Lockley, W. J. S.; Mather, A. N.; Spink, E.; Thompson, S. P.; Wilkinson, D. J. *Tetrahedron Lett.* **2000**, *41*, 2705.
- (108) McAuley, B.; Hickey, M. J.; Kingston, L. P.; Jones, J. R.; Lockley, W. J. S.; Mather, A. N.; Spink, E.; Thompson, S. P.; Wilkinson, D. J. *J. Label. Compd. Radiopharm.* **2003**, *46*, 1191.
- (109) Vázquez-Serrano, L. D.; Owens, B. T.; Buriak, J. M. *Chem. Commun.* **2002**, 2518.
- (110) Powell, M. E.; Elmore, C. S.; Dorff, P. N.; Heys, J. R. *J. Label. Compd. Radiopharm.* **2007**, *50*, 523.
- (111) Cross, P. W. C. PhD Thesis, University of Strathclyde, **2004**.
- (112) Brown, J. A. PhD Thesis, University of Strathclyde, **2007**.
- (113) Brown, J. A.; Irvine, S.; Kennedy, A. R.; Kerr, W. J.; Andersson, S.; Nilsson, G. N. *Chem. Commun.* **2008**, 1115.
- (114) Brown, J. A.; Cochrane, A. R.; Irvine, S.; Kerr, W. J.; Mondal, B.; Parkinson, J. A.; Paterson, L. C.; Reid, M.; Tuttle, T.; Andersson, S.; Nilsson, G. N. *Adv. Synth. Catal.* **2014**, *356*, 3551.
- (115) Cochrane, A. R.; Idziak, C.; Kerr, W. J.; Mondal, B.; Paterson, L. C.; Tuttle, T.; Andersson, S.; Nilsson, G. N. *Org. Biomol. Chem.* **2014**, *12*, 3598.
- (116) Kerr, W. J.; Mudd, R. J.; Paterson, L. C.; Brown, J. A. *Chem. Eur. J.* **2014**, *20*, 14604.
- (117) Simmons, E. M.; Hartwig, J. F. *Angew. Chem. Int. Ed.* **2012**, *51*, 3066.
- (118) Parmentier, M.; Hartung, T.; Pfaltz, A.; Muri, D. *Chem. Eur. J.* **2014**, *20*, 11496.
- (119) Tolman, C. A. *J. Am. Chem. Soc.* **1969**, *92*, 2953.
- (120) Kelly III, R. A.; Clavier, H.; Giudice, S.; Scott, N. M.; Stevens, E. D.; Bordner, J.; Samardjiev, I.; Hoff, C. D.; Cavallo, L.; Nolan, S. P. *Organometallics* **2008**, *27*, 202.
- (121) Nelson, D. J.; Nolan, S. P. *Chem. Soc. Rev.* **2013**, *42*, 6723.
- (122) Tolman, C. A. *J. Am. Chem. Soc.* **1970**, *92*, 2956.
- (123) Herrmann, W. A. *Angew. Chem. Int. Ed.* **2002**, *41*, 1290.

- (124) Díez-González, S.; Marion, N.; Nolan, S. P. *Chem. Rev.* **2009**, *109*, 3612.
- (125) Nolan, S. P. *Eur. J. Inorg. Chem.* **2009**, *2009*, 1664.
- (126) Dröge, T.; Glorius, F. *Angew. Chem. Int. Ed.* **2010**, *49*, 6940.
- (127) Benhamou, L.; Chardon, E.; Lavigne, G.; Bellemin-Laponnaz, S.; Cesar, V. *Chem. Rev.* **2011**, *111*, 2705.
- (128) Clavier, H.; Nolan, S. P. *Chem. Commun.* **2010**, *46*, 841.
- (129) Hopkinson, M. N.; Richter, C.; Schedler, M.; Glorius, F. *Nature* **2014**, *510*, 485.
- (130) Arduengo III, A. J.; Harlow, R. L.; Kline, M. *J. Am. Chem. Soc.* **1991**, *113*, 363.
- (131) Scholl, M.; Ding, S.; Lee, C. W.; Grubbs, R. H. *Org. Lett.* **1999**, *1*, 953.
- (132) Frey, G. D.; Rentzsch, C. F.; von Preysing, D.; Scherg, T.; Mühlhofer, M.; Herdtweck, E.; Herrmann, W. A. *J. Organomet. Chem.* **2006**, *691*, 5725.
- (133) Organ, M. G.; Chass, G.; Fang, D.-C.; Hopkinson, A.; Valente, C. *Synthesis* **2008**, 2776.
- (134) Valente, C.; Calimsiz, S.; Hoi, K. H.; Mallik, D.; Sayah, M.; Organ, M. G. *Angew. Chem. Int. Ed.* **2012**, *51*, 3314.
- (135) Dorta, R.; Stevens, E. D.; Scott, N. M.; Costabile, C.; Cavallo, L.; Hoff, C. D.; Nolan, S. P. *J. Am. Chem. Soc.* **2005**, *127*, 2485.
- (136) Back, O.; Henry-Ellinger, M.; Martin, C. D.; Martin, D.; Bertrand, G. *Angew. Chem. Int. Ed.* **2013**, *125*, 3011.
- (137) Nolan, S. P.; Nelson, D. J.; Slawin, A.; Cordes, D. B.; Poater, A.; Cavallo, L.; Vummaleti, S.; Gomez Suarez, A. *Chem. Sci.* **2015**.
- (138) Poater, A.; Cosenza, B.; Correa, A.; Giudice, S.; Ragone, F.; Scarano, V.; Cavallo, L. *Eur. J. Inorg. Chem.* **2009**, 1759.
- (139) Fey, N.; Orpen, A. G.; Harvey, J. N. *Coord. Chem. Rev.* **2009**, *253*, 704.
- (140) Fey, N.; Haddow, M. F.; Harvey, J. N.; McMullin, C. L.; Orpen, A. G. *Dalton Trans.* **2009**, 8183.
- (141) Lightfoot, A.; Schnider, P.; Pfaltz, A. *Angew. Chem. Int. Ed.* **1998**, *37*, 2897.
- (142) Drago, D.; Pregosin, P. S.; Pfaltz, A. *Chem. Commun.* **2002**, 286.
- (143) Martinez-Viviente, E.; Pregosin, P. S. *Inorg. Chem.* **2003**, *42*, 2209.
- (144) Smidt, S. P.; Zimmermann, N.; Studer, M.; Pfaltz, A. *Chem. Eur. J.* **2004**, *10*, 4685.

- (145) Tsang, A. S.-K.; Sanhueza, I. A.; Schoenebeck, F. *Chem. Eur. J.* **2014**, *20*, 16432.
- (146) Cui, B.; Zheng, B.; He, K.; Zheng, Q. *J. Nat. Prod.* **2003**, *66*, 1101.
- (147) Cochrane, A. R. PhD Thesis, University of Strathclyde, **2011**.
- (148) Hirano, K.; Urban, S.; Wang, C.; Glorius, F. *Org. Lett.* **2009**, *11*, 1019.
- (149) Urban, S.; Tursky, M.; Frohlich, R.; Glorius, F. *Dalt. Trans.* **2009**, 6934.
- (150) Ellames, G. J.; Gibson, J. S.; Herbert, J. M.; Kerr, W. J.; McNeill, A. H. *J. Label. Compd. Radiopharm.* **2004**, *47*, 1.
- (151) Irvine, S. PhD Thesis, University of Strathclyde, **2009**.
- (152) Leuthäusser, S.; Schwarz, D.; Plenio, H. *Chem. Eur. J.* **2007**, *13*, 7195.
- (153) Reid, M. 9 Month Report, University of Strathclyde, **2012**.
- (154) Triphenylphosphine(1,5-cyclooctadiene)[1,3-bis(2,4,6-trimethylphenyl)imidazol-2-ylidene]iridium(I) hexafluorophosphate, min. 98%
http://www.strem.com/catalog/v/77-1825/31/iridium_1019852-99-3 (accessed Jan 11, 2015).
- (155) Tribenzylphosphine(1,5-cyclooctadiene)[1,3-bis(2,4,6-trimethylphenyl)imidazol-2-ylidene]iridium(I) hexafluorophosphate, min. 98%
http://www.strem.com/catalog/v/77-1810/31/iridium_1019853-01-0 (accessed Jan 11, 2015).
- (156) (Dimethylphenylphosphine)(1,5-cyclooctadiene)[1,3-bis(2,4,6-trimethylphenyl)imidazol-2-ylidene]iridium(I) hexafluorophosphate, min. 98%
http://www.strem.com/catalog/v/77-1830/31/iridium_1019853-03-2 (accessed Jan 11, 2015).
- (157) Macchioni, A. *Chem. Rev.* **2005**, *105*, 2039.
- (158) Pregosin, P. S.; Kumar, P. G. A.; Fernández, I. *Chem. Rev.* **2005**, *105*, 2977.
- (159) Krossing, I.; Reisinger, A. *Coord. Chem. Rev.* **2006**, *250*, 2721.
- (160) Macchioni, A.; Bellachioma, G.; Cardaci, G.; Travaglia, M.; Zuccaccia, C.; Milani, B.; Corso, G.; Zangrando, E.; Mestroni, G.; Carfagna, C.; Formica, M. *Organometallics* **1999**, *18*, 3061.
- (161) Evans, L. A.; Fey, N.; Harvey, J. N.; Hose, D.; Lloyd-Jones, G. C.; Murray, P.; Orpen, A. G.; Osborne, R.; Owen-Smith, G. J. J.; Purdie, M. *J. Am. Chem. Soc.* **2008**, *130*, 14471.
- (162) Moreau, C.; Hague, C.; Weller, A. S.; Frost, C. G. *Tetrahedron Asymm.* **2001**, *42*, 6957.

- (163) Vazquez-Serrano, L. D.; Owens, B. T.; Buriak, J. M. *Inorg. Chim. Acta* **2006**, 359, 2786.
- (164) Nelson, D. J.; Truscott, B. J.; Egbert, J. D.; Nolan, S. P. *Organometallics* **2013**, 32, 3769.
- (165) Powell, J.; Lough, A.; Saeed, T. *J. Chem. Soc., Dalton. Trans.* **1997**, 4137.
- (166) O'Connor, A. R.; White, P. S.; Brookhart, M. *Organometallics* **2010**, 29, 5382.
- (167) Phan, D. H. T.; Kim, B.; Dong, V. M. *J. Am. Chem. Soc.* **2009**, 131, 15608.
- (168) Pike, S. D.; Weller, A. S. *Dalton. Trans.* **2013**, 42, 12832.
- (169) Roy, A. H.; Hartwig, J. F. *Organometallics* **2004**, 23, 194.
- (170) Appelhans, L. N.; Zuccaccia, D.; Kovacevic, A.; Chianese, A. R.; Miecznikowski, J. R.; Macchioni, A.; Clot, E.; Eisenstein, O.; Crabtree, R. H. *J. Am. Chem. Soc.* **2005**, 127, 16299.
- (171) Davies, P. W.; Martin, N. *Org. Lett.* **2009**, 11, 2293.
- (172) Hesk, D.; Das, P. R.; Evans, B. *J. Label. Compd. Radiopharm.* **1995**, 36, 497.
- (173) Passays, J.; Ayad, T.; Ratovelomanana-Vidal, V.; Gaumont, A.-C.; Jubault, P.; Leclerc, E. *Tetrahedron Asymm.* **2011**, 22, 562.
- (174) Winkhaus, G.; Singer, H. *Chem. Ber.* **1966**, 3610.
- (175) Constable, D. J. C.; Dunn, P. J.; Hayler, J. D.; Humphrey, G. R.; Leazer, Jr., J. L.; Linderman, R. J.; Lorenz, K.; Manley, J.; Pearlman, B. A.; Wells, A.; Zaks, A.; Zhang, T. Y. *Green Chem.* **2007**, 9, 411.
- (176) Tucker, J. L. *Org. Proc. Res. Dev.* **2006**, 10, 315.
- (177) Sheldon, R. A. *Chem. Soc. Rev.* **2012**, 41, 1437.
- (178) Krossing, I. *Chem. Eur. J.* **2001**, 7, 490.
- (179) Nishida, H.; Takada, N.; Yoshimura, M.; Sonoda, T.; Kobayashi, H. *Bull. Chem. Soc. Japn.* **1984**, 57, 2600.
- (180) Drost, R. M.; Bouwens, T.; van Leest, N. P.; de Bruin, B.; Elsevier, C. J. *ACS Catal.* **2014**, 4, 1349.
- (181) Kalgutkar, A. S.; Daniels, J. S. In *Metabolism, Pharmacokinetics and Toxicology of Functional Groups: Impact of Chemical Building Blocks on ADMET*; Smith, D. A., Ed.; Royal Society of Chemistry: Cambridge, **2010**; pp. 119–122.

- (182) Matsuura, Y.; Tamura, M.; Kochi, T.; Sato, M.; Chatani, N.; Kakiuchi, F. *J. Am. Chem. Soc.* **2007**, *129*, 9858.
- (183) Sadhu, P.; Alla, S. K.; Punniyamurthy, T. *J. Org. Chem.* **2013**, *78*, 6104.
- (184) Wang, L.; Wu, W.; Chen, Q.; He, M. *Org. Biomol. Chem.* **2014**, *12*, 7923.
- (185) McGlacken, G. P.; Bateman, L. M. *Chem. Soc. Rev.* **2009**, *38*, 2447.
- (186) Villa, G.; Thuy-boun, P. S.; Homs, A.; Yu, J. **2013**.
- (187) Zhu, S.-F.; Xie, J.-B.; Zhang, Y.-Z.; Li, S.; Zhou, Q.-L. *J. Am. Chem. Soc.* **2006**, *128*, 12886.
- (188) Li, S.; Zhu, S.-F.; Zhang, C.-M.; Song, S.; Zhou, Q.-L. *J. Am. Chem. Soc.* **2008**, *130*, 8584.
- (189) Song, S.; Zhu, S.-F.; Yang, S.; Li, S.; Zhou, Q.-L. *Angew. Chem. Int. Ed.* **2012**, *51*, 2708.
- (190) Song, S.; Zhu, S.-F.; Yu, Y.-B.; Zhou, Q.-L. *Angew. Chem. Int. Ed.* **2013**, *125*, 1596.
- (191) Owen, M. R.; Luscombe, C.; Godbert, S.; Crookes, D. L.; Emiabata-Smith, D. *Org. Proc. Res. Dev.* **2001**, *5*, 308.
- (192) Leardi, R. *Anal. Chim. Acta* **2009**, *652*, 161.
- (193) Murray, P. M.; Tyler, S. N. G.; Moseley, J. D. *Org. Proc. Res. Dev.* **2013**, *17*, 40.
- (194) Hansch, C.; Leo, A.; Taft, R. W. *Chem. Rev.* **1991**, *91*, 165.
- (195) Fawcett, J.; Harding, D. A. J.; Hope, E. G.; Singh, K.; Solan, G. A. *Dalton Trans.* **2010**, *39*, 10781.
- (196) Mantilli, L.; Gérard, D.; Besnard, C.; Mazet, C. *Eur. J. Inorg. Chem.* **2012**, *2012*, 3320.
- (197) Chang, Y.-H.; Fu, C.-F.; Liu, Y.-H.; Peng, S.-M.; Chen, J.-T.; Liu, S.-T. *Dalton Trans.* **2009**, 861.
- (198) Nelson, D. J.; Truscott, B. J.; Slawin, A. M. Z.; Nolan, S. P. *Inorg. Chem.* **2013**, *52*, 12674.
- (199) Zahalka, H. A.; Alper, H. *Organometallics* **1986**, *5*, 2497.
- (200) Vaska, L.; Jun, J. P. *Chem. Commun.* **1971**, 418.
- (201) Dunbar, K. R.; Haefner, S. C. *Inorg. Chem.* **1992**, *31*, 3676.
- (202) Torres, O.; Martín, M.; Sola, E. *Organometallics* **2009**, *28*, 863.

- (203) Ringnér, M. *Nat. Biotechnol.* **2008**, *26*, 303.
- (204) Jover, J.; Fey, N.; Harvey, J. N.; Lloyd-Jones, G. C.; Orpen, A. G.; Owen-Smith, G. J. J.; Murray, P.; Hose, D. R. J.; Osborne, R.; Purdie, M. *Organometallics* **2012**, *31*, 5302.
- (205) Fey, N.; Tsipis, A. C.; Harris, S. E.; Harvey, J. N.; Orpen, A. G.; Mansson, R. A. *Chem. Eur. J.* **2005**, *12*, 291.
- (206) Fey, N.; Tsipis, A. C.; Harris, S. E.; Harvey, J. N.; Orpen, A. G.; Mansson, R. A. *Chem. Eur. J.* **2005**, *12*, 291.
- (207) Ragone, F.; Poater, A.; Cavallo, L. *J. Am. Chem. Soc.* **2010**, *132*, 4249.
- (208) Serpell, C. J.; Kilah, N. L.; Costa, P. J.; Félix, V.; Beer, P. D. *Angew. Chem. Int. Ed.* **2010**, *49*, 5322.
- (209) Wang, H.; Lin, I. *Organometallics* **1998**, *17*, 972.
- (210) Perutz, R. N.; Sabo-Etienne, S. *Angew. Chem. Int. Ed.* **2007**, *46*, 2578.
- (211) Drews, J. *Science* **2000**, *287*, 1960.
- (212) Walsh, C. *Nat. Rev. Microbiol.* **2003**, *1*, 65.
- (213) Domagk, G. *Dtsch. Med. Wochenschr.* **1935**, *61*, 250.
- (214) Collins, K. D.; Glorius, F. *Nat. Chem.* **2013**, *5*, 597.
- (215) Penning, T. D.; Talley, J. J.; Bertenshaw, S. R.; Carter, J. S.; Collins, P. W.; Docter, S.; Graneto, M. J.; Lee, L. F.; Malecha, J. W.; Miyashiro, J. M.; Rogers, R. S.; Rogier, D. J.; Yu, S. S.; AndersonGD; Burton, E. G.; Cogburn, J. N.; Gregory, S. A.; Koboldt, C. M.; Perkins, W. E.; Seibert, K.; Veenhuizen, A. W.; Zhang, Y. Y.; Isakson, P. C. *J. Med. Chem.* **1997**, *40*, 1347.
- (216) Whitesides, G. M.; Hackett, M.; Brainard, R. L.; Lavalleye, J.-P. P. M.; Sowinski, A. F.; Izumi, A. N.; Moore, S. S.; Brown, D. W.; Staudt, E. M. *Organometallics* **1985**, *4*, 1819.
- (217) Poater, A.; Falivene, L.; Urbina-Blanco, C. a.; Manzini, S.; Nolan, S. P.; Cavallo, L. *Procedia Comput. Sci.* **2013**, *18*, 845.
- (218) Wiberg, K. B. *Chem. Rev.* **1955**, *55*, 713.
- (219) Westheimer, F. H. *Chem. Rev.* **1961**, *61*, 265.
- (220) Westaway, K. C. *J. Label. Compd. Radiopharm.* **2007**, *50*, 989.
- (221) Swiderek, K.; Paneth, P. *Chem. Rev.* **2013**, *113*, 7851.

- (222) Gómez-Gallego, M.; Sierra, M. A. *Chem. Rev.* **2011**, *111*, 4857.
- (223) Ariza, X.; Asins, G.; Garcia, J.; Hegardt, F. G.; Makowski, K.; Serra, D.; Velasco, J. J. *J. Label. Compd. Radiopharm.* **2010**, *53*, 556.
- (224) Barnett, D. W.; Refaei, M. S.; Curley, R. W. *J. Label. Comp. Radiopharm.* **2013**, *56*, 6.
- (225) Boga, S. B.; Alhassan, A. B.; Hesk, D. *Tetrahedron Lett.* **2014**, *55*, 4442.
- (226) Chappelle, M. R.; Hawes, C. R. *J. Label. Compd. Radiopharm.* **2010**, *53*, 745.
- (227) Korsager, S.; Taaning, R. H.; Lindhardt, A. T.; Skrydstrup, T. *J. Org. Chem.* **2013**, *78*, 6112.
- (228) Skaddan, M. B.; Yung, C. M.; Bergman, R. G. *Org. Lett.* **2004**, *6*, 11.
- (229) Yung, C. M.; Skaddan, M. B.; Bergman, R. G. *J. Am. Chem. Soc.* **2004**, *126*, 13033.
- (230) Beck, C. M.; Rathmill, S. E.; Park, Y. J.; Chen, J.; Crabtree, R. H.; Liable-Sands, L. M.; Rheingold, A. L. *Organometallics* **1999**, *18*, 5311.
- (231) Kwong, F. Y.; Lee, H. W.; Lam, W. H.; Qiu, L.; Chan, A. S. C. *Tetrahedron Asymm.* **2006**, *17*, 1238.
- (232) Fristrup, P.; Kreis, M.; Palmelund, A.; Norrby, P.-O.; Madsen, R. *J. Am. Chem. Soc.* **2008**, *130*, 5206.
- (233) Iwai, T.; Fujihara, T.; Tsuji, Y. *Chem. Commun.* **2008**, 6215.
- (234) Olsen, E. P. K.; Madsen, R. *Chem. Eur. J.* **2012**, *18*, 16023.
- (235) Olsen, E. P. K.; Singh, T.; Harris, P.; Andersson, P. G.; Madsen, R. *J. Am. Chem. Soc.* **2015**, *137*, 834.
- (236) Willis, M. C. *Chem. Rev.* **2010**, *110*, 725.
- (237) Castaing, M.; Wason, S. L.; Estepa, B.; Hooper, J. F.; Willis, M. C. *Angew. Chem. Int. Ed.* **2013**, *125*, 13522.
- (238) Leung, J. C.; Krische, M. J. *Chem. Sci.* **2012**, *3*, 2202.
- (239) Poingdestre, S.-J.; Goodacre, J. D.; Weller, A. S.; Willis, M. C. *Chem. Commun. (Camb)*. **2012**, *48*, 6354.
- (240) Hooper, J. F.; Young, R. D.; Weller, A. S.; Willis, M. C. *Chem. Eur. J.* **2013**, *19*, 3125.
- (241) Pawley, R. J.; Huertos, M. a.; Lloyd-Jones, G. C.; Weller, A. S.; Willis, M. C. *Organometallics* **2012**, *31*, 5650.
- (242) Murphy, S. K.; Bruch, A.; Dong, V. M. *Angew. Chem. Int. Ed.* **2014**, *53*, 2455.

- (243) Murphy, S. K.; Bruch, A.; Dong, V. M. *Chem. Sci.* **2014**, *6*, 174.
- (244) Murphy, S. K.; Dong, V. M. *Chem. Commun.* **2014**, *50*, 13645.
- (245) Nelson, D. J.; Collado, A.; Manzini, S.; Meiries, S.; Slawin, A. M. Z.; Cordes, D. B.; Nolan, S. P. *Organometallics* **2014**, *33*, 2048.
- (246) Mudd, R. J. 9 Month Report, University of Strathclyde, **2014**.
- (247) Black, P. J.; Cami-Kobeci, G.; Edwards, M. G.; Slatford, P. A.; Whittlesey, M. K.; Williams, J. M. J. *Org. Biomol. Chem.* **2006**, *4*, 116.
- (248) Sherrill, C. D. vergil.chemistry.gatech.edu/notes/cp.pdf (accessed Jan 11, **2015**).
- (249) Wolf, J.; Labande, A.; Daran, J.-C.; Poli, R. *J. Organomet. Chem.* **2006**, *691*, 433.
- (250) Kerr, W. J.; Reid, M.; Tuttle, T. *ACS Catal.* **2015**, *5*, 402.
- (251) Kennedy, A. R.; Kerr, W. J.; Moir, R.; Reid, M. *Org. Biomol. Chem.* **2014**, *12*, 7927.
- (252) Pan, S.; Shibata, T. *ACS Catal.* **2013**, *3*, 704.
- (253) Abu-hasanayn, F.; Krogh-jespersen, K.; Coldman, A. S.; Brunswick, N. *Inorg. Chem.* **1993**, *32*, 495.
- (254) Kubota, M.; Bencala, K. E.; Kiefer, G. W. *Inorg. Chim. Acta* **1973**, *7*, 195.
- (255) Chai, C.; Armarego, W. R. F. *Purification of Laboratory Chemicals*; Butterworth-Heinemann, **2012**.
- (256) Coles, S. J.; Gale, P. A. *Chem. Sci.* **2012**, *3*, 683.
- (257) Sheldrick, G. M. *Acta Cryst.* **2008**, *64*, 112.
- (258) Spek, A. L. *Act Cryst.* **2009**, *65*, 148.
- (259) Yuan, D.; Tang, H.; Xiao, L.; Huynh, H. V. *Dalton. Trans.* **2011**, *40*, 8788.
- (260) Landaeta, V. R.; Peruzzini, M.; Herrera, V.; Bianchini, C.; Sánchez-Delgado, R. a.; Goeta, A. E.; Zanobini, F. *J. Organomet. Chem.* **2006**, *691*, 1039.
- (261) Li, F.; Zhang, H.; Jiang, L.; Zhang, W.; Nie, J.; Feng, Y.; Yang, M.; Liu, M. *Magn. Reson. Chem.* **2007**, *45*, 929.
- (262) Jiménez, M. V.; Fernández-Tornos, J.; Pérez-Torrente, J. J.; Modrego, F. J.; Winterle, S.; Cunchillos, C.; Lahoz, F. J.; Oro, L. A. *Organometallics* **2011**, *30*, 5493.
- (263) Cochrane, A. R.; Irvine, S.; Kerr, W. J.; Reid, M.; Andersson, S.; Nilsson, G. N. *J. Label. Compd. Radiopharm.* **2013**, *56*, 451.

- (264) Ahammed, S.; Saha, A.; Ranu, B. C. *J. Org. Chem.* **2011**, *76*, 7235.
- (265) Hinklin, R. J.; Kiessling, L. L. *Org. Lett.* **2002**, *4*, 1131.
- (266) Gentile, G.; Hamprecht, D.; Micheli, F.; Prandi, A.; Terreni, S. International Patent. WO2007/022935 A1, **2007**.
- (267) Morimoto, H.; Shimadzu, H.; Kushiya, E.; Kawanishi, H.; Hosaka, T.; Kawase, Y.; Yasuda, K.; Kikkawa, K.; Yamauchi-Kohno, R.; Yamada, K. *J. Med. Chem.* **2001**, *44*, 3355.
- (268) Veisi, H.; Ghorbani-Vaghei, R.; Hemmati, S.; Mahmoodi, J. *Synlett* **2011**, *2011*, 2315.
- (269) De Benedetti, P. G.; Iarossi, D.; Menziani, M. C.; Frassinetti, C.; Benedetti, A. *J. Mole. Struc.* **1988**, *175*, 37.
- (270) Guntrip, B. S. International Patent. WO 2004/039762 A1, **2004**.
- (271) Yoichi, K.; Sato, K.; Sato, T. US Patent. 6610853 B1, **2003**.
- (272) Lobb, K. L.; Hipskind, P. A.; Aikins, J. A.; Alvarez, E.; Cheung, Y.-Y.; Considine, E. L.; De Dios, A.; Durst, G. L.; Ferritto, R.; Grossman, C. S.; Giera, D. D.; Hollister, B. A.; Huang, Z.; Iversen, P. W.; Law, K. L.; Li, T.; Lin, H.-S.; Lopez, B.; Lopez, J. E.; Cabrejas, L. M. M.; McCann, D. J.; Molero, V.; Reilly, J. E.; Richett, M. E.; Shih, C.; Teicher, B.; Wikel, J. H.; White, W. T.; Mader, M. M. *J. Med. Chem.* **2004**, *47*, 5367.
- (273) Arnsward, M.; Neumann, W. P. *Chem. Ber.* **1991**, *124*, 1997.
- (274) Cai, C.; Rivera, N. R.; Balsells, J.; Sidler, R. R.; McWilliams, J. C.; Shultz, C. S.; Sun, Y. *Org. Lett.* **2006**, *8*, 5161.
- (275) Alper, H.; Xu, T. *Tetrahedron Lett.* **2013**, *54*, 5496.
- (276) De Morin, F. F. International Patent. WO 2007/076092 A2, 2007.
- (277) Pompeo, M.; Froese, R. D. J.; Hadei, N.; Organ, M. G. *Angew. Chem. Int. Ed.* **2012**, *51*, 11354.
- (278) Su, H.-L.; Pérez, L. M.; Lee, S.-J.; Reibenspies, J. H.; Bazzi, H. S.; Bergbreiter, D. E. *Organometallics* **2012**, *31*, 4063.
- (279) Wolf, J.; Labande, A.; Daran, J.; Poli, R. *Eur. J. Inorg. Chem.* **2008**, 3024.
- (280) Kohn, W.; Sham, L. *Phys. Rev.* **1965**, *140*, 1133.
- (281) Zhao, Y.; Truhlar, D. G. *Theor. Chem. Acc.* **2008**, *120*, 215.
- (282) Francl, M. M.; Pietro, W. J.; Hehre, W. J.; Binkley, J. S.; DeFrees, D. J.; Pople, J. A.; Gordon, M. S. *J. Chem. Phys.* **1982**, *77*, 3654.

- (283) Andrae, D.; Häußermann, U.; Dolg, M.; Stoll, H.; Preuß, H. *Theor. Chim. Acta* **1990**, *77*, 123.
- (284) Weigend, F.; Ahlrichs, R. *Phys. Chem. Chem. Phys.* **2005**, *7*, 3297.
- (285) Weigend, F. *Phys. Chem. Chem. Phys.* **2006**, *8*, 1057.
- (286) Frisch, M. J.; Trucks, G. W.; Schlegel, H. B.; Scuseria, G. E.; Robb, M. A.; Cheeseman, J. R.; Scalmani, G.; Barone, V.; Mennucci, B.; Petersson, G. A.; Nakatsuji, H.; Caricato, M.; Li, X.; Hratchian, H. P.; Izmaylov, A. F.; Bloino, J.; Zheng, G.; Sonnenberg, J. L.; Hada, M.; Ehara, M.; Toyota, K.; Fukuda, R.; Hasegawa, J.; Ishida, M.; Nakajima, T.; Honda, Y.; Kitao, O.; Nakai, H.; Vreven, T.; J. A. Montgomery, J.; Peralta, J. E.; Ogliaro, F.; Bearpark, M.; Heyd, J. J.; Brothers, E.; Kudin, K. N.; Staroverov, V. N.; Kobayashi, R.; Normand, J.; Raghavachari, K.; Rendell, A.; Burant, J. C.; Iyengar, S. S.; Tomasi, J.; Cossi, M.; Rega, N.; Millam, J. M.; Klene, M.; Knox, J. E.; Cross, J. B.; Bakken, V.; Adamo, C.; Jaramillo, J.; Gomperts, R.; Stratmann, R. E.; Yazyev, O.; Austin, A. J.; Cammi, R.; Pomelli, C.; Ochterski, J. W.; Martin, R. L.; Morokuma, K.; Zakrzewski, V. G.; Voth, G. A.; Salvador, P.; Dannenberg, J. J.; Dapprich, S.; Daniels, A. D.; Farkas, O.; Foresman, J. B.; Ortiz, J. V.; Cioslowski, J.; Fox, D. J. Gaussian, Inc., 2009.
- (287) Tomasi, J.; Mennucci, B.; Cammi, R. *Chem. Rev.* **2005**, *105*, 2999.
- (288) Macrae, C. F.; Bruno, I. J.; Chisholm, J. A.; Edgington, P. R.; McCabe, P.; Pidcock, E.; Rodriguez-Monge, L. Taylor, R.; Streek, J. v. d.; Wood, P. A. Mercury, **2008**.
- (289) Macrae, C. F.; Bruno, I. J.; Chisholm, J. A.; Edgington, P. R.; McCabe, P.; Pidcock, E.; Rodriguez-Monge, L.; Taylor, R.; Streek, J. v. d.; Wood, P. A. *J. Appl. Cryst.* **2008**, *41*, 466.
- (290) Reed, A. E.; Weinstock, R. B.; Weinhold, F. *J. Chem. Phys.* **1985**, *83*, 735.
- (291) XLSTAT Version 2015.1.01 <http://www.xlstat.com/en/>.
- (292) Gusev, D. G. *Organometallics* **2013**, *32*, 4239.
- (293) Kirschner, K. *J. Chem. Ed.* **2007**, *84*, 1225.